Drosophila versus *Mycobacteria*: Host-pathogen interactions between *Drosophila melanogaster* and *Mycobacterium abscessus*.

Eleanor Kirsten Phyllis Marshall

MRC Centre for Molecular Bacteriology and Infection

Imperial College London

Supervisor:

Professor Marc Dionne

Thesis submitted to the Department of Life Sciences, Imperial College London for the degree of Doctor of Philosophy.

Statement of originality

I confirm the work presented in this thesis is my own. Any work and external contributions performed by others has been referenced and acknowledged.

A significant part of the work presented in Chapter 1: Introduction has been published as Eleanor K.P. Marshall and Marc S. Dionne. *Drosophila* versus *Mycobacteria*: A model for mycobacterial host–pathogen interactions. Molecular Microbiology,117(3):600–609, 3 2022.

Eleanor Marshall

Copyright declaration

The copyright of this thesis rests with the author. Unless otherwise indicated, its contents are licensed under a Creative Commons Attribution-Non Commercial 4.0 International Licence (CC BY-NC).

Under this licence, you may copy and redistribute the material in any medium or format. You may also create and distribute modified versions of the work. This is on the condition that: you credit the author and do not use it, or any derivative works, for a commercial purpose.

When reusing or sharing this work, ensure you make the licence terms clear to others by naming the licence and linking to the licence text. Where a work has been adapted, you should indicate that the work has been changed and describe those changes.

Please seek permission from the copyright holder for uses of this work that are not included in this licence or permitted under UK Copyright Law.

Abstract

Host-pathogen interactions are shaped by many factors and can determine infection outcomes, often by influencing the host immune response and bacterial virulence. This project applied the genetic tractability of *D. melanogaster* to explore the interactions with *M. abscessus* in the context of the innate and cellular immune responses. *M. abscessus* is an emerging pathogen that represents a major threat to individuals with cystic fibrosis, with infection rates increasing globally. The genetic determinants of *M. abscessus* virulence are poorly understood, partly due to a lack of genetic tools.

Using CRISPR-Cas9, I produced *M. abscessus* knockout strains targeting a variety of genes to study their role during infection and identify host factors they may interact with. This included the *M. abscessus tad* locus, loss of which causes increased pellicle biofilm formation, decreased intercellular adhesion and prolonged *D. melanogaster* survival. By manipulating host and microbial genetics, I found the increase in *D. melanogaster* survival during infection with *tad* knockout strains was due to TNFα signalling. This suggests the *tad* deletion mutations acquired in a dominant circulating clone of *M. abscessus* may promote initial colonisation and transmission at the expense of resistance against immune responses.

Amino acid uptake by *M. abscessus* was also found to influence *D. melanogaster* immune responses, identified by knockout of an asparagine permease. Asparagine-limited *M. abscessus* resulted in longer-lived flies without significant change in bacterial loads. This survival increase can be attributed to cytokine signalling in *D. melanogaster*, with possible links to dysregulated insulin signalling. This demonstrates that asparagine uptake in *M. abscessus* prior to infection is not required for replicative fitness *in vivo* but does influence the interaction with the host.

This work has characterised *D. melanogaster* as a model for *M. abscessus* infection,

highlighting the importance of the physical properties and metabolic status of a microbe in influencing host-pathogen interactions.

Acknowledgements

I would first like to thank my supervisor, Professor Marc Dionne. I am immensely grateful for the opportunity to undertake this project and for your support, guidance, and kindness throughout everything that has happened in the past years. You've taught me what it means to be a good scientist, and always supplied excellent snacks.

I'd also like to thank my friends and colleagues within the Dionne lab. Dr Jake Jacobson, for patching me up on multiple occasions, Dr Crystal Vincent, for teaching me French and TLCs, Dr Carolina Simoes da Silva Pereira, for teaching me the secrets of Western Blots and fulfilling my dreams of being a Ghostbuster, Dr Catarina Nunes, for your help with experiments and introducing me to mixed effects regression models, Dr Will Pearson, for your kindness and saving my car, Dr Ashima Wadhawan, for teaching me about all things bacteria and always telling me when I've gone red, Dr Krista Grimes, for helping me understand *Drosophila* genetics and crosses, and Natalie Munroe (hello Clarice), for being so much fun. You've all contributed so much feedback and advice to the project, and it has been wonderful to work with you. You've made Imperial feel like home.

My thanks also go to the members of the Floto lab, especially Dr Sophie Burbaud and Jasper Sangen, for looking after me during my time in Cambridge, teaching me about all things *abscessus*, and showing me the importance of daily coffee breaks.

Thanks to the South Kensington Fly Forum and the broader CMBI community, for the collective support, constructive feedback, and a vacuum manifold so I could perform 192 PCR purifications at once. Special thanks to Dr Marta Rudzite and Andrea Majstorovic for their friendship and dedication to improving the CMBI.

The support from my family has made it possible to pursue a PhD. I will be forever grateful to my parents for their support, patience, and strength during these years. And also for filling up

my washer fluid and supplying me with Costa. My siblings, Kim, for doing excellent science drawings to make figures, Frances, for introducing me to my two biggest distractions (A Song of Ice and Fire, and Formula 1), and Luke, for keeping me humble. Finally, Louis - you've been here every step of the way, and have made every part of it better. Thank you for the great fun, and the great food.

Table of Contents

Statement of originality **2**

Copyright declaration **3**

Abstract **4**

Acknowledgements **6**

List of Figures **14**

List of Tables **18**

Abbreviations **19**

Chapter 1: Introduction **25**

1.1 The pathogen: *Mycobacterium abscessus* 25

1.1.1 The mycobacterial cell envelope 26

1.1.1.1 Morphotypes 27

1.1.1.2 Morphotype conversion 28

1.1.1.3 Type VII secretion system 30

1.1.2 Biofilms 32

1.1.3 Immune Response to *M. abscessus* 34

1.1.3.1 Cellular response and phagocytosis 35

1.1.3.2 Innate immune response 37

1.1.3.3 Adaptive immune response 38

1.1.4 Evolution and emergence of *Mycobacterium abscessus* 39

1.1.4.1 A note on taxonomy 41

1.1.4.2 Infection sources and transmission 43

1.1.5 Epidemiology 45

1.1.5.1 Risk factors 46

1.1.5.2 Clinical relevance 48

1.1.6 Treatment and Antimicrobial resistance 50

1.1.6.1 Intrinsic resistance 51

1.1.6.2 Adaptive resistance 51

1.1.6.3 Acquired resistance 52

1.1.7 Models for studying *M. abscessus* 52

1.1.7.1 *In vitro* models 52

1.1.7.2 *In vivo* models 53

1.2 The model organism: *Drosophila melanogaster* 54

1.2.1 *Drosophila melanogaster* immunity and defence 55

1.2.1.1 Humoral immunity 56
1.2.1.2 Toll signalling pathway and melanisation 58
1.2.1.3 Imd signalling pathway 61
1.2.1.4 Eiger signalling and apoptosis 61
1.2.1.5 JAK/STAT signalling 67
1.2.1.6 Cellular immunity 69
1.2.2 Immunometabolism 70
1.2.2.1 Insulin signalling 71
1.2.3 Modelling mycobacterial infection in *Drosophila melanogaster* 72
1.2.3.1 Detection of mycobacteria by *Drosophila melanogaster* 73
1.2.3.2 Uptake of mycobacteria by *Drosophila melanogaster* phagocytic cells 75
1.2.3.3 *Drosophila melanogaster* host factors restricting intracellular mycobacterial growth 76
1.2.3.4 Role of autophagy during mycobacterial infection 79
1.2.3.5 Mycobacterial virulence factors 81
1.2.3.6 Resistance, tolerance, virulence 82
1.3 Genetic editing in mycobacteria 83
1.3.1 Homologous recombination 84
1.3.2 CRISPRi and CRISPR 85
1.4 Phenogenomics of *M. abscessus* 89
1.5 Project aims and thesis outline 90
Chapter 2: Materials and methods 92
2.1 Bacterial strains, plasmids, and culture conditions 92
2.1.1 Bacterial strains and plasmids 92
2.1.2 Culture conditions 100
2.1.3 Generating CRISPR knockout mutants 102
2.1.3.1 Plasmid construction and cloning 102
2.1.3.2 Transformation of electrocompetent *M. abscessus* 106
2.1.3.3 CRISPR-Cas9 induction 107
2.1.3.4 Screening *M. abscessus* CRISPR strains 107
2.2 Bacterial growth experiments 109
2.2.1 Growth curves 109
2.2.2 Biofilm assay 109
2.2.3 Biofilm imaging 110
2.3 *Drosophila melanogaster* experiments 110

2.3.1 Fly husbandry 110
2.3.2 Stocks and crosses 111
2.3.2.1 UAS-Gal4 System 114
2.3.3 Transgenic flies 115
2.3.4 *Drosophila* injection 117
2.3.5 Survival experiments 117
2.3.6 Bacterial load quantifications 118
2.3.7 Live *in vivo* confocal imaging 118
2.3.8 *D. melanogaster* adult eye imaging 118
2.4 Molecular biology techniques 119
2.4.1 Generating electrocompetent *M. abscessus* 119
2.4.2 Polymerase chain reaction 119
2.4.3 Gel electrophoresis 121
2.4.4 PCR purification 121
2.4.5 Gel extraction 122
2.4.6 Sanger sequencing 122
2.4.7 RT-qPCR 122
2.4.7.1 Bacterial gene expression 123
2.4.7.2 *Drosophila* gene expression 123
2.4.7.3 RNA isolation 123
2.4.7.4 DNAse treatment and reverse transcription 124
2.4.7.5 RT-qPCR reaction 125
2.4.8 Thin layer chromatography 127
2.4.9 SDS PAGE 127
2.4.10 Western Blots 128
2.5 Statistical analysis and data visualisation 131
Chapter 3: *Drosophila melanogaster* as a model for *Mycobacterium abscessus* infection 132
3.1 Introduction 132
3.2 Aims 133
3.3 Results 134
3.3.1 *Drosophila melanogaster* is susceptible to infection with *Mycobacterium abscessus* 134
3.3.2 Activation of Toll pathway signalling during *M. abscessus* infection 138
3.3.2.1 Toll pathway antimicrobial peptides 138
3.3.2.2 Bomanin antibacterial effectors and Immune-induced molecules 141

3.3.2.3 Melanisation response 144
3.3.3 Activation of Imd pathway signalling during *M. abscessus* infection. ... 145
3.3.4 Eiger signalling during *M. abscessus* infection 149
3.3.5 Cytokine signalling during *M. abscessus* infection..... 152
3.3.6 Uptake of *M. abscessus* by *D. melanogaster* haemocytes 155
3.4 Discussion 160
3.4.1 Optimisation of *M. abscessus* injection..... 160
3.4.2 Detection of *M. abscessus* by *D. melanogaster* immune signalling pathways..... 163
3.4.3 *M. abscessus* induces an ineffective immune response in *D. melanogaster* 165
3.4.4 The role of the cellular response during *M. abscessus* infection 166
3.4.5 Differences between *M. abscessus* morphotypes 167
Chapter 4: Screening *Mycobacterium abscessus* CRISPR knockout mutants 169
4.1 Introduction 169
4.2 Aims 172
4.3 Results 172
4.3.1 Generating CRISPR frameshift mutations 172
4.3.2 MAB_0169c: Exported repetitive protein..... 178
4.3.3 MAB_0471 and MAB_0472: Hypothetical transmembrane proteins 181
4.3.4 MAB_1012c: YrbE family protein 185
4.3.5 MAB_1132c: L-asparagine permease..... 188
4.3.6 MAB_1283c: WXG100 family type VII secretion target 190
4.3.7 MAB_2262c: Mycobactin import ATP-binding/permease protein IrtA ... 192
4.3.8 MAB_3522c and MAB_3523c: Assimilatory sulfite reductase and Integral membrane nitrite extrusion protein NarK3 194
4.3.9 MAB_4163c: Fatty-acid-CoA ligase FadD 198
4.3.10 MAB_4588c: Enoyl-CoA hydratase/isomerase 201
4.4 Discussion 203
4.4.1 CRISPR editing of *M. abscessus* and gene essentiality 203
4.4.2 Future work using the *M. abscessus* knockout strains 205
Chapter 5: Putative type-IVb pilus in *Mycobacterium abscessus* and its interactions with host signalling pathways..... 209
5.1 Introduction 209
5.2 Aims 212
5.3 Results 213

5.3.1 Possible functions of MAB_0471 and MAB_0472 213
5.3.2 MAB_0471 and MAB_0472 mutants show exaggerated pellicle biofilm formation 216
5.3.3 MAB_0471 and MAB_0472 inhibit eiger signalling in *D. melanogaster*. 220
5.3.4 Interaction of MAB_0471 and MAB_0472 with Imd signalling 225
5.3.5 Expressing MAB_0473, MAB_0474, or MAB_0475 in haemocytes does not rescue survival phenotype of *M. abscessus* MAB_0471 and MAB_0472 mutant strains 231
5.4 Discussion 235
5.4.1 Role of MAB_0471 and MAB_0472 in biofilm formation 236
5.4.2 Role of MAB_0471 and MAB_0472 in host interactions 239

Chapter 6: Asparagine limitation in *M. abscessus* leads to changes in *D. melanogaster* cytokine signalling and metabolism 242

6.1 Introduction 242
6.2 Aims 244
6.3 Results 244
6.3.1 MAB_1132c functions as an asparagine permease in *M. abscessus* ... 244
6.3.2 Asparagine acquisition by *M. abscessus* impacts bacterial virulence and host tolerance 247
6.3.3 Nitrogen limitation is not driving changes in virulence caused by asparagine limitation 249
6.3.4 Innate immune signalling is diminished in flies infected with asparagine permease mutant *M. abscessus* strains 253
6.3.5 Cytokine signalling in *D. melanogaster* is responsible for changes in host susceptibility to asparagine-limited *M. abscessus* 259
6.3.6 Asparagine uptake by *M. abscessus* drives changes in host insulin/Akt signalling 260
6.4 Discussion 262

Chapter 7: Discussion 266

7.1 Summary of work presented 266
7.1.1 Background and aim of the project 266
7.1.2 Key findings 267
7.2 *D. melanogaster* as a model for *M. abscessus* infection 269
7.2.1 The role of haemocytes 270
7.2.2 *M. abscessus* interactions with *D. melanogaster* differ from those with *M. marinum* 272
7.3 Insights into *M. abscessus* pathogenesis 273
7.3.1 Pathogenic evolution of *M. abscessus* 273

7.3.2 Impact of microbial metabolic status on host-pathogen interactions 274
7.4 Conclusions, future questions, and outlook 275
References 277
Appendix 344

List of Figures

Figure 1.1 Structure of the mycobacterial cell envelope 26

Figure 1.2 *M. abscessus* morphotypes 28

Figure 1.3 Advances in cystic fibrosis treatment and the emergence of *M. abscessus* dominant circulating clones 41

Figure 1.4 *Mycobacterium abscessus* complex taxonomic changes 42

Figure 1.5 Toll pathway signalling and melanisation cascade 59

Figure 1.6 Imd pathway signalling 62

Figure 1.7 Eiger signalling pathway 64

Figure 1.8 JAK/STAT signalling pathway 68

Figure 1.9 Insulin signalling 72

Figure 1.10 CRISPR for mycobacterial gene editing 88

Figure 2.1 UAS-Gal4 system for tissue specific expression of transgenes in *D. melanogaster* 115

Figure 2.2 Outline of crosses performed to generate experimental and control genotypes 116

Figure 3.1 Dose-dependent effects of initial *M. abscessus* inoculum on *D. melanogaster* survival 136

Figure 3.2 Selecting a suitable detergent for *M. abscessus* bacterial load quantifications 138

Figure 3.3 *In vitro* growth characteristics of *M. abscessus* morphotypes 139

Figure 3.4 Survival of Dif^{1} flies with *M. abscessus* 140

Figure 3.5 Transcript levels of canonical Toll pathway AMPs during *M. abscessus* infection 142

Figure 3.6 Survival of $Bom^{\Delta 55c}$ flies with *M. abscessus* 143

Figure 3.7 Transcript levels of Bomanins and Immune-induced molecules during *M. abscessus* infection 145

Figure 3.8 Survival of $PPO1^{\Delta}$, $PPO2^{\Delta}$ flies with *M. abscessus* 146

Figure 3.9 Survival of imd^{10191} flies with *M. abscessus* 147

Figure 3.10 Transcript levels of canonical Imd pathway AMPs during *M. abscessus* infection 148

Figure 3.11 Survival of $Tak1^{1}$ flies with *M. abscessus* 149

Figure 3.12 Survival of egr^{1ag} and egr^{3ag} flies with *M. abscessus* 150

Figure 3.13 Transcript levels of *egr-RA* and *Tace* during *M. abscessus* infection 151
Figure 3.14 Survival of *Upd2*$^{\Delta}$, *Upd3*$^{\Delta}$, and *Upd2*$^{\Delta}$ *Upd3*$^{\Delta}$ flies with *M. abscessus* .. 153
Figure 3.14 Survival of *Upd2*$^{\Delta}$, *Upd3*$^{\Delta}$, and *Upd2*$^{\Delta}$ *Upd3*$^{\Delta}$ flies with *M. abscessus* continued 154
Figure 3.15 Transcript levels of cytokines and JAK/STAT targets during *M. abscessus* infection 156
Figure 3.16 Confocal images of *D. melanogaster* haemocytes infected with *M. abscessus* 158
Figure 3.16 Confocal images of *D. melanogaster* haemocytes infected with *M. abscessus* continued 159
Figure 3.17 Survival of flies lacking haemocytes or lacking phagocytic capability following *M. abscessus* infection 161
Figure 4.1 Sankey diagram showing *M. abscessus* CRISPR screening process and progress 173
Figure 4.2 MAB_0169c contributes to *M. abscessus* virulence *in vivo* 180
Figure 4.3 MAB_0471 knockout leads to decreased virulence and decreased replication *in vivo* 182
Figure 4.3 MAB_0471 knockout leads to decreased virulence and decreased replication *in vivo* continued 183
Figure 4.4 MAB_0472 knockout leads to decreased virulence and decreased replication *in vivo* 184
Figure 4.4 MAB_0472 knockout leads to decreased virulence and decreased replication *in vivo* continued 185
Figure 4.5 MAB_1012c is required for *M. abscessus* virulence *in vivo* 187
Figure 4.6 Loss of MAB_1132c leads to decreased *M. abscessus* virulence 189
Figure 4.7 MAB_1283c contributes to *M. abscessus* virulence *in vivo* 191
Figure 4.8 Loss of MAB_2262c severely impairs *in vivo* growth 194
Figure 4.9 Nitrite reduction by MAB_3522c is involved in *in vivo* growth of *M. abscessus* 197
Figure 4.10 Nitrite extrusion by MAB_3523c contributes to *M. abscessus* virulence .. 198
Figure 4.11 MAB_4163c knockout strongly attenuates growth in *D. melanogaster* 201
Figure 4.12 MAB_4588c does not appear to be required for infection of *D. melanogaster* by *M. abscessus* 203
Figure 5.1 Phenogenomics of MAB_0471 in *M. abscessus* 210

Figure 5.2 Hypothetical structure of Tad secretion system in Gram-negative bacteria 212
Figure 5.3 MAB_0471 operon in *M. abscessus* and homologous counterparts in other mycobacterial species 214
Figure 5.4 Loss of MAB_0471 or MAB_0472 increases biofilm formation 217
Figure 5.5 Loss of MAB_0471 or MAB_0472 increases pellicle biofilm formation 218
Figure 5.6 Loss of MAB_0471 reduces intercellular adhesion 219
Figure 5.7 No difference in GPL production in Δ0471 and Δ0472 strains 220
Figure 5.8 *egr*^{3} flies show no difference in survival during infection with wild-type *M. abscessus* or Δ0472-1 221
Figure 5.9 Egr is required for survival increase of flies infected with Δ0471-1 and Δ0472-1 222
Figure 5.10 Akt activity is reduced in infected flies to a greater extent by *M. abscessus* ATCC 19977 than Δ0471-2 and Δ0472-4 224
Figure 5.11 Role of Wgn in increased fly survival when infected with Δ0471 and Δ0472 strains 225
Figure 5.12 Imd contributes to fly defense against Δ0471 and Δ0472 strains 227
Figure 5.13 *Tak1*^{1} flies maintain survival increase during infection with Δ0471-1 and Δ0472-1 229
Figure 5.14 Role of Tak1 in survival increase during infection with Δ0471 and Δ0472 strains 230
Figure 5.15 SDS-PAGE gel of proteins precipitated from *M. abscessus* culture supernatant 232
Figure 5.16 Survival of transgenic flies expressing MAB_0473, MAB_0474, or MAB_0475 during *M. abscessus* infection 233
Figure 5.16 Survival of transgenic flies expressing MAB_0473, MAB_0474, or MAB_0475 during *M. abscessus* infection continued 234
Figure 5.17 Expression of MAB_0474 and MAB_0475 individually does not inhibit eiger-induced cell death 235
Figure 6.1 MAB_1132c is important but not essential for growth with asparagine as the sole nitrogen source 245
Figure 6.2 Increasing asparagine concentrations rescues growth of Δ1132c strains 246
Figure 6.3 Asparagine availability in *M. abscessus* impacts host survival but not bacterial *in vivo* growth 248
Figure 6.4 Triacylglycerol accumulation in asparagine-limited *M. abscessus* strains . 251

Figure 6.5 Transcription of triacylglycerol synthase genes 252
Figure 6.6 Glycopeptidolipid gene transcription in Δ1132c strains 253
Figure 6.7 Reduction in transcription of Toll pathway targets during infection with Δ1132c strains 255
Figure 6.8 Reduction in transcription of Imd pathway targets during infection with Δ1132c strains 256
Figure 6.9 Transcription of other immune signalling pathway genes during infection with Δ1132c strains 258
Figure 6.9 Transcription of other immune signalling pathway genes during infection with Δ1132c strains continued 259
Figure 6.10 Increased susceptibility of unpaired mutant *D. melanogaster* to Δ1132c *M. abscessus* 260
Figure 6.11 Reduction of *D. melanogaster* Akt activity by *M. abscessus* is dependent on asparagine uptake 262
Figure S2.1 Plasmids used to produce *M. abscessus* knockout mutants using CRISPR-Cas9 344
Figure S2.2 Sequence of *S. pyogenes cas9* enzyme expressed by plasmid pTetInt-*cas9*PYO 345
Figure S2.2 Sequence of *S. pyogenes cas9* enzyme expressed by plasmid pTetInt-*cas9*PYO continued 346
Figure S2.3 Python script for design of PCR primers to amplify *M. abscessus* target genes 347
Figure S3.1 Confocal images of *D. melanogaster* haemocytes infected with *M. abscessus* 350
Figure S4.1 Isocitrate lyase enzymes in *Mycobacteria* 351
Figure S4.2 Multiple sequence alignment of isocitrate lyase 1 in *M. abscessus* and *M. tuberculosis* 352

List of Tables

Table 1.1 Mendelian susceptibility to mycobacterial disease-associated genes 47

Table 2.1 Bacterial strains used in this study 92

Table 2.2 Bacterial plasmids used in this study 97

Table 2.3 *Mycobacterium abscessus* CRISPR single guide RNAs 103

Table 2.4 *Mycobacterium abscessus* PCR primers used in this study 108

Table 2.5 *D. melanogaster* food composition 111

Table 2.6 *Drosophila melanogaster* lines used in this study 112

Table 2.7 PCR primers used to amplify *M. abscessus* genes for production of transgenic *D. melanogaster* 116

Table 2.8 PCR reaction components 120

Table 2.9 *Drosophila melanogaster* PCR primers used in this study 120

Table 2.10 *Mycobacterium abscessus* PCR primers used in this study 120

Table 2.11 PCR reaction conditions 121

Table 2.12 DNAse reaction components 124

Table 2.13 Reverse transcription reaction components 124

Table 2.14 RT-qPCR reaction conditions 125

Table 2.15 *Drosophila melanogaster* RT-qPCR primers used in this study 125

Table 2.16 *Mycobacterium abscessus* RT-qPCR primers used in this study 126

Table 2.17 Western Blot buffers 130

Table 2.18 Western Blot antibodies 130

Table 4.1 *M. abscessus* CRISPR Knockout Target Genes 171

Table 4.2 Gene editing efficiency of each of the sgRNA plasmids 173

Table 4.3 List of *M. abscessus* mutations identified following CRISPR induction and sequencing 177

Table 5.1 Percent identify of MAB_0471 operon proteins in various mycobacterial species relative to *M. abscessus* 215

Table 7.1 Comparison of *M. abscessus* and *M. marinum* infection of *D. melanogaster* 272

Table S2.1 R studio packages. 348

Table S6.1 Statistically significant comparisons for Figure 6.7. 353

Table S6.2 Statistically significant comparisons for Figure 6.8. 358

Table S6.3 Statistically significant comparisons for Figure 6.9. 361

Abbreviations

ABC	ATP-binding cassette
ACFS	Artificial cystic fibrosis sputum
AIDS	Acquired immunodeficiency syndrome
AKH	Adipokinetic hormone
AMP	Antimicrobial peptide
Atf	Acetyltransferase
Atg	Autophagy-related
AttA	Attacin A
BCG	Bacillus Calmette-Guérin
BDSC	Bloomington *Drosophila* Stock Centre
BSA	Bovine serum albumin
Bsk	Basket
Cas	CRISPR associated protein
cDNA	Complementary DNA
Cec	Cecropin
CF	Cystic fibrosis
CFU	Colony forming units
cMBT	Carboxymycobactin
COPD	Chronic obstructive pulmonary disease
COX	Cyclooxygenase
CRISPR	Clustered regularly interspaced palindromic repeats
CRISPRi	CRISPR interference
crRNA	CRISPR RNA
Dark	Death-associated APAF1-related killer
DBHS	*Drosophila* behaviour, human splicing
DCC	Dominant circulating clone
Dcp-1	Death caspase-1
DCT	Distributive conjugal transfer
Def	Defensin
Diap	Death-associated inhibitor of apoptosis
Dif	Dorsal-related immunity factor

dILP	*Drosophila* insulin-like peptide
DNA	Deoxyribose nucleic acid
Dome	Domeless
Dpt	Diptericin
Dredd	Death-related ced-3/Nedd2-like caspase
Drice	Death related ICE-like caspase
Dro	Drosocin
Dronc	Death regulator Nedd2-like caspase
Drs	Drosomycin
EDA	Ectodysplasia
eDNA	Extracellular DNA
EDTA	Ethylenediamine tetra-acetic acid
Egr	Eiger, EDA-like cell death trigger
Erp	Exported repetitive protein
ESAT-6	6-kDa early secretory antigenic target
ESCRT	Endosomal sorting complex required for transport
Esp	ESX-1 secretion-associated proteins
ESX	ESAT-6 secretion
Fadd	Fas-associated death domain
Flp	Fimbrial low-molecular weight protein
GAG	Granuloma activated gene
GDND	Glycosyl diacylated nonadecyl diol
GFP	Green fluorescent protein
GNBP	Gram-negative binding protein
GPL	Glycopeptidolipid
Grnd	Grindelwald
Gtf	Glycosyltransferase
GWAS	Genome-wide associated study
Hep	Hemipterous
HGT	Horizontal gene transfer
HIV	Human immunodeficiency virus
Hop	Hopscotch
IFNγ	Interferon γ

IκB	Inhibitor of NF-κB
IKK	Inhibitor of κB kinase
IL-1β	Interleukin 1β
ILI	Intracellular lipid inclusion
IM	Immune-induced molecule
Imd	Immune deficiency
Indel	Insertion or deletion
iNOS	Nitric oxide synthase
IPC	Insulin producing cell
IR	Inverted repeat
JAK	Janus kinase
JNK	Jun-N-terminal kinase
JNKK	Jun-N-terminal kinase kinase
JNKKK	Jun-N-terminal kinase kinase kinase
LAM	Lipoarabinomannan
LB	Lysogeny broth
LD	Lipid droplet
LM	Lipomannan
m-DAP	*meso*-diaminopimelic acid
MAPK	Mitogen activated protein kinase
MAPKK	Mitogen activated protein kinase kinase
MAPKKK	Mitogen activated protein kinase kinase kinase
MBT	Mycobactin
Mce	Mammalian cell entry
MES	2-(N-morpholino)ethanesulfonic acid
MOPS	3-(N-morpholino)propanesulfonic acid
MP1	Melanisation protease 1
MPT	Mitochondrial permeability transition
MSMD	Mendelian susceptibility to mycobacterial disease
Msn	Mishapen
Mtk	Metchnikowin
MyD88	Myeloid differentiation primary response 88
NET	Neutrophil extracellular trap

NF-κB	Nuclear factor κ-light chain enhancer of activated B cells
NHEJ	Non-homologous end joining
Nopo	No poles
NTM	Nontuberculous mycobacteria
OADC	Oleic acid, dextrose, catalase
OD_{600}	Optical density at 600 nm
PAGE	Polyacrymalide gel electrophoresis
PAM	Protospacer adjacent motif
PAMP	Pathogen associated molecular pattern
PBS	Phosphate buffered saline
PCR	Polymerase chain reaction
PDIM	Phthiocerol dimycocerosates
PFGE	Pulsed-field gel electrophoresis
PGL	Phenolic glycolipids
PGRP	Peptidoglycan recognition protein
PIM	Phosphatidyl-*myo*-inositol mannoside
PPO	Prophenoloxidase
PPR	Pattern recognition receptor
PSF	Protein-associated splicing factor
RGM	Rapid growing mycobacteria
ROS	Reactive oxygen species
Rpl4	Ribosomal protein L4
RT-qPCR	Reverse transcription quantitative polymerase chain reaction
SCID	Severe combined immunodeficient
SDS	Sodium dodecyl sulphate
SFPQ	Splicing factor proline and glutamine rich
SGM	Slow growing mycobacteria
sgRNA	Small guide RNA
SL-1	Sulfolipid-1
SNP	Single nucleotide polymorphism
Socs	Suppressor of cytokine signalling
Sp7	Serine protease 7
SSTI	Skin and soft tissue infection

STAT	Signal transducer and activator of transcription
SPE	Spätzle processing enzyme
Tab2	TAK1-associated binding protein 2
Tace	TNFα converting enzyme
Tad	Tight adherence
TAG	Triacylglycerol
Tak1	TGF-β activated kinase 1
TCS	Two component system
TDM	Trehalose dimycolate
Tep	Thioester-containing protein
TGFβ	Transforming growth factor β
TLC	Thin layer chromatography
TLR	Toll-like receptor
TNFα	Tumour necrosis factor α
TNFR	Tumour necrosis factor receptor
TORC	Target of rapamycin complex
TPP	Trehalose polyphleate
Traf	Tumour necrosis factor receptor associated factor
TRIP	Tumour necrosis factor receptor associated factor-interacting protein
UAS	Upstream activation sequence
Upd	Unpaired
VDRC	Vienna *Drosophila* Resource Centre
Wgn	Wengen
WGS	Whole genome sequencing

The Fly

Little Fly,

Thy summer's play

My thoughtless hand

Has brushed away.

Am not I

A fly like thee?

Or art not thou

A man like me?

For I dance

And drink and sing,

Till some blind hand

Shall brush my wing.

If thought is life

And strength and breath

And the want

Of thought is death,

Then am I

A happy fly,

If I live,

Or if I die.

William Blake (1757 - 1827)

Chapter 1: Introduction

1.1 The pathogen: *Mycobacterium abscessus*

Mycobacterium abscessus, a rapid-growing nontuberculous mycobacteria (NTM) species, has emerged as a significant threat to individuals with cystic fibrosis (CF) and other chronic lung diseases, such as bronchiectasis or chronic obstructive pulmonary disease (COPD)[1,2]. NTM refers to the over 180 species of mycobacteria besides the two obligate human pathogens *Mycobacterium tuberculosis* and *Mycobacterium leprae*, the majority of which are environmental saprophytes with some species, such as *M. abscessus*, capable of causing opportunistic infections[3]. Mycobacteria species are further classified into two groups based on whether colonies form on solid agar medium within 7 days or in more than 7 days, the rapid-growing mycobacteria (RGM) and slow-growing mycobacteria (SGM), respectively[4].

Globally, rates of NTM infection are increasing[2,5,6], largely driven by two species that are responsible for 70 - 95% of all pulmonary NTM infections, the SGM *Mycobacterium avium*, and *M. abscessus*, which is considered to be the most pathogenic of the RGM[7,8]. Infections with *M. abscessus* are highly challenging - sometimes impossible - to treat, owing to extremely high levels of both intrinsic and acquired resistance[2,7,9,10]. *M. abscessus* infection can cause accelerated inflammatory lung damage[11,12] and prevent safe lung transplantation in patients who urgently require transplants[13]. To date very little is understood about the molecular mechanisms underlying *M. abscessus* pathology relating to intracellular invasion or phagocytosis, virulence factors, or adaptations to the intracellular environment, and how these translate into inflammatory lung damage and resistance to antibiotics in patients[14].

In this section, I will present what is currently understood about *M. abscessus* biology, including how it interacts with infected hosts and the subsequent immune responses to an *M. abscessus* infection, its epidemiology and transmission, and discuss the current models used to study *M. abscessus* infections.

1.1.1 The mycobacterial cell envelope

The cell envelope architecture of mycobacteria is unique and unlike typical Gram-positive monoderm bacteria within the *Actinobacteria* phylum. In addition to the cell membrane, members of the order *Corynebacteriales*, which includes mycobacteria, also possess a layer of arabinogalactan attached to the peptidoglycan. The arabinogalactan then adheres to mycolic acids, which form the inner leaflet of a bilayer called the mycomembrane[15–18], shown in Figure 1.1. This capsule structure is a matrix that contains a variety of glucans, lipids, and secreted proteins. Membrane proteins such as transporters, kinases, cell wall precursor enzymes, and sensory signalling factors are also present to build and regulate the mycobacterial cell envelope[18]. This cell wall-like structure has led some authors to make comparisons between mycobacteria and Gram-negative diderm bacteria[16,17,19,20]. Evidence indicates that the mycobacterial cell envelope varies amongst mycobacterial species, but nevertheless is highly plastic and tightly regulated[21–26]. It plays an essential role in mycobacterial biology, determining transmission[27], host-pathogen interactions, persistence and dormancy in chronic infection, and resistance to antimicrobials[18].

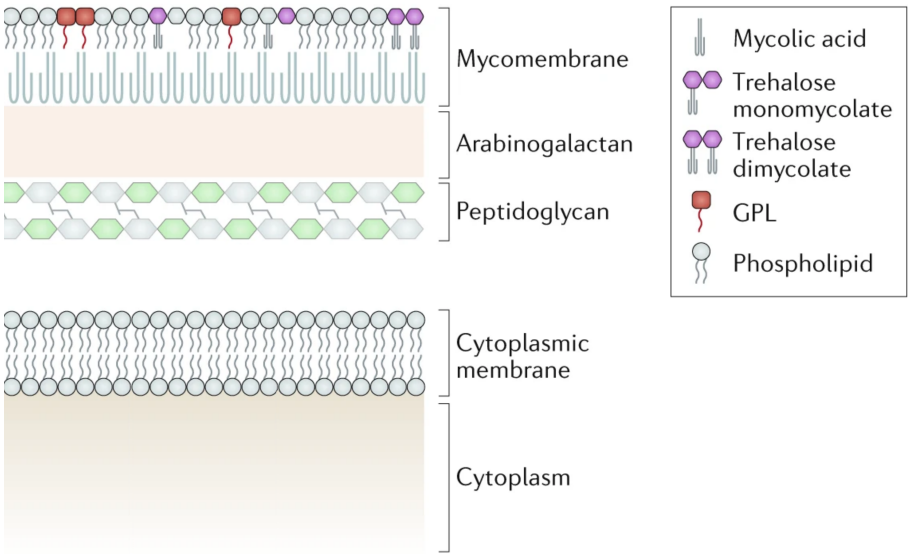


Figure 1.1. Structure of the mycobacterial cell envelope. Figure adapted from Johansen, M.D., Herrmann, JL. & Kremer, L. Non-tuberculous mycobacteria and the rise of Mycobacterium abscessus. Nat Rev Microbiol 18, 392–407 (2020)[14].

1.1.1.1 Morphotypes

M. abscessus can form two phenotypically distinct morphotypes, termed smooth and rough, based on the presence or absence of glycopeptidolipids (GPLs), which form a layer surrounding the mycomembrane. Smooth morphotypes form a well-rounded, uniform and glossy colony, whereas rough morphotype colonies appear dry and irregular, as seen in Figure 1.2. The capacity to produce distinct morphotypes is not unique to *M. abscessus*, other NTM including *M. avium*[28], *Mycobacterium kansasii*[29], and *Mycobacterium parafortuium*[30] can also display similar smooth and rough morphotypes. *M. tuberculosis* and other tuberculous mycobacteria only form rough morphotype colonies as these species produce phenolic glycolipids (PGL) and not GPLs[31].

The presence or absence of GPLs has considerable influence on the physiology and pathology of *M. abscessus*, changing properties related to biofilm formation and sliding motility, interactions with host cells[32,33], virulence[34], intracellular behaviour within phagocytes[33], and clinical outcomes[35]. In addition to the changes in the levels of GPL in *M. abscessus* morphotypes, there are also differences in the levels of trehalose dimycolate (TDM), which is a known cording factor and contributor to *M. tuberculosis* virulence[36]. TDM is present in minimal amounts within the smooth *M. abscessus* morphotype but produced at much higher levels by the rough morphotype[32,37].

The prevailing view is that the smooth morphotype represents the primary colonising and infective morphotype as the GPLs reduce hydrophobicity[38–40] and promote biofilm formation, which facilitates environmental survival, transmission, and host colonisation. In contrast, the rough morphotype is described as being more virulent and invasive. It is more frequently isolated from patients with established or persistent infections[41,42] and causes a more rapid decline in lung function compared to the smooth morphotype[11]. The morphotype of *M. abscessus* is an essential factor during infection, as it is this outermost layer that is the primary

interface with infected host cells, and this dictates adhesion, detection, immune response and bacterial modulation of the immune response[43].

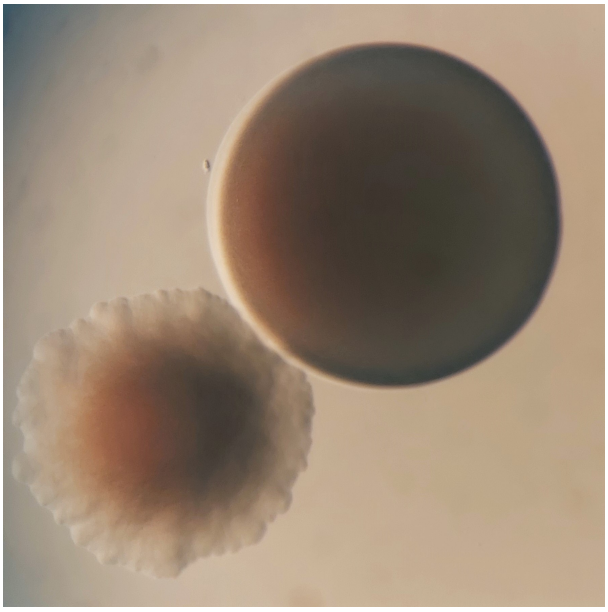


Figure 1.2. *M. abscessus* morphotypes. Image of a rough morphotype *M. abscessus* colony (lower left) and a smooth morphotype *M. abscessus* colony (upper right). Image taken using a digital camera through a microscope eyepiece. Colonies grown on 7H11 agar.

1.1.1.2 Morphotype conversion

M. abscessus has been shown to switch between the two morphotypes, predominantly in the direction of smooth to rough. This occurs due to mutations in genes involved in the synthesis or transport of GPLs, such as *mmpL4A* and *mmpL4B*[44,45], resulting in an irreversible switch to the rough morphotype and acquisition of the associated rough morphotype characteristics such as reduced sliding motility[46], cord formation[47], and increased stimulation of Toll-like receptor (TLR)2[46]. Recently it was also found that changes in GPL glycosylation also results in a smooth-to-rough conversion. This was observed in strains with mutations in glycosyltransferase 1 (*Gtf1*), which transfers 6-deoxy-talose to the threonine of the peptide core, and *Gtf2*, which transfers rhamnose to alaninol. The authors speculated that GPL glycosylation may mask components required for the smooth-to-rough transition, in addition to altering bacterial surface properties and host-pathogen interactions[43]. Following this work, the acetylation state of GPL was also studied as the 6-dTal transferred by Gtf1 is also O-acetylated,

however deletion of the identified O-acetyltransferases (Atf) within the GPL biosynthetic locus, *atf1* (MAB_4106c) and *atf2* (MAB_4110c), produced only subtle changes in colony morphology and no change in macrophage infection dynamics[48]. Another putative acetyltransferase, MAB_3168c, was found to cause changes in *M. abscessus* cell wall structure, with mutations in MAB_3168c causing a rough-to-smooth morphotype switch, however there were no identified differences in the lipid profiles[49].

Importantly, there is evidence that morphotype switching can be driven by transcriptional regulation of the GPL locus without irreversible genetic mutations, allowing for bidirectional switching. This has been observed with temperature changes, strains that do not produce GPLs at 37°C do produce the full complement of GPL at 23°C, further supporting the idea that the smooth morphotype is the environmental variant[32,50]. Other stresses have also induced morphotype switching in *M. abscessus*. Growth in Lysogeny broth (LB) causes *M. abscessus* to uniformly adopt the rough morphotype, likely due to insufficient nutrients. Nitric oxide donor DETA-NONOate also induced switching to the rough morphotype, leading the authors to propose that the rough morphotype was induced by stress conditions[51]. The importance of this effect is highlighted by findings that subinhibitory doses of amikacin also induce smooth-to-rough transitioning of *M. abscessus*, driven by *M. abscessus* transcriptional regulator WhiB7 (MAB_3508c)[52]. This can cause increased inflammatory responses and increased antibiotic resistance, important implications for patients[52,53]. Another important regulon may be involved in morphotype switching in response to stress, the DosRS two-component system (TCS) is well characterised in *M. tuberculosis*, driving an approximately 50 gene regulon to respond to hypoxia, NO, and CO both *in vitro* and *in vivo*[54,55]. In *M. abscessus* 127 differentially expressed genes were identified in a DosRS mutant strain in hypoxic conditions, and it was also observed that deletion of DosRS from *M. abscessus* resulted in a smooth-to-rough morphotype conversion[56]. The gene MAB_3083c, identified as RNase J, has also been identified as a factor in morphotype switching, with a rough-to-smooth transition

observed in transposon mutants. The mechanism of this switch remains unclear as no changes in GPL were identified, however it is possibly related to the role of RNase J in mRNA turnover or other deficiencies in the mycobacterial cell wall structure[57].

The general consensus is that the smooth morphotype is associated with an environmental lifestyle, forming protective biofilms which aid in host colonisation and persistent infections within CF patients, whereas the rough morphotype is very rarely isolated from environmental samples[58]. The stress of the hostile host environment then acts as a selective pressure to promote conversion to the rough morphotype, which may result in increased clearance of any smooth morphotype *M. abscessus* by increasing the host immune responses[44,59,60]. This would account for the greater isolation of rough morphotypes from chronically infected patients[41,42].

1.1.1.3 Type VII secretion system

Specialised secretion systems can promote bacterial pathogenesis by transporting virulence factors required for intracellular survival or manipulation of the host environment, transporting cell wall components, or by removing antimicrobial compounds. The major secretion system in mycobacteria is the type VII 6-kDa early secretory antigenic target (ESAT-6) secretion (ESX) system (ESX-1 to ESX-5)[61,62]. The substrates of the ESX systems are divided into 3 groups: Esx proteins (EsxA, EsxB, EsxT, EsxU) which are part of the WXG-100 protein family, ESX-1 secretion-associated proteins (EspA, EspB, EspC), and PE-PPE proteins (PE4-PPE5) with Pro-Glu and Pro-Pro-Glu N-terminal motifs[61,62].

Of the five different ESX systems identified, only two are present in *M. abscessus*[63]; ESX-3 which is conserved across the *Mycobacterium* genus and is required for iron acquisition[64,65], and ESX-4 which is thought to be the ancestral locus from which the other ESX systems evolved[66]. An additional plasmid-encoded ESX locus (ESX-P) has been described from a clinical isolate of *M. abscessus* subsp. *bolletii* on a large plasmid (pMBOL)[66]. The evolutionary

trajectory of *M. abscessus* has allowed it to utilise these two ESX systems to potentially fulfil the roles of the other ESX systems used in other mycobacteria. In the majority of mycobacteria, the ESX-4 system is non-functional due to the *esx-4* gene cluster lacking the *eccE* gene, likely due to redundancy from other ESX systems and subsequent genome reductions[67]. In contrast, *M. abscessus* requires ESX-4 for intracellular survival, and has retained *eccE* within the *esx-4* gene cluster[68]. The *M. abscessus* ESX-4 substrates EsxU and EsxT, predicted homologues of ESX-1 substrates EsxA and EsxB in *M. tuberculosis*, form a heterodimer to cause phagosomal membrane damage in host cells[69]. Together this suggests that the ESX-4 system may function analogously to the ESX-1 system by blocking phagosomal acidification and promoting intracellular survival of *M. abscessus*[68–70] in a very similar mechanism to that of ESX-1 in *M. tuberculosis*[68] and *Mycobacterium marinum*[71].

The ESX-3 system is the most conserved of the type VII secretion systems and has been widely studied in *M. tuberculosis*. ESX-3 system genes are expressed in response to iron limitation to maintain homeostasis, with an essential role in intracellular survival by acquiring nutrients during infection, and also in delaying phagolysosome fusion[62,64]. The ESX-3 operon also encodes for the ESX-3 substrates, EsxG, EsxH, and PE5-PPE4 proteins. In *M. tuberculosis*, EsxH impedes endomembrane repair and lysosomal trafficking by interacting with hepatocyte growth factor-regulated tyrosine kinase substrate (HGS/HRS), a component of the endosomal sorting complex required for transport (ESCRT) repair system[72,73]. In *M. abscessus*, ESX-3 promotes the production of pro-inflammatory cytokines such as TNFα, IL-1β, IL-6 and IL-12p40 in both murine and human macrophages, and is also associated with activation of MAPK and NF-κB signalling; deletion of ESX-3 caused a reduction in pro-inflammatory cytokine production, decreased cyclooxygenase 2 (COX-2), decreased nitric oxide synthase (iNOS), and also decreased neutrophil recruitment[74].

In addition to the role of the ESX systems in *M. abscessus* intracellular survival and

pathogenesis, they may have additional roles regulating other mycomembrane properties such as capsule integrity, biofilm formation, and hydrophobicity. This has been exemplified by numerous studies in *M. marinum* where the ESX-5 system secretes the PPE-10 substrate to maintain surface hydrophobicity and capsule integrity, and is essential for growth[75], deletion of ESX-1 substrates attenuates sliding motility and biofilm formation[76], and loss of ESX-3 also decreases permeability and impacts biofilm formation[77]. It remains to be seen if the ESX-3 and ESX-4 systems in *M. abscessus* also fulfill these roles to compensate for the lack of ESX-1 and ESX-5[78].

1.1.2 Biofilms

The formation of ”pellicles” or ”aggregates” by mycobacteria was observed very early in the study of mycobacteriology[79–81], similar to what is now described as a biofilm[82]. Despite these observations by Robert Koch and others, the majority of microbiological work centered around culturing bacteria in uniformly dispersed planktonic cultures. This form of planktonic growth was only achieved several decades after the identification of the tubercle bacilli in the case of mycobacteria, and required the addition of detergents, such as Tween80, as dispersing agents in culture media[83–85]. Tween80 remains a key ingredient in mycobacterial cultures, despite the known impact on the physical and biological characteristics of mycobacteria[86–88]. Recent work has highlighted the importance of biofilms as the predominant microbial lifestyle in the environment and within clinical settings, with important phenotypic and genetic alterations that dictate host-pathogen interactions and treatment options during infection.

Mycobacteria are capable of forming biofilms in a manner very similar to that of other organisms, starting with adhesion to a solid surface and developing through sessile growth, production of an extracellular matrix, and subsequently dispersal, with intracellular communication via quorum-sensing. Mycobacteria, in the absence of detergent, display a strong propensity to attach to surfaces and to one another, forming clumps, cords, or other

multicellular structures[88,89]. Additionally, many NTM have been identified within multispecies environmental biofilms, often found in water treatment facilities[90,91], showerheads[92], and faucets[93]. These polymicrobial biofilms represent a significant public health challenge owing to their high tolerance of disinfectants[94–96] and have led to numerous infections with NTM including *M. abscessus*, some of which proved fatal. Key sources of iatrogenic infections are heater-cooler units which contain a water tank to provide temperature-controlled fluids during cardiothoracic surgeries[97], and contaminated water sources in dental clinics[98].

Additionally, mycobacteria are capable of forming so-called pellicle or pellicular biofilms at air-liquid interfaces in static conditions, as floating aggregated bacterial communities[82]. This represents an important aspect of bacterial growth distinct from the traditional adherent biofilm paradigm, and is especially relevant in pulmonary infections. As with traditional biofilms, pellicle biofilms undergo distinct developmental stages and act as reservoirs for bacilli which are phenotypically tolerant to high concentrations of antibiotics[82,99–104]. Formation of the mycobacterial pellicle biofilm appears to be enhanced by eutrophy, high carbon dioxide and low oxygen tensions, rather than oligotrophic conditions that conventionally induce biofilm formation in other bacteria[105]. However, it has been suggested that biofilm formation by SGM species such as *M. avium* is less dependent on nutrient conditions, providing an advantage in low-nutrient environments[106].

Biofilm formation is an important component of *M. abscessus* infections and has been shown to occur within the lung cavity of infected patients[107]. The notion of the smooth *M. abscessus* morphotype forming biofilms during host colonisation whilst the rough morphotype is non-biofilm producing was recently disproved, with both morphotypes capable of producing unique biofilms with distinct characteristics. Whilst biofilms produced by both morphotypes display increased tolerance to antimicrobial treatments, smooth morphotype biofilms are more pliant under mechanical force[108], whereas rough biofilms are stiffer[108] and hyperaggregative[109]. Similar

to *M. tuberculosis* pellicle biofilms, *M. abscessus* biofilms are also associated with changes in transcriptional responses related to stress response genes, lipid profiles and nutrient homeostasis[104,110,111].

Studies have identified various environmental cues that appear to promote biofilm formation by *M. abscessus*, including carbon-to-nitrogen ratios[112], however recent work has found that these results can differ significantly based on the medium used to grow *M. abscessus* biofilms. Formation of *M. abscessus* biofilms occurred more readily in artificial cystic fibrosis sputum (ACFS) medium- mimicking the conditions inside airways of CF patients, and is less dependent on previously identified environmental cues, likely due to the abundance of different nutrient sources[113]. These biofilms also produced greater levels of TDM than biofilms grown in standard medium and displayed greater levels of tolerance to antimicrobials relative to planktonic bacteria grown in the same ACFS media. In standard media, no tolerance difference was identified between the biofilm population and the planktonic population[37,113,114]. Additionally, *M. abscessus* biofilms grown in ACFS medium produce unique matrices with greater levels of extracellular DNA (eDNA) and glycans within the extracellular matrix as opposed to proteins and mycolic acids identified from biofilms formed in standard lab media[113].

1.1.3 Immune Response to *M. abscessus*

The *M. abscessus* morphotypes produce distinct immune responses following infection of both *in vitro* and *in vivo* models, with the 'unmasking' model widely accepted to explain these differences. This proposes that loss of GPL in rough *M. abscessus* morphotypes leads to greater exposure of immunostimulatory factors such as phosphatidyl-*myo*-inositol mannosides (PIMs) and lipoproteins which act as potent TLR2 agonists[50,115–117]. In the smooth *M. abscessus* morphotype, the GPL layer hides these cell wall components which possibly delays detection of *M. abscessus* by the host immune systems. This delay in immune activation then facilitates host colonisation, as observed in *in vitro* studies of respiratory epithelial cells[116]. It

has been confirmed in murine macrophages that GPLs are not potent inducers of inflammatory cytokines such as TNFα[34].

1.1.3.1 Cellular response and phagocytosis

M. abscessus is considered a facultative intracellular bacteria, however the different morphotypes display unique intracellular behaviours and induce distinct responses by macrophages during phagocytosis. Following phagocytosis, the smooth morphotype is most often found contained within so-called loner-phagosomes as single bacilli[33]. It is noteworthy that both morphotypes have been described to replicate within phagosomes[33,118]. The smooth morphotype is capable of restricting phagosomal maturation, possibly related to the disruption observed in the phagosomal membrane suggesting that the smooth morphotype can establish cytosolic contact[33]. This ability to block phagosomal acidification requires the ESX-4 system[68] and mmpL8MAB (MAB_0855), the latter being essential for the production of a glycosyl diacylated nonadecyl diol (GDND) alcohol[119]. Additionally, the production of GDND by mmpL8MAB is also involved in adhesion of the smooth morphotype to macrophage membranes to aid phagocytosis[119]. No homologue of MAB_0855 was identified in any other mycobacteria, with the exception of the closely related *Mycobacterium chelonae*, implying this locus was lost during genomic reduction in *M. tuberculosis*[119]. Cells infected with the smooth *M. abscessus* morphotype are less likely to undergo apoptosis compared to cells infected with the rough morphotype, in part due to the direct action of GPLs. The polar GPL produced by *M. abscessus* that are diglycosylated and diacetylated on the core GPL structure were found to localise in the mitochondrial compartment, interact with cyclophilin D, and inhibit mitochondrial permeability transition (MPT) pore formation, preventing apoptosis[120].

In contrast, phagocytic cups form around larger clumps of rough morphotype *M. abscessus* which are difficult to internalise, resulting in fewer phagosomes containing greater numbers of bacteria, possibly exceeding the bactericidal capacities of the cell[33,121]. These phagosomes

appear to mature into phagolysosomes and autophagic vacuoles, unlike cells infected with the smooth morphotype, leading to greater levels of apoptosis. Despite this, the rough morphotype is capable of resisting degradation, and it has been suggested that apoptotic cell death of infected cells may facilitate spread of the rough morphotype by releasing it into the extracellular environment[33]. The formation of cords by rough morphotype *M. abscessus*, much like those produced by *M. tuberculosis*, is highly inflammatory and damaging. In a larval zebrafish model, rough *M. abscessus* was released from apoptotic macrophages and formed extracellular cords and abscesses, leading to rapid death of infected animals[122]. Several factors have been identified to play a role in rough *M. abscessus* cord formation including a dehydratase (MAB_4780), the deletion of which abrogated all aspects of rough *M. abscessus* pathology in the zebrafish model[123], and trehalose polyphleates (TPPs) which have been shown to localise at the external surface of *M. abscessus* cords[124].

Neutrophils have been shown to play a role in the killing of both smooth and rough *M. abscessus* morphotypes. The role of neutrophils in antimicrobial responses is primarily in generating reactive oxygen species (ROS), releasing antimicrobial peptides (AMPs), and forming neutrophil extracellular traps (NETs). NETs are composed of chromatin and enzymes including elastase and myeloperoxidase from neutrophil granules and are released into the extracellular space to immobilise pathogens and facilitate their clearance by immune cells[125]. Although production of ROS appears to have no impact on either morphotype, NET formation was required for killing of both smooth and rough morphotypes, albeit via different mechanisms. By inhibiting phagocytosis, killing of smooth morphotype *M. abscessus* by neutrophils was abrogated, however, there was no effect on killing of the rough morphotype. This divergence indicates that extracellular killing mechanisms are important for targeting the rough morphotype, whereas phagocytosis and intracellular killing mechanisms are more important for targeting the smooth morphotype[126]. This has also been observed in macrophage infections which found that the smooth morphotype was more susceptible to immune control by macrophages[32,34,127].

1.1.3.2 Innate immune response

Innate immune signalling in response to *M. abscessus* infection is primarily driven via TLR2 activation. Whilst loss of TLR2 in murine macrophages did not alter bacterial load during infection with either the smooth or the rough morphotype, it was required for cytokine production and initiation of Th1-type T-cell immunity[128]. TLR2 is required for production of IFNγ, TNFα, IL-12p70, and IL-6 during *M. abscessus* infection via signalling and activation of the Jun-N-terminal kinase (JNK) pathway[128–130]. TLR2 knockout mice were also found to have significantly reduced early recruitment of neutrophils, macrophages, and dendritic cells into the lungs during *M. abscessus* infection, which is a key contributor to the control of other mycobacterial infections such as *Mycobacterium fortuitum*[128].

The exact *M. abscessus* cell wall component that acts as the TLR2 agonist remains unknown and is debated. Rhoades *et al.* found that the rough *M. abscessus* morphotype stimulates TLR2 activity whereas the smooth morphotype does not, and physical removal of GPLs from the smooth morphotype then increases its capability for TLR2 agonism[50]. They also found that PIM2 and PIM6, which are abundant within the *M. abscessus* cell wall, show TLR2-agonist activity[50]. However, despite the increase in TNFα production seen in GPL-deficient smooth *M. abscessus* compared to the original GPL-intact smooth *M. abscessus* strain, levels of TNFα produced in response to infection with the rough *M. abscessus* strain were still approximately seven times higher[50,115]. This implies that there are additional components in the rough morphotype responsible for the increased cytokine activity. Later work by Roux *et al.* identified a complex cell surface fraction that was more abundant in the rough *M. abscessus* morphotype which was largely responsible for TLR2 activation. The authors identified lipoproteins to be the primary TLR2 agonist within the cell surface fraction, as no PIMs, lipomannans (LMs) or lipoarabinomannans (LAMs) were isolated[115]. Lipoproteins were the first molecules found to play a key role in the detection of *M. tuberculosis* by the innate immune response, also via TLR2[131], and are still considered one of the strongest TLR2 agonists[115,132]. The

understanding of *M. abscessus* lipoproteins is limited, however, there are a comparable number of lipoprotein annotated genes within the *M. abscessus* genome (118[63]) as in the *M. tuberculosis* genome (99[133]), including numerous homologues such as four Lpq-H-like proteins. One of these *lpqH* genes, MAB_2379, is absent from non-pathogenic mycobacteria such as *Mycobacterium smegmatis*, suggesting a role for this gene in the inflammatory immune response to pathogenic mycobacteria[63,115].

1.1.3.3 Adaptive immune response

In terms of the adaptive immune response to *M. abscessus*, there is a similar pattern to that seen in other mycobacterial infections, with an important role of CD4+ T-cells and a less pronounced B-cell response[134]. The importance of CD4 T-cells in mycobacterial infections is highlighted in HIV/AIDS patients in which CD4 T-cell counts can be used to predict progression of a latent *M. tuberculosis* infection into an active one[135]. HIV/AIDS patients are also at greater risk of disseminated infections caused by *M. abscessus*[136,137]. The role of B-cells during *M. abscessus* infection is very poorly understood. Anti-*M. abscessus* IgG antibodies have been found in patients months or years before signs of clinical infection or isolation of *M. abscessus* from cultures[138], suggesting latent or subclinical infections - a well-characterised phenomenon in *M. tuberculosis* infection[139]. There is also evidence of a lymphocyte cross-reactive response against *M. abscessus* induced by Bacillus Calmette-Guérin (BCG) vaccination in mice and humans[140]. Whilst this has not been extensively studied, in countries where the BCG vaccine is routinely given to infants within the first month of life, such as Brazil, there are relatively low levels of NTM infections in CF centres[141]. In contrast in Denmark, where general BCG vaccination was ended in 1986, at the Copenhagen CF centre *M. abscessus* infection is a growing problem[142]. Despite the observations of cross-reactivity, there is very little evidence to suggest that there is any protective effect of BCG vaccination against *M. abscessus* or NTM infection, which is unsurprising given its poor protection against latent *M. tuberculosis*

infection[143]. Nevertheless, there is anecdotal evidence in small numbers of CF patients that those who are BCG-vaccinated are more able to clear NTM infections[134,144]. Very little is known about how these immune responses may change depending on the *M. abscessus* morphotype. Whilst it has been reported that anti-GPL-core IgA antibodies are raised in patients and to greater levels in patients with smooth *M. abscessus* cultures than rough[145], it is unclear what effect these antibodies have against *M. abscessus* and whether morphotype switching can overcome any such effects.

1.1.4 Evolution and emergence of *Mycobacterium abscessus*

RGM within the "*Abscessus-Chelonae*" clade are considered the earliest branching lineage within the *Mycobacterium* genus[146]. As such, whilst *M. abscessus* shares some virulence factors with other pathogenic mycobacteria such as mammalian cell entry (mce) proteins and LpqH-like proteins[63], these can show greater variability in terms of sequence similarity and some are proposed to serve different functions in RGM species[147]. Equally, there are some virulence factors, such as the ESX systems, which have undergone gene duplication events in other mycobacterial species after the separation from the RGM branch[66]. It has been proposed that the two ESX systems present in the *M. abscessus* genome may act to fulfill the roles of the five different ESX systems present in other pathogenic mycobacteria[68–71]. It has also been reported that *M. abscessus* has acquired genes from non-mycobacterial sources, likely from *Pseudomonas* sp. and *Burkholderia* sp. encountered during infection of CF patients. These include cysteine desulfurases related to a DNA degradation phenotype (possibly due to high levels of DNA in CF sputum[63,148–150]), homogentisate catabolism proteins, phenylacetic acid degradation proteins, and phenazine biosynthesis proteins involved in persistence and virulence of *Pseudomonas aeruginosa* in CF patients[63,151]. *M. abscessus* has also acquired additional phospholipase C proteins related to those in *P. aeruginosa* and *Streptomyces* sp., which are required for intracellular survival and virulence[63,149,152].

It has recently been suggested that allopatric within-host evolution during chronic infection of susceptible individuals can drive adaptation and evolution of pathogenic mycobacterial species such as *M. abscessus*, along a similar evolutionary trajectory as *M. tuberculosis*. However, this within-host adaptation and increased pathogenicity of *M. abscessus* is currently constrained by reduced transmission fitness, but there are concerns that increasing opportunities may allow for direct transmission and evolution towards being an obligate pathogen, as *M. tuberculosis* did 4000 to 6000 years ago[153]. An important driver of saltational evolution is horizontal gene transfer (HGT), and a comparison of 20 mycobacterial species identified *M. abscessus* as the most prolific participant in HGT events[149]. A form of HGT unique to mycobacteria is distributive conjugal transfer (DCT)[153–155] which generates mosaicism across mycobacterial genomes[156,157]. Transposon mutagenesis studies have identified various genes involved in DCT, in particular, ESX systems appear to play a central role[158–160], however, the exact mechanism of transfer remains unknown. DNA transfer by DCT was found to require stable, extended cell-cell contact either on solid medium or in the form of a pellicle biofilm, but did not occur in planktonic culture[154,161]. Previous studies in *M. smegmatis* found that ESX-1 and ESX-4 were both required for DNA transfer to a recipient strain, whereas in donor strains ESX-4 was not required[160,162]. Paradoxically, mutations in ESX-1 led to hyper-conjugative donor strains[158]. More recent work using *M. tuberculosis* and *Mycobacterium canettii* did not replicate this finding and concluded that DCT in *M. tuberculosis* occurred independently of ESX-1[155]. This is consistent with the recombinogenic mosaic patterns observed in the genomes of mycobacterial species devoid of an ESX-1 system, such as *M. abscessus*[155,157].

Global dominant circulating clones (DCCs) of *M. abscessus* have been described and are associated with improved intracellular survival, increased antibiotic resistance, worse clinical outcomes and the formation of transmission chains[163]. Such genetically clustered isolates of *M. abscessus* represent over 70% of *M. abscessus* infections within CF patients, the majority of which come from DCCs 1 - 3[163]. The expansion of these DCCs appears to have begun in the

1950s, contemporary to the introduction of CF treatment centres and use of antipseudomonal and antistaphylococcal antibiotics. This diminished the presence of competitive bacterial species and increased CF patient life expectancy, creating a niche for *M. abscessus*[153,163–166] (Figure 1.3). It has also been suggested that non-CF lung niches can act as additional reservoirs for *M. abscessus*, such as in people who smoke, contributing to the global distribution of the DCCs[153,167]. It has been suggested that these DCCs have undergone several cycles of within-host evolution, increasing their pathogenic potential[163,166].

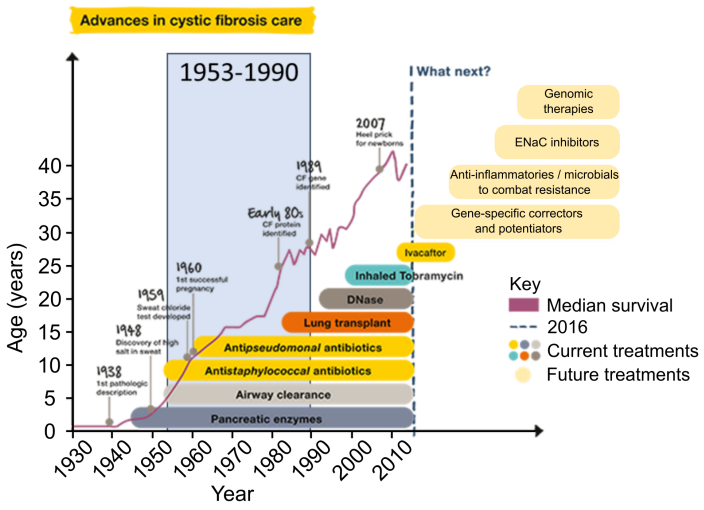


Figure 1.3. Advances in cystic fibrosis treatment and the emergence of *M. abscessus* dominant circulating clones. Line graph shows the increase in CF patient life expectancy, overlaid with introduction of new treatment options. The blue box indicates the approximate emergence and expansion period of *M. abscessus* DCCs 1 - 3[163,166]. Figure adapted from the Cystic Fibrosis Trust.

1.1.4.1 A note on taxonomy

The phylogeny and classification of *M. abscessus* has changed many times since its identification from a subcutaneous abscess in 1953 as a result of a knee wound[168]. Originally classified as a subspecies of *M. chelonae*, a closely related species with an identical 16S rRNA sequence, and grouped under the *M. fortuitum* complex[169], *M. abscessus* was later recognised as its own species in 1992[170,171] In 2006, *M. abscessus* was subdivided into three subspecies forming the *M. abscessus* complex: *M. abscessus* subsp. *abscessus*, *M. abscessus* subsp. *bolletii* and *M. abscessus* subsp. *massiliense*[172]. In 2011 this classification

was questioned and *M. abscessus* subsp. *bolletii* and *M. abscessus* subsp. *massiliense* were united under the subspecies name *bolletii*[173], however subsequent genome sequencing and phylogenetic studies confirmed the existence of *M. abscessus* subsp. *massiliense* as its own subspecies[174–178]. The taxonomic changes are shown in Figure 1.4. Differences between the subspecies have important clinical implications; *M. abscessus* subsp. *bolletii* is rarely isolated from clinical infections, suggesting variability between the subspecies in terms of their adaptations towards a pathogenic lifestyle[179–181]. Additionally, whilst *M. abscessus* subsp. *abscessus* and *M. abscessus* subsp. *bolletii* both possess a functional erythromycin ribosome methyltransferase *erm(41)* gene providing resistance to macrolides[182,183], *M. abscessus* subsp. *massiliense* carries a truncated and non-functional *erm(41)* gene rendering it more susceptible to macrolides, improving clinical treatment options[183,184]. Recently, taxonomic changes have stemmed from a proposal to split the *Mycobacterium* genus into five separate genera, reclassifying *M. abscessus* as *Mycobacteroides abscessus*[146], however this has been generally rebuffed by the mycobacteriology community[185,186].

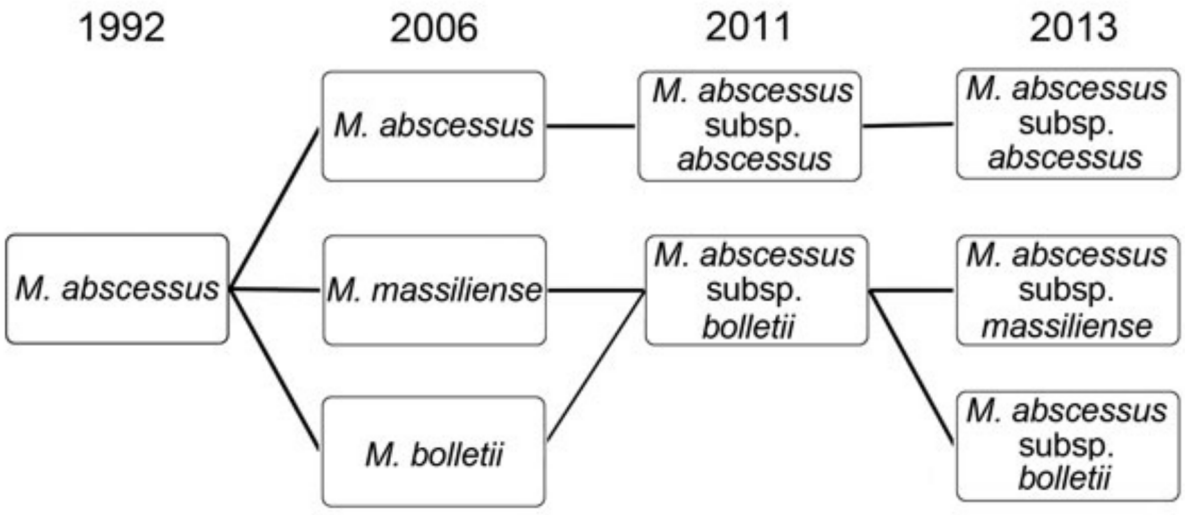


Figure 1.4. *Mycobacterium abscessus* complex taxonomic changes. Changes in the taxonomic classification and nomenclature of the *Mycobacterium abscessus* complex and its subspecies from its classification as a species in 1992 until 2013. Figure taken from Lee MR, Sheng WH, Hung CC, Yu CJ, Lee LN, Hsueh PR. Mycobacterium abscessus Complex Infections in Humans. Emerg Infect Dis. 2015[187].

1.1.4.2 Infection sources and transmission

NTM are found ubiquitously throughout the environment in natural waters and soil, including in niche environments with low oxygen or nutrient availability such as metalworking fluids, brown water swamps, peat-rich soil and boreal soil[188,189]. Variation in environmental conditions likely accounts for the differences in predominant NTM species and diversity by geographic region[190,191]. The lipid-rich outer mycomembrane is fundamental to the survival of NTM by increasing resistance to acidity[192], salinity, high temperatures[94], disinfectants[193] and antibiotics[194]. Mycolic acids increase hydrophobicity which promotes adherence to surfaces, biofilm formation[195] and contributes to the propensity of NTM to aerosolize. NTM isolates detected from potting soil[196] and showers[197,198] matched those in patients with NTM pulmonary disease, suggesting inhalation of aerosols is a major source of NTM infection[199].

In addition to environmental sources of NTM, these species have also adapted to occupy man-made niches such as municipal water distribution and plumbing systems[195,200,201]. The use of chlorine and other disinfectants in water systems kills other competing bacterial species, thus increasing resources available for the remaining resistant NTM, leading to increased levels of NTM being detected[193,201–203]. Alarmingly many studies detected NTM in hospital water systems[204] including inside patient ice machines[205], water used for preparation of medical solutions, heater-cooler devices[206] and water used for dialysis[207,208].

Historically, the acquisition of *M. abscessus* was thought to occur independently via exposure to environmental sources such as contaminated water or soil[198,209,210]. This was consistent with studies from the 1990s and 2000s examining *M. abscessus* and other NTM species collected from CF patients using pulsed-field gel electrophoresis (PFGE) and *hsp65* sequencing, which showed genetically diverse strains of *M. abscessus* being isolated[211–213]. Suspicions of person-to-person transmission of *M. abscessus* following the transfer of a *M. abscessus*-positive CF patient to a CF centre in Seattle and a subsequent outbreak within

the centre[214]. Other studies also began to suggest that patients within the same hospital had very genetically similar *M. abscessus* strains[215–217]. Additionally, there were reports of patients infected with clarithromycin- and amikacin-resistant *M. abscessus* strains, despite never previously receiving macrolide treatment[217]. Use of whole-genome sequencing (WGS) to study *M. abscessus* transmission offers far higher genomic resolution compared to previous techniques used to compare isolates, overcoming limitations in comparing mycobacterial strains due to slow mutation rates[148,218,219]. WGS was performed on 168 *M. abscessus* isolates collected from 31 infected patients at a CF centre in Papworth Hospital, UK, to better understand the acquisition of *M. abscessus*. This identified three modes of acquisition of *M. abscessus* by CF patients: independent acquisition of genetically diverse strains from the environment, independent acquisition of a prevalent strain circulating in the area with roughly 50-200 base pair differences between isolates in loosely grouped clusters and person-to-person transmission, either directly or indirectly, of genetically identical or near-identical strains[217]. The likelihood of direct person-to-person transmission within CF centres is low due to strict infection control procedures[217], so it is suggested that indirect transmission via aerosols and fomites is more likely with only low levels of inoculum needed to be infectious[217,220,221].

Another WGS study used 1080 clinical isolates from 517 patients from CF centres across the globe. Bryant *et al.* found evidence of independent acquisition of genetically unrelated *M. abscessus* strains likely from environmental sources and also identified the DCCs - clades of highly related isolates from a wide range of locations[163]. The DCCs were shown to have improved survival within macrophages and increased virulence in mice, consistent with the observation that CF patients infected with a DCC strain tend to have worse clinical outcomes[163]. DCC1 was the most prevalent clone across Europe and Australia and has since been found in 39% of non-CF patients with both pulmonary and extrapulmonary *M. abscessus* subsp. *massiliense* infection and 17% of CF patient isolates in the United States[222]. Strains from other outbreaks, such as in the Seattle CF centre and a post-surgical soft tissue *M.*

abscessus outbreak in Brazil, have shown high genetic relatedness to DCC3, which was also identified in isolates collected from Papworth[217,223,224]. DCC3 also appears to be increasingly prevalent in Asia[225]. Currently, the long-distance spread of these DCCs remains unexplained with no clear evidence of the transfer of CF patients, doctors or equipment moving between the centres involved in the study[163]. The possibility of transient colonisation of immunocompetent individuals or other vectors of transmission has not yet been determined. Mutational signatures associated with smoking have been identified in the *M. abscessus* DCCs[166]. Individuals who smoke are more susceptible to NTM infection due to structural damage within the lung and impaired immune responses[226], and *M. abscessus* has been isolated from the lungs of people who smoke[167,184,227]. It is therefore possible that people who smoke contribute to the transmission of *M. abscessus* and the global spread of the DCCs[166].

Some studies using WGS continue to dispute person-to-person transmission of *M. abscessus*. One study argues that a set threshold of single nucleotide polymorphism (SNP) differences across the core genome is too restrictive to assess relatedness between isolates, and so incorporated accessory genome information into their analysis. This study concluded that inter-patient isolate diversity was too great to attribute to person-to-person transmission, however, it used far fewer patients and isolates. The authors acknowledge that the full potential of WGS in studying *M. abscessus* transmission can only be reached by combining large-scale screening of patients as well as environmental reservoirs[228].

1.1.5 Epidemiology

M. abscessus is the most common cause of NTM infection by a RGM, responsible for 3-13% of all NTM pulmonary disease cases in the United States[187]. *M. abscessus* is most commonly isolated in Asia and Oceania, representing 16% and 12% of all NTM isolates from each region, respectively, in contrast to South America (5.7%), North America (3.2%), and Europe (2.9%)[229]. In the United States, *M. abscessus* most frequently causes disease in Hawai'i,

Florida, and other parts of the south-eastern United States[230,231], in Europe, RGM such as *M. abscessus* are commonly found in the United Kingdom and Greece[232], and in Asia *M. abscessus* is widespread in India[233], Singapore[232], and Taiwan[234,235]. Information about the prevalence of NTM in Africa is very limited, however, there are reports of *M. abscessus* being among the most frequently isolated NTM species in Zambia[236]. In Australia, *M. abscessus* is commonly found in southern territories[232], and NTM are notifiable infections in Queensland, allowing for ongoing surveillance of potentially virulent and transmissible NTM[237]. Unfortunately, for the majority of the world, NTM are not notifiable infections and the lack of fully representative samples in epidemiological studies makes it extremely challenging to understand the current state or monitor changes in NTM infections. NTM infection is also frequently misdiagnosed as TB, especially in high TB-burden areas[238,239]. In one centre in Brazil, 79% of all patients diagnosed with a NTM infection were initially treated for TB infection for up to 6 months before the NTM diagnosis was confirmed[240].

Despite these limitations, it is generally accepted that the incidence of NTM infection, including *M. abscessus* infection, is rising globally[226,241–246]. This may be partly due to increased awareness of NTM, improved microbiological detection methods such as antigenic skin sensitization tests[243,247] (however these can be impacted by false-positive reactions from prior BCG vaccination[248]), a growing population of susceptible individuals, changes in BCG vaccination schedules[140,243,249] and increased exposure to NTM[197–199].

1.1.5.1 Risk factors

CF patients are the population most at risk of *M. abscessus* infection, with an estimated prevalence within CF patients of 13% in Europe and 16% in the United States[212,218]. It has been observed that the relative proportion of *M. abscessus* isolated from mycobacterial cultures from CF patients has increased over the past decade, with *M. abscessus* becoming almost as prevalent within CF patients as *M. avium*[2,250]. Other chronic structural lung diseases such

as non-CF bronchiectasis and COPD are other common risk factors[251,252]. Disseminated *M. abscessus* infection tends to occur in immunocompromised patients, such as those with HIV/AIDS[136,137].

It has been found that 81% of HIV-negative individuals with disseminated NTM-infection produced neutralising anti-interferon-γ (IFNγ) autoantibodies, leading to adult-onset immunodeficiency similar to that of HIV infection[137]. The criticality of IFNγ and associated signalling by IL-12 and IL-23 in defence against mycobacterial infection is further highlighted by Mendelian susceptibility to mycobacterial disease (MSMD), a rare inherited condition that predisposes individuals to infection with NTM. Mutations in nineteen genes, almost all of which are involved in IFNγ-mediated immunity, have been associated with MSMD (Table 1.1)[253,254]. Individuals with MSMD are also susceptible to infection with *M. bovis* BCG and so are unable to receive the BCG vaccine[254]. Immunosuppressant medications such as TNFα inhibitors also increase the risk of *M. abscessus* and other NTM infections[241,255].

Table 1.1. Mendelian susceptibility to mycobacterial disease-associated genes. AR - autosomal recessive. AD - autosomal dominant. XR - X-linked recessive[253,254].

Gene symbol	Protein	Mode of inheritance
CYBB	Major component of phagocyte NADPH oxidase (PHOX) complex	XR
IFNG	IFNγ	AR
IFNGR1	Ligand-binding chain of (IFNγ) receptor (IFNγR1)	AR / AD
IFNGR2	Accessory chain of IFNγR	AR / AD
IL12B	p40 subunit common to IL-12 and IL-23	AR
IL12RB1	β1 chain common to receptor complexes for IL-12 and IL-23	AR
IL12RB2	β2 chain for IL-12 receptor complex	AR
IL23R	Component of IL-23 receptor complex	AR
IRF8	Transcription factor induced by IFNγ	AR / AD
ISG15	Induces IFNγ which acts synergistically with IL-12	AR
JAK1	Janus kinase 1	AR

NEMO (IKBKG)	Nuclear factor κ B (NF-κB) essential modulator, encodes regulatory subunit of inhibitor of κB kinase (IKK)	XR
RORC	Nuclear receptor isoforms RAR-related orphan receptor γ and ROR-γT	AR
SPLL2A	Signal peptide peptidase-like 2A, intracellular transmembrane protease	AR
STAT1	Signal transducer and activator of transcription 1	AR / AD
TBX21	T-box protein 21, transcription factor involved in development and function of IFNγ-producing lymphocytes	AR
TYK2	A JAK involved in signalling responses to IL-10, IL-12, IL-23, and IFNα/β	AR
USP18	Ubiquitin-specific protease 18	AR
ZNFX1	Zinc finger NFX1-type containing 1, important for induction of IFNα/β-stimulated gene (ISG)	AR

1.1.5.2 Clinical relevance

The population most affected by *M. abscessus* infection is undeniably those with CF. CF is an autosomal recessive disorder caused by mutations in the CF transmembrane conductance gene regulator (CFTR) gene leading to dysfunction in various organs, predominantly chronic lung infection. Unfortunately, despite advances in the treatment of CF, the majority of patients die as a result of respiratory failure stemming from chronic bacterial infections[256]. Prior to the 1990s NTM infection was not typically associated with CF, however since then the number of infections of *M. abscessus* and other NTM have been rising steadily[257]. In the UK, NTM infection within the CF population increased from 1.3% in 2010 to 3.8% in 2015[258].

There is evidence that *M. abscessus* infects CF patients with more severe disease and at an earlier age compared to the other dominant NTM found in CF patients, *M. avium*. This is particularly concerning due to the rapid decline in lung function caused by *M. abscessus* infection, which results in end-stage lung disease in 13.6 years following infection on average. The median age at the time of *M. abscessus* acquisition is 13 years old[250,259]. The risk

of acquiring NTM infection then continues to increase with age[1]. Significant symptoms accompanying *M. abscessus* pulmonary infection include considerable weight loss, fever, haemoptysis, difficulty sleeping, and difficulty breathing[260].

Bilateral lung transplantation is hugely important as a treatment option for CF patients, providing significant improvements to survival and quality of life[261]. Previous studies have found that CF is the third leading cause of lung transplantation, accounting for 16.8% of all lung transplants worldwide[262,263]. The presence of *M. abscessus* infection and its contraindication for lung transplantation is strongly debated. Some studies have shown that bilateral lung transplantation is possible despite the presence of an *M. abscessus* infection, however, this requires aggressive treatment to clear the infection to avoid the risk of *M. abscessus* spreading and developing into a disseminated infection[264–267]. Nevertheless, the majority of patients who have received bilateral lung transplants with a pre-transplant isolation of *M. abscessus* have died, often as a result of overwhelming *M. abscessus* infection[268]. Improvements in the treatment of CF such as triple combination therapy using elexacaftor–tezacaftor–ivacaftor and the associated improvements in lung function do appear to be reducing the need for lung transplants in CF patients, as seen by a reduction in the number of lung transplantations in CF patients in France, however, it is unclear whether this effect will be long-term or simply delay the need for lung transplantation[269].

M. abscessus is capable of infecting immunocompetent individuals, typically in the form of skin and soft tissue infections (SSTIs). These can range from localised infections to deep tissue infections with the risk of becoming disseminated. These are typically acquired from environmental sources such as contaminated water that comes into contact with a wound or is introduced into the skin. Such infections are associated with contaminated needles or surgical equipment and so are often caused by cosmetic surgery[270,271] and procedures such as mesotherapy[272,273], botox[274,275], acupuncture[276,277], or tattooing[278,279]. *M. abscessus*

SSTIs are also reported following time spent in hot tubs and spa pools[280,281]. *M. abscessus* SSTIs cause the name-sake abscesses which can spread cutaneously and subcutaneously beyond the area of infection, non-healing ulcers, and purulent draining nodules[270]. Treatment requires a combination of at least two antibiotics over a period of 4 months, and can also require surgical intervention to remove granulomas and infected tissue[1].

1.1.6 Treatment and Antimicrobial resistance

Treatment of *M. abscessus* is extremely challenging owing to both intrinsic and acquired resistance mechanisms conferring resistance to most classes of antibiotics, including aminoglycosides, β-lactams, macrolides, rifamycins and tetracyclines. Treatment success can also vary greatly depending on the subspecies, sputum conversion and maintenance of negative cultures is reported to range between 82% and 96% for *M. abscessus* subsp. *massiliense* but only between 25% and 42% for *M. abscessus* subsp. *abscessus*[184,282–285]. According to the 2007 ATS/IDSA guidelines, ”At present, there is no reliable or dependable antibiotic regimen, even based on in vitro susceptibilities, including parenteral agents, to produce a cure for M. abscessus lung disease”[1]. This was very similar to the 2020 guidelines which stated ”the optimal drugs, regimens, and duration of therapy are not known” for the treatment of *M. abscessus* pulmonary disease[10]. Phage therapy appears to offer great promise in the treatment of *M. abscessus*. The first reported use of mycobacteriophage, and the first use of engineered phage, utilised derivatives of Muddy, ZoeJ, and BP, to treat a young CF patient following a lung transplant that had resulted in disseminated *M. abscessus* infection despite being treated for 8 years previously. Treatment was successful[266], and since then phage therapy has been administered to at least five other patients to treat *M. abscessus* infections[267,286].

1.1.6.1 Intrinsic resistance

The first aspect of intrinsic resistance in *M. abscessus* is the hydrophobic barrier formed by the mycomembrane, reducing the permeability of hydrophilic compounds into the bacilli[200,287], including β-lactams and aminoglycosides[288]. Porins and multidrug efflux pumps also contribute by removing compounds that have entered the cell. These include MmpL transporters and ABC transporters and these confer resistance against bedaquiline and clofazimine[289,290]. Drug-modifying enzymes are also prevalent in *M. abscessus* and serve to degrade or modify antibiotics to inactivate them. An example is MAB_0591 which catalyses the ADP-ribosylation of rifampicin rendering it inactive[291]. This is in contrast to the more common mechanism of rifampicin resistance which is acquired by genetic mutations in the drug target, the β-subunit of RNA polymerase *rpoB*[292]. The *M. abscessus* β-lactamase MAB_2875 also hydrolyses imipenem and cefoxitin, which are both currently part of *M. abscessus* treatment regimes[293], however combination with a non β-lactam inhibitor avibactam can extend the spectrum of β-lactams with activity against *M. abscessus*[294,295]. An acetyltransferase MAB_4395 acetylates aminoglycosides including gentamicin, tobramycin and kanamycin to inhibit their activity[296], and a phosphotransferase MAB_2385 is the primary determinant of streptomycin resistance[297]. Additionally, a gene involved in intracellular survival, MAB_4532c (eis2)[298], has been shown to modify amikacin, hygromycin, kanamycin[299], and confer resistance to capreomycin[296]. Finally, the lack of drug-activating enzymes is the reason for the lack of activity of isoniazid against *M. abscessus*, as the catalase-peroxidase KatG is unable to produce the active metabolite[300].

1.1.6.2 Adaptive resistance

Adaptive resistance is triggered by environmental conditions, including exposure to antibiotics, and is driven by changes in gene or protein expression rather than mutations or acquisition of novel resistance genes. An important example of this in *M. abscessus* is *erm(41)* which

is induced by macrolide exposure, especially clarithromycin and azithromycin which are fundamental parts of *M. abscessus* treatment. *erm(41)* encodes a ribosome methylase which induces macrolide resistance by methylating the 23S rRNA[182,301]. The modulation of *erm(41)* expression is regulated by the multidrug-inducible transcriptional activator WhiB7[302]. WhiB7 (MAB_3508c) controls expression of over 100 genes and is induced by structurally unrelated antibiotics, including aminoglycosides, macrolides, and tetracycline[53], as well as in response to iron starvation and redox changes[303]. WhiB7 also regulates expression of eis2[304] and SigH (MAB_3543c), a sigma factor linked to tigecycline resistance[305]. An analogue of rifampicin, rifabutin, was recently shown to inhibit transcriptional induction of *erm(41)* by WhiB7 and so suppressed the inducible clarithromycin resistance[306].

1.1.6.3 Acquired resistance

As with other bacterial species, prolonged exposure to antibiotics can lead to the selection of *M. abscessus* isolates with genetic changes for drug resistance. The most prevalent of these are mutations in *rrl*, the 23S rRNA gene, and *rrs*, the 16S rRNA gene. Such mutations create high levels of resistance to kanamycin, amikacin, tobramycin, and macrolides[307–309]. Despite the intensive antibiotic treatment regimes used against *M. abscessus*, genetic changes driving resistance are reported relatively rarely[310–312]. This is possibly because the selective pressure applied by antibiotic treatment is not particularly strong given the various mechanisms of intrinsic and inducible resistance against the antibiotics in clinical use.

1.1.7 Models for studying *M. abscessus*

1.1.7.1 *In vitro* models

In vitro models provided insight into differences between *M. abscessus* S and R morphotypes during early invasion of phagocytic cells[313], and tumour-derived cell lines (THP-1 and U937) are commonly used for studying mycobacterial infection[314–316]. These lines exhibit key metabolic differences such as the Warburg effect which are not representative of normal host

metabolic responses to infection by an intracellular pathogen[317]. Furthermore, murine cell lines (J774A.1 and RAW264.7)[313] have important differences in innate immune responses such as increased production of NO[318] and differences in inflammasome activation[319]. Recently an experimental model of foamy macrophages was derived from murine bone-marrow macrophages[320,321]. In human hosts, foamy macrophages are characterised by their high lipid content and are thought to act as a reservoir for *M. tuberculosis* for dormancy and persistence[322]. This model was used to shed light on the capacity of *M. abscessus* to acquire host lipids and the role of diacylglycerol transferases in intracellular lipid inclusion (ILI) formation. Production of ILIs by *M. abscessus* may act as a long-term energy store to support persistence in a manner similar to *M. tuberculosis*[323].

Other cellular host models of *M. abscessus* infection include amoebae such as *Dictyostelium discoideum*[324] and *Acanthamoeba castellanii*[325]. *M. abscessus* is primarily an environmental microorganism and is thought to frequently infect free-living amoebae within the environment, and evidence suggests that *M. abscessus* evolved in close contact with environmental protozoa. These provide an intracellular niche similar to that of phagocytes and may contribute to adaptation of *M. abscessus* towards a more pathogenic lifestyle[152,326]. Use of these infection models has also identified virulence determinants in *M. abscessus*, including MgtC and phospholipase C[152,326]. These *in vitro* models offer insight into the intracellular behaviour of *M. abscessus* during infection, however, do not fully reflect the complexity of an *in vivo* infection and host immune response.

1.1.7.2 *In vivo* models

Development of murine models for *M. abscessus* infection has been challenging. Immunocompetent mice clear *M. abscessus* infection within a few weeks[327,328] and chronic *M. abscessus* infection can only occur in mouse models with multiple innate or acquired immunity defects such as severe combined immunodeficient (SCID) and nude mice lacking

mature B and T-lymphocytes[327,329,330]. Recent work to create a chronic infection model in immunocompetent mice has used intratracheal infection with *M. abscessus* entrapped in small agar beads, physically retaining the bacteria within the airways and allowing for growth. This has had mixed results, with one study reporting that introduction of agar beads led to high mortality in mice[331], and another reporting successful chronic infection of mice for at least 6 months post-infection[332].

Zebrafish (*Danio rerio*) embryos are commonly used to study acute *M. abscessus* infection and the innate immune response. Non-invasive imaging and fluorescent reporter zebrafish lines identified mechanisms of cording by *M. abscessus* R morphotypes, the impact of cording on pathogenesis[123] and the role of TNFα signalling in protection against *M. abscessus*[333]. Injection of *M. abscessus* into the spinal cord results in formation of abscesses disseminated in the central nervous system (CNS), which may behave differently to pulmonary infection[122]. There is debate about whether zebrafish models accurately depict granuloma formation. Clumps of bacterial cells and macrophages have been observed in zebrafish following *M. abscessus* and *M. marinum* infection. Granuloma-activated genes (GAGs) were activated in *M. marinum* following aggregation of infected macrophages and bacteria suggesting some degree of similarity between these aggregates and *bona fide* granulomas[334]. The same has not yet been shown for *M. abscessus* infection.

The use of *Drosophila melanogaster* as a model for mycobacterial infection will be discussed in Section 1.2.3.

1.2 The model organism: *Drosophila melanogaster*

Drosophila melanogaster, commonly known as the fruit fly, is one of the most widely used model organisms in fields ranging across genetics, neuroscience, developmental biology and immunology. First reared in the laboratory at the start of the 20th century at Harvard by Charles Woodwoth, the short generation time and large numbers of offspring produced

by *D. melanogaster* made them appealing research tools. Later research into the role of chromosomes in inherited traits by Thomas Hunt Morgan and Herman J. Muller led to the development of *Drosophila* genetics as an experimental field and the first of six Nobel prizes to be awarded for work using *D. melanogaster* as a model organism. The genome of *D. melanogaster* was the second ever to be sequenced from a multicellular organism[335] and is now very well annotated following continuous refinement and study. This has allowed a suite of experimental tools to be developed for use with the *D. melanogaster* model, established protocols for tissue-specific genetic manipulation and several banks with every available genetically modified or mutant line ready to be shipped.

Beyond the experimental practicalities of using *D. melanogaster* as a model organism, there is also a high degree of conservation between *D. melanogaster* and mammals in terms of genetics, cellular signalling pathways, innate immunity and metabolism. 77% of human disease-related genes are estimated to have highly related genes within *D. melanogaster*[336]. As a result, *D. melanogaster* has become a well-established model for the study of innate immunity, the relationship between the innate immune response and metabolic changes during infection, and increasingly the exploration of host-pathogen interactions.

1.2.1 *Drosophila melanogaster* immunity and defence

D. melanogaster can resist infection using various mechanisms, all of which show degrees of conservation with mammalian responses to infection. Importantly, unlike vertebrate immune responses, there is no adaptive immune response in *D. melanogaster*. They are unable to produce antibodies or have any form of immune memory, and there are no *D. melanogaster* immune cells analogous to B-cells, T-cells, or natural killer (NK) cells.

To prevent pathogen entry there are physical barriers in *D. melanogaster*, which primarily consist of epithelial systems beneath the cuticle, within the gut and within the trachea. These are lined with a chitinous matrix and can secrete lysozymes, AMPs and ROS, creating a

hostile environment to deter microbial colonisation[337–339]. Should the *D. melanogaster* cuticle be damaged or broken, clotting and melanisation is immediately induced by the haemolymph to initiate wound healing and to act as a secondary barrier to immobilise invading pathogens[339–343].

In the event that a pathogen evades the initial barriers to infection, the *D. melanogaster* innate immune system is activated to target the invading microbes. This innate immune response is comprised of two main arms: an inducible humoral response and cellular immunity, which communicate with one another via several known cytokine signal transduction pathways.

1.2.1.1 Humoral immunity

The humoral immune response in *D. melanogaster* is primarily represented by 21 AMPs. These are peptides which show antimicrobial activity both *in vitro* and *in vivo* by targeting and destabilising negatively charged membranes of microorganisms, however the exact mechanism of action of these peptides is not fully understood. The AMPs encoded within the *D. melanogaster* genome are grouped into seven families, each with different expression patterns and efficacies against various bacteria and fungi. The Attacins, Diptericins, and Drosocin are primarily anti-bacterial, Drosomycin and Metchnikowin are anti-fungal, and Cecropins and Defensin show both anti-bacterial and anti-fungal activity[344]. AMPs can also act synergistically with one another to enhance the response against certain microbes[345].

During a systemic immune response, AMP expression is strongly induced by signalling via the Toll and Immune deficiency (Imd) pathways upon detection of a pathogen which results in rapid synthesis and secretion of large amounts of AMPs into the haemolymph from fat body cells, reaching concentrations up to 100 μM[344,346]. The *D. melanogaster* fat body is a diffuse organ arranged in lobes primarily located lining the cuticle of the abdomen, but can also be found within the head and thorax. It is analogous to mammalian adipose tissue and liver, playing important roles in nutrient sensing, lipid storage, and immune response signalling via

the haemolymph[347]. Another class of inducible effectors that contribute to the *D. melanogaster* humoral response are the Bomanins. These are a separate family of 12 secreted peptides, also termed immune-induced molecules (IMs), and are specific to the *Drosophila* genus[348]. These effectors are specifically induced by the Toll pathway, with anti-fungal and anti-bacterial activity *in vivo*[348], but no antimicrobial activity *in vitro*, suggesting a requirement for post-translational modifications[349].

A systemic immune response in *D. melanogaster* can be triggered upon detection of bacterial or fungal infection by two signalling pathways, Toll or Imd, which act primarily via activation of NF-κB-related transcription factors to trigger the expression of a suite of immune-responsive genes including the AMPs and Bomanins[348,350,351]. Specific gene expression is controlled by specific pathway activation and can be differentially triggered by different pathogens, with some AMP genes preferentially induced by one pathway or the other[352,353]. Generally, these two pathways are both activated by bacterial and fungal components, including bacterial peptidoglycans. The long-held view is that the divergent activation of these pathways, with Toll activated by Gram-positive bacteria and fungi and Imd activated by Gram-negative bacteria, is based on differing recognition of lysine-containing (Lys-type) peptidoglycan or *meso*-diaminopimelic acid (*m*-DAP) by pattern recognition receptors (PRRs), respectively[353]. The discrimination between differences in peptidoglycan is based on the amino acid present at position 3 of the stem peptide, however, several factors may influence peptidoglycan detection, such as cross-linking in polymeric peptidoglycan fragments as opposed to monomers, the *in vivo* prevalence of which is unclear[354,355]. Levels of accessibility to peptidoglycan, influenced by wall teichoic acids which conceal the peptidoglycan layer, have also been shown to alter peptidoglycan detection by *D. melanogaster* PRRs[355].

1.2.1.2 Toll signalling pathway and melanisation

The Toll pathway in *D. melanogaster* is activated by binding of pathogen associated molecular patterns (PAMPs) such as Lys-type peptidoglycan, primarily found in Gram-positive bacteria, or β1,3-glucan, found in fungal cell walls. Toll pathway signalling is outlined in Figure 1.5. The PRR peptidoglycan recognition protein (PGRP)-SA primarily detects Lys-type peptidoglycan, but has also been shown to weakly respond to Gram-negative *m*-DAP peptidoglycan independently of any Imd pathway activation[355,356]. This has also been shown in other insect species, including *Tenebrio molitor*, the mealworm beetle[357]. PGRP-SA and Gram-negative binding protein-1 (GNBP1) have been shown to form a complex[356,358–361], however, it is unknown if GNBP1 hydrolyses peptidoglycan to present glycan reducing ends to PGRP-SA[362], or if it acts as a linker between PGRP-SA and Modular serine protease (ModSP)[363]. Another PRR capable of inducing Toll pathway signalling is PGRP-SD which functions independently of PGRP-SA and GNBP1, and has also been shown to bind *m*-DAP peptidoglycan[364,365]. The antifungal immune response driven by Toll signalling is activated by GNBP3, a PRR for β1,3-glucan found in fungal cell walls[366].

Signalling via these activated PRRs converges in an extracellular proteolytic cascade of serine proteases from the initiator ModSP, which activates Gram-positive specific serine protease (Grass), which further activates serine protease paralogues Hayan and Persephone (Psh), leading to cleavage and activation of Spätzle processing enzyme (SPE)[363,367,368]. This extracellular proteolytic cascade can also be induced by the presence of microbial proteases[369,370]. Activated SPE then cleaves Spätzle[371], allowing it to bind the Toll receptor by releasing the C-terminal domain required for binding[372]. The subsequent conformational change and dimerisation of the Toll receptor[373] allows the signalling pathway to continue intracellularly via recruitment of Myeloid differentiation primary response 88 (MyD88)[374,375], an adaptor protein which facilitates the formation of a protein complex by binding Tube via death-domains, and the serine-threonine kinase protein Pelle[376–379]. This complex

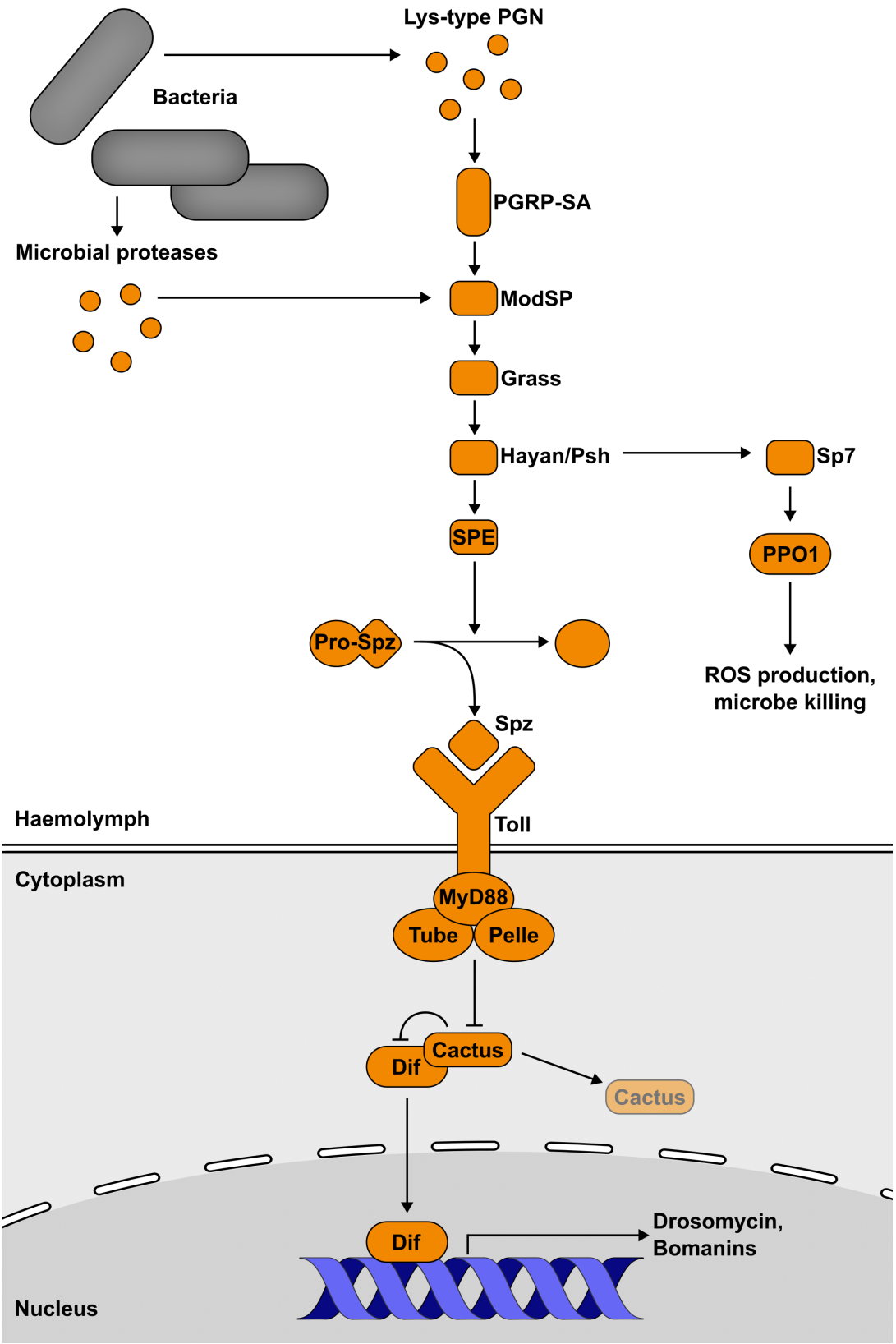


Figure 1.5. Toll pathway signalling and melanisation cascade. See text for details.

then targets Cactus, an IκB homologue, for phosphorylation and degradation[380], removing inhibition on NF-κB-related transcription factor Dorsal-related immunity factor (Dif). Dif then translocates into the nucleus and can regulate a set of immune-responsive genes including Drosomycin AMPs and Bomanins[348,381,382].

Melanisation is an arthropod-specific immune response which relies on prophenoloxidase (PPO) enzymes to polymerise and deposit melanin due to the oxidation of phenols. There are three PPO enzymes described in *D. melanogaster*, PPO1 and PPO2 are involved in haemolymph melanisation, and PPO3 is lamellocyte-derived during encapsulation[383,384]. In larval *D. melanogaster*, a subset of haemocytes called crystal cells mediate the melanisation response by being lysed upon JNK signalling and releasing large stores of PPO1 and PPO2 enzymes into the haemolymph[385]. In adult flies there is no population of crystal cells, despite the clear importance of melanisation in the adult *D. melanogaster* immune response as PPO mutants are considerably more susceptible to Gram-positive and fungal infections[368,383], and so the source of PPO is unclear. The exact antimicrobial mechanism of action involved which contribute to the killing of bacteria and fungi is also unclear, however, it possibly relies on the production of ROS. Notably, there is interaction between the melanisation and Toll pathways, as outlined in Figure 1.5. Both pathways can be activated by common serine proteases[386–388], however, the serine proteases required for melanisation are not essential for Toll pathway activation and vice versa. Additionally, the immune-responsive genes regulated by Toll signalling include many of the serine proteases and serpins (serine protease inhibitors) involved in melanisation[368,389]. It has also been shown that the melanisation pathway can be activated by the same PRRs that sense fungal pathogens, such as GNBP3, independently of Toll pathway activation[366]. Three serine proteases have been described with a role in activation of PPO1 and PPO2 in the haemolymph: Hayan, Melanisation protease 1 (MP1), and Serine protease 7 (Sp7)[368,390–392].

1.2.1.3 Imd signalling pathway

The Imd signalling pathway, shown in Figure 1.6, is responsive to *m*-DAP-type peptidoglycan typically found in Gram-negative bacteria[356,393–395], which can be detected by PRRs at both the cell surface by PGRP-LC and intracellularly by PGRP-LE. Both of these receptors can then activate a cell signalling pathway similar to mammalian tumour necrosis factor receptor (TNFR) signalling, by dimerising and recruiting the Imd adaptor protein[353,354,396–402]. In addition to activation via the PRRs, Imd can also be activated by *D. melanogaster* orthologue of STING (dmSTING), an intracellular detector of cyclic dinucleotides[403]. In turn, Imd recruits Fas-associated death domain (Fadd)[404,405] to allow binding and activation of the caspase-8 homologue Death-related ced-3/Nedd2-like caspase (Dredd)[396,406] which acts at two points in the pathway. Firstly Dredd is involved in the cleavage of the NF-κB-related transcription factor Relish which removes a C-terminal ankyrin-repeat autoinhibitory domain, freeing the N-terminal Rel domain to translocate to the nucleus and drive transcription of a variety of immune responsive genes such as Diptericin and Drosocin AMPs[407,408]. Additionally, Dredd can cleave Imd resulting in K63-ubiquitination of Imd which allows recruitment of TGF-β activated kinase 1 (Tak1) and its regulatory partner Tak1-associated binding protein 2 (Tab2)[409–413]. This results in Tak1 phosphorylating and activating the inhibitor of κB kinase (IKK) complex[414], which is formed by a regulatory subunit Kenny (IKKγ, also known as NEMO) and a catalytic subunit IRD5 (IKKβ)[415–417]. IKK complex then activates Relish by phosphorylation, removing the autoinhibitory ankyrin-repeat domain, and driving the relevant gene expression programme[416]. Tak1 signalling is also capable of inducing an alternative stress response pathway by JNK signalling.

1.2.1.4 Eiger signalling and apoptosis

Eiger (EDA-like cell death trigger, Egr), named in memory of all the mountaineers who perished on the Eiger Nordwand ”Wall of Death”, was identified as a homologue of TNFα in

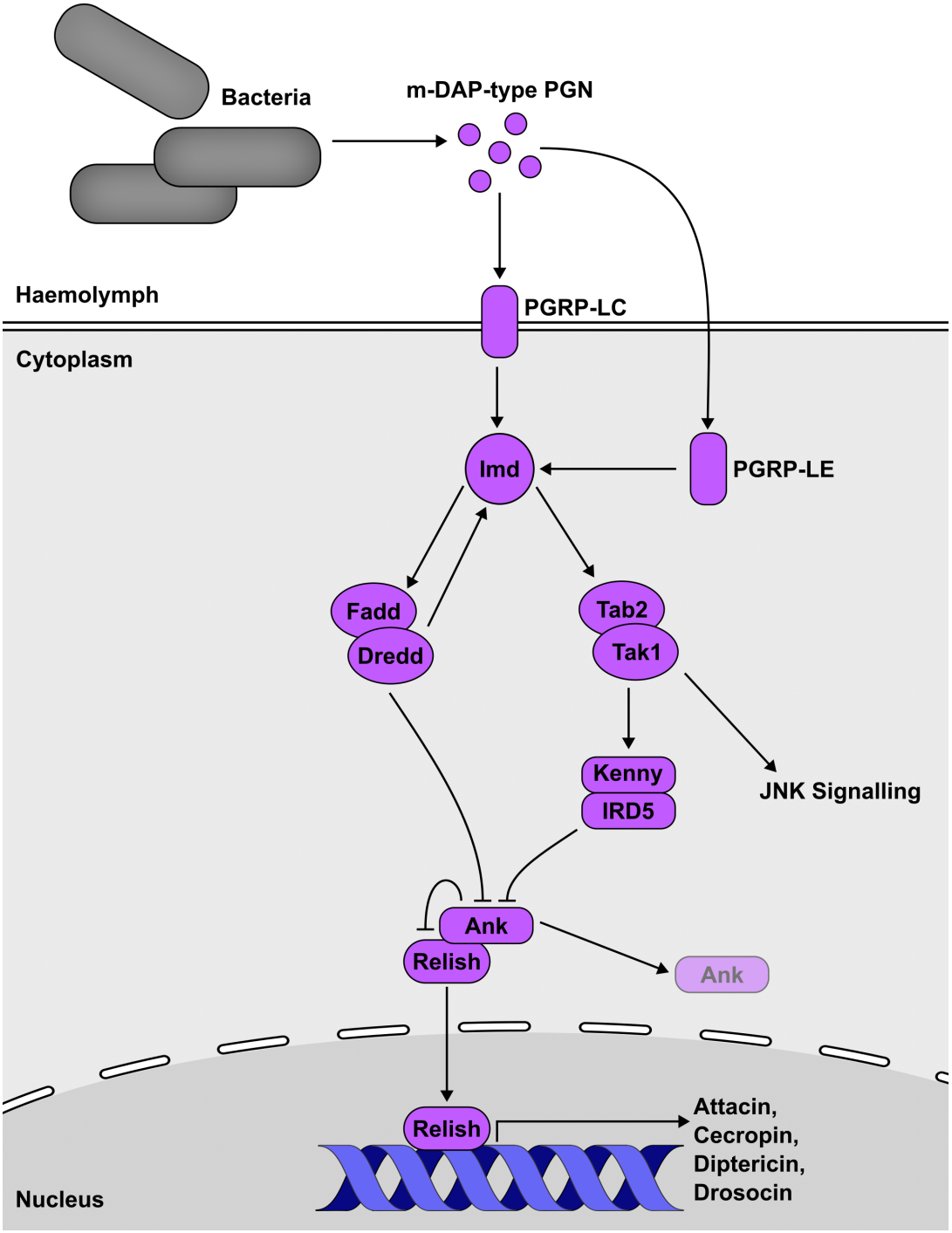


Figure 1.6. Imd pathway signalling. See text for details.

D. melanogaster, and was the first invertebrate TNF superfamily ligand to be described[418,419]. TNFα plays a pivotal role in regulating the innate immune response during infection in many species by orchestrating immune cell functions such as transcription of immune-related genes, activity of inflammatory cascades, and inducing apoptosis. Apoptosis is an essential host

defence mechanism against invading pathogens by allowing controlled destruction and removal of infected cells, reducing the possible replication and further spread of the pathogen and decreasing the damaging inflammatory response associated with dying and necrotic cells. This apoptotic signalling is driven by various caspases. In mammals, ligand-induced apoptosis is referred to as the extrinsic apoptosis pathway and is driven by caspase 8, in contrast to the intrinsic apoptosis pathway which is triggered by intracellular death signals and requires caspase 9 activity and apoptosome formation[419].

In *D. melanogaster*, Egr signalling also plays an important role in host innate immune function. Egr is a type II transmembrane protein with a TNF homology domain within the C-terminal, which can be produced as a short-form or long-form isoform. The C-terminal domain is cleaved and released as a soluble mature cytokine by the *D. melanogaster* TNFα converting enzyme (Tace)[418,420,421]. Egr can then signal via two receptors, Wengen (Wgn)[422] and Grindelwald (Grnd)[423], named for villages near Eiger in the Swiss Jungfrau region. While both receptors form heterohexamers which bind with trimeric Egr ligands, the affinity with which they bind Egr varies by three orders of magnitude. Grnd shows much higher affinity for Egr binding, which occurs at the cell surface and is required for apoptotic signalling by Egr. In contrast, Wgn is localised within intracellular vesicles and lacks the intracellular death-death domain required for TNF receptor associated factor (Traf)-interacting motif and canonical JNK signalling, suggesting that signalling via the different receptors may serve different functions, dependent upon differing ligand availability[424].

Egr signalling can trigger cell death through multiple pathways. JNK signalling, Figure 1.7, is one of these pathways, which is activated upon Egr binding to Grnd allowing Tab2 to act as an adaptor protein linking Traf4 (also known as Traf1) to Tak1 (JNKKK)[418,419,425,426]. Traf6 (also known as Traf2) has also been reported to induce JNK signalling via Egr, likely with a consistent mechanism as Traf4[424,426,427]. Misshapen (Msn, MAPKKK) can then interact

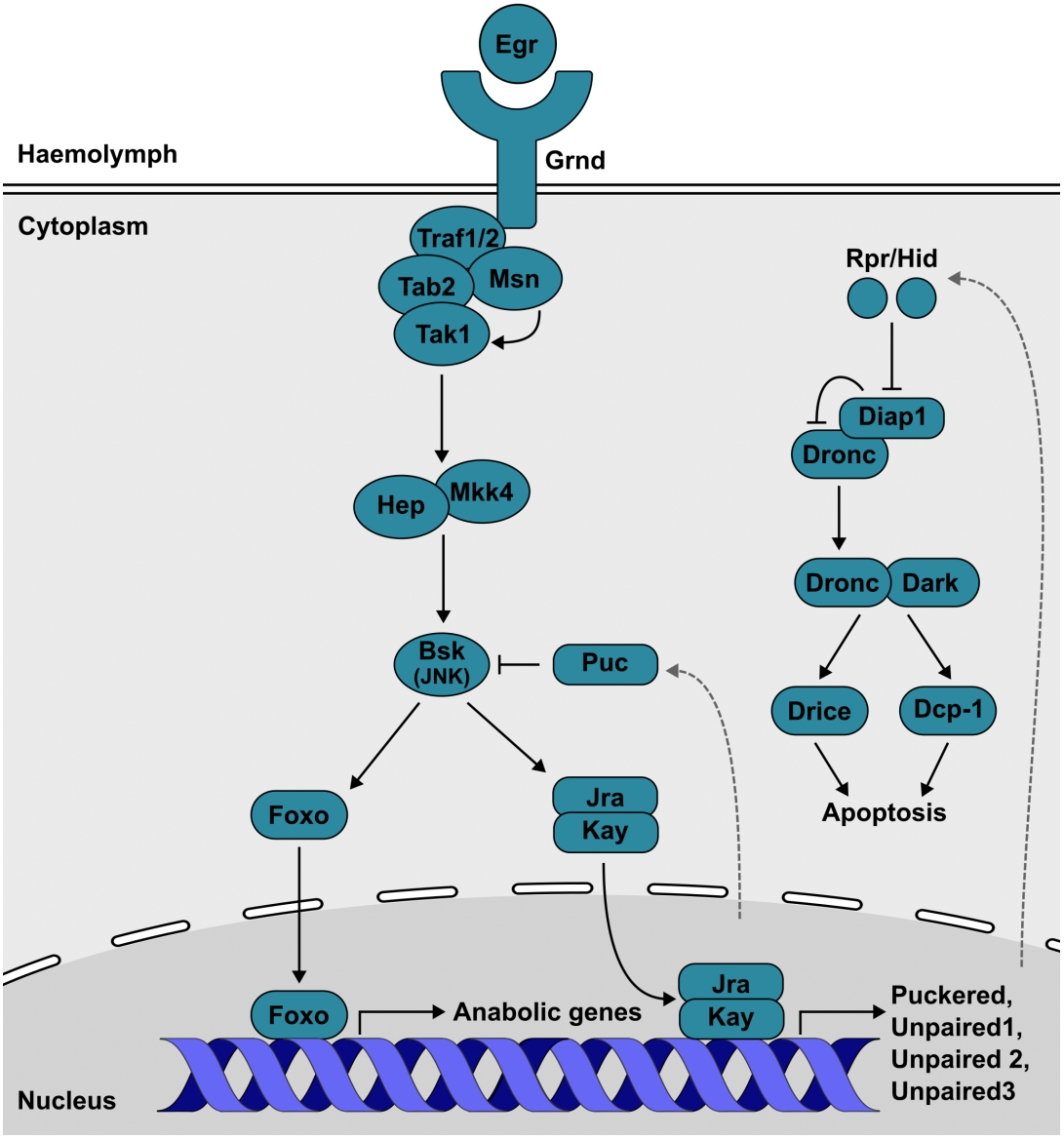


Figure 1.7. Eiger signalling pathway. See text for details.

with Traf4 linking Msn to Tab2 forming a transcient complex, subsequently allowing Msn to phosphorylate Tak1[418,419,425,426]. This results in a cascade activating Hemipterous (Hep, JNKK, also known as Mkk7), Map kinase kinase 4 (Mkk4), and subsequently Basket (Bsk, JNK)[418]. Unlike in mammals, two MAPKKs are required to activate JNK in *D. melanogaster*, Hep and Mkk4, with non-redundant roles acting in parallel[428]. Activated JNK is capable of driving a wide range of cellular responses, relating to metabolism, immune responses, cell proliferation and apoptosis, which is driven through different transcription factors. Firstly, JNK can phosphorylate Jun-related antigen (Jra), the *D. melanogaster* Jun[429,430], and Kayak (Kay),

the *D. melanogaster* Fos[431], which together form the AP-1 transcription factor. Transcriptional targets of this include inducing expression of *puckered* (*puc*), which forms a negative feedback loop by dephosphorylating and inhibiting Bsk[432]. Activated JNK can also drive transcriptional changes via Foxo. These transcription factors can cause a huge variety of context-specific and tissue-specific cellular responses relating to metabolism and growth (*dILP2*), autophagy (*sestrin*), cellular proliferation and tissue repair (*upd1, upd2, upd3*)[433,434].

Activated JNK is also capable of inducing transcriptional activation of immune genes such as *Punch*, *Malvolio*, and *Sulfated*[410], as well as triggering cell death via Death regulator Nedd2-like caspase (Dronc). Dronc is the *D. melanogaster* caspase 9 homologue, which is capable of associated with the protein cofactor Apaf-1 homologue Death-associated APAF1-related killer (Dark) to form the apoptosome. JNK signalling can trigger the activation of Dronc by causing transcriptional upregulation of genes such as *head involution defective* (*hid*), *reaper* (*rpr*), and *grim*, which form small proteins that bind and inactivate Death-associated inhibitor of apoptosis 1 (Diap1), thus removing inhibition of Dronc[419,435]. This releases Dronc to form the apoptosome with Dark and activate the effector caspases Death-related ICE-like caspase (Drice) and Death caspase-1 (Dcp-1)[436–438]. JNK signalling can be rapidly terminated by proteasomal degradation of Tak1 caused by activation of Relish by the Imd pathway, promoting a pro-survival response[439]. The *D. melanogaster* homologue of tumour suppressor mutated in familial cylindromatosis, Cylindromatosis (CYLD) is also thought to activate JNK signalling via Traf6 by deubiquitinating and thereby stabilising the Traf6 protein[427].

Egr signalling has also been described to activate apoptosis independently of JNK signalling. This pathway involves the activation of No poles (NOPO), an E3 ubiquitin ligase which is the *D. melanogaster* orthologue of Traf-interacting protein (TRIP). A heterodimer complex formed by Bendless (Ben), the *D. melanogaster* orthologue of Ubc13, and Ubiquitin-conjugating enzyme variant 1A (Uev1A), which functions as an E2 ubiquitin-conjugating enzyme to activate

NOPO, which also causes a transcriptional upregulation of *rpr* and *hid*[440]. There is also some evidence that this Ben-Uev1A complex can elicit JNK-dependent cell death via Traf6[441,442]. In the event that apoptosis is inhibited, Egr can also induce cell death via necrosis in addition to controlled apoptosis. Egr expression was still capable of inducing cell death when the effector caspases Drice and Dcp-1 were inhibited. This process was still dependent on initiator caspase Dronc and JNK signalling, as overexpression of Dronc alone was not sufficient to cause necrosis when apoptosis was blocked[443,444].

It is unclear to what extent there is cross-talk between the Imd and the JNK signalling pathways. Whilst activation of Tak1 by Imd can activate JNK signalling, it is unclear if there is any involvement of Egr signalling in the regulation of Relish activity. Recent work has suggested that in homeostatic conditions Egr signalling via Wgn suppresses Relish immune signalling in a Traf6-dependent manner, acting upstream of Tak1[445]. This immune suppression is then overcome by Imd signalling during infection, whereby Traf6 facilitates translocation of NF-κ transcription factors Dif and Relish into the nucleus[425,445,446]. It is unclear if changes in Egr secretion during infection also remove this inhibitory action through Wgn in order to increase Relish activity due to the changes in the cellular localisation of Egr, and differences in affinity between the two Egr receptors Wgn and Grnd[424,445]. It is also unclear how Wgn may partner with Traf6 to inhibit Tak1 activity, as Wgn lacks the canonical death-death domain required for interacting with Traf[424].

In addition to its role in regulating innate immune responses, Egr signalling has been implicated in regulating energy homeostasis, consistent with the action of TNFα in mammals[447–450]. In *D. melanogaster* Egr can act as an adipokine, in response to low protein conditions detected by amino acid sensor Target of rapamycin C1 (TORC1) within the fat body, Tace expression is increased resulting in cleavage of Egr from the cell surface. The released soluble Egr then travels to insulin-producing cells (IPCs) within the brain, whereby JNK signalling via Grnd

increases Foxo activity, inhibiting expression of *Drosophila* insulin-like peptide (dILP)-2 and dILP-5 in order to reduce growth[421]. Wgn was also found to restrict autophagy-mediated lipolysis in homeostatic conditions by reducing intracellular levels of Traf3, independently of Egr, possibly by promoting degradation of Traf3 by NOPO[445,451].

Previous work has highlighted the role of Egr in the *D. melanogaster* response to a range of pathogens, such as *Escherichia coli*, *Enterococcus faecalis*, and *Coxiella burnetii*[452,453], possibly related to its requirement for proper AMP production within the fat body[454]. However, these previous studies must be carefully considered as it was recently found that the widely used Egr mutant *D. melanogaster* lines, egr^{1} and egr^{3} also carried additional mutations in the Nimrod C1 (*NimC1*) gene, a phagocytosis receptor. Imprecise excisions of the $Regg1^{GS9830}$ P-element which resulted in the deletions in the first coding exon of the *egr* gene also resulted in truncation of *NimC1* before the transmembrane domain of the receptor. NimC1 is normally found on plasmatocytes, and loss of NimC1 function impairs the capacity of the plasmatocytes to phagocytose microbes, clouding the results from studies using the egr^{1} and egr^{3} lines[455].

1.2.1.5 JAK/STAT signalling

Janus kinase/signal transducer and activator of transcription (JAK/STAT) signalling is associated with key aspects of innate immune regulation, in both mammals and *D. melanogaster*. In *D. melanogaster*, the JAK/STAT pathway, shown in Figure 1.8, is activated by three cytokine-like ligands called Unpaired (Upd), Upd2, and Upd3, which display differing activation potentials[456–460]. All three ligands bind a common gp130-like receptor, Domeless (Dome), which shares similarities to the mammalian cytokine class I receptors such as the presence of a cytokine-binding module and an extracellular fibronectin type III domain[461,462]. In *D. melanogaster*, binding of an Upd ligand to Dome induces dimerisation of Dome and activation of the sole *D. melanogaster* JAK, called Hopscotch (Hop)[463]. The JAKs are associated with the cytoplasmic tail of Dome, and so upon dimerisation, they activate and

phosphorylate one another, as well as specific tyrosine residues on the cytoplasmic tail of Dome. This allows for the sole *D. melanogaster* STAT, Stat92E[464], to bind using the Src homology 2 (SH2) domains. The STATs are then tyrosine phosphorylated by the JAKs, releasing the STATs as a dimer to translocate into the nucleus and drive transcription of target genes[465,466]. This process is negatively regulated by Suppressor of cytokine signalling (SOCS) proteins, in *D. melanogaster* this is by Socs36E[467,468].

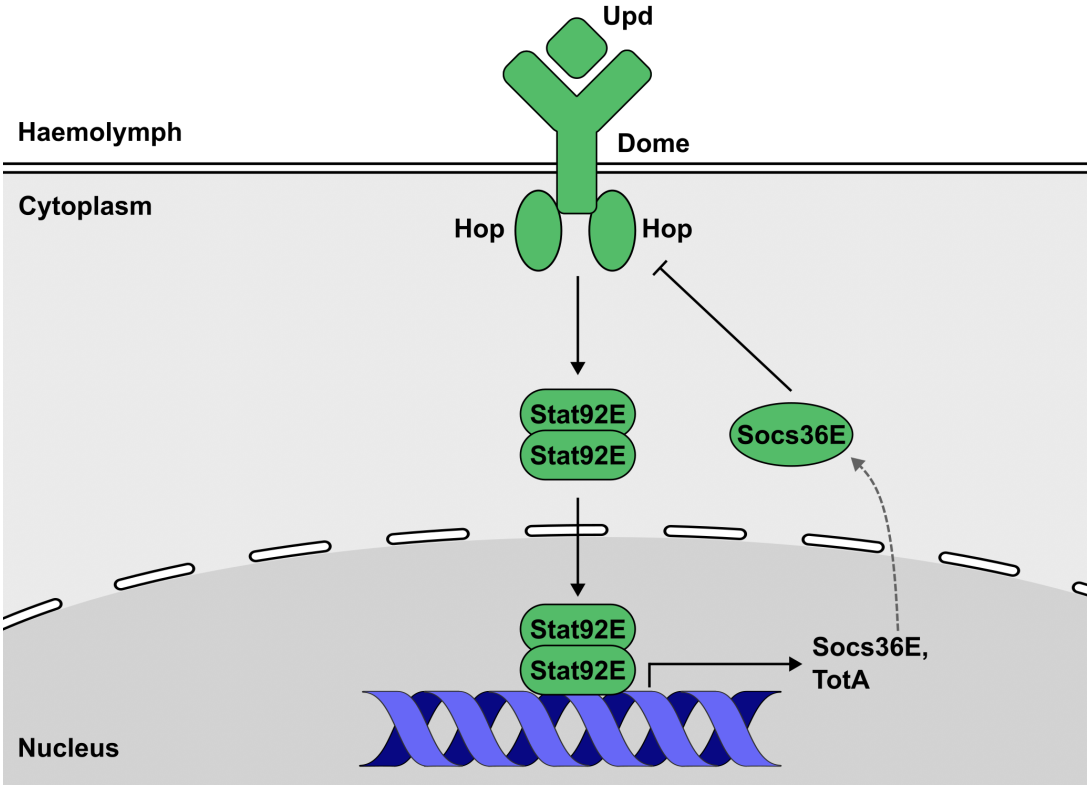


Figure 1.8. JAK/STAT signalling pathway. See text for details.

In response to infection, *D. melanogaster* JAK/STAT signalling is required for antiviral defence, maintaining gut integrity during bacterial infection, and production of stress proteins such as TotA and Tep1[457,469]. Upd3 signalling in haemocytes during *M. marinum* infection in *D. melanogaster* has been shown to induce *Autophagy-related 2* (*Atg2*) expression. This resulted in accumulation of intracellular lipid droplets, increased *in vivo* growth of *M. marinum*, and decreased survival of the host[470]. JAK/STAT signalling also has a role in regulating host metabolism, Upd2 signalling in GABAergic neurons removes inhibition on IPCs, allowing for

the production and secretion of dILPs such as dILP2 to promote fat storage[471,472].

1.2.1.6 Cellular immunity

In addition to the conserved cell signalling pathways involved in innate immune responses, *D. melanogaster* is also capable of cellular immune responses via the blood cells, termed haemocytes. Haemocytes can be grouped into three different subtypes, each of which serve different immunological functions and have varying presence dependent on the life stage of *D. melanogaster*. Due to the higher quantity of haemocytes during the larval stage, the composition and function of haemocytes within larvae has been extensively characterised, whereas the same cannot be said of adult *D. melanogaster*[473].

Within larvae, 95% of the circulating haemocyte population is made up of plasmatocytes, professional phagocytes analogous to mammalian macrophages or monocytes that are responsible for destroying foreign pathogens by phagocytosis, coordinating innate immune signalling by secreting cytokines and other signals, and clearing apoptotic cells or other cellular debris[473–477]. Plasmatocytes emerge from two lineages, mainly the haematopoietic pockets[478–481] but also from the lymph gland within the larvae from blood cell progenitors (prohaemocytes)[477,482,483]. It is thought that the entirety of the adult haemocyte population is retained from this population of plasmatocytes throughout their lifespan, without replacement[484]. While larval plasmatocytes are described as both circulating and sessile, adult plasmatocytes have only been described as sessile and attached to different tissues within the adult fly[485].

The other subtypes of haemocytes are found only within the larval stages. Crystal cells represent the remaining 5% of circulating haemocytes within larvae under normal conditions, named for the large crystalline inclusions of PPO that they carry to facilitate melanisation responses[473,474,477]. The final subtype is lamellocytes, which are only produced in response to large pathogens that are unable to be phagocytosed, such as parasitic wasp eggs.

Lamellocytes are then produced in large numbers to bind and encapsulate the wasp egg in multiple layers in order to kill the invading parasite[473,474,477,486].

Phagocytosis by plasmatocytes is initiated upon detection of a PAMP such as β-1,3 glucans, lipopolysaccharides, peptidoglycans[487], by a PRR such as opsonins[488], Nimrods[489], or scavenger receptors[490]. F-actin branching forms a phagocytic cup, which is then extended by actin polymerisation around the microbe until it is contained within a newly formed phagosome[487]. Following internalisation, the phagosome undergoes a process of maturation by fusing with early endosomes, late endosomes, and lysosomes, regulated by GTPases such as Rab5 and Rab7. This culminates in a highly acidic phagolysosome containing proteases and DNAses in order to destroy the phagocytosed microbe[487].

1.2.2 Immunometabolism

Immunometabolism refers to the interplay between the host immune responses and metabolic changes during an infection. *D. melanogaster* is an ideal model for studying this relationship due to the tight integration of the immune and metabolic responses orchestrated by a single organ, the fat body. In addition to its role in the production of key immune signalling molecules and AMPs, the fat body acts as an energy store, mainly containing triglycerides stored within intracellular lipid droplets (LDs)[491]. These are synthesised primarily from dietary fatty acids, proteins or carbohydrates, and are released as free fatty acids for energy production by β-oxidation. Glycogen is also stored within the fat body and can be used as glycolytic fuel to meet energy demands. Glucose is also used to synthesise trehalose, the primary circulating sugar in *D. melanogaster*[491]. The balance of these energy stores is regulated by insulin and glucagon-like adipokinetic hormone (AKH) signalling[491–493]. Using these accumulated energy stores, the fat body can mobilise key metabolites, lipids, carbohydrates and amino acids, when necessary, for example during an energetically demanding immune response requiring the production of large amounts of AMPs.

The use of *D. melanogaster* as a model for immunometabolism is exemplified by the work by Dionne *et al.*, which found that *D. melanogaster* infected with *M. marinum* displayed a wasting phenotype whereby the infected flies became hyperglycaemic alongside progressive loss of lipid stores and glycogen[494]. This is very similar to the infection-induced cachexia seen in mammals infected with mycobacteria. In *D. melanogaster*, this phenotype was found to be dependent on the transcription factor Forkhead box sub-group O (Foxo), which inhibits insulin signalling. It was shown that during *M. marinum* infection, insulin signalling became defective and caused an over-activation of Foxo leading to widespread metabolic pathology and disease[494].

1.2.2.1 Insulin signalling

Insulin signalling is conserved across metazoans[495], and plays an essential role in nutrient sensing in *D. melanogaster* by promoting anabolism during high nutrient conditions in order to promote growth as well as production and storage of glycogen and lipids[496]. The seven dILPs in *D. melanogaster* show differing patterns of expression and regulation, and as such vary in their function[496]. An outline of insulin signalling in *D. melanogaster* is shown in Figure 1.9. dILPs produced by IPCs, median neurosecretory cells[497–499], can act on the fat body by binding the insulin receptor (InR)[500], which results in the intracellular binding of Chico[501]. Phosphatidylinositol-3-kinase (PI3K) is then recruited to the cell membrane and activated, driving an accumulation of phosphatidylinositol (3, 4, 5)-triphosphate (PIP_3). This acts as a binding site for phosphoinositide-dependent kinase (Pdk1) and Akt kinase[496]. This binding causes a conformational change[502], allowing for the phosphorylation of the Akt activation loop by Pdk1[503]. Akt can also be phosphorylated by TORC2, at a different site, which may facilitate the phosphorylation and activation by Pkd1 however does not seem essential for Akt activity[504,505]. Activated Akt can then regulate a suite of anabolic processes induced by insulin signalling, including inhibiting the nuclear translocation of Foxo[506]. Foxo

regulates a large transcriptional programme to counteract anabolism and favour catabolism, over 30% of nutrient-responsive genes are controlled by Foxo in *D. melanogaster* S2 cells[507] and over 1250 genes are differentially expressed due to the action of Foxo during fasting in *D. melanogaster* adults[508]. In addition to inhibiting Foxo, Akt can inhibit glycogen synthase kinase (GSK3) to promote production of glycogen[509], or activate TOC1 to increase nucleotide, protein, and lipid synthesis[510].

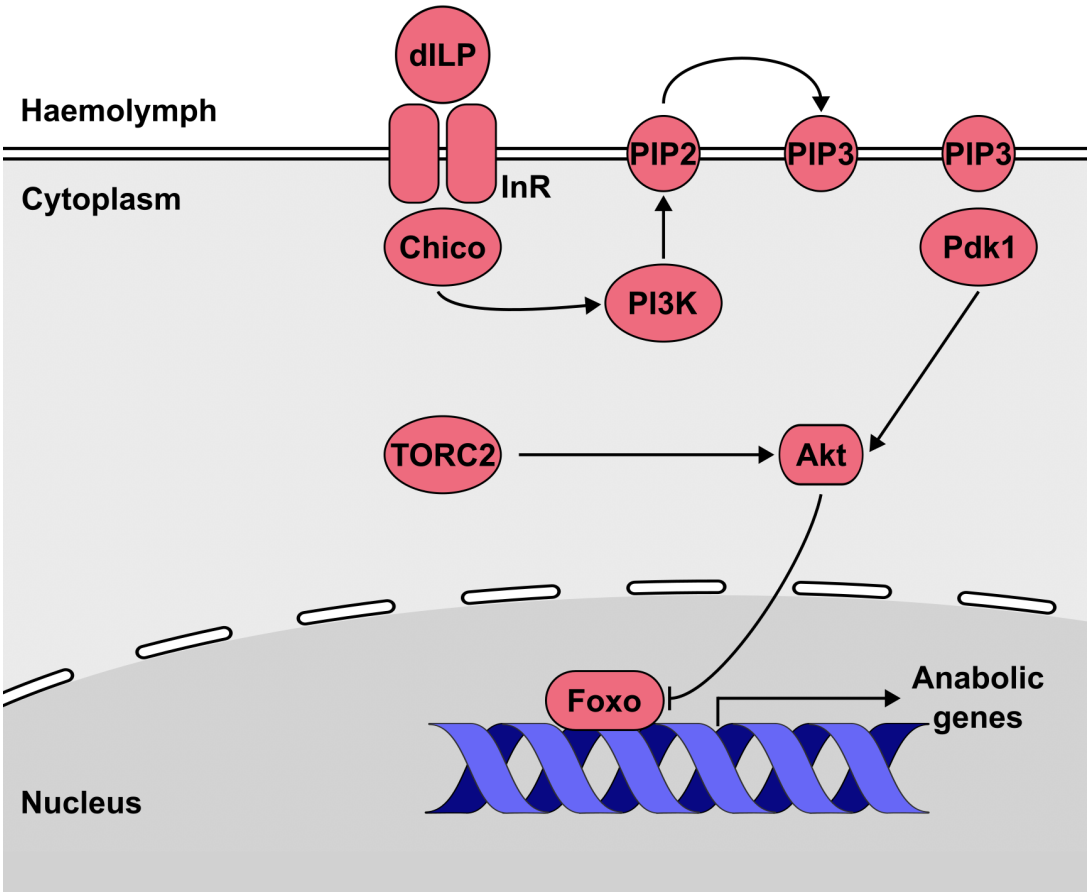


Figure 1.9. Insulin signalling. See text for details.

1.2.3 Modelling mycobacterial infection in *Drosophila melanogaster*

The increasing understanding of the *D. melanogaster* innate immune system and its relationship to other host processes, such as metabolic responses during infection, has led to growing interest in the use of *D. melanogaster* as a model for host-pathogen interactions. The highly conserved cell signalling pathways which comprise the innate immune response

are frequently targeted by pathogens during infection. Cell-autonomous host factors have also been identified that interact with a range of pathogens from RNAi screens with *D. melanogaster* cell lines[511], which can then be studied further using *in vivo* infection models combining eukaryotic and prokaryotic genetic manipulation.

Studies using both *in vitro* and *in vivo* approaches with the *D. melanogaster* model have led to interesting findings about mycobacterial infection. *In vitro* studies make use of cultured *D. melanogaster* phagocytes, typically the S2 cell line and its derivatives, which are particularly well-suited for pseudo-genetic RNAi screens and have been highly informative in identifying key host factors responsible for controlling mycobacterial infection. S2 cells recapitulate *in vivo* behaviour of several mycobacterial species; pathogenic species such as *M. marinum* and *M. fortuitum* are capable of intracellular growth and lead to cell death, mirroring their lethality *in vivo*, whereas non-pathogenic species such as *M. smegmatis* have their growth restricted[512–514]. For the study of nontuberculous mycobacteria such as *M. marinum*, typically found in environmental sources, the ideal culture temperature of S2 cells at 28°C closely matches the ideal growth temperature of these mycobacterial species. This makes S2 cells well suited for studying nontuberculous mycobacteria, however, they are limited in studying obligate human pathogens such as *M. tuberculosis*, as the optimum growth temperature for these species is 37°C, which causes cytotoxic heat shock response in S2 cells[514,515]. The same is true of intact *D. melanogaster*, which are typically maintained at their ideal temperature of 25°C.

1.2.3.1 Detection of mycobacteria by *Drosophila melanogaster*

An essential aspect of studying mycobacterial infections with the *D. melanogaster* model is considering which humoral immune signalling pathways are activated and how. Studies with different mycobacterial species in *in vivo D. melanogaster* infection have found differing results with regard to the activation of the *D. melanogaster* humoral signalling pathways and the

possible role of these pathways during infection, particularly the Toll pathway. Infection of *D. melanogaster* with *M. marinum* failed to induce production of any AMPs at levels higher than a sterile-injury control during the first 50 hours post-infection. Transcriptomics did show some Toll pathway activation much later during the infection, at 96 hours post-infection, shortly before death[494]. Nonetheless, fly lines lacking the Toll or Imd signalling pathways showed no change in susceptibility to infection with *M. marinum* compared to wild-type *D. melanogaster*[516], indicating that to whatever extent the Toll pathway is induced has no meaningful impact on the infection outcome, possibly due to high intrinsic resistance to Toll-mediated killing by *M. marinum* or that Toll activation occurs too late and too weakly to alter the progression of the *M. marinum* infection. This contrasts with *D. melanogaster* infections with other mycobacterial species. *Mycobacterium smegmatis* is a non-pathogenic mycobacterium in humans and is non-lethal to wild-type *D. melanogaster* and Imd mutant *D. melanogaster*. However, Toll mutant *D. melanogaster* are susceptible to *M. smegmatis* infection with increased bacterial burdens compared to wild-type flies and death at approximately one week post-infection (unpublished data, Dionne Lab)[514]. Toll pathway activation has also been implicated during infection with *M. abscessus*. Oh *et al.* reported a 26-fold increase in *Drosomycin* (*Drs*) expression 4-days post-infection and that flies with mutations in PGRP-SA, the PRR responsible for peptidoglycan detection in the Toll pathway, were more susceptible to *M. abscessus* infection compared to wild-type flies[517]. It should be noted that the findings of Oh *et al.* are limited, in part by the use of mixed male and female flies in experiments, which are known to have differing immune activity including in response to mycobacterial infection (unpublished data, Dionne Lab)[518,519].

Recent work by Touré *et al.* found that in *D. melanogaster* lacking phagocytic plasmatocytes, which causes *M. abscessus* to remain extracellular, there was strong induction of AMPs associated with both the Toll and the Imd signalling pathways, including *Attacin-A* (*AttA*), *Cecropin C* (*CecC*), *Defensin* (*Def*), and *Metchnikowin* (*Mtk*). Additionally, phagocyte-depleted flies were considerably more susceptible to *M. abscessus* infection when they were also

carrying mutations in *Relish* (*Rel*), *spätzle* (*spz*), *Def*, or a *Mtk Drs* double mutant[488]. This suggests that the Toll pathway is detecting and responding to extracellular *M. abscessus* and that production of AMPs is somewhat effective at slowing the infection. Nevertheless, it cannot be considered entirely effective as nearly all infected wild-type flies still succumb to *M. abscessus* infection, albeit at a later time-point. Unfortunately, despite the very interesting result that phagocyte-depleted *Rel* mutant flies infected with *M. abscessus* died more rapidly, the authors concluded that there was no involvement of the Imd pathway as flies with mutations in *AttA* and *Drosocin* (*Dro*) did not increase susceptibility, and so did not follow up about the possible role of Rel during *M. abscessus* infection[488].

Despite this work, it remains unclear how mycobacterial species are detected by the *D. melanogaster* humoral signalling pathways. Mycobacteria produce *m*-DAP-type peptidoglycan[520,521] which should be detected by the Imd pathway[356,393–395], however previous work has shown that Imd mutant flies show no increase in susceptibility to *M. abscessus* infection[118,517]. The activation of Toll pathway signalling may be driven by PGRP-SA, as reported by Oh *et al.*[517], PGRP-SD, or by the action of microbial proteases. Other detection mechanisms may include cyclic dinucleotides detected by dmSTING, synergy between Toll and Imd pathway signalling[403,522], alternative PAMPs such as factors within the mycomembrane, or widespread tissue damage and inflammatory responses[514]. The apparent delay in recognition of mycobacteria by the *D. melanogaster* humoral immune system compared to infections with other bacteria indicates a degree of immune evasion by the mycobacteria, which may be facilitated by the intracellular localisation, or shielding of mycobacterial peptidoglycan by the mycomembrane[514].

1.2.3.2 Uptake of mycobacteria by *Drosophila melanogaster* phagocytic cells

Little is known about specific receptors and host factors responsible for the phagocytic uptake of mycobacteria in the *D. melanogaster* infection model, and this seemingly varies by

mycobacterial species. Two proteins have been identified, firstly the CD36 family scavenger receptor Peste (Pes) was found to be required for uptake of *Mycobacterium fortuitum* by *D. melanogaster* S2 cells. It was also found to play a role in uptake of *M. smegmatis* and *Listeria monocytogenes* but had no effect on uptake of *S. aureus* or *E. coli*. Human embryonic kidney 293 (HEK293) cells are normally resistant to *M. fortuitum* infection, however expression of *pes* within these cells allowed them to be infected[512]. The second host factor identified was the opsonin Thioester-containing protein 4 (Tep4), which was shown to be involved in the phagocytic uptake of *M. abscessus* by plasmatocytes in an *in vivo* infection of adult *D. melanogaster*. *Tep4* loss-of-function mutant flies show increased susceptibility to *M. abscessus* infection[488], suggesting *M. abscessus* utilises phagocytosis and its adaptations to an intracellular lifestyle as a method of immune evasion. *Tep4* mutant flies did not show any difference in survival when infected with *M. marinum*, either because Tep4 is not involved in phagocytic uptake of *M. marinum*, or because any AMP response to extracellular *M. marinum* is ineffective[488].

1.2.3.3 *Drosophila melanogaster* host factors restricting intracellular mycobacterial growth

An RNAi screen using *D. melanogaster* S2 cells was used to identify host factors that affected intracellular growth of *M. fortuitum*. This was detected using green fluorescent protein (GFP) expression under the control of *map24* and *map49* promoters in *M. fortuitum*, which are induced when mycobacteria that survive within phagocytes are phagocytosed[523]. 81 host factors were identified to be required for infection of S2 cells by *M. fortuitum*, however, 54 of these were considered to be for general phagocytosis as they also impaired uptake of *E. coli*. Most of these general phagocytosis genes were involved in the actin cytoskeleton and vesicle trafficking, such as the Arp2/3 complex, Arp14D, Cdc42, Rab5, and actin capping proteins. Other host factors were found to play an additional role specifically in the uptake of mycobacteria, such as

Rab5 and Rac2, as targeting these genes with dsRNA caused a significant intracellular growth defect in *M. fortuitum* infection, but only a mild defect in phagocytosis of *E. coli*. This study also identified host factors important for controlling the intracellular growth of *M. fortuitum* without any direct role in phagocytosis, such as components of the vacuolar ATPase and chromatin factors[512].

D. melanogaster S2 cells have also identified host lysosomal enzymes which are effective at controlling mycobacterial infection, which typically pathogenic mycobacteria resist by inhibiting phagosome maturation and fusion with lysosomes. Lysosomal enzyme β-hexosaminidase was found to control intracellular growth of *M. marinum*, as RNAi knockdown of the β-hexosaminidase β-subunit (the homologue of mammalian HEXO2), in S2 cells led to a distinct increase in intracellular *M. marinum*. This was then replicated in murine bone marrow-derived macrophages (BMDMs), with HexB-deficiency leading to a similar increase in intracellular growth of *M. marinum*. The action of β-hexosaminidase against *M. marinum* was found to be extracellular killing of *M. marinum* at the cell surface following secretion of β-hexosaminidase, and not because of a more generalised phagocytic response[514,515]. Interestingly, this protective effect of β-hexosaminidase is mirrored in human patients. Tay-Sachs disease, an inherited neurodegenerative disorder, is caused by genetic loss of the α-subunit of hexosaminidase; instead of producing an $\alpha\beta$-heterodimer, Tay-Sachs patients have increased production of the β-subunit of hexosaminidase. These patients also display increased resistance to tuberculosis[515,524–526]. This is consistent with the results that RNAi knockdown of the homologue of the α-subunit in *D. melanogaster*, HEXO1, had no impact on *M. marinum* infection in S2 cells. It was also found that β-hexosaminidase had no bactericidal effect against *Salmonella typhimurium* or *Listeria monocytogenes*, suggesting a specific mycobactericidal effect possibly due to specific interactions with a mycobacterial factor or the much slower replication rate of *M. marinum*[514,515].

Once mycobacteria have been taken up by phagocytic cells, the ESCRT proteins play a key role in restricting the intracellular growth of mycobacteria. *M. smegmatis* constitutively expressing GFP was inoculated into S2 cells, which were treated with dsRNA targeting *D. melanogaster* host factors to identify which genes are normally responsible for controlling the growth of non-pathogenic *M. smegmatis*. The targeted host factors which led to an increase in intracellular *M. smegmatis* growth included a component of the ESCRT I complex, dVps28, and a component of the ESCRT III complex, CG8055, a homologue of CHMP4B/SNF7[513,514,527]. Other components of different ESCRT complexes were then specifically targeted with dsRNAs. The dsRNAs targeting Vps4, Vps20, Vps24, Vps25, Vps26, and dTsg101 all caused deficiencies in ESCRT function, measured by the impact on ubiquitin trafficking, and also led to increased intracellular growth of *M. smegmatis*. Some of these host factors, those that caused the most disruption to ESCRT function (Vps4, Vps28, dTsg101, CG8055), also altered the phagosome environment within S2 cells, shown by decreased induction of *map24* and *map49* by *M. fortuitum*[513,514]. Immunofluorescence of S2 cells infected with *M. smegmatis* found that ESCRT machinery acts directly on the intracellular bacterial compartment, and that loss of ESCRT function can cause a profound change in the host susceptibility to infection with non-pathogenic *M. smegmatis*. Following this work it was found in a *Dictyostelium discoideum* model of infection that ESCRT machinery is recruited to phagosomes containing pathogenic *M. marinum* or *M. tuberculosis* depending on the presence of ESX-1, likely in response to the small membrane perforations caused by the ESX-1 system and an attempt by the host to repair them[73,514,528]. *M. tuberculosis* is also capable of secreting virulence factors via ESX-3, EsxG and EsxH, as a countermeasure to inhibit ESCRT function and subsequent phagosomal maturation[72,73,512,514,515]. ESCRT function has also been linked to a possible role in antigen presentation, as inhibition of ESCRT function by *M. abscessus* EsxH undermines the recognition of infected macrophages by CD4+ T-cells[514,529].

1.2.3.4 Role of autophagy during mycobacterial infection

Autophagy is a key intracellular degradation pathway and plays an important role in cellular and systemic defence against intracellular pathogens such as mycobacteria, however the precise nature of this involvement is not entirely clear[530]. Virulent mycobacteria such as *M. tuberculosis* have been shown to actively impair autophagic functions within the cell alongside inhibiting phagosomal maturation, by the action of secreted virulence factors ESAT6/EsxA, EsxG, and EsxH[72,73,531]. Despite the apparent association between autophagy-related genes and mycobacterial pathogenesis, it seems increasingly likely individual autophagy genes are not significantly contributing towards protection against pathogenic mycobacteria, but rather that they act in roles beyond autophagy to help control infection[514,530]. There may also be a link between autophagic factors and systemic pathology caused by mycobacterial infection. Autophagy is controlled by endocrine signals regulating systemic metabolism, particularly the insulin signalling pathway[532,533], and so the disruptions to insulin signalling during mycobacterial infection and potential changes in autophagy are likely connected. While the exact nature of this relationship remains unclear, it is possibly mediated by JNK and Foxo. Whilst insulin signalling inhibits Foxo activity via Akt[506], JNK signalling positively regulates Foxo activity[433,434], and increased Foxo activity has been shown to induce autophagy, alongside Foxo target gene *Thor* (also known as *4E-BP*)[534,535]. In an *in vivo D. melanogaster* infection with *M. marinum*, flies with mutated Foxo survived for longer following infection, and also showed a reduction in metabolic pathology. The authors concluded that during *M. marinum* infection the observed decrease in activated Akt, possibly caused by a reduction in circulating insulin or increased turnover of activated Akt, and the ensuing exacerbation of Foxo activity causes a progressive loss of energy stores and increasing pathology[494]. It was not addressed in this study whether autophagic factors were contributing to the observed phenotypes or being altered by the changes in Foxo activity, however, several other studies have used *D. melanogaster* to investigate the various roles of ATGs in mycobacterial infection.

During *in vivo* infection of adult *D. melanogaster* with *M. marinum*, it was found that JAK/STAT signalling via the cytokine Upd3 inhibited expression of *Atg2*. Flies with mutations in *upd3* had elevated *Atg2* transcript levels, and increased survival with decreased bacterial load during *M. marinum* infection. This was mirrored in S2R+ cultured cells, overexpression of *Atg2* halved levels of intracellular *M. marinum* and drastically reduced cell death, with no changes in initial bacterial uptake. This protective effect of Atg2 is likely due to the effect on intracellular triglyceride levels. Increased *Atg2* expression led to reduced numbers of large intracellular lipid droplets, preventing the accumulation of lipids that are highly beneficial for intracellular mycobacterial survival under normal conditions[470]. In addition to this role in regulating host cell lipid droplets, the role of *Atg2* in autophagy is to transport lipids during autophagosome formation. Loss of *Atg2* in *D. melanogaster* causes autophagic membranes to become enriched in phosphatidylinositol (PI) and other polyunsaturated lipid species, altering membrane fluidity. Accumulation of PI3P within autophagosomal membranes is important for recruitment of downstream effectors, and also for facilitating lipid transfer by Atg2 by aiding the unidirectionality of lipid transfer from the endoplasmic reticulum to the negatively charged autophagosomal membrane[536,537]. Mycobacteria possess multiple virulence factors to prevent this accumulation of PI3P and subsequently the proper function of Atg2, including SapM, a PI3P phosphatase[538], and LAM, which intercalates into autophagosomal membranes and blocks PI3P kinase hVPS34 recruitment, thus preventing the initial production of PI3P[514,539,540].

Atg7 was also identified as an autophagy factor with a role in mycobacterial infection using *D. melanogaster*. *Atg7* mutant *D. melanogaster* showed decreased survival during *M. marinum* infection compared to wild-type flies[541,542]. *Atg7* encodes the sole *D. melanogaster* E1-like enzyme which activates Atg8 (LC3) and Atg12, ubiquitin-like protein conjugation systems that are essential for the formation and closure of autophagosome membrane structures[543,544]. In mammals, these autophagy factors are involved in a noncanonical autophagy pathway termed

LC3-associated phagocytosis, linking PRRs and phagosomal maturation. While the role of this LAP pathway in clearance of mycobacteria is unclear, it was found that during a mouse infection, *M. tuberculosis* evades LAP-mediated killing by producing CpsA to inhibit NADPH oxidase 2 (NOX2) recruitment to the phagosome[514,545].

ATGs have also been shown to be required for the action of several antimycobacterial drugs. Isoniazid and pyrazinamide were shown to induce autophagy in *in vitro M. tuberculosis* infection of macrophages, whereas chloramphenicol and tetracycline did not[541]. Both Isoniazid and pyrazinamide are pro-drugs, converted to their active form by the action of mycobacteria[541,546]. Following treatment with Isoniazid and pyrazinamide, the subsequent production of bacterial ROS induced the production of cellular and mitochondrial ROS by the host cell, and this was found to be required for the induction of autophagy by Isoniazid and pyrazinamide. These findings were supported by an *in vivo* study, in which *D. melanogaster* larvae infected with *M. marinum* were treated with amikacin or rifampicin, which caused an increase in autophagy marker Atg8a in the fat body. Using GFP-tagged Atg8a, the Atg8a labelled vesicles were found to be colocalised with lysosomes in the antibiotic treated larvae, suggesting that treatment with these antimycobacterial drugs promotes degradation of the Atg8A labelled vesicles[541]. Using a *M. marinum* infection in adult *D. melanogaster*, this finding was extended to Atg7. Treating wild-type flies with amikacin or rifampicin increased survival following *M. marinum* infection, however in *Atg7* mutant flies the antibiotic treatment offered only a mild protective effect, highlighting the importance of autophagy in the action of antimycobacterial drugs[514,541].

1.2.3.5 Mycobacterial virulence factors

Despite the potential of using *D. melanogaster* to screen for key bacterial virulence factors, as has been done for other pathogens such as *Bacillus anthracis*[547], *P. aeruginosa*[548–550], *Staphylococcus aureus*[551], and *Vibrio cholerae*[552], there is only a single example of this for mycobacteria. This showed that *mag24*, a *M. marinum* promoter, is induced by phagocytosis

following infection. Blocking *D. melanogaster* phagocytosis, expression of GFP induced by *mag24* was not activated, and *M. marinum* strain L1D in which the *mag24* locus is deleted, is considerably less virulent in infected *D. melanogaster* compared with wild-type *M. marinum*. This highlights that the process of phagocytosis and subsequent induction of *mag24* in *M. marinum* enhances virulence[516].

1.2.3.6 Resistance, tolerance, virulence

It has become increasingly clear that disease is not simply correlated with pathogen burden and many factors contribute towards pathogenesis during an infection from both the pathogen side and the host side. Firstly, host resistance is defined as the host ability to reduce pathogen burden; this is the primary goal of the different aspects of the innate immune response in *D. melanogaster*, to detect and eliminate invading microbes[553]. Secondary to this is host tolerance, mechanisms to limit the detrimental consequences of infection without directly impacting the pathogen load[553]. Tolerance may include activating repair mechanisms to counter the damage inflicted by inflammatory immune responses or managing metabolic processes to sustain the energetically costly immune activation. Such tolerance mechanisms have been previously described in *D. melanogaster* in response to numerous infections in order to promote survival, in some cases more effectively than others. Together, resistance and tolerance represent the total defensive capacity of the host[553].

When considering host-pathogen interactions, the relationship between host tolerance and microbial virulence can be difficult to determine and is frequently debated. This is in part due to shifting definitions of virulence. Following the development of germ theory and the advent of microbiology, virulence was considered to be inversely proportional to the number of organisms required to cause an infection[554]. This has evolved over the decades and now, based on the damage framework, the definition of virulence can be considered as the relative ability of a microbe to cause damage and disease within a host[554,555]. Based on this concept of

virulence, almost any microbial factor that promotes adhesion to host cells or survival within the host by immune evasion facilitates the prerequisites for persistence and replication, and so can be described as a virulence factor owing to the subsequent pathogenesis. A pathogen such as *M. tuberculosis* can be considered highly virulent due to its ability to evade host immune responses, establish chronic infections, spread throughout the host environment and to new hosts, and cause severe illness.

Additionally, the level of virulence is a continuous variable based on the amount of damage manifested within a host, which is dependent on host factors such as differing susceptibility and immune responses leading to variation in the damage caused by a microbe. This is exemplified by the near lack of pulmonary disease caused by *M. abscessus* and other NTM in immunocompetent individuals, but severe disease seen in immunocompromised or CF patients. Virulence therefore is a measure of host-pathogen interactions, rather than a microbial-specific factor. It is increasingly recognised that microbial virulence can be decoupled from *in vivo* replication and microbial burden.

Microbial toxicity is a different aspect that can be encompassed within virulence. Toxicity refers to the production of specific products (toxins) by microbes during an infection that have a direct interaction with host factors in order to cause damage or disrupt host processes. For example, *M. tuberculosis* secretes tuberculosis necrotising toxin (TNT) to induce death of infected macrophages by necrosis, promoting further spread[556].

1.3 Genetic editing in mycobacteria

Genetic editing tools have become foundational in the study of bacterial pathogens in order to interrogate the genetic drivers of bacterial physiology, metabolism, and virulence. The ability to produce strains with specific gene knockouts or conditional expression is essential to understanding the function of that gene product and can contribute to the identification of novel drug targets. Introducing more specific mutations such as amino acid substitutions

or single-point mutations provides information about the relationship between a proteins structure and function, which can shed light on drug resistance mechanisms or host-pathogen interactions[557–560]. The most common approach to study the function of specific bacterial genes has been the use of allelic exchange by homologous recombination to introduce genomic deletions, however, such methods have been difficult to perform in mycobacteria as a result of their slow growth and thick outer mycomembrane preventing efficient DNA transfer[560,561].

1.3.1 Homologous recombination

Homologous recombination is a form of genetic recombination used for DNA repair in which genetic information is exchanged between two similar regions of DNA, which provides a means to replace an allele of interest with a mutated counterpart. A piece of DNA carrying the desired mutation, often an allele disrupted by an inserted antibiotic resistance gene, is flanked by regions homologous to the targeted locus. The mutated allele is then introduced to the bacteria using a delivery vector such as a suicide vector with no origin of replication[560,562]. The presence of the antibiotic resistance gene acts as a selective marker to identify when a double cross-over occurs between the homologous regions both upstream and downstream of the mutant allele, replacing the original target allele with the mutated allele. This is termed one-step allelic exchange[560,562]. In two-step allelic exchange, the mutant allele carries an additional negative selection marker that results in death of the bacteria. This allows clones that have undergone a single cross-over to be identified using positive selection with the antibiotic resistance marker. These strains carry both the wild-type allele and the introduced mutated allele, and so a second recombination event is identified using the negative selection[563,564]. An example of two-step alleleic exchange made use of two positive selection markers, antibiotic resistance and *lacZ* for β-galactosidase activity, and *sacB* as a negative selection marker which results in sucrose sensitivity due to the production of a toxic metabolite[565–567]. To remove the antibiotic resistance genes that become integrated into the bacterial genome, which may have

impacts on the bacterial phenotype, a *Saccharomyces cerevisiae* FLP recombinase can be used to mediate site-specific recombination between two FLP recognition target sites flanking the introduced antibiotic resistance gene[560,568].

The use of this process in mycobacteria was hampered due to extremely low transformation efficiency when electroporating plasmid vectors[562,569,570]. The use of mycobacteriophages to deliver mutant alleles was introduced as a strategy to overcome this. Following transduction, bacteria that have undergone recombination are selected at a temperature that is non-permissive to the replication of the delivery phage[560]. This method of recombination was found to result in a high number of spontaneous antibiotic resistance mutants, which creates challenges when screening for successful recombination and requires optimisation to reduce clumping for each mycobacterial species[564,571]. Mycobacteriophages were also made use of for recombineering, a process of site-specific recombination using specific DNA sites recognised by bacteriophage-encoded recombinase enzymes rather than homologous regions. The recombinase enzymes form a synaptic complex and then drives cleavage of chromosomal DNA, rearrangement, and ligation of the cleaved ends. There are very few reports of recombineering being used successfully in NTM[564].

1.3.2 CRISPRi and CRISPR

The clustered regularly interspaced palindromic repeats (CRISPR) and CRISPR-associated protein (Cas) system is a form of prokaryotic immunity against phage. Foreign phage DNA is digested by the host and incorporated into the CRISPR locus as spacers[572,573]. During subsequent infection, the integrated spacer DNA is used to produce short CRISPR RNAs (crRNAs) to target the sequence complementary to the spacer. This then acts as a guide for the recruitment of Cas proteins with nuclease activity to cleave either RNA or DNA. Self-recognition is prevented by the presence of a protospacer adjacent motif (PAM) sequence that is present in the viral genome but absent from the CRISPR spacer[572,573].

The use of CRISPR as a genetic editing tool in mycobacteria was first reported in 2015, using CRISPR interference (CRISPRi) to silence targeted genes[561]. This was achieved by using a catalytically inactive Cas9 protein, dCas9, lacking endonuclease activity. Small guide RNAs (sgRNAs) are designed to mimic the crRNAs targeting a specific DNA sequence and forming a complex with the dCas9 via the Cas9 handle. Despite being unable to cleave the target DNA, the sgRNA-dCas9 complex remains bound to the target site and blocks the action of RNA polymerase, causing transcriptional repression of the targeted gene[561,574]. This was achieved initially in *M. smegmatis* and *M. tuberculosis* using dCas9 from *Streptococcus pyogenes*[561], however, later evaluation of 11 different Cas9 proteins identified dCas9 from *Streptococcus thermophilus* to be the most efficacious[575]. *S. pyogenes* Cas9 or dCas9 was found to be toxic to mycobacteria when expressed under the control of a potent constitutive promoter, *hsp60*, however use of a tetracycline-regulated promoter prevented overproduction and toxicity[560,575,576]. *S. thermophilus* dCas9 was found to be nontoxic, however active Cas9 under the *hsp60* promoter was toxic to *M. smegmatis*, highlighting the importance of controlled expression when using this system in mycobacteria[560,575]. This system is highly flexible, expression of the system can be controlled in an ATc dose-dependent manner due to the control of tetracycline transcriptional regulators, allowing gene silencing to be driven at different levels as needed[561]. It also allows for the silencing of multiple genes simultaneously, without the need for multiple antibiotic resistance markers. A major drawback to the use of CRISPRi in the study of mycobacterial gene function is that when targeted genes are located within a single operon, all downstream genes also show repressed transcription[561].

To achieve frameshift mutations within a target gene and create a knockout mutant lacking that gene function altogether requires the use of catalytically active Cas9 endonucleases. Similar to the process in CRISPRi, Cas9 binds to a targeted gene via a sgRNA and Cas9 handle sequence and creates a double-stranded break in the DNA sequence. Such breaks are highly genotoxic and so are rapidly repaired by host DNA repair mechanisms. These include homologous

recombination, which requires a homologous DNA template for repair, or non-homologous end joining (NHEJ), which is highly error-prone and likely to introduce random insertions or deletions (INDELS) and cause frameshift mutations[564]. Most bacteria lack a NHEJ repair system and so a double-stranded DNA break often results in cell death as they cannot efficiently repair the damage. However, mycobacteria do possess a NHEJ repair system[577,578], meaning a CRISPR-based method for introducing frameshift mutations into specific target genes is feasible. Expression of mycobacterial NHEJ repair proteins Ku and Ligase D (LigD) was used to produce indel mutations and gene deletions in *E. coli*, and then also used to create mutations in *M. smegmatis*, *M. marinum*, and *M. tuberculosis* by overexpressing NHEJ proteins and inhibiting homologous recombination repair proteins[579]. One-step CRISPR-Cas9 editing of mycobacteria was then achieved, without altering endogenous NHEJ or homologous recombination protein levels, in *M. marinum* and *M. tuberculosis*[580]. *S. thermophilus* Cas9 was used, and while short-term induction produced almost no off-target mutations, longer-term induction of the system began to introduce undesirable mutations. Additionally, there was a degree of leakage as edited colonies were identified in the absence of an inducer, however, this was possibly caused by the integration of the Cas9 machinery into the mycobacterial genome by phage L5 integrase. This was later removed from the genome with an integrative plasmid containing fluorescent tdTomato[580].

At the start of my project, the papers describing the use of CRISPR and catalytically active Cas9 to create knockout strains in mycobacteria were not yet published, and to date, this has not been reported in *M. abscessus*. This method was developed by Dr Sophie Burbaud and Dr Josephine Bryant within the Floto group at the University of Cambridge, with whom I worked to create *M. abscessus* knockout strains targeting various genes of interest. This is a two-plasmid system, with one plasmid encoding *S. pyogenes* Cas9 under the control of a tetracycline transcriptional regulator, and the other plasmid carrying the sgRNA sequence upstream of the Cas9 handle also under the control of a tetracycline transcriptional regulator. The *S. pyogenes*

Cas9 PAM sequence is 5′-NGG-3′ that is found directly downstream of the target sequence. These plasmids also carry kanamycin and zeocin resistance cassettes, respectively. Both plasmids are transformed into *M. abscessus* by electroporation, and growth in antibiotic medium acts as a selective pressure to maintain the plasmids as mycobacteria are particularly prone to plasmid loss. Expression of Cas9 and the sgRNA with the Cas9 handle is induced by the addition of doxycycline, whereby the sgRNA binds to the target sequence, recruits Cas9 via the Cas9 handle, and Cas9 creates a double strand break in the DNA. NHEJ repair activity by *M. abscessus* then creates the possibility of introducing indels and frameshift mutations, resulting in loss-of-function of the encoded protein. Once strains carrying successful frameshift mutations are identified, the bacteria can then be cultured without the addition of antibiotics as maintenance of the CRISPR-Cas9 plasmids is no longer required. Recent analysis of this system in *M. abscessus* has found that induction of the CRISPR-Cas9 system and creation of double-strand breaks within the DNA leads to upregulation of all DNA repair mechanisms in *M. abscessus*, i.e. homologous recombination, NHEJ, and single-strand annealing (Unpublished data, Dr Sophie Burbaud, Floto Group).

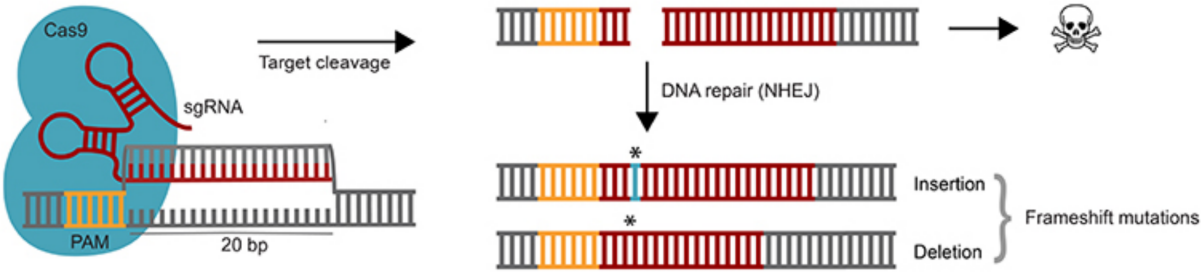


Figure 1.10. CRISPR for mycobacterial gene editing. Overview of gene editing by CRISPR-Cas9. Upon induction the designed sgRNA and Cas9 enzyme are expressed. The sgRNA recognises and binds the target site next to the PAM, allowing for binding of Cas9 which induces a double-stranded DNA break. The break is repaired by error-prone NHEJ which can introduce frameshift mutations and loss-of-function of the targeted gene. If the double-stranded DNA break is not repaired it can result in bacterial death. Figure adapted from Meijers AS, Troost R, Ummels R, Maaskant J, Speer A, Nejentsev S, Bitter W, Kuijl CP. Efficient genome editing in pathogenic mycobacteria using Streptococcus thermophilus CRISPR1-Cas9. Tuberculosis (Edinb). 2020[580].

1.4 Phenogenomics of *M. abscessus*

As a result of the lack of genetic editing tools available in *M. abscessus*, the classical systems-level approach to understand the genetic determinants of *M. abscessus* behaviour using transposon-insertions to create mutant libraries for screening was not feasible. An alternative approach is to use bacterial genome wide association studies (GWAS), using large-scale sequencing of clinical isolates to capture the genetic and phenotypic variation within the population and identify potential causal associations. This approach however is also limited as the majority of bacterial phenotypes are a complex interplay involving functional interactions between a group of proteins, rather than simple monogenetic features. Linkage disequilibrium, which describes the degree to which an allele of one gene is inherited in association with another allele of a nearby gene, can also lead to ambiguity as to which gene variants are associated with certain phenotypes. In the case of *M. abscessus*, linkage disequilibrium is extensive and genome-wide [581].

This led Boeck *et al.* to develop a phenogenomics approach to study *M. abscessus*, using multidimensional phenotyping, WGS, computational modelling and epistatic analysis to understand key genetic determinants of *M. abscessus* virulence [581]. 331 clinical *M. abscessus* isolates were obtained from patients with chronic pulmonary disease and respiratory *M. abscessus* infection from all major CF centres in the UK, as well as hospitals in the Republic of Ireland, the US, Sweden, Denmark, Australia, and the Netherlands. These isolates were characterised across 58 phenotypic dimensions to consider five key pathogen traits: planktonic growth in various carbon sources; antibiotic resistance against clinically relevant drugs; *in vitro* infection of human macrophages (THP-1 cells); *in vivo* infection of *D. melanogaster*; and clinical outcomes following patient infection. This led to the identification of phenotypic clusters each associated with different clinical outcomes, which were clustered phylogenetically indicating distinct heritable traits, however, these groups were not associated with differences in macrolide

resistance, morphotype, or subspecies.

Another limitation of GWAS approaches is the inability to determine how the specific mutations identified within a gene may impact protein function. To address this, Boeck *et al.* used a structure-guided GWAS approach to evaluate and predict the functional impact of the non-synonymous SNPs identified across the *M. abscessus* genome. This was combined with epistatic analysis to identify any groups of mutations across the genome that may have co-evolved, which would indicate possible epistatic interactions between those genes. Homoplastic mutations were also identified, including deletions in MAB_0471 which occurred in the ancestor of DCC2 which is now widespread. Following this work, a CRISPRi approach was used to validate some of the identified GWAS hit by knocking down gene expression of MAB_0471 and MAB_3317c and assessing their virulence *in vivo* using *D. melanogaster*, which confirmed the role of these *M. abscessus* genes in regulating virulence[581]. This highly intensive approach identified clinically relevant genetic determinants of *M. abscessus* virulence, including in genes that may be associated with the adaptations of *M. abscessus* towards a more virulent human pathogen[153,166,581].

1.5 Project aims and thesis outline

M. abscessus is a growing threat, with the possibility of becoming an increasingly prevalent human pathogen. However, due to the lack of genetic tools study into the genetic determinants of *M. abscessus* pathogenesis has been severely restricted. The primary aim of my project is to combine both prokaryotic and eukaryotic genetic manipulation tools to probe specific host-pathogen interactions between *M. abscessus* and *D. melanogaster* and explore the virulence mechanisms of *M. abscessus*. The *D. melanogaster* model will allow us to focus on interactions with *M. abscessus* entirely within the context of the innate immune response, which is a fundamental determinant in human infection outcomes.

To achieve this, my project is subdivided into smaller aims. Firstly, to characterise the *D.*

melanogaster immune response to *M. abscessus* infection (Chapter 3). This will provide important context to understand how the *D. melanogaster* immune response may change during infection with various *M. abscessus* mutant strains, how it differs from the response to other mycobacterial pathogens such as *M. marinum*, and to assess its suitability as a model for *M. abscessus* infection.

Secondly, to use the CRISPR methodology described in Section 1.3.2 to generate frameshift mutations of targeted *M. abscessus* genes, knocking out the function of the protein product (Chapter 4). *M. abscessus* genes selected for knockout were chosen based on the previous phenogenomics study[581] (Section 1.4), homologues of key *M. tuberculosis* virulence factors, and genes involved in important metabolic processes for intracellular survival such as nitrate respiration and fatty acid metabolism. This chapter will describe the efficiency of the CRISPR methodology, provide insight into the role of each of the targeted genes during *D. melanogaster* infection, and then assess which mutant strains to continue studying in greater detail.

The final aim is to understand specific host-pathogen interactions relating to the selected *M. abscessus* genes of interest, MAB_0471 and MAB_0472 (Chapter 5), and MAB_1132c (Chapter 6). These strains are used to understand the changes in the *D. melanogaster* immune response as a result of these mutated genes and identify host factors driving these changes. Additional *in vitro* experiments to understand the bacterial physiology that may underlie these differences are also used to better understand the function of these *M. abscessus* genes.

Chapter 7 will discuss the results of the previous chapters, consider the results in the context of our current understanding of *M. abscessus* infection, and suggest future experiments that could be used to answer outstanding questions.

Chapter 2: Materials and methods

2.1 Bacterial strains, plasmids, and culture conditions

2.1.1 Bacterial strains and plasmids

The bacterial strains used in this study are shown in Table 2.1. Glycerol stocks of all bacterial strains were produced using a mixture of bacterial culture and a 50% glycerol solution, and stored in cryo vials at -80°C. The plasmids used in this study are shown in Table 2.2.

Table 2.1. Bacterial strains used in this study. List of bacterial strains used in experiments or to generate CRISPR mutants. 'Strain' indicates the name used throughout this thesis.

Strain	Description	Source
ATCC 19977	*Mycobacterium abscessus* type strain	NCTC
ATCC 19977-*cas9*	*Mycobacterium abscessus* type strain transformed with plasmid pTetInt-*cas9*PYO	Andres Floto
tdTomato Smooth	*Mycobacterium abscessus* transformed with fluorescent tdTomato and hygromycin resistance plasmid pTec27	Andres Floto
tdTomato Rough	*Mycobacterium abscessus* transformed with fluorescent tdTomato and hygromycin resistance plasmid pTec27	Andres Floto
0169c g1	*Mycobacterium abscessus* transformed with plasmids pTetInt-*cas9*PYO and pGRNAz-*0169c* g1	This study
0169c g2	*Mycobacterium abscessus* transformed with plasmids pTetInt-*cas9*PYO and pGRNAz-*0169c* g2	This study
0169c g3	*Mycobacterium abscessus* transformed with plasmids pTetInt-*cas9*PYO and pGRNAz-*0169c* g3	This study
0169c g4	*Mycobacterium abscessus* transformed with plasmids pTetInt-*cas9*PYO and pGRNAz-*0169c* g4	This study
0169c g5	*Mycobacterium abscessus* transformed with plasmids pTetInt-*cas9*PYO and pGRNAz-*0169c* g5	This study
0471 g1	*Mycobacterium abscessus* transformed with plasmids pTetInt-*cas9*PYO and pGRNAz-*0471* g1	This study
0471 g2	*Mycobacterium abscessus* transformed with plasmids pTetInt-*cas9*PYO and pGRNAz-*0471* g2	This study
0471 g3	*Mycobacterium abscessus* transformed with plasmids pTetInt-*cas9*PYO and pGRNAz-*0471* g3	This study
0471 g4	*Mycobacterium abscessus* transformed with plasmids pTetInt-*cas9*PYO and pGRNAz-*0471* g4	This study

Strain	Description	Source
0471 g5	*Mycobacterium abscessus* transformed with plasmids pTetInt-*cas9*PYO and pGRNAz-*0471* g5	This study
0472 g1	*Mycobacterium abscessus* transformed with plasmids pTetInt-*cas9*PYO and pGRNAz-*0472* g1	This study
0472 g2	*Mycobacterium abscessus* transformed with plasmids pTetInt-*cas9*PYO and pGRNAz-*0472* g2	This study
0472 g3	*Mycobacterium abscessus* transformed with plasmids pTetInt-*cas9*PYO and pGRNAz-*0472* g3	This study
0472 g4	*Mycobacterium abscessus* transformed with plasmids pTetInt-*cas9*PYO and pGRNAz-*0472* g4	This study
0472 g5	*Mycobacterium abscessus* transformed with plasmids pTetInt-*cas9*PYO and pGRNAz-*0472* g5	This study
1012c g1	*Mycobacterium abscessus* transformed with plasmids pTetInt-*cas9*PYO and pGRNAz-*1012c* g1	This study
1012c g2	*Mycobacterium abscessus* transformed with plasmids pTetInt-*cas9*PYO and pGRNAz-*1012c* g2	This study
1012c g3	*Mycobacterium abscessus* transformed with plasmids pTetInt-*cas9*PYO and pGRNAz-*1012c* g3	This study
1012c g4	*Mycobacterium abscessus* transformed with plasmids pTetInt-*cas9*PYO and pGRNAz-*1012c* g4	This study
1012c g5	*Mycobacterium abscessus* transformed with plasmids pTetInt-*cas9*PYO and pGRNAz-*1012c* g5	This study
1132c g1	*Mycobacterium abscessus* transformed with plasmids pTetInt-*cas9*PYO and pGRNAz-*1132c* g1	This study
1132c g2	*Mycobacterium abscessus* transformed with plasmids pTetInt-*cas9*PYO and pGRNAz-*1132c* g2	This study
1132c g3	*Mycobacterium abscessus* transformed with plasmids pTetInt-*cas9*PYO and pGRNAz-*1132c* g	This study
1132c g4	*Mycobacterium abscessus* transformed with plasmids pTetInt-*cas9*PYO and pGRNAz-*1132c* g4	This study
1132c g5	*Mycobacterium abscessus* transformed with plasmids pTetInt-*cas9*PYO and pGRNAz-*1132c* g5	This study
1283c g1	*Mycobacterium abscessus* transformed with plasmids pTetInt-*cas9*PYO and pGRNAz-*1283c* g1	This study
1283c g2	*Mycobacterium abscessus* transformed with plasmids pTetInt-*cas9*PYO and pGRNAz-*1283c* g2	This study
1283c g3	*Mycobacterium abscessus* transformed with plasmids pTetInt-*cas9*PYO and pGRNAz-*1283c* g3	This study

Strain	Description	Source
1933c g1	*Mycobacterium abscessus* transformed with plasmids pTetInt-*cas9*PYO and pGRNAz-*1933c* g1	This study
1933c g2	*Mycobacterium abscessus* transformed with plasmids pTetInt-*cas9*PYO and pGRNAz-*1933c* g2	This study
1933c g3	*Mycobacterium abscessus* transformed with plasmids pTetInt-*cas9*PYO and pGRNAz-*1933c* g3	This study
1933c g4	*Mycobacterium abscessus* transformed with plasmids pTetInt-*cas9*PYO and pGRNAz-*1933c* g4	This study
1933c g5	*Mycobacterium abscessus* transformed with plasmids pTetInt-*cas9*PYO and pGRNAz-*1933c* g5	This study
2228c g1	*Mycobacterium abscessus* transformed with plasmids pTetInt-*cas9*PYO and pGRNAz-*2228c* g1	This study
2228c g2	*Mycobacterium abscessus* transformed with plasmids pTetInt-*cas9*PYO and pGRNAz-*2228c* g2	This study
2228c g3	*Mycobacterium abscessus* transformed with plasmids pTetInt-*cas9*PYO and pGRNAz-*2228c* g3	This study
2262c g1	*Mycobacterium abscessus* transformed with plasmids pTetInt-*cas9*PYO and pGRNAz-*2262c* g1	This study
2262c g2	*Mycobacterium abscessus* transformed with plasmids pTetInt-*cas9*PYO and pGRNAz-*2262c* g2	This study
2262c g3	*Mycobacterium abscessus* transformed with plasmids pTetInt-*cas9*PYO and pGRNAz-*2262c* g3	This study
2262c g4	*Mycobacterium abscessus* transformed with plasmids pTetInt-*cas9*PYO and pGRNAz-*2262c* g4	This study
2262c g5	*Mycobacterium abscessus* transformed with plasmids pTetInt-*cas9*PYO and pGRNAz-*2262c* g5	This study
2728c g1	*Mycobacterium abscessus* transformed with plasmids pTetInt-*cas9*PYO and pGRNAz-*2728c* g1	This study
2728c g2	*Mycobacterium abscessus* transformed with plasmids pTetInt-*cas9*PYO and pGRNAz-*2728c* g2	This study
2728c g3	*Mycobacterium abscessus* transformed with plasmids pTetInt-*cas9*PYO and pGRNAz-*2728c* g3	This study
2728c g4	*Mycobacterium abscessus* transformed with plasmids pTetInt-*cas9*PYO and pGRNAz-*2728c* g4	This study
2728c g5	*Mycobacterium abscessus* transformed with plasmids pTetInt-*cas9*PYO and pGRNAz-*2728c* g5	This study
3029 g1	*Mycobacterium abscessus* transformed with plasmids pTetInt-*cas9*PYO and pGRNAz-*3029* g1	This study

Strain	Description	Source
3029 g2	*Mycobacterium abscessus* transformed with plasmids pTetInt-*cas9*PYO and pGRNAz-*3029* g2	This study
3029 g3	*Mycobacterium abscessus* transformed with plasmids pTetInt-*cas9*PYO and pGRNAz-*3029* g3	This study
3029 g4	*Mycobacterium abscessus* transformed with plasmids pTetInt-*cas9*PYO and pGRNAz-*3029* g4	This study
3029 g5	*Mycobacterium abscessus* transformed with plasmids pTetInt-*cas9*PYO and pGRNAz-*3029* g5	This study
3473c g1	*Mycobacterium abscessus* transformed with plasmids pTetInt-*cas9*PYO and pGRNAz-*3473c* g1	This study
3473c g2	*Mycobacterium abscessus* transformed with plasmids pTetInt-*cas9*PYO and pGRNAz-*3473c* g2	This study
3473c g3	*Mycobacterium abscessus* transformed with plasmids pTetInt-*cas9*PYO and pGRNAz-*3473c* g3	This study
3473c g4	*Mycobacterium abscessus* transformed with plasmids pTetInt-*cas9*PYO and pGRNAz-*3473c* g4	This study
3473c g5	*Mycobacterium abscessus* transformed with plasmids pTetInt-*cas9*PYO and pGRNAz-*3473c* g5	This study
3521c g1	*Mycobacterium abscessus* transformed with plasmids pTetInt-*cas9*PYO and pGRNAz-*3521c* g1	This study
3521c g2	*Mycobacterium abscessus* transformed with plasmids pTetInt-*cas9*PYO and pGRNAz-*3521c* g2	This study
3521c g3	*Mycobacterium abscessus* transformed with plasmids pTetInt-*cas9*PYO and pGRNAz-*3521c* g3	This study
3521c g4	*Mycobacterium abscessus* transformed with plasmids pTetInt-*cas9*PYO and pGRNAz-*3521c* g4	This study
3521c g5	*Mycobacterium abscessus* transformed with plasmids pTetInt-*cas9*PYO and pGRNAz-*3521c* g5	This study
3522c g1	*Mycobacterium abscessus* transformed with plasmids pTetInt-*cas9*PYO and pGRNAz-*3522c* g1	This study
3522c g2	*Mycobacterium abscessus* transformed with plasmids pTetInt-*cas9*PYO and pGRNAz-*3522c* g2	This study
3522c g3	*Mycobacterium abscessus* transformed with plasmids pTetInt-*cas9*PYO and pGRNAz-*3522c* g3	This study
3522c g4	*Mycobacterium abscessus* transformed with plasmids pTetInt-*cas9*PYO and pGRNAz-*3522c* g4	This study
3522c g5	*Mycobacterium abscessus* transformed with plasmids pTetInt-*cas9*PYO and pGRNAz-*3522c* g5	This study

Strain	Description	Source
3523c g1	*Mycobacterium abscessus* transformed with plasmids pTetInt-*cas9*PYO and pGRNAz-*3523c* g1	This study
3523c g2	*Mycobacterium abscessus* transformed with plasmids pTetInt-*cas9*PYO and pGRNAz-*3523c* g2	This study
3523c g3	*Mycobacterium abscessus* transformed with plasmids pTetInt-*cas9*PYO and pGRNAz-*3523c* g3	This study
3523c g4	*Mycobacterium abscessus* transformed with plasmids pTetInt-*cas9*PYO and pGRNAz-*3523c* g4	This study
3523c g5	*Mycobacterium abscessus* transformed with plasmids pTetInt-*cas9*PYO and pGRNAz-*3523c* g5	This study
4095c g1	*Mycobacterium abscessus* transformed with plasmids pTetInt-*cas9*PYO and pGRNAz-*4095c* g1	This study
4095c g2	*Mycobacterium abscessus* transformed with plasmids pTetInt-*cas9*PYO and pGRNAz-*4095c* g2	This study
4095c g3	*Mycobacterium abscessus* transformed with plasmids pTetInt-*cas9*PYO and pGRNAz-*4095c* g3	This study
4095c g4	*Mycobacterium abscessus* transformed with plasmids pTetInt-*cas9*PYO and pGRNAz-*4095c* g4	This study
4095c g5	*Mycobacterium abscessus* transformed with plasmids pTetInt-*cas9*PYO and pGRNAz-*4095c* g5	This study
4163c g1	*Mycobacterium abscessus* transformed with plasmids pTetInt-*cas9*PYO and pGRNAz-*4163c* g1	This study
4163c g2	*Mycobacterium abscessus* transformed with plasmids pTetInt-*cas9*PYO and pGRNAz-*4163c* g2	This study
4163c g3	*Mycobacterium abscessus* transformed with plasmids pTetInt-*cas9*PYO and pGRNAz-*4163c* g3	This study
4163c g4	*Mycobacterium abscessus* transformed with plasmids pTetInt-*cas9*PYO and pGRNAz-*4163c* g4	This study
4163c g5	*Mycobacterium abscessus* transformed with plasmids pTetInt-*cas9*PYO and pGRNAz-*4163c* g5	This study
4588c g1	*Mycobacterium abscessus* transformed with plasmids pTetInt-*cas9*PYO and pGRNAz-*4588c* g1	This study
4588c g2	*Mycobacterium abscessus* transformed with plasmids pTetInt-*cas9*PYO and pGRNAz-*4588c* g2	This study
4588c g3	*Mycobacterium abscessus* transformed with plasmids pTetInt-*cas9*PYO and pGRNAz-*4588c* g3	This study
4588c g4	*Mycobacterium abscessus* transformed with plasmids pTetInt-*cas9*PYO and pGRNAz-*4588c* g4	This study

Strain	Description	Source
4588c g5	*Mycobacterium abscessus* transformed with plasmids pTetInt-*cas9*PYO and pGRNAz-*4588c* g5	This study
Δ0169c-1	*Mycobacterium abscessus* with mutation in MAB_0169c	This study
Δ0169c-2	*Mycobacterium abscessus* with mutation in MAB_0169c	This study
Δ0169c-3	*Mycobacterium abscessus* with mutation in MAB_0169c	This study
Δ0471-1	*Mycobacterium abscessus* with mutation in MAB_0471	This study
Δ0471-2	*Mycobacterium abscessus* with mutation in MAB_0471	This study
Δ0472-1	*Mycobacterium abscessus* with mutation in MAB_0472	This study
Δ0472-2	*Mycobacterium abscessus* with mutation in MAB_0472	This study
Δ0472-3	*Mycobacterium abscessus* with mutation in MAB_0472	This study
Δ0472-4	*Mycobacterium abscessus* with mutation in MAB_0472	This study
Δ1012c-1	*Mycobacterium abscessus* with mutation in MAB_1012c	This study
Δ1012c-2	*Mycobacterium abscessus* with mutation in MAB_1012c	This study
Δ1132c-1	*Mycobacterium abscessus* with mutation in MAB_1132c	This study
Δ1132c-2	*Mycobacterium abscessus* with mutation in MAB_1132c	This study
Δ1132c-3	*Mycobacterium abscessus* with mutation in MAB_1132c	This study
Δ1283c	*Mycobacterium abscessus* with mutation in MAB_1283c	This study
Δ2262c	*Mycobacterium abscessus* with mutation in MAB_2262c	This study
Δ3522c	*Mycobacterium abscessus* with mutation in MAB_3522c	This study
Δ3523c	*Mycobacterium abscessus* with mutation in MAB_3523c	This study
Δ4163c	*Mycobacterium abscessus* with mutation in MAB_4163c	This study
Δ4588c-1	*Mycobacterium abscessus* with mutation in MAB_4588c	This study
Δ4588c-2	*Mycobacterium abscessus* with mutation in MAB_4588c	This study
Δ4588c-3	*Mycobacterium abscessus* with mutation in MAB_4588c	This study
DH5α	*Escherichia coli* cloning strain	NEB

Table 2.2. Bacterial plasmids used in this study. List of bacterial plasmids used to generate fluorescent bacterial strains or to produce CRISPR mutant strains.

Plasmid	Description	Source
pGRNAz	Plasmid producing Cas9 handle and terminator sequence under transcriptional control of tetracycline, contains zeocin resistance gene	Andres Floto
pGRNAz-*0169c* g1	pGRNAz plasmid containing *0169c* g1 guide RNA	This study
pGRNAz-*0169c* g2	pGRNAz plasmid containing *0169c* g2 guide RNA	This study

Plasmid	Description	Source
pGRNAz-*0169c* g3	pGRNAz plasmid containing *0169c* g3 guide RNA	This study
pGRNAz-*0169c* g4	pGRNAz plasmid containing *0169c* g4 guide RNA	This study
pGRNAz-*0169c* g5	pGRNAz plasmid containing *0169c* g5 guide RNA	This study
pGRNAz-*0471* g1	pGRNAz plasmid containing *0471* g1 guide RNA	This study
pGRNAz-*0471* g2	pGRNAz plasmid containing *0471* g2 guide RNA	This study
pGRNAz-*0471* g3	pGRNAz plasmid containing *0471* g3 guide RNA	This study
pGRNAz-*0471* g4	pGRNAz plasmid containing *0471* g4 guide RNA	This study
pGRNAz-*0471* g5	pGRNAz plasmid containing *0471* g5 guide RNA	This study
pGRNAz-*0472* g1	pGRNAz plasmid containing *0472* g1 guide RNA	This study
pGRNAz-*0472* g2	pGRNAz plasmid containing *0472* g2 guide RNA	This study
pGRNAz-*0472* g3	pGRNAz plasmid containing *0472* g3 guide RNA	This study
pGRNAz-*0472* g4	pGRNAz plasmid containing *0472* g4 guide RNA	This study
pGRNAz-*0472* g5	pGRNAz plasmid containing *0472* g5 guide RNA	This study
pGRNAz-*1012c* g1	pGRNAz plasmid containing *1012c* g1 guide RNA	This study
pGRNAz-*1012c* g2	pGRNAz plasmid containing *1012c* g2 guide RNA	This study
pGRNAz-*1012c* g3	pGRNAz plasmid containing *1012c* g3 guide RNA	This study
pGRNAz-*1012c* g4	pGRNAz plasmid containing *1012c* g4 guide RNA	This study
pGRNAz-*1012c* g5	pGRNAz plasmid containing *1012c* g5 guide RNA	This study
pGRNAz-*1132c* g1	pGRNAz plasmid containing *1132c* g1 guide RNA	This study
pGRNAz-*1132c* g2	pGRNAz plasmid containing *1132c* g2 guide RNA	This study
pGRNAz-*1132c* g3	pGRNAz plasmid containing *1132c* g3 guide RNA	This study
pGRNAz-*1132c* g4	pGRNAz plasmid containing *1132c* g4 guide RNA	This study
pGRNAz-*1132c* g5	pGRNAz plasmid containing *1132c* g5 guide RNA	This study
pGRNAz-*1283c* g1	pGRNAz plasmid containing *1283c* g1 guide RNA	This study
pGRNAz-*1283c* g2	pGRNAz plasmid containing *1283c* g2 guide RNA	This study
pGRNAz-*1283c* g3	pGRNAz plasmid containing *1283c* g3 guide RNA	This study
pGRNAz-*1933c* g1	pGRNAz plasmid containing *1933c* g1 guide RNA	This study
pGRNAz-*1933c* g2	pGRNAz plasmid containing *1933c* g2 guide RNA	This study
pGRNAz-*1933c* g3	pGRNAz plasmid containing *1933c* g3 guide RNA	This study
pGRNAz-*1933c* g4	pGRNAz plasmid containing *1933c* g4 guide RNA	This study
pGRNAz-*1933c* g5	pGRNAz plasmid containing *1933c* g5 guide RNA	This study
pGRNAz-*2228c* g1	pGRNAz plasmid containing *2228c* g1 guide RNA	This study

Plasmid	Description	Source
pGRNAz-*2228c* g2	pGRNAz plasmid containing *2228c* g2 guide RNA	This study
pGRNAz-*2228c* g3	pGRNAz plasmid containing *2228c* g3 guide RNA	This study
pGRNAz-*2262c* g1	pGRNAz plasmid containing *2262c* g1 guide RNA	This study
pGRNAz-*2262c* g2	pGRNAz plasmid containing *2262c* g2 guide RNA	This study
pGRNAz-*2262c* g3	pGRNAz plasmid containing *2262c* g3 guide RNA	This study
pGRNAz-*2262c* g4	pGRNAz plasmid containing *2262c* g4 guide RNA	This study
pGRNAz-*2262c* g5	pGRNAz plasmid containing *2262c* g5 guide RNA	This study
pGRNAz-*2728c* g1	pGRNAz plasmid containing *2728c* g1 guide RNA	This study
pGRNAz-*2728c* g2	pGRNAz plasmid containing *2728c* g2 guide RNA	This study
pGRNAz-*2728c* g3	pGRNAz plasmid containing *2728c* g3 guide RNA	This study
pGRNAz-*2728c* g4	pGRNAz plasmid containing *2728c* g4 guide RNA	This study
pGRNAz-*2728c* g5	pGRNAz plasmid containing *2728c* g5 guide RNA	This study
pGRNAz-*3029* g1	pGRNAz plasmid containing *3029* g1 guide RNA	This study
pGRNAz-*3029* g2	pGRNAz plasmid containing *3029* g2 guide RNA	This study
pGRNAz-*3029* g3	pGRNAz plasmid containing *3029* g3 guide RNA	This study
pGRNAz-*3029* g4	pGRNAz plasmid containing *3029* g4 guide RNA	This study
pGRNAz-*3029* g5	pGRNAz plasmid containing *3029* g5 guide RNA	This study
pGRNAz-*3473c* g1	pGRNAz plasmid containing *3473c* g1 guide RNA	This study
pGRNAz-*3473c* g2	pGRNAz plasmid containing *3473c* g2 guide RNA	This study
pGRNAz-*3473c* g3	pGRNAz plasmid containing *3473c* g3 guide RNA	This study
pGRNAz-*3473c* g4	pGRNAz plasmid containing *3473c* g4 guide RNA	This study
pGRNAz-*3473c* g5	pGRNAz plasmid containing *3473c* g5 guide RNA	This study
pGRNAz-*3521c* g1	pGRNAz plasmid containing *3521c* g1 guide RNA	This study
pGRNAz-*3521c* g2	pGRNAz plasmid containing *3521c* g2 guide RNA	This study
pGRNAz-*3521c* g3	pGRNAz plasmid containing *3521c* g3 guide RNA	This study
pGRNAz-*3521c* g4	pGRNAz plasmid containing *3521c* g4 guide RNA	This study
pGRNAz-*3521c* g5	pGRNAz plasmid containing *3521c* g5 guide RNA	This study
pGRNAz-*3522c* g1	pGRNAz plasmid containing *3522c* g1 guide RNA	This study
pGRNAz-*3522c* g2	pGRNAz plasmid containing *3522c* g2 guide RNA	This study
pGRNAz-*3522c* g3	pGRNAz plasmid containing *3522c* g3 guide RNA	This study
pGRNAz-*3522c* g4	pGRNAz plasmid containing *3522c* g4 guide RNA	This study
pGRNAz-*3522c* g5	pGRNAz plasmid containing *3522c* g5 guide RNA	This study

Plasmid	Description	Source
pGRNAz-*3523c* g1	pGRNAz plasmid containing *3523c* g1 guide RNA	This study
pGRNAz-*3523c* g2	pGRNAz plasmid containing *3523c* g2 guide RNA	This study
pGRNAz-*3523c* g3	pGRNAz plasmid containing *3523c* g3 guide RNA	This study
pGRNAz-*3523c* g4	pGRNAz plasmid containing *3523c* g4 guide RNA	This study
pGRNAz-*3523c* g5	pGRNAz plasmid containing *3523c* g5 guide RNA	This study
pGRNAz-*4095c* g1	pGRNAz plasmid containing *4095c* g1 guide RNA	This study
pGRNAz-*4095c* g2	pGRNAz plasmid containing *4095c* g2 guide RNA	This study
pGRNAz-*4095c* g3	pGRNAz plasmid containing *4095c* g3 guide RNA	This study
pGRNAz-*4095c* g4	pGRNAz plasmid containing *4095c* g4 guide RNA	This study
pGRNAz-*4095c* g5	pGRNAz plasmid containing *4095c* g5 guide RNA	This study
pGRNAz-*4163c* g1	pGRNAz plasmid containing *4163c* g1 guide RNA	This study
pGRNAz-*4163c* g2	pGRNAz plasmid containing *4163c* g2 guide RNA	This study
pGRNAz-*4163c* g3	pGRNAz plasmid containing *4163c* g3 guide RNA	This study
pGRNAz-*4163c* g4	pGRNAz plasmid containing *4163c* g4 guide RNA	This study
pGRNAz-*4588c* g5	pGRNAz plasmid containing *4588c* g5 guide RNA	This study
pGRNAz-*4588c* g1	pGRNAz plasmid containing *4588c* g1 guide RNA	This study
pGRNAz-*4588c* g2	pGRNAz plasmid containing *4588c* g2 guide RNA	This study
pGRNAz-*4588c* g3	pGRNAz plasmid containing *4588c* g3 guide RNA	This study
pGRNAz-*4588c* g4	pGRNAz plasmid containing *4588c* g4 guide RNA	This study
pTetInt-*cas9*PYO	Plasmid producing Cas9 under transcriptional control of tetracycline, contains kanamycin resistance gene	Andres Floto
pTec27	Plasmid constitutively expressing tdTomato, contains hygromycin resistance gene	Andres Floto
pUASTattB	Used to generate donor plasmids to insert an open reading frame of interest under UASt regulatory control into an attP-containing site in the *Drosophila melanogaster* genome, using the bacteriophage ΦC31 integrase system	Dionne Lab

2.1.2 Culture conditions

Mycobacterium abscessus ATCC 19977 was used as the wild-type bacteria for all experiments, and the parental strain for the CRISPR knockout strains produced. *M. abscessus* strains were cultured in Middlebrook 7H9 broth supplemented with 10% oleic

acid-albumin-dextrose-catalase (OADC), 0.5% glycerol, and 0.05% Tween80, unless otherwise specified. Middlebrook 7H9 broth contains inorganic compounds to supply potassium sulphur, magnesium, and phosphorus for mycobacterial growth. Oleic acid contains long-chain fatty acids essential for mycobacterial metabolism, albumin protects from toxic free fatty acids, dextrose is a fermentable carbohydrate and energy source, and catalase removes toxic peroxides. Glycerol supplies an energy and a carbon source. Detergent Tween80 is added to reduce clumping of mycobacteria and promote planktonic growth. Some experiments required growth in medium without detergent, such as biofilm assays, or without catalase, such as conditions requiring the addition of hydrogen peroxide. 7H9 broth was sterile filtered before use, and prior to the addition of antibiotics. When required, 300 μg/mL zeocin was added for maintenance of plasmid pGRNAz, 200 μg/mL kanamycin was added for maintenance of plasmid pTetInt-*cas9*PYO, 100 ng/mL doxycycline for induction of genes under transcriptional control of tetracycline on plasmids pGRNAz and pTetInt-*cas9*PYO, or 1 mg/mL hygromycin B was added for maintenance of plasmid pTec27. For growth in a minimal media, *M. abscessus* was grown in Sauton's Modified Medium containing 0.5 g/L monopotassium phosphate, 0.5 g/L magnesium sulphate, 2 g/L citric acid, 10 g/L glycerol, 0.05% Tween80. The nitrogen source was controlled, and was supplied as one of 5 mM asparagine, 10 mM asparagine, 20 mM asparagine, 40 mM asparagine, 5 mM aspartate, 5 mM glutamine, 5 mM glutamate, 0.05 g/L ammonium chloride, or 1 g/L ammonium chloride, as specified. pH was adjusted using 5 mM NaOH to either pH 7.0 or pH 5.5 as specified. Minimal medium was autoclaved before use, prior to the addition of Tween80. Cultures were typically started from a single colony grown on a 7H11 agar plate stored at 4°C, elsewise from a glycerol stock stored at -80°C. Cultures were grown at 37°C shaking (180 - 200 rpm) unless otherwise specified. Some experiments required static growth, such as biofilm assays.

For growth on solid media, *M. abscessus* was grown on Middlebrook 7H11 agar supplemented with 10% OADC and 0.5% glycerol. Middlebrook 7H11 agar base contains inorganic salts to aid

the growth of mycobacteria, and malachite green which partially inhibits other contaminating bacterial species. 7H11 agar was autoclaved prior to adding OADC and antibiotics. When necessary, 300 μg/mL zeocin was added for maintenance of plasmid pGRNAz, 200 μg/mL kanamycin was added for maintenance of plasmid pTetInt-*cas9*PYO, or 1 mg/mL hygromycin B was added for maintenance of plasmid pTec27. 7H11 agar plates were typically incubated at 29°C, and sometimes at 37°C to increase colony growth rate.

Escherichia coli DH5α was used for pGRNAz plasmid construction and cloning, cultured in Lysogeny broth (LB) broth at room temperature statically or 37°C shaking, supplemented with 50 μg/mL zeocin when necessary for maintenance of the pGRNAz plasmid.

2.1.3 Generating CRISPR knockout mutants

2.1.3.1 Plasmid construction and cloning

In order to produce *M. abscessus* CRISPR knockout mutants, we first designed single guide RNAs (sgRNAs) targeting the *M. abscessus* genes of interest, aiming for at least five pairs of sgRNAs per target gene. This work was performed in collaboration with Prof. Andres Floto at the University of Cambridge Molecular Immunity Unit within the MRC Laboratory of Molecular Biology, with extensive help and support from Sophie Burbaud, Jasper Sangen, and the rest of the Floto group. The sgRNAs designed and produced are listed in Table 2.3. The forward sgRNAs are 20-bp long, while the complementary reverse sequence has an additional 6-bp to complement the sticky ends produced by restriction enzymes. sgRNAs were designed using a macro written by Dr Josephine Bryant by reading the gene of interest from the 5' end and identifying the PAM motif (NCC) on the sense strand, leaving one nucleotide space from the PAM site, then extracting the 20 nucleotides downstream as the guide. This is checked to ensure the GC content is between 45 and 75%, whether there are off-target hits elsewhere in the genome with less than four mismatches, and also check secondary structure and reject any guide with one or more hairpins.

pGRNAz plasmid, shown in Supplementary Figure S2.1A, was transformed into *E. coli* DH5α competent cells by heat shock, incubating the plasmid and bacteria together on ice for 20 - 30 minutes, placing the reaction mix in a 42°C heat block for 30 seconds. *E. coli* are then allowed to recover in 500 μL SOC at 37°C shaking for 1 hour, then plated onto LB agar containing 50 μg/mL zeocin to select colonies that have been transformed with the pGRNAz plasmid, to grow at room temperature overnight. Single colonies were selected from the plates and grown in LB broth supplemented with 50 μg/mL zeocin at 37°C shaking overnight to amplify the pGRNAz plasmid. QIAprep Miniprep Kits were then used to purify pGRNAz from the overnight *E. coli* cultures, based upon alkaline lysis of *E. coli* bacterial cells and binding of plasmid DNA onto a silica membrane.

sgRNAs could then be annealed and cloned into the purified pGRNAz plasmid at restriction enzyme SphI and AclI sites, upstream of the terminator and Cas9 handle sequence. Firstly the purified pGRNAz plasmid was digested by incubating the plasmid DNA with the restriction enzymes and appropriate buffer at 37°C for 1 hour. Gel electrophoresis was then used to identify plasmids that were successfully digested by running on a 1% agarose gel, and conducting a gel purification to purify the digested plasmid backbone. Each sgRNA is then ligated into a pGRNAz backbone with T4 DNA ligase and ligase buffer, incubating at room temperature for 2 hours. Recombinant pGRNAz plasmids are then transformed and amplified in *E. coli* DH5α and purified using QIAprep Miniprep kits, as described previously. A diagnostic restriction digest was then performed again using SphI and AclI and gel electrophoresis was used to identify successfully recombinant plasmids containing the inserted sgRNA.

Table 2.3. *Mycobacterium abscessus* CRISPR single guide RNAs. 5 pairs of guide RNAs were designed per targeted *M. abscessus* gene, with the exception of *MAB_1283c* and *MAB_2228c* for which only 3 pairs were designed due to the small size of these genes.

Gene	Forward sgRNA	Reverse sgRNA
0169c g1	GAGCTCAAGGCTGTCGAAAG	CGCTTTCGACAGCCTTGAGCTCCATG
0169c g2	ACGGACTTGCGACGGCCAGC	CGGCTGGCCGTCGCAAGTCCGTCATG

Gene	Forward sgRNA	Reverse sgRNA
0169c g3	GGTCGCGAGGGCAATGGCAA	CGTTGCCATTGCCCTCGCGACCCATG
0169c g4	CTTGGGTCATGTTGGTCGCG	CGCGCGACCAACATGACCCAAGCATG
0169c g5	GACCGCGCCCATGACCTCTC	CGGAGAGGTCATGGGCGCGGTCCATG
0471 g1	GGCGAGCAGCACTAAGGCCT	CGAGGCCTTAGTGCTGCTCGCCCATG
0471 g2	GCGGCACCAGAAGCAACGCG	CGCGCGTTGCTTCTGGTGCCGCCATG
0471 g3	GTCCAGCCGCCGATACCTTT	CGTGGAGCTGGCCCGAATCCTCCATG
0471 g4	CGTCAGCACCAGCGCACTCA	CGTGAGTGCGCTGGTGCTGACGCATG
0471 g5	TCCGATTCGACGCGAGATCT	CGAGATCTCGCGTCGAATCGGACATG
0472 g1	TCGAAAGAAGCAGGAAGCCG	CGCGGCTTCCTGCTTCTTTCGACATG
0472 g2	GTCGTCCCGCTCGAAAGAAG	CGCTTCTTTCGAGCGGGACGACCATG
0472 g3	GAGGATTCGGGCCAGCTCCA	CGTGGAGCTGGCCCGAATCCTCCATG
0472 g4	CCCCCGCTCGACGGAGGATT	CGAATCCTCCGTCGAGCGGGGGCATG
0472 g5	GCAAGCATCTCCCCCGCTCG	CGCGAGCGGGGGAGATGCTTGCCATG
1012c g1	GCGACGCCATCATTGGTAGC	CGGCTACCAATGATGGCGTCGCCATG
1012c g2	TGCCGCACGAATTCCTGCCA	CGTGGCAGGAATTCGTGCGGCACATG
1012c g3	GGCAGCGTGACCAGAATGAC	CGGTCATTCTGGTCACGCTGCCCATG
1012c g4	GATCGAGAGTGTGACGCCGA	CGTCGGCGTCACACTCTCGATCCATG
1012c g5	CCAGGATCATGTCGCCGGGG	CGCCCCGGCGACATGATCCTGGCATG
1132c g1	GGCCGACACATCGTAATTAG	CGCTAATTACGATGTGTCGGCCCATG
1132c g2	ACACCACGAACAGTCCGGGC	CGGCCCGGACTGTTCGTGGTGTCATG
1132c g3	CGCAGCATGAAGAAGACGAA	CGTTCGTCTTCTTCATGCTGCGCATG
1132c g4	ACGAAGGAGCCGGAGGAGGG	CGCCCTCCTCCGGCTCCTTCGTCATG
1132c g5	GAGCATAGGAGACGAAGGAG	CGCTCCTTCGTCTCCTATGCTCCATG
1283c g1	GGAGCGCTTCCAGCTTGTCC	CGGGACAAGCTGGAAGCGCTCCCATG
1283c g2	TGCTCGAACGACTCCGCATT	CGAATGCGGAGTCGTTCGAGCACATG
1283c g3	TCTGCGCGACCTTGGCCCAC	CGGTGGGCCAAGGTCGCGCAGACATG
1933c g1	AAGTGCTGCACGACGCCCGG	CGCCGGGCGTCGTGCAGCACTTCATG
1933c g2	CTCTGATCGAAGGCCGAAGC	CGGCTTCGGCCTTCGATCAGAGCATG
1933c g3	CGTCGAAAACGCTCTGATCG	CGCGATCAGAGCGTTTTCGACGCATG
1933c g4	ACCGAGGAACCGTCGAACGC	CGGCGTTCGACGGTTCCTCGGTCATG
1933c g5	TCGACTGGAAACCACGGACC	CGGGTCCGTGGTTTCCAGTCGACATG
2228c g1	CGGCCAGGTCAGCACCCAGT	CGACTGGGTGCTGACCTGGCCGCATG
2228c g2	TCATCGAGGTATCACCGTGC	CGGCACGGTGATACCTCGATGACATG

Gene	Forward sgRNA	Reverse sgRNA
2228c g3	AGGCGCGGATGAGTTCTTCC	CGGGAAGAACTCATCCGCGCCTCATG
2262c g1	CATCGTGATACGTACGCAGT	CGACTGCGTACGTATCACGATGCATG
2262c g2	GGTCTTCGAAGAGCGTCGGC	CGGCCGACGCTCTTCGAAGACCCATG
2262c g3	CATTCAGCCGGGGTGTGTAA	CGTTACACACCCCGGCTGAATGCATG
2262c g4	TCGGGATCGGGGAACCAGAA	CGTTCTGGTTCCCCGATCCCGACATG
2262c g5	GATGCTCGCTGGTTCCCCCA	CGTGGGGGAACCAGCGAGCATCCATG
2728c g1	CGTTTGCCCCGCACCGCGAA	CGTTCGCGGTGCGGGGCAAACGCATG
2728c g2	TCGTGGGAAACATCATCAGC	CGGCTGATGATGTTTCCCACGACATG
2728c g3	CGGCCAGCTGCGTGATCAAC	CGGTTGATCACGCAGCTGGCCGCATG
2728c g4	GTTCGATCTGCTGGTTCGTA	CGTACGAACCAGCAGATCGAACCATG
2728c g5	CCTTGTTGATGGACTCTTGC	CGGCAAGAGTCCATCAACAAGGCATG
3029 g1	GCTCAAGCCTCTCGGCGATG	CGCATCGCCGAGAGGCTTGAGCCATG
3029 g2	CGCTCCATGCGTGCCACCGT	CGACGGTGGCACGCATGGAGCGCATG
3029 g3	CCAGCCGGTGCTTACGCATC	CGGATGCGTAAGCACCGGCTGGCATG
3029 g4	TGATGTCGACCAGCAGGCAC	CGGTGCCTGCTGGTCGACATCACATG
3029 g5	CGTGTTCCCAGCGGCATGCC	CGGGCATGCCGCTGGGAACACGCATG
3473c g1	GATGACTTTTCGTCCGTCGG	CGCCGACGGACGAAAAGTCATCCATG
3473c g2	AGTTGTGTCGTGCCTTGCGA	CGTCGCAAGGCACGACACAACTCATG
3473c g3	CCTCGCGCAGTGTCTTGACC	CGGGTCAAGACACTGCGCGAGGCATG
3473c g4	GCAGCGGAGCGTGATTGGTC	CGGACCAATCACGCTCCGCTGCCATG
3473c g5	CCGTCGGCCGGTTTCTTACT	CGAGTAAGAAACCGGCCGACGGCATG
3521c g1	ACAAGGCGGCCTGTACGTCG	CGCGACGTACAGGCCGCCTTGTCATG
3521c g2	CGCTGGGCATGAGGAACAAG	CGCTTGTTCCTCATGCCCAGCGCATG
3521c g3	TACAACTCCCCGCTGGGCAT	CGATGCCCAGCGGGGAGTTGTACATG
3521c g4	GAGCAGCGGCGATGCCACAG	CGCTGTGGCATCGCCGCTGCTCCATG
3521c g5	CGAGAAGACCTGCTTGAGCA	CGTGCTCAAGCAGGTCTTCTCGCATG
3522c g1	TCACGCAGCACCTGGACAAA	CGTTTGTCCAGGTGCTGCGTGACATG
3522c g2	CCGTCACCTGCCACTGATCG	CGCGATCAGTGGCAGGTGACGGCATG
3522c g3	ACAACGCCACCCGGTCATAG	CGCTATGACCGGGTGGCGTTGTCATG
3522c g4	GGTCCCAGCTGTCGATGTAC	CGGTACATCGACAGCTGGGACCCATG
3522c g5	GGTCTTCCGCGTAGTCGTTT	CGAAACGACTACGCGGAAGACCCATG
3523c g1	AGCGTCCGCGCCGTGCAATT	CGAATTGCACGGCGCGGACGCTCATG
3523c g2	GTCCCACGCGACGACGTCCT	CGAGGACGTCGTCGCGTGGGACCATG

Gene	Forward sgRNA	Reverse sgRNA
3523c g3	ACCACGGACCAGATCAGGTT	CGAACCTGATCTGGTCCGTGGTCATG
3523c g4	ACAGCACCATCACCGACCAG	CGCTGGTCGGTGATGGTGCTGTCATG
3523c g5	GCGCTGAAAACGGTCCAGTT	CGAACTGGACCGTTTTCAGCGCCATG
4095c g1	CTGGATTTCGGCCGCGGTGC	CGGCACCGCGGCCGAAATCCAGCATG
4095c g2	GGGTTGGTGTCCCAGTCCTG	CGCAGGACTGGGACACCAACCCCATG
4095c g3	TGATGCCCTTCCAGCGGGGG	CGCCCCCGCTGGAAGGGCATCACATG
4095c g4	TGCCCTGCAGCTCCTCAACC	CGGGTTGAGGAGCTGCAGGGCACATG
4095c g5	TGACGGCGTCCCACAGGATC	CGGATCCTGTGGGACGCCGTCACATG
4163c g1	CGATTGCATGCTCAATGAGG	CGCCTCATTGAGCATGCAATCGCATG
4163c g2	GCTTTCGGTCACCGGAAATG	CGCATTTCCGGTGACCGAAAGCCATG
4163c g3	GATTGGACTGCTCCTCAAGC	CGGCTTGAGGAGCAGTCCAATCCATG
4163c g4	GGAGATAGTGCCCGAGCCGA	CGTCGGCTCGGGCACTATCTCCCATG
4163c g5	TTCACGTTGACCGAGATCGC	CGGCGATCTCGGTCAACGTGAACATG
4588c g1	TACGCGCGTCCGGACGGTTG	CGCAACCGTCCGGACGCGCGTACATG
4588c g2	CCGGTAATGATGGCGACGGA	CGTCCGTCGCCATCATTACCGGCATG
4588c g3	ACACCGCCTCGCCACTCACA	CGTGTGAGTGGCGAGGCGGTGTCATG
4588c g4	TCGGCTTGCGTGGCGGCACA	CGTGTGCCGCCACGCAAGCCGACATG
4588c g5	GGAATGCCGAACTTCGCGCT	CGAGCGCGAAGTTCGGCATTCCCATG

2.1.3.2 Transformation of electrocompetent *M. abscessus*

The recombinant plasmids containing the sgRNAs were then transformed into *M. abscessus* ATCC 19977-*cas9* containing pTetInt-*cas9*PYO, shown in Supplementary Figure S2.1B, which expresses *S. pyogenes cas9* (Supplementary Figure S2.2), by electroporation. Briefly, 200 μL of electrocompetent *M. abscessus* ATCC 19977-*cas9* was mixed with 1 μg of each recombinant pGRNAz ligation reaction, no more than 10 μL, in a 2 mm electroporating cuvette and electroporated at 2.5 kV, 1000 Ω, 25 μF. The mixture was then transferred into 5 mL fresh 7H9, without antibiotic, in a 50 mL falcon and allowed to recover at 37°C shaking for 24 hours. Cultures were then plated onto 7H11 agar plates containing both 300 μg/mL zeocin and 200 μg/mL kanamycin and incubated at 37°C for 3 - 4 days.

2.1.3.3 CRISPR-Cas9 induction

To induce expression of the CRISPR-Cas9 system, single colonies were selected from the electroporated *M. abscessus* 7H11 agar plates and grown in 5 mL 7H9 supplemented with 300 μg/mL zeocin and 200 μg/mL kanamycin, and incubated at 37°C shaking for 3 - 4 days. Glycerol stocks were produced to store at -80°C. Each culture was diluted to OD_{600} = 0.2, and 3 mL of the diluted culture was added to 12 mL of fresh 7H9 supplemented with 300 μg/mL zeocin and 200 μg/mL kanamycin. Doxycycline was added to a final concentration of 100 ng/mL to induce expression of the sgRNA and cas9 handle on each pGRNAz, and expression of cas9 on pTetInt-*cas9*PYO. These cultures were then incubated at 37°C shaking for 48 hours. Following growth, each culture was serially diluted in fresh 7H9 supplemented with 300 μg/mL zeocin and 200 μg/mL kanamycin and plated onto 7H11 agar plates containing both 300 μg/mL zeocin and 200 μg/mL kanamycin, and left to grow at 37°C for 3 - 4 days.

2.1.3.4 Screening *M. abscessus* CRISPR strains

To identify *M. abscessus* colonies in which the CRISPR-Cas9 system was successfully induced and resulted in a frameshift mutation in the gene of interest, at least ten colonies per guide RNA were selected from the 7H11 agar plates grown with serially diluted *M. abscessus* strains following induction of the CRISPR-Cas9 system with doxycycline. Each colony was grown in 5 mL 7H9 containing 300 μg/mL zeocin and 200 μg/mL kanamycin at 37°C shaking for 3 - 4 days, which was used to produce glycerol stocks to store at -80°C and for genomic DNA (gDNA) extraction. Briefly, cultures were centrifuged at 3000 x g for 10 minutes to pellet the bacteria. The bacterial pellet was then resuspended in 250 μL TE buffer, and transferred into a 2 mL tube containing 500 mL of 0.1 mm silica beads. These were placed into a bead beater and beat for 2 minutes, rested for 1 minute on ice, and beat for another 2 minutes. The tubes were centrifuged at 13,000 rpm for 2 minutes and the supernatant was collected in a 1.5 mL microcentrifuge tube. gDNA extraction was then performed using Qiaamp DNA minikit.

PCR amplification was then used to amplify the targeted *M. abscessus* gene of interest for each pGRNAz plasmid. The PCR primers used for amplification of *M. abscessus* genes of interest are listed in Table 2.4. PCR products were then run on a 1% agarose gel by gel electrophoresis to confirm the primers had successfully amplified the target gene, and the DNA was purified from the remaining PCR reaction using the Qiagen PCR purification kit. The purified DNA was then sent for Sanger sequencing to characterise the mutations induced by the CRISPR-Cas9 in each *M. abscessus* strain produced, sequencing was performed using the same primers as were used for PCR.

Table 2.4. *Mycobacterium abscessus* PCR primers used in this study. Primers used to validate CRISPR-induced mutations in *M. abscessus*.

Gene	Forward	Reverse
MAB_0169c	GTAAGACTCGGTGTGGTGG	AGTCACACCAGTAACTCTGG
MAB_0471	GTGGAATCTCCAGAGATTCG	CCGATCTACGTTCACTCCC
MAB_0472	TGGGACAGATGATCGGAGC	GATGGCAGAAAGCACAGCC
MAB_1012c	GTTCACCGTCATCAGCAGC	GATGTCCGAGACGTACTCG
MAB_1132c	TGGTCAACACGATGATCAGG	CGTGGCCAATCTCATACCG
MAB_1283c	GTCAACAAGGTTGAGGCGG	CAAACATGTCCGCACGACC
MAB_1933c	TGCCGTTCATCTTGGAATCG	CATCGCGCGGTCATTATCC
MAB_2228c	ACGCGTTGAGCATTGAATCC	GATATCGCGCAGGTCAACC
MAB_2262c	ATACCTCGATATCCACCTCG	TAGGATGGGCTAAGTACTGG
MAB_2728c	GATCGAACTTGCCCTGAGC	GTTGCAAAAGTGACGTACGG
MAB_2914	ATTGGTCATCGTCACCTCGG	CGATGGACCACTGAGGGATG
MAB_3029	AGTGGACCTACTACCCTGC	CTTGAGTCGGGACAACAGG
MAB_3473c	ACTCCACCTTGACCTTGCC	GACCATCCTCAATGGAGCG
MAB_3521c	AGCGGGATGATCCTGATGG	AGGCCGGAGATGACAATCC
MAB_3522c	GCATCGAGGTCATCCATGG	GCGTTCTGGGTGTTTCTCG
MAB_3523c	GAACCGTTGTGGGTAAAAGG	GTGGATGTGACGTGATCGG
MAB_4095c	GTTGTTGATGCGGCGAACC	AACAGTCAACGCAGTGAACG
MAB_4163c	GTCTTGACATTGGGGGTGC	CACGATGAGGACGTGATCG
MAB_4588c	ATAAACCCGTACTTGGCAGC	CATCTTGCCGGTACTACCG

2.2 Bacterial growth experiments

2.2.1 Growth curves

Pre-cultures of *M. abscessus* strains were grown in 7H9 at 37°C shaking for 3 - 4 days. Cultures were pelleted by centrifugation at 4000 x g for 5 minutes, and washed in 2 mL PBS Tween80 0.1% three times, to remove as much remaining 7H9 as possible. The bacterial pellet was then resuspended in 2 mL PBS Tween80 0.1% and centrifuged at 200 x g for 5 minutes in order to collect single bacterial cells with minimal clumping from the top of the supernatant. This was then diluted to OD_{600} = 1 in PBS Tween80 0.1%. Growth curves were set up in sterile 96-well plates, 198 μL of the tested medium was added to wells, and 2 μL of each *M. abscessus* strain being tested was added to the media. Each condition was surrounded by at least one empty row and column on all sides to prevent contamination from other conditions. Empty wells were filled with 200 μL of Milli-Q distilled water to prevent evaporation of the media. Negative controls were included using wells filled with 198 μL of medium and 2 μL of PBS Tween80 0.1%. Plates were then sealed with parafilm, and placed into a 37°C shaking incubator at 180 rpm for 4 - 5 days. Twice daily, the plates were removed and each well was gently mixed using a multichannel pipette inside a biosafety cabinet, to resuspend the bacteria settled on the bottom of the wells. Absorbance of each well was measured in a plate reader at OD_{592}, and the plates were sealed and returned to the incubator. Each condition was measured in quadruplicate for every experiment. The absorbance of each measurement for *M. abscessus* bacterial strains was normalised against the respective medium negative control, by subtracting the average of the negative control absorbance from each bacterial strain measurement at each timepoint.

2.2.2 Biofilm assay

Precultures of *M. abscessus* were grown in 7H9 at 37°C shaking for 3 days, and washed three times by pelleting by centrifugation at 4000 x g for 5 minutes and resuspending in 2 mL 7H9 without Tween80. Bacterial suspensions were diluted with 7H9 without Tween80 to OD_{600} =

1.0, and 100 μL of this preparation was transferred into three sterile 96-well plates, with at least four sample replicates per plate. Plates were sealed with a sterile lid and parafilm, and incubated at 37°C standing for 3, 5, or 7 days. At each time point, a plate was removed for a crystal violet assay to measure biofilm growth. Planktonic cells were removed by briskly shaking out the medium into a waste tray, then the plate was washed by submerging in Milli-Q water. Water was shaken out, and 125 μL of 0.1% crystal violet was added to each well and left at room temperature for 10 minutes. The crystal violet solution was removed, and the plate washed twice more in clean Milli-Q water. Excess liquid was removed by tapping the plates on paper towels and plates left to air dry. Once dry, 200 μL of 30% acetic acid was added to each well to solubilise adhered crystal violet and incubated for 10 - 15 minutes at room temperature. The contents of each well was then mixed by gentle pipetting, and 125 μL of the crystal violet acetic acid solution was transferred to a new 96-well plate to measure the OD at 592 nm.

2.2.3 Biofilm imaging

Precultures of *M. abscessus* were grown in 7H9 at 37°C shaking for 3 days, and washed three times by pelleting by centrifugation at 4000 x g for 5 minutes and resuspending in 2 mL 7H9 without Tween80. Bacterial suspensions were diluted with 7H9 without Tween80 to OD_{600} = 1.0, and 30 μL of this preparation was used to inoculate 3 mL of fresh 7H9 without Tween80 in sterilised PRYEX 11.5 mL culture tubes and sealed with sterilised screw cap lids. Four replicates of each bacterial strain tested were set up. These were incubated at 37°C standing, and photographed using a digital camera on day 2, day 5, and day 7 of growth.

2.3 *Drosophila melanogaster* experiments

2.3.1 Fly husbandry

D. melanogaster stocks were maintained on food containing 10% Brewer's yeast, 8% fructose, 2% polenta, and 0.8% agar, as outlined in Table 2.5. Food was prepared in 12 L batches, distributed into vials, sealed with flugs and generally stored at room temperature until use,

otherwise kept at 4°C. *D. melanogaster* lines were kept in these vials in incubators at either 18°C, 25°C, 29°C, or room temperature as required, with 12-hour light-dark cycles for *D. melanogaster* circadian rhythms.

Table 2.5. *D. melanogaster* food composition. Composition of 12 L batch of *D. melanogaster* food.

Ingredient	Amount	Percent (w/v)
Tap water	12 L	-
Brewer's yeast	1200 g	10
Fructose	960 g	8
Polenta	240 g	2
Agar	96 g	0.8
Propionic acid	90 mL	0.75
Nigapin (15% w/v in ethanol)	60 mL	0.075

To collect and sort *D. melanogaster*, adults were anaesthetised using CO_2 through gas-porous pads and fine paint brushes for manipulating the flies. Males and females were identified based on anatomical differences, such as smaller, darker, and more rounded abdomens and genitalia in males, and the presence of sex combs on males. All experiments used adult male *D. melanogaster* that were between 5 and 10 days post-eclosion, which were collected and maintained at 25°C with approximately 20 - 30 individuals per vial.

2.3.2 Stocks and crosses

All experimental *D. melanogaster* lines were kept in duplicate at 18°C and tipped onto fresh food every four weeks. Lines used in this study are listed in Table 2.6, including the full genotype and the source of the line which includes the Bloomington *Drosophila* Stock Centre (BDSC) and the Vienna *Drosophila* Resource Centre (VDRC).

When required, *D. melanogaster* lines were expanded at room temperature or 25°C. If the experimental genotype required was homozygous, such as w^{1118} wild-type control or mutant lines, male *D. melanogaster* would be collected from these stock populations. If the

experimental genotype required was heterozygous, these would be generated by performing crosses. Virgin females were collected, identified by the presence of meconium in the abdomen containing waste products from the pupal stage, indicating that the female was too recently eclosed to have mated, as *D. melanogaster* typically do not mate within the first eight hours post-eclosion. Use of virgin females was required as female *D. melanogaster* are capable of storing sperm once mated. These would be housed with males, with 3 or 4 of each sex, in a single vial for 2 - 4 days to allow mating and egg laying. These adult flies were then tipped onto fresh food, and the vials containing the progeny kept at 25°C.

Balancer chromosomes were used to identify specific genotypes of the progeny produced by crosses. These are used to track an allele of interest by carrying a phenotypic marker, and help maintain deleterious mutations by preventing recombination as balancers are inverted and rearranged chromosomes which are homozygous lethal[582]. Male *D. melanogaster* were collected from crosses by selecting those without the balancer chromosome phenotypic marker.

Table 2.6. *Drosophila melanogaster* lines used in this study. List of fly lines used in experiments, or used for crosses to generate experimental and control genotypes. 'Line' indicates the abbreviated name of each fly line used throughout this thesis, with the full genotype listed in the 'Genotype' column.

Line	Genotype	Description	Source
$Bom^{\Delta 55c}$	w^{1118} ; $Bom^{\Delta 55c}$	Lacking 10 of 12 Bomanin effector peptides, 9 kb deletion within 'Bom' cluster	S. Wasserman, UCSD[348]
Dif^{1}	w^{1118} ; Dif^{1}	Loss of function allele of *Dif*	BDSC (36559)
Dronc-IR	+ ; *UAS-Dronc-IR*	*Dronc*-targeting RNAi driving expression of 500 bp inverted repeat	NIG (8091R-1)
egr^{1}	w^{1118} ; egr^{1}	Loss of function allele of *egr*, deletion of first coding exon	M. Miura, University of Tokyo
egr^{3}	w^{1118} ; egr^{3}	Loss of function allele of *egr*, deletion of first coding exon	M. Miura, University of Tokyo

Line	Genotype	Description	Source
egr^{1ag}	*w^{1118} ; egr^{1ag}*	Loss of function allele of *egr*	L. Johnston, Columbia University[455]
egr^{3ag}	*w^{1118} ; egr^{3ag}*	Loss of function allele of *egr*	L. Johnston, Columbia University[455]
GMR-Gal4-regg1^{GS9830}	*+ ; GMR-Gal4-regg1^{GS9830}*	Increased expression of Egr due to insertion of upstream P-element under control of eye specific driver GMR-Gal4	T. Clandinin, Stanford University
Hml$^{\Delta}$-Gal4, UAS-2x-eGFP	*+ ; Hml$^{\Delta}$-Gal4, UAS-2x-eGFP*	Haemocyte specific Gal4 driver line, also expressing enhanced GFP under UAS control	S. Sineko[583]
Hml$^{\Delta}$-Gal4, UAS-2x-eGFP; tub-Gal80^{ts}	*w^{1118} ; Hml$^{\Delta}$-Gal4, UAS-2x-eGFP; tub-Gal80^{ts}*	Haemocyte specific Gal4 driver line, with constitutive expression of Gal80^{ts} driven by tubulin, also expressing enhanced GFP under UAS control	Dionne Lab
imd^{10191}	*w^{1118} ; imd^{10191}*	Loss of function allele of *imd*	Dionne Lab
NimC1^{1};eater^{1}	*w^{1118} ; NimC1^{1} ; eater^{1}*	Double mutant with deletion removing ATG translation start site and following 852 bp of NimC1, and 745 bp deletion removing ATG start site, first and second exons, and 18 bp of third exon of eater	B. Lemaitre, EPFL
PPO1$^{\Delta}$PPO2$^{\Delta}$	*w^{1118} ; PPO1$^{\Delta}$ PPO2$^{\Delta}$*	Loss of function alleles of *PPO1* and *PPO2*	M. Hanson, B. Lemaitre, EPFL[383]
Tak1^{1}	*w^{1118} Tak1*^{1}	Loss of function allele of *Tak1*, amino acid replacement D159G within the kinase domain	Dionne Lab
Tak1^{1}	*w Tak1*^{1}	Loss of function allele of *Tak1*, amino acid replacement D159G within the kinase domain	B. Lemaitre, EPFL

Line	Genotype	Description	Source
Tak1^{2527}	*w Tak1*^{2527}	Loss of function allele of *Tak1*, amino acid replacement W178term, stop codon in the activation loop of the kinase domain	D. Schneider
tub-Gal80^{ts} *; UAS-reaper*	*w*^{1118} *; tub-Gal80*^{ts} *; UAS-reaper*	Expression of pro-apoptotic gene *reaper* under the control of UAS, with temperature sensitive inhibition	Dionne Lab
Upd2$^{\Delta}$	*w*^{1118} *Upd2*$^{\Delta}$	4.7 kb deletion removing the *upd2* transcription unit	B. Lemaitre, EPFL
Upd3$^{\Delta}$	*w*^{1118} *Upd3*$^{\Delta}$	13,464 bp deletion removing the first three exons of *upd3*	B. Lemaitre, EPFL
Upd2$^{\Delta}$*Upd3*$^{\Delta}$	*w*^{1118} *Upd2*$^{\Delta}$*Upd3*$^{\Delta}$	Double mutant containing deletion alleles of *Upd2* and *Upd3*	B. Lemaitre, EPFL
w^{1118}	*w*^{1118}	Isogenic wild-type control	BDSC
wgn^{KO}	*w*^{1118} *wgn*^{KO}	Loss of function allele of *wgn*	D. Andersen, J. Colombani, University of Copenhagen [423,445]
UAS-473	*w*^{1118} *; ; UAS-473*	Expression of *MAB_0473* under the control of UAS	This study
UAS-474	*w*^{1118} *; ; UAS-474*	Expression of *MAB_0474* under the control of UAS	This study
UAS-475	*w*^{1118} *; ; UAS-475*	Expression of *MAB_0475* under the control of UAS	This study

2.3.2.1 UAS-Gal4 System

The UAS-Gal4 system is an important *D. melanogaster* genetic tool used to manipulate gene expression within specific target tissues[584]. This could be expression of a transgenic construct, or an RNA inverted repeat (IR) to express double-stranded RNA and knock down expression of a gene of interest. This system makes use of the yeast transcriptional activator Gal4 which is placed under the control of an endogenous tissue-specific enhancer with the required pattern of expression in a *D. melanogaster* driver line. A second *D. melanogaster*

line contains an upstream activation sequence (UAS) linked to the transgene product. The progeny of these two lines containing both the Gal4 and UAS constructs then drive expression of the transgene product in the desired tissue, as shown in Figure 2.1. This system can be further controlled with the use of a temperature-sensitive repressor Gal80 ($Gal80^{ts}$). At 18°C $Gal80^{ts}$ binds Gal4 and prevents it from promoting transcription of the transgene product. At 29°C $Gal80^{ts}$ is degraded, allowing Gal4 to drive expression of the transgene product. By maintaining flies at 18°C and then moving them to 29°C when necessary, the activation of transgene expression can be controlled, for example at a specific point during *D. melanogaster* development.

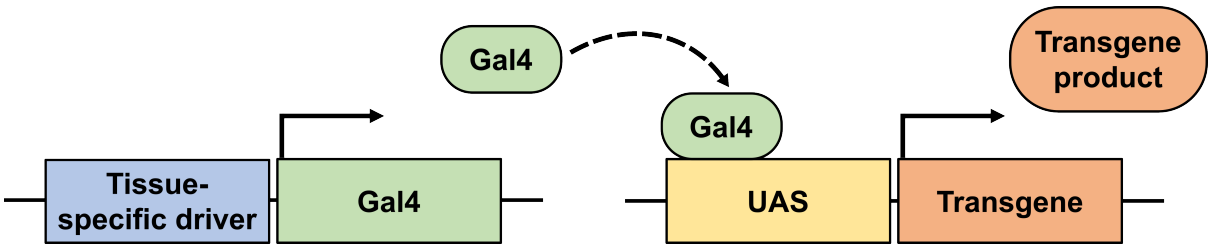


Figure 2.1. UAS-Gal4 system for tissue specific expression of transgenes in *D. melanogaster*.

For experiments making use of the UAS-Gal4 system, an additional genotype control will use a line carrying only the UAS construct, as some UAS constructs can drive low levels of expression of the transgene product in the absence of Gal4. An example of crosses set up to produce experimental genotypes is shown in Figure 2.2.

2.3.3 Transgenic flies

To produce flies expressing *M. abscessus* genes MAB_0473, MAB_0474, or MAB_0475, the genes were amplified by PCR (primers shown in Table 2.7), and purified with the Qiagen PCR purification kit. The plasmid pUASt AttB and purified PCR products were then digested with Cutsmart buffer and restriction enzymes BglII and XhoI at 37°C for 1 hour. The digested products were run on a 1% agarose gel by gel electrophoresis, and the DNA fragments excised and purified using the Qiagen gel purification kit. Each *M. abscessus* gene PCR product was

Experimental genotype Hml^{Δ}-Gal4 > UAS-474	Cross w^{1118} ; Hml^{Δ}-Gal4 x w^{1118} ; UAS-474 Offspring w^{1118} ; $\frac{Hml^{\Delta}\text{-}Gal4}{UAS\text{-}474}$
Driver-only control genotype Hml^{Δ}-Gal4 > +	Cross w^{1118} ; Hml^{Δ}-Gal4 x w^{1118} Offspring w^{1118} ; $\frac{Hml^{\Delta}\text{-}Gal4}{+}$
UAS-only control genotype + > UAS-474	Cross w^{1118} x w^{1118} ; UAS-474 Offspring w^{1118} ; $\frac{UAS\text{-}474}{+}$

Figure 2.2. Outline of crosses performed to generate experimental and control genotypes.

then individually ligated into pUASt AttB with T4 DNA ligase and T4 DNA ligase buffer, and transformed into competent DH5α *E. coli* by heat shock. Bacteria were allowed to recover in SOC medium for one hour, then plated onto LB agar containing 100 μg/mL ampicillin and incubated at 37°C overnight. Single transformed colonies were then selected and streaked onto fresh LB Amp 100 μg/mL agar plates to grow, then a single colony from this was grown overnight at 37°C shaking in LB Amp 100 μg/mL media. The amplified plasmid was extracted using the Qiagen QIAprep Miniprep kit, and the plasmids were sent for sequencing to confirm that insertion of the *M. abscessus* genes was successful. Finally, the successfully transformed plasmids were injected into *D. melanogaster* embryos by the Cambridge Fly Facility. This made use of bacteriophage ϕC31 integrase-mediated recombination for insertion of the genetic material at a specific attP site.

Table 2.7. PCR primers used to amplify *M. abscessus* genes for production of transgenic *D. melanogaster*.

Gene	Forward	Reverse
MAB_0473	ATATAGATCTACCATGATACACAACGGTATGTTGACC	ATATCTCGAGCATCTCCGTCTAGACGCTG
MAB_0474	ATAGAGATCTACCATGCTGGTGATGTGTGCAG	ATAGCTCGAGGCGCCGCCGTCAGCCCT

Gene	Forward	Reverse
MAB_0475	ATAGAGATCTACCATGCGATTGCCGCCGAGTCAA	ATAGCTCGAGGGTACTACCGTCACCCACCCT

2.3.4 *Drosophila* injection

Cultures of *M. abscessus* were grown in 5 mL 7H9 supplemented with Tween80 at 37°C shaking for 3 - 4 days. The bacterial culture was then centrifuged at 4000 x g for 5 minutes, bacterial pellets were resuspended in 2 mL of sterile filtered PBS Tween80 0.1%, and centrifuged again at 200 x g for 5 minutes. The top 1 mL of supernatant was collected to select for single bacilli with minimal clumping, and the optical density was measured at 600 nm. *M. abscessus* was diluted in sterile filtered PBS Tween80 0.1% to OD_{600} = 0.05 unless otherwise stated.

Flies were anesthetised with CO_2 and injected with the prepared *M. abscessus* inoculum using a pulled borosilicate glass capillary needle. A picospritzer III system was used to inject 50 nL of either bacterial suspension or sterile PBS Tween80 0.1% for sterile injury controls. The volume of the injection was calibrated by measuring a drop injected into a mixture of mineral oil with Halocarbon oil 700 (Sigma-Aldrich H8898) and measuring the width of the droplet using the microscope eyepiece reticule. The injection volume could then be adjusted by changing the duration that liquid is pumped from the needle, in milliseconds. Flies were injected close to the dorsal-ventral midline in the abdomen, near the haltere, with the needle facing the posterior to avoid piercing the thorax. Post-infection flies were maintained at 29°C and 65% humidity. Vials were stored horizontally and flies were transferred to new vials with fresh food every 3 or 4 days to reduce death caused by flies becoming stuck within the food.

2.3.5 Survival experiments

Survival experiments were performed on male flies, aged 5 - 10 days post-eclosion. Groups of 20 - 30 male flies per condition were injected either with bacterial suspension or sterile-filtered PBS Tween80 0.1% as sterile-injury controls, or uninjected flies that were anesthetised for a similar length of time as injected groups. Vials were checked at least once daily to record the

number of dead and living flies. These data are presented as Kaplan-Meier curves, compared using Log-Rank test for pairwise comparisons.

2.3.6 Bacterial load quantifications

Male flies, aged 5 - 10 days post-eclosion, were injected with *M. abscessus* bacterial suspension. At each time point, 8 flies were collected and homogenised in 100 μL of PBS Tween80 1% with a sterilised pestle, followed by 1 in 10 serial dilutions in PBS Tween80 1% in a 96-well plate. 10 μL per dilution was plated onto 7H11 plates and incubated at 29°C for 3 to 4 days, and colonies were counted to calculate the colony-forming units (CFU) per fly.

2.3.7 Live *in vivo* confocal imaging

D. melanogaster infected with *M. abscessus* tdTomato Smooth or tdTomato Rough were collected at various time points, anaesthetised, and placed onto microscope slides by placing the dorsal side in glue. Care was taken to not to submerge the fly, only to immobilise it. Flies were then covered with a cover slip resting on Vaseline in each of the four corners, and slides kept on ice. Confocal images were obtained using a Zeiss LSM510 microscope equipped with a 63x NA 1.25 oil objective. Fluorophores were excited using 488 nm (eGFP) and 543 nm (tdTomato) laser lines and emission signals were collected using bandpass filters of 505-550 nm and 585-615 nm respectively. The red channel in images showing tdTomato fluorescence was changed to magenta in ImageJ.

2.3.8 *D. melanogaster* adult eye imaging

Adult fly eye images were taken using a Nikon SMZ1000 stereomicroscope equipped with a GXCAM HICHROME-MET digital microscope camera.

2.4 Molecular biology techniques

2.4.1 Generating electrocompetent *M. abscessus*

Electrocompetent *M. abscessus* was kindly provided by Dr Sophie Burbaud, Floto Group, University of Cambridge. Briefly, a 100 mL culture of *M. abscessus* was grown at 37°C shaking in 7H9 to no later than mid-log phase. The culture was centrifuged at 3000 rpm for 8 minutes in two 50 mL falcon tubes, and each pellet recovered in 40 mL Milli-Q water with 10% glycerol and 0.05% Tween80. Centrifugation and resuspension was repeated once more, centrifuged again and the pellet resuspended in 200 μL Milli-Q water with 10% glycerol and 0.05% Tween80 per transformation. This was centrifuged for a final time and resuspended in the same volume of Milli-Q water with 10% glycerol and 0.05% Tween80.

2.4.2 Polymerase chain reaction

Polymerase chain reaction (PCR) was used to amplify *M. abscessus* target genes for Sanger sequencing validation of CRISPR mutations, and to confirm *D. melanogaster* genotypes. For PCR amplification of *M. abscessus* genes, extracted gDNA was used as template DNA, with reactions prepared in 200 μL PCR tubes as outlined in Table 2.8. DMSO was added to improve amplification by reducing secondary structures, which is common in DNA with high GC contents such as the genomes of mycobacteria. Primers for amplification of *M. abscessus* target genes were designed using Python3 (script shown in Supplementary Figure S2.3), and are listed in Table 2.10. For PCR amplification of *D. melanogaster* genes, 3 flies were homogenised in 100 μL of smashing buffer, which was used as template DNA. Primers for *D. melanogaster* target genes are listed in Table 2.9. PCR reactions were performed using an Applied Biosciences 2720 or a G-storm gradient thermocycler using the conditions outlined in Table 2.11. PCR products were then visualised by gel electrophoresis (2.4.3), and/or stored at -20°C until PCR purification (2.4.4).

Table 2.8. PCR reaction components. Volume shown is per sample.

Reagent	Volume (μL)
Dreamtaq buffer (5X)	5
DMSO	2.5
dNTPs (10 mM)	1
Forward primer (20 μM)	1
Reverse primer (20 μM)	1
Dreamtaq polymerase	0.25
Water	37.25 (or volume required to reach final volume of 50)
Template DNA	2
Total volume	**50**

Table 2.9. *Drosophila melanogaster* PCR primers used in this study. Primers used to confirm genotype of *D. melanogaster*.

Gene	Forward	Reverse
wgn	AAAACTGGGCAGCTGCTTC	ACTGGGCTAACTGGGAAAG
NimC1	CCGGGCTACGTAATGAGAAA	CAATTTGAGTGCGGAACCTC

S2.3.

Table 2.10. *Mycobacterium abscessus* PCR primers used in this study. Primers used to validate CRISPR-induced mutations in *M. abscessus*. Designed using Python3 script that I wrote, shown in Supplementary Figure

Gene	Forward	Reverse
MAB_0169c	GTAAGACTCGGTGTGGTGG	AGTCACACCAGTAACTCTGG
MAB_0471	GTGGAATCTCCAGAGATTCG	CCGATCTACGTTCACTCCC
MAB_0472	TGGGACAGATGATCGGAGC	GATGGCAGAAAGCACAGCC
MAB_1012c	GTTCACCGTCATCAGCAGC	GATGTCCGAGACGTACTCG
MAB_1132c	TGGTCAACACGATGATCAGG	CGTGGCCAATCTCATACCG
MAB_1283c	GTCAACAAGGTTGAGGCGG	CAAACATGTCCGCACGACC
MAB_1933c	TGCCGTTCATCTTGGAATCG	CATCGCGCGGTCATTATCC
MAB_2228c	ACGCGTTGAGCATTGAATCC	GATATCGCGCAGGTCAACC
MAB_2262c	ATACCTCGATATCCACCTCG	TAGGATGGGCTAAGTACTGG
MAB_2728c	GATCGAACTTGCCCTGAGC	GTTGCAAAAGTGACGTACGG
MAB_2914	ATTGGTCATCGTCACCTCGG	CGATGGACCACTGAGGGATG
MAB_3029	AGTGGACCTACTACCCTGC	CTTGAGTCGGGACAACAGG

Gene	Forward	Reverse
MAB_3473c	ACTCCACCTTGACCTTGCC	GACCATCCTCAATGGAGCG
MAB_3521c	AGCGGGATGATCCTGATGG	AGGCCGGAGATGACAATCC
MAB_3522c	GCATCGAGGTCATCCATGG	GCGTTCTGGGTGTTTCTCG
MAB_3523c	GAACCGTTGTGGGTAAAAGG	GTGGATGTGACGTGATCGG
MAB_4095c	GTTGTTGATGCGGCGAACC	AACAGTCAACGCAGTGAACG
MAB_4163c	GTCTTGACATTGGGGGTGC	CACGATGAGGACGTGATCG
MAB_4588c	ATAAACCCGTACTTGGCAGC	CATCTTGCCGGTACTACCG

Table 2.11. PCR reaction conditions.

Reaction stage	Temperature	Time	Number of cycles
Initial denaturation	95°C	30 s	1
Denaturation	95°C	30 s	30
Annealing	55°C	30 s	30
Extension	68°C	1 min	30
Final extension	68°C	5 min	1
Cooling	4°C	Hold	

2.4.3 Gel electrophoresis

Gel electrophoresis was used to visualise and compare DNA fragments following amplification of PCR products or restriction enzyme digestion. Agarose powder (Fisher) was dissolved in Tris-acetate-EDTA (TAE) buffer by boiling to produce a 1% agarose gel. SYBR Safe DNA gel stain (Stratech) was added at a 1:10,000 dilution once the agarose gel solution was cooled, and the gel was poured into a gel box with a well comb. Once completely solidified, samples were mixed with 6 X loading dye and 10 μL per sample was loaded into wells along the top of the gel, as well as a DNA ladder (NEB). Gels were covered in TAE buffer and run at 100 mV for 30 minutes to 1 hour, and bands were visualised using a Syngene InGenius gel imaging system.

2.4.4 PCR purification

Following confirmation of successful PCR amplification of *M. abscessus* target genes by visualising PCR products on an agarose gel, the remaining PCR product was purified either

using the QIAquick PCR purification kit (Qiagen) or the QIAquick 96 PCR Purification Kit (Qiagen), depending on the number of samples being processed. Purified DNA was eluted in Milli-Q water, a Nanodrop was used to assess DNA purity and concentration, and purified PCR DNA was stored at -20°C.

2.4.5 Gel extraction

To extract DNA fragments or plasmid backbones following digestion with restriction enzymes that were successfully visualised on an agarose gel, a scalpel was used to cut out the band of interest from the gel. Gel extraction was performed using the Qiagen gel extraction kit (Qiagen), and the purified DNA was quantified using a Nanodrop.

2.4.6 Sanger sequencing

DNA samples selected for Sanger sequencing were diluted to 10 ng per μL in Milli-Q water and 6 μL was loaded into microcentrifuge tubes and sealed with parafilm. Primers used to generate the PCR product for sequencing of target genes (Table 2.10) were diluted to 3.2 pmol per μL, and loaded into microcentrifuge tubes and sealed with parafilm. Samples were sent to Source Biosciences to perform Sanger sequencing. Sequences were viewed using SnapGene Viewer (6.0.2) and compared to wild-type *M. abscessus* gene sequence (ATCC 19977) using Basic Local Alignment Search Tool (BLAST). Samples showing nucleotide insertions or deletions in the gene of interest were aligned to the wild-type gene using Clustal Omega multiple sequence alignment to annotate the mutation, and mutations were confirmed by sequencing the sample again using the second PCR primer.

2.4.7 RT-qPCR

RT-qPCR was used to measure RNA transcript levels of both *D. melanogaster* genes and *M. abscessus* genes. The initial collection of these samples differs and is described below, and is followed by a common RNA isolation, DNAse treatment and reverse transcription protocol.

2.4.7.1 Bacterial gene expression

10 mL cultures were grown to stationary or mid-exponential phase and bacterial pellets were collected by centrifugation at 3000 x g for 10 minutes. The supernatant was discarded and the pellets resuspended in 400 μL TRI reagent (Sigma T9424). Samples were transferred to a 2 mL tube containing 500 mL of 0.1 mm silica beads (Lysing Matrix B tubes, MP Biomedicals) and placed into a FastPrep 24 (MP Biomedicals) beadbeater for 2 minutes, rested for 1 minute on ice, and beat for another 2 minutes. Samples were then centrifuged at 13,400 x g for 5 minutes and at least 100 μL supernatant transferred to fresh microcentrifuge tubes. Samples were stored at -20°C before RNA isolation.

2.4.7.2 *Drosophila* gene expression

Three flies per sample were collected in 100 μL TRI reagent and homogenised with a sterilised pestle in a microcentrifuge tube. A minimum of four samples per condition per time point were collected. Samples were stored at -20°C before RNA isolation.

2.4.7.3 RNA isolation

RNA was isolated from each sample by adding 20 μL chloroform per 100 μL TRI reagent in each sample. Samples were then shaken thoroughly for 30 seconds and incubated for 5 minutes at 4°C. Samples were centrifuged at 13,400 x g for 15 minutes at 4°C, then the upper aqueous phase was collected into a new microcentrifuge tube and the organic phase discarded. 50 μL isopropanol was added to each sample, followed by incubation at room temperature for 10 minutes. Samples were centrifuged again at 13,400 x g for 10 minutes and the supernatant was discarded. The remaining pellet was covered in 200 μL of 75% ethanol, and stored at -20°C if necessary.

2.4.7.4 DNAse treatment and reverse transcription

Samples were centrifuged at max speed for 5 minutes and the ethanol discarded. A second round of centrifugation was performed to remove any remaining ethanol. The RNA pellet was then covered in 40 μL of the DNAse reaction mix shown in Table 2.12 and incubated at 37°C for 30 minutes. The reaction was stopped by the addition of 4 μL of 25 mM EDTA and incubation at 65°C for 10 minutes. 10 μL of each DNAse treated sample was used for reverse transcription, the remaining volume was stored at -80°C.

Table 2.12. DNAse reaction components. Volume shown is per sample.

Reagent	Volume (μL)
DNAse buffer (10X)	4
RNAse-free DNAse I	2
Water	34

10 μL of each DNAse treated sample was added to 1 μL of random hexamers (200 μg/μL) and incubated at 70°C for 5 minutes. 9.9 μL of reverse transcription reaction mix, shown in Table 2.13, was added to each sample and incubated for 10 minutes at room temperature then for 1 - 2 hours at 37°C. Reverse transcription was stopped by incubation at 70°C for 10 minutes. 10 μL of each complementary DNA (cDNA) sample was added to a single microcentrifuge tube to create a pool of all samples. This pool was diluted 1 in 5 in TE (10 mM Tris, 1 mM EDTA) eight times, creating a series used to generate standard curves. The remaining volume of each cDNA sample was diluted 1 in 40 in TE and stored with the pool and serial dilution series at -20°C.

Table 2.13. Reverse transcription reaction components. Volume shown is per sample.

Reagent	Volume (μL)
Reverse transcriptase buffer (5X)	4
Water	1.9
RiboLock (RNAse inhibitor)	1

Reagent	Volume (μL)
RevertAid M-MuLc reverse transcriptase	1
dNTPs (10 mM)	2

2.4.7.5 RT-qPCR reaction

The RT-qPCR reactions were prepared on ice with a reaction mix of 5 μL SensiMix SYBR Green (Biolnie QT650) and 0.2 μL 10 μM primer mix containing forward and reverse primers in TE. This was added to 4.8 μL cDNA samples or the pool serial dilution series. Amplification was performed using a Corbett RG-6000 or Qiagen Rotor-Gene Q thermocycler using the conditions listed in Table 2.14. Primer sequences used for *D. melanogaster* genes are listed in Table 2.15 and primer sequences used for *M. abscessus* genes are listed in Table 2.16.

The pooled samples and serial dilution series were used to produce a standard curve for each gene. This was used to calculate the gene expression of each of the samples which was then normalised to a housekeeping gene, *Rpl4* for *D. melanogaster* gene expression and *MAB_3869c* (RNA polymerase β subunit *rpoB*) for *M. abscessus* gene expression.

Table 2.14. RT-qPCR reaction conditions.

Reaction stage	Temperature	Time	Number of cycles
Initial denaturation	95°C	10 min	1
Denaturation	95°C	15 s	40
Annealing	57 °C	30 s	40
Extension	72°C	30 s	40
Cooling	4°C	Hold	

Table 2.15. *Drosophila melanogaster* RT-qPCR primers used in this study. Primers used to amplify *D. melanogaster* cDNA transcripts.

Gene	Forward	Reverse
Atg2	CAAAAGACCTGTACGCAGAGC	TACTGAGCAACAGGTTTCGTC
AttA	CACAATGTGGTGGGTCAGG	GGCACCATGACCAGCATT
CecA1	TCTTCGTTTTCGTCGCTCTC	CTTGTTGAGCGATTCCCAGT

Gene	Forward	Reverse
Def	TTCTCGTGGCTATCGCTTTT	GGAGAGTAGGTCGCATGTGG
Dipt	ACCGCAGTACCCACTCAATC	CCCAAGTGCTGTCCATATCC
Dro	CCATCGAGGATCACCTGACT	CTTTAGGCGGGCAGAATG
Drs	GTACTTGTTCGCCCTCTTCG	CTTGCACACACGACGACAG
egr-RA	GAGGCAACTTCCAAAGAGAGC	CGGATCTGGCTGAAAGAAGA
IM1	CGTCACCGTTTTTGTGCTC	TGATCACATTTCCTGGATCG
IM2	ACCGTCTTTGTGTTCGGTCT	GATTACCACATTTCCTGGATCG
IM4	CAAACCTCAGAAATCAACATGAA	GGATGAGCACGGTTCCAG
IM10	ATAAGGGGCCAGAATGAAGG	CTCATCGGTGTACACATGCTC
Mtk	TCTTGGAGCGATTTTTCTGG	TCTGCCAGCACTGATGTAGC
Rpl4	TCCACCTTGAAGAAGGGCTA	TTGCGGATCTCCTCAGACTT
Socs36E	AAAAAGCCAGCAAACCAAAA	AGGTGATGACCCATTGGAAG
Stat92E	ACTAGTGGAACACCGCATCA	AGTCCGCCATTCCAAAGTC
Tace	CTGATGTCCTACCCGATGGC	CCTCAAGGTCTTGGCCACAT
TotA	CCAAAATGAATTCTTCAACTGC	GAATAGCCCATGCATAGAGGAC
Upd2	CGGAACATCACGATGAGCGAAT	TCGGCAGGAACTTGTACTCG
Upd3	ACTGGGAGAACACCTGCAAT	GCCCGTTTGGTTCTGTAGAT

Table 2.16. *Mycobacterium abscessus* RT-qPCR primers used in this study. Primers used to amplify *M. abscessus* cDNA transcripts.

Gene	Forward	Reverse
MAB_0934	ATTCCTGTCCGGTGGGTTTG	ATCCGGTCGATACATTGCGA
MAB_0935c	GGATCATCGACAGCGACACT	CGGGGGACTTACGCCAATAG
MAB_0936c	GCAACATCGTGACCGAAACC	CACCCCGAGGTACTTGAAGC
MAB_0937c	CGGACTATGCCGTCTTCCTC	CTGACGGCTTGGTCGTAGTT
MAB_0938c	CGGTTCTCCTACCAGCTGAC	CTGATTTCTCGGCGATCGGA
MAB_0939	CATGAGAGCCCGCTGGATAG	GCACGTTTGACGGTGAACTC
MAB_1917	CTTGGTGGTTTCCAACGTGC	CGGATACATGCCGATCACCT
MAB_2914	ATTGGTCATCGTCACCTCGG	TGTCAGGGTTTTCGGTCTCG
MAB_3508c	GATTCTTGAGCAGGGGACCA	GGGCAGTGGGTTCTTGCG
MAB_3551c	CGGTGAGATCGGAGAGTTGG	GACACACGTTGATTGAGCGG
MAB_3869c	TGATCAACATCCGTCCCGTC	CTGGTCCATGAACTGCGACA
MAB_4097c	GTCGTCATAGCCGTGTGGAT	GTCCAGTACCAAGACCGACG

Gene	Forward	Reverse
MAB_4100c	CCTGCCTGGAGTACATCGAA	CCACCTTGCGCCAATCTCTC
MAB_4115c	GATGAACGGTCGGTATCGCT	TGTCCGAGTTCGACTCGTTG
MAB_4116c	AGCGAGAGCATTCGGTTTCA	AAAGACCTTCCCCATCTGCG
MAB_4117c	GATTCCGCTGCTGGTGATTG	TCTCGTTACCGAATACGCCG
MAB_4454c	TTCTGGATCATCAACGCCCC	CACCTCTACGGCCTCTTCAC
MAB_4459c	GAGCCGATCTCGACCGTTAC	TTCTCGGTCAGTTCCAAGGC
MAB_4544c	ATGTCCACCACCGAAGTGTC	TGAGATTTCCCATCACCGCC

2.4.8 Thin layer chromatography

Thin layer chromatography (TLC) was used to measure bacterial triacylglycerol. Briefly, *M. abscessus* cultures were diluted to a consistent OD with fresh media, pelleted by centrifugation at 4000 x g for 10 minutes, and dried in a 50°C incubator. Pellets were then resuspended in 100 μL of a chloroform (3): methanol (1) solution, and spun for 3 minutes at 13,000 rpm at 4°C. The pellets were homogenised using a sterile pestle, spun again, and maintained on ice. Standards were produced using lard dissolved in the same chloroform: methanol mix, diluting each standard to known concentrations. For each experiment, at least three replicates of each sample were run. 2 μL of each standard and 20 μL of each sample were loaded onto silica gel glass plates, placed into a chamber containing the solvent hexane (4): ethyl ether (1), and run until the solvent was 1 cm below the top edge of the plate. Plates were removed from the chamber and dried. To visualise triacylglycerol, the plates were stained with cerium ammonium molybdate (CAM) solution, baked at 80°C for 20 minutes, and scanned.

2.4.9 SDS PAGE

SDS PAGE was performed on bacterial cell pellets and culture supernatant. Cultures were grown to stationary phase in 10 mL Sauton's minimal medium (Asn 4 g/L), then centrifuged at 2000 x g for 5 minutes at 4°C. The supernatant was collected and passed through a 0.22 μM filter, and proteins were precipitated by adding 3.5 mL pre-chilled 20% w/v trichloroacetic acid (TCA) and leaving it at 4°C overnight. The samples were centrifuged at 4500 x g for 15

minutes at 4°C, the supernatant carefully discarded, and the remaining TCA was washed away by adding 200 μL cold acetone slowly along the sides of the tube. The sample was centrifuged again at 4500 x g for 15 minutes at 4°C, the supernatant carefully discarded, and the pellet was left to air dry for 10 minutes. The protein pellet was resuspended in 60 μL 2x Laemmli sodium dodecyl sulphate (SDS)-polyacrylamide gel electrophoresis (PAGE) buffer, using a 65°C water bath to aid resuspension when necessary. If the samples turned yellow due to incomplete removal of TCA, a few microlitres of 1 M Tris-Cl pH 7.5 was added until they became blue again. Samples were stored at -80°C. Four samples per strain were collected.

Samples were heated at 85°C for 5 minutes along with a protein ladder (NEB P7706), vortexed, and 5 μL added to 4-12 % gradient pre-cast gels (Invitrogen NuPAGE NP0329). Electrophoresis was performed using a running buffer based on the mass of the target protein - less than 75 kDa used 2-(N-morpholino)ethanesulfonic acid (MES), greater than 75 kDa used 3-(N-morpholino)propanesulfonic acid (MOPS) (Table 2.17). Gels were run at 300 mA, 200 V, and 50 W, for 35 minutes if using MES, or 50 minutes if using MOPS. The gel was then washed 3 times for 5 minutes with Milli-Q water on a tilting table to remove SDS and buffer salts, and stained with 25 mL Simply Blue stain on the tilting table for 1 hour. The gel was washed again with 100 mL Milli-Q water and 20 mL 20% NaCl solution for 1 hour. Gel images were taken using a digital camera.

2.4.10 Western Blots

Three flies per sample were collected in 75 μL 2x Laemmli SDS-PAGE buffer in a microcentrifuge tube and homogenised with a sterilised pestle. Four samples per condition per time point were collected, and samples were stored at -80°C. Samples were heated at 85°C for 5 minutes along with a protein ladder (NEB P7706), vortexed, and 5 μL added to 4-12 % gradient pre-cast gels (Invitrogen NuPAGE NP0329). Electrophoresis was performed using a running buffer based on the mass of the target protein - less than 75 kDa used MES, greater

than 75 kDa used MOPS (Table 2.17). Gels were run at 300 mA, 200 V, 50 W, for 35 minutes if using MES, or 50 minutes if using MOPS.

Proteins were then transferred onto polyvinylidene fluoride (PVDF) Immobilon Transfer membrane (Millipore) in transfer buffer (Table 2.17) via electroblotting in a transfer chamber (Biorad). This was kept at 4°C and continually stirred using a magnetic stirrer. The transfer power pack was set to 400 mA, 250 V, 50 W, and run for 1 hour.

Following transfer, the membrane was blocked at room temperature for 1 hour using 5% milk (Cell Signalling) in TBS containing 0.1% Tween20 (TBS-T). Once blocked, the solution was discarded and the membrane was washed in TBS-T for 5 minutes at least 3 times. Primary antibody incubation was overnight at 4°C in 5% bovine serum albumin (BSA) in TBS-T. Membranes were washed again in TBS-T for 5 minutes at least 3 times and then incubated with the secondary antibody, conjugated with Horseradish peroxidase (HRP), in 5% milk in TBS-T for 2 hours at room temperature. Antibodies used are listed in Table 2.18. The membrane was washed 5 times in TBS-T for 5 minutes, then incubated with chemiluminescent HRP-substrate solution (SuperSignal West Pico PLUS, Thermo Scientific 34580) for 5 minutes at room temperature. The blots were imaged using a Fuji LAS-3000 luminescent image analyser.

To normalise the sample blots, the antibodies bound to the membrane were stripped by incubating the membrane in 0.2 M NaOH for 1 hour at room temperature. The membrane was washed in TBS-T, and the steps above were repeated using the anti α-tubulin antibody for the primary antibody. Images were analysed using ImageJ, the mass of the sample bands were compared to bands of known mass in the protein ladder, and bands were normalised by dividing the signal from the sample bands of the target protein by the signal from the α-tubulin bands.

Table 2.17. Western Blot buffers.

Buffer	Components	Notes
2x Laemmli SDS-PAGE buffer	4% SDS 20% glycerol 10% 2-mercaptoethanol 0.004% bromophenol blue in 0.125 M Tris HCl (pH 6.8)	Stored at -80°C
MES running buffer (20x stock solution)	97.6 g Anydrous MES 60.6 g Tris-Base 10 g SDS 3 g EDTA in Milli-Q water to 500 mL	Diluted 1 in 20 in Milli-Q water before use
MOPS running buffer (20x stock solution	104.6 g MOPS 60.6 g Tris-Base 10 g SDS 3 g EDTA in Milli-Q water to 500 mL	Diluted 1 in 20 in Milli-Q water before use
Transfer buffer	6.06 g Tris-Base 28.8 g Glycine 400 mL MeOH 1600 mL Milli-Q water	MeOH added last, cooled to 4°C before use
TBS (10x stock solution)	24.2 g Tris-Base 80 g NaCl in Milli-Q water to 1 L	Adjusted to pH 7.6 with HCl or NaOH as needed
TBS-T	100 mL 10 x TBS stock solution 10 mL 10% Tween20 in 890 mL Milli-Q water	

Table 2.18. Western Blot antibodies.

Target	Source and type	Supplier	Concentration used
Phospho-AKT	Rabbit, polyclonal	Cell Signalling Technologies 4054	1:1000
Total-AKT	Rabbit, monoclonal	Cell Signalling Technologies 4691	1:1000
α-Tubulin	Mouse, monoclonal	Developmental Studies Hybridoma Bank 12G10	1:5000
Rabbit IgG	Goat, HRP-linked, polyclonal	Cell Signalling Technologes 7074	1:5000

Target	Source and type	Supplier	Concentration used
Mouse IgG	Horse, HRP-linked, polyclonal	Cell Signalling Technologies 7076	1:10,000

2.5 Statistical analysis and data visualisation

All data visualisation and statistical analyses were performed using R studio with R version 4.2.3. A list of R studio packages used is shown in Supplementary Table S2.1.

For boxplots, the box denotes the interquartile range (IQR), with a heavy line showing the median and whiskers indicating the range of all data points within 1.5 x the IQR or the most extreme value, whichever is closest to the median. Survival curves were plotted using the Kaplan-Meier method, using Log-Rank for pairwise comparisons. For other data, a Shapiro-Wilk test was used to test for normality to select the appropriate statistical test. Normally distributed data was compared using ANOVA with Tukey's test for multiple comparisons, and non-normally distributed data was compared using either the Wilcoxon rank-sum test (also known as Mann-Whitney test) for comparisons between two conditions or using Kruskal-Wallis test with Bonferroni's adjustment for comparisons involving more than two conditions.

When necessary, *p*-values are represented in figures using the standard asterisk method: $*$, P < 0.05; $**$, P < 0.01; $***$, P < 0.001; $****$, P < 0.0001.

Diagrams were produced using Inkscape.

Chapter 3: *Drosophila melanogaster* as a model for *Mycobacterium abscessus* infection

3.1 Introduction

The *D. melanogaster* model for bacterial infection has become widely used for the study of host-pathogen interactions, owing to its well-characterised immune response, ease of use, and the tools available to manipulate its genetics. This has facilitated the identification of host factors that interact with a range of pathogens, as well as bacterial virulence factors that manipulate the cell signalling pathways driving the innate immune response[511]. Studies using the *D. melanogaster* model have contributed to the understanding of mycobacterial infections, primarily from *in vitro* studies using the S2 cell line to identify which host factors restrict intracellular growth of species such as *M. fortuitum*[512–514]. However, immune responses to different mycobacterial species can vary greatly and very little is known about the *D. melanogaster* immune response to an *in vivo M. abscessus* infection.

To the best of my knowledge, at the start of my work, there were two published papers using an *in vivo D. melanogaster* model to study *M. abscessus* infection[517,585]. In the first, Oh *et al.* found that flies with mutations in PGRP-SA and Dif were shorter lived than wild-type flies during *M. abscessus* infection, whereas there was no impact on survival of flies with loss-of-function of Imd. They concluded that PGRP-SA was responsible for the detection of *M. abscessus* in *D. melanogaster*, and this activated Toll signalling which culminated in the production of AMPs[517]. The second, by the same authors, used *D. melanogaster* fed with various combinations of antibiotics to screen drug efficacy against *M. abscessus* infection[585]. Given the importance of the innate immune response in controlling *M. abscessus* infection in other animal models[128–130] and in patients with MSMD[253,254], I wanted to understand more about the *D. melanogaster* immune response to *M. abscessus* infection and what pathways were being activated throughout the course of infection.

During my project, two more papers were published using the *D. melanogaster* model for *in vivo M. abscessus* infection. These also showed Toll pathway activation during infection, but this occurred very late during the infection suggesting that the Toll pathway was not being activated in response to the initial detection of the bacteria, with the exception of forcing *M. abscessus* to remain extracellular by removing opsonisation protein Tep4[118,488]. There is also evidence of Imd pathway activation with the transcription of AMPs associated with Imd but again at very late stages in the infection[118,581], consistent with the conventional view that Imd pathway PRRs PGRP-LE and PGRP-LC detect *m*-DAP-type peptidoglycan as produced by *M. abscessus*[520,521].

These studies only made use of the *M. abscessus* type strain, ATCC 19977, for infection of *D. melanogaster*, which is morphotypically smooth. I also wanted to consider whether the unmasking model of *M. abscessus* GPLs reducing or preventing immune responses was also occurring during infection of *D. melanogaster* by concealing immunostimulatory factors such as lipoproteins within the mycomembrane[50,115–117]. This would indicate whether the *D. melanogaster* model recapitulates the increased virulence of the rough morphotype as seen in other infection models.

3.2 Aims

The aim of this chapter was to characterise how the *D. melanogaster* model responds to infection with *M. abscessus*, providing important context about what constitutes a typical *D. melanogaster* immune response to *M. abscessus* for comparison when studying *M. abscessus* mutant strains with various *D. melanogaster* mutant lines in future chapters. Additionally, this would provide insight into which innate immune mechanisms, if any, detect and respond to *M. abscessus*, how effective these responses are against *M. abscessus*, and if there are any detrimental effects on the host caused by these responses. Finally, the location and behaviour of *M. abscessus* during infection can also be considered, indicating where to direct

D. melanogaster drivers for tissue-specific genetic manipulation of the host in later work. To achieve this, I infected various *D. melanogaster* lines, each with mutations in different aspects of the immune response, with different doses of *M. abscessus* strains displaying both the smooth and the rough morphotype, to assess differences in survival. I also performed RT-qPCR to measure the transcriptional response of many targets of the different *D. melanogaster* immune signalling pathways and used *in vivo* confocal imaging to visualise *M. abscessus* and its localisation throughout the infection.

3.3 Results

3.3.1 *Drosophila melanogaster* is susceptible to infection with *Mycobacterium abscessus*

To characterise the typical immune response of *D. melanogaster* during infection with *M. abscessus*, I initially had to design and optimise the experimental infection conditions. The primary factors I considered were the initial dose of the bacterial inoculums being injected into flies and the use of detergents to prevent clumping of the *M. abscessus* when quantifying the number of colony forming units (CFU) per fly over the course of an infection.

I also had to decide on whether to use male or female *D. melanogaster* for my experiments. To the best of my knowledge, at the start of my project, there were only two published papers using *D. melanogaster* as a model for *M. abscessus* infection [517,585], and to date, only two more papers have been published since [118,488], all of which use female flies. Sex-specific differences in immune responses have been described in *D. melanogaster* for a variety of infections, including *M. abscessus* [519] (Dionne Lab, unpublished data). Whilst the sex-specific differences in *M. abscessus* infection outcomes offer very interesting questions about the pathogenesis of *M. abscessus* in terms of host metabolic and immune regulation differences, for all of my experiments I have used single-sex groups of male *D. melanogaster*. This is primarily driven by biosafety concerns. Eggs laid into the food by female flies result in liquefied food once the

larvae hatch, causing an increase in the number of flies dying as a result of drowning rather than death due to the infection conditions. This requires infected female flies to be moved onto fresh food on a more regular basis compared to male flies, increasing the risk of escape during the transfer. As *M. abscessus* is a human pathogen, the biosafety risk of escaped infected flies can be reduced by using male flies and transferring these groups onto fresh food less frequently.

Firstly I performed a dose response experiment to characterise the infection dynamics with different numbers of *M. abscessus* being injected into flies. I prepared *M. abscessus* bacterial suspensions in PBS Tween80 0.1%, the addition of Tween80 was to reduce clumping between the bacterial cells and ensure injection of consistent numbers of bacteria. I prepared a range of doses from OD_{600} = 0.1 to OD_{600} = 0.001 and quantified the number of CFU per mL of each of these preparations using growth on 7H11 agar plates (Figure 3.1A). The OD_{600} measurements correlated well with the CFU (Figure 3.1B), indicating that using OD_{600} measurements is a suitable and rapid method for preparing *M. abscessus* inoculums for *D. melanogaster* injections.

I then used these various initial doses to inject into *D. melanogaster* (Figure 3.1C). I observed a clear dose-dependent effect on *D. melanogaster* survival, with the median survival time ranging from 99.5 to 142.9 hours post-infection, respectively. Even the lowest dose, approximately 25 CFU per fly based on the CFU per mL of the initial inoculum, resulted in the death of 93.1% of the infected *D. melanogaster* population. Groups of flies were also injected with PBS Tween80 0.1% which acted as both a sterile-injection control and ensured there was no impact on *D. melanogaster* survival caused by the Tween80 0.1% used to prepare the bacterial inoculums. I then used these survival data to select an appropriate initial dose to use for comparing *M. abscessus* infection in different *D. melanogaster* immune-signalling mutant lines. This is an important factor to consider as having too high a dose could result in large numbers of *M. abscessus* overwhelming the *D. melanogaster* immune system and prevent any effective

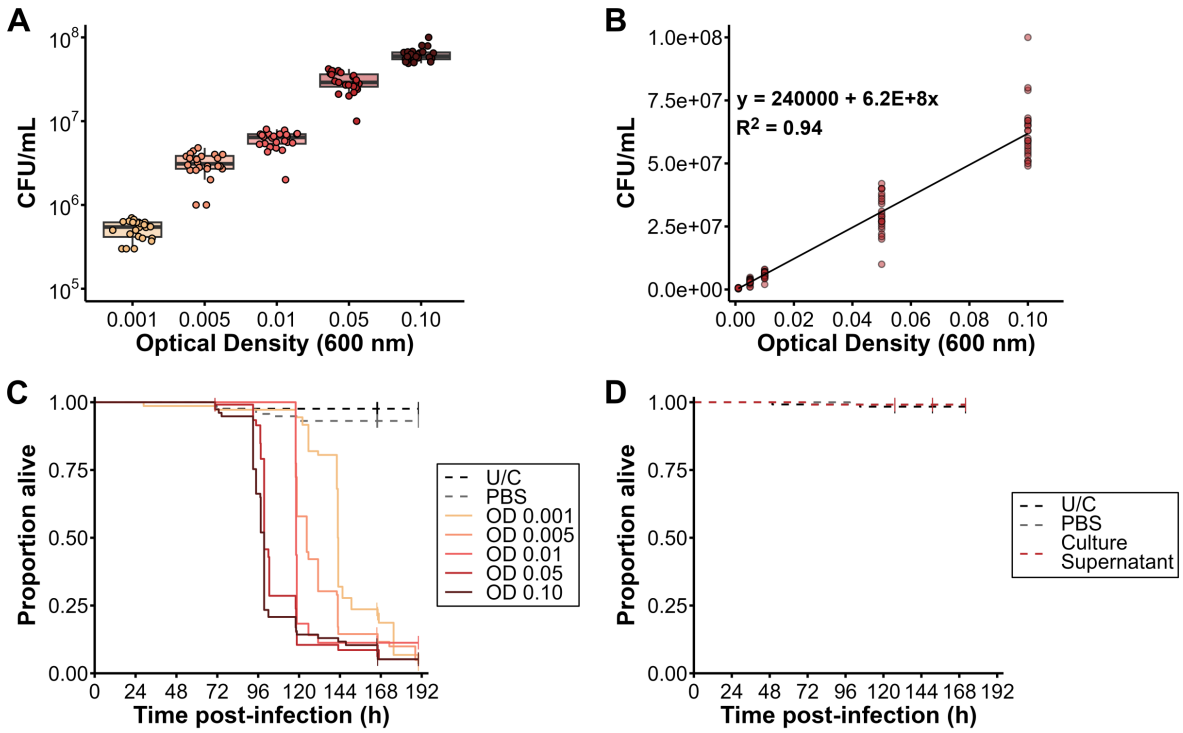


Figure 3.1. Dose-dependent effects of initial *M. abscessus* inoculum on *D. melanogaster* survival. (**A**) The number of colony forming units per mL in initial *M. abscessus* inoculum preparation ranging from OD_{600} = 0.001 to OD_{600} = 0.10. Data represent the mean ± s.d of three independent experiments, n = 24 per dose. (**B**) The OD-CFU standard curve based on the number of colony forming units per mL in initial *M. abscessus* inoculum preparation ranging from OD_{600} = 0.001 to OD_{600} = 0.10. Data represent three independent experiments, n = 24 per dose. (**C**) w^{1118} *D. melanogaster* survival following injection with increasing doses of *M. abscessus* ATCC 19977, OD_{600} = 0.001 (yellow), OD_{600} = 0.005 (orange), OD_{600} = 0.01 (dark orange), OD_{600} = 0.05 (red), OD_{600} = 0.10 (dark red), compared with PBS Tween80 0.1% sterile injury control (grey), or uninjected control (U/C) (black). Data represent three independent experiments, $125 \geq n \geq 71$ per condition. (**D**) w^{1118} *D. melanogaster* survival following injection with sterile filtered supernatant from *M. abscessus* culture spent medium (red), PBS Tween80 0.1% sterile injury control (grey), or uninjected control (U/C) (black). Data represent three independent experiments, $122 \geq n \geq 113$ per condition.

immune response, leading to rapid death and no opportunity to identify survival differences between different *D. melanogaster* immune-signalling mutants. Alternatively, having too low a dose may result in a weak or unobservable immune response and again prevent identification of survival differences. Taking this into consideration, I selected a high dose (OD_{600} = 0.05) and a low dose (OD_{600} = 0.005), as these two doses showed consistent survival phenotypes with the median time to death approximately one day apart. I also injected *D. melanogaster* with sterile filtered spent 7H9 medium from *M. abscessus* cultures, which resulted in no death of *D.*

melanogaster, indicating that the death of infected flies is due to the presence of the bacteria and not a secreted factor present in the culture supernatant (Figure 3.1D).

I also wanted to consider which detergent was most suitable for serially diluting *M. abscessus* extracted from infected flies in order to quantify the bacterial load during the course of an infection. I infected *D. melanogaster* with OD_{600} = 0.05 of *M. abscessus* and immediately smashed and collected flies (0 hr time point) in either PBS with Tween80 or PBS with sodium dodecyl sulfate (SDS), the concentrations of detergent ranging from 0.1% to 2% (Figure 3.2A). The CFU per fly was calculated for each group and compared, flies smashed in PBS Tween80 0.1% to Tween80 1% showed consistent numbers of CFU whereas all flies smashed with PBS SDS showed considerably fewer CFU, with no growth of any colonies at PBS SDS 2% indicating the toxicity of SDS against *M. abscessus*. Due to the apparent toxicity of the SDS, I decided to use PBS with Tween80 as a detergent for the purposes of bacterial quantification experiments, and I selected PBS Tween80 1% as this showed the least variation in the number of colonies, clear 10-fold differences in the number of colonies at each 10-fold serial dilution, and gave the closest value to the number of CFU per fly predicted based on the CFU per mL of *M. abscessus* at OD_{600} = 0.05, with 50 nL being injected into each fly. Using this method, I then quantified bacterial numbers during the course of an *M. abscessus* infection with flies infected with OD_{600} = 0.05 (Figure 3.2B). I observed exponential growth of *M. abscessus* for the first 72 hours of the infection, with a fairly consistent bacterial doubling time of approximately 10 hours.

Another factor to consider when screening *D. melanogaster* immune-signalling mutants is possible differences caused by the *M. abscessus* morphotypes. Isogenic *M. abscessus* strains derived from ATCC 19977 displaying either the smooth or the rough morphotype, both carrying the tdTomato fluorescent plasmid, were kindly gifted to us by Prof. Andres Floto from University of Cambridge, and these strains were used to evaluate the differences in *D. melanogaster* responses to the *M. abscessus* morphotypes. While the number of CFU for OD_{600} = 0.05 and

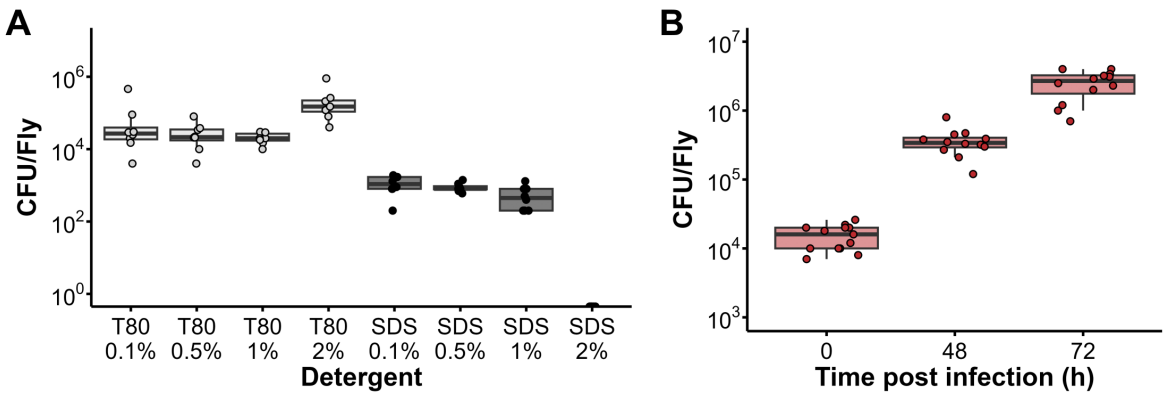


Figure 3.2. Selecting a suitable detergent for *M. abscessus* bacterial load quantifications. (**A**) Number of colony forming units per fly (CFU/Fly) from w^{1118} *D. melanogaster* following injection with *M. abscessus* ATCC 19977 at OD_{600} = 0.05 0 hours post-infection, calculated following collection and serial dilution of infected flies with various concentrations of either PBS Tween80 (light grey) or PBS SDS (dark grey). Data represent the mean ± s.d of one independent experiment, n = 8 per condition. (**B**) Bacterial load quantification showing growth of *M. abscessus* ATCC 19977 when injected at OD_{600} = 0.05 into w^{1118} *D. melanogaster*. Flies were collected and serially diluted in PBS Tween80 1%. Data represent the mean ± s.d of two independent experiments, n $\geq$ 12 per timepoint.

OD_{600} = 0.005 was the same for the type strain ATCC 19977 (which is morphotypically smooth) and the tdTomato Smooth strain, there was an approximately 4-fold and 5-fold decrease in the number of CFU at these same OD_{600} measurements for the tdTomato Rough strain, respectively (Figure 3.3A). This meant the number of CFU in the low dose of tdTomato Smooth was closer to the number of CFU in the high dose of tdTomato Rough. This difference between the strains is also observed in an *in vitro* growth curve of these strains in 7H9 media, while the growth of ATCC 19977 and tdTomato Smooth are very similar, the tdTomato Rough has a lower OD_{592} throughout log phase growth (Figure 3.3B).

3.3.2 Activation of Toll pathway signalling during *M. abscessus* infection

3.3.2.1 Toll pathway antimicrobial peptides

To understand which aspects of the *D. melanogaster* humoral immune response may be responding to *M. abscessus* infection, I began infecting fly lines with mutations in key immune signalling pathways with *M. abscessus*. I infected flies using both a high (OD_{600} = 0.05) and a low (OD_{600} = 0.005) dose of the *M. abscessus* type strain (ATCC 19977), and with

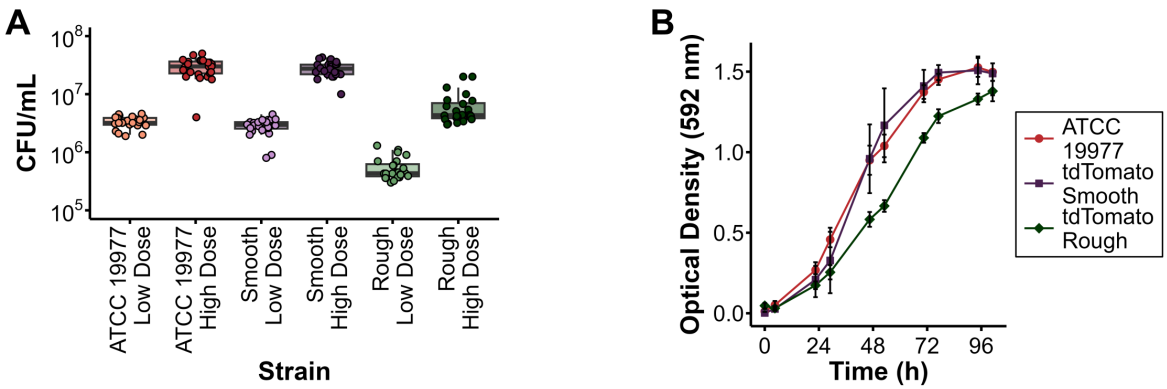


Figure 3.3. *In vitro* growth characteristics of *M. abscessus* morphotypes. (**A**) The number of colony forming units per mL in initial *M. abscessus* inoculum preparation for ATCC 19977 (red), tdTomato Smooth (purple) and tdTomato Rough (green) at high (OD_{600} = 0.05) and low (OD_{600} = 0.005) doses. Data represent the mean ± s.d of three independent experiments, n = 24 per group. (**B**) *In vitro* growth of *M. abscessus* strains ATCC 19977 (red), tdTomato Smooth (purple), and tdTomato Rough (green), grown in 7H9 at 37°C shaking, growth measured by absorbance at OD_{592}. Data represents the mean ± s.d of four technical replicates, and is representative of three independent experiments.

the two isogenic morphotype variants tdTomato Smooth and tdTomato Rough, which would allow me to identify any differences in fly survival and if any such differences were associated with a specific *M. abscessus* morphotype. I began by considering the Toll pathway, which is essential for the *D. melanogaster* response against Gram-positive bacteria and fungi. Despite *Mycobacteria* being phylogenetically more closely related to other Gram-positive bacterial species[586], *Mycobacteria* species produce *meso*-DAP type peptidoglycan[520,521,587,588], rather than Lys-type peptidoglycan typical for Gram-positive bacteria. Because of this it was unclear if the Toll pathway would be responsible for the initial detection and response to *M. abscessus* infection in *D. melanogaster*[356,394,517,589].

The fly line I used to assess the role of Toll signalling during *M. abscessus* infection was Dif^1, a line with a loss-of-function allele in the gene *Dif*, encoding the transcription factor responsible for transcription of Toll-pathway target genes[590]. I observed that Dif^1 flies displayed no difference in survival when infected with *M. abscessus* ATCC 19977 (Figure 3.4A), tdTomato Smooth (Figure 3.4B), or tdTomato Rough (Figure 3.4C) at either high or low infection doses when compared to w^{1118} flies. This suggests that either *M. abscessus* is not being detected by the

Toll signalling system, possibly due to immune evasion techniques by the bacteria, or that whatever response is induced by Toll signalling during an *M. abscessus* infection is insufficient to have any control on *M. abscessus in vivo* growth and thus have no impact on the outcome of the infection.

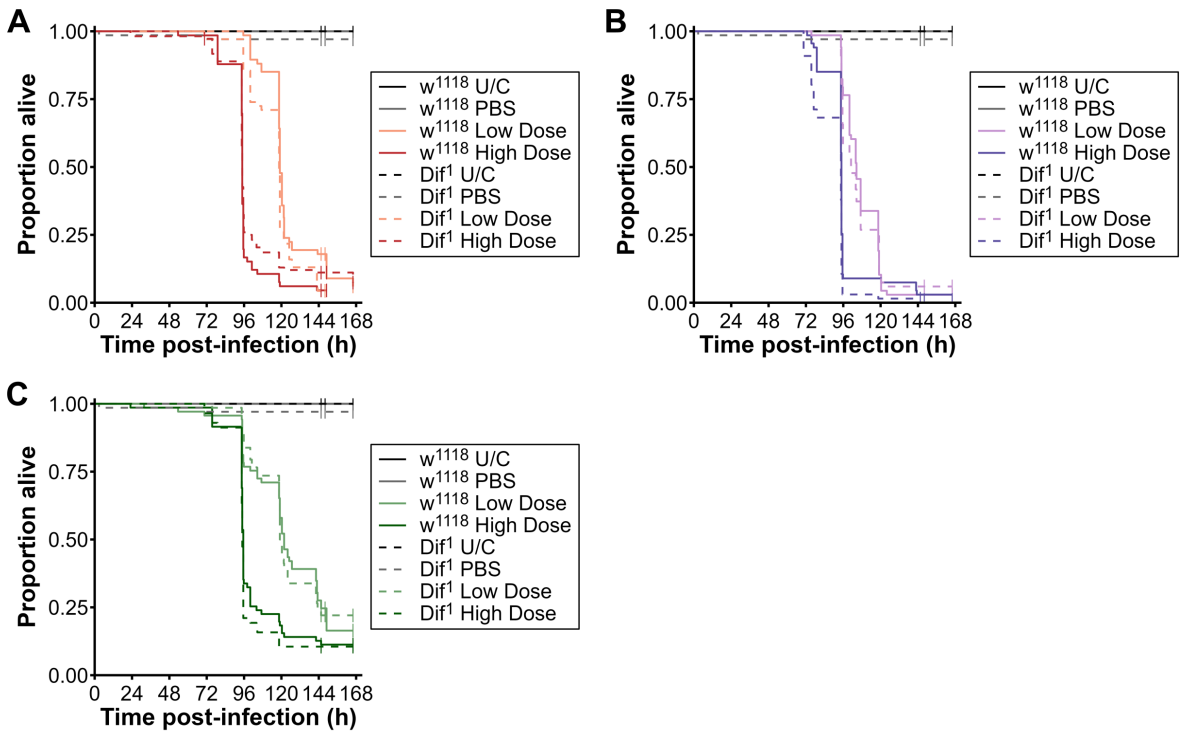


Figure 3.4. Survival of *Dif*^{1} flies with *M. abscessus*. Survival of *w*^{1118} (solid lines) and *Dif*^{1} (dashed lines) *D. melanogaster* when infected with either a high (OD_{600} = 0.05, dark colour) or a low (OD_{600} = 0.005, light colour) dose of *M. abscessus* (**A**) ATCC 19977 (red, orange), (**B**) tdTomato Smooth (dark purple, light purple), or (**C**) tdTomato Rough (dark green, light green). Data is pooled from three independent experiments, experiments shown in **A**, **B**, and **C** were performed with common controls, PBS Tween80 0.1% sterile injury control (grey), or uninjected control (U/C, black). $110 \geq n \geq 65$ per group, groups were compared using Log-Rank test.

To establish whether the Toll signalling pathway was being activated by *M. abscessus* infection or not, I used RT-qPCR to assess transcript levels of AMPs typically associated with Toll pathway activation at different time points during an *M. abscessus* infection. *w*^{1118} flies were infected with the high dose of *M. abscessus* ATCC 19977 and collected at 6 hours, 48 hours, and 80 hours post-infection in order to see immune responses that would be associated with initial detection of the bacteria during the early 6 hour timepoint, and also late-stage infection

responses shortly before the flies begin dying at 96 hours post-infection. For the AMPs *Drosomycin* (*Drs*) (Figure 3.5A) and *Metchnikowin* (*Mtk*) (Figure 3.5B), there was no early response at 6 hours post-infection, with transcripts of neither of these AMPs increasing beyond the levels seen in the sterile injury control group. By 48 hours post-infection transcript levels of these AMPs are beginning to increase above that of the sterile injury control group, which then increases further by 80 hours post-infection. For the other AMPs *Cecropin A1* (*CecA1*) (Figure 3.5C) and *Defensin* (*Def*) (Figure 3.5D), both of which can also be induced via Imd pathway signalling, there is little to no transcriptional response, with only a small increase in *CecA1* transcript levels at 80 hours post-infection. These data suggest that there is very little activation of the canonical Toll pathway AMPs during the initial phase of the *M. abscessus* infection. During an infection with a classic Toll pathway activator, such as *Staphylococcus aureus*, there is a strong early response 6 - 12 hours post-infection resulting in high AMP transcript levels. It is not until later in the *M. abscessus* infection that signs of Toll pathway activation are seen, which may be due to detection of *M. abscessus* peptidoglycans by the Toll PRRs, or possibly alternative mechanisms of Toll pathway activation.

3.3.2.2 Bomanin antibacterial effectors and Immune-induced molecules

Next, I tested if other antibacterial effectors of the Toll pathway besides the AMPs were being activated during an *M. abscessus* infection, such as the Bomanin peptides. These effectors lack sequence similarity to other AMPs and are specific to the genus *Drosophila*, but have been found to be important in the *D. melanogaster* immune response against fungi and some bacterial species, such as *E. faecalis*[348]. To test if the Bomanin peptides were involved in the *D. melanogaster* response to *M. abscessus* I infected $Bom^{\Delta 55c}$, a line with a 9 kb deletion encompassing ten of the twelve *Bom* genes[348]. When infected with *M. abscessus* ATCC 19977 at both the high and low dose (Figure 3.6A) there was no statistically significant difference between the w^{1118} and $Bom^{\Delta 55c}$ flies, but I observed a small fraction of the $Bom^{\Delta 55c}$ flies

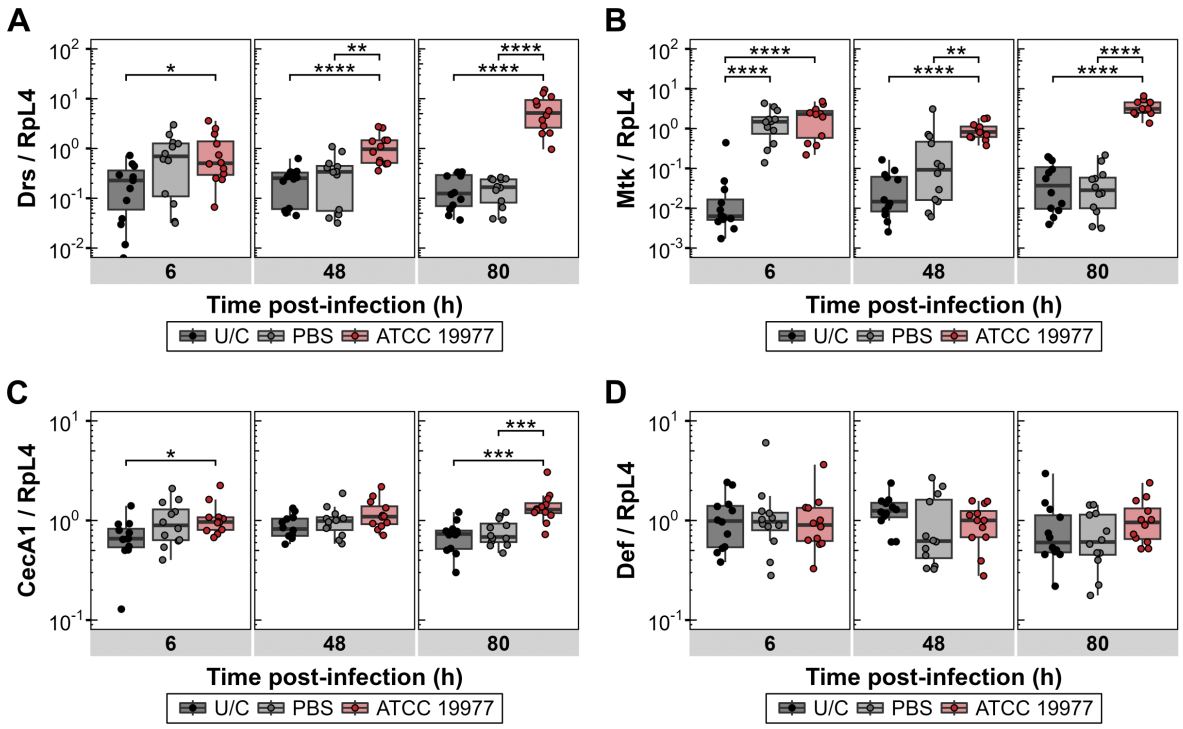


Figure 3.5. Transcript levels of canonical Toll pathway AMP during *M. abscessus* infection. RT-qPCR measurements of (**A**) *Drosomycin*, (**B**) *Metchnikowin*, (**C**) *Cecropin A1*, and (**D**) *Defensin*, normalised to housekeeping gene *RpL4*, of w^{1118} flies. Flies were uninjected (U/C, black), or injected with PBS Tween80 0.1% (grey) or *M. abscessus* ATCC 19977 OD_{600} = 0.05 (red) and transcript levels were measured at 6, 48, and 80 hours post-infection. Data is pooled from three independent experiments, n = 12 per group, statistical comparisons were made using Wilcoxon rank-sum test. This data shown is also shown in RT-qPCR experiments in Chapter 6, Figure 6.7 and Figure 6.8, as controls to compare *M. abscessus* knockout strains. ∗, P < 0.05; ∗∗, P < 0.01; ∗∗∗, P < 0.001; ∗∗∗∗, P < 0.0001.

surviving for approximately a day longer than the rest. This increase in $Bom^{\Delta 55c}$ survival was most strongly seen in flies infected with tdTomato Smooth (Figure 3.6B). There was no difference observed for the high-dose infected flies, but $Bom^{\Delta 55c}$ flies infected with low-dose tdTomato Smooth survived significantly longer (median time to death 118.17 hours) than the w^{1118} group (median time to death 100.75 hours, P = 6.9e-06). A slight difference in survival was also seen in flies infected with tdTomato Rough (Figure 3.6C), however in this case there was no difference between flies infected with the low dose. Instead, $Bom^{\Delta 55c}$ flies infected with high dose tdTomato Rough were surviving significantly longer than the w^{1118} group (P = 8.4e-05). The lack of consistency between increased survival in the $Bom^{\Delta 55c}$ flies during

M. abscessus infection depending on morphotype and dose makes this phenotype difficult to fully understand, possibly the level of Bomanin activity is highly variable during the infection. Nevertheless, these data suggest that during an *M. abscessus* infection there is activation of Bomanin peptides to some degree, and the activity of these peptides is detrimental to the host as lacking these peptides is leading to increases in survival time.

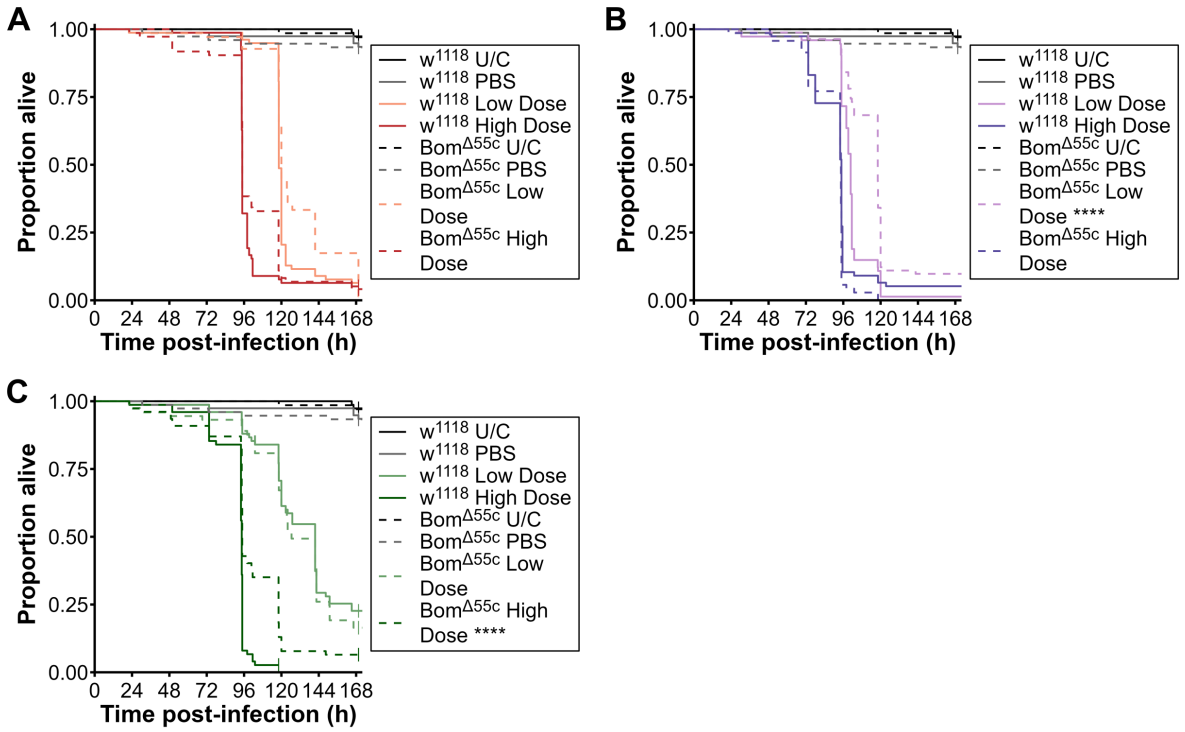


Figure 3.6. Survival of *Bom*$^{\Delta 55c}$ flies with *M. abscessus*. Survival of *w*^{1118} (solid lines) and *Bom*$^{\Delta 55c}$ (dashed lines) *D. melanogaster* when infected with either a high (OD_{600} = 0.05, dark colour) or a low (OD_{600} = 0.005, light colour) dose of *M. abscessus* (**A**) ATCC 19977 (red, orange), (**B**) tdTomato Smooth (dark purple, light purple), or (**C**) tdTomato Rough (dark green, light green). Data is pooled from three independent experiments, experiments shown in **A**, **B**, and **C** were performed with common controls, PBS Tween80 0.1% sterile injury control (grey), or uninjected control (U/C, black). $84 \geq n \geq 68$ per group, groups were compared using Log-Rank test. Asterisks in the legend indicate the *p*-value compared to *w*^{1118} flies infected with the same *M. abscessus* strain and dose. $*$, $P < 0.05$; $**$, $P < 0.01$; $***$, $P < 0.001$; $****$, $P < 0.0001$.

I measured transcript levels of *Bom* genes *IM1*, also known as *BomS1*, (Figure 3.7A), and *IM2*, also known as *BomS2*, (Figure 3.7B). Both showed an increasing trend of transcript levels in the *M. abscessus* ATCC 19977 infected flies slightly above the level of the sterile injury control group at 6 hours post-infection, despite not being statistically significant, suggesting that there is

some level of detection of *M. abscessus* by the Toll pathway during the early stages of infection. The levels of these transcripts then continue to increase steadily over the course of the infection in infected flies. I also considered transcript levels of *IM4*, also known as *Daisho1*, (Figure 3.7C), and *IM10*, encoded within *BaraA*, both of which are also regulated by the Toll pathway and are involved in the *D. melanogaster* antifungal response, but are not considered Bomanins as they lack the CXXC motif[348,591,592]. These showed the same pattern of expression as the *Bom* genes, with flies infected with ATCC 19977 showing a slight increase in transcript levels above that of sterile injury controls at 6 hours post-infection, which continues to increase gradually over time. This suggests that *M. abscessus* is being detected by *D. melanogaster* during the early stages of infection, and inducing effectors via Toll signalling that are typically considered to be antifungal.

3.3.2.3 Melanisation response

The *D. melanogaster* melanisation pathway can be triggered by the same PRRs that detect Gram-positive bacteria and fungi upstream of Toll signalling, PGRP-SA and GNBP1. Additionally, the serine proteases that regulate melanisation, such as Sp7, are themselves regulated by other serine proteases capable of activating the Toll pathway, such as ModSP and Serpin27A[366,368,383,389]. Given the transcription of Toll pathway AMPs late during *M. abscessus* infection but lack of survival difference in Toll pathway mutant flies, I wanted to assess the possible role of melanisation during an *M. abscessus* infection. I infected the $PPO1^{\Delta}$, $PPO2^{\Delta}$ double mutant fly line, as these are the two *PPO* genes responsible for all PO activity within adult *D. melanogaster* which occurs in the haemolymph[383]. Similar to the phenotype observed in Dif^{1} flies, there was no difference in survival between $PPO1^{\Delta}$, $PPO2^{\Delta}$ and w^{1118} flies when infected with either a high or low dose of *M. abscessus* ATCC19977 (Figure 3.8A), tdTomato Smooth (Figure 3.8B), or tdTomato Rough (Figure 3.8C). While I cannot conclude whether or not the melanisation cascade is being activated concurrently with the

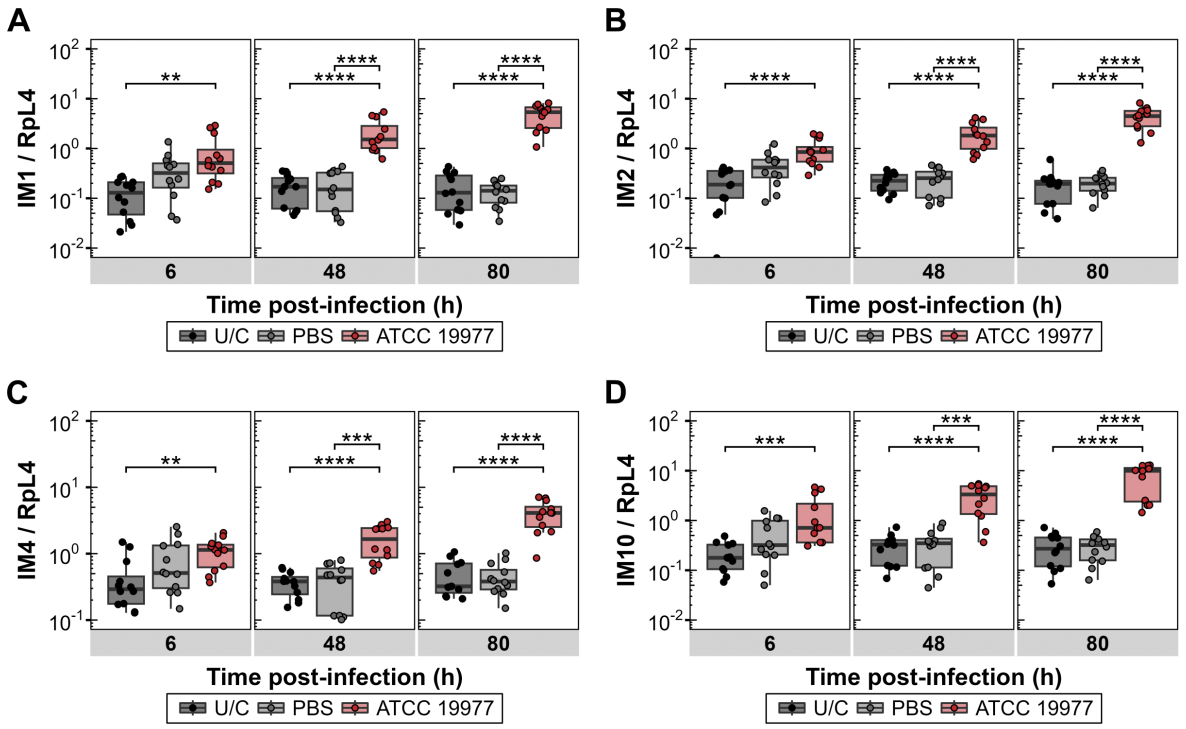


Figure 3.7. Transcript levels of Bomanins and Immune-induced molecules during *M. abscessus* infection. RT-qPCR measurements of (**A**) *IM1*, (**B**) *IM2*, (**C**) *IM4*, and (**D**) *IM10*, normalised to housekeeping gene *RpL4*, of w^{1118} flies. Flies were uninjected (U/C, black), or injected with PBS Tween80 0.1% (grey) or *M. abscessus* ATCC 19977 OD_{600} = 0.05 (red) and transcript levels were measured at 6, 48, and 80 hours post-infection. Data is pooled from three independent experiments, n = 12 per group, statistical comparisons were made using Wilcoxon rank-sum test. This data shown is also shown in RT-qPCR experiments in Chapter 6, Figure 6.7, as controls to compare *M. abscessus* knockout strains. $*$, P < 0.05; $**$, P < 0.01; $***$, P < 0.001; $****$, P < 0.0001.

Toll pathway during *M. abscessus* infection, if there is any melanisation activity it is clearly insufficient to have any impact on the outcome of the *M. abscessus* infection in *D. melanogaster*.

3.3.3 Activation of Imd pathway signalling during *M. abscessus* infection.

The Imd signalling pathway represents the other major branch of the humoral immune response in *D. melanogaster* and is considered to resemble the mammalian tumour necrosis factor receptor pathway. It is typically associated with the detection of Gram-negative bacteria due to activation upon detection of DAP-type peptidoglycan by PRRs PGRP-LC and PGRP-LE. As *M. abscessus* produces *m*-DAP-type peptidoglycan, I felt it was important to also identify any possible response to *M. abscessus* infection by the Imd pathway. Infections were performed using the imd^{10191} line, a loss of function allele caused by a frameshift in the coding region due to

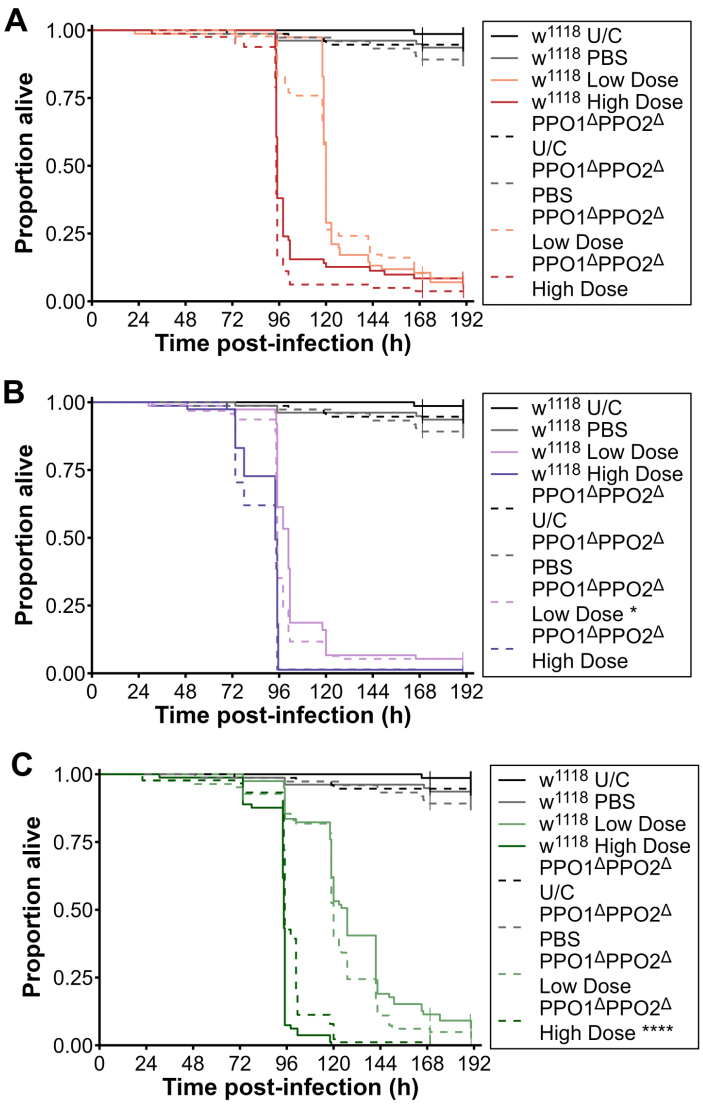


Figure 3.8. Survival of *PPO1*$^{\Delta}$*, PPO2*$^{\Delta}$ flies with *M. abscessus*. Survival of *w*^{1118} (solid lines) and *PPO1*$^{\Delta}$*, PPO2*$^{\Delta}$ (dashed lines) *D. melanogaster* when infected with either a high (OD_{600} = 0.05, dark colour) or a low (OD_{600} = 0.005, light colour) dose of *M. abscessus* (**A**) ATCC 19977 (red, orange), (**B**) tdTomato Smooth (dark purple, light purple), or (**C**) tdTomato Rough (dark green, light green). Data is pooled from three independent experiments, experiments shown in **A**, **B**, and **C** were performed with common controls, PBS Tween80 0.1% sterile injury control (grey), or uninjected control (U/C, black). $94 \geq n \geq 71$ per group, groups were compared using Log-Rank test. Asterisks in the legend indicate the *p*-value compared to *w*^{1118} flies infected with the same *M. abscessus* strain and dose. $*$, $P < 0.05$; $**$, $P < 0.01$; $***$, $P < 0.001$; $****$, $P < 0.0001$.

a 26-bp deletion, resulting in significantly increased sensitivity to infection with Gram-negative bacteria[593]. As with the Toll pathway mutant lines tested, there was no survival difference in *imd*^{10191} flies compared to wild-type flies when infected with *M. abscessus* for either the smooth or the rough morphotypes, with either a high or a low dose (Figure 3.9).

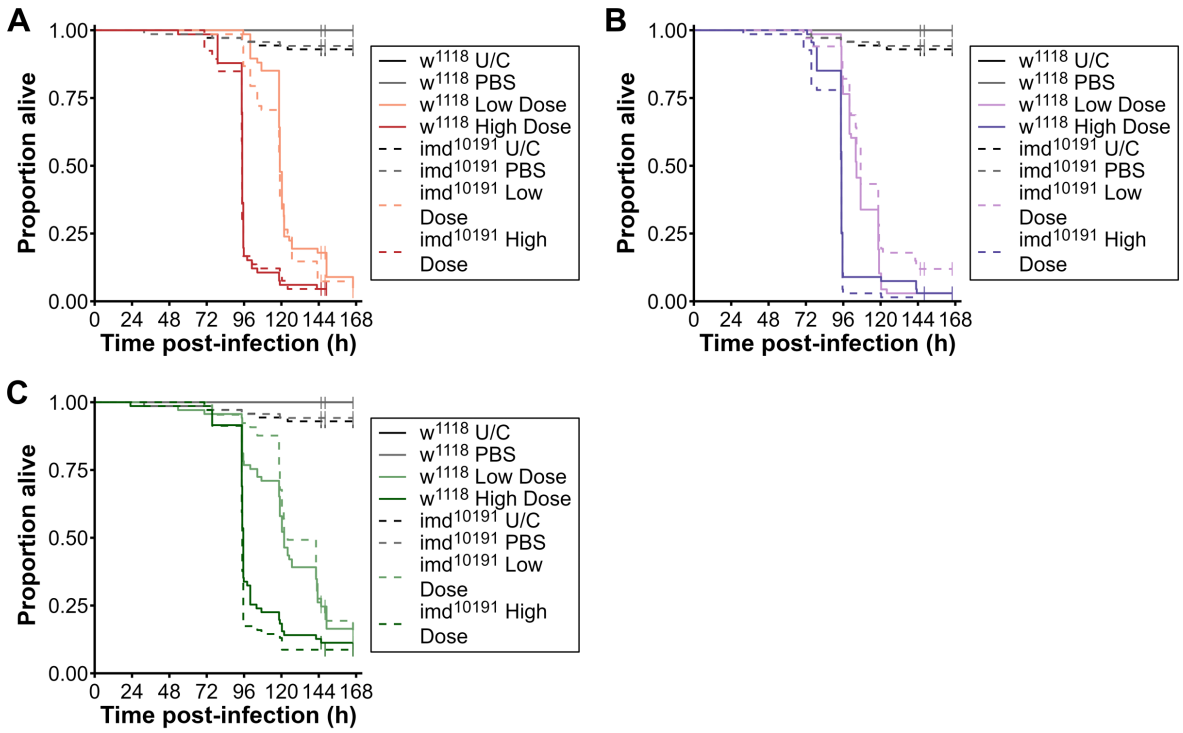


Figure 3.9. Survival of *imd*^{10191} flies with *M. abscessus*. Survival of *w*^{1118} (solid lines) and *imd*^{10191} (dashed lines) *D. melanogaster* when infected with either a high (OD_{600} = 0.05, dark colour) or a low (OD_{600} = 0.005, light colour) dose of *M. abscessus* (**A**) ATCC 19977 (red, orange), (**B**) tdTomato Smooth (dark purple, light purple), or (**C**) tdTomato Rough (dark green, light green). Data is pooled from three independent experiments, experiments shown in **A**, **B**, and **C** were performed with common controls, PBS Tween80 0.1% sterile injury control (grey), or uninjected control (U/C, black). $71 \geq n \geq 65$ per group, groups were compared using Log-Rank test.

Interestingly, with regards to the transcriptional response of Imd pathway-associated AMPs, whilst there was an increase in transcription of these AMPs, it occurred later during the infection compared to the Toll pathway-associated AMPs and Bomanins. For all of the Toll pathway genes that showed transcriptional activation during *M. abscessus* infection (all except Cecropin A1 and Defensin, both of which can also be induced by the Imd pathway), the transcript levels were increased for *M. abscessus* infected flies compared with PBS sterile-injury control flies by 48 hours post-infection. For the Imd pathway AMP transcript levels, only Attacin shows a statistically significant increase in *M. abscessus* flies compared to PBS control flies at 48 hours post-infection (Figure 3.10 A), the other AMP genes are only increased in *M. abscessus* flies at 80 hours post-infection (Figure 3.10 B, C).

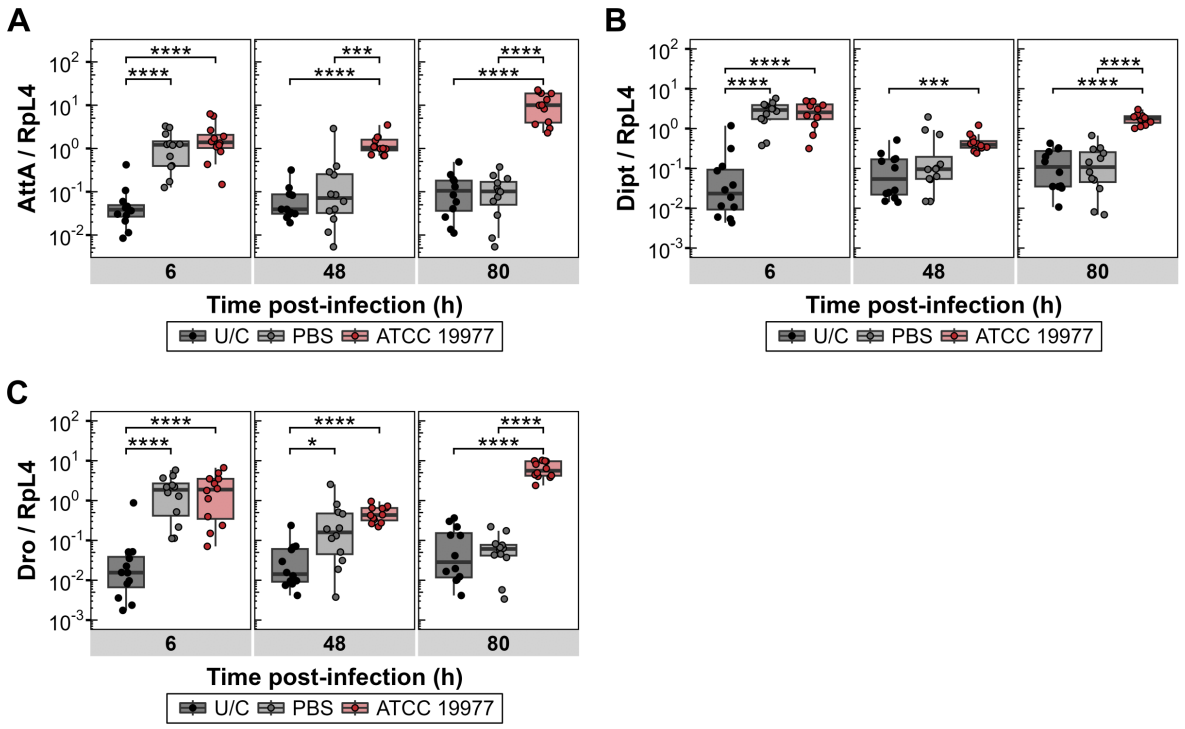


Figure 3.10. Transcript levels of canonical Imd pathway AMPs during *M. abscessus* infection. RT-qPCR measurements of (**A**) *Attacin*, (**B**) *Diptericin*, and (**C**) *Drosocin*, normalised to housekeeping gene *RpL4*, of w^{1118} flies. Flies were uninjected (U/C, black), or injected with PBS Tween80 0.1% (grey) or *M. abscessus* ATCC 19977 OD_{600} = 0.05 (red) and transcript levels were measured at 6, 48, and 80 hours post-infection. Data is pooled from three independent experiments, n = 12 per group, statistical comparisons were made using Wilcoxon rank-sum test. This data shown is also shown in RT-qPCR experiments in Chapter 6, Figure 6.8, as controls to compare *M. abscessus* knockout strains. ∗, P < 0.05; ∗∗, P < 0.01; ∗∗∗, P < 0.001; ∗∗∗∗, P < 0.0001.

I also decided to infect flies with mutations in *Tak1*, the *D. melanogaster* homologue of MAP kinase kinase kinase, which is involved in both Imd signalling as well as JNK activation. For this I used the $Tak1^{1}$ line, which contains an amino acid replacement mutation (D159G) within the kinase domain and are highly susceptible to Gram-negative bacterial infections, with no difference in survival compared to wild-type flies when infected with Gram-positive or fungal infections[404,409,594]. As with the survival of imd^{10191} flies, $Tak1^{1}$ flies showed no differences in survival compared to w^{1118} wild-type flies during infection with *M. abscessus* when infected with either morphotype or either dose (Figure 3.11), consistent with the imd^{10191} survival results.

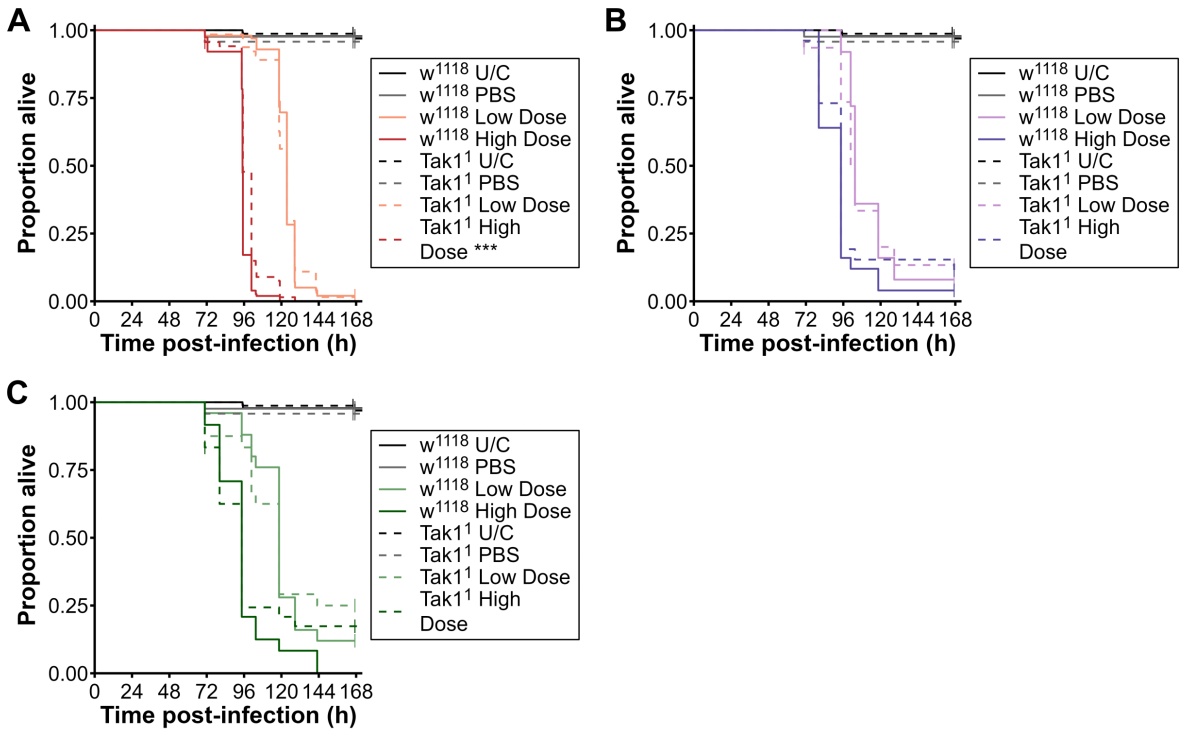


Figure 3.11. Survival of *Tak1*^{1} flies with *M. abscessus*. Survival of *w*^{1118} (solid lines) and *Tak1*^{1} (dashed lines) *D. melanogaster* when infected with either a high (OD_{600} = 0.05, dark colour) or a low (OD_{600} = 0.005, light colour) dose of *M. abscessus* (**A**) ATCC 19977 (red, orange), (**B**) tdTomato Smooth (dark purple, light purple), or (**C**) tdTomato Rough (dark green, light green). For **A**, data is pooled from three independent experiments, $64 \geq n \geq 127$ per group. For **B** and **C** data represents one independent experiment, $24 \geq n \geq 32$ per group. Experiments shown in **A**, **B**, and **C** were performed with common controls, PBS Tween80 0.1% sterile injury control (grey), or uninjected control (U/C, black). Groups were compared using Log-Rank test.

3.3.4 Eiger signalling during *M. abscessus* infection

Following the survivals with *Tak1*^{1} mutant *D. melanogaster*, I examined the role of TNFα and JNK signalling in *D. melanogaster* during *M. abscessus* infection. TNFα and JNK signalling play important protective roles against *M. abscessus* in infected host cells. This is in contrast to previous work in *D. melanogaster* that found flies with mutations in *egr*, the TNF homologue, were longer lived compared to wild-type flies when infected with *M. marinum*[452], however, this study made use of the *egr*^{1} and *egr*^{3} mutant alleles which carried additional mutations in NimC1[455]. To study the role of *D. melanogaster* TNF signalling during *M. abscessus* infection, I made use of the *egr*^{1ag} and *egr*^{3ag} lines, derived from *egr*^{1} and *egr*^{3} respectively, carrying deletions in the first coding exon of *egr* but retaining *NimC1*[455]. For *egr*^{1ag}, there was no

difference in survival compared to w^{1118} in any of the *M. abscessus* infection conditions (Figure 3.12A - C), which is unsurprising considering the $Tak1^{1}$ survival results.

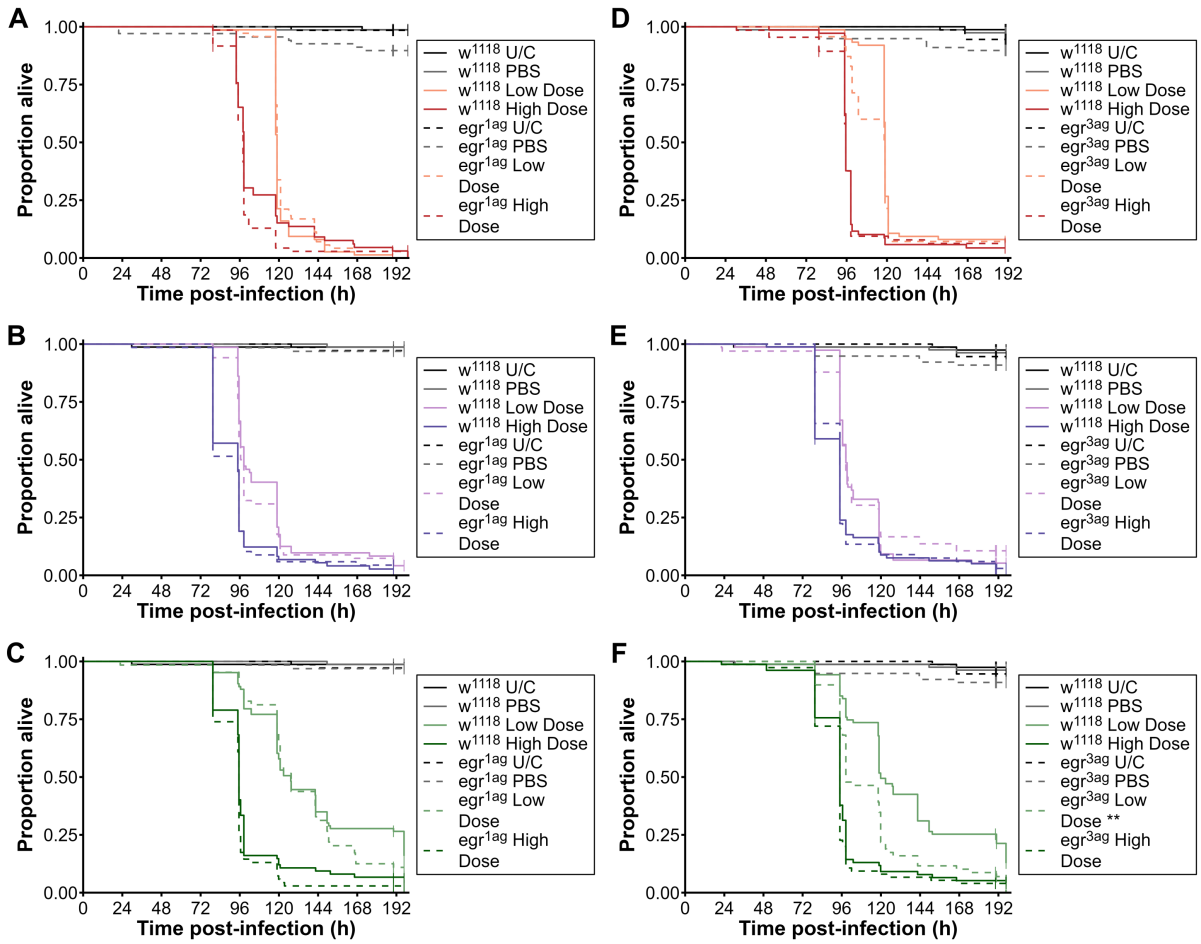


Figure 3.12. Survival of *egr*^{1ag} and *egr*^{3ag} flies with *M. abscessus*. (**A - C**) Survival of w^{1118} (solid lines) and *egr*^{1ag} (dashed lines) *D. melanogaster* when infected with either a high (OD_{600} = 0.05, dark colour) or a low (OD_{600} = 0.005, light colour) dose of *M. abscessus* (**A**) ATCC 19977 (red, orange), (**B**) tdTomato Smooth (dark purple, light purple), or (**C**) tdTomato Rough (dark green, light green). (**D - F**) Survival of w^{1118} (solid lines) and *egr*^{3ag} (dashed lines) *D. melanogaster* when infected with either a high (OD_{600} = 0.05, dark colour) or a low (OD_{600} = 0.005, light colour) dose of *M. abscessus* (**D**) ATCC 19977 (red, orange), (**E**) tdTomato Smooth (dark purple, light purple), or (**F**) tdTomato Rough (dark green, light green). Data is pooled from three independent experiments, experiments shown in **A**, **B**, **C**, **D**, **E**, and **F** were performed with common controls, PBS Tween80 0.1% sterile injury control (grey), or uninjected control (U/C, black). $87 \geq n \geq 64$ per group, groups were compared using Log-Rank test. Asterisks in the legend indicate the *p*-value compared to w^{1118} flies infected with the same *M. abscessus* strain and dose. $*$, $P < 0.05$; $**$, $P < 0.01$; $***$, $P < 0.001$; $****$, $P < 0.0001$.

egr^{3ag} also displayed no survival difference when infected with *M. abscessus* ATCC 19977 (Figure 3.12D) or tdTomato Smooth (Figure 3.12E), however at the low dose of tdTomato Rough the median survival time was reduced to 98.50 hours post-infection in *egr*^{3ag} flies compared to

119.83 hours post-infection in w^{1118} flies (Figure 3.12F). This would suggest that Egr is mildly protective against low doses of rough morphotype *M. abscessus*, however, as this does not occur in both Egr mutant *D. melanogaster* lines I cannot exclude the possibility that this result is an artefact caused by unknown problems in the egr^{3ag} line.

I used RT-qPCR to assess if there was any transcriptional evidence of Egr signalling, by measuring transcripts of *egr-RA* (Figure 3.13A), one of the two *egr* splice variants, and *Tace* (Figure 3.13B), which cleaves and releases a soluble form of Egr from the surface of the fat body. *Tace* expression has been previously shown to increase within the fat body in response to amino acid restriction[421]. There was no detectable change in transcript levels of either *egr-RA* or *Tace* in response to *M. abscessus* infection at any point in the course of the infection. This may be due to Egr that has already been produced being released during infection with no requirement for new mRNA transcripts and production, and that transcriptional changes of *Tace* within the fat body are relatively small and not observed when measuring transcripts from the whole fly. Equally, there may simply be no signalling via Egr during an *M. abscessus* infection.

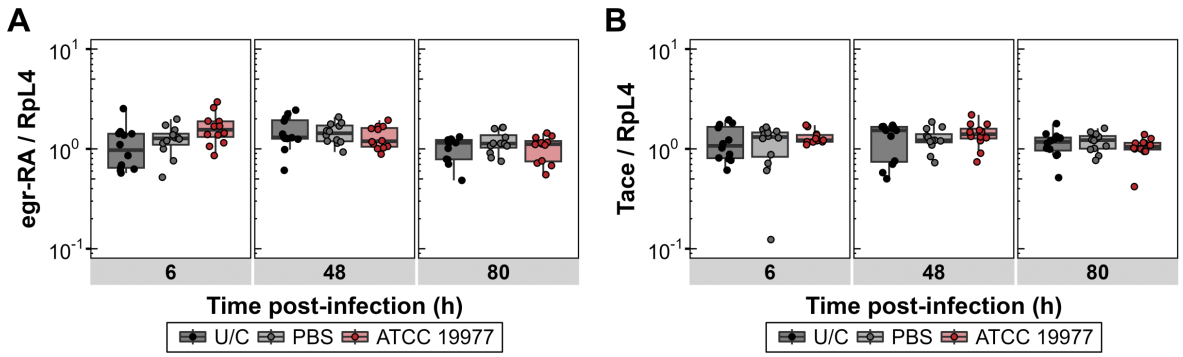


Figure 3.13. Transcript levels of *egr-RA* and *Tace* during *M. abscessus* infection. RT-qPCR measurements of (**A**) *egr-RA*, and (**B**) *Tace* normalised to housekeeping gene *RpL4*, of w^{1118} flies. Flies were uninjected (U/C, black), or injected with PBS Tween80 0.1% (grey) or *M. abscessus* ATCC 19977 OD_{600} = 0.05 (red) and transcript levels were measured at 6, 48, and 80 hours post-infection. Data is pooled from three independent experiments, n = 12 per group, statistical comparisons were made using one-way ANOVA with Tukey's test. This data shown is also shown in RT-qPCR experiments in Chapter 6, Figure 6.9, as controls to compare *M. abscessus* knockout strains.

3.3.5 Cytokine signalling during *M. abscessus* infection.

The final *D. melanogaster* immune signalling pathway I tested for a role in *M. abscessus* infection was the JAK/STAT signalling pathway. In *D. melanogaster*, JAK/STAT signalling by Upd ligands plays an important role in innate immune signalling and metabolic changes during an infection by causing dILP secretion[471,472]. During *M. marinum* infection in *D. melanogaster*, Upd3 activity promotes intracellular mycobacterial growth by inhibiting *Atg2* expression and leading to dysregulation of intracellular lipid droplets[470]. Mutations in *upd3* subsequently increased host survival and reduced *M. marinum* burden during the infection[470]. I therefore wanted to assess if the same phenotype could be seen during *M. abscessus* infection. For these survivals I made use of the *Upd2*$^{\Delta}$ line which contains a 4.7 kb deletion removing the *upd2* coding region, the *Upd3*$^{\Delta}$ line with a 13.5 kb deletion removing the first three exons of *upd3*[595] and an *Upd2*$^{\Delta}$ *Upd3*$^{\Delta}$ double mutant. Unlike *M. marinum* infection in which *Upd3*$^{\Delta}$ flies are longer lived than wild-type flies, there was no change in survival for the *Upd2*$^{\Delta}$ (Figure 3.14A - C), *Upd3*$^{\Delta}$ (Figure 3.14D - F), or *Upd2*$^{\Delta}$ *Upd3*$^{\Delta}$ (Figure 3.14G - I) mutant flies compared to wild-type during *M. abscessus* infection. This was true for both the smooth and the rough morphotype at either a high or a low injection dose.

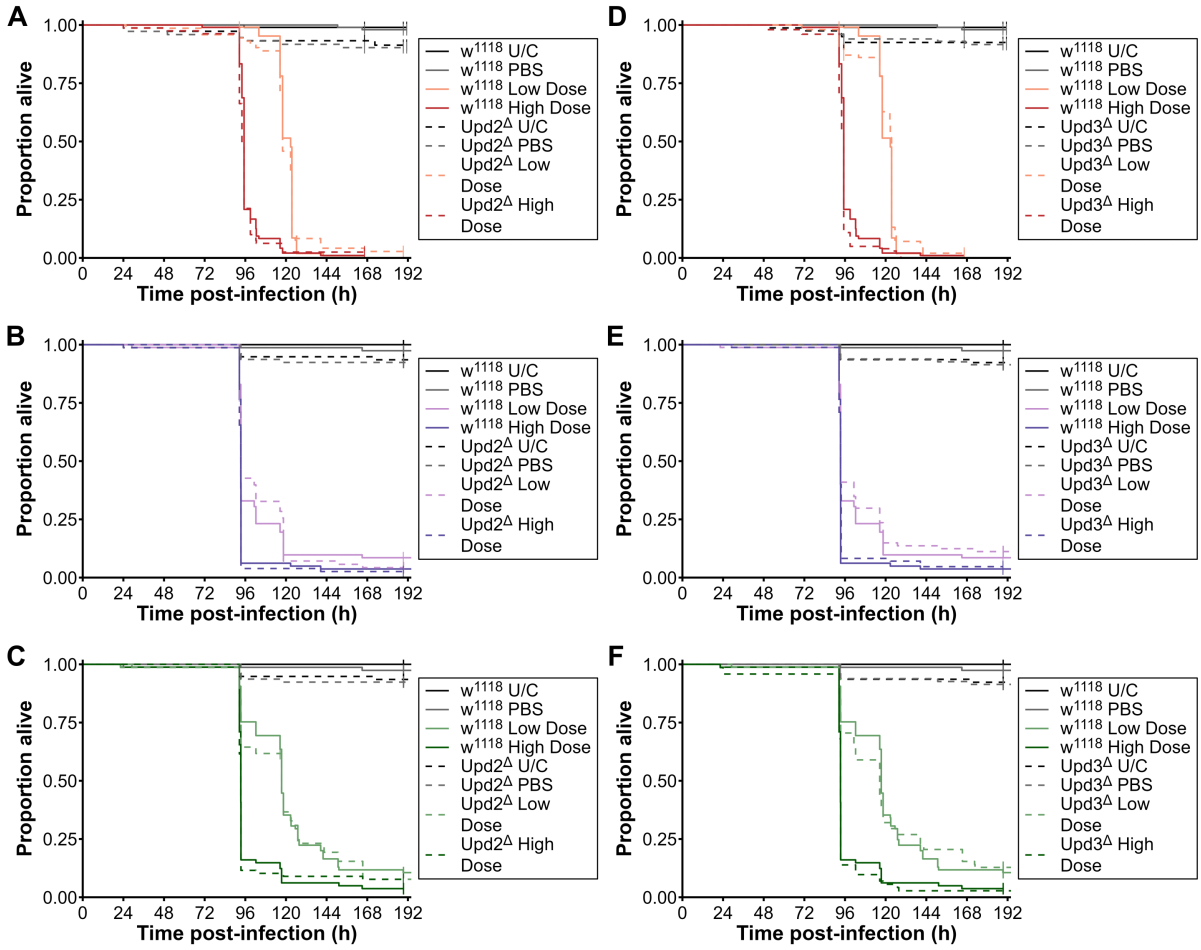


Figure 3.14. Survival of *Upd2*$^{\Delta}$, *Upd3*$^{\Delta}$, and *Upd2*$^{\Delta}$ *Upd3*$^{\Delta}$ flies with *M. abscessus*. (**A - F**) See legend on page 154.

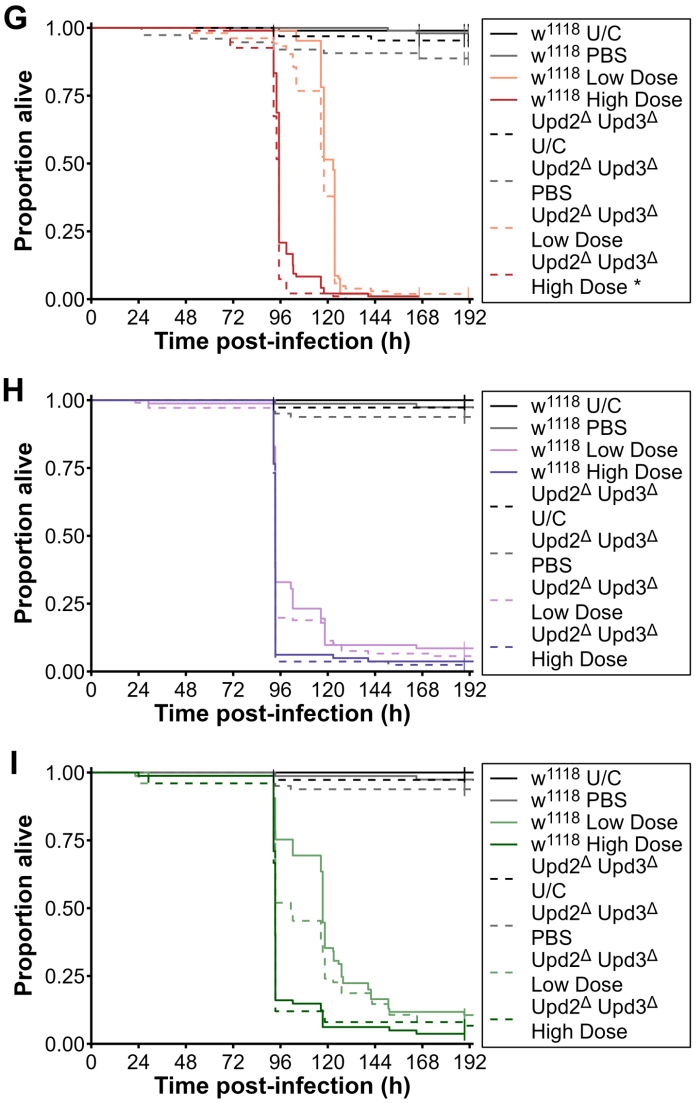


Figure 3.14. Survival of *Upd2*$^{\Delta}$, *Upd3*$^{\Delta}$, and *Upd2*$^{\Delta}$ *Upd3*$^{\Delta}$ flies with *M. abscessus* continued. (**A - C**) Survival of *w*^{1118} (solid lines) and *Upd2*$^{\Delta}$ (dashed lines) *D. melanogaster* when infected with either a high (OD_{600} = 0.05, dark colour) or a low (OD_{600} = 0.005, light colour) dose of *M. abscessus* (**A**) ATCC 19977 (red, orange), (**B**) tdTomato Smooth (dark purple, light purple), or (**C**) tdTomato Rough (dark green, light green). (**D - F**) Survival of *w*^{1118} (solid lines) and *Upd3*$^{\Delta}$ (dashed lines) *D. melanogaster* when infected with either a high (OD_{600} = 0.05, dark colour) or a low (OD_{600} = 0.005, light colour) dose of *M. abscessus* (**D**) ATCC 19977 (red, orange), (**E**) tdTomato Smooth (dark purple, light purple), or (**F**) tdTomato Rough (dark green, light green). (**G - I**) Survival of *w*^{1118} (solid lines) and *Upd2*$^{\Delta}$ *Upd3*$^{\Delta}$ (dashed lines) *D. melanogaster* when infected with either a high (OD_{600} = 0.05, dark colour) or a low (OD_{600} = 0.005, light colour) dose of *M. abscessus* (**G**) ATCC 19977 (red, orange), (**H**) tdTomato Smooth (dark purple, light purple), or (**I**) tdTomato Rough (dark green, light green). Data is pooled from three independent experiments, experiments shown in **A**, **B**, **C**, **D**, **E**, **F**, **G**, **H**, and **I** were performed with common controls, PBS Tween80 0.1% sterile injury control (grey), or uninjected control (U/C, black). $109 \geq n \geq 65$ per group, groups were compared using Log-Rank test. Asterisks in the legend indicate the *p*-value compared to *w*^{1118} flies infected with the same *M. abscessus* strain and dose. $*$, $P < 0.05$; $**$, $P < 0.01$; $***$, $P < 0.001$; $****$, $P < 0.0001$.

The previous study of *M. marinum* infection in *D. melanogaster* found a strong increase in the transcription of *upd3* during infection, which impaired *Atg2* expression[470]. I used RT-qPCR to measure the transcriptional response of multiple genes involved in JAK/STAT signalling in *D. melanogaster* to identify any transcriptional changes occurring during *M. abscessus* infection, including *upd2*, *upd3*, the JAK/STAT negative regulator *Socs36E* and the transcription factor *Stat92E*. I also measured transcript levels of *Atg2* and *Turnadot A* (*TotA*), a stress protein expressed in the fat body by activation of JAK/STAT signalling[457]. At 48 hours post-infection, levels of *upd2* transcripts were decreased in *M. abscessus* infected flies, which then increased to levels slightly above the controls by 80 hours post-infection (Figure 3.15A). Expression of *upd3* showed a similar pattern, albeit not statistically significant (Figure 3.15B). *Socs36E* was also slightly increased at 80 hours post-infection, but again not significantly (Figure 3.15C). Comparison of *Stat92E* expression at 48 hours post-infection also revealed a very small decrease in *M. abscessus* infected flies compared to uninjected controls, but no differences later during infection (Figure 3.15D). Unsurprisingly, based on the survival phenotypes and lack of changes in *upd3* expression, there was no change in *Atg2* expression at any time point (Figure 3.15E). Additionally, at 80 hours post-infection, *TotA* expression was mildly increased in PBS sterile-injury flies and reduced in *M. abscessus* flies, relative to the uninfected controls (Figure 3.15F).

3.3.6 Uptake of *M. abscessus* by *D. melanogaster* haemocytes

Cellular immunity is another key aspect of *D. melanogaster* defence against pathogens. Since *M. abscessus* is an intracellular pathogen in amoeba and mammalian infection models, and *M. marinum* was shown to reside within *D. melanogaster* haemocytes and likely grow within them intracellularly, I wanted to confirm that the same process was occurring during *D. melanogaster* infection with *M. abscessus*. Additionally, visualising the location of *M. abscessus* throughout the infection would help direct tissue-specific genetic manipulation of

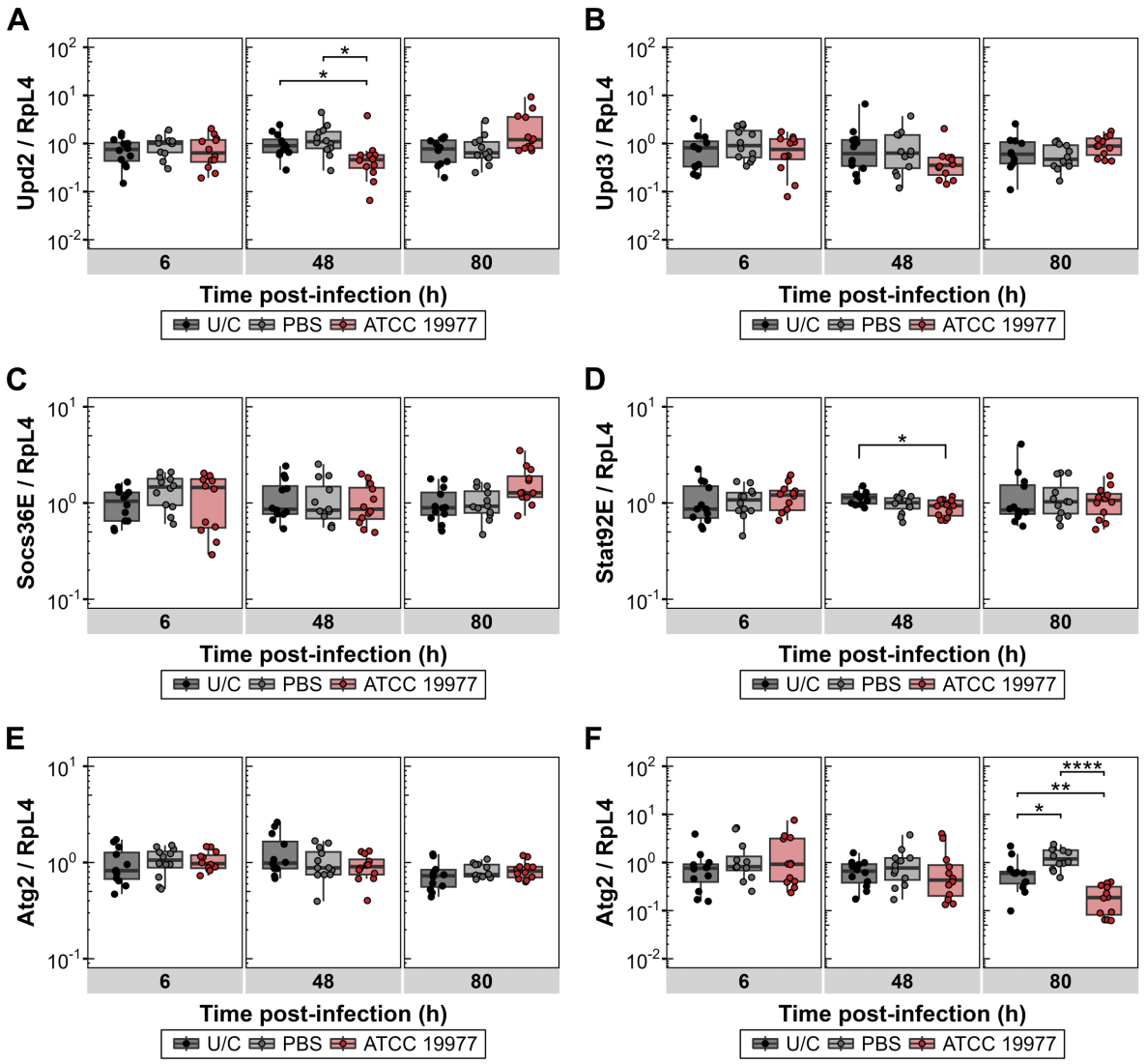


Figure 3.15. Transcript levels of cytokines and JAK/STAT targets during *M. abscessus* infection. RT-qPCR measurements of (**A**) *upd2*, (**B**) *upd3*, (**C**) *Socs36E*, (**D**) *Stat92E*, (**E**) *Atg2*, and (**F**) *TotA* normalised to housekeeping gene *RpL4*, of w^{1118} flies. Flies were uninjected (U/C, black), or injected with PBS Tween80 0.1% (grey) or *M. abscessus* ATCC 19977 OD_{600} = 0.05 (red) and transcript levels were measured at 6, 48, and 80 hours post-infection. Data is pooled from three independent experiments, n = 12 per group, statistical comparisons were made using Wilcoxon rank-sum test. This data shown is also shown in RT-qPCR experiments in Chapter 6, Figure 6.9, as controls to compare *M. abscessus* knockout strains. ∗, P < 0.05; ∗∗, P < 0.01; ∗∗∗, P < 0.001; ∗∗∗∗, P < 0.0001.

the host in future experiments. To achieve this I used a fly line with a haemocyte-specific driver inducing expression of GFP, *Hml$^{\Delta}$-Gal4, UAS-2x-eGFP*, and infected flies with the *M. abscessus* smooth and rough morphotype strains containing the fluorescent tdTomato plasmid, pTec27. Unfortunately, these experiments were performed prior to identifying the difference in the OD-CFU between the two *M. abscessus* morphotypes, and so both morphotypes were

injected into flies at an OD_{600} = 0.05. This equates to approximately 4-fold fewer *M. abscessus* tdTomato Rough being injected than *M. abscessus* tdTomato Smooth (Figure 3.3A).

Nevertheless, flies infected with both the tdTomato Rough (Figure 3.16A) and tdTomato Smooth (Figure 3.16B) show *M. abscessus* is present within haemocytes throughout the course of the infection. Red fluorescence appears to show *M. abscessus* internalised within intracellular vesicles inside haemocytes as early as 90 minutes post-infection, suggesting that *M. abscessus* is rapidly phagocytosed (shown in Figure S3.1). Levels of red fluorescence then appear to increase, in terms of intensity and the number of intracellular vesicles observed in haemocytes, from 24 hours post-infection through to 72 hours post-infection, indicating that *M. abscessus* is likely surviving within the intracellular environment, and possibly growing, although these images cannot exclude the possibility of continued *M. abscessus* uptake by haemocytes. Extracellular bacteria were also observed in one experiment in large numbers at 48 hours post-infection, however, I was unable to repeat this observation.

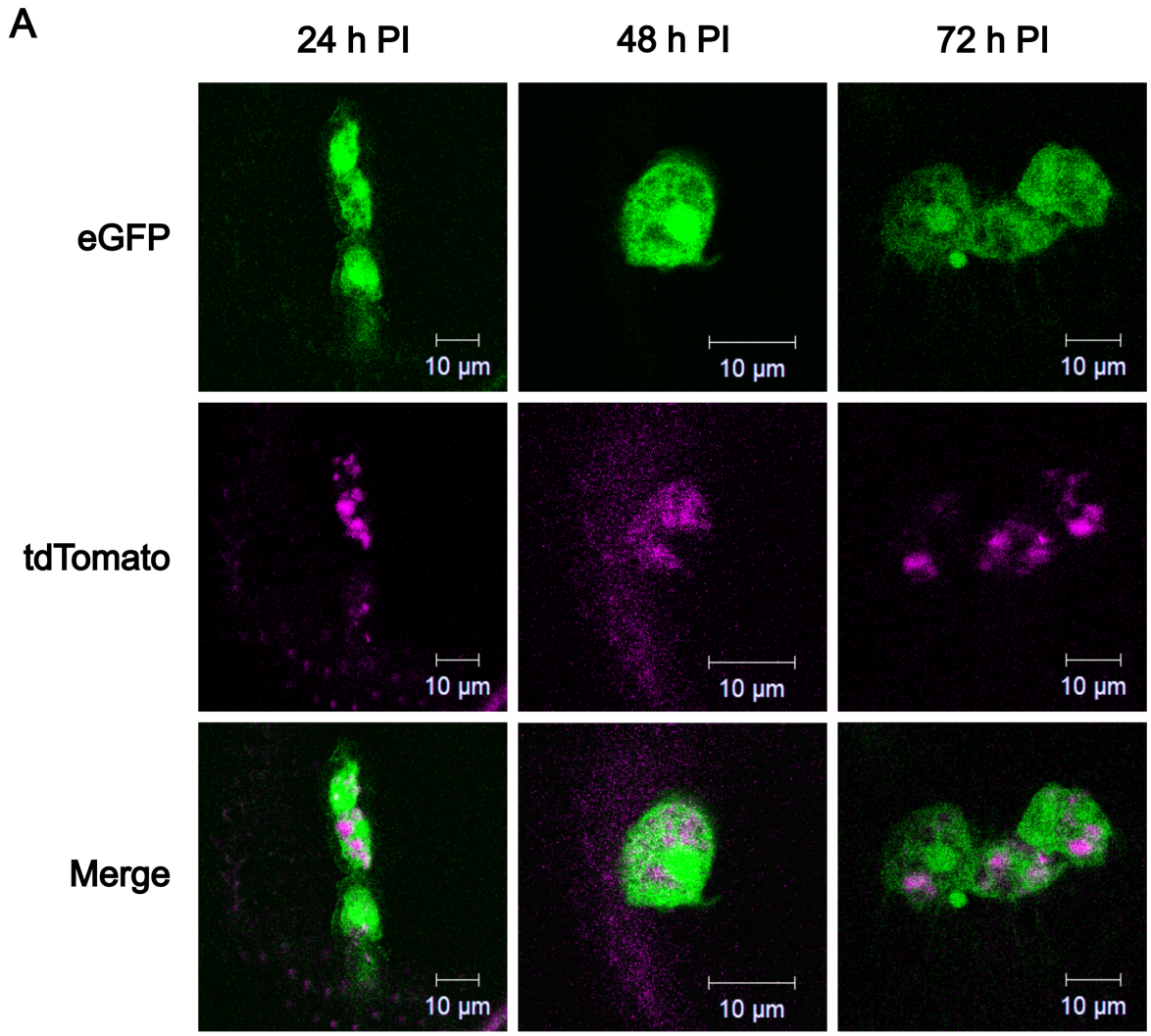


Figure 3.16. Confocal images of *D. melanogaster* haemocytes infected with *M. abscessus*. (**A**) See legend on page 159.

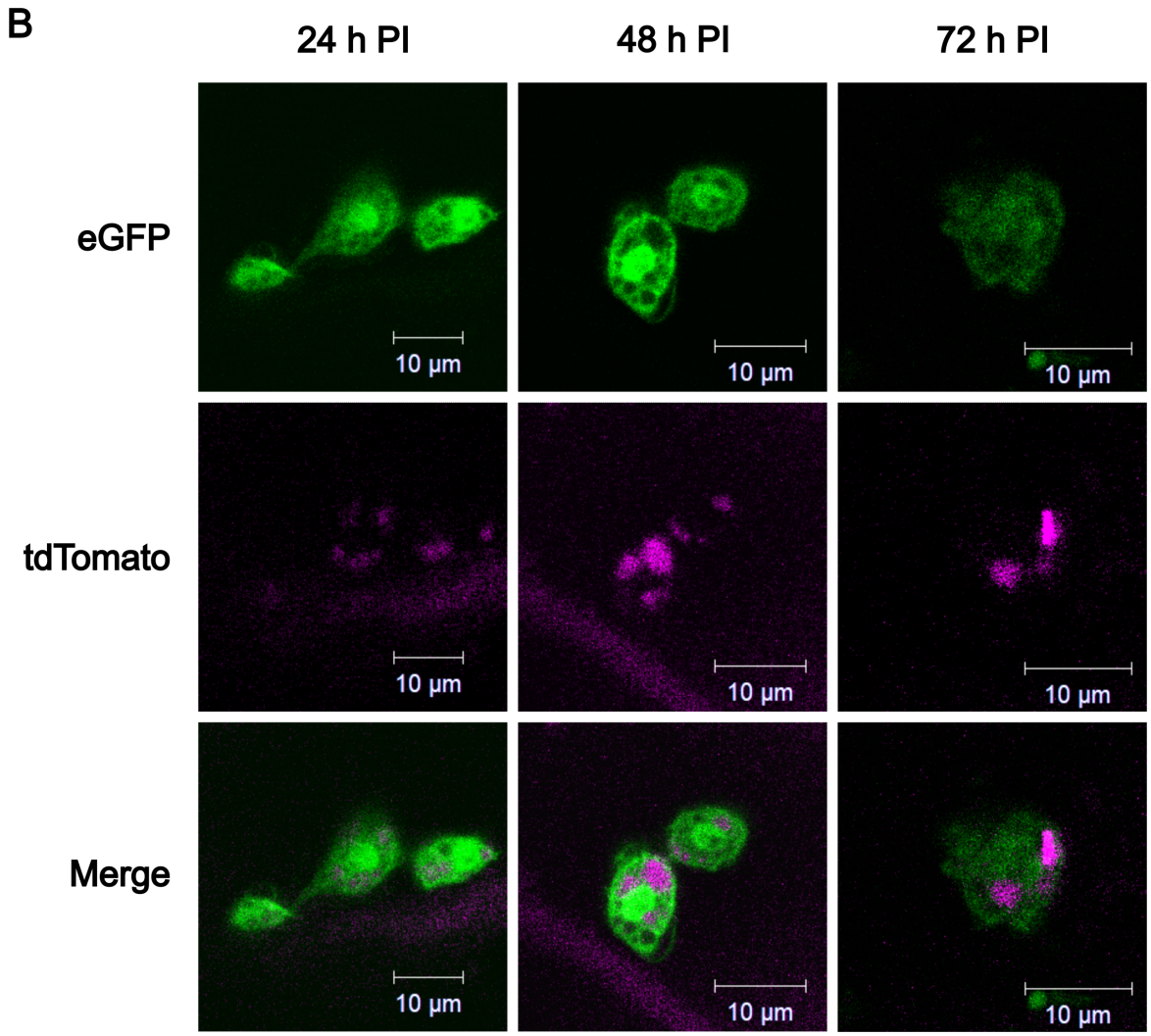


Figure 3.16. Confocal images of *D. melanogaster* haemocytes infected with *M. abscessus* continued. (**A**) Confocal images taken of live *D. melanogaster* with *in vivo M. abscessus* tdTomato Rough infection. Flies with haemocytes expressing eGFP (Hml$^{\Delta}$-Gal4, UAS-2x-eGFP) were injected with *M. abscessus* tdTomato Rough (magenta) and imaged every 24 hours for the first 3 days post infection. Scale bar represents 10 μm. (**B**) Confocal images taken of live *D. melanogaster* with *in vivo M. abscessus* tdTomato Smooth infection. Flies with haemocytes expressing eGFP (Hml$^{\Delta}$-Gal4, UAS-2x-eGFP) were injected with *M. abscessus* tdTomato Smooth (magenta) and imaged every 24 hours for the first 3 days post infection. Scale bar represents 10 μm.

To confirm the role of haemocytes in *M. abscessus* infection of *D. melanogaster*, I made use of the UAS-Gal4 system to generate flies lacking haemocytes by driving expression of *reaper*, a pro-apoptotic gene, within haemocytes of adult flies. Surprisingly there was no change in survival of flies lacking haemocytes compared to control lines during *M. abscessus* infection,

implying that despite the observation that *M. abscessus* is phagocytosed by haemocytes, they do not offer any benefit in terms of host survival (Figure 3.17A). Unfortunately, due to limited numbers of flies, I was unable to perform confocal imaging on these flies to confirm that they were lacking haemocytes.

I also infected flies that were double mutants lacking two Nimrod-family receptors which contribute to bacterial phagocytosis in *D. melanogaster*, NimC1 and Eater[596]. Infecting flies with either a high (Figure 3.17B) or a low dose (Figure 3.17C) of *M. abscessus* resulted in the *NimC1*^{1}*;Eater*^{1} double mutant flies dying a day earlier than wild-type flies. This suggests that haemocytes contribute to the progression of infection in two ways: by phagocytosing the bacteria, they perform a function that is, on net, beneficial to the host, but they also perform some function that is detrimental to the host. This would explain why the entire loss of haemocytes has no effect on survival, whereas the loss of phagocytic capability in the presence of otherwise functional haemocytes decreases time-to-death.

3.4 Discussion

3.4.1 Optimisation of *M. abscessus* injection

In the first part of this chapter, I compared different experimental injection conditions in order to select parameters for robust and consistent *M. abscessus* infection of *D. melanogaster* in later experiments. This primarily involved selecting an initial injection dose that would be capable of inducing *D. melanogaster* immune responses without being so high that the immune signalling pathways are overwhelmed and infected flies die very rapidly. Infecting flies with increasing doses of *M. abscessus* led to clear dose-dependent decreases in longevity, however, there was relatively little difference between flies infected with OD_{600} = 0.05 and OD_{600} = 0.1. This may indicate that the OD_{600} = 0.05 dose represents a limit in terms of damage inflicted on the fly, or the dose at which any host clearance mechanisms are too costly or ineffective, meaning higher infection doses have little additional impact on survival time. It is also possible that there

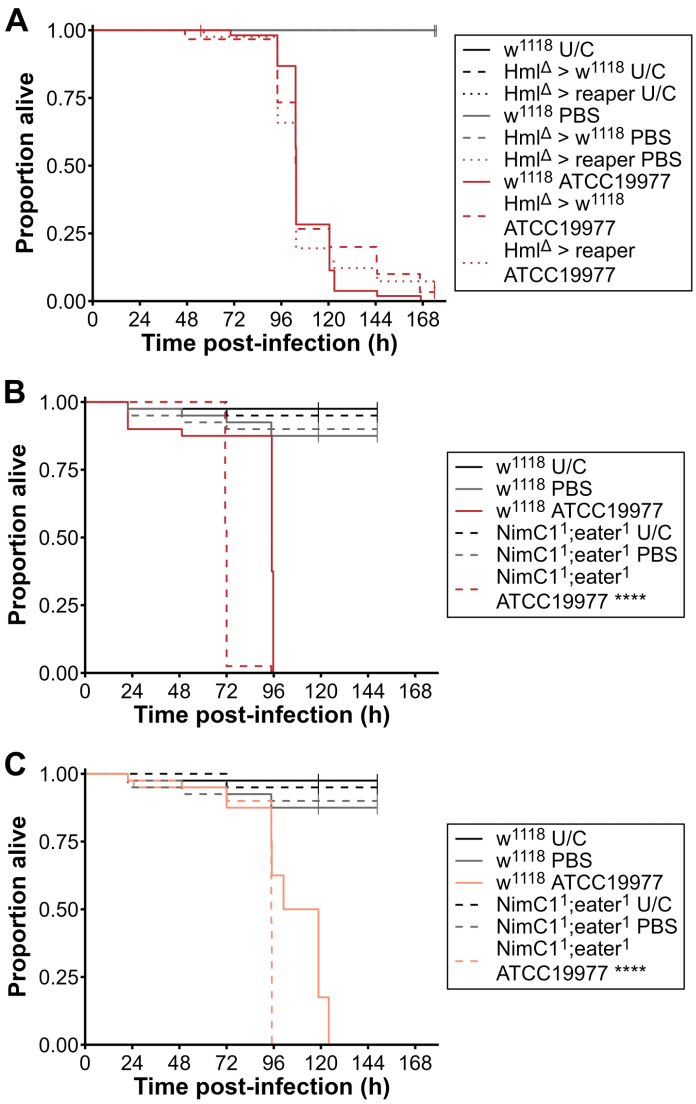


Figure 3.17. Survival of flies lacking haemocytes or lacking phagocytic capability following *M. abscessus* infection. (**A**) The Gal80^{ts} system was used to remove haemocytes after eclosion to prevent any developmental defects as a result of loss of haemocytes. Pro-apoptotic gene *reaper* was expressed in haemocytes (*Hml$^{\Delta}$-Gal4 > UAS-reaper*, dotted lines) prior to infection with a high dose (OD_{600} = 0.05) of *M. abscessus* ATCC19977 (red). *w^{1118}* (solid lines) and a driver-only genotype control (*Hml$^{\Delta}$-Gal4 > w^{1118}*, dashed lines) are also shown. Flies were also injected with PBS Tween80 0.1% as a sterile injury control (grey), or uninjected control (U/C, black). Data is pooled from two independent experiments, 21 $\geq$ n $\geq$ 54 per group, groups were compared using Log-Rank test. Survival of *w^{1118}* (solid lines) and *NimC1^{1};Eater^{1}* double mutant flies (dashed lines) following injection with a (**B**) high dose (OD_{600} = 0.05) *M. abscessus* ATCC19977 (red) or (**C**) low dose (OD_{600} = 0.005) *M. abscessus* ATCC19977 (orange). Flies were also injected with PBS Tween80 0.1% as a sterile injury control (grey), or uninjected control (U/C, black). Data is pooled from two independent experiments, n = 40 per group, groups were compared using Log-Rank test. Asterisks in the legend indicate the *p*-value compared to *w^{1118}* flies infected with the same *M. abscessus* strain and dose. $*$, P < 0.05; $**$, P < 0.01; $***$, P < 0.001; $****$, P < 0.0001. Setting up of the *D. melanogaster* crosses and collecting flies with the experimental genotypes was performed by Dr Catarina Nunes.

is a small difference in the survival time of flies infected with OD_{600} = 0.05 or OD_{600} = 0.10 which is not reflected in the Kaplan-Meier survival curves caused by flies infected with the higher dose dying early and rapidly during the overnight window between being checked. These times to death of flies infected with various doses of *M. abscessus* are consistent with results from other work using *D. melanogaster* as a model for *M. abscessus* infection[118,517]. Additionally, I confirmed that the sterile-filtered supernatant of *M. abscessus* cultures did not cause any death in *D. melanogaster*, indicating that pathology in infected *D. melanogaster* is caused by the presence of *M. abscessus*, and not contributed to by a secreted protein or toxic component of the media. This is again consistent with previous studies which found that heat-killed and PFA-killed *M. abscessus* showed greatly reduced mortality in infected *D. melanogaster*[118,517], confirming that pathology and mortality in infected flies is caused by active *M. abscessus* and not simply the presence of virulence factors or PAMPs.

For survival experiments in different *D. melanogaster* immune signalling mutant lines, I selected two different doses, OD_{600} = 0.05 and OD_{600} = 0.005, in order to identify any possible subtle survival differences in immune mutant fly lines. I also considered different detergents for performing bacterial load quantifications in order to prevent clumping of *M. abscessus* and produce clear 10-fold differences in the number of colonies from each serial dilution without toxicity to *M. abscessus*. For bacterial load quantifications, I selected PBS Tween80 1% for homogenising and serially diluting infected flies, as this showed the most consistent ten-fold decreases in the number of colonies across dilutions. The bacterial load quantification of *M. abscessus* injected at OD_{600} = 0.05 shows exponential growth in *D. melanogaster* over the course of the infection, confirming that the host clearance mechanisms are ineffective against *M. abscessus*.

3.4.2 Detection of *M. abscessus* by *D. melanogaster* immune signalling pathways

It has previously been reported that infection of *D. melanogaster* with mutations in PGRP-SA or Dif with *M. abscessus* led to more rapid mortality of mutant flies relative to wild-type flies, leading the authors to conclude that PGRP-SA was responsible for the detection of *M. abscessus* and that subsequent activation of the Toll pathway was protective against the infection, to a degree[517]. Based on my survival results, I found that flies with mutations in Dif are no more susceptible to *M. abscessus* infection than wild-type flies, similar to the results found by Touré *et al.* using Spz mutant flies and Mtk Drs double mutant flies[118]. Whilst my study did not replicate the previously described decrease in survival of Dif mutant flies and did not perform any survival experiments using PGRP-SA mutant flies, I did observe evidence of Toll pathway activation based on transcriptional increases in AMPs by 48 hours post-infection. That said, the transcriptional response that is observed is relatively weak and occurs late during the infection, similar to the observations by Touré *et al.* and Oh *et al.*[118,517]. For comparison, during *D. melanogaster* infection with other bacterial pathogens such as *E. coli* or *Francisella novicida*, AMP transcript levels reach 100-fold increases above that of uninfected controls, typically peaking between 6 and 12 hours post-infection[352,519,597]. Whilst some of the AMP and Bomanin transcriptional responses do reach these high levels, this only occurs at 80 hours post-infection.

The lateness of this Toll pathway activation can be explained by the lack of extracellular *M. abscessus* available to detect within the haemolymph during the early stages of infection owing to its rapid phagocytosis and uptake by haemocytes, as observed in Figure 3.16. Following intracellular growth of *M. abscessus* and subsequent apoptosis or necrosis of infected cells, bacteria may be released into the haemolymph[118] and then be detected by the Toll pathway, resulting in the late-stage transcriptional response. Touré *et al.* also found that extracellular *M. abscessus* in Tep4 mutant flies induced significantly higher transcription of *Cecropin C*

Defensin, *Attacin*, *Drosocin*, and *Metchnikowin* despite having lower bacterial loads compared to wild-type flies capable of phagocytosing *M. abscessus*[488], suggesting detection of *M. abscessus* is improved when the bacteria is extracellular.

While not statistically significant in comparison to PBS sterile-injury control flies, there was a trend of increasing transcription of immune-induced molecules (IMs) in *M. abscessus* infected flies at 6 hours post-infection, which continued to increase over the course of the infection. This may be indicative of early Toll pathway activation[348,591], activation of Toll by an alternative route related to fungal immune responses as IM4 has only previously been reported for its protective effect against certain filamentous fungi[598], or possibly that transcription of these genes occurs at a lower threshold compared to transcription of AMPs. The comparative lack of Imd pathway activation early in infection, despite intracellular PRR PGRP-LE, may be related to the containment of *M. abscessus* within the phagolysosome, in which *M. abscessus* inhibits phagosome maturation and degradation, preventing release of peptidoglycan for PGRP-LE detection within the cytosol. The thick mycomembrane layer and additional GPL layer in *M. abscessus* ATCC19977 may also prevent any PGRP from accessing *M. abscessus* peptidoglycan[355]. Activation of Imd pathway AMPs Attacin and Diptericin did occur, but not until 80 hours post-infection, possibly by independent activation of the Imd pathway following detection of *M. abscessus*, cross-talk between the Toll and Imd pathways, or in response to widespread inflammatory damage occurring within the fly. This is consistent with the study by Touré *et al.* which found that flies lacking Attacins, Drosocins, and Diptericin or flies with mutations in Rel show no difference in survival compared to wild-type flies when infected with *M. abscessus*. However, in another study, they did find that phagocyte-depleted flies with mutations in *Rel* have increased susceptibility to *M. abscessus* infection, despite no apparent increase in susceptibility in phagocyte-depleted flies with mutations in Imd-associated AMPs. This suggests an alternative role of Rel beyond AMP transcription in response to extracellular *M. abscessus*[488]. Indeed in vertebrates, Rel signalling has an antiapoptotic effect, so it is

possible that Rel serves an important protective role for the phagocytes remaining following injection of clodronate liposomes during *M. abscessus* infection[599].

3.4.3 *M. abscessus* induces an ineffective immune response in *D. melanogaster*

The majority of *D. melanogaster* immune mutant lines infected with *M. abscessus* showed no change in susceptibility to the infection compared to wild-type *D. melanogaster*, regardless of infection dose or *M. abscessus* morphotype. Dif^{1} and imd^{10191} mutant flies, which have defective Toll and Imd pathway signalling, respectively, are unable to drive transcription of AMPs, confirming that the transcriptional activation of AMPs during *M. abscessus* infection does not play a meaningful role in *D. melanogaster* resistance against *M. abscessus*. Whilst this differs from the decreased survival of Dif^{1} flies described by Oh *et al.*[517], it is in line with the results from Touré *et al.*, who showed that AMP-deficient flies and flies with mutations in Rel and Spz showed equivalent survival to wild-type flies when infected with *M. abscessus*. *M. abscessus* strains with mutations in *mmpL8* (MAB_0855), which has reduced intracellular viability, reduced adhesion and reduced cytosol-phagosome contact resulting in decreased virulence in zebrafish, and MAB_4532c, which also has impaired intracellular viability due to inability to induce phagosomal membrane damage and prevent ROS production in macrophages, show reduced virulence in *D. melanogaster*. This reduced virulence is maintained in the AMP deficient, Rel, or Spz mutant lines, indicating that the increased host survival seen in infection with these *M. abscessus* mutant strains is independent of the host AMP response[118].

Contrary to the findings of Touré *et al.* who reported that $Bom^{\Delta 55c}$ mutant flies also showed no change in susceptibility to infection with *M. abscessus*, I did observe an increase in survival of $Bom^{\Delta 55c}$ flies when infected with a low dose (OD_{600} = 0.005) of *M. abscessus* tdTomato Smooth, and a high dose (OD_{600} = 0.05) of *M. abscessus* tdTomato Rough. It is worth noting that the number of CFU between these two bacterial inoculums is only approximately two-fold

different, based on the CFU per mL, meaning there is possibly a specific *M. abscessus* dose range at which production of Bomanin peptides is detrimental to host survival. The low dose of *M. abscessus* tdTomato Rough may be too low to induce significant transcription of Bomanins, and at higher doses, the survival difference may be more subtle and not captured by the twice-daily survival checks. However, as Bomanin peptide transcription is downstream of Toll signalling, this same survival increase should also be observed in Dif^{1} flies which would also lack Bomanin production. Possible explanations for this discrepancy include that Bomanin peptides can be activated independently of Dif, or that the observed increase in survival of $Bom^{\Delta 55c}$ flies is not because of a direct detrimental effect of Bomanin peptides, but because of a secondary change such as a compensatory upregulation in other AMPs which requires greater energy and resources creating an immune tradeoff with other metabolic functions.

3.4.4 The role of the cellular response during *M. abscessus* infection

The rapid phagocytosis of *M. abscessus* by *D. melanogaster* haemocytes and the observation of possible intracellular growth has also been reported by Touré *et al.*[118]. Removal of haemocytes by expression of pro-apoptotic gene *Death executioner Bcl-2* (*Debcl*) under the control of the driver *croquemort* (*crq*) led to more rapid death of *M. abscessus* infected flies compared to controls as well as increased bacterial loads, suggesting that these phagocytic cells do play an important role in controlling bacterial growth and slowing the progression of *M. abscessus* pathogenesis[118]. The authors also reported that depletion of phagocytes by expressing *Debcl* under the control of different drivers, *Hemese* (*He*) or *Angiotensin converting enzyme* (*Ance*) led to decreased *M. abscessus* growth and increased *D. melanogaster* survival[118], and so the discrepancies between my findings and the previously published results may lie in the use of different tissue drivers creating variation in which subpopulations of haemocytes are being targeted.

M. marinum infection was found to be cytotoxic to *D. melanogaster* haemocytes, both *in vitro*

and *in vivo*, with a progressive reduction in haemocyte numbers in the last days of *in vivo* *M. marinum* infection. Shortly before death, no visible haemocytes could be identified, and mutations that prolonged haemocyte survival also prolonged overall survival. This indicates the importance of haemocytes in controlling *M. marinum* infection, and equally the importance of haemocyte apoptosis or necrosis in *M. marinum* pathogenicity[470]. An important outstanding question is if the same is true of *M. abscessus* infection. Increased caspase activity has been reported, and inhibition of caspase activity in plasmatocytes by expression of p35 led to increased fly survival during *M. abscessus* infection[118], however direct evidence of apoptosis, necrosis or haemocyte depletion has not been shown, and it remains unclear how loss of haemocytes may contribute to death of *D. melanogaster*.

Whilst the different roles of haemocytes during *M. abscessus* infection of *D. melanogaster* are not clear, my findings suggest that phagocytic uptake of *M. abscessus* is protective to the host, however, the presence of haemocytes unable to phagocytose is harmful. This implies that another haemocyte response occurring during *M. abscessus* infection is damaging, possibly due to the downstream effects of haemocyte signalling or the balance of apoptosis and necrosis leading to inflammatory damage. This hypothesis is consistent with the results of previous studies, including that *M. abscessus* infection of flies with depleted phagocytes by clodronate liposomes, which leaves some phagocytes remaining, also decreases survival compared to wild-type flies[118].

3.4.5 Differences between *M. abscessus* morphotypes

Unfortunately due to the differences in the CFU per mL of the ODs for *M. abscessus* tdTomato Smooth and tdTomato Rough, I was unable to make a direct comparison between the *D. melanogaster* response to the different morphotypes. Despite having fewer CFU in the initial dose at the same OD_{600}, the tdTomato Rough strain typically kills infected flies at the same time as the tdTomato Smooth and wild-type ATCC 19977 strain with the equivalent OD_{600}.

This may suggest a slight increase in virulence of the rough morphotype compared to the smooth, as reported in other *in vitro* cell models[33] and *in vivo* infection models[600]. The tdTomato Rough strain also appears to be more readily phagocytosed, with greater levels of tdTomato fluorescence within haemocytes 24 hours post-infection compared to tdTomato Smooth infected flies, again despite a lower initial inoculum.

The *D. melanogaster* model may be capable of identifying different factors between the two *M. abscessus* morphotypes and how they may alter interactions with the host and virulence. This will require a better understanding of how *D. melanogaster* detects and responds to the different morphotypes through the use of different GPL mutant *M. abscessus* strains combined with *D. melanogaster* PRR mutant lines.

Together, the results from this chapter suggest that *M. abscessus* is well suited to evading and resisting the *D. melanogaster* immune response, and is capable of manipulating the intracellular environment of phagocytes to promote its own survival and growth. This makes *D. melanogaster* an excellent model system for studying the interaction between *M. abscessus* and host phagocytes, and for identifying both bacterial and host factors involved in this interaction, contributing to understanding how *M. abscessus* resists host innate immune responses. I have found that despite activation of Toll pathway signalling and later Imd pathway signalling leading to the production of AMPs, this response is ineffective against *M. abscessus*. Additionally, the *D. melanogaster* immune response to *M. abscessus* is distinct from the response to *M. marinum*, suggesting that there are key differences in how these pathogens behave in this host environment.

Chapter 4: Screening *Mycobacterium abscessus* CRISPR knockout mutants

4.1 Introduction

Genome editing is a fundamental tool in the study of bacterial pathogens as the production of mutant strains with knockouts, conditional knockdowns or overexpression of target genes is essential in understanding gene function and to possibly identify novel drug targets. More specific mutations such as single-point amino acid substitutions can allow for the study of drug resistance mechanisms, transcriptional regulation and specific protein domain structure-function relationships[557–560]. Unfortunately, such genetic manipulations are difficult to perform in mycobacteria, partly due to their slow growth and thick outer mycomembrane which prevents efficient DNA transfer[560,601,602].

The development of genetic tools for use in other bacteria have since been extensively modified and engineered for use in mycobacterial species, allowing for the characterisation of key *M. tuberculosis* genes and their role in pathogenesis. These methods include homologous recombination and mycobacteriophage recombinases, which are generally considered to work in almost all mycobacterial species[567,603]. However, this is not the case for *M. abscessus*[604,605]. Allelic exchange by recombineering occurs at a much lower frequency in *M. abscessus* compared to *M. smegmatis* (7% efficiency vs 100% efficiency), and the ts-*sacB* system or use of mycobacteriophage both failed to produce any allelic exchange mutants in *M. abscessus* despite being successful in *M. smegmatis* (0% efficiency vs 100% efficiency)[604]. The lack of efficient or effective tools for the genetic manipulation of *M. abscessus* has severely hampered research into this pathogen. The first *M. abscessus* knockout mutant was produced in 2009 by recombineering[604]. In 2011 a TetR/PipOFF system was tested and produced a fadD32 conditional mutant, however, this was an intensive process[605]. It was not until 2018 that a more rapid method of gene knockout was developed to work in *M. abscessus* using a

single cross-over homologous recombination system[606].

The development of CRISPR-based tools offered new opportunities for the genetic manipulation of *M. abscessus*. CRISPR interference (CRISPRi) was first described in *M. tuberculosis* and *M. smegmatis*, using small guide RNA (sgRNA) to hybridise with the target DNA sequence and allow binding of an endonuclease-deficient dCas9 in order to suppress gene expression[561]. This technique was applied to *M. abscessus* to study the role of peptidoglycan biosynthesis genes in β-lactam resistance[607]. In 2020, using an active *Streptococcus thermophilus* Cas9, CRISPR was used to efficiently and rapidly generate frameshift mutations in *M. smegmatis*, *M. marinum*, and *M. tuberculosis*[579,580].

To date, use of CRISPR to produce *M. abscessus* mutant strains with targeted gene knockouts has not been reported. Using the method described in Section 1.3.2, two plasmids encoding *S. pyogenes* Cas9 and a sgRNA sequence upstream of the Cas9 handle, I aimed to produce frameshift mutations in genes of interest in *M. abscessus* by inducing NHEJ repair activity to create indels. Target genes were selected from the phenogenomics study described in Section 1.4. Briefly, using 331 clinical *M. abscessus* isolates collected from CF patients across the globe to perform GWASs combined with intensive phenotypic studies, computational analyses to predict the functional impact of mutations and epistatic analyses, clinically relevant genetic determinants of *M. abscessus* virulence were identified[581]. Six of these GWAS hits were then selected as target genes for my study to be knocked out using the CRISPR-Cas9 approach (Table 4.1).

Other target genes were selected based on their homology to key, well-characterised *M. tuberculosis* virulence factors. This would allow for a direct comparison between mechanisms of *M. tuberculosis* and *M. abscessus* virulence. The final group of target genes were selected for their involvement in key metabolic pathways: nitrite reduction and extrusion which is an essential aspect of nitrate respiration in hypoxic conditions, and fatty acid metabolism. These

mutants would provide information about the role of these pathways during *M. abscessus* infection in *D. melanogaster*, and could also be used to understand how bacterial metabolism can drive changes in host metabolism.

Table 4.1. *M. abscessus* CRISPR Knockout Target Genes. Successful knockout mutants are shown in bold.

Gene	Function	Reason
MAB_0169c	**Exported repetitive protein**	Homologue of *M. tuberculosis* virulence factor Rv3810[63]
MAB_0471	**Conserved hypothetical transmembrane protein**	GWAS & knockdown study
MAB_0472	**Conserved hypothetical membrane protein**	GWAS & knockdown study
MAB_1012c	**YrbE family protein**	GWAS & knockdown study
MAB_1132c	**Probable L-asparagine permease 1 (Transport protein)**	GWAS & knockdown study
MAB_1283c	**WXG100 family type VII secretion target**	GWAS & knockdown study
MAB_1933c	Glutamine synthetase	Homologue of *M. tuberculosis* virulence factor Rv2220[63]
MAB_2228c	ESAT-6-like protein	GWAS & knockdown study
MAB_2262c	**Mycobactin import ATP-binding/permease protein IrtA**	Homologue of *M. tuberculosis* virulence factor Rv1348[63]
MAB_2728c	Hypothetical invasion protein Inv1	Homologue of *M. tuberculosis* virulence factor Rv1477[63]
MAB_3029	Iron-dependent repressor IdeR	Homologue of *M. tuberculosis* virulence factor Rv2711[63]
MAB_3473c	SsrA-binding protein	Homologue of *M. tuberculosis* virulence factor Rv3100c[63]
MAB_3521c	Probable nitrite reductase	Involvement in key metabolic pathway
MAB_3522c	**Assimilatory sulfite reductase (ferredoxin)**	Involvement in key metabolic pathway
MAB_3523c	**Probable integral membrane nitrite extrusion protein NarK3**	Involvement in key metabolic pathway
MAB_4095c	Isocitrate lyase	Homologue of *M. tuberculosis* virulence factor Rv0467[63]

Gene	Function	Reason
MAB_4163c	**Probable fatty acid CoA ligase FadD**	Involvement in key metabolic pathway
MAB_4588c	**Probable enoyl-CoA hydratase/isomerase**	Involvement in key metabolic pathway

4.2 Aims

The first aim of this chapter was to produce frameshift mutations resulting in loss-of-function of the *M. abscessus* target genes using a CRISPR-Cas9 approach. To the best of my knowledge, this has not previously been described in *M. abscessus*. Following this, the experiments described in this chapter aimed to assess how each of these *M. abscessus* target genes contribute to pathogenicity during infection of *D. melanogaster* by comparing survival and bacterial load to flies infected with wild-type *M. abscessus*. This would then allow us to select which of these *M. abscessus* genes to continue studying in more depth to understand its role during infection.

4.3 Results

4.3.1 Generating CRISPR frameshift mutations

The initial step in generating the *M. abscessus* CRISPR mutant strains was performed at the MRC Laboratory of Molecular Biology in collaboration with the Floto group. The design of sgRNAs, plasmid construction, cloning, and transformation of *M. abscessus* strains was performed with help from Dr. Sophie Burbaud and Jasper Sangen. *M. abscessus* strains transformed with a pGRNAz plasmid carrying a sgRNA targeting a gene of interest alongside the Cas9 handle and a second plasmid, pTetInt-*cas9*PYO containing the Cas9 sequence, were grown in medium containing doxycycline to activate the components of the CRISPR-Cas9 system. Cultures were then serially diluted and plated onto 7H11 agar plates to select single colonies. A minimum of 10 single colonies per sgRNA were selected, cultured, and

frozen as a glycerol stock at -80°C. This resulted in the production of 940 *M. abscessus* strains to be screened to identify strains with successful frameshift mutations in the genes of interest. The screening process is outlined in Figure 4.1, showing the number of strains which progressed through the screening process: gDNA extraction, PCR amplification of the target gene, purification of the PCR product, Sanger sequencing of the PCR product, and identification of mutations including frameshift mutations. The editing efficiency of each of the sgRNA plasmids is calculated in Table 4.2. Once a successful frameshift mutation was identified for a target gene, screening was stopped for any remaining strains targeting the same gene, hence the low numbers of strains sequenced for some sgRNA plasmids.

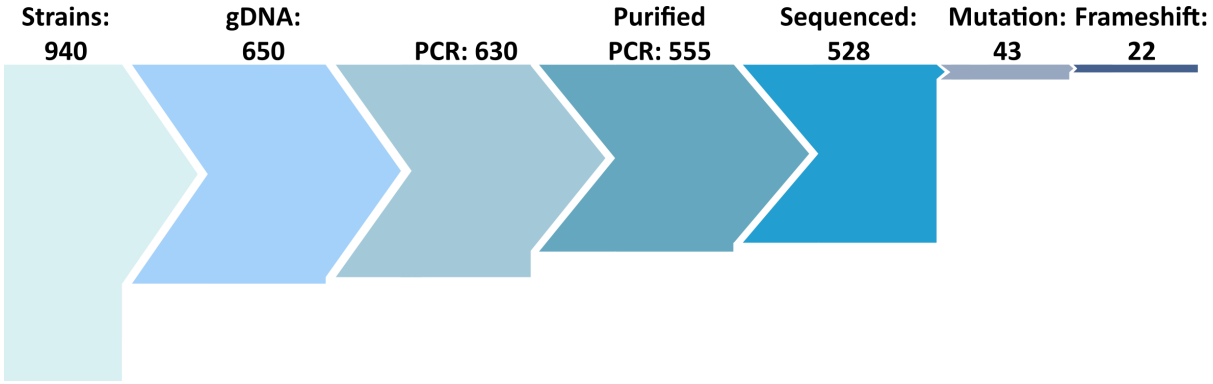


Figure 4.1. Sankey diagram showing *M. abscessus* CRISPR screening process and progress.

Table 4.2. Gene editing efficiency of each of the sgRNA plasmids. Gene editing efficiency is calculated as a percentage of the number of strains with a mutation in the target gene out of the total number of strains sequenced. Frameshift editing efficiency is the percentage of strains with a frameshift mutation out of the total number of strains sequenced.

Target gene	Plasmid	Number strains sequenced	Gene editing efficiency	Frameshift generation efficiency
MAB_0169c	pGRNAz-*0169c* g1	5	20%	20%
MAB_0169c	pGRNAz-*0169c* g2	5	0%	0%
MAB_0169c	pGRNAz-*0169c* g3	4	0%	0%
MAB_0169c	pGRNAz-*0169c* g4	4	0%	0%
MAB_0169c	pGRNAz-*0169c* g5	4	75%	50%
MAB_0471	pGRNAz-*0471* g1	10	0%	0%

Target gene	Plasmid	Number strains sequenced	Gene editing efficiency	Frameshift generation efficiency
MAB_0471	pGRNAz-*0471* g2	10	0%	0%
MAB_0471	pGRNAz-*0471* g3	36	8.33%	5.56%
MAB_0471	pGRNAz-*0471* g4	10	0%	0%
MAB_0471	pGRNAz-*0471* g5	10	0%	0%
MAB_0472	pGRNAz-*0472* g1	1	0%	0%
MAB_0472	pGRNAz-*0472* g2	12	41.67%	33.33%
MAB_0472	pGRNAz-*0472* g3	2	0%	0%
MAB_0472	pGRNAz-*0472* g4	1	100%	0%
MAB_0472	pGRNAz-*0472* g5	3	0%	0%
MAB_1012c	pGRNAz-*1012c* g1	7	0%	0%
MAB_1012c	pGRNAz-*1012c* g2	7	71.43%	28.57%
MAB_1012c	pGRNAz-*1012c* g3	3	0%	0%
MAB_1012c	pGRNAz-*1012c* g4	5	0%	0%
MAB_1012c	pGRNAz-*1012c* g5	3	0%	0%
MAB_1132c	pGRNAz-*1132c* g1	1	0%	0%
MAB_1132c	pGRNAz-*1132c* g2	2	50%	50%
MAB_1132c	pGRNAz-*1132c* g3	2	100%	50%
MAB_1132c	pGRNAz-*1132c* g4	1	0%	0%
MAB_1132c	pGRNAz-*1132c* g5	1	100%	100%
MAB_1283c	pGRNAz-*1283c* g1	17	0%	0%
MAB_1283c	pGRNAz-*1283c* g2	16	0%	0%
MAB_1283c	pGRNAz-*1283c* g3	10	10%	10%
MAB_1933c	pGRNAz-*1933c* g1	4	0%	0%
MAB_1933c	pGRNAz-*1933c* g2	5	0%	0%
MAB_1933c	pGRNAz-*1933c* g3	5	0%	0%
MAB_1933c	pGRNAz-*1933c* g4	5	0%	0%
MAB_1933c	pGRNAz-*1933c* g5	3	0%	0%
MAB_2228c	pGRNAz-*2228c* g1	20	20%	0%
MAB_2228c	pGRNAz-*2228c* g2	20	10%	0%
MAB_2228c	pGRNAz-*2228c* g3	19	5.26%	0%
MAB_2262c	pGRNAz-*2262c* g1	2	0%	0%

Target gene	Plasmid	Number strains sequenced	Gene editing efficiency	Frameshift generation efficiency
MAB_2262c	pGRNAz-*2262c* g2	1	0%	0%
MAB_2262c	pGRNAz-*2262c* g3	1	0%	0%
MAB_2262c	pGRNAz-*2262c* g4	1	0%	0%
MAB_2262c	pGRNAz-*2262c* g5	1	100%	100%
MAB_2728c	pGRNAz-*2728c* g1	10	0%	0%
MAB_2728c	pGRNAz-*2728c* g2	10	50%	0%
MAB_2728c	pGRNAz-*2728c* g3	10	0%	0%
MAB_2728c	pGRNAz-*2728c* g4	10	0%	0%
MAB_2728c	pGRNAz-*2728c* g5	10	0%	0%
MAB_3029	pGRNAz-*3029* g1	2	0%	0%
MAB_3029	pGRNAz-*3029* g2	3	0%	0%
MAB_3029	pGRNAz-*3029* g3	2	0%	0%
MAB_3029	pGRNAz-*3029* g4	2	0%	0%
MAB_3029	pGRNAz-*3029* g5	2	0%	0%
MAB_3473c	pGRNAz-*3473c* g1	10	40%	0%
MAB_3473c	pGRNAz-*3473c* g2	10	0%	0%
MAB_3473c	pGRNAz-*3473c* g3	10	0%	0%
MAB_3473c	pGRNAz-*3473c* g4	5	60%	0%
MAB_3473c	pGRNAz-*3473c* g5	5	0%	0%
MAB_3521c	pGRNAz-*3521c* g1	10	0%	0%
MAB_3521c	pGRNAz-*3521c* g2	7	0%	0%
MAB_3521c	pGRNAz-*3521c* g3	6	16.67%	0%
MAB_3521c	pGRNAz-*3521c* g4	7	0%	0%
MAB_3521c	pGRNAz-*3521c* g5	8	0%	0%
MAB_3522c	pGRNAz-*3522c* g1	10	10%	0%
MAB_3522c	pGRNAz-*3522c* g2	4	0%	0%
MAB_3522c	pGRNAz-*3522c* g3	5	0%	0%
MAB_3522c	pGRNAz-*3522c* g4	5	0%	0%
MAB_3522c	pGRNAz-*3522c* g5	7	14.29%	14.29%
MAB_3523c	pGRNAz-*3523c* g1	1	100%	100%
MAB_3523c	pGRNAz-*3523c* g2	0	0%	0%

Target gene	Plasmid	Number strains sequenced	Gene editing efficiency	Frameshift generation efficiency
MAB_3523c	pGRNAz-*3523c* g3	1	0%	0%
MAB_3523c	pGRNAz-*3523c* g4	3	0%	0%
MAB_3523c	pGRNAz-*3523c* g5	3	0%	0%
MAB_4095c	pGRNAz-*4095c* g1	10	10%	0%
MAB_4095c	pGRNAz-*4095c* g2	10	0%	0%
MAB_4095c	pGRNAz-*4095c* g3	9	11.11%	0%
MAB_4095c	pGRNAz-*4095c* g4	10	20%	0%
MAB_4095c	pGRNAz-*4095c* g5	10	0%	0%
MAB_4163c	pGRNAz-*4163c* g1	2	0%	0%
MAB_4163c	pGRNAz-*4163c* g2	6	16.67%	16.67%
MAB_4163c	pGRNAz-*4163c* g3	3	0%	0%
MAB_4163c	pGRNAz-*4163c* g4	6	0%	0%
MAB_4163c	pGRNAz-*4163c* g5	1	0%	0%
MAB_4588c	pGRNAz-*4588c* g1	4	0%	0%
MAB_4588c	pGRNAz-*4588c* g2	3	66.67%	66.67%
MAB_4588c	pGRNAz-*4588c* g3	3	33.33%	33.33%
MAB_4588c	pGRNAz-*4588c* g4	0	0%	0%
MAB_4588c	pGRNAz-*4588c* g5	0	0%	0%

Some *M. abscessus* target genes showed very low levels of gene editing efficiency and 0% frameshift editing efficiency across all sgRNA plasmids. While it is likely some of these genes are essential, such as MAB_1933c glutamine synthetase and MAB_3473c SsrA-binding protein[608], the lack of mutations produced in other targeted genes such as MAB_2228c ESAT-6-like protein, MAB_2728c hypothetical invasion protein Inv1, MAB_3029 iron-dependent repressor IdeR, MAB_3521c probable nitrite reductase, and MAB_4095c isocitrate lyase is possibly due to failure of the designed sgRNAs. Strains with mutations induced by the activation of the CRISPR-Cas9 are described in Table 4.3.

Table 4.3. List of *M. abscessus* mutations identified following CRISPR induction and sequencing. Strains with successful frameshift mutations were given a strain ID used throughout this thesis. Strains lacking a detailed mutation annotation is due to unsuccessful sequence alignment.

Strain ID	Target Gene	Plasmid	Mutation	Mutation Description
Δ0169c-1	MAB_0169c	pGRNAz-*0169c* g1	c.115-117 del c.142-143 del	3 bp deletion 2 bp deletion
	MAB_0169c	pGRNAz-*0169c* g5	c. 173-184del	12 bp deletion
Δ0169c-2	MAB_0169c	pGRNAz-*0169c* g5	c.171-172del	2 bp deletion
Δ0169c-3	MAB_0169c	pGRNAz-*0169c* g5	c.134-135ins TCGC	4 bp insertion
	MAB_0471	pGRNAz-*0471* g3	c.56-64del	9 bp deletion
Δ0471-1	MAB_0471	pGRNAz-*0471* g3	c.55-56insG	1 bp insertion
Δ0471-2	MAB_0471	pGRNAz-*0471* g3	c.55-56insG	1 bp insertion
	MAB_0471	pGRNAz-*0471* g3	c.56-61del	6 bp deletion
Δ0472-1	MAB_0472	pGRNAz-*0472* g2	c.97del	1 bp deletion
	MAB_0472	pGRNAz-*0472* g2	c.95-97del	3 bp deletion
Δ0472-2	MAB_0472	pGRNAz-*0472* g2	c.97del	1 bp deletion
Δ0472-3	MAB_0472	pGRNAz-*0472* g2	c.97del	1 bp deletion
Δ0472-4	MAB_0472	pGRNAz-*0472* g2	c.97-100del	4 bp deletion
	MAB_0472	pGRNAz-*0472* g4	c.242-250del	9 bp deletion
Δ1012c-1	MAB_1012c	pGRNA-*1012c* g2	c.182-194del	13 bp deletion
	MAB_1012c	pGRNA-*1012c* g2	c.183-191del	9 bp deletion
	MAB_1012c	pGRNA-*1012c* g2	c.186-197del	12 bp deletion
Δ1012c-2	MAB_1012c	pGRNA-*1012c* g2	c.185-195del	11 bp deletion
	MAB_1012c	pGRNA-*1012c* g2	c.186-197del	12 bp deletion
Δ1132c-1	MAB_1132c	pGRNAz-*1132c* g2	c.160del	1 bp deletion
	MAB_1132c	pGRNAz-*1132c* g3	c.198-203del	6 bp deletion
Δ1132c-2	MAB_1132c	pGRNAz-*1132c* g3	c.199-218del	20 bp deletion
Δ1132c-3	MAB_1132c	pGRNAz-*1132c* g5	c.256-257insG	1 bp insertion
Δ1283c	MAB_1283c	pGRNAz-*1283c* g3	c.271del	1 bp deletion
Δ2262c	MAB_2262c	pGRNAz-*2262c* g5	c.189-190insG	1 bp insertion
	MAB_2728c	pGRNAz-*2728c* g2	c.92-97del	6 bp deletion
	MAB_2728c	pGRNAz-*2728c* g2	c.92-97del	6 bp deletion

Strain ID	Target Gene	Plasmid	Mutation	Mutation Description
	MAB_2728c	pGRNAz-*2728c* g2	c.91-102del	12 bp deletion
	MAB_2728c	pGRNAz-*2728c* g2	c.91-96del	6 bp deletion
	MAB_2728c	pGRNAz-*2728c* g2	c.92-100del	9 bp deletion
	MAB_3473c	pGRNAz-*3473c* g1		15 bp deletion
	MAB_3473c	pGRNAz-*3473c* g1		3 bp insertion
	MAB_3473c	pGRNAz-*3473c* g1		3 bp deletion
	MAB_3473c	pGRNAz-*3473c* g1		3 bp deletion
	MAB_3473c	pGRNAz-*3473c* g4	c.229-231del	3 bp deletion
	MAB_3473c	pGRNAz-*3473c* g4	c.230-238del	9 bp deletion
	MAB_3473c	pGRNAz-*3473c* g4	c.230-238del	9 bp deletion
Δ3522c	MAB_3522c	pGRNAz-*3522c* g5	c.191-204del	14 bp deletion
Δ3523c	MAB_3523c	pGRNAz-*3523c* g1	c.20-21insA	1 bp insertion
Δ4163c	MAB_4163c	pGRNAz-*4163c* g2	c.70del	1 bp deletion
Δ4588c-1	MAB_4588c	pGRNAz-*4588c* g2	c.471del	1 bp deletion
Δ4588c-2	MAB_4588c	pGRNAz-*4588c* g2	c.471del	1 bp deletion
Δ4588c-3	MAB_4588c	pGRNAz-*4588c* g3	c.471del	1 bp deletion

4.3.2 MAB_0169c: Exported repetitive protein

MAB_0169c was selected as a target for knockout due to its homology to Rv3810[63], the *M. tuberculosis* virulence factor exported repetitive protein (Erp, also known as P36 and Pirg)[609]. Erp was the first mycobacterial virulence protein to be studied using targeted deletion[610] and has been characterised as a cell surface protein specific to the *Mycobacterium* genus found in both pathogenic and non-pathogenic mycobacterial species[611]. In *M. tuberculosis*, Erp is produced during phagosomal growth and although disruption of the *erp* gene in *M. tuberculosis* and *M. bovis* BCG impairs intracellular replication in cultured macrophages[610], expression of the *M. tuberculosis* Erp allele in non-pathogenic *M. smegmatis* does not confer any survival advantage[612]. Mutation of Erp in *M. bovis* BCG, *M. smegmatis* and *M. marinum* has been reported to cause altered colony morphology, producing smaller and more raised colonies than wild-type counterparts[610,611,613,614].

Three independent MAB_0169c knockout strains were produced using CRISPR-Cas9 targeting. The first, Δ0169c-1, carries frameshift mutations at two separate locations within the gene. As these mutations have occurred within the central domain of the protein, it is likely this double mutation is due to off-target action of the sgRNA caused by repeated PGLTS modules within this domain[609,610]. Δ0169c-2 carries a frameshift mutation at the start of the highly conserved carboxy-terminal domain, a hydrophobic region which anchors the Erp protein into the mycomembrane. Whilst this C-terminal domain is not required to restore wild-type colony morphology or virulence of Erp mutant strains, it is required for restoring resistance to SDS detergent[613,615]. Δ0169c-3, produced using the same sgRNA plasmid as Δ0169c-2, carries a frameshift mutation within the central domain, again suggesting a lack of specificity caused by the PGLTS repeats.

Infecting *D. melanogaster* with the three Δ0169c strains considerably prolonged survival compared to flies infected with wild-type *M. abscessus*, however ultimately still proved almost entirely fatal, as shown in Figure 4.2A. This is consistent with the study of Erp mutants of other pathogenic mycobacteria, *M. bovis*, *M. tuberculosis*, and *M. marinum*, in which loss of Erp function impairs intracellular growth in macrophages and replication in mice[610,612,615]. Zebrafish embryos infected with an *M. marinum* Erp mutant also show prolonged survival compared to wild-type infected embryos, however, still succumb to the infection[614]. Additionally, Erp mutant strains of *M. bovis* show normal *in vitro* growth despite the *in vivo* growth defect[616], consistent with my findings in Figure 4.2B in which growth of the Δ0169c strains in standard conditions was very similar to that of the wild-type strain

Studies of Erp mutants in other mycobacterial species such as *M. tuberculosis* and *M. marinum* found that the decreased virulence was caused by defects in their ability to replicate intracellularly. This is likely due to permeability defects, as *M. smegmatis* Erp mutants show increased sensitivity to detergents such as SDS[613], and *M. marinum* Erp mutants are

more susceptible to hydrophobic antibiotics without any change in resistance to hydrophilic compounds[614]. Bacterial load quantification within *D. melanogaster* did not show a reduction in Δ0169c-3 levels compared to that of wild-type at 72 hours post-infection (Figure 4.2C). This suggests that the Δ0169c strains do not have an *in vivo* growth defect, however, a caveat of this interpretation is that the flies injected with Δ0169c-3 show a higher initial dose. This may be due to structural changes in the mycomembrane leading to differences in the number of CFU in the same OD_{600} compared to the wild-type strain.

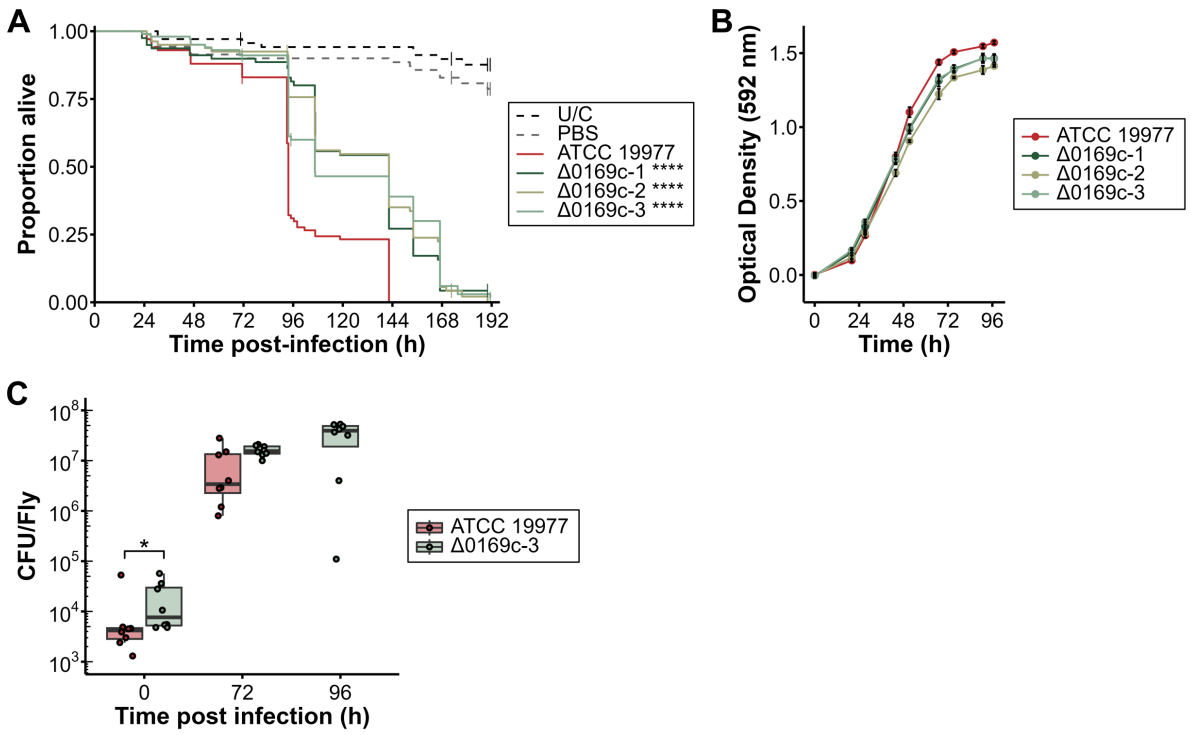


Figure 4.2. MAB_0169c contributes to *M. abscessus* virulence *in vivo*. (**A**) *In vivo* infection of w^{1118} flies with wild type *M. abscessus* ATCC 19977 (red) and three Δ0169c strains (green). Control groups (dotted lines) are uninjected controls U/C (black) and PBS Tween80 0.1% sterile injury control (grey). Data is pooled from three independent experiments, $103 \geq n \geq 70$ per group. Asterisks in the legend indicate the *p*-value compared to flies infected with ATCC 19977, compared using the Log-Rank test. (**B**) *In vitro* growth curve of wild type *M. abscessus* ATCC 19977 (red) and three Δ0169c strains (green) grown in standard 7H9 medium at 37°C shaking. Data represent the mean ± s.d of quadruplicate samples and are representative of three independent experiments. (**C**) Bacterial load quantification of w^{1118} flies infected with wild type *M. abscessus* ATCC 19977 (red) and Δ0169c-3 (green) at 0, 72, and 96 hours post-infection. Data represents one independent experiment, n = 8 per condition per time point. Statistical significance was determined using the Wilcoxon Rank-Sum test to compare strains at each time point. ∗, $P < 0.05$; ∗∗, $P < 0.01$; ∗∗∗, $P < 0.001$; ∗∗∗∗, $P < 0.0001$.

4.3.3 MAB_0471 and MAB_0472: Hypothetical transmembrane proteins

MAB_0471 and MAB_0472 were both identified from the phenogenomics study[581], in which clinical isolates with deletions in MAB_0471 were associated with increased *D. melanogaster* survival and more persistent infection in CF patients. These deletion mutations have also occurred in the ancestor of DCC2[581], which has spread to CF patients globally and shows greater levels of resistance and increased intracellular replication[163]. Epistatic analysis revealed an interaction between MAB_0471 and MAB_0472, and a CRISPRi knockdown of these genes confirmed the increase in *D. melanogaster* survival[581]. These genes show homology to *tad*/*flp* genes, and are discussed in greater detail in Chapter 5.

Initially, one MAB_0471 mutant strain was produced using CRISPR, Δ0471-1. Consistent with the survivals using MAB_0471 knockdown strains, *D. melanogaster* infected with Δ0471-1 show prolonged survival (Figure 4.3A). *In vitro* growth showed the Δ0471-1 strain reached a slightly lower OD_{600} at stationary phase (Figure 4.3B), but showed a significant *in vivo* growth defect in infected flies (Figure 4.3B). At 72 hours post-infection, flies infected with Δ0471-1 showed an approximately 7-fold decrease in CFU compared to flies infected with wild-type *M. abscessus*. There was a slight difference in the number of CFU per mL at OD_{600} = 0.05 between Δ0471-1 and wild-type, however, this was likely due to the large variation in the wild-type *M. abscessus* CFUs. Later work led to another MAB_0471 knockout strain being produced, Δ0471-2. This also showed increased survival of infected *D. melanogaster* (Figure 4.3E), and no difference in the number of CFU per mL at OD_{600} = 0.05 (Figure 4.3F).

These results were mirrored using the MAB_0472 knockout strains produced, supporting the idea that these two genes functionally interact. Again, initially, one *M. abscessus* MAB_0472 knockout strain was produced, Δ0472-1, which showed increased *D. melanogaster* survival (Figure 4.4A), slightly reduced stationary phase OD_{600} (Figure 4.4B), a strongly reduced bacterial load in infected flies at 72 hours post-infection (Figure 4.4C), and similar albeit

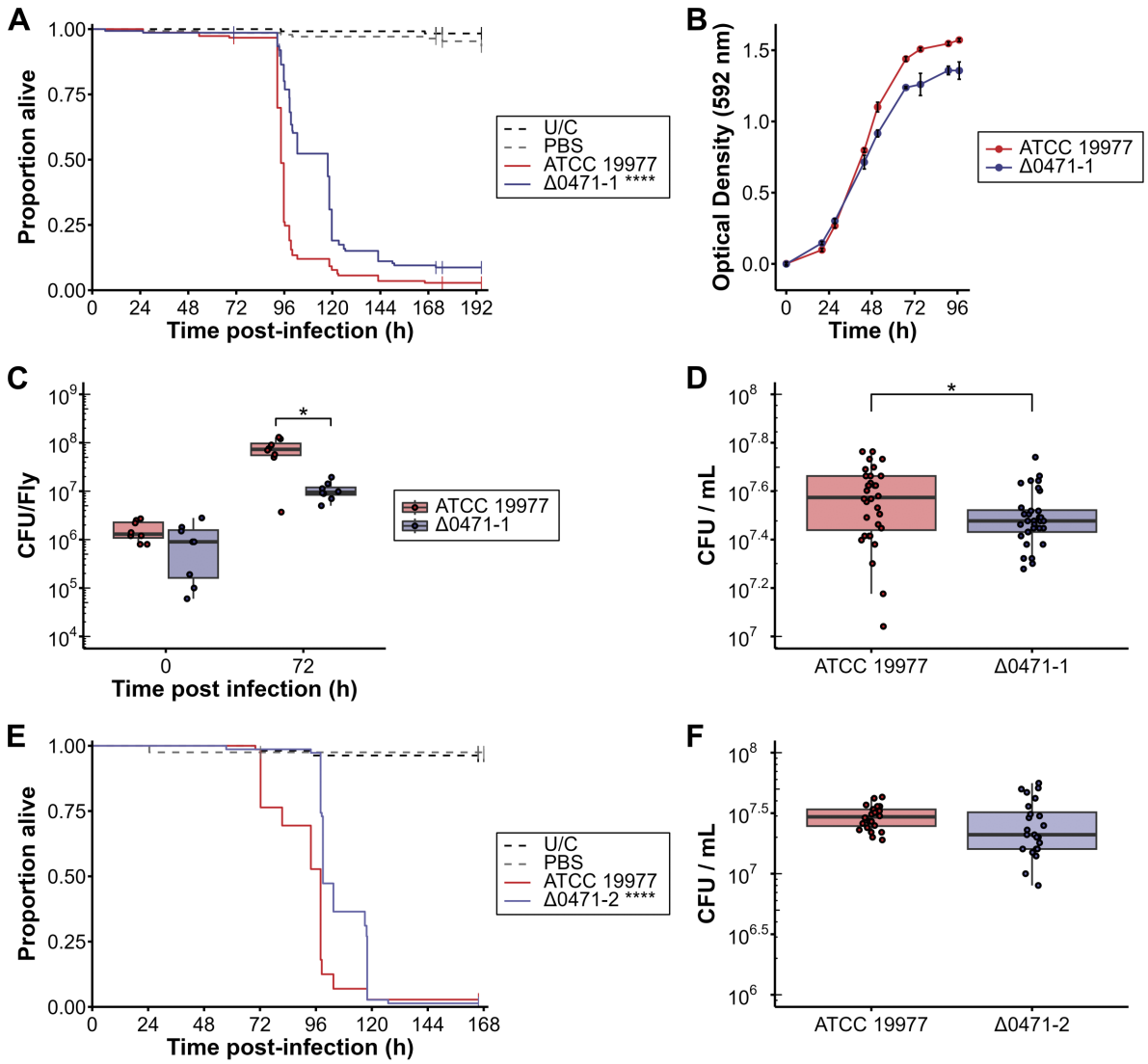


Figure 4.3. MAB_0471 knockout leads to decreased virulence and decreased replication *in vivo*. (**A**) *In vivo* infection of w^{1118} flies with wild type *M. abscessus* ATCC 19977 (red) and Δ0471-1 (purple). Control groups (dotted lines) are uninjected controls U/C (black) and PBS Tween80 0.1% sterile injury control (grey). Data is pooled from three independent experiments, $153 \geq n \geq 120$ per group. Asterisks in the legend indicate the *p*-value compared to flies infected with ATCC 19977, compared using the Log-Rank test. (**B**) *In vitro* growth curve of wild type *M. abscessus* ATCC 19977 (red) and Δ0471-1 (purple) grown in standard 7H9 medium at 37°C shaking. Data represent the mean ± s.d of quadruplicate samples and are representative of three independent experiments. (**C**) Bacterial load quantification of w^{1118} flies infected with wild type *M. abscessus* ATCC 19977 (red) and Δ0471-1 (purple) at 0, and 72 hours post-infection. Data represents one independent experiment, n = 8 per condition per time point. Statistical significance was determined using the Wilcoxon Rank-Sum test to compare strains at each time point. (**D**) Number of CFU per mL of *M. abscessus* ATCC 19977 (red) and Δ0471-1 (purple) at OD_{600} = 0.05, prepared in PBS Tween80 0.1%. Data is pooled from four independent experiments, n = 8 per strain per independent experiment. Caption continued on page 183.

Figure 4.3. MAB_0471 knockout leads to decreased virulence and decreased replication *in vivo* continued. Statistical significance was calculated by comparing the mutant strains to ATCC 19977 using unpaired two sample t-test. (**E**) *In vivo* infection of w^{1118} flies with wild type *M. abscessus* ATCC 19977 (red) and Δ0471-2 (purple). Control groups (dotted lines) are uninjected controls U/C (black) and PBS Tween80 0.1% sterile injury control (grey). Data is pooled from three independent experiments, $80 \geq n \geq 54$ per group. Asterisks in the legend indicate the *p*-value compared to flies infected with ATCC 19977, compared using the Log-Rank test. (**F**) Number of CFU per mL of *M. abscessus* ATCC 19977 (red) and Δ0471-2 (purple) at OD_{600} = 0.05, prepared in PBS Tween80 0.1%. Data is pooled from three independent experiments, n = 8 per strain per independent experiment. Statistical significance was calculated by comparing the mutant strains to ATCC 19977 using unpaired two sample t-test. $*$, P < 0.05; $**$, P < 0.01; $***$, P < 0.001; $****$, P < 0.0001.

marginally lower CFU per mL at OD_{600} = 0.05. Later strains produced, Δ0472-2, Δ0472-3 and Δ0472-4 also showed prolonged *D. melanogaster* survival (Figure 4.4E), however, this was not as pronounced as the original Δ0472-1 strain. Additionally, the CFU per mL of the Δ0472-2, Δ0472-3 and Δ0472-4 strains was distinctly lower than that of wild-type *M. abscessus* at OD_{600} = 0.05 (Figure 4.4F).

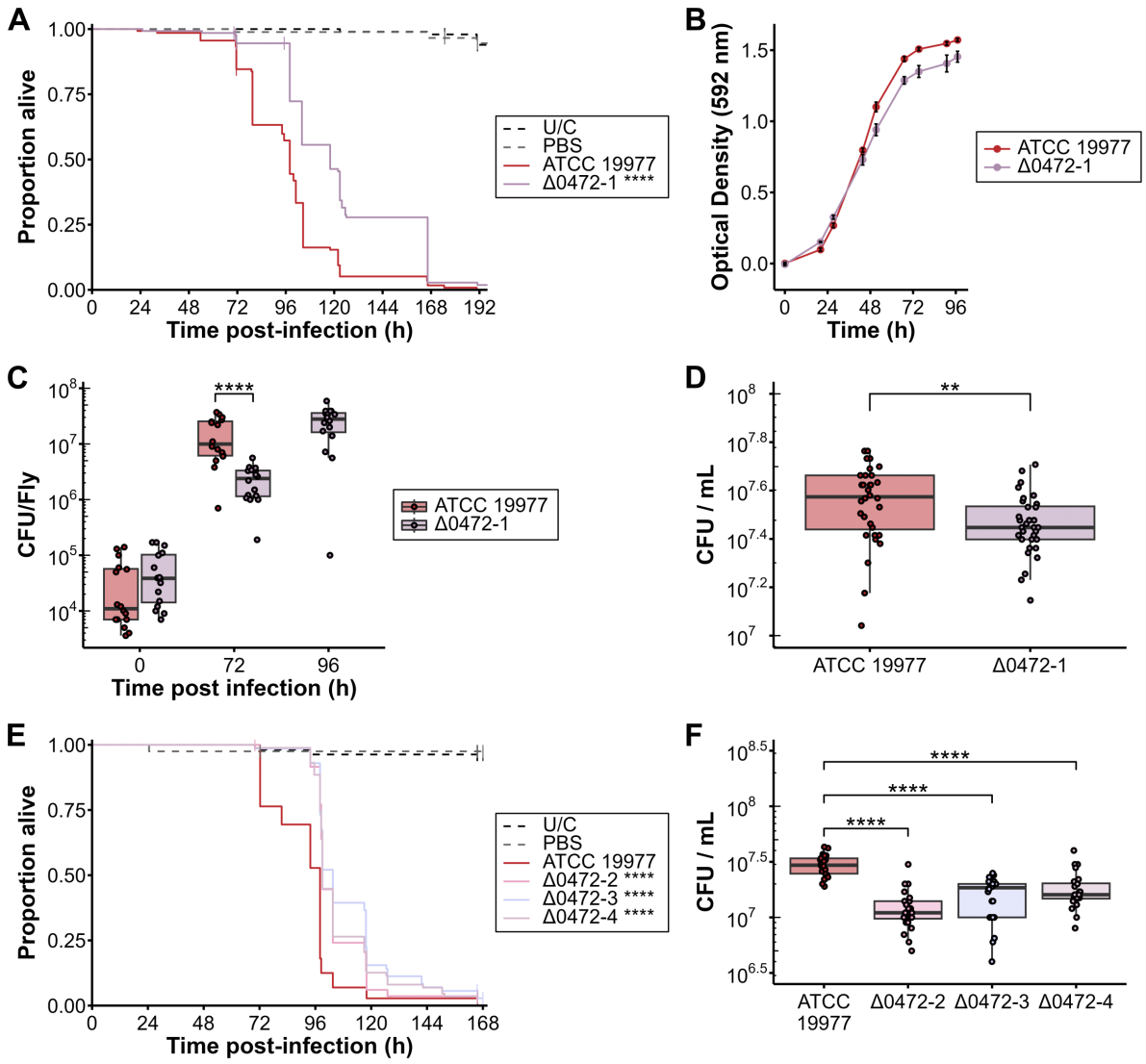


Figure 4.4. MAB_0472 knockout leads to decreased virulence and decreased replication *in vivo*. (**A**) *In vivo* infection of w^{1118} flies with wild type *M. abscessus* ATCC 19977 (red) and Δ0472-1 (pink). Control groups (dotted lines) are uninjected controls U/C (black) and PBS Tween80 0.1% sterile injury control (grey). Data is pooled from three independent experiments, $136 \geq n \geq 88$ per group. Asterisks in the legend indicate the *p*-value compared to flies infected with ATCC 19977, compared using the Log-Rank test. (**B**) *In vitro* growth curve of wild type *M. abscessus* ATCC 19977 (red) and Δ0472-1 (pink) grown in standard 7H9 medium at 37°C shaking. Data represent the mean ± s.d of quadruplicate samples and are representative of three independent experiments. (**C**) Bacterial load quantification of w^{1118} flies infected with wild type *M. abscessus* ATCC 19977 (red) and Δ0472-1 (pink) at 0, 72 and 96 hours post-infection. Data represents two independent experiments, n = 16 per condition per time point. Statistical significance was determined using the Wilcoxon Rank-Sum test to compare strains at each time point. (**D**) Number of CFU per mL of *M. abscessus* ATCC 19977 (red) and Δ0472-1 (pink) at OD_{600} = 0.05, prepared in PBS Tween80 0.1%. Data is pooled from four independent experiments, n = 8 per strain per independent experiment. Caption continued on 185.

Figure 4.4. MAB_0472 knockout leads to decreased virulence and decreased replication *in vivo* continued. Statistical significance was calculated by comparing the mutant strains to ATCC 19977 using unpaired two sample t-test. (**E**) *In vivo* infection of w^{1118} flies with wild type *M. abscessus* ATCC 19977 (red), Δ0472-2, Δ0472-3 and Δ0472-4 (pink). Control groups (dotted lines) are uninjected controls U/C (black) and PBS Tween80 0.1% sterile injury control (grey). Data is pooled from three independent experiments, $87 \geq n \geq 54$ per group. Asterisks in the legend indicate the *p*-value compared to flies infected with ATCC 19977, compared using the Log-Rank test. (**F**) Number of CFU per mL of *M. abscessus* ATCC 19977 (red), Δ0472-2, Δ0472-3 and Δ0472-4 (pink) at OD_{600} = 0.05, prepared in PBS Tween80 0.1%. Data is pooled from three independent experiments, n = 8 per strain per independent experiment. Statistical significance was calculated by comparing the mutant strains to ATCC 19977 using Wilcoxon Rank-Sum test. $*$, P < 0.05; $**$, P < 0.01; $***$, P < 0.001; $****$, P < 0.0001.

4.3.4 MAB_1012c: YrbE family protein

MAB_1012c was originally identified from the phenogenomics study due to mutations in this gene being associated with changes in *D. melanogaster* survival and intracellular replication[581]. MAB_1012c is annotated as a YrbE family protein, meaning it is likely part of one of the seven mammalian cell entry (mce) operons within the *M. abscessus* genome[63]. These operons typically consist of eight core genes, YrbE A-B and Mce A-F, and are named from a study which found that introducing the *mce1A* gene from *M. tuberculosis* into a nonpathogenic strain of *E. coli* conferred the ability to invade and replicate intracellularly within the nonphagocytic HeLa cell line[617]. These operons were initially considered virulence factors[618–620], with the number of mce operons being reported to correlate with virulence[621], however, whilst these operons are certainly an important determinant in virulence of pathogenic mycobacterial species[619,620,622,623] they are also present in comparable numbers in non-pathogenic species[624]. The *M. tuberculosis* genome contains four *mce* operons, *M. smegmatis* contains six, and *M. leprae* contains only one[624,625]. This has led to the suggestion that *mce* operons are involved in adaptation to adverse environmental conditions as their expression is dependent on stress conditions such as hypoxia, oxidative stress, carbon sources and starvation[626].

The *mce* operons encode a subfamily of ATP-binding cassette (ABC) transporters, with Mce

proteins showing homology to substrate-binding proteins and YrbE proteins showing homology to permeases with ATPase interacting domains[624]. Evidence suggests these operons are involved in the transport of lipids and homeostasis of the mycobacterial cell wall, transporting cholesterol from the host, or mycolic acids and other mycobacterial lipids, possibly by forming multi-protein complexes[623,627–630]. The role of the *mce* operons in cell wall homeostasis is evident in studies in *M. smegmatis*, in which loss of all six *mce* operons induced profound changes in colony morphology and biofilm formation[628]. Despite this understanding of *mce* operons as a whole, the physiological function of YrbE proteins remains unclear. One study found that expression of the *M. tuberculosis* YrbE3A gene in *M. smegmatis* and *M. bovis* BCG led to altered colony morphology and reduced intracellular survival in macrophages, likely due to increased expression of TNFα via phosphorylation of p-JNK by YrbE3A[631]. In *M. tuberculosis mce1* operon, YrbE1B is the target of a negative regulator protein Mce1N which physically prevents interaction of the transmembrane domain and nucleotide binding domain[632]. Whilst the two *M. tuberculosis mce1* YrbE genes, YrbE1A and YrbE1B, show sequence similarity between 65 and 75% in the majority of mycobacterial species, the YrbE genes from RGM species within the Abscessus-Chelonae clade show less than 14% sequence similarity. This suggests that the *mce* operons in these species, and in ancestral RGM species, may have a different function[147]. Despite *M. abscessus* having seven mce operons, none of these are directly syntenic to the *mce1* operon of *M. tuberculosis*[323].

In *M. abscessus*, the gene MAB_1012c is part of an *mce* operon with six *mce* genes (MAB_1005c - MAB_1010c) and two YrbE genes (MAB_1011c and MAB_1012c). This *mce* operon, along with four other *M. abscessus mce* operons, were found to be strongly upregulated in response to hypoxia[56]. Two independent Δ1012c strains were produced using CRISPR-Cas9, both using the same sgRNA plasmid with deletions of different sizes in the same gene location. *D. melanogaster* infected with either of the Δ1012c strains show increased survival relative to flies infected with wild-type *M. abscessus*, shown in Figure 4.5A. The *in vitro*

growth of the Δ1012c strains shows slower log phase growth and a reduced stationary phase level (Figure 4.5B). This impaired *in vitro* growth appears to be mirrored *in vivo*, with a small reduction in bacterial load at 72 hours post-infection, albeit not statistically significant (Figure 4.5C).

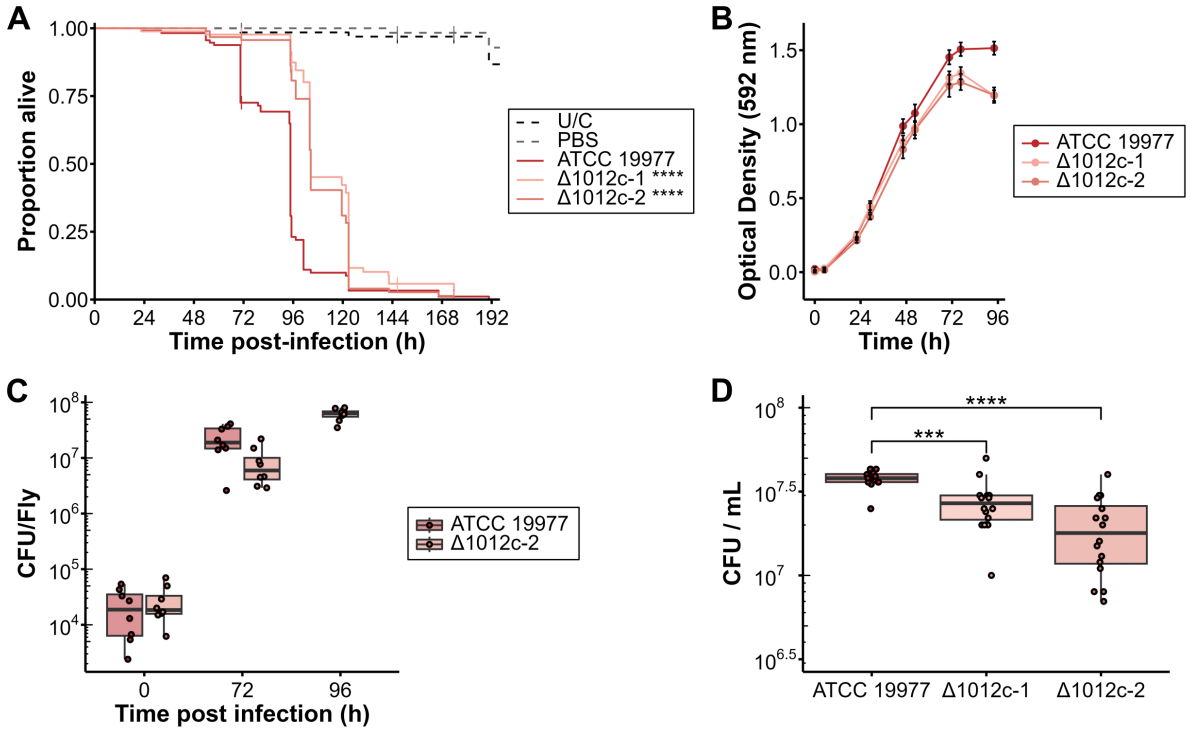


Figure 4.5. MAB_1012c is required for *M. abscessus* virulence *in vivo*. (**A**) *In vivo* infection of w^{1118} flies with wild type *M. abscessus* ATCC 19977 (red), Δ1012-1 or Δ1012-2 (orange). Control groups (dotted lines) are uninjected controls U/C (black) and PBS Tween80 0.1% sterile injury control (grey). Data is pooled from three independent experiments, $113 \geq n \geq 64$ per group. Asterisks in the legend indicate the *p*-value compared to flies infected with ATCC 19977, compared using the Log-Rank test. (**B**) *In vitro* growth curve of wild type *M. abscessus* ATCC 19977 (red), Δ1012-1 and Δ1012-2 (orange) grown in standard 7H9 medium at 37°C shaking. Data represent the mean ± s.d of quadruplicate samples and are representative of three independent experiments. (**C**) Bacterial load quantification of w^{1118} flies infected with wild type *M. abscessus* ATCC 19977 (red) or Δ1012-2 (orange) at 0, 72 and 96 hours post-infection. Data represents one independent experiment, n = 8 per condition per time point. Statistical significance was determined using the Wilcoxon Rank-Sum test to compare strains at each time point. (**D**) Number of CFU per mL of *M. abscessus* ATCC 19977 (red), Δ1012-1 and Δ1012-2 (orange) at OD_{600} = 0.05, prepared in PBS Tween80 0.1%. Data is pooled from two independent experiments, n = 8 per strain per independent experiment. Statistical significance was calculated by comparing the mutant strains to ATCC 19977 using unpaired two sample t-test. ∗, P < 0.05; ∗∗, P < 0.01; ∗∗∗, P < 0.001; ∗∗∗∗, P < 0.0001.

The number of CFU per mL of the two Δ1012c strains at the same OD_{600} was slightly lower than

that of the wild-type *M. abscessus* (Figure 4.5D), possibly indicating differences in the cell wall. This difference in the CFU to OD_{600} ratio may further exaggerate the differences seen between the Δ1012c strains and wild-type *M. abscessus* in the *in vitro* growth curve, but despite this difference, *D. melanogaster* were injected with comparable initial loads of either wild-type *M. abscessus* or Δ1012c-2.

4.3.5 MAB_1132c: L-asparagine permease

MAB_1132c was also originally identified as a hit from the phenogenomics study[581] and selected for knockout. The alleles identified were present only in clinical isolates of the *M. abscessus massiliense* clade and were associated with changes in *D. melanogaster* survival, *D. melanogaster* immune response, and resistance to antibiotics[581]. It is annotated as a probable asparagine permease, and the role and function of this gene is discussed in greater detail in Chapter 6.

Three independent Δ1132c strains were produced using CRISPR knockout, each using a different sgRNA producing frameshift mutations in different locations within the gene. Infecting *D. melanogaster* with the Δ1132c strains resulted in a very consistent increase in fly survival compared to infection with wild-type *M. abscessus*, with flies dying approximately a day later (Figure 4.6A). The *in vitro* growth of the Δ1132c strains was also very similar to that of wild-type *M. abscessus* (Figure 4.6B). Bacterial load quantification showed a very slight decrease in the number of CFU per fly for Δ1132c-1 and Δ1132c-2 of approximately 2-fold compared to wild-type *M. abscessus* infected flies. This difference is not sufficient to explain the increase in survival, based on the dose response experiments from the previous chapter (Figure 3.1C). Additionally, by 96 hours post-infection flies infected with the Δ1132c strains show considerably greater numbers of bacteria than the wild-type reached by 72 hours post-infection, both 24 hours before the respective groups began dying. This suggests that the observed increase in fly survival due to loss of MAB_1132c function is caused by a decrease in *M. abscessus*

virulence rather than a change in *in vivo* growth. Finally, I confirmed that the number of CFU per mL at OD_{600} = 0.05 for the Δ1132c strains was similar to that of wild-type *M. abscessus*, shown in Figure 4.6D).

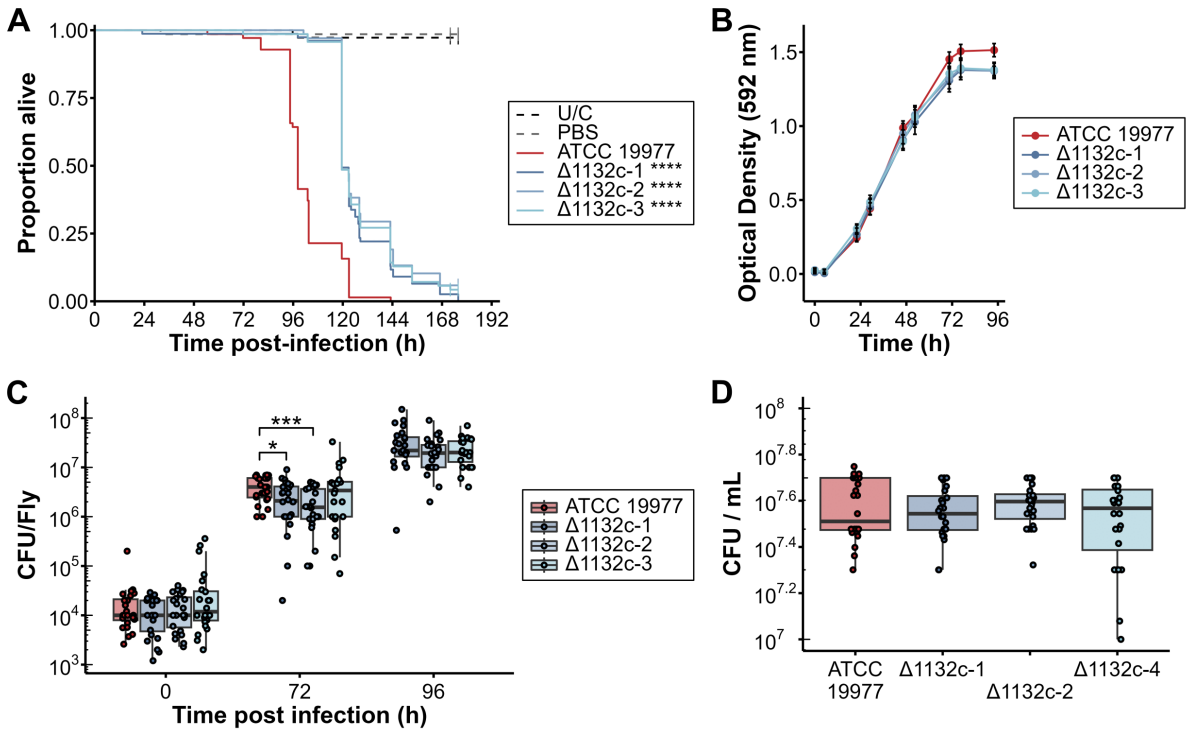


Figure 4.6. Loss of MAB_1132c leads to decreased *M. abscessus* virulence. (**A**) *In vivo* infection of w^{1118} flies with wild type *M. abscessus* ATCC 19977 (red), Δ1132c-1, Δ1132c-2 or Δ1132c-3 (blue). Control groups (dotted lines) are uninjected controls U/C (black) and PBS Tween80 0.1% sterile injury control (grey). Data is pooled from three independent experiments, 77 ≥ n ≥ 68 per group. Asterisks in the legend indicate the *p*-value compared to flies infected with ATCC 19977, compared using the Log-Rank test. (**B**) *In vitro* growth curve of wild type *M. abscessus* ATCC 19977 (red), Δ1132c-1, Δ1132c-2 and Δ1132c-3 (blue) grown in standard 7H9 medium at 37°C shaking. Data represent the mean ± s.d of quadruplicate samples and are representative of three independent experiments. (**C**) Bacterial load quantification of w^{1118} flies infected with wild type *M. abscessus* ATCC 19977 (red), Δ1132c-1, Δ1132c-2 or Δ1132c-3 (blue) at 0, 72 and 96 hours post-infection. Data represents three independent experiments, n = 8 per condition per time point per experiment. Statistical significance was determined using the Wilcoxon Rank-Sum test to compare strains at each time point. (**D**) Number of CFU per mL of *M. abscessus* ATCC 19977 (red), Δ1132c-1, Δ1132c-2 or Δ1132c-3 (blue) at OD_{600} = 0.05, prepared in PBS Tween80 0.1%. Data is pooled from three independent experiments, n = 8 per strain per independent experiment. Statistical significance was calculated by comparing the mutant strains to ATCC 19977 using the Wilcoxon Rank-Sum test. ∗, P < 0.05; ∗∗, P < 0.01; ∗∗∗, P < 0.001; ∗∗∗∗, P < 0.0001.

4.3.6 MAB_1283c: WXG100 family type VII secretion target

MAB_1283c was also selected as a target for knockout in *M. abscessus* based on the results from the phenogenomics and knockdown study, with knockdown of MAB_1283c associated with increased *D. melanogaster* survival[581]. Unfortunately, it was originally annotated as an uncharacterised protein, with no predicted domains and no hits from blast searches to identify similar proteins in other species. Recently the protein name for MAB_1283c was updated to WXG100 family type VII secretion target. These ESX (type VII) system substrates are short α-helical proteins, exemplified by the well-characterised EsxA and EsxB (also known as ESAT-6 and CFP10, respectively) of *M. tuberculosis*[633], and are grouped into three subfamilies: CFP-10, ESAT-6-like, and *sag*EsxA-like[634]. As these proteins are typically secreted as heterodimers, the genes encoding the two products are often located together as bicistrons upstream of the ESX structural components[635–638]. MAB_1283c appears to lack the characteristic WxG motif that this family of proteins is named for, however, it does contain the reported secretion signal motif YxxxD/E (YDNTE)[639] and is also predicted to form the characteristic four-helix bundle structure. It is genomically close to another WXG100 family type VII secretion target (MAB_1280c) and ESX-1 secretion-associated protein EspA/EspE-like domain-containing protein (MAB_1285c), but does not appear to be in close proximity to the *M. abscessus* ESX-3 locus (MAB_2224c - MAB_2234c)[74] or the ESX-4 locus (MAB_3573c - MAB_3760)[68]. It is also possible that MAB_1283c functions as a homodimer, which the mono-cistronic *sag*EsxA-like WXG100 proteins are reported to do[634].

The *M. abscessus* Δ1283c strain produced contained a single base pair deletion, likely leading to disruption of the C-terminal domain including the secretion signal motif and helical structures. During infection of *D. melanogaster*, flies infected with Δ1283c survived considerably longer than wild-type *M. abscessus* infected flies (Figure 4.7A), consistent with the original knockdown studies[581].

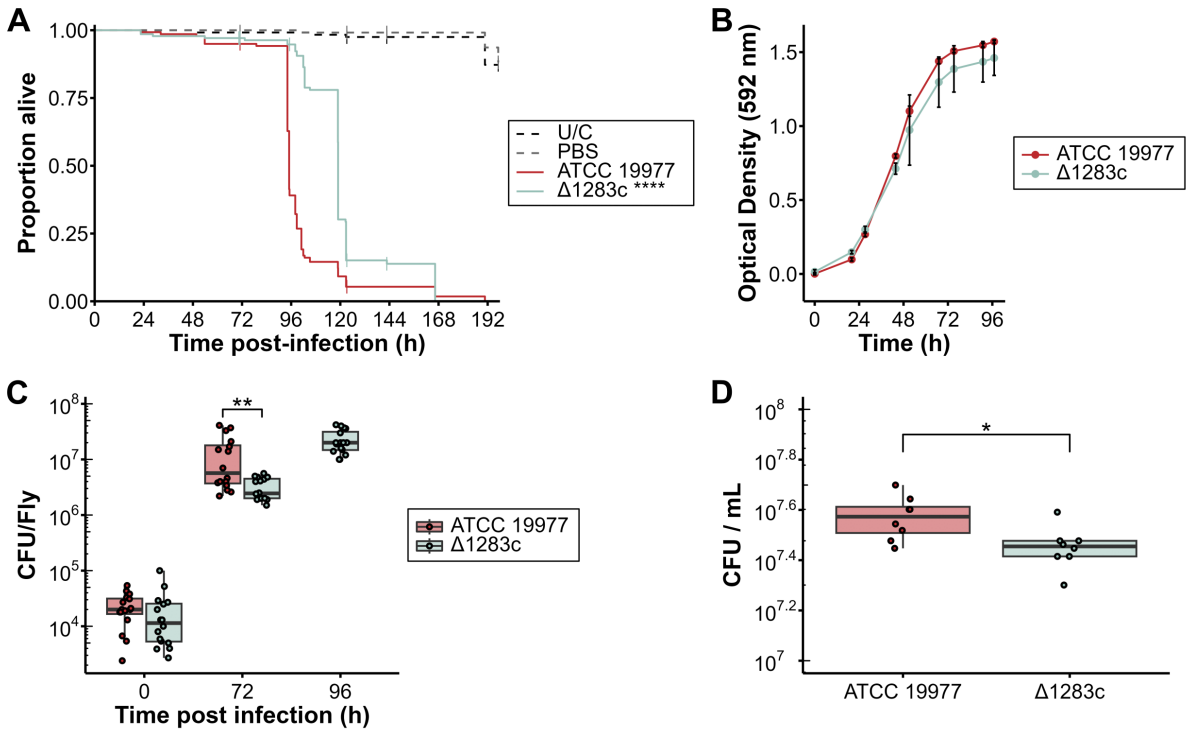


Figure 4.7. MAB_1283c contributes to *M. abscessus* virulence *in vivo*. (**A**) *In vivo* infection of w^{1118} flies with wild type *M. abscessus* ATCC 19977 (red) and Δ1283c (green). Control groups (dotted lines) are uninjected controls U/C (black) and PBS Tween80 0.1% sterile injury control (grey). Data is pooled from three independent experiments, $139 \geq n \geq 119$ per group. Asterisks in the legend indicate the *p*-value compared to flies infected with ATCC 19977, compared using the Log-Rank test. (**B**) *In vitro* growth curve of wild type *M. abscessus* ATCC 19977 (red) and Δ1283c (green) grown in standard 7H9 medium at 37°C shaking. Data represent the mean ± s.d of quadruplicate samples and are representative of three independent experiments. (**C**) Bacterial load quantification of w^{1118} flies infected with wild type *M. abscessus* ATCC 19977 (red) and Δ1283c (green) at 0, 72 and 96 hours post-infection. Data represents two independent experiments, n = 8 per condition per time point per experiment. Statistical significance was determined using the Wilcoxon Rank-Sum test to compare strains at each time point. (**D**) Number of CFU per mL of *M. abscessus* ATCC 19977 (red) and Δ1283c (green) at OD_{600} = 0.05, prepared in PBS Tween80 0.1%. Data is pooled from one independent experiment, n = 8 per strain. Statistical significance was calculated by comparing the mutant strains to ATCC 19977 using unpaired two sample t-test. ∗, P < 0.05; ∗∗, P < 0.01; ∗∗∗, P < 0.001; ∗∗∗∗, P < 0.0001.

In vitro growth also showed very little difference between Δ1283c and wild-type *M. abscessus* (Figure 4.7B). At 72 hours post-infection, the bacterial load of wild-type *M. abscessus* flies was slightly higher than that of flies infected with Δ1283c, and by 96 hours post-infection flies infected with Δ1283c had comparable bacterial loads to flies infected with wild-type *M. abscessus* at 72 hours post-infection (Figure 4.7C). This suggests that there is a mild *in vivo* growth defect and that the increase in *D. melanogaster* survival is predominantly being driven

by a decrease in virulence in the Δ1283c strain. The number of CFU at OD_{600} = 0.05 was marginally lower for Δ1283c compared to wild-type *M. abscessus* (Figure 4.7D), however the 1.3-fold difference is unlikely to have a significant impact and indeed the bacterial load quantification at 0 hours post-infection shows comparable initial doses for each stain.

4.3.7 MAB_2262c: Mycobactin import ATP-binding/permease protein IrtA

MAB_2262c encodes a mycobactin import ATP-binding/permease protein IrtA, and was selected for knockout due to its similarity to *M. tuberculosis* virulence factor Rv1348 which is required for growth in iron-deficient conditions[63]. Iron is an essential nutrient for almost all living organisms particularly due to its role as an enzyme cofactor. For intracellular pathogens such as *M. abscessus* and *M. tuberculosis*, availability of iron is severely restricted during infection as it is stored by host metal-binding proteins such as heme and ferritin[640–642]. This requires mycobacterial pathogens to scavenge iron away from the host using two high-affinity iron siderophores unique to mycobacteria. These are mycobactin (MBT) which is lipid-anchored to the cell wall, and carboxymycobactin (cMBT) which is a water-soluble secreted form[643,644]. MAB_2262c encodes a putative IdeR binding site suggesting its regulation is controlled by IdeR, the iron response transcriptional regulator[645].

In *M. tuberculosis*, IrtA is part of a heterodimeric ABC transporter alongside IrtB which facilitates import of iron-bound mycobacterial siderophores from the periplasm across the cytoplasmic membrane[646,647]. The IrtAB ABC transporter contains two transmembrane domains and two nucleotide binding domains, one of each in IrtA and IrtB. Additionally, IrtA contains an N-terminal siderophore interaction domain that is required for the uptake of Fe^{3+}-MBT, but not Fe^{3+}-cMBT. This also controls the reduction of Fe^{3+}-MBT by a flavin-adenine dinucleotide electron donor, releasing acquired iron into the cytoplasm[647,648]. Despite functioning as an ABC importer, the IrtAB complex is folded in the typical manner of an ABC exporter[647] and it has been suggested that IrtA can function as an independent ABC transporter to export

non-ferrated siderophores[649]. In acidic conditions the solubility of transition metals such as iron is increased, allowing iron to cross biological membranes and contribute to ROS generation via the Fenton reaction. It was recently found that in acidic conditions, IrtA, IrtB, mycobactin biosynthesis genes and the ESX-3 genes required for mycobactin import were all downregulated in *M. abscessus*, possibly in an effort to mitigate stress from ROS[650].

The Δ2262c *M. abscessus* strain showed the strongest change in phenotype of all of the *M. abscessus* knockout mutants produced. Infected *D. melanogaster* survived for 3 days longer than wild-type infected flies (Figure 4.8A), despite being injected with approximately 14-fold more bacteria based on the bacterial load quantification (Figure 4.8C). This likely suggests a significant change in OD_{600} to CFU ratio. Based on the bacterial load quantification, *in vivo* growth of the Δ2262c strain is severely impaired, by 72 hours post-infected wild-type *M. abscessus* has reached numbers of CFU per fly over 6-fold higher than that of Δ2262c. The Δ2262c strain continues to show very slow growth between 72 hours and 120 hours post-infection with a doubling time of 22.5 hours, over twice as long as wild-type *M. abscessus* (Figure 3.2B). There appears to be no growth defect in *in vitro* growth (Figure 4.8B), although without knowing the OD_{600} to CFU ratio this cannot be confirmed. Nevertheless, the fact that the Δ2262c strain does grow within and ultimately kill infected *D. melanogaster* suggests that the bacteria are still capable of acquiring iron. Import of mycobactin possibly occurs via the ESX-3 system[64,65] and reduction to release iron may be achieved by another ferric-siderophore reductase such as ViuB which has been described in *M. tuberculosis* and is homologous to IrtA-NTD[648,651], MAB_3205c in *M. abscessus*.

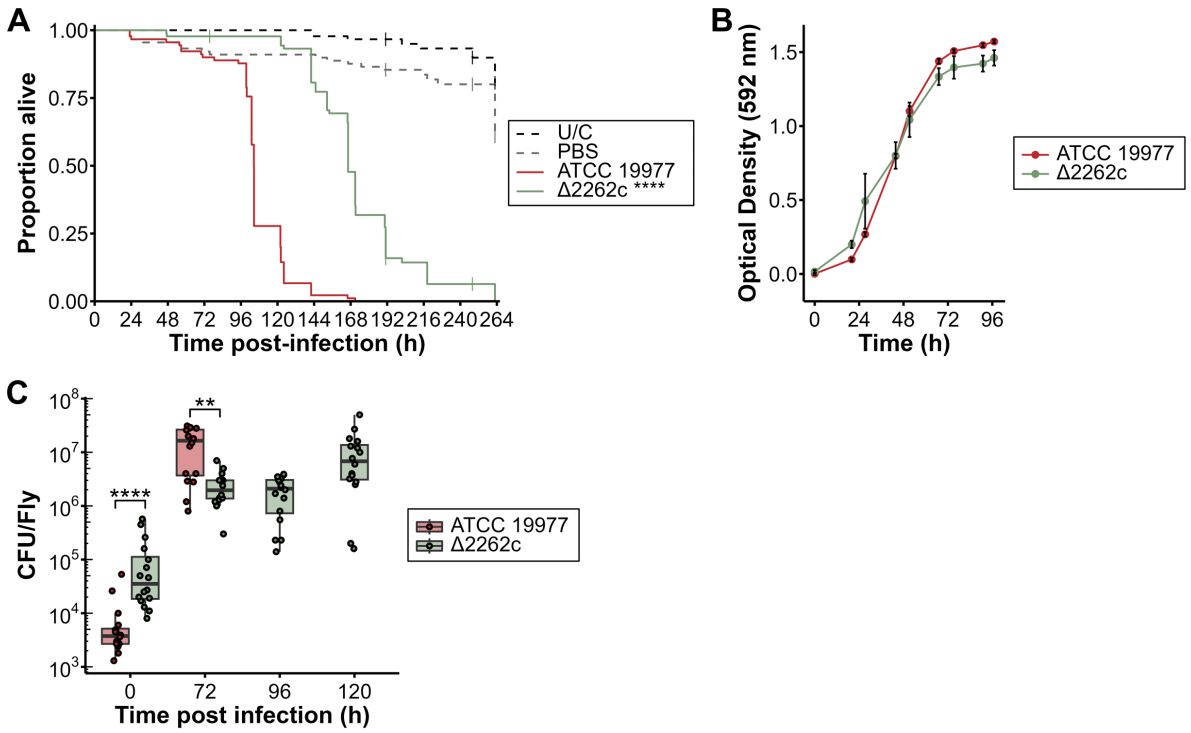


Figure 4.8. Loss of MAB_2262c severely impairs *in vivo* growth. (**A**) *In vivo* infection of w^{1118} flies with wild type *M. abscessus* ATCC 19977 (red) and Δ2262c (green). Control groups (dotted lines) are uninjected controls U/C (black) and PBS Tween80 0.1% sterile injury control (grey). Data is pooled from three independent experiments, n = 90 per group. Asterisks in the legend indicate the *p*-value compared to flies infected with ATCC 19977, compared using the Log-Rank test. (**B**) *In vitro* growth curve of wild type *M. abscessus* ATCC 19977 (red) and Δ2262c (green) grown in standard 7H9 medium at 37°C shaking. Data represent the mean ± s.d of quadruplicate samples and are representative of three independent experiments. (**C**) Bacterial load quantification of w^{1118} flies infected with wild type *M. abscessus* ATCC 19977 (red) and Δ2262c (green) at 0, 72, 96 and 120 hours post-infection. Data represents two independent experiments, n = 8 per condition per time point per experiment. Statistical significance was determined using the Wilcoxon Rank-Sum test to compare strains at each time point. ∗, P < 0.05; ∗∗, P < 0.01; ∗∗∗, P < 0.001; ∗∗∗∗, P < 0.0001.

4.3.8 MAB_3522c and MAB_3523c: Assimilatory sulfite reductase and Integral membrane nitrite extrusion protein NarK3

Nitrate reduction has been described in *M. tuberculosis* due to hypoxia, serving as a respiratory function to support a non-replicating dormant population[652]. There is very little information about whether *M. abscessus* uses nitrate reduction genes to support pathogenesis and persistence in a similar manner, so MAB_3522c and MAB_3532c were targeted for CRISPR knockout.

MAB_3522c is annotated as assimilatory sulfite reductase, but is homologous to NirB[653], the small subunit of the NirBD NADH-dependent nitrite reductase. In *M. tuberculosis*, NirBD functions to assimilate nitrogen, however, this only occurs *in vitro* when nitrate or nitrite are provided as the sole nitrogen source as nitrite reduction to ammonium is energetically costly and consumes 6 electrons. This may also explain the apparent preference *M. tuberculosis* has for asparagine as a nitrogen source over nitrite[654,655]. NirBD mutant *M. tuberculosis* strains are attenuated during hypoxic dormancy even in the presence of alternative nitrogen sources, suggesting an additional role beyond nitrogen assimilation by aiding removal of toxic nitrite. The production of ammonium also serves to increase the pH of the acidic phagosome environment, promoting survival[656]. NirB is also required for biofilm formation and maturation in *M. tuberculosis*[103,657]. MAB_3523c is annotated as integral membrane nitrite extrusion protein NarK3. In *M. tuberculosis* during nitrate respiration, NarK3 is another mechanism to protect against nitrite toxicity by exporting nitrite out of the cell[656,658]. NirB and NarK3 are both regulated by GlnR and are upregulated in response to nitrogen stress, and it has been shown that the metabolism of nitrate and nitrite are both important adaptations for intracellular survival of pathogenic mycobacteria regardless of oxygen status[659,660].

A study into the transcriptional response of *M. abscessus* to hypoxia and the DosRS two component system found contrary findings to the production of these nitrite reduction and extrusion genes. In hypoxic conditions, MAB_3522c and MAB_3523c, along with orphan response regulator MAB_3520c and the NirD subunit MAB_3521c, were among the most strongly downregulated genes. However, in a DosRS mutant *M. abscessus* strain in hypoxic conditions, MAB_3521c and MAB_3523c were among the most strongly upregulated genes, suggesting that DosRS may act to repress transcription of these nitrate reduction genes during hypoxia[56]. These differences in the role of nitrate reduction during hypoxia between *M. abscessus* and *M. tuberculosis* may be a product of experimental conditions caused by whether or not nitrogen limitation is induced and nitrate is provided as the sole nitrogen source.

M. smegmatis strains transformed with MAB_3521c and MAB_3522c, the NirBD subunits, showed significantly delayed bacterial killing time by amikacin, clarithromycin, and linezolid, both in liquid culture and in intracellular infection of macrophages[653]. As with *M. tuberculosis*, transcriptional regulation of NirB and NarK3 is controlled by GlnR[654,660–662], and regulation of these genes and others within the GlnR regulon also facilitates biofilm formation in *M. abscessus*[662].

Infecting flies with Δ3522c or Δ3523c both led to prolonged *D. melanogaster* survival compared to infection with wild-type *M. abscessus* (Figures 4.9A and 4.10A), and neither mutant strain showed any difference in *in vitro* growth characteristics (Figures 4.9B and 4.10B). However, whilst the Δ3522c strain shows reduced *in vivo* growth based on the bacterial load quantification compared to wild-type *M. abscessus* (Figure 4.9C), Δ3523c appears to grow at the same rate as wild-type and so reaches higher bacterial loads within the fly before death (Figure 4.10C). This suggests that nitrite reduction by MAB_3522c is required for proper *in vivo* growth of *M. abscessus*, whereas nitrite extrusion by MAB_3523c is not. It is, therefore, possible that nitrite extrusion is contributing to *M. abscessus* virulence, either by the effect of secreted nitrite on the host, or by changes in *M. abscessus* metabolism due to accumulating levels of intracellular nitrite.

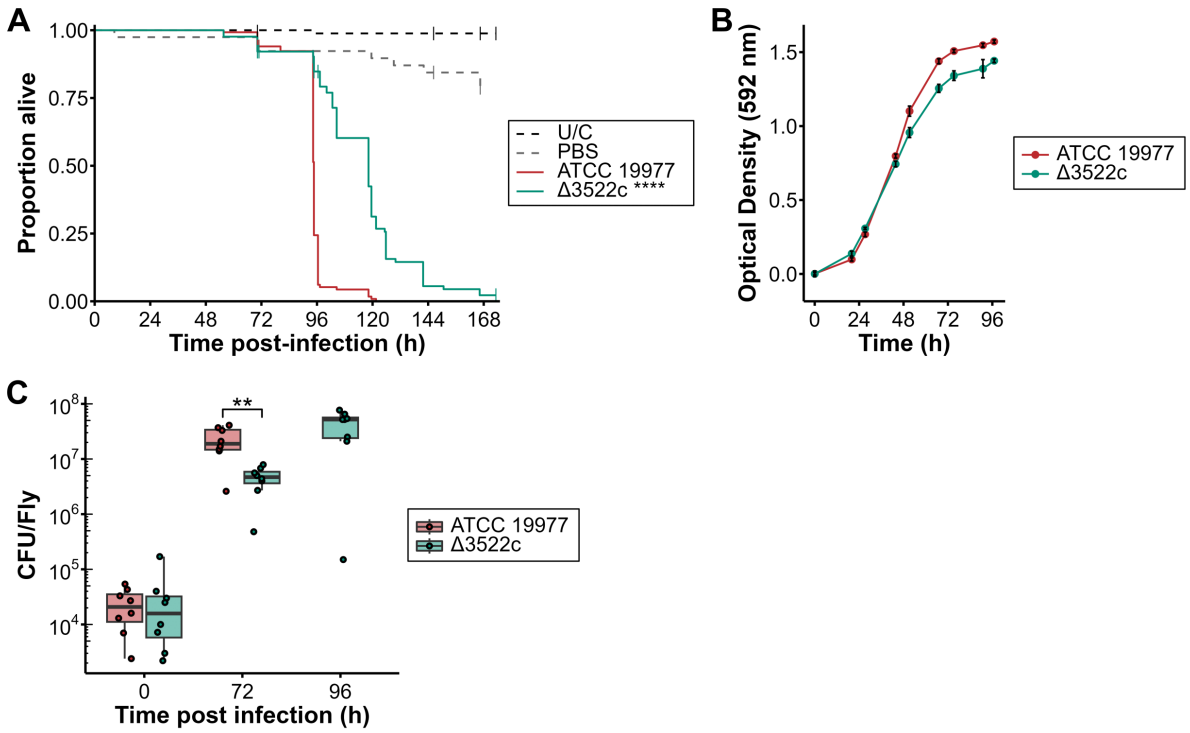


Figure 4.9. Nitrite reduction by MAB_3522c is involved in *in vivo* growth of *M. abscessus*. (**A**) *In vivo* infection of w^{1118} flies with wild type *M. abscessus* ATCC 19977 (red) and Δ3522c (blue). Control groups (dotted lines) are uninjected controls U/C (black) and PBS Tween80 0.1% sterile injury control (grey). Data is pooled from three independent experiments, $135 \geq n \geq 86$ per group. Asterisks in the legend indicate the *p*-value compared to flies infected with ATCC 19977, compared using the Log-Rank test. (**B**) *In vitro* growth curve of wild type *M. abscessus* ATCC 19977 (red) and Δ3522c (blue) grown in standard 7H9 medium at 37°C shaking. Data represent the mean ± s.d of quadruplicate samples and are representative of three independent experiments. (**C**) Bacterial load quantification of w^{1118} flies infected with wild type *M. abscessus* ATCC 19977 (red) and Δ3522c (blue) at 0, 72 and 96 hours post-infection. Data represents one independent experiment, n = 8 per condition per time point. Statistical significance was determined using the Wilcoxon Rank-Sum test to compare strains at each time point. $*$, $P < 0.05$; $**$, $P < 0.01$; $***$, $P < 0.001$; $****$, $P < 0.0001$.

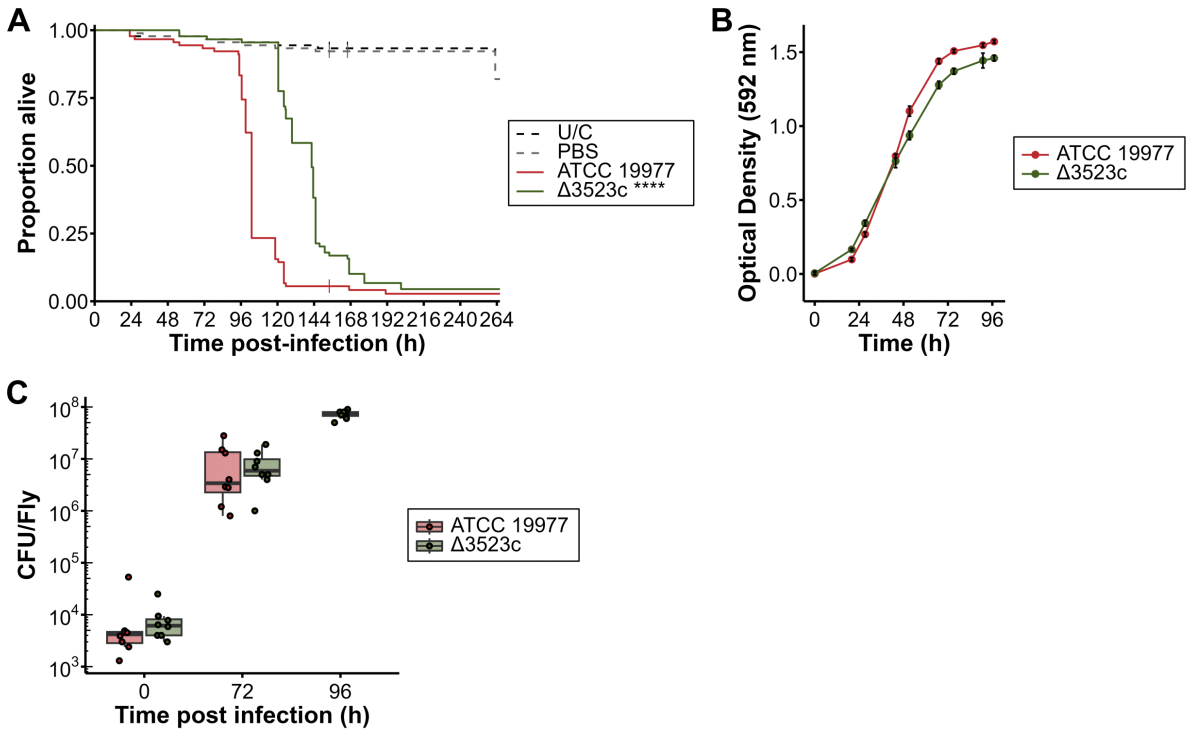


Figure 4.10. Nitrite extrusion by MAB_3523c contributes to *M. abscessus* virulence. (**A**) *In vivo* infection of w^{1118} flies with wild type *M. abscessus* ATCC 19977 (red) and Δ3523c (green). Control groups (dotted lines) are uninjected controls U/C (black) and PBS Tween80 0.1% sterile injury control (grey). Data is pooled from three independent experiments, n = 90 per group. Asterisks in the legend indicate the *p*-value compared to flies infected with ATCC 19977, compared using the Log-Rank test. (**B**) *In vitro* growth curve of wild type *M. abscessus* ATCC 19977 (red) and Δ3523c (green) grown in standard 7H9 medium at 37°C shaking. Data represent the mean ± s.d of quadruplicate samples and are representative of three independent experiments. (**C**) Bacterial load quantification of w^{1118} flies infected with wild type *M. abscessus* ATCC 19977 (red) and Δ3523c (green) at 0, 72 and 96 hours post-infection. Data represents one independent experiment, n = 8 per condition per time point. Statistical significance was determined using the Wilcoxon Rank-Sum test to compare strains at each time point. ∗, P < 0.05; ∗∗, P < 0.01; ∗∗∗, P < 0.001; ∗∗∗∗, P < 0.0001.

4.3.9 MAB_4163c: Fatty-acid-CoA ligase FadD

A defining characteristic of pathogenic mycobacteria is the unique ability to assimilate lipids from hosts such as fatty acids and cholesterol. These lipids not only serve as an important carbon source, but their catabolic products serve functions in persistence and virulence of the mycobacteria. MAB_4163c was selected as a *M. abscessus* gene target due to its homology to *M. tuberculosis* FadD19 (Rv3515c), a fatty-acid-CoA ligase involved in cholesterol metabolism. Cholesterol is required for *in vivo* growth and persistence of *M. tuberculosis* in mice models[623]. Strains with impaired cholesterol processing exhibit considerable defects in

intracellular growth[663–668]. The ability to completely degrade cholesterol requires a cluster of approximately 96 genes involved in cholesterol import, degradation and regulation[669–671]. The degradation of cholesterol can be considered in three parts: oxygen-dependent cleavage of the A and B rings, oxidative degradation of the C and D rings, and β-oxidation of the acyl side chain[670] for which FadD19 is required[672,673]. Firstly, the side chain is hydroxylated by monooxygenases at the terminal C26 or C27 carbon of cholesterol. FadD19 then ligates a coenzyme-A (CoA) which is necessary to initiate the first of several rounds of β-oxidation and the subsequent release of a propionyl-CoA unit[667,674,675].

Propionyl-CoA can act as a precursor to potentially toxic metabolites. *M. tuberculosis* is extremely sensitive to changes in levels of propionyl-CoA, so uses various metabolic pathways to manage this[668,676–678]. Firstly, using isocitrate lyases. Isocitrate lyase 1 (ICL1) and isocitrate lyase 2 (ICL2) are the first enzymes in the glyoxylate cycle for growth on even-chain fatty acids[679]. These ICL enzymes show 2-methylisocitrate lyase (MCL) activity[680], acting within the methylcitrate cycle for growth on odd-chain and branched-chain fatty acids[679]. This activity is essential in *M. tuberculosis* which does not contain a distinct MCL. In contrast, *M. abscessus* and the other species within the "*Abscessus-Chelonae*" clade only possess a single ICL homologous to *M. tuberculosis* ICL1, and a distinct MCL enzyme (Supplementary Figure S4.1). Multiple sequence alignment of *M. abscessus* ICL MAB_4095c and *M. tuberculosis* ICL1 shows 83% similarity[63] between the two proteins, with a conserved active site (black boxes), suggesting the *M. abscessus* ICL enzyme also has MCL activity (Supplementary Figure S4.2). It is this MCL activity that converts propionyl-CoA to succinate and pyruvate as the last reaction of the methylcitrate cycle, which then enters the TCA cycle[676,681].

The alternative method of removing propionyl-CoA is via a propionyl-CoA carboxylase which produces methylmalonyl-CoA. This can then either feed the methylmalonyl pathway to produce succinyl-CoA[678] or contribute to the synthesis of bioactive cell wall lipids alongside

malonyl-CoA produced from acetyl-CoA[682,683]. These cell wall lipids produced from the three-carbon intermediates derived from cholesterol include phthiocerol dimycocerosates (PDIM) and sulfolipid-1 (SL-1), which are highly potent virulence factors due to modulation of host cell and tissue responses[684–689]. This production of polyketide lipids also requires excess fatty acid-AMP primers, which intracellular mycobacteria likely also acquire from host sources[686]. Supply of excess fatty acids can overcome growth inhibition of an ICL1 *M. tuberculosis* mutant[668] and also counter growth inhibition caused by itaconic acid produced by macrophages to inhibit ICL1 and ICL2 activity[679,690].

D. melanogaster is a cholesterol auxotroph meaning sterols are dietarily acquired[691,692]. Due to the use of yeast-based food to maintain *D. melanogaster*, the dietary sterol provided is predominantly ergosterol. Flies infected with Δ4163c show increased survival compared to wild-type *M. abscessus* (Figure 4.11A) and reduced *in vivo* growth as seen by the over 10-fold reduction in bacterial load at 72 hours post-infection (Figure 4.11C). By 96 hours post-infection, flies infected with Δ4163c have a similar bacterial load to flies infected with wild-type *M. abscessus* at 72 hours post-infection. This indicates that MAB_4163c is required for *in vivo* growth of *M. abscessus*, possibly functioning to degrade host-acquired ergosterol, but does not appear to alter the virulence of *M. abscessus*. There are no significant differences between Δ4163c and wild-type *M. abscessus* in terms of *in vitro* growth (Figure 4.11B) or OD_{600} to CFU ratio (Figure 4.11D).

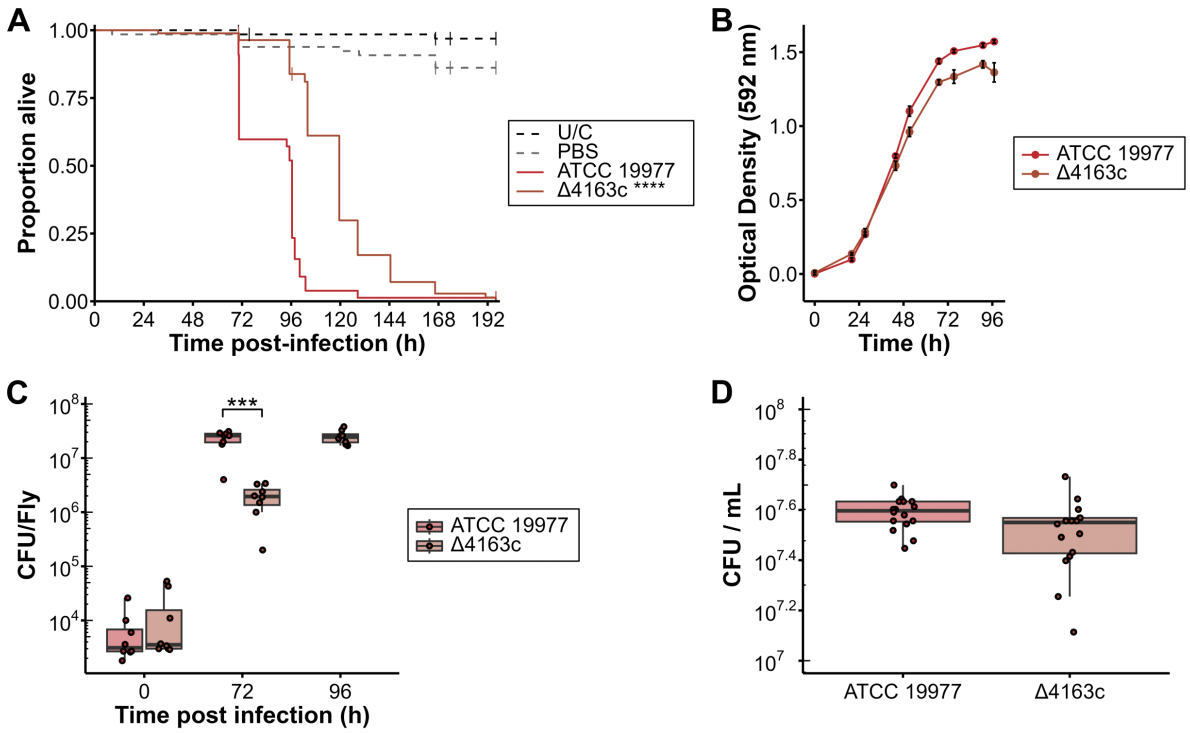


Figure 4.11. MAB_4163c knockout strongly attenuates growth in *D. melanogaster*. (**A**) *In vivo* infection of w^{1118} flies with wild type *M. abscessus* ATCC 19977 (red) and Δ4163c (brown). Control groups (dotted lines) are uninjected controls U/C (black) and PBS Tween80 0.1% sterile injury control (grey). Data is pooled from three independent experiments, $89 \geq n \geq 65$ per group. Asterisks in the legend indicate the *p*-value compared to flies infected with ATCC 19977, compared using the Log-Rank test. (**B**) *In vitro* growth curve of wild type *M. abscessus* ATCC 19977 (red) and Δ4163c (brown) grown in standard 7H9 medium at 37°C shaking. Data represent the mean ± s.d of quadruplicate samples and are representative of three independent experiments. (**C**) Bacterial load quantification of w^{1118} flies infected with wild type *M. abscessus* ATCC 19977 (red) and Δ4163c (brown) at 0, 72 and 96 hours post-infection. Data represents one independent experiment, n = 8 per condition per time point. Statistical significance was determined using the Wilcoxon Rank-Sum test to compare strains at each time point. (**D**) Number of CFU per mL of *M. abscessus* ATCC 19977 (red) and Δ4163c (brown) at OD_{600} = 0.05, prepared in PBS Tween80 0.1%. Data is pooled from two independent experiments, n = 8 per strain per independent experiment. Statistical significance was calculated by comparing the mutant strains to ATCC 19977 using unpaired two sample t-test. ∗, P < 0.05; ∗∗, P < 0.01; ∗∗∗, P < 0.001; ∗∗∗∗, P < 0.0001.

4.3.10 MAB_4588c: Enoyl-CoA hydratase/isomerase

MAB_4588c, annotated as an enoyl-CoA hydratase/isomerase, was selected for targeting due to its predicted role in fatty acid metabolism. MAB_4588c shares 68.67% identity to Rv0222 (also known as echA1) in *M. tuberculosis*, which is required within the bacterial cytosol to hydrate double bonds in *cis*-unsaturated fatty acids. This is followed by degradation by FadAB to produce acetyl-CoA for use in the TCA cycle[693]. Rv0222 has also been identified as a

diagnostic biomarker for *M. tuberculosis*[694,695].

A recent study used a panel of 208 secreted mycobacterial proteins and lipoproteins expressed in HEK293T cells to identify factors that inhibit inflammatory responses via NF-κB or AP-1[696]. Rv0222 was identified to inhibit NF-κB activation, and an *M. tuberculosis* Rv0222-deletion mutant was found to induce significantly higher levels of pro-inflammatory cytokines in primary peritoneal macrophages and showed lower bacterial burdens in an *in vivo* mouse infection. The authors suggested that Rv0222 had a second role within the host cytoplasm as it is ubiquitinated at K76 by a host ubiquitin ligase anaphase promoting complex subunit 2 (ANAPC2), which then allows Rv0222 to recruit SHP1 protein tyrosine phosphatase to TRAF6 and inhibit its ubiquitination, impairing NF-κB activation. Although it is unclear how Rv0222 may be secreted into the host cytosol as there is no discernible signal peptide, it does contain a WxG motif which raises the possibility that it can be secreted by an ESX system. Alternatively, the protein may be released into the host cytosol by the lysis of some intracellular bacilli, aiding the remaining bacteria[696,697]. As there is no other information regarding this protein in *M. abscessus*, it is not clear that MAB_4588c is a homologue for Rv0222. Another *M. abscessus* gene, MAB_0606c, is also annotated as a probable enoyl CoA hydratase and was reported to be similar to Rv0222, however the protein similarity between MAB_0606c and Rv0222 is only 44%[698].

Three Δ4588c *M. abscessus* strains were produced, however all three carried the same frameshift mutation. Δ4588c-1 and Δ4588c-2 were both produced using the same sgRNA plasmid, whereas Δ4588c-3 was produced with a different sgRNA plasmid. Unlike the other genetic knockout strains produced, there was no difference between any of the Δ4588c strains and wild-type *M. abscessus* in terms of *D. melanogaster* survival (Figure 4.12A), *in vitro* growth (Figure 4.12C), or bacterial load (Figure 4.12C). This is possibly due to redundancy caused by the large number of other enoyl-CoA hydratases involved in β-oxidation. There was a slight reduction in the number of CFU per mL at OD_{600} = 0.05 for all three Δ4588 strains compared

to wild-type *M. abscessus* (Figure 4.12D), however the difference was very small.

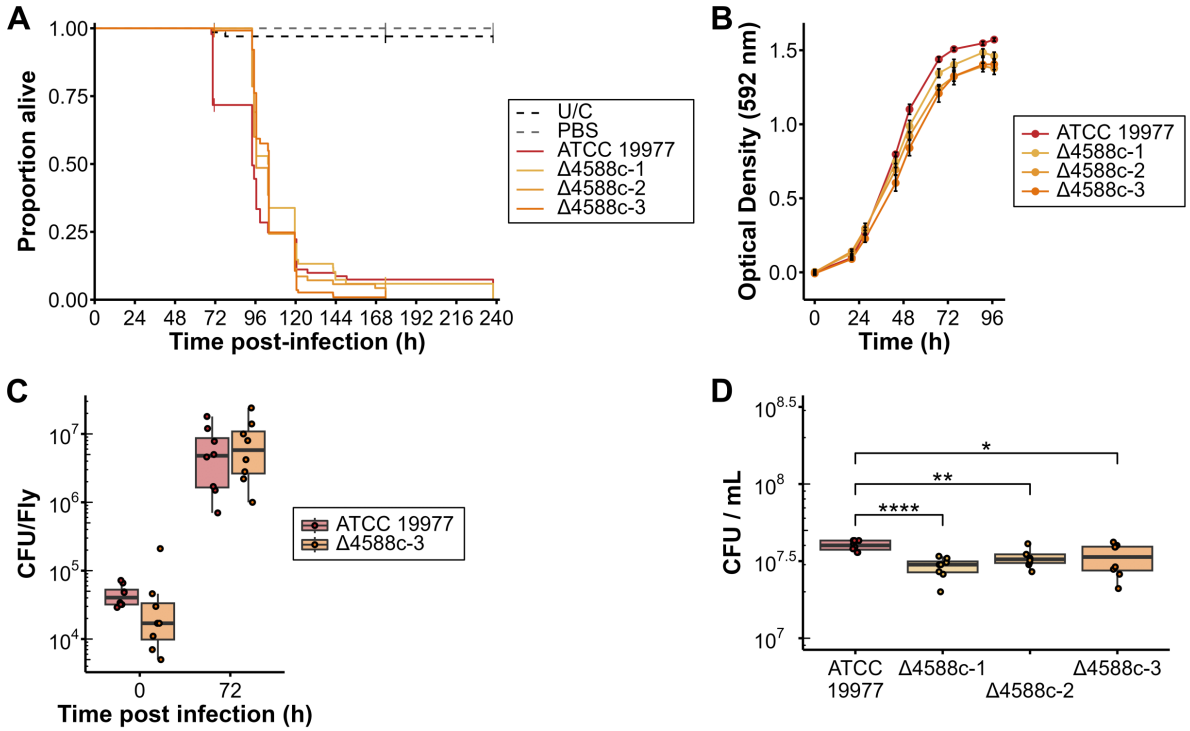


Figure 4.12. MAB_4588c does not appear to be required for infection of *D. melanogaster* by *M. abscessus*. (**A**) *In vivo* infection of w^{1118} flies with wild type *M. abscessus* ATCC 19977 (red), Δ4588c-1, Δ4588c-2 and Δ4588c-3 (yellow). Control groups (dotted lines) are uninjected controls U/C (black) and PBS Tween80 0.1% sterile injury control (grey). Data is pooled from three independent experiments, 123 ≥ n ≥ 65 per group. Asterisks in the legend indicate the *p*-value compared to flies infected with ATCC 19977, compared using the Log-Rank test. (**B**) *In vitro* growth curve of wild type *M. abscessus* ATCC 19977 (red), Δ4588c-1, Δ4588c-2 and Δ4588c-3 (yellow) grown in standard 7H9 medium at 37°C shaking. Data represent the mean ± s.d of quadruplicate samples and are representative of three independent experiments. (**C**) Bacterial load quantification of w^{1118} flies infected with wild type *M. abscessus* ATCC 19977 (red) and Δ4588c-3 (yellow) at 0 and 72 hours post-infection. Data represents one independent experiment, n = 8 per condition per time point. Statistical significance was determined using the Wilcoxon Rank-Sum test to compare strains at each time point. (**D**) Number of CFU per mL of *M. abscessus* ATCC 19977 (red), Δ4588c-1, Δ4588c-2 and Δ4588c-3 (yellow) at OD_{600} = 0.05, prepared in PBS Tween80 0.1%. Data represents one independent experiment, n = 8 per strain. Statistical significance was calculated by comparing the mutant strains to ATCC 19977 using unpaired two sample t-test. ∗, P < 0.05; ∗∗, P < 0.01; ∗∗∗, P < 0.001; ∗∗∗∗, P < 0.0001.

4.4 Discussion

4.4.1 CRISPR editing of *M. abscessus* and gene essentiality

In this chapter I have shown that the two plasmid CRISPR-Cas9 method used is capable of inducing frameshift mutations in *M. abscessus*, without overexpression of the NHEJ repair

machinery[579] and without requiring the removal of antibiotic resistance cassettes[699] or integrated plasmids[580] from the genome.

Using the two plasmid CRISPR-Cas9 method for gene editing in *M. abscessus* was straightforward and relatively efficient. Of the 18 genes targeted, 11 were successfully knocked out to produce loss-of-function mutant strains. A recent study using transposon mutagenesis found that 2 gene targets, MAB_1933 glutamine synthetase and MAB_3473c SsrA-binding protein, are essential in *M. abscessus*[608], explaining the 0% frameshift generation efficiency for all sgRNAs targeting MAB_1933 and MAB_3473c. It is unclear why there was no frameshift editing in the 5 remaining genes targeted. MAB_2228c, a homologue of EsxH in *M. tuberculosis*, and MAB_2728c, a homologue of invasion protein Inv1 in *M. tuberculosis* (Rv1477), are unlikely to be essential genes and some sgRNAs did show levels of gene editing, but no frameshift generation. It is also unclear why no knockout mutants were produced for MAB_3521c, the NirD subunit of nitrite reductase NirBD, despite the successful knockout of MAB_3522c NirD. This likely represents a failure of the sgRNAs used, and it is possible that generating and screening more stains will produce frameshift knockouts of these genes. Although MAB_3029 IdeR and MAB_4095c Icl are not reported to be essential in *M. abscessus* based on the transposon mutagenesis study, the function of these genes has been reported to be essential in *M. tuberculosis*[700–702].

Based on the 11 genes that had successful frameshift mutations, there was an overall frameshift generation efficiency of 22%, however, this may be an underestimation as the method of identifying mutants could overlook large deletion events[580]. As this method used a longer induction time than that reported for CRISPR-Cas9 editing of *M. marinum*[580], it is important to perform WGS on the strains produced to check for off-target genomic mutations and to consider optimising the doxycycline induction conditions if necessary. This method for the production of loss-of-function mutant strains of *M. abscessus* will enable future research into

genetic determinants of pathogenesis, accelerating our understanding of this bacterium and aid development of novel treatments.

4.4.2 Future work using the *M. abscessus* knockout strains

Using the *M. abscessus* CRISPR knockout strains produced there is huge potential in studying the role each of these genes has in *M. abscessus* during infection. The initial experiments to describe the *in vivo D. melanogaster* survival phenotypes of each of these mutants have led to many outstanding questions for each target gene.

Firstly, is there a structural change in the cell wall of the Δ0169c Erp mutant strains? *M. smegmatis* Erp mutants show an altered colony morphology which is smaller and more raised than wild-type colonies[613], and mutations in Erp lead to permeability defects[613,614]. Recent work in *M. tuberculosis* has also found that Erp interacts with an unknown protein, Rv2617c, and these two proteins are required for resisting oxidative stress by hydrogen peroxide[703]. Similar studies using the *M. abscessus* Δ0169c strains could assess changes in resistance to SDS, hydrophilic versus hydrophobic antibiotics, and hydrogen peroxide, along with colony imaging to visualise morphological changes. Repeat experiments are required to understand if there is an *in vivo* growth defect of the Δ0169c strains in *D. melanogaster*, using OD_{600} to CFU ratios to ensure a consistent initial dose is injected into each fly. Further studies could make use of the S2 *D. melanogaster* cell line to understand the role of Erp in the intracellular behaviour of *M. abscessus*, and identify host factors that it may interact with to better understand the function of this protein during infection. The Erp protein of *M. tuberculosis* was found to interact with an adenylyl cyclase, Rv2212, and this interaction increased the intracellular survival of *M. smegmatis* in THP-1 macrophages[704]. This raises additional questions about whether the cAMP levels of the *M. abscessus* Δ0169c strains are altered, and whether this is responsible for the observed changes in virulence.

The Δ1012c strains can be used to study the role of this particular mce (MAB_1005c -

MAB_1012c) operon in *M. abscessus*. Expression levels of these genes can be measured in various conditions, such as oxidative stress or starvation to see how they are induced, and possibly identify the transcriptional regulators responsible for their control[626]. Possible differences in colony morphology may explain the reduction in OD_{600} to CFU ratio observed, as has been described in *M. smegmatis*[628]. The potential role of this mce operon in cholesterol or lipid uptake may be responsible for such morphological changes, and could also be assessed by measuring growth in minimal medium with various lipids as sole carbon sources. *D. melanogaster* could also be used to identify if *M. abscessus* also drives changes in immune responses by manipulating JNK activity[631] and whether this requires MAB_1012c activity. This would make use of *D. melanogaster* lines with mutations in different aspects of JNK signalling, RT-qPCRs to measure transcriptional changes in the immune response, and Western Blots to assess phosphorylation levels of the various JNK signalling components.

Unfortunately very little is known about MAB_1283c. Based on the survival and bacterial load quantification of flies infected with Δ1283c, it appears to be involved in virulence, possibly as a virulence factor secreted by an ESX system. Cell culture and imaging studies using this knockout mutant strain would indicate if this gene product is secreted into the intracellular environment and interferes with phagosomal maturation in some manner, similar to that of other Esx proteins.

The importance of iron acquisition for intracellular growth of *M. abscessus* is clearly highlighted by the severe *in vivo* growth defect of the Δ2262c knockout strains. As the Δ2262c strain did still grow in *D. melanogaster* and eventually kill all infected flies, it is clear *M. abscessus* is still capable of acquiring iron via other mechanisms, as has been reported in *M. tuberculosis*[646]. Using tools such as RT-qPCR or RNAseq, we could assess transcriptional changes in the Δ2262c strain compared to wild-type *M. abscessus* when grown in low-iron conditions to identify other systems that may be responsible for iron uptake in the absence

of IrtA. Further information about the role of IrtA can be gleaned using Δ2262c, such as whether IrtA is required in some capacity for siderophore export[649]. Blue agar chrome azurol S (CAS) assay can be used to detect siderophores which scavenge iron from an Fe-CAS-hexadecyltrimethylammonium bromide complex, causing the agar to change colour from blue to orange. Proper mycobactin biosynthesis and transport is also required for normal cell wall structure and permeability, and *M. tuberculosis* strains with mutations in mycobactin biosynthesis show distinct colony morphology[705]. If IrtA is also involved in transporting mycobactin to the cell surface, Δ2262c would likely show similar changes in morphology. Finally, the Δ2262c strain can be used to study the role of iron acquisition in *M. abscessus* biofilm formation. Iron is critical for robust pellicle biofilm formation by *M. smegmatis*, independent from planktonic growth requirements, possibly due to the induction of genes involved in producing fatty acid matrix components[101].

To confirm the function of MAB_3522c as a nitrite reductase to assimilate nitrogen, experiments measuring growth in a minimal medium with a defined nitrogen source such as nitrate, nitrite or ammonium[654] can be used. Recent work has found that knockout of the global nitrogen regulator GlnR (MAB_0744) from *M. abscessus* reduced biofilm formation and resistance to antibiotics, but both these phenotypes were rescued by the addition of glutamine or glutamate. Among the seven genes most decreased in the *glnR* knockout mutant were MAB_3522c and MAB_3523c, suggesting these genes are crucial components in the early formation of pellicle biofilms[662]. Whilst overexpression of each gene individually within the *glnR* knockout was not sufficient to increase the production of biofilm[662], the Δ3522c and Δ3523c strains could be used to explore the role these genes play in biofilm formation and antibiotic resistance.

Cholesterol metabolism is a fundamental aspect of *M. tuberculosis* metabolism to promote intracellular survival and contributes to the production of PDIM and SL-1 whilst imposing the need for removal of toxic propionyl-CoA. In *M. abscessus*, MAB_4163c is upregulated in

response to hypoxia[56] and within amoeba and macrophages[298], along with other genes involved in β-oxidation of fatty acids. Whilst MAB_4163c is clearly important for *in vivo* growth of *M. abscessus* within *D. melanogaster*, its role in cholesterol degradation can be tested by performing growth experiments with defined carbon sources, including cholesterol and ergosterol. Additionally, the Δ4163c strain can be used to study how cholesterol metabolism is regulated in *M. abscessus*. In *M. tuberculosis*, cAMP production[706,707] and iron chelator sAEL057[708] both cause defects in cholesterol metabolism. Comparing the growth of Δ4163c and Δ2262c to wild-type *M. abscessus* in iron-deplete or iron-replete minimal medium with cholesterol as the sole carbon source could show the possible role of iron acquisition in cholesterol metabolism in *M. abscessus*.

Despite there being no observable survival or *in vivo* growth difference between wild-type *M. abscessus* and the Δ4588c strains, the *D. melanogaster* model could continue to be used to study these mutants. Considering the findings that Rv0222 in *M. tuberculosis* impairs NF-κB signalling by interfering with TRAF6 activity[696], it would be interesting to test if MAB_4588c acts in a similar manner in *M. abscessus*. The results from Chapter 3 indicate that loss of AMP production in *D. melanogaster*, controlled by NF-κB proteins Rel and Dif, does not have any impact on fly survival during *M. abscessus* infection, and so if MAB_4588c is inhibiting their action it is unsurprising that we see no difference in host survival with the Δ4588c strains. Use of RT-qPCR would indicate whether there are changes in AMP transcription during infection with the Δ4588c strains compared to wild-type *M. abscessus*, and whether any such changes are dependent on *D. melanogaster* Traf6 could be assessed using mutant fly lines.

Chapter 5: Putative type-IVb pilus in *Mycobacterium abscessus* and its interactions with host signalling pathways

5.1 Introduction

In the previous chapter, I assessed the impact of loss of each of the *M. abscessus* target genes on *D. melanogaster* survival. Based on these results and the previous findings from the phenogenomics study[581], I decided to further investigate the role of MAB_0471 and MAB_0472 in *M. abscessus* pathogenesis. These genes are annotated as conserved hypothetical transmembrane proteins and were initially described by Boeck *et al* as components of a putative Type II secretion system. Phylogenetic analysis revealed that deletion mutations in MAB_0471 and a deleterious mutation in a peptide synthetase MAB_3317c have both arisen in the ancestor of DCC2 (Figure 5.1A), which is responsible for several transmission networks within CF patients. Epistatic analysis also revealed a distant connection between MAB_0471 and MAB_3317c (Figure 5.1B), and the authors speculated that these genes form part of a discrete network involved in secretion, metabolism, transcriptional regulation and cell wall biosynthesis. Consistent with previous reports that *M. abscessus* DCCs are associated with worse clinical outcomes[163], patients with strains containing a deletion in MAB_0471 showed greater levels of persistent respiratory infections and were less likely to clear the infection[581] (Figure 5.1C). This suggests that loss of MAB_0471 function increases the virulence of *M. abscessus* in CF patients, however, this is not the result seen in *D. melanogaster* in which knockdown or knockout of MAB_0471 led to increased fly survival (Figures 4.3A, E and 5.1D).

Given the clinical importance of these *M. abscessus* genes and the possibility of them contributing towards a mechanism of bacterial secretion previously undescribed in *M. abscessus*, I wanted to understand more about the function of MAB_0471 and MAB_0472. I also wanted to characterise the possible interactions of these genes with *D. melanogaster* host factors to identify possible causes for the discrepancy between loss of MAB_0471 contributing

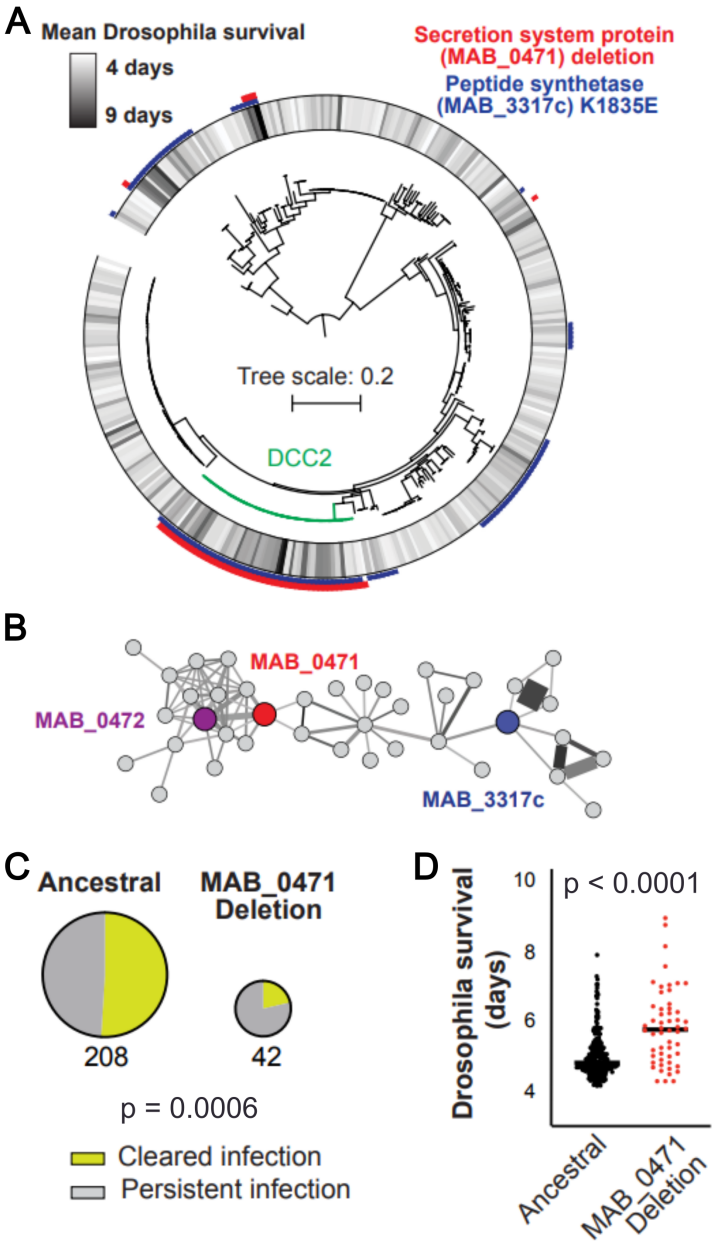


Figure 5.1. Phenogenomics of MAB_0471 in *M. abscessus*. (**A**) Phylogenetic tree of *M. abscessus* clinical isolates tested and corresponding mean *D. melanogaster* survival. Mutations in MAB_0471 and MAB_3317c align with clinical isolates with increased *D. melanogaster* survival and DCC2, within the subspecies *M. abscessus* supsp. *abscessus*. (**B**) Epistatic gene network showing association of MAB_0471 with other putative secretion system genes such as MAB_0472, and distant connection to MAB_3317c. Derived from correlation-compressed direct coupling analysis. (**C**) MAB_0471 deletion was associated with more persistent infection within CF patients compared to ancestral strains, compared with two-sided unpaired *t*-test. (**D**) Infection of *D. melanogaster* with clinical *M. abscessus* strains containing MAB_0471 deletion led to increased survival compared to flies infected with ancestral strains. Figure adapted from Boeck L, Burbaud S, Skwark M, Pearson WH, Sangen J, Wuest AW, Marshall EKP, Weimann A, Everall I, Bryant JM, Malhotra S, Bannerman BP, Kierdorf K, Blundell TL, Dionne MS, Parkhill J, Andres Floto R. Mycobacterium abscessus pathogenesis identified by phenogenomic analyses. Nat Microbiol. 2022[581].

to *M. abscessus* pathogenesis in CF patients but diminishing pathogenesis in *D. melanogaster*.

I found that MAB_0471 and MAB_0472 form part of a conserved operon which appears to be a tight adherence (*tad*) locus, described in Section 5.3.1. The *tad* genes encode components of a macromolecular transport system involved in the assembly of a type IVb pilin, the fimbrial low-molecular-weight protein (Flp) pilus[709,710]. Type IV pili are widely distributed across genera and species, and perform a variety of functions contributing to bacterial pathogenicity including twitching motility, biofilm formation, host cell adherence, bacteria-bacteria interactions, and DNA uptake[711–713]. The *tad* operon originally identified in *Actinobacillus actinomycetemcomitans* (also known as *Aggregatibacter actinomycetemcomitans*) contained 14 genes[712], however only seven have been reported in *M. tuberculosis*[714,715]: *tadZ*, an inner membrane protein with a cytoplasmic ATPase-like domain that is possibly involved in pilin localisation; *tadA*, an inner membrane ATPase required for pilin assembly; *tadB* and *tadC*, two membrane proteins involved in pilus assembly and possibly act as secretion aparatus; *flp*, the major pilin gene; and *tadE* and *tadF*, pseudopilins that lack the conserved N-terminal motif (GxxxxEF) found in other pseudopilins[710,711]. In addition, *M. tuberculosis* encodes two Flp pre-pilin peptidases away from the rest of the gene cluster, encoded by Rv0990c and Rv2551c, which are responsible for processing the pre-pilins into functional mature pilins[713,714,716]. A hypothetical structure of the Tad secretion system is shown in Figure 5.2 in the context of a Gram-negative bacterium. Given the lack of any known RcpA, RcpB, RcpC, or TadD genes in *M. tuberculosis* and other mycobacteria, it is unclear if or how an outer membrane secretin channel may form[710,717], or if this is necessary for the function of this pilin/secretion system through the mycomembrane. To date, very little is known about how the *tad* locus contributes to mycobacterial virulence in pathogenic species such as *M. tuberculosis* and *M. abscessus*.

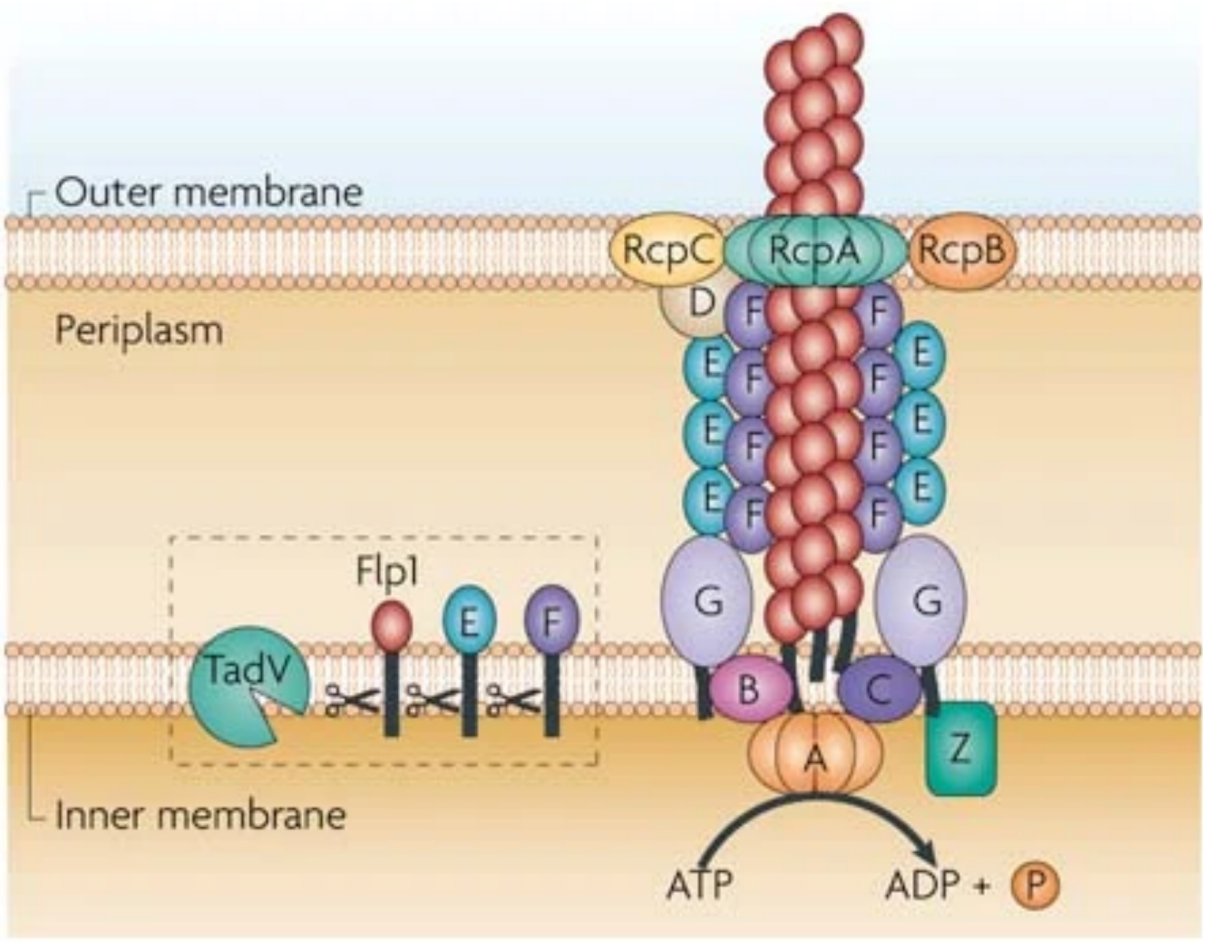


Figure 5.2. Hypothetical structure of Tad secretion system in Gram-negative bacteria. This model is based on homologues of Tad proteins within bacterial and archaeal systems. The Tad proteins are labelled with the fourth letter of their names. Rcp, rough colony protein. Figure taken from Tomich, M., Planet, P. and Figurski, D. The tad locus: postcards from the widespread colonization island. Nat Rev Microbiol 5, 363–375 (2007)[710].

5.2 Aims

The aim of this chapter was to gain a better understanding of the roles of MAB_0471 and MAB_0472 in *M. abscessus* infection. Firstly, I wanted to identify similar genes and proteins in related mycobacterial species such as *M. tuberculosis* to try to predict possible functions of these genes in *M. abscessus*. Once I identified these genes as part of a *tad* locus, I assessed the biofilm formation of the Δ0471 and Δ0472 strains, given the role of the *tad* locus in biofilm formation and cellular adhesion in other bacterial species. Following this, I used SDS-PAGE to test if small peptides within this gene operon were secreted and then if expression of these genes within *D. melanogaster* haemocytes would restore the wild-type

survival phenotype during infection with the knockout mutant strains. I also used various *D. melanogaster* mutant lines to identify host factors that would restore the wild-type survival phenotype during infection, which may represent host targets of the MAB_0471 operon. Finally, I performed RT-qPCR experiments to understand what, if any, transcriptional changes were occurring in the MAB_0471 and MAB_0472 *M. abscessus* knockout strains *in vitro* and how these changes may contribute to infection outcomes.

5.3 Results

5.3.1 Possible functions of MAB_0471 and MAB_0472

The epistatic analysis revealed associations with other genes that appeared to form an operon encoding a putative Type II or Type IV secretion system, MAB_0471, MAB_0472, MAB_0473, MAB_0474, and MAB_0475, as well as two other genes upstream in the genome, MAB_0432 and MAB_0433. To predict possible functions of these genes, I began by searching for homologous genes in other mycobacterial species. I identified this operon in multiple pathogenic and non-pathogenic species, shown in Figure 5.3, and found that this operon was identified as the tad/flp operon in *M. tuberculosis*. MAB_0471 shares sequence similarity with tadB, and MAB_0472 shares sequence similarity with tadC. In the majority of species, the tadZ and tadA genes (MAB_0432 and MAB_0433, respectively) were not separated from the rest of the operon, however, in *M. abscessus*, *M. fortuitum* (a RGM) and *M. avium* (a SGM) the operon appears to have split. It is unclear if the proteins produced still functionally interact with one another or if splitting the operon has impacted the function of the putative secretion systems encoded.

There is varying degrees of conservation for each of the genes across the mycobacterial species considered, shown in Table 5.1. The greatest levels of similarity are seen in tadA and flp, with each of the *flp* genes encoding a highly conserved GxxxxEY sequence required for TadV peptidase activity which is essential for Flp processing and subsequent pilin assembly

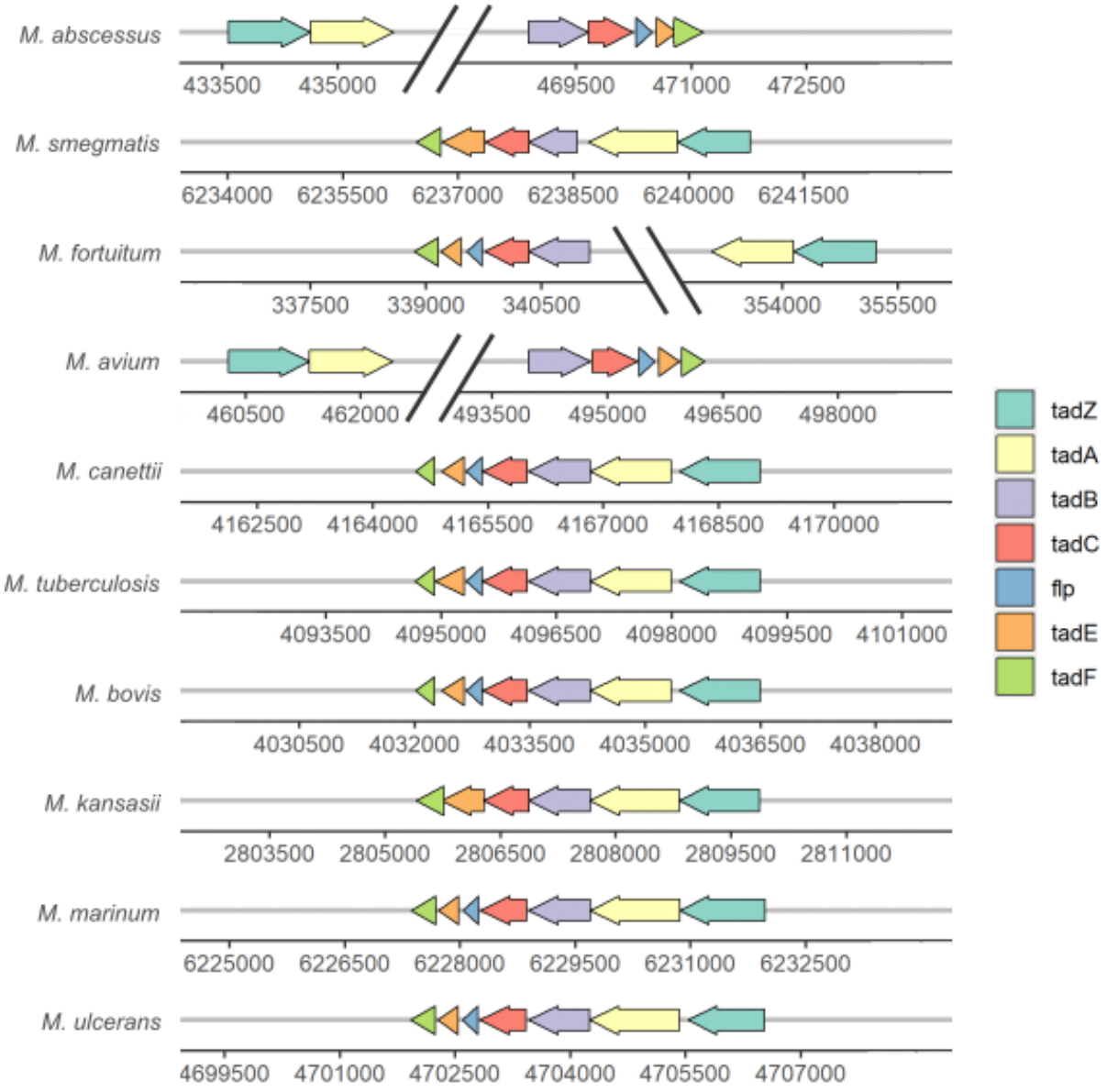


Figure 5.3. MAB_0471 operon in *M. abscessus* and homologous counterparts in other mycobacterial species. Gene organisation and genome localisation of the tad/flp operon within *M. abscessus*, *M. smegmatis*, *M. fortuitum*, *M. avium*, *M. canettii*, *M. tuberculosis*, *M. bovis*, *M. kansasii*, *M. marinum*, and *M. ulcerans*. Each operon is centered on MAB_0471 (tadB) homologues. The operon contains seven genes, including four that resemble pilus assembly proteins (tadZ, tadA - tadC), an flp prepilin (flp), and two secreted proteins (tadE and tadF). Produced using R package 'gggenes'.

and function[718], with the exception of *M. smegmatis* and *M. kansasii* which are lacking the *flp* gene. That said, despite the similarity of these genes amongst mycobacterial species, there is very little similarity to known *tad* genes from other bacterial species such as *P. aeruginosa* or *A. actinomycetemcomitans*[712].

Table 5.1. Percent identify of MAB_0471 operon proteins in various mycobacterial species relative to *M. abscessus*. Multiple sequence alignment of genes was performed using Clustal Omega, and percent identity matrices created using Clustal2.1. Percent identity is relative to the respective *M. abscessus* gene. * MUL_4227 is annotated as a pseudogene due to a frameshift mutation.

Species	tadZ	tadA	tadB	tadC	flp	tadE	tadF
M. abscessus ATCC 19977	MAB_0432 100.00%	MAB_0433 100.00%	MAB_0471 100.00%	MAB_0472 100.00%	MAB_0473 100.00%	MAB_0474 100.00%	MAB_0475 100.00%
M. smegmatis Mc^2 155	MSMEG_6171 52.40%	MSMEG_6169 68.54%	MSMEG_6168 52.17%	MSMEG_6167 48.15%		MSMEG_6165 60.47%	MSMEG_6164 62.04%
M. fortuitum ATCC 6841	MFORT_06947 46.15%	MFORT_06942 71.14%	MFORT_06882 47.58%	MFORT_06877 48.42%	MFORT_06872 70.15%	MFORT_06867 50.59%	MFORT_06862 56.31%
M. avium 104	MAV_0470 46.22%	MAV_0471 72.36%	MAV_0509 48.00%	MAV_0510 50.26%	MAV_0511 72.73%	MAV_0512 62.50%	MAV_0514 50.00%
M. canettii CIPT 140010059	MCAN_36801 46.22%	MCAN_36791 66.87%	MCAN_36781 49.40%	MCAN_36771 49.73%	MCAN_36761 66.18%	MCAN_36751 62.07%	MCAN_36741 52.56%
M. tuberculosis H37Rv	Rv3660c 46.22%	Rv3659c 66.87%	Rv3658c 49.00%	Rv3657c 49.19%	Rv3656c 66.18%	Rv3655c 60.23%	Rv3654c 52.56%
M. bovis BCG	BCG_3718c 46.22%	BCG_3717c 66.87%	BCG_3716c 49.00%	BCG_3715c 49.19%	BCG_3714c 66.18%	BCG_3713c 60.92%	BCG_3712c 52.65%
M. kansasii ATCC 12478	MKAN_12735 45.75%	MKAN_12730 69.27%	MKAN_12725 45.82%	MKAN_12720 48.70%		MKAN_12715 59.77%	MKAN_12710 55.65%
M. marinum M	MMAR_5148 44.66%	MMAR_5147 69.55%	MMAR_5146 45.60%	MMAR_5145 47.42%	MMAR_5144 65.15%	MMAR_5577 57.47%	MMAR_5143 53.12%
M. ulcerans Agy99	MUL_4233 43.61%	MUL_4232 67.60%	MUL_4231 42.04%	MUL_4230 46.39%	MUL_4229 65.15%	MUL_4228 57.47%	MUL_4227* 49.51%

5.3.2 MAB_0471 and MAB_0472 mutants show exaggerated pellicle biofilm formation

The *tad* locus is widely reported to be involved in biofilm formation in many bacteria, including *A. actinomycetemcomitans*[711,712], *P. aeruginosa*[719–721] and *Acinetobacter baumannii*[722]. The formation of bundled Flp pili contributes towards attachment to solid surfaces, allowing the formation of extremely tenacious biofilms[711,720]. However, despite the expression of the seven *tad*/*flp* genes being 17.8-fold higher during biofilm formation compared to planktonic growth in *M. tuberculosis*[723], Δ*tadAB* and Δ*tadC-flp* mutant strains showed no difference in pellicle biofilm development compared to wild-type when observed after three weeks of growth[715].

Therefore, I decided to assess biofilm formation using the *M. abscessus* Δ0471 and Δ0472 strains, expecting biofilm formation to either be diminished or similar to wild-type *M. abscessus*. The results I obtained were the opposite of this - deletion of MAB_0471 or MAB_0472 resulted in accelerated biofilm formation compared to wild-type. All of the Δ0471 and Δ0472 strains showed more robust biofilm formation, as seen by measurement of crystal violet staining shown in Figure 5.4, after 3, 5 and 7 days of biofilm growth. During these assays, particularly during the washing steps to remove planktonic bacteria, I observed that the biofilms were not always robustly attached to the solid surface of the 96-well plates. They had a tendency to float and form biofilm at the surface, which resulted in the loss of a considerable amount of biofilm mass during the washing steps.

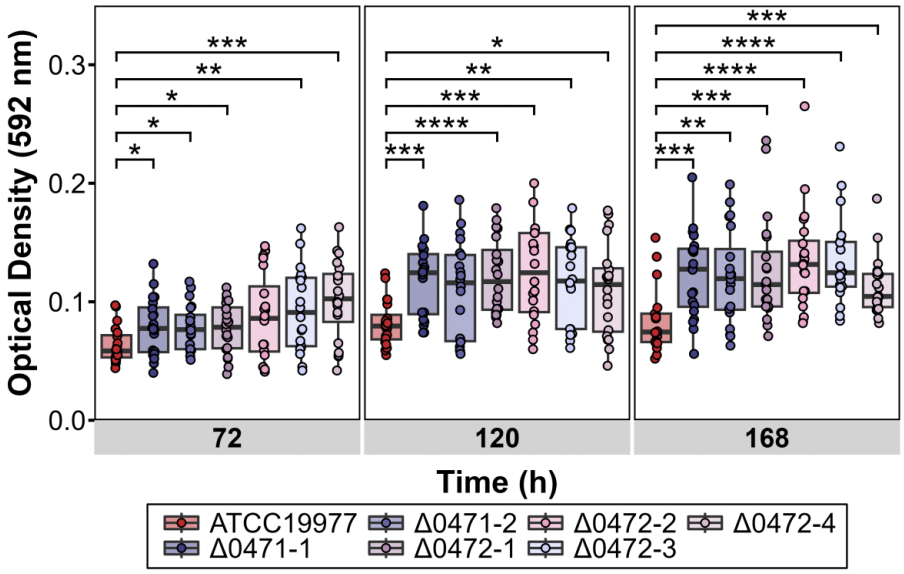


Figure 5.4. Loss of MAB_0471 or MAB_0472 increases biofilm formation. Crystal violet quantification of biofilm formation in 96-well plates of *M. abscessus* ATCC19977 (red), Δ0471-1 and Δ0471-2 (purple), and Δ0472-1, Δ0472-2, Δ0472-3 and Δ0472-4 (pink). Data is pooled from three independent experiments, $4 \geq n \geq 8$ technical replicates per strain per experiment. Statistical significance was calculated using the Wilcoxon Rank-Sum test to compare strains at each time point. ∗, $P < 0.05$; ∗∗, $P < 0.01$; ∗∗∗, $P < 0.001$; ∗∗∗∗, $P < 0.0001$.

I next decided to visualise pellicle biofilm formation, as this appeared to be primary biofilm forming at the air-liquid interface by the Δ0471 and Δ0472 strains during the crystal violet assay in 96-well plates. I observed a time-dependent increase in pellicle formation. All Δ0471 and Δ0472 strains showed initial formation of pellicle at day 2 of growth in borosilicate glass tubes, shown in Figure 5.5A, most notably Δ0472-4. Pellicle formation was further increased in these strains at day 4 post-incubation, at which point there was still minimal pellicle formation by wild-type *M. abscessus* (Figure 5.5B). It was only at day 8 post-incubation that wild-type *M. abscessus* showed substantial pellicle biofilm formation, and it was noted that upon handling the wild-type cultures the pellicle formed by ATCC 19977 was easily disturbed. In contrast, the Δ0471 and Δ0472 formed robustly attached pellicle biofilms that showed enhanced ability to extend upwards along the glass tubes, as seen in Figure 5.5C. This same phenotype was also observed in plastic 50 mL falcon tubes during preparation of RT-qPCR samples (data not shown).

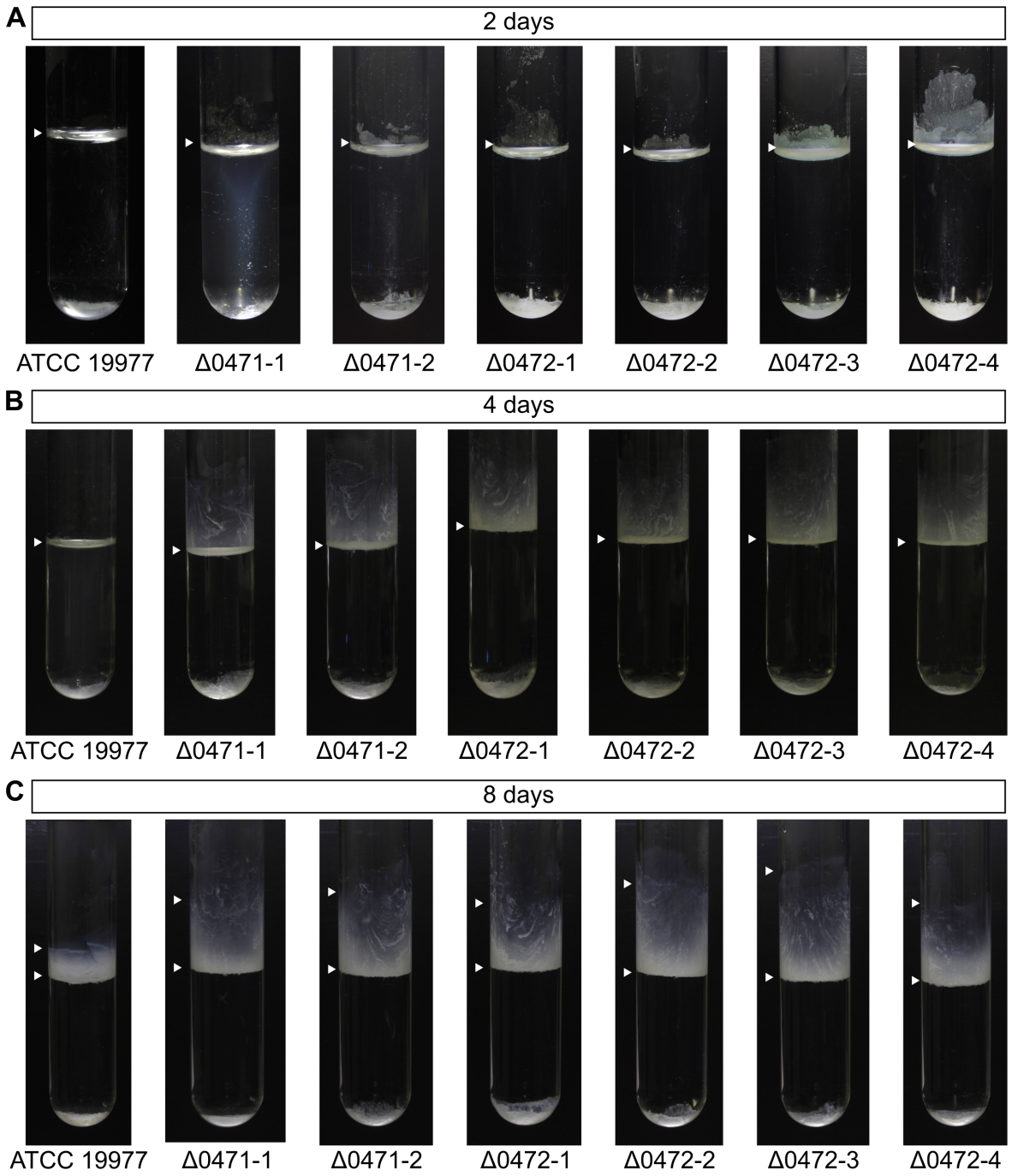


Figure 5.5. Loss of MAB_0471 or MAB_0472 increases pellicle biofilm formation. *M. abscessus* ATCC 19977 and the Δ0471 and Δ0472 strains were grown in 3 mL 7H9 without addition of Tween80 in static culture in borosilicate glass tubes and imaged with a digital camera after (**A**) 2 days, (**B**) 4 days, and (**C**) 8 days of growth. Images are representative of four replicates per strain from a single experiment.

To observe the phenotype of biofilms forming on the surface of the media, I grew wild-type *M. abscessus* ATCC 19977 and Δ0471-2 in detergent-free medium in 6-well plates. These were grown at 37°C standing and imaged after 3 and 7 days of growth. Growth in the 6-well plates

resulted in no surface attachment by either the wild-type or Δ0471-2 *M. abscessus* strain, possibly due to the tissue culture treatment of the plate. The wild-type strain showed much greater levels of intercellular adhesion, forming large clumps and a thin sheet-like structure after 3 days of growth, seen in Figure 5.6A. In contrast, Δ0471-2 produced many small clumps dispersed throughout the medium and was unable to form a similar continuous structure even after 7 days of growth (Figure 5.6B).

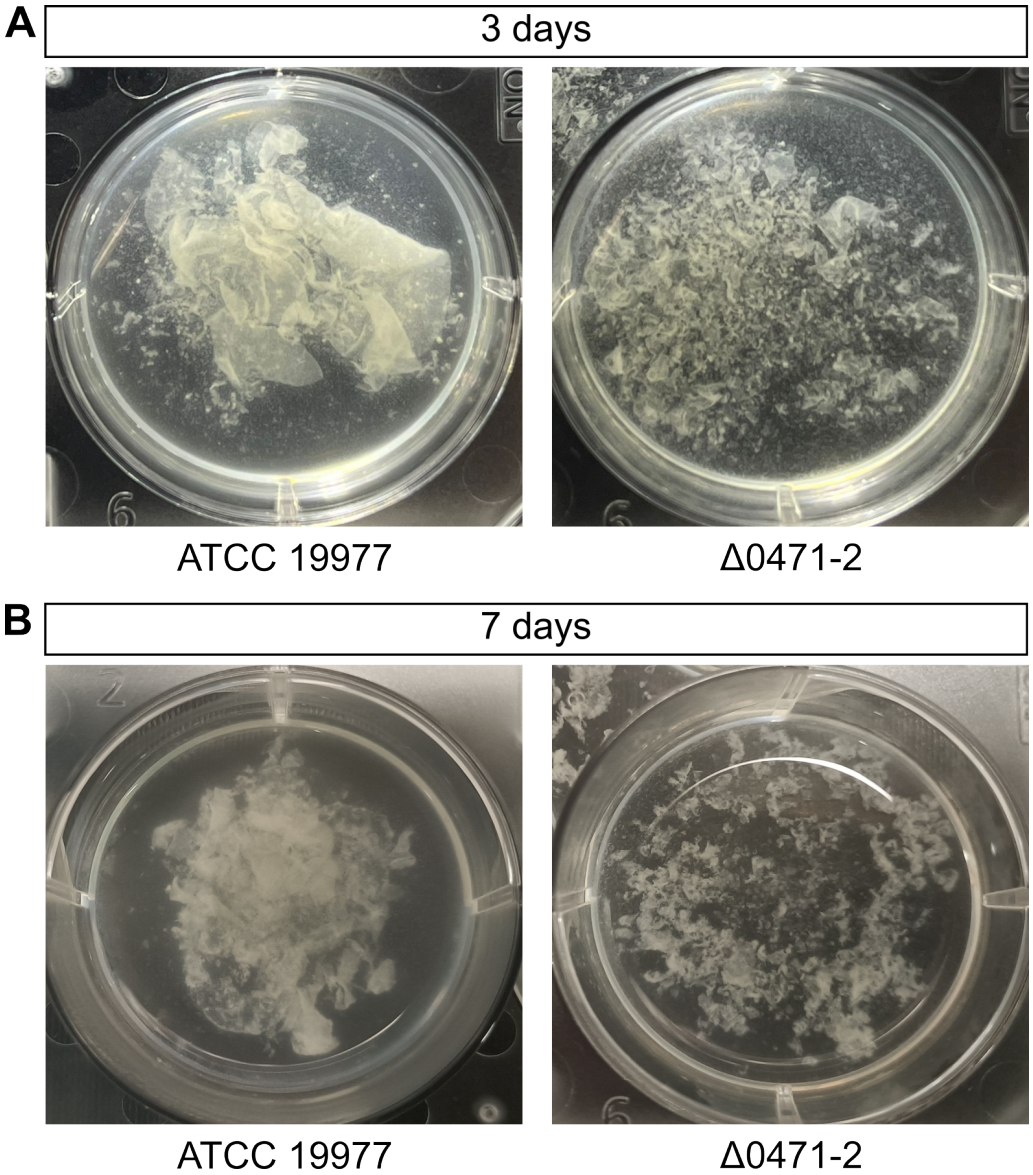


Figure 5.6. Loss of MAB_0471 reduces intercellular adhesion. *M. abscessus* ATCC 19977 and the Δ0471-2 strains were grown in 3 mL 7H9 without addition of Tween80 in static culture in tissue-culture treated 6-well plates and imaged with a digital camera after (**A**) 3 days and (**B**) 7 days of growth. Images are representative of six replicates per strain from a single experiment.

I also considered whether the changes in attachment capabilities between wild-type *M. abscessus* and the Δ0471 and Δ0472 strains was due to differences in GPL production. I grew cultures to late exponential phase in medium with detergent and performed RT-qPCR to measure the transcript levels of 13 genes involved in GPL production and transportation, shown in Figure 5.7. No differences between the parental strain ATCC 19977 and the Δ0471 and Δ0472 strains were identified in any of the genes.

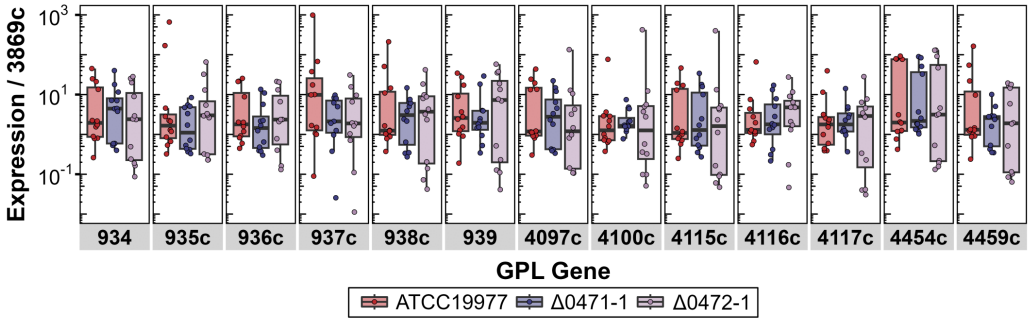


Figure 5.7. No difference in GPL production in Δ0471 and Δ0472 strains. RT-qPCRs show gene expression of genes involved in glycopeptidolipid (GPL) production in *M. abscessus* wild type ATCC 19977, Δ0471-1 and Δ0472-1 strains during log phase growth in 7H9 complete media. Data are pooled from two independent experiments, n = 8 per strain, normalised against MAB_3869c (*rpoB*), statistical comparisons were made using Wilcoxon rank-sum test.

5.3.3 MAB_0471 and MAB_0472 inhibit eiger signalling in *D. melanogaster*

I next wanted to identify host factors that were responsible for the increase of *D. melanogaster* survival during infection with the Δ0471 and Δ0472 strains. A previous study of *M. tuberculosis* found that the *tad* locus inhibited TNFα-induced apoptosis in infected macrophages. An Rv3659c (tadA) mutant strain induced much greater levels of apoptosis compared to wild-type *M. tuberculosis*. The percentage of apoptotic cells was not decreased by complementation with the genes Rv3656c - Rv3659c (flp - tadA), but was reduced by complementation with Rv3654c - Rv3659c (tadF - tadA). This inhibition of apoptosis was found to be caused by suppression of caspase-8 activation, a component of the extrinsic apoptosis pathway, with no differences in intrinsic apoptosis[714]. Rv3654c and Rv3655c were reported to be secreted into the intracellular environment and interact with polypyrimidine tract binding protein-associated

splicing factor (PSF) and ALK lymphoma oligomerisation partner on chromosome 17 (ALO17), respectively[714]. Additionally, the Rv3659c mutant *M. tuberculosis* strain was attenuated during macrophage infection[714], mirroring the attenuation of the Δ0471 and Δ0472 strains in *D. melanogaster*. All seven *M. tuberculosis tad* locus genes were upregulated following interaction with macrophages or alveolar epithelical cells[714,723]

I therefore considered whether the MAB_0471 locus was also suppressing TNFα-induced apoptosis, and so infected flies with mutations in the *D. melanogaster* TNFα homologue, egr. These experiments were initially performed using the *egr*^{3} line infected with Δ0472-1, shown in Figure 5.8. Whilst wild-type *w*^{1118} flies live longer during infection with Δ0472-1 compared to infection with wild-type *M. abscessus* ATCC 19977, dying at 118.83 hours post-infection versus 96.00 hours post-infection, respectively (Figure 5.8A, P = 1.8e-0.9), there is no difference in the survival of *egr*^{3} flies (Figure 5.8B). The *egr*^{3} flies are no more susceptible to infection with wild-type *M. abscessus*, succumbing to infection at 94.75 hours post-infection, however infection with Δ0472-1 leads to death at the same time as wild-type *M. abscessus* at 95.00 hours post-infection (P = 0.091, ns). This indicates that the survival increase seen in *w*^{1118} flies infected with Δ0472-1 is dependent on egr.

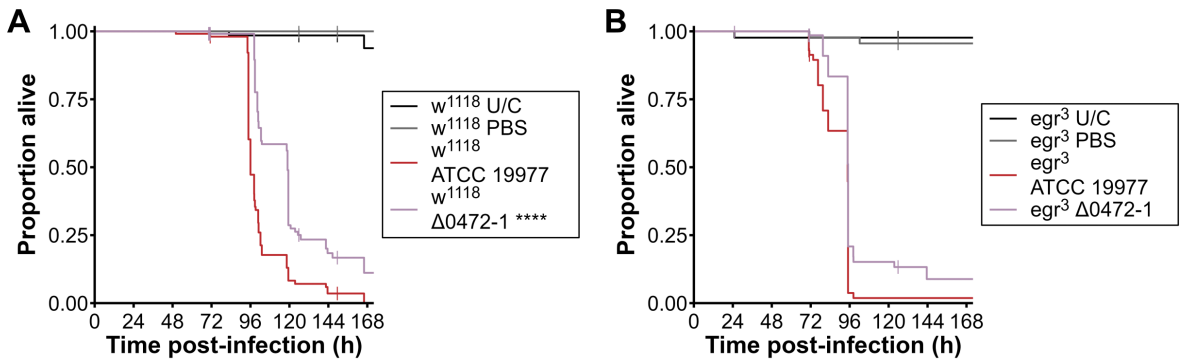


Figure 5.8. *egr*^{3} flies show no difference in survival during infection with wild-type *M. abscessus* or Δ0472-1. Survival of (**A**) *w*^{1118} and (**B**) *egr*^{3} flies infected with wild-type *M. abscessus* ATCC 19977 (red) or Δ0472-1 (pink). Data is pooled from three independent experiments, 111 ≥ n ≥ 64 per group. Asterisks in the legend indicate the *p*-value compared to flies of the same genotype infected with ATCC 19977, compared using the Log-Rank test. ∗, P < 0.05; ∗∗, P < 0.01; ∗∗∗, P < 0.001; ∗∗∗∗, P < 0.0001.

Following the finding that the *egr*^{3} *D. melanogaster* line carries additional mutations in the phagocytosis receptor NimrodC1[455], I wanted to validate the previous result using the *egr*^{1ag} and *egr*^{3ag} lines. This confirmed the result that the increase in survival seen in *w*^{1118} flies infected with Δ0471-1 and Δ0472-1 (Figure 5.9A) is lost in *egr*^{1ag} (Figure 5.9B) and *egr*^{3ag} (Figure 5.9C) flies. Infection with Δ0471-1 and Δ0472-1 *M. abscessus* decreases time-to-death from 118.00 and 98.50 hours post-infection, respectively, in *w*^{1118} flies to 100.00 and 95.75 hours post-infection in *egr*^{1ag} and 95.75 and 95.75 hours post-infection in *egr*^{3ag}. This suggests that the function of the MAB_0471 locus is to suppress or inhibit TNFα or its downstream signalling events, and that loss of MAB_0471 or MAB_0472 reduces *M. abscessus* pathogenicity possibly by increasing host apoptotic signalling.

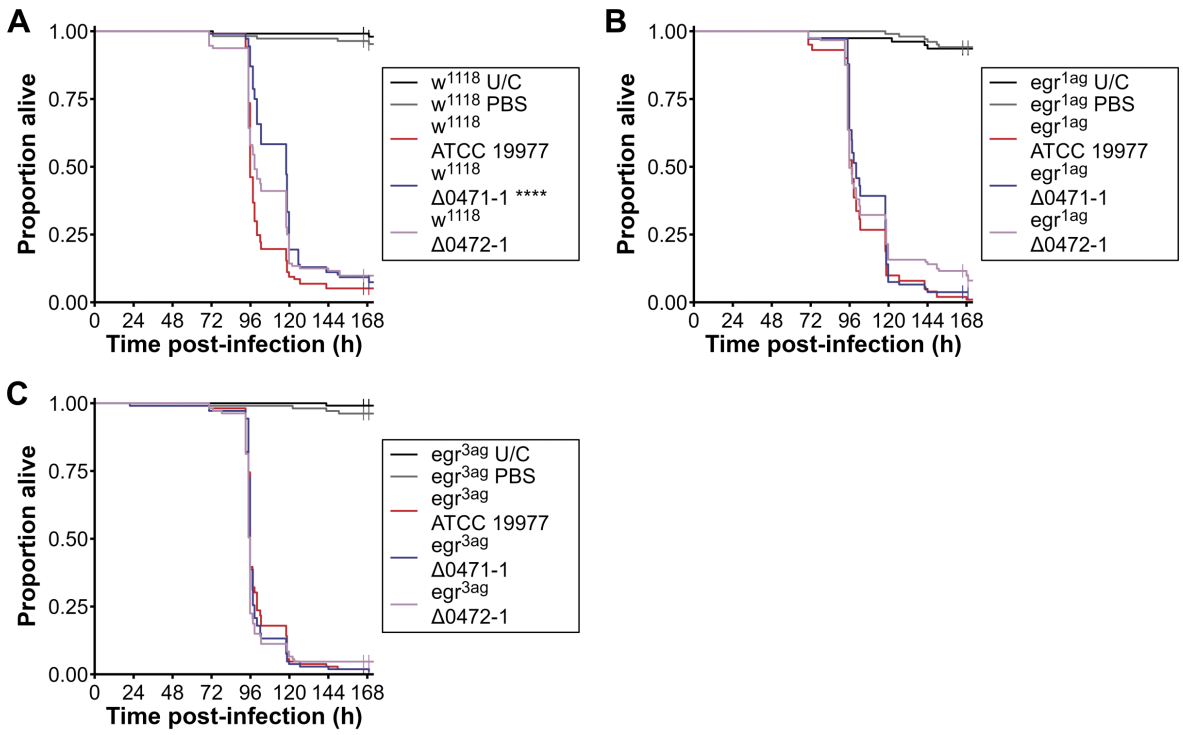


Figure 5.9. Egr is required for survival increase of flies infected with Δ0471-1 and Δ0472-1. Survival of (**A**) *w*^{1118}, (**B**) *egr*^{1ag} and (**C**) *egr*^{3ag} flies infected with wild-type *M. abscessus* ATCC 19977 (red), Δ0471-1 (purple) or Δ0472-1 (pink). Data is pooled from three independent experiments, $121 \geq n \geq 78$ per group. Asterisks in the legend indicate the *p*-value compared to flies of the same genotype infected with ATCC 19977, compared using the Log-Rank test. $*$, $P < 0.05$; $**$, $P < 0.01$; $***$, $P < 0.001$; $****$, $P < 0.0001$.

In addition to the role of Egr in activating JNK-dependent apoptosis, it also acts as an adipokine

on IPCs within the brain to inhibit the production of dILPs[421]. Mycobacterial infections are known to drive insulin signalling disruption in humans, and this has also been shown in *D. melanogaster* in which insulin signalling via Akt is reduced during infection with *M. marinum*. This leads to a wasting phenotype, progressive loss of glycogen and triglyceride levels combined with hyperglycaemia. This pathology is driven by the transcription factor Foxo, which is inhibited by insulin and AKT activity[494]. I therefore asked whether there were differences in Akt activity between *M. abscessus* ATCC 19977 and the Δ0471 and Δ0472 strains.

Full Akt activity requires phosphorylation of Ser505 within a C-terminal hydrophobic motif by TOR[504,724,725], and so Akt activity can be assessed by measuring levels of Akt phosphorylation of Ser505 by Western Blot. Figure 5.10 shows levels of phospho-Akt in w^{1118} flies at 80 hours post-infection. Consistent with the previous observations of *M. marinum* infection in *D. melanogaster*[494], there is a reduction of the 60 kDa isoform of phospho-AKT without a change in the levels of total Akt relative to sterile-injury control flies. This same reduction is not observed in flies infected with Δ0471-2 or Δ0472-4, suggesting these strains have an impaired ability to inhibit insulin signalling or this may not occur until later in the infection, once the bacterial load of the Δ0471-2 or Δ0472-4 strains reaches a similar level to that of ATCC 19977. Additional experiments at later time points to measure phospho-Akt levels in the Δ0471-2 and Δ0472-4 strains are necessary to determine if these strains are also capable of inhibiting insulin signalling and whether the difference observed is due to a difference in bacterial load.

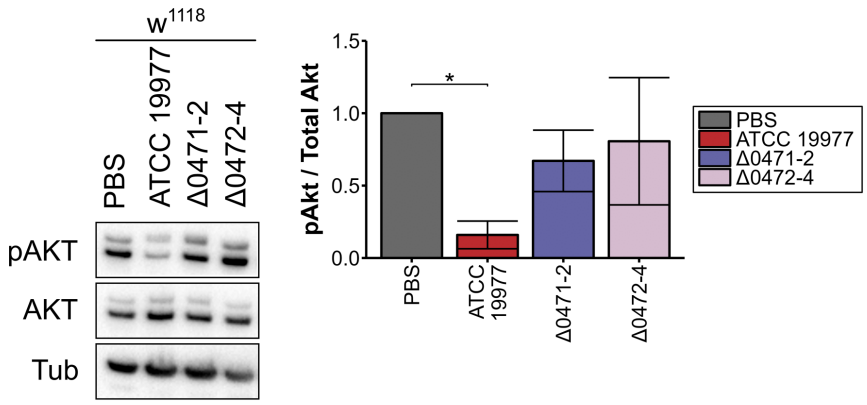


Figure 5.10. Akt activity is reduced in infected flies to a greater extent by *M. abscessus* ATCC 19977 than Δ0471-2 and Δ0472-4. Systemic levels of Ser505 phosphorylated and total Akt protein of w^{1118} flies at 80 hours post-infection with *M. abscessus* ATCC 19977 (red), Δ0471-2 (purple) or Δ0472-4 (pink), measured by Western Blot. Data represents one experiment, n = 3 per condition. Groups were compared with one-way ANOVA with Tukey's test. ∗, P < 0.05; ∗∗, P < 0.01; ∗∗∗, P < 0.001; ∗∗∗∗, P < 0.0001.

D. melanogaster Egr signals via two receptors, Wgn[422] and Grnd[423], which show different subcellular localisations and different affinities for egr, suggesting that signalling via the different receptors may serve different functions[424]. Egr signalling in *D. melanogaster* is discussed in detail in Section 1.2.1.4. I next considered whether the inhibition of Egr signalling via the MAB_0471 locus was associated with either of these receptors. Infecting a wgn^{KO} line with Δ0471-2 again eliminated the survival difference seen in w^{1118} flies (Figure 5.11A, B), suggesting that the aspect of Egr signalling targeted by *M. abscessus* MAB_0471 operon is downstream of Wgn. However, the loss of survival difference between wild-type *M. abscessus* and the Δ0472 strains (Figure 5.11C) was only observed in wgn^{KO} during infection with Δ0472-2, not Δ0472-3 or Δ0472-4 (Figure 5.11D). This lack of consistency between the Δ0472 strains during infection of wgn^{KO} suggests that Egr signalling via Wgn is not responsible, at least not entirely, for the reduced pathogenicity of the Δ0471 and Δ0472 strains. Similar experiments were performed using a $grnd^{KO}$ *D. melanogaster* line, however these experiments could not be included due to a failure of control groups.

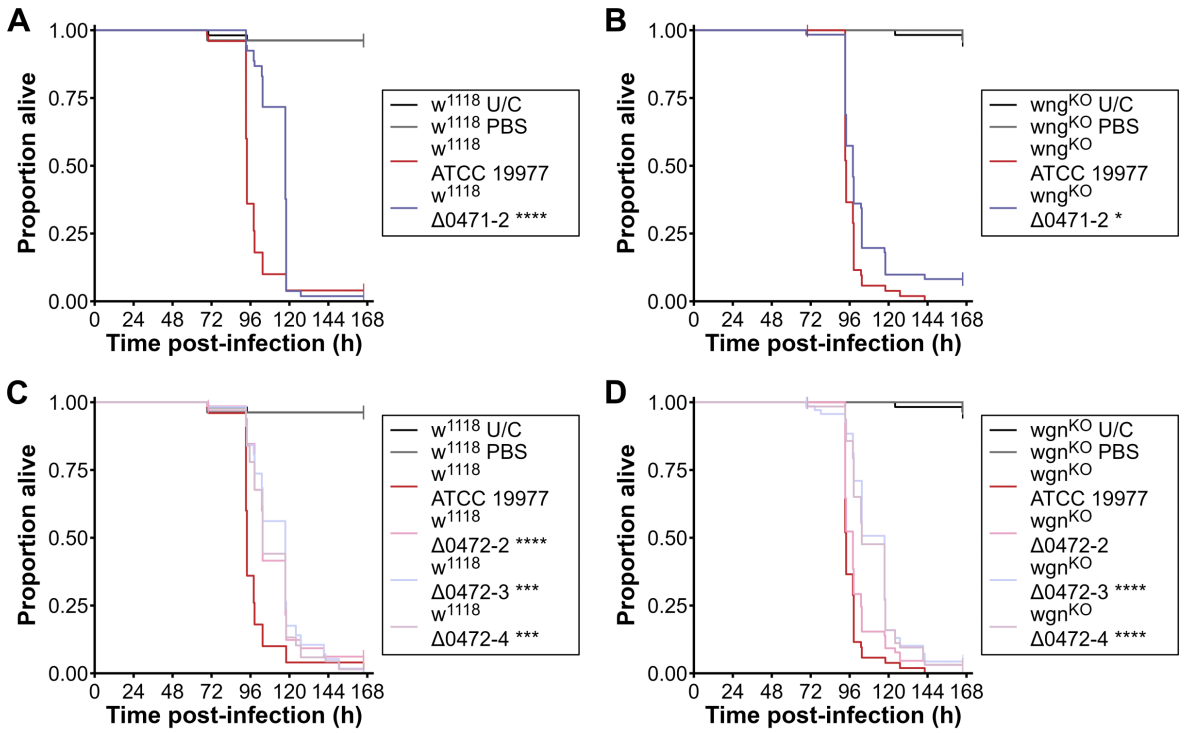


Figure 5.11. Role of Wgn in increased fly survival when infected with Δ0471 and Δ0472 strains. Survival of (**A**) *w*^{1118} and (**B**) *wgn*^{KO} flies infected with wild-type *M. abscessus* ATCC 19977 (red) or Δ0471-2 (purple), and survival of (**C**) *w*^{1118} and (**D**) *wgn*^{KO} flies infected with wild-type *M. abscessus* ATCC 19977 (red), Δ0472-2, Δ0472-3, or Δ0472-4 (pink). Data is pooled from three independent experiments with common controls, $95 \geq n \geq 72$ per group. Asterisks in the legend indicate the *p*-value compared to flies of the same genotype infected with ATCC 19977, compared using the Log-Rank test. $*$, $P < 0.05$; $**$, $P < 0.01$; $***$, $P < 0.001$; $****$, $P < 0.0001$.

5.3.4 Interaction of MAB_0471 and MAB_0472 with Imd signalling

In mammals, the extrinsic apoptosis pathway is driven by caspase 8 and is ligand-induced, in contrast to intrinsic apoptosis which is triggered by intracellular signals and is driven by caspase 9 activity and apoptosome formation[419]. The reduction of TNFα mediated apoptosis by *M. tuberculosis tad* locus was found to be by suppression of extrinsic apoptosis and caspase 8 activity, with no change in intrinsic apoptotic signals or caspase 9 activity[714]. However, in *D. melanogaster*, the initiator caspase induced by Egr signalling and subsequent JNK activation is Dronc, an orthologue of caspase 9[726]. The *D. melanogaster* caspase 8 homologue, Dredd[727], is a component of Imd signalling and is responsible for the cleavage of both Rel[407,408] and Imd[409–413], discussed in Section 1.2.1.3. In addition to this, Dredd has

been shown to be involved in bacteria-induced JNK signalling as RNAi-knockdown of Dredd in S2 cells reduces phosphorylation and activation of JNK[728,729]. Rel also contributes to the control of JNK signalling by inducing degradation of Tak1, terminating JNK signalling[439]. In addition to its role in regulation of inflammatory responses, Dredd has also been implicated in direct apoptotic signalling by activating Rpr, Grim and Hid[730,731].

Dredd is activated following the recruitment of Fadd to imd[396,404–406]. Considering this, I infected flies with a loss-of-function mutation in imd, upstream of Dredd activation, with the Δ0471 and Δ0472 strains to assess the role of Dredd and other downstream Imd signalling in the decrease of pathogenicity. Loss of Imd function also restored Δ0471-1 and Δ0472-1 to full pathogenicity (Figure 5.12A, B), as well as for Δ0471-2 (Figure 5.12C, D) and Δ0472-2, Δ0472-3 and Δ0472-4 (Figure 5.12E, F).

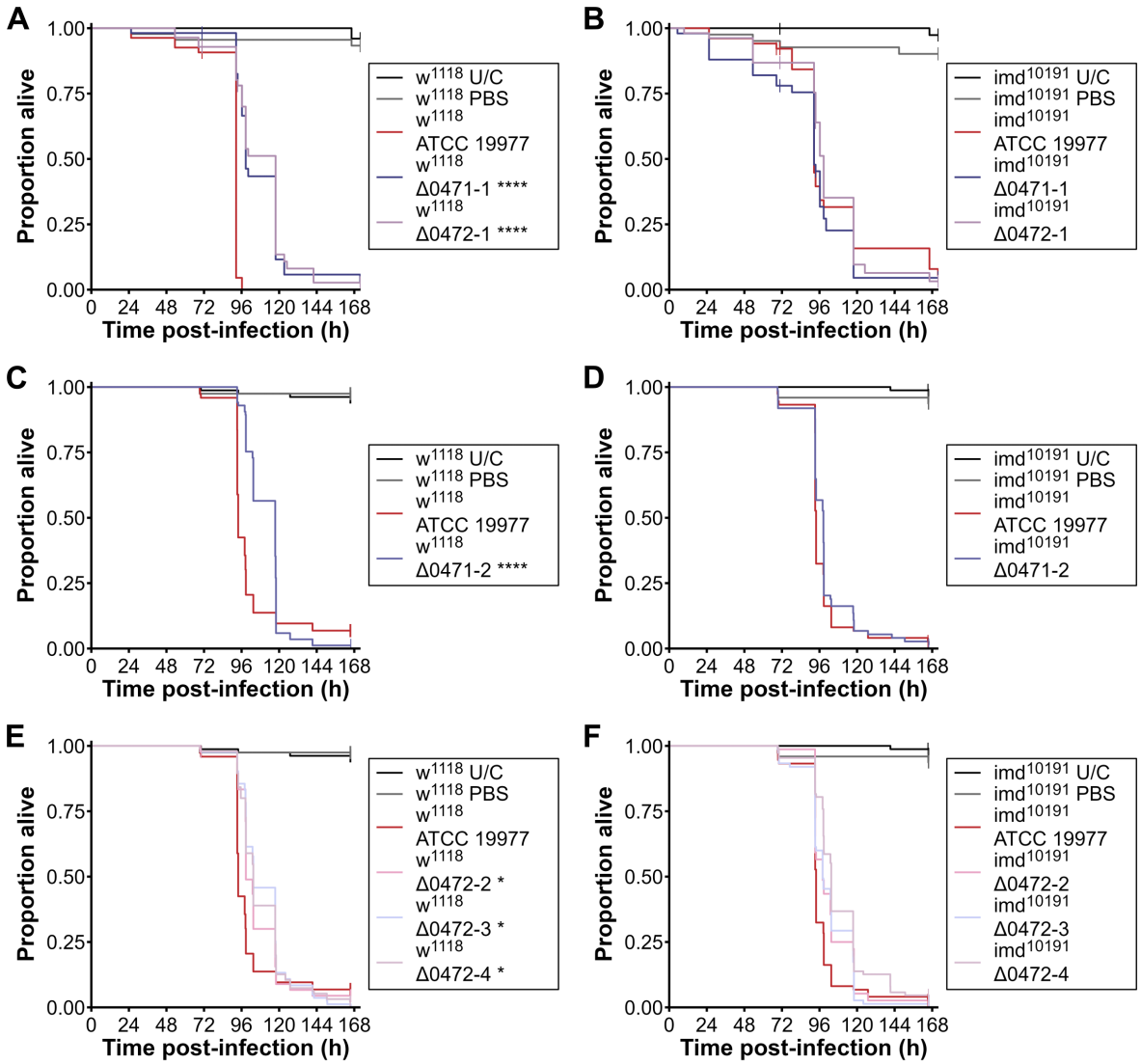


Figure 5.12. Imd contributes to fly defense against Δ0471 and Δ0472 strains. Survival of (**A**) *w*^{1118} and (**B**) *imd*^{10191} flies infected with wild-type *M. abscessus* ATCC 19977 (red), Δ0471-1 (purple) or Δ0472-1 (pink). Data represents one independent experiment, 56 $\geq$ n $\geq$ 25 per group. Asterisks in the legend indicate the *p*-value compared to flies of the same genotype infected with ATCC 19977, compared using the Log-Rank test. Survival of (**C**) *w*^{1118} and (**D**) *imd*^{10191} flies infected with wild-type *M. abscessus* ATCC 19977 (red) or Δ0471-2 (purple), and survival of (**E**) *w*^{1118} and (**F**) *imd*^{10191} flies infected with wild-type *M. abscessus* ATCC 19977 (red), Δ0472-2, Δ0472-3 or Δ0472-4 (pink). Data is pooled from three independent experiments with common controls, 95 $\geq$ n $\geq$ 74 per group. Asterisks in the legend indicate the *p*-value compared to flies of the same genotype infected with ATCC 19977, compared using the Log-Rank test. $*$, P < 0.05; $**$, P < 0.01; $***$, P < 0.001; $****$, P < 0.0001.

It was unclear whether the role of Imd signalling in increasing host survival during infection with the Δ0471 and Δ0472 strains was due to the activity of Dredd or due to cross-talk with JNK signalling via Tak1. I next infected Tak1 mutant flies, *Tak1*^{1} and *Tak1*^{2527} with the Δ0471 and Δ0472 strains. For these initial experiments, the Tak1 mutant fly lines carried a + wild-type genetic background rather than *w*^{1118}. The + wild-type genetic background lacks the deletion mutation in the *white* gene that gives the *w*^{1118} line its characteristic white eye, which can be used as a visual genetic marker to identify flies on the correct genetic background. As with the *w*^{1118} flies, *Tak1*^{1} and *Tak1*^{2527} infected with Δ0471-1 (Figure 5.13A, B, C) and Δ0472-1 (Figure 5.13D, E, F) lived longer compared to infection with wild-type *M. abscessus* ATCC 19977. This would suggest that the reduced survival of *imd*^{10191} infected with Δ0471 and Δ0472 strains is not due to a reduction of JNK signalling, but perhaps because of a loss of Dredd activation.

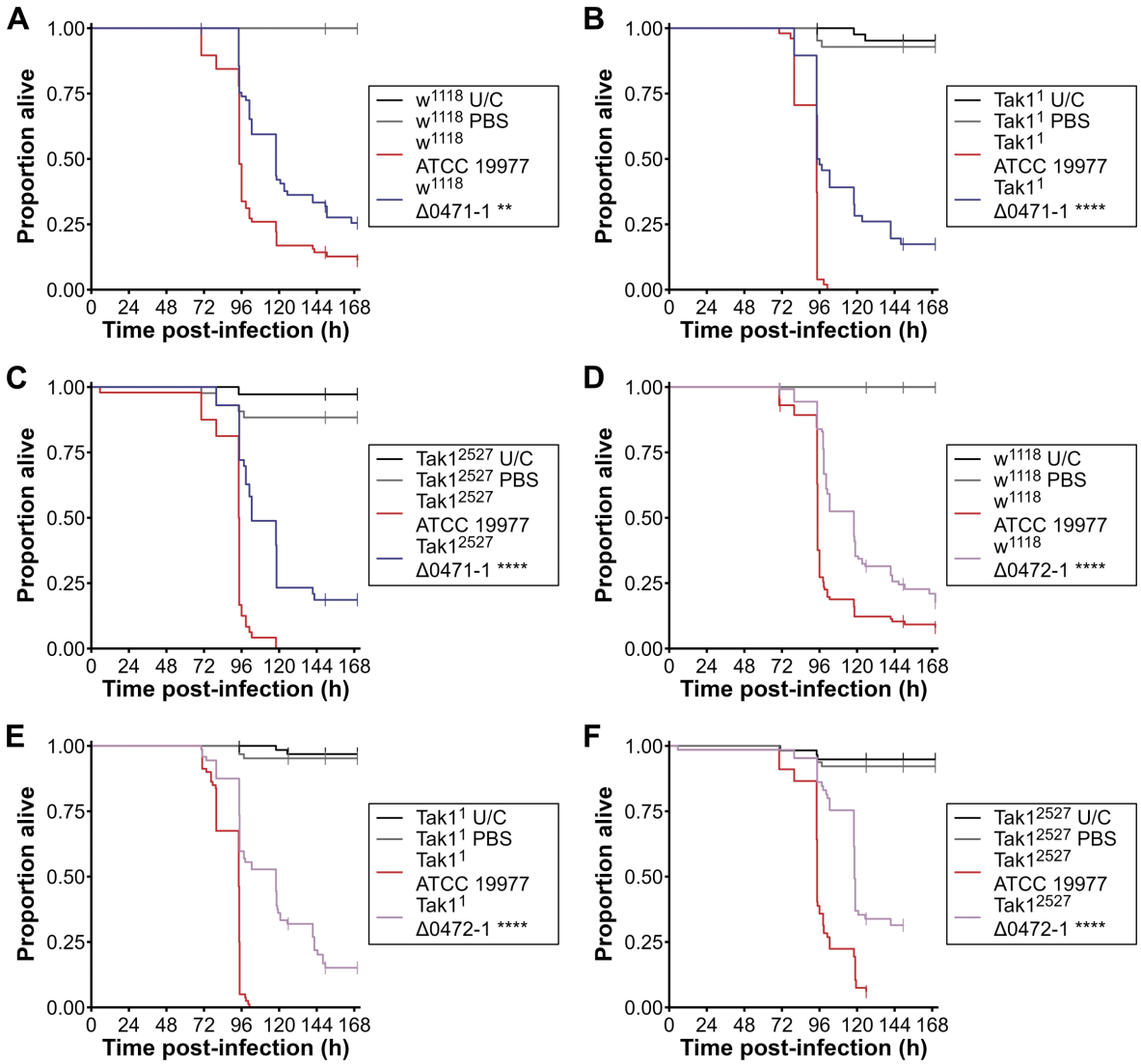


Figure 5.13. *Tak1[1]* flies maintain survival increase during infection with Δ0471-1 and Δ0472-1. Survival of (**A**) *w[1118]*, (**B**) *Tak1[1]* and (**C**) *Tak1[2527]* flies infected with wild-type *M. abscessus* ATCC 19977 (red) or Δ0471-1 (purple). Data is pooled from two independent experiments, 77 ≥ n ≥ 36 per group. Asterisks in the legend indicate the *p*-value compared to flies of the same genotype infected with ATCC 19977, compared using the Log-Rank test. Survival of (**D**) *w[1118]*, (**E**) *Tak1[1]* and (**F**) *Tak1[2527]* flies infected with wild-type *M. abscessus* ATCC 19977 (red) or Δ0472-1 (pink). Data is pooled from three independent experiments, 123 ≥ n ≥ 58 per group. Asterisks in the legend indicate the *p*-value compared to flies of the same genotype infected with ATCC 19977, compared using the Log-Rank test. ∗, P < 0.05; ∗∗, P < 0.01; ∗∗∗, P < 0.001; ∗∗∗∗, P < 0.0001.

Following backcrossing of the *Tak1*^{1} line onto the *w*^{1118} genetic background by Prof Marc Dionne, I performed new survival experiments. As with the previous Wgn experiments, the results were inconsistent. During infection with Δ0471-2 (Figure 5.14A, B), the survival of *Tak1*^{1} flies was reduced compared to *w*^{1118} flies infected with Δ0471-2, but not entirely reduced to the same point as infection with wild-type *M. abscessus* ATCC 19977. During infection with Δ0472 strains, *Tak1*^{1} flies infected with Δ0472-3 and Δ0472-4 maintained the increased survival seen in *w*^{1118} flies, but not for infection with Δ0472-2 (Figure 5.14C, D). This lack of consistency again makes it unfeasible to draw conclusions about how the *M. abscessus* MAB_0471 locus is inhibiting Egr signalling using this data.

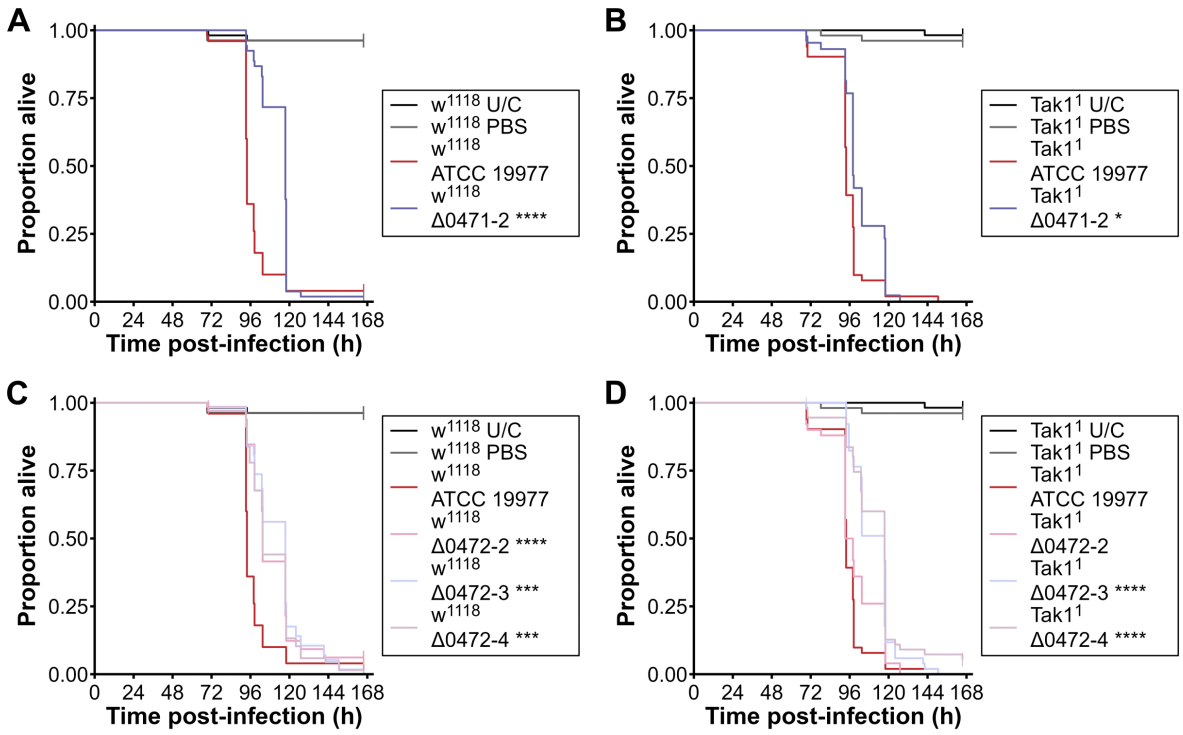


Figure 5.14. Role of Tak1 in survival increase during infection with Δ0471 and Δ0472 strains. Survival of (**A**) *w*^{1118} and (**B**) *Tak1*^{1} flies infected with wild-type *M. abscessus* ATCC 19977 (red) or Δ0471-2 (purple), and survival of (**C**) *w*^{1118} and (**D**) *Tak1*^{1} flies infected with wild-type *M. abscessus* ATCC 19977 (red), Δ0472-2, Δ0472-3 or Δ0472-4 (pink). Data is pooled from three independent experiments with common controls, $95 \geq n \geq 66$ per group. Asterisks in the legend indicate the *p*-value compared to flies of the same genotype infected with ATCC 19977, compared using the Log-Rank test. ∗, $P < 0.05$; ∗∗, $P < 0.01$; ∗∗∗, $P < 0.001$; ∗∗∗∗, $P < 0.0001$.

5.3.5 Expressing MAB_0473, MAB_0474, or MAB_0475 in haemocytes does not rescue survival phenotype of *M. abscessus* MAB_0471 and MAB_0472 mutant strains

As Rv3654c and Rv3655c (TadE and TadF, homologues of MAB_0474 and MAB_0475) are reported to be secreted into the intracellular environment of infected cells[714], I used SDS PAGE to assess if the secreted products were missing in the Δ0471 and Δ0472 strains. Briefly, cultures were grown to stationary phase in Sauton's minimal media, as the expression of the *M. tuberculosis tad* locus genes was greatest at stationary phase[723]. The bacterial pellet and supernatant were collected, the supernatant was sterile filtered and proteins were precipitated using TCA. The resulting SDS PAGE gel from the supernatant of *M. abscessus* ATCC 19977, Δ0471-1 and Δ0472-1 cultures is shown in Figure 5.15. The predicted sizes of the MAB_0474 and MAB_0475 protein products are 9.06 kDa and 12.71 kDa, respectively. Use of the 4 - 12% gradient gels meant I was unable to resolve proteins below 11 kDa in size. Whilst there was no observable difference in protein levels between 11 kDa and 17 kDa, there was a distinct increase of a protein at approximately 95 kDa in the Δ0471-1 and Δ0472-1 samples compared to ATCC 19977 that has not been identified.

To evaluate if expression of MAB_0473, MAB_0474 or MAB_0475 within haemocytes would restore the pathogenicity of the Δ0471 and Δ0472 strains, we produced transgenic *D. melanogaster* lines. This allowed us to drive expression of these *M. abscessus* virulence factors within *D. melanogaster*. As *M. abscessus* is primarily located within haemocytes during infection, I used the Hml^{Δ}-Gal4 line crossed with males carrying either UAS-MAB_0473, UAS-MAB_0474, or UAS-MAB_0475. For all of the genetic control lines, both UAS-only (Figure 5.16A - D) and driver-only (Figure 5.16E), flies survived longer when infected with Δ0471-1 or Δ0472-1 compared to wild-type *M. abscessus*. In the case of w^{1118} > *UAS-473* (Figure 5.16B), the difference between the knockout strains and wild-type *M. abscessus* was not statistically significant. It is possible that the UAS-473 line is 'leaky' and that there is some

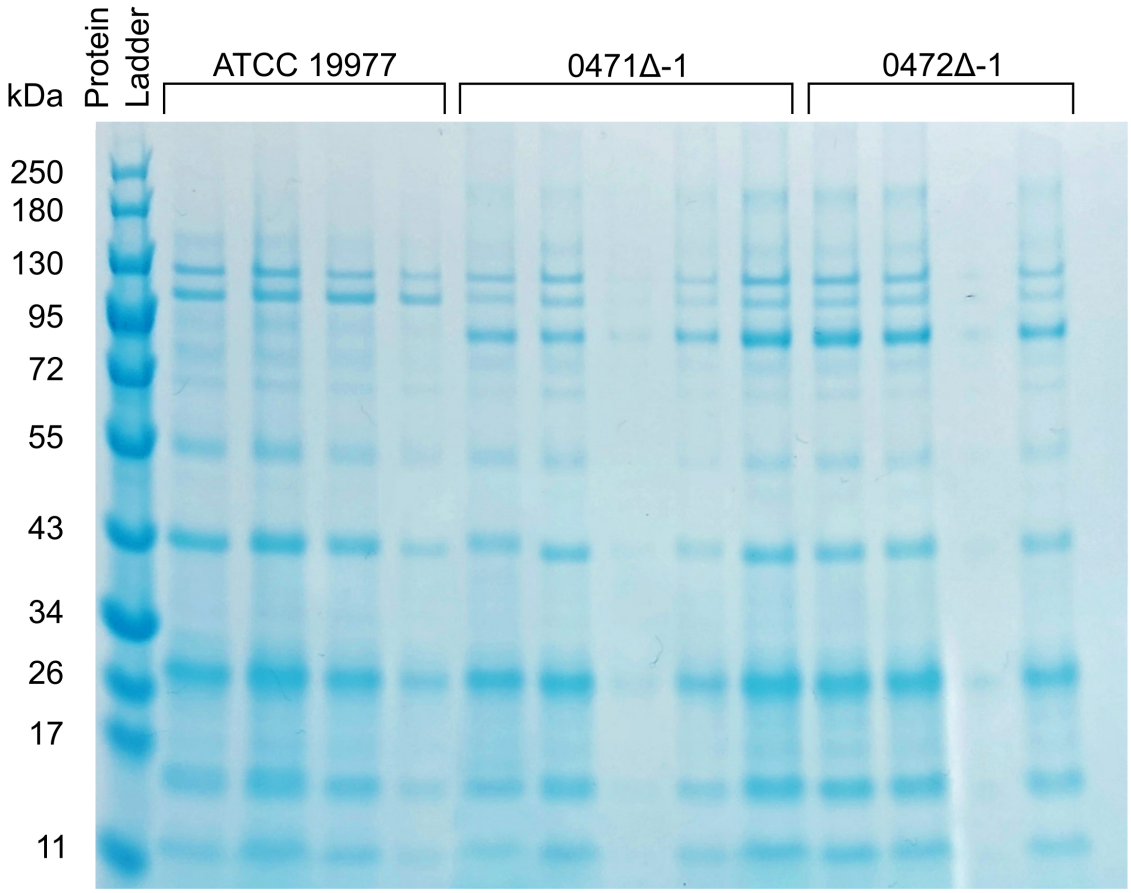


Figure 5.15. SDS-PAGE gel of proteins precipitated from *M. abscessus* culture supernatant. *M. abscessus* ATCC 19977 (Lanes 2 - 5), Δ0471-1 (Lanes 6, 7, 9, 10) and Δ0472-1 (Lanes 11 - 14) were cultured in Sauton's minimal media, supernatant proteins were precipitated by TCA and analysed by SDS-PAGE. Each lane shows one of four biological replicates, lane 8 is empty due to loading error. Gel is representative of two independent experiments, performed with the help of Chiara Wuelfing.

level of expression of MAB_0473 within these flies in the absence of a Gal-4 driver line. Driving expression of MAB_0473 (Figure 5.16F), MAB_0474 (Figure 5.16G), or MAB_0475 (Figure 5.16H, I) within haemocytes did not lead to any clear increases in the virulence of Δ0471-1 or Δ0472-1, indicating that expression of these *M. abscessus* genes individually is not sufficient to overcome the loss of MAB_0471 or MAB_0472.

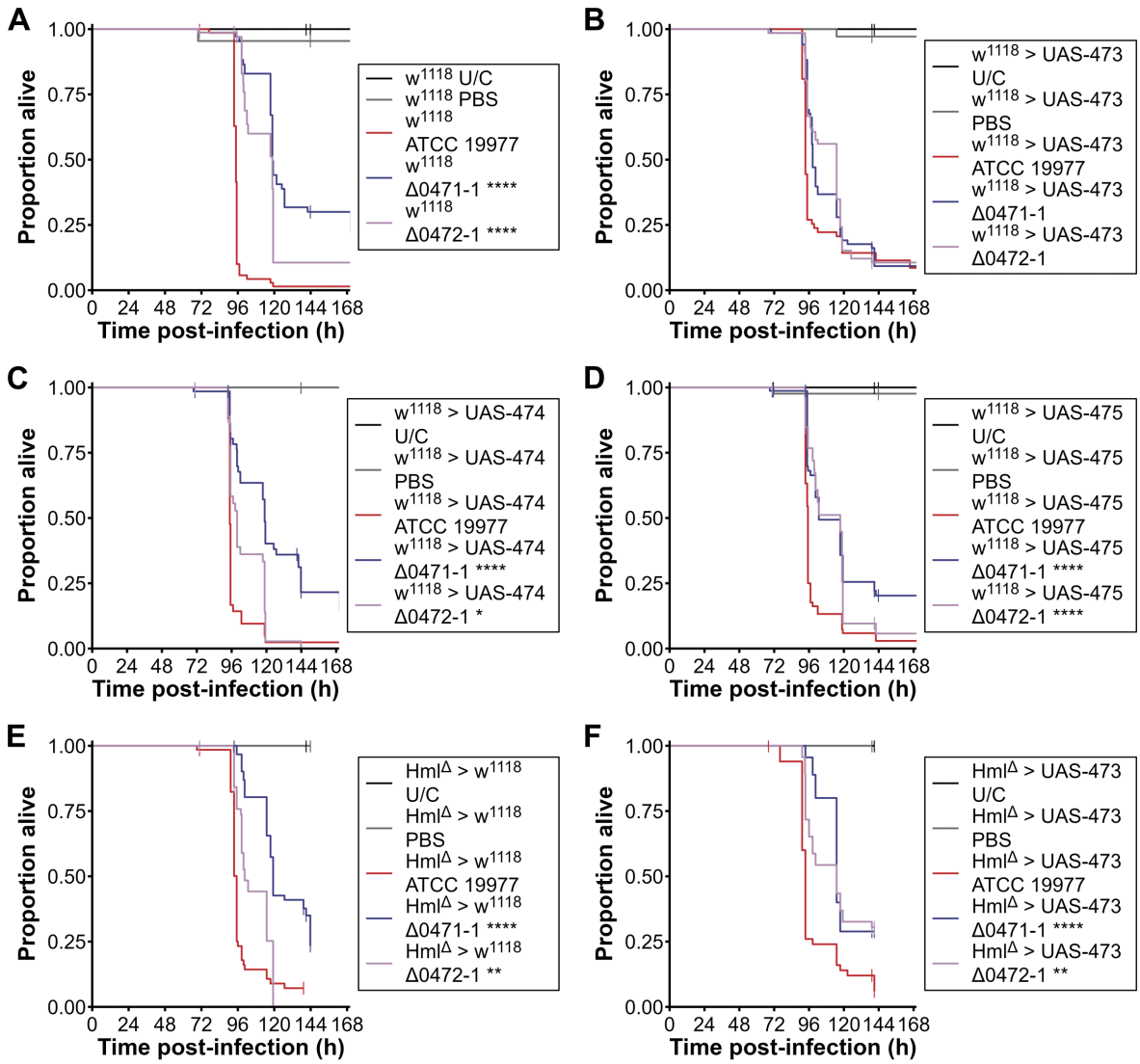


Figure 5.16. Survival of transgenic flies expressing MAB_0473, MAB_0474, or MAB_0475 during *M. abscessus* infection. (**A - F**) See legend on page 234.

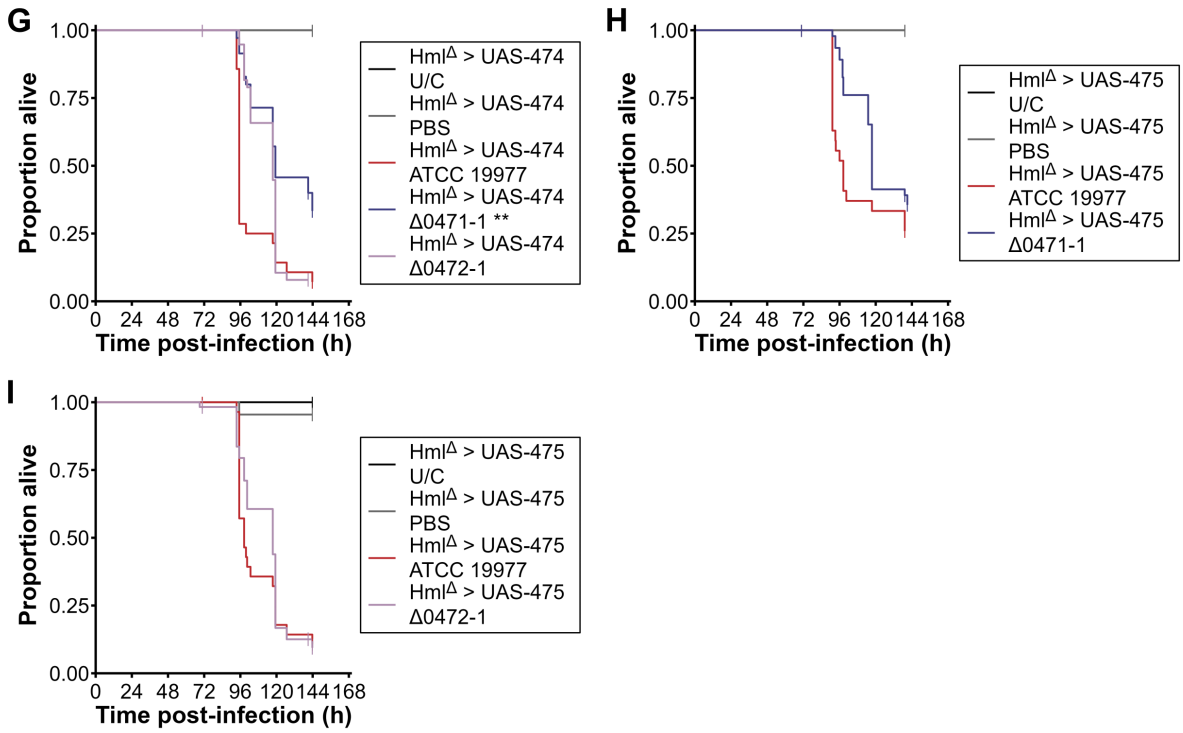


Figure 5.16. Survival of transgenic flies expressing MAB_0473, MAB_0474, or MAB_0475 during *M. abscessus* infection continued. Survival of (**A**) w^{1118}, (**B**) w^{1118} > *UAS-0473*, (**C**) w^{1118} > *UAS-0474*, (**D**) w^{1118} > *UAS-0475*, (**E**) *Hml*$^{\Delta}$ > w^{1118}, (**F**) *Hml*$^{\Delta}$ > *UAS-0473* flies infected with *M. abscessus* ATCC 19977 (red), Δ0471-1 (purple) or Δ0472-1 (pink). (**G**) *Hml*$^{\Delta}$ > *UAS-0474*, (**H**) *Hml*$^{\Delta}$ > *UAS-0475* and (**I**) *Hml*$^{\Delta}$ > *UAS-0475* flies infected with *M. abscessus* ATCC 19977 (red), Δ0471-1 (purple) or Δ0472-1 (pink). Data is pooled from two independent experiments with common controls, 81 ≥ n ≥ 21 per group. Asterisks in the legend indicate the *p*-value compared to flies of the same genotype infected with ATCC 19977, compared using the Log-Rank test. ∗, P < 0.05; ∗∗, P < 0.01; ∗∗∗, P < 0.001; ∗∗∗∗, P < 0.0001.

In order to specifically assess the role of MAB_0474 and MAB_0475 in the inhibition of apoptosis, as is reported to be the function of Rv3654c and Rv3655c[714], we made use of the *GMR-Gal4-regg1*^{GS9830} line. Regg stands for reduced-eye generator with a GMR-Gal4 driver, and the eye-specific GMR driver results in a reduced eye phenotype caused by increased eiger-induced apoptosis, due to overexpression of egr[418]. *Regg1*^{GS9830} is the parental strain of *egr*^{1} and *egr*^{3}, and also contains the additional NimC1 mutations[455]. By co-expressing *regg1*^{GS9830} with inhibitors of Egr signalling, such as dominant-negative forms of Bsk (JNK) or Tak1, the reduced-eye phenotype is ablated. Figure 5.17 shows images of the *D. melanogaster* genotypes tested. Firstly, all UAS-only controls show normal sized eyes (Figure 5.17A - D).

Figure 5.17E shows the reduced-eye phenotype of the *GMR-Gal4-regg1*^{GS9830} > *w*^{1118} control. Knockdown of dronc was used as a positive control, and shows a partial recovery of eye size (Figure 5.17F). This is consistent with previous experiments that used overexpression of a dominant-negative form of dronc in *GMR-Gal4-regg1*^{GS9830}, leading the authors to conclude the eiger-induced cell death does not require caspase activity[418], possibly via inducing necrosis[444]. Expression of MAB_0474 (Figure 5.17G) or MAB_0475 (Figure 5.17H) had no noticeable effect on eye size, meaning that individually neither is capable of inhibiting egr-induced apoptosis.

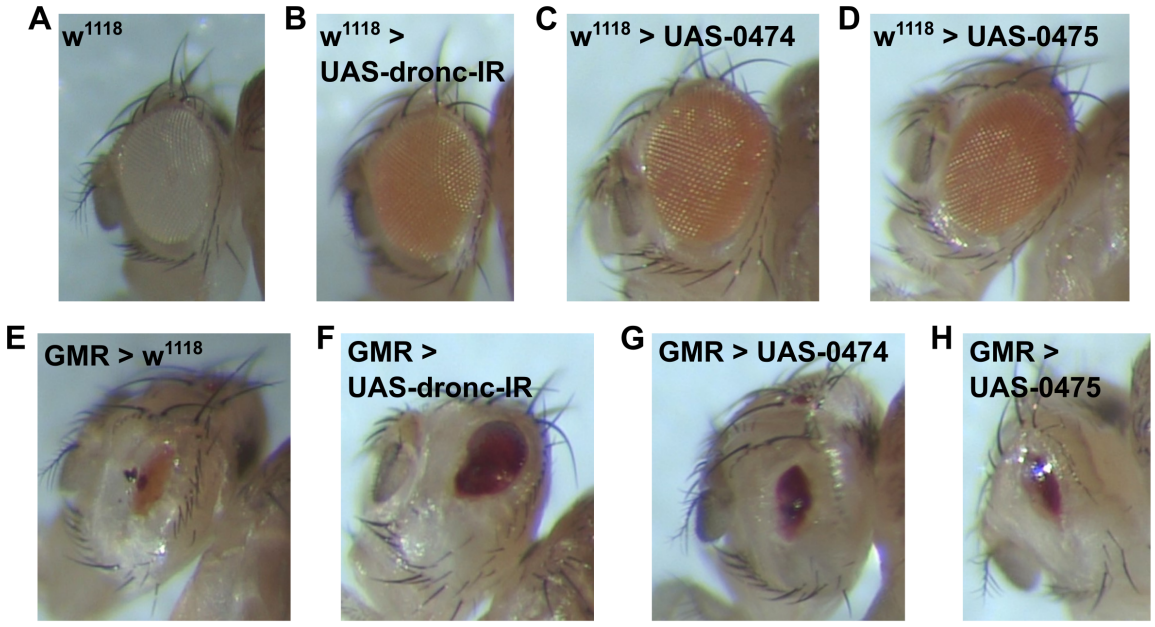


Figure 5.17. Expression of MAB_0474 and MAB_0475 individually does not inhibit eiger-induced cell death. Adult eye images of (**A**) *w*^{1118}, (**B**) *w*^{1118} > *UAS-dronc-IR*, (**C**) *w*^{1118} > *UAS-0474*, (**D**) *w*^{1118} > *UAS-0475*, (**E**) *GMR-Gal4-regg1*^{GS9830} > *w*^{1118}, (**F**) *GMR-Gal4-regg1*^{GS9830} > *UAS-dronc-IR*, (**G**) *GMR-Gal4-regg1*^{GS9830} > *UAS-0474*, and (**H**) *GMR-Gal4-regg1*^{GS9830} > *UAS-0475*. Images are representative of at least 5 individuals per genotype from one experiment, performed with the help of Annie Zhang.

5.4 Discussion

MAB_0471 was originally identified from clinical isolates of *M. abscessus* from CF patients, deletion mutations in this gene had occurred in the lineage of DCC2 and were associated with more persistent infection[581]. Loss of MAB_0471 or MAB_0472 function results in extended survival of *D. melanogaster* with lower bacterial loads during infection. In this chapter I have

identified that MAB_0471 and MAB_0472 are tadB and tadC proteins, part of the operonic tad/flp locus forming a putative secretion system likely involved in the secretion of MAB_0474 (tadE) and MAB_0475 (tadF), and possibly involved in the formation of an flp pilus consisting of MAB_0473 (flp) polypeptide. Two types of pili have been described in *M. tuberculosis*, the single gene *M. tuberculosis* pilus (Mtp)[732], and the Tad locus[714]. The role of each of these pili in *M. tuberculosis* virulence is debated and very poorly understood. It has been reported that species of NTM lack functional orthologues of the Mtp and Tad pilus[733], however, an orthologue of Mtp has been identified in *M. abscessus* (MAB_0270c) which is thought to participate in the formation of pili-like structures, and is under the regulational control of PhoP[650]. The tad locus has never previously been described in *M. abscessus*, and its role in pathogenesis is unknown.

5.4.1 Role of MAB_0471 and MAB_0472 in biofilm formation

The tad locus has been implicated in bacterial adherence and biofilm formation in multiple species[711–713], and these processes play a pivotal role in the establishment and persistent of infections in the lungs of CF patients. I identified that all Δ0471 and Δ0472 strains displayed a consistent biofilm phenotype, unique to that of wild-type *M. abscessus*. Growth in borosilicate glass tubes revealed that the Δ0471 and Δ0472 strains produced pellicle biofilm at the air-liquid interface more rapidly than wild-type *M. abscessus*, which was more securely attached to the solid surface and quickly extended up the insides of the glass tubes. However, growth in six-well plates showed that Δ0471-2 grew in many small dispersed clumps, and was less able to form the continuous sheet structure seen in wild-type *M. abscessus*. This suggests that attachment to solid surfaces is unchanged in the Δ0471 and Δ0472 strains, but that the tad locus is involved in adherence to other bacteria.

One factor that may contribute to this is the presence of eDNA, a component of biofilm extracellular matrices[734]. eDNA plays a fundamental role in the formation of stable biofilm

structures due to the binding capacity of the highly charged DNA molecule, promoting intercellular aggregation[735] and biofilm self-organisation[736]. The presence of eDNA enables adhesion to abiotic materials, increasing bacterial surface colonisation of less adhesive hydrophobic surfaces such as medical implants[737]. Within the environment of the CF lung, concentrations of eDNA have been reported up to 4 mg/mL, almost an order of magnitude greater than in healthy tissues[738]. eDNA also aids in promoting the increased resistance of the biofilm by neutralising cationic effector molecules such as AMPs[739,740], restricting the diffusion of antimicrobials[741–744], acidifying the local environment[745], and mediating horizontal gene transfer[746]. It was initially believed that eDNA was released from lysed cells within the interior of biofilms as a result of genotoxic stress[735,747,748], however, more recent work shows that the complex mechanisms of release and regulation of eDNA are unknown in many species[737,749] and these can be quorum-sensing-dependent and -independent[750].

The extracellular matrix of *M. abscessus* biofilms has been shown to contain eDNA dispersed throughout the biofilm, but more abundant in areas with lower cell counts pointing to its role in aggregation and adhesion[110]. It has also been suggested that *M. abscessus* actively releases DNA during biofilm development due to the dramatic increase in eDNA levels within *M. abscessus* biofilms relative to comparable planktonic growth[113].

The possible role of eDNA in the changes to Δ0471 and Δ0472 biofilm phenotypes stems from the finding that an insertion in the *M. smegmatis* TadA homologue, MSMEG_6169, disrupted DNA transfer[160]. The authors originally identified DNAse-resistant unidirectional transfer of extensive regions of the chromosome, with distinct donor and recipient strains - distributive conjugal transfer[154]. Insertions into the *esx-1* locus resulted in a hyper-conjugative phenotype of the donor strain, indicating that ESX-1 negatively regulates DCT. The authors speculated that a possible mechanism was a form of quorum sensing in which the proteins secreted by the ESX-1 system prevent transfer until the appropriate conditions are met[158]. Recipient strains

with mutations within the *esx-1* locus are transfer-defective also, underscoring a role of ESX-1 activity in the recipient strain[160]. In a similar manner, insertions into MSMEG_6169 resulted in a hyper-conjugative donor strain and abolished recipient function. The strongly elevated transfer frequencies of the tadA mutant strains rules out a direct role in DNA transfer[160], despite the fact that TadA is a homologue for VirB11[751], an essential component of DNA transfer by plasmid-mediated conjugation[752]. The authors then speculated that the Tad locus may contribute to DNA transfer by maintaining cell-cell contact with the flp pilus[160], however later work found that DNA transfer frequency was greatest within pellicle biofilms at the air-liquid interface, despite higher numbers of cells clumped together within the sediment[161]. This suggests that a specific aspect of the biofilm environment promotes DNA transfer, and the role of the Flp pilus in this process could be explored further using the Δ0471 and Δ0472 strains given the increased pellicle biofilm formation in these strains. It was also speculated that the Tad system functions similarly to ESX-1 and that proteins secreted by the Tad system modulate DNA transfer. No change in EsxB secretion was observed in the TadA mutant, and so it is likely that the Tad system secretes a unique set of proteins from ESX-1 which may functionally interact[160]. The secreted Tad proteins may also be involved in binding and detection of eDNA and be involved in a quorum sensing mechanism involved in biofilm formation in a manner similar to type IV pilin subunits in *Clostridioides difficile*[753].

Whilst it is unlikely that the *M. abscessus* Tad locus is directly involved in DNA transfer or release of eDNA, it is possible that disruption to cell-cell adhesion due to the loss of the flp pilus and changes in intercellular communication via the TadE and TadF secreted proteins results in altered quorum sensing and subsequent downstream pathways. In *P.aeruginosa* the PprAB TCS, a master regulator of quorum sensing, was found to directly regulate expression of the *tad* locus[754]. Identifying how the *tad* locus is regulated in *M. abscessus* during biofilm formation and its possible involvement in quorum sensing would shed light on the downstream changes occurring in the Δ0471 and Δ0472 strains. Given the hyperconjugative nature of

the *M. smegmatis* tadA mutant[160], there may be increased eDNA release in the Δ0471 and Δ0472 strains promoting adhesion to solid surfaces but reduced cell-cell adhesion due to the loss of the Flp pilus. This may also involve the unidentified 95 kDa protein secreted into the supernatant by the Δ0471 and Δ0472 strains, if this is a protein that is normally adhered to the Flp pilus. Alternatively, the 95 kDa protein may be produced in greater levels in the Δ0471 and Δ0472 strains due to changes in transcriptional regulation even during planktonic growth. SDS-PAGE analysis of biofilm supernatant would identify whether this protein is also produced in biofilm conditions by *M. abscessus*.

5.4.2 Role of MAB_0471 and MAB_0472 in host interactions

The loss of the *tad* locus has clear implications on the host-pathogen interactions of *M. abscessus*, as seen in the clinical outcomes of patients infected with DCC2 strains with MAB_0471 deletions or in *D. melanogaster* survival experiments. The biofilm phenotype of the Δ0471 and Δ0472 strains offers an explanation as to why in CF patients MAB_0471 deletions are associated with more persistent infections, whereas in *D. melanogaster* infection with Δ0471 and Δ0472 strains prolongs fly survival compared to wild-type *M. abscessus*. The environment of the CF lung is ideal for the formation of mycobacterial pellicle biofilms which contributes to increased antimicrobial tolerance and increased virulence[755], however, the lack of a comparable air-liquid interface in *D. melanogaster* makes it unlikely that pellicle biofilm formation is occurring. Instead, the results from infection of *D. melanogaster* with the Δ0471 and Δ0472 strains shed light on the more specific molecular role of the *tad* locus in *M. abscessus* interactions with host cells.

Our results show that the increased survival observed in flies infected with the Δ0471 and Δ0472 strains is dependent on Egr activity, consistent with the hypothesis that the *tad* locus inhibits TNFα-induced apoptosis[714]. Whilst the results suggest that signalling via the receptor Wgn is part of the Egr activity inhibited by MAB_0471 and MAB_0472, I cannot exclude the

role of Grnd. Loss of Imd also restores the Δ0471 and Δ0472 survival phenotype to that of wild-type *M. abscessus*, however loss of Tak[1] function does not. Tak[1] is a JNKKK in the cascade triggering JNK activation by egr and also acts independently within the Imd pathway to regulate Rel by activating the IKK complex. This indicates that the increase in fly survival during infection with the Δ0471 and Δ0472 strains is not due to cross-talk between Imd and Egr signalling, and possibly not due to JNK signalling. The role of JNK signalling in the survival increase should be assessed using *D. melanogaster* lines with mutations in Bsk (JNK) and Hep (JNKK). Instead, the increase in fly survival during Δ0471 or Δ0472 infection may be contributed to separately by JNK-independent caspase-mediated cell death via NOPO and Ben-dUEV1a downstream of egr[440], and Dredd caspase activity downstream of Imd[396,404–406]. Alternatively, Egr signalling may be involved in the activation of Dredd via Traf4 and Traf6 adaptor proteins. Although signalling via Traf4 is predominantly directed towards JNK signalling, both Traf4 and Traf6 have been associated with NF-κB signalling by interacting with Pelle[425,446,756]. Further studies focusing on the role of caspase-8 homologue Dredd during infection with the Δ0471 and Δ0472 strains would indicate whether the *M. abscessus tad* locus is functioning to suppress apoptosis in a similar way to that of *M. tuberculosis*[714].

It is also possible that MAB_0474 and MAB_0475 are interacting with other host factors. The *M. tuberculosis* homologue of MAB_0475, Rv3654c, was found to bind and cleave PSF (also known as splicing factor proline and glutamine rich, SFPQ)[714]. Two orthologues of PSF are present in *D. melanogaster*, no on or off transient A (nonA) and nonA-like (nonA-l). Nuclear proteins within the *Drosophila* behaviour, human splicing (DBHS) group, which includes PSF, nonA and nonA-l, bind DNA and RNA *in vitro* and are linked to pre-mRNA splicing and transcriptional regulation[757]. Knockdown of nonA in *D. melanogaster* did not result in changes to transcription or splicing but did suggest a possible role in messenger ribonucleoprotein (mRNP) mobility within the nucleus. It is also possible that the lack of change to transcription and splicing is due to partially redundant functions of nonA and nonA-l[757]. Making use of

the UAS-Gal4 system to knockdown expression of either nonA, nonA-l, or both, in specific *D. melanogaster* tissues and infecting with the Δ0471 and Δ0472 *M. abscessus* strains may indicate whether there is a meaningful interaction occurring.

The use of transgenic flies showed that expression of MAB_0474 or MAB_0475 within haemocytes did not restore the survival phenotype of Δ0471 and Δ0472. It is possible that haemocytes are not the primary location for the pathways being targeted and expressing these factors in the fat body would show an effect, or that expression of MAB_0474 and MAB_0475 individually is not sufficient to overcome the loss of function of MAB_0471 and MAB_0472 and combined expression of these factors would restore the wild-type phenotype. This reasoning can also be applied to the lack of inhibition of eiger-induced apoptosis observed in GMR-Gal4-regg1^{GS9830} flies expressing either MAB_0474 or MAB_0475.

Chapter 6: Asparagine limitation in *M. abscessus* leads to changes in *D. melanogaster* cytokine signalling and metabolism

6.1 Introduction

Metabolic adaptations are central to the virulence and antibiotic resistance profiles of pathogenic mycobacteria[758]. A key example of this is nitrogen metabolism. As intracellular pathogens, mycobacteria are often located within the harsh, nitrogen-limited environment of the phagosome during infection, and so acquiring nitrogen and other nutrients represents an important facet of intracellular survival. Nitrogen limitation leads to widespread metabolic reprofiling in mycobacteria, often transcriptionally regulated by GlnR[660,759]. This is associated with important clinical phenotypes such as dormancy, formation of granulomas[760], biofilm development[761], and antibiotic tolerance[762]. It has been shown that nitrogen limitation in *M. abscessus* leads to increased triacylglycerol intracellular lipid inclusions within the bacteria, elevated drug tolerance, and increased virulence in zebrafish embryos[762]. In *M. tuberculosis*, the uptake of amino acids asparagine and aspartate and the subsequent nitrogen assimilation plays an important role in intracellular survival by increasing resistance to acid stress within the phagosome[763,764].

Mycobacterial infection also leads to changes in the metabolism of the host, which in turn changes the abundance of key metabolites available to the infecting mycobacterium. On a systemic level, mycobacterial infection generally causes disruptions in insulin signalling, leading to hyperglycaemia and wasting of metabolic stores in many animal hosts[494,765,766]. On a cellular level, there is increased triglyceride deposition within infected macrophages[470,767,768]. In *D. melanogaster*, infection with *M. marinum* leads to elevated JAK/STAT signalling via the cytokine Upd3, which in turn inhibited expression of *Atg2*. This led to dysregulation of intracellular lipid bodies[470], increasing the available triglyceride to the benefit of the microbe[322,687,769].

The metabolic adaptations of host and pathogen during infection are both important determinants of infection outcome. However, the interactions between host metabolism and microbial metabolism are, in general, not well understood. Key questions include:

1. Which host metabolites are most important for microbes and how do these metabolites specifically contribute to microbial survival?

2. Does microbial exploitation of host metabolites interact with host metabolic regulation or have direct consequences for the host?

3. How does the metabolic status of a microbe influence host-pathogen interactions and subsequent host responses?

There are all important factors to consider, especially for opportunistic pathogens such as *M. abscessus* that are predominantly acquired from environmental sources. The relationship between the metabolic adaptations of *M. abscessus* and host immune responses is particularly poorly understood, and these interactions may inform novel therapeutic strategies.

The results in Chapter 4 identified that *M. abscessus* strains with mutations in MAB_1132c, a putative asparagine permease transporter, caused prolonged infection in *D. melanogaster* without an equivalent decrease in bacterial load. This decoupling between bacterial load and host survival suggests that the reduced virulence of these strains is due to the metabolic impact due to impaired asparagine acquisition. MAB_1132c was also originally identified from the phenogenomics screen of clinical *M. abscessus* isolates, and was only identified in clinical isolates of the *M. abscessus* subsp. *massiliense* clade. The alleles identified were associated with changes in *D. melanogaster* survival, *D. melanogaster* immune response, and resistance to antibiotics[581]. I therefore decided to study the function of MAB_1132c, which I confirmed to be an asparagine transporter, and subsequently the role of asparagine during *M. abscessus* infection.

6.2 Aims

The aim of this chapter was to study the immune and metabolic consequences of interactions between *D. melanogaster* and *M. abscessus*, and specifically how MAB_1132c and asparagine uptake by *M. abscessus* contribute to pathogenicity. Firstly I needed to identify the function of MAB_1132c using growth curves in minimal medium with defined nitrogen sources. Next, I assessed how asparagine availability in culture medium impacted bacterial virulence and host tolerance with *D. melanogaster* survival and bacterial load measurements. The metabolic changes in *M. abscessus* were compared using TLC, and the immune and metabolic responses in *D. melanogaster* were evaluated with RT-qPCR and Western Blots.

6.3 Results

6.3.1 MAB_1132c functions as an asparagine permease in *M. abscessus*

MAB_1132c encodes one of two predicted L-asparagine permeases in *M. abscessus*. However, in *M. tuberculosis*, one of its two predicted L-asparagine permeases functions as an aspartate transporter[763,764]. I therefore tested which amino acids MAB_1132c has a role in transporting by evaluating the growth of Δ1132c strains in complete medium (Figure 6.1A) and minimal medium containing 5 mM of one of the structurally related amino acids, aspartate (Figure 6.1B), asparagine (Figure 6.1C), glutamate (Figure 6.1D), or glutamine (Figure 6.1E). In rich media, the Δ1132c strains exhibited no growth defect relative to the parental strain, and this was also observed in minimal medium containing aspartate as the sole nitrogen source. A mild growth defect was observed in the Δ1132c strains grown with only glutamate or glutamine, however, there was a strong growth defect in medium containing only asparagine as the sole nitrogen source. This requirement suggests that MAB_1132c functions as an asparagine transporter in *M. abscessus*, and possibly contributes to the uptake of glutamine and glutamate also.

The fact that the Δ1132c strains were capable of growing in medium with asparagine as the sole nitrogen source clearly indicates that MAB_1132c is not the only transport system involved

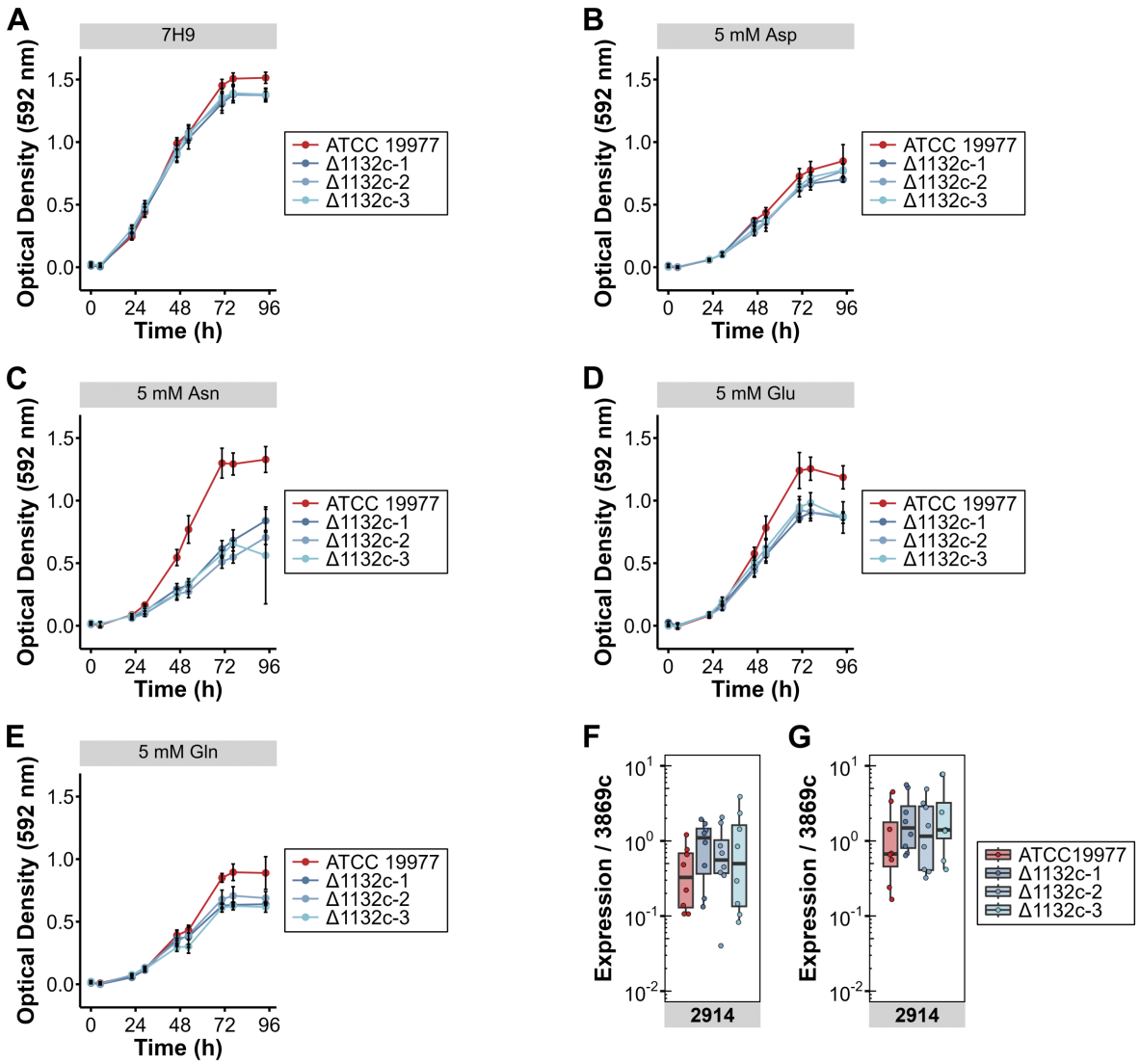


Figure 6.1. MAB_1132c is important but not essential for growth with asparagine as the sole nitrogen source. Growth of *M. abscessus* ATCC 19977 (red) and Δ1132c strains (blue) in various nutrient conditions, measured by optical density at 592 nm. Data represent the mean ± s.d of quadruplicate samples and are representative of three independent experiments. Bacteria grown in (**A**) complete 7H9 medium, or minimal medium containing 5 mM of (**B**) aspartate (Asp), (**C**) asparagine (Asn), (**D**) glutamate (Glu), or (**E**) glutamine (Gln) as the sole nitrogen source. RT-qPCRs show gene expression of gene MAB_2914, also annotated as an asparagine permease, during log phase growth in (**F**) 7H9 complete medium or in (**G**) minimal medium with 5 mM asparagine as the sole nitrogen source. Data are representative of two independent experiments (N = 8), normalised against housekeeping gene MAB_3869c (*rpoB*), statistical comparisons were made using Wilcoxon rank-sum test.

in uptake of asparagine. I measured transcript levels of the other predicted L-asparagine permease within the *M. abscessus* genome, MAB_2914, following growth in either 7H9 complete medium (Figure 6.1F) or in minimal medium with 5 mM asparagine (Figure 6.1G). There was no difference between wild-type *M. abscessus* or the Δ1132c strains in either

media, indicating that there is no compensatory upregulation of MAB_2914 when MAB_1132c function is lost. There was a slight increase in transcription of MAB_2914 in all strains grown in low-asparagine medium compared to the complete media, possibly driven by GlnR regulation in response to limited nitrogen availability[662]. The activity of other asparagine uptake mechanisms in *M. abscessus* was confirmed by growing the Δ1132c strains in minimal medium with increasing concentrations of asparagine (5 mM to 40 mM), as shown in Figure 6.2. While growth of wild-type *M. abscessus* was not particularly impacted by increasing asparagine availability (Figure 6.2A), Δ1132c-1 (Figure 6.2B), Δ1132c-2 (Figure 6.2C) and Δ1132c-3 (Figure 6.2D) all showed increasing ability to grow correlating with the concentration of asparagine, reaching similar levels of growth as the wild-type strain at 40 mM.

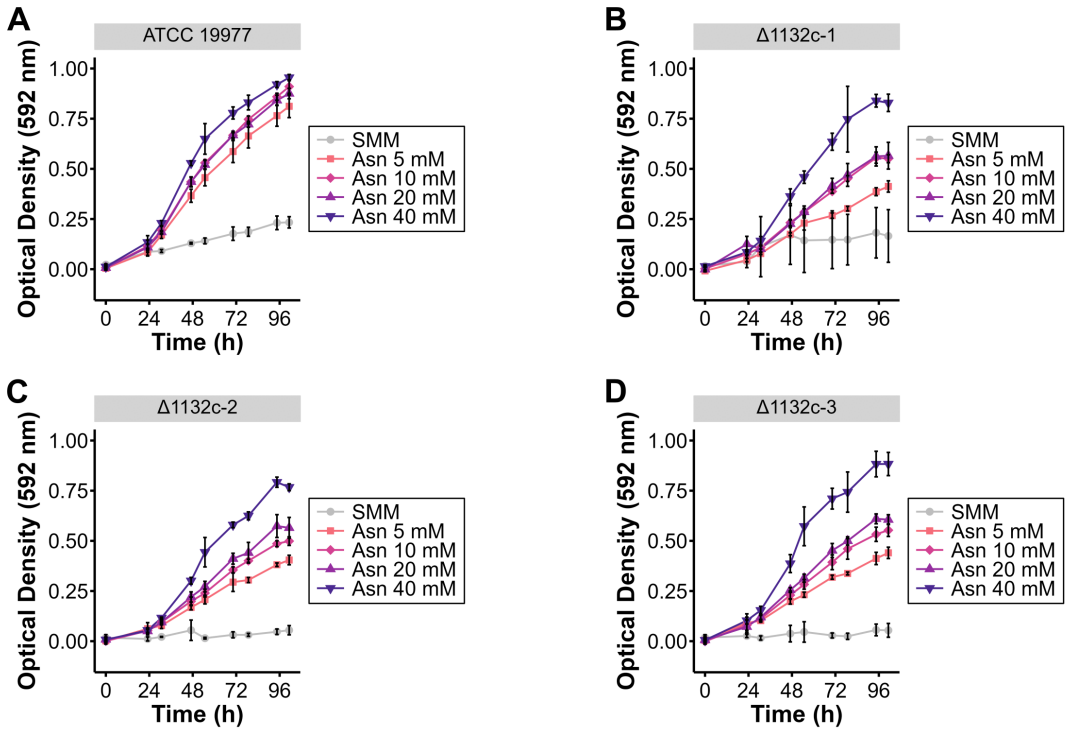


Figure 6.2. Increasing asparagine concentrations rescues growth of Δ1132c strains. Growth of *M. abscessus* wild type (ATCC 19977) (**A**) and Δ1132c strains (**B, C, D**) in minimal medium with increasing concentrations of asparagine as the sole nitrogen source. SMM (grey) shows growth in minimal medium with no nitrogen source provided. Measured by optical density at 592 nm. Data represent the mean ± s.d of quadruplicate samples and are representative of three independent experiments.

These data suggest that MAB_2914 is unlikely to compensate for reduced asparagine uptake

caused by loss of MAB_1132c during *in vitro* growth. This shows that MAB_1132c functions as one of several asparagine transporters in *M. abscessus* which function non-redundantly from one another, highlighting the importance of asparagine uptake in this bacterium.

6.3.2 Asparagine acquisition by *M. abscessus* impacts bacterial virulence and host tolerance

Previous work studying amino acid uptake in *M. tuberculosis* found that expression of asparagine transporter AnsP2 (Rv0346c) was strongly induced in the lungs of patients[770], suggesting a role for this gene during infection. Later work stated that AnsP2 was not required for pathogenicity of *M. tuberculosis* as an AnsP2-KO strain showed no difference in its ability to grow in the lungs and spleen of infected mice compared with wild-type, however, mouse survival was not reported[764]. As previously described in Section 4.3.5, the Δ1132c strains exhibited significantly delayed host death compared with wild-type *M. abscessus* (Figure 6.3A). In *M. tuberculosis*, asparagine metabolism is specifically required for ability to survive acid stress; I reasoned that a similar effect might underlie the observed delay in host death caused by MAB_1132c mutation[764]. In this case, I expected that Δ1132c bacteria should be present in lower numbers. Unexpectedly, I found a minimal difference in the bacterial load between Δ1132c strains and wild-type control bacteria in infected flies over the course of the infection (Figure 6.3B). Flies infected with wild-type bacteria began to die in large numbers at 96 hours post-infection, whilst flies infected with Δ1132c bacteria continued to survive despite increasing bacterial loads (Figure 6.3B). This indicates that MAB_1132c promotes pathogenicity without contributing to the net increase in bacterial numbers, decoupling pathogen virulence with *in vivo* replication.

I next reasoned that nitrogen limitation, induced by asparagine deprivation in the Δ1132c grown in minimal medium with asparagine as the sole nitrogen source, may increase the virulence of the Δ1132c strains due to an increase in intracellular lipid inclusions[762]. In order to

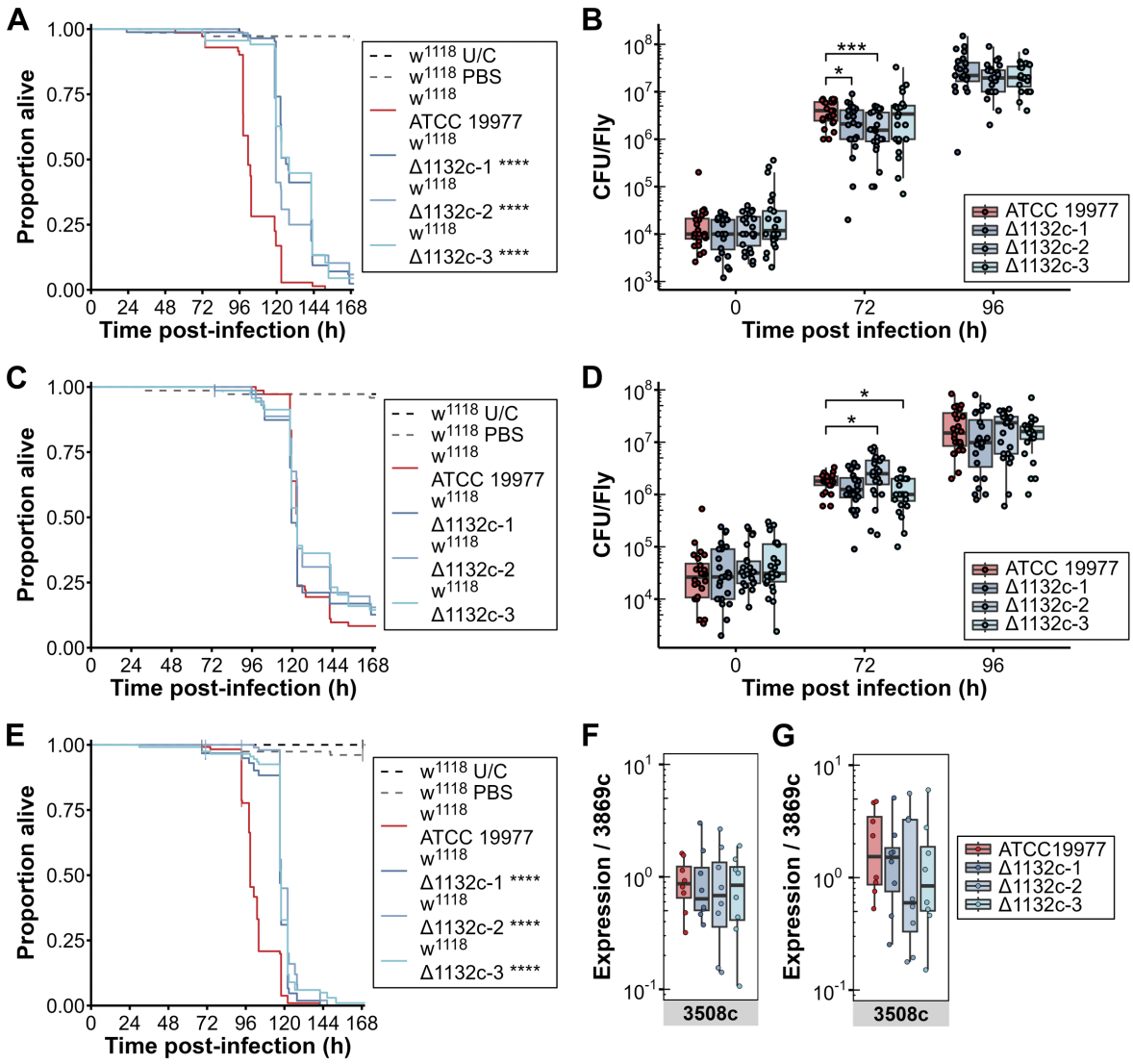


Figure 6.3. Asparagine availability in *M. abscessus* impacts host survival but not bacterial *in vivo* growth. Survival curves of w^{1118} flies infected with *M. abscessus* ATCC 19977 (red) or Δ1132c strains (blue) grown in (**A**) complete medium (7H9), or minimal medium with (**C**) 5 mM asparagine or (**E**) 40 mM asparagine as the sole nitrogen source. Control groups are uninfected flies (black) and PBS Tween80 0.1% injected flies (grey). Data is pooled from three independent experiments performed with common controls, $123 \geq n \geq 68$ per group. Asterisks in the legend indicate the *p*-value compared to flies infected with ATCC 19977, compared using the Log-Rank test. Bacterial load quantifications of w^{1118} flies infected with *M. abscessus* ATCC 19977 (red) or Δ1132c strains (blue) grown in (**B**) complete medium (7H9), or (**D**) minimal medium with 5 mM asparagine as the sole nitrogen source. Data is pooled from three independent experiments, n = 8 per strain per condition per independent experiment. Statistical significance was calculated by comparing the mutant strains to ATCC 19977 within the same time point and medium using the Wilcoxon Rank-Sum test. RT-qPCRs show gene expression of gene MAB_3508c, WhiB7, during log phase growth in (**F**) 7H9 complete medium or in (**G**) minimal medium with 5 mM asparagine as the sole nitrogen source. Data are representative of two independent experiments (N = 8), normalised against housekeeping gene MAB_3869c (*rpoB*), statistical comparisons were made using Wilcoxon rank-sum test. $*$, $P < 0.05$; $**$, $P < 0.01$; $***$, $P < 0.001$; $****$, $P < 0.0001$.

determine how asparagine deprivation would affect *M. abscessus* virulence, I infected flies with wild-type or Δ1132c *M. abscessus* grown in minimal medium supplemented with low (5 mM) or high (40 mM) asparagine as the sole nitrogen source. Despite their *in vitro* growth defect in low-asparagine medium (Figure 6.1C), the survival of flies infected with the Δ1132c strains was unchanged when grown in rich medium or low-asparagine medium with median times to death of 119.5 - 128.0 hours to 119.5 - 123.0 hours, respectively. However, growth in low-asparagine medium caused the wild-type strain to recapitulate the behaviour of Δ1132c strains: host death was delayed without any change in the numbers of viable *M. abscessus* present at any point in infection (Figure 6.3D). Growth in low-asparagine medium led to flies infected with wild-type *M. abscessus* reaching greater bacterial loads at 96 hours post-infection, consistent with the Δ1132c strains, which is not seen in flies infected with wild-type *M. abscessus* grown in rich media. Increasing the asparagine availability with the high-asparagine medium restored the wild-type phenotype to that seen in initial growth in rich media, again with no change in the survival time of flies infected with the Δ1132c strains (Figure 6.3E). This indicates that asparagine availability prior to infection, regardless of *in vitro* growth capacity, contributes to differences in bacterial pathogenicity or host tolerance to infection.

To evaluate whether the change in virulence was associated with an altered stress response, I measured the transcript levels of *M. abscessus* WhiB7, a transcriptional regulator involved in the activation of over 100 genes including determinants of drug resistance and virulence factors[53,771]. There was no change in the transcription of WhiB7 (MAB_3508c) between any of the strains in either complete medium (Figure 6.3F) or low-asparagine medium (Figure 6.3G).

6.3.3 Nitrogen limitation is not driving changes in virulence caused by asparagine limitation

Previous work found that nitrogen-limited *M. abscessus* showed increased virulence in zebrafish embryos which was driven by the accumulation of intracellular triacylglycerol

stores[762]. As Figure 6.3 showed that the Δ1132c strains had no change in virulence, and asparagine limitation reduced wild-type *M. abscessus* virulence, I wanted to test whether triacylglycerol accumulation was occurring in these conditions. This was visualised by growing *M. abscessus* cultures to stationary phase, diluting cultures to the same OD_{600}, and extracting lipids with chloroform and methanol. These were then run on silica gel glass plates and triglycerides visualised using CAM solution. I reproduced the observation of increased triacylglycerol in wild-type bacteria grown with an alternative high and low nitrogen minimal medium (ammonium chloride as the sole nitrogen source), shown in Figure 6.4A. I also observed that the Δ1132c strains grown in low-asparagine medium showed increased triacylglycerol accumulation (Figure 6.4B), suggesting that the impaired *in vitro* growth of these strains in this medium was due to nitrogen limitation. However, as there was no triacylglycerol accumulation in the Δ1132c strains grown in complete 7H9 medium (Figure 6.4C), the observed survival phenotypes are likely independent of triacylglycerol accumulation as there were no changes in host survival during infection with the Δ1132c strains grown in low-asparagine medium relative to growth in rich media. Additionally, there was no triacylglycerol accumulation in wild-type *M. abscessus* grown in low-asparagine medium (Figure 6.4B), which showed a profound increase in fly survival during infection. This further supports the argument that decreased virulence associated with decreased asparagine uptake, either due to MAB_1132c mutation or growth in low-asparagine media, is not a product of general nitrogen limitation and instead results from a specific requirement for asparagine transport prior to infection.

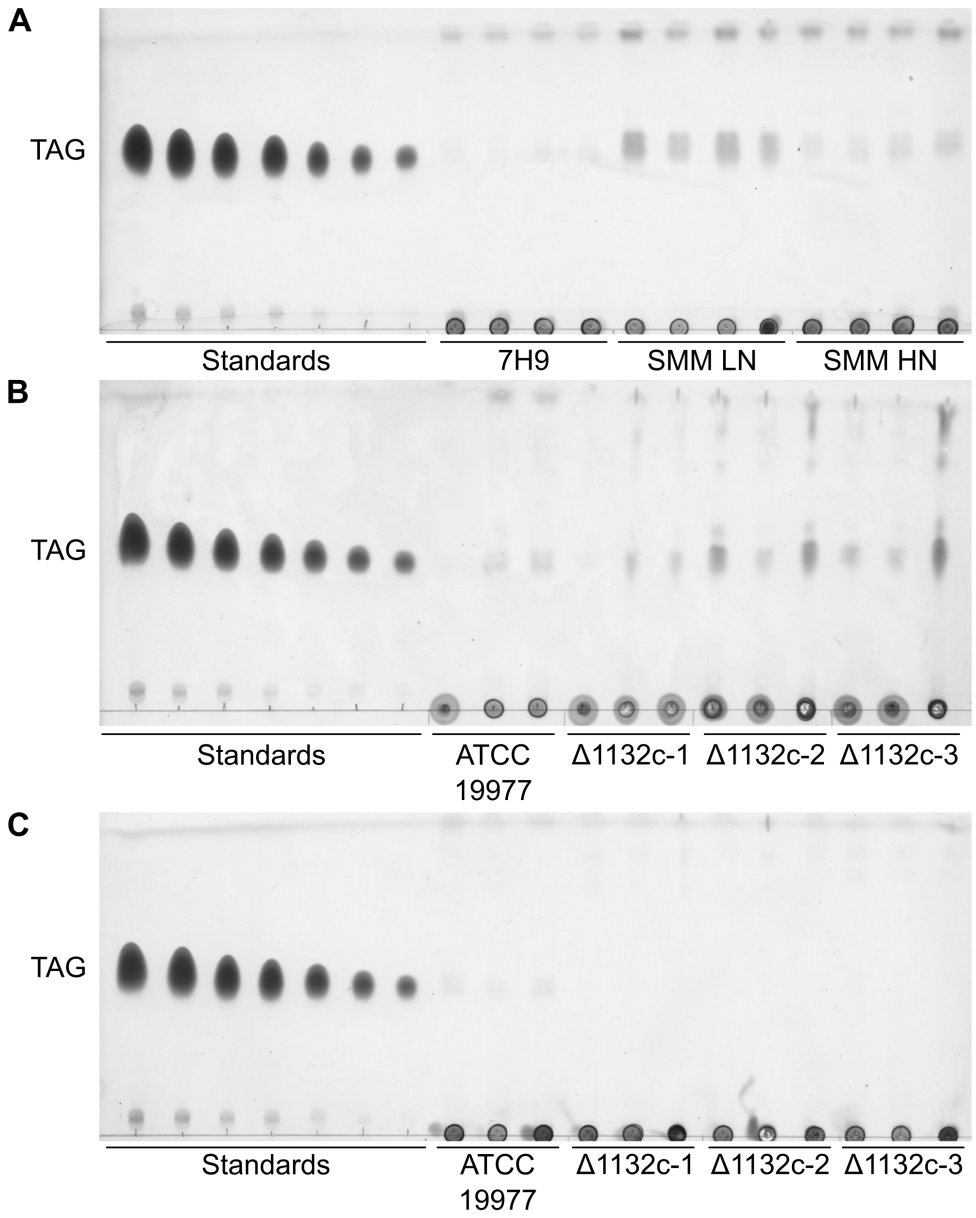


Figure 6.4. Triacylglycerol accumulation in asparagine-limited *M. abscessus* strains. (**A**) Cultures of wild-type (ATCC 19977) *M. abscessus* were grown in 7H9 complete media, or minimal medium containing either high (SMM HN) or low (SMM LN) nitrogen concentrations (1 g/L or 0.05 g/L ammonium chloride, respectively), triacylglycerols were extracted and TLC plates were run with lard standards. Plate is representative of three independent experiments, n = 4 per medium per experiment. Cultures of wild-type (ATCC 19977) *M. abscessus* and Δ1132c strains were grown in (**B**) SMM 5 mM Asn or (**C**) 7H9 complete media, triacylglycerols were extracted and TLC plates were run with lard standards. Plates are representative of three independent experiments, n = 3 per strain per medium per experiment.

As there was an increase in triacylglycerol levels in the Δ1132c strains grown in low-asparagine media, I measured the transcript levels of three triacylglycerol synthase genes, of seven predicted within the genome, MAB_3551c (Tgs1), MAB_1917 (Tgs2) and MAB_4544c

(Tgs4)[323]. Unsurprisingly, there was no difference between the wild-type and Δ1132c strains when grown in complete media, shown in Figure 6.5A, but also no difference between the strains when grown in low-asparagine media, Figure 6.5B. The observed increase in triacylglycerol in the Δ1132c strains grown in low-asparagine medium is therefore likely a result of increased triacylglycerol synthase activity, rather than transcriptional regulation of the triacylglycerol synthase genes.

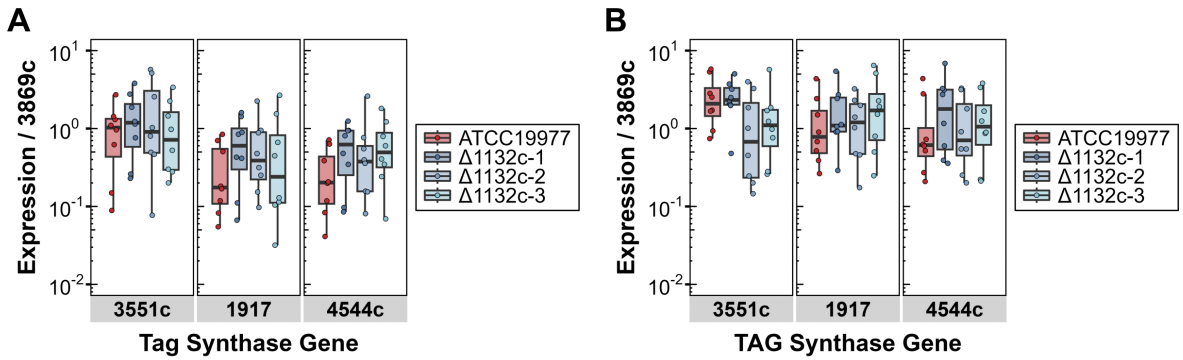


Figure 6.5. Transcription of triacylglycerol synthase genes. (**A**) RT-qPCRs show gene expression of triacylglycerol synthase genes MAB_3551c, MAB_1917 and MAB_4544c, during log phase growth in (**A**) 7H9 complete medium or in (**B**) minimal medium with 5 mM asparagine as the sole nitrogen source. Data are representative of two independent experiments (N = 8), normalised against housekeeping gene MAB_3869c (*rpoB*), statistical comparisons were made using Wilcoxon rank-sum test.

I also confirmed that the observed survival phenotypes were not a product of differences in the morphotype of the *M. abscessus* strains. *M. abscessus* is capable of producing a thick layer of glycopeptidolipids (GPLs) surrounding the mycomembrane, which can result in highly variable host immune responses based on the presence or absence of these GPLs due to differences in cord formation and exposed immunogenic proteins[122,126,333]. To determine if the observed survival differences associated with decreased asparagine availability prior to infection were caused by differences in GPL production I measured transcript levels of 13 key genes required for the production and transport of GPLs, and found no difference between wild-type bacteria and Δ1132c strains in either rich (Figure 6.6A) or low asparagine medium (Figure 6.6B). Additionally, there was no observable morphotype difference between these bacterial strains.

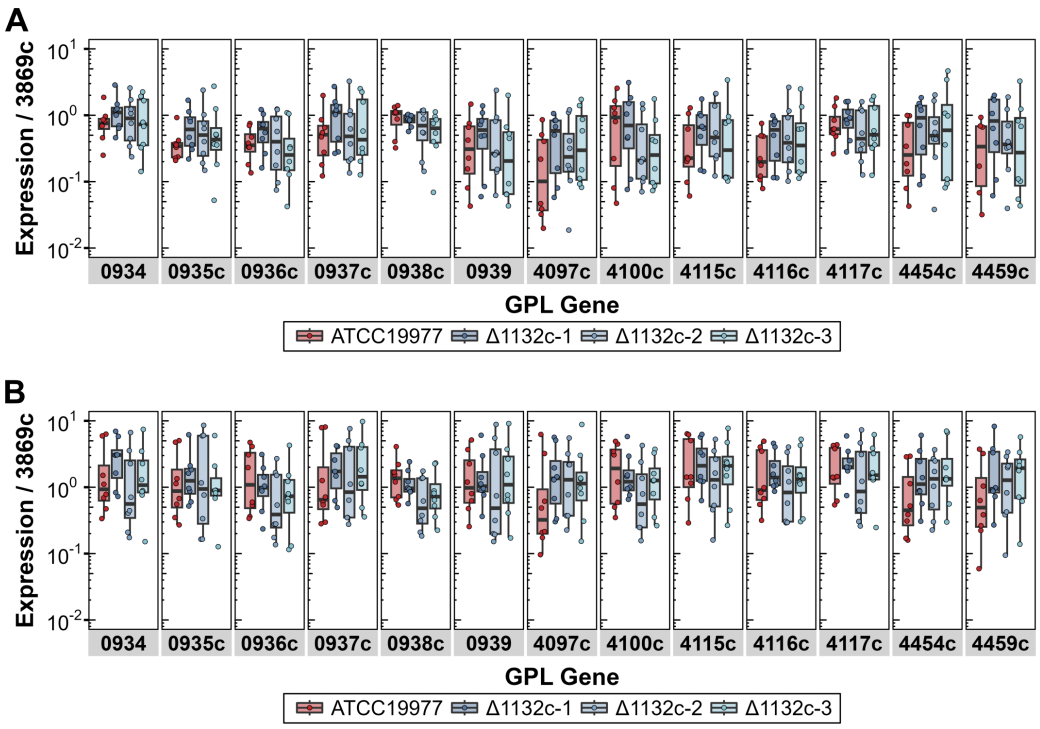


Figure 6.6. Glycopeptidolipid gene transcription in Δ1132c strains. RT-qPCRs show gene expression of genes involved in glycopeptidolipid (GPL) production in *M. abscessus* wild type (ATCC 19977) and Δ1132c strains during log phase growth in (**A**) 7H9 complete medium or in (**B**) minimal medium with 5 mM asparagine as the sole nitrogen source. Data are pooled from two independent experiments, n = 8 per strain, normalised against MAB_3869c (*rpoB*), statistical comparisons were made using Wilcoxon rank-sum test.

6.3.4 Innate immune signalling is diminished in flies infected with asparagine permease mutant *M. abscessus* strains

The fact that Δ1132c bacteria caused significantly delayed host death despite being present in similar numbers indicated that their interaction with the host was fundamentally different. In order to get a better understanding of the nature of this difference, I assayed the expression of antimicrobial peptides, well-defined transcriptional targets of innate immune detection pathways, after infection with wild-type and Δ1132c *M. abscessus*.

As described in Chapter 3 and as with other mycobacteria, *M. abscessus* drivers slower and weaker immune activation than most other tested bacteria in *D. melanogaster*[516]. Infection does not activate antimicrobial peptide expression above or beyond that induced by the sterile-injury PBS control within the first 6 hours post-infection. However, by 48 hours

post-infection, antimicrobial peptide transcript levels are significantly higher in the *M. abscessus* infected flies than in PBS controls, an effect that is strengthened at 80 hours post-infection. This late antimicrobial peptide induction is significantly blunted in flies infected with Δ1132c bacteria; it is not until 80 hours post-infection that antimicrobial peptide transcription in flies infected with Δ1132c strains exceeds that seen in the PBS sterile-injury control group. Interestingly, this pattern is true of antimicrobial peptides associated with both Toll (Figure 6.7A, B) and Imd pathway activation (Figure 6.8A - E). Bomanins produced as a result of Toll signalling activity showed the same trend as the other AMPs (Figure 6.7C - F).

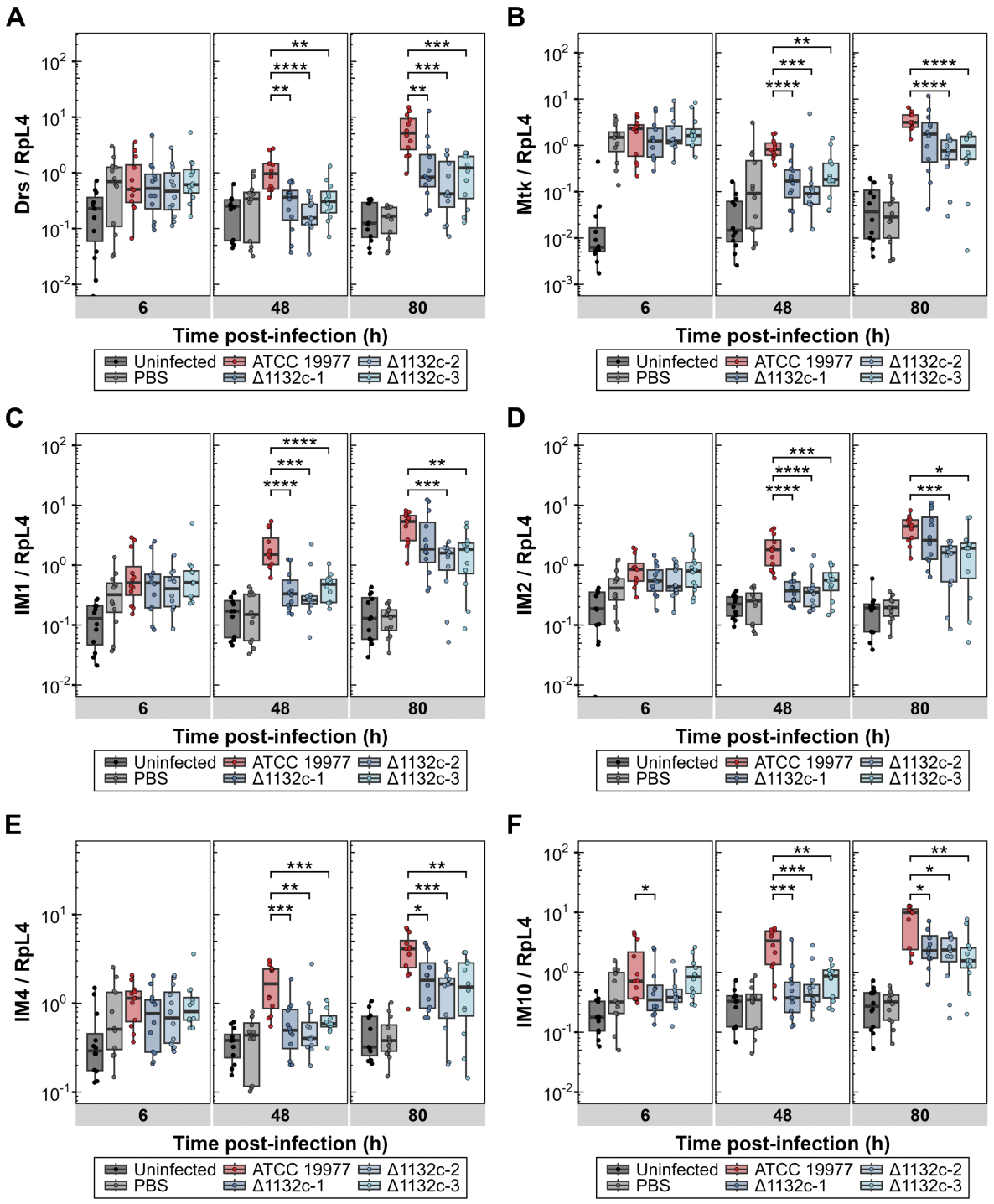


Figure 6.7. Reduction in transcription of Toll pathway targets during *M. abscessus* infection with Δ1132c strains. RT-qPCR measurements of (**A**) *Drosomycin*, (**B**) *Metchnikowin*, (**C**) *IM1*, (**D**) *IM2*, (**E**) *IM4*, and (**F**) *IM10* normalised to housekeeping gene *RpL4*, of w^{1118} flies. Flies were uninjected (U/C, black), or injected with PBS Tween80 0.1% (grey), *M. abscessus* ATCC 19977 OD_{600} = 0.05 (red), Δ1132c-1, Δ1132c-2, or Δ1132c-3 (blue) and transcript levels were measured at 6, 48, and 80 hours post-infection. Data is pooled from three independent experiments, n = 12 per group, statistical comparisons were made using Wilcoxon rank-sum test. All statistically significant comparisons are shown in Table S6.1. ∗, P < 0.05; ∗∗, P < 0.01; ∗∗∗, P < 0.001; ∗∗∗∗, P < 0.0001.

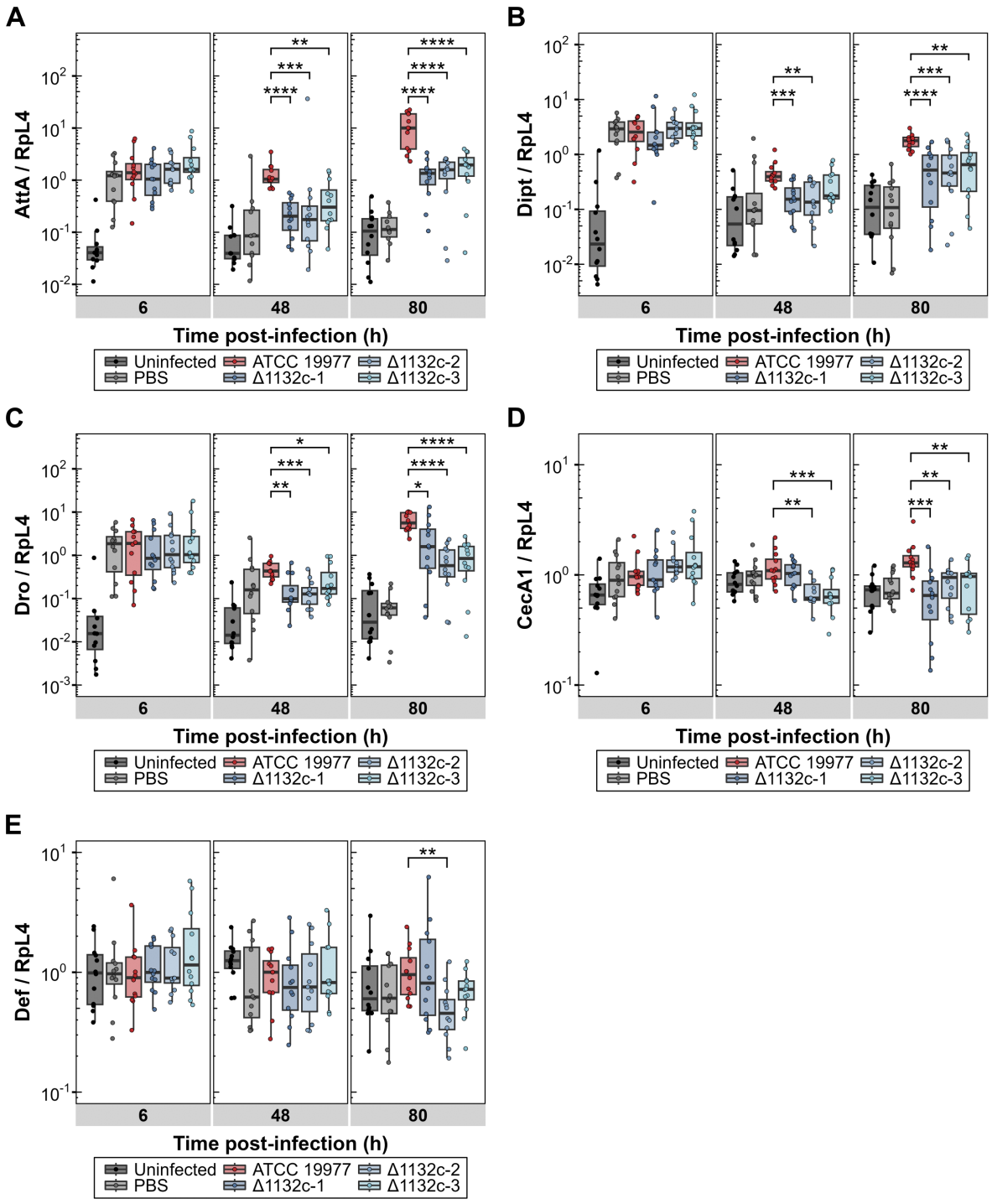


Figure 6.8. Reduction in transcription of Imd pathway targets during infection with Δ1132c strains. RT-qPCR measurements of (**A**) *Attacin*, (**B**) *Diptericin*, (**C**) *Drosocin*, (**D**) *Cecropin A1* and (**E**) *Defensin* normalised to housekeeping gene *RpL4*, of w^{1118} flies. Flies were uninjected (U/C, black), or injected with PBS Tween80 0.1% (grey), *M. abscessus* ATCC 19977 OD_{600} = 0.05 (red), Δ1132c-1, Δ1132c-2, or Δ1132c-3 (blue) and transcript levels were measured at 6, 48, and 80 hours post-infection. Data is pooled from three independent experiments, n = 12 per group, statistical comparisons were made using Wilcoxon rank-sum test. All statistically significant comparisons are shown in Table S6.2. ∗, P < 0.05; ∗∗, P < 0.01; ∗∗∗, P < 0.001; ∗∗∗∗, P < 0.0001.

In addition to assessing transcript levels of antimicrobial peptides, I also measured other *D. melanogaster* immunity-related genes. Expression of cytokines Upd2 and Upd3 and their downstream JAK/STAT signalling targets Socs36E, Stat92E and Atg2 were unchanged across all groups (Figure 6.9A - E). Despite showing statistical significance, the differences between groups were very mild and are unlikely to hold any biological relevance. Stress protein Turandot A (TotA) is induced in the fat body upon JAK/STAT signalling by Upd2 and Upd3[457,469]. At 80 hours post-infection, *TotA* expression was mildly increased in PBS sterile-injury flies and reduced in *M. abscessus* flies, relative to the uninfected controls. Consistent with the reduced transcription responses of antimicrobial peptides in flies infected with Δ1132c strains, the expression of TotA in these flies was reduced compared to the PBS sterile-injury flies, but not as low as the wild-type *M. abscessus* infected flies (Figure 6.9F). Other immune signalling pathway genes, such as Eiger and TACE involved in TNFα signalling, were also unchanged (Figure 6.9G, H).

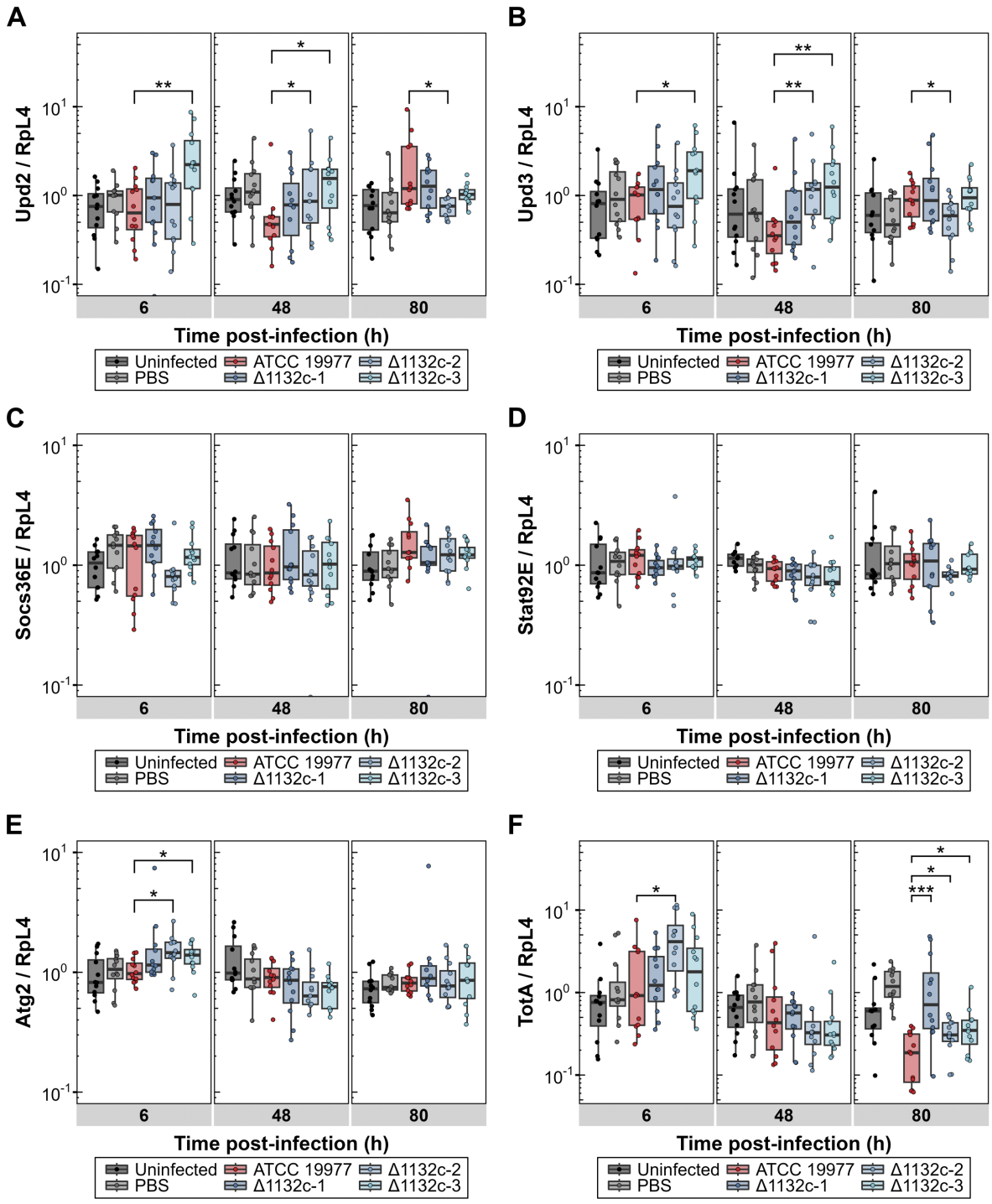


Figure 6.9. Transcription of other immune signalling pathway genes during infection with Δ1132c strains. (**A - F**) See legend on page 259.

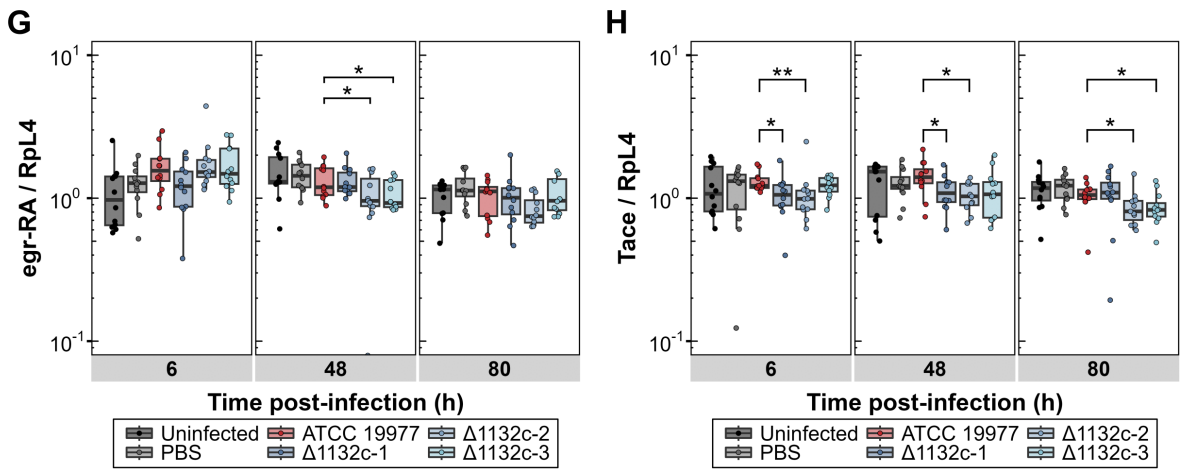


Figure 6.9. Transcription of other immune signalling pathway genes during infection with Δ1132c strains continued. RT-qPCR measurements of (**A**) *Unpaired 2*, (**B**) *Unpaired 3*, (**C**) *Socs36E*, (**D**) *Stat92E*, (**E**) *Atg2*, (**F**) *TotA*, (**G**) *egr-RA* and (**H**) *Tace* normalised to housekeeping gene *RpL4*, of w^{1118} flies. Flies were uninjected (U/C, black), or injected with PBS Tween80 0.1% (grey), *M. abscessus* ATCC 19977 OD_{600} = 0.05 (red), Δ1132c-1, Δ1132c-2, or Δ1132c-3 (blue) and transcript levels were measured at 6, 48, and 80 hours post-infection. Data is pooled from three independent experiments, n = 12 per group, statistical comparisons were made using Wilcoxon rank-sum test. All statistically significant comparisons are shown in Table S6.3. ∗, P < 0.05; ∗∗, P < 0.01; ∗∗∗, P < 0.001; ∗∗∗∗, P < 0.0001.

6.3.5 Cytokine signalling in *D. melanogaster* is responsible for changes in host susceptibility to asparagine-limited *M. abscessus*

Immune-induced cytokine signalling is an important cause of pathology in many infections. The reduced immune activation I observed with Δ1132c strains suggested the possibility that differences in time to death might be a product of changes in cytokine signalling. It was previously observed that the cytokine Upd3 was an important regulator of the *D. melanogaster* immune response to *Mycobacterium marinum*[470], so I tested the role of Upd3 and its relative Upd2 in infections with wild-type and Δ1132c *M. abscessus*.

I observed that wild-type *M. abscessus* did not show the same effect as *M. marinum*: flies lacking either *upd2* or *upd3*, or both cytokines, exhibited identical time-to-death as controls. However, the difference in time-to-death between flies infected with wild-type and Δ1132c *M. abscessus* was significantly reduced in *upd2* mutants (Figure 6.10B) and *upd3* mutants (Figure

6.10C), and almost completely eliminated in *upd2 upd3* double mutants (Figure 6.10D), relative to wild-type flies (Figure 6.10A). This suggests that an important role of asparagine transport via MAB_1132c in this infection is to inhibit the activity of Upd2 and Upd3; genetic elimination of these cytokines is sufficient to almost entirely suppress the Δ1132c survival phenotype. It is also possible that the action of Upd2 and Upd3 contributes to increased host tolerance during infection with the Δ1132c strains, but is ineffective against wild-type *M. abscessus*.

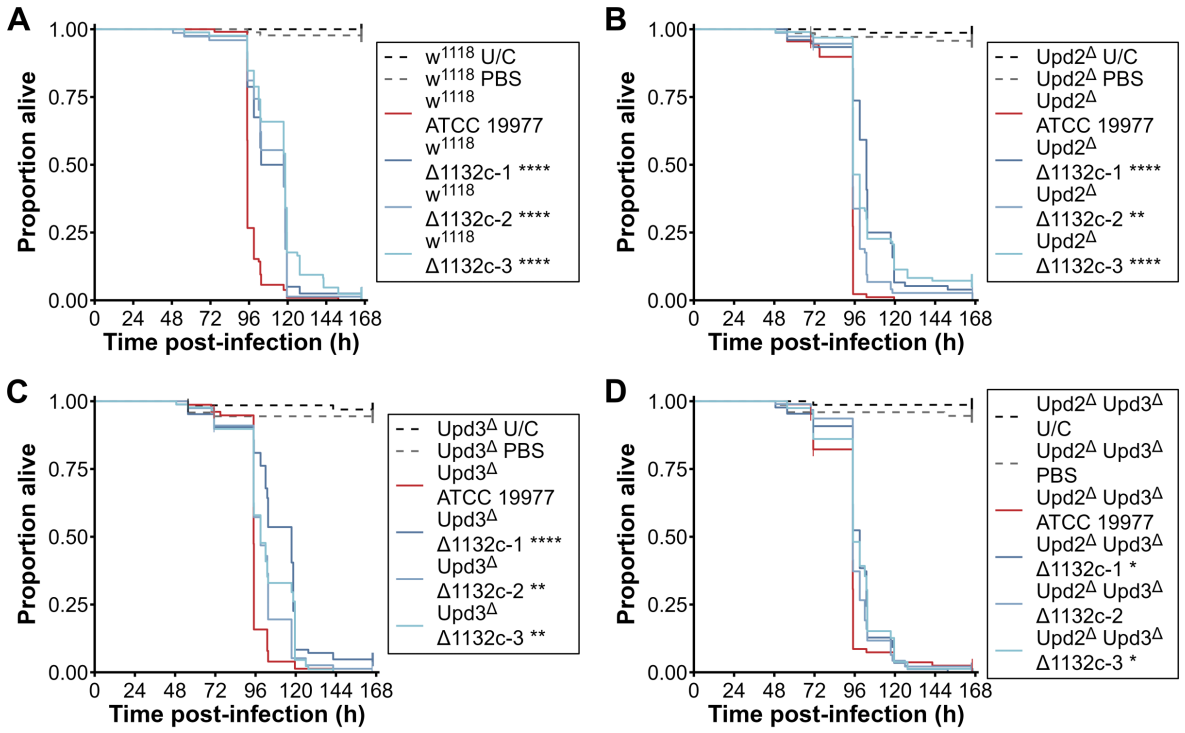


Figure 6.10. Increased susceptibility of unpaired mutant *D. melanogaster* to Δ1132c *M. abscessus*. Survival curves of (**A**) w^{1118} (control), (**B**) *upd2´*, (**C**) *upd3´* and (**D**) *upd2´upd3´* flies infected with *M. abscessus* ATCC 19977 (red) or Δ1132c strains (blue) grown in complete medium (7H9). Control groups are uninfected flies (black) and PBS Tween80 0.1% injected flies (grey). Data is pooled from three independent experiments performed with common controls, $106 \geq n \geq 66$ per group. Asterisks in the legend indicate the *p*-value compared to flies infected with ATCC 19977, compared using the Log-Rank test. Asterisks in legends indicate significant differences compared against flies of the same genotype infected with ATCC 19977. $*$, $P < 0.05$; $**$, $P < 0.01$; $***$, $P < 0.001$; $****$, $P < 0.0001$.

6.3.6 Asparagine uptake by *M. abscessus* drives changes in host insulin/Akt signalling

Infection with pathogenic mycobacteria results in disrupted insulin signalling, both in humans and many animal models. In *D. melanogaster* infection with *M. marinum*, a wasting response

occurs due to failure of Akt activation and the subsequent increase in transcription factor Foxo activity, causing hyperglycaemia, and a reduction in glycogen and triglyceride stores[494]. Upd cytokine signalling is an important regulator of insulin/Akt pathway activity in *D. melanogaster* via effects on insulin-like peptide production, release, and peripheral sensitivity[471,772,773]. Therefore, I next tested the effects of MAB_1132c on Akt activity by assaying levels of Akt phosphorylation on Ser505[494,504].

Assaying levels of Akt phosphorylation of Ser505 by Western Blot allows comparison of Akt activity, as phosphorylation is required for full Akt activity[504,724,725]. Consistent with previous observations of *D. melanogaster* infected with *M. marinum*[494], wild-type *M. abscessus* caused a progressive decrease in the levels of the 60 kDa isoform of phospho-AKT with no changes in the amount of total AKT in wild-type flies. In contrast, wild-type flies infected with Δ1132c-2 showed a slight initial decrease in the levels of phospho-AKT compared with sterile-injury control flies at 48 hours post-infection, but by 96 hours post-infection there was no difference between Δ1132c-2 infected flies and sterile injury controls (Figure 6.11A). The reduction in phospho-AKT was retained, though somewhat blunted, in *upd2* mutant flies infected with wild-type bacteria, but the behaviour of Δ1132c-2 infection was completely unaltered in *upd2* mutant hosts (Figure 6.11B). Overall, these data suggest that the dysregulation in insulin signalling caused by *M. abscessus* requires asparagine uptake by the bacteria. This may be driven in part by changes in signalling via Upd2. In any case, it is clear from the decoupling between bacterial numbers, host survival, and phospho-AKT levels seen in Δ1132c-2 infection that changes in microbial metabolism can have direct impacts on the metabolic pathology seen during infection, likely in part due to changes in molecules detected by the host and the subsequent host response.

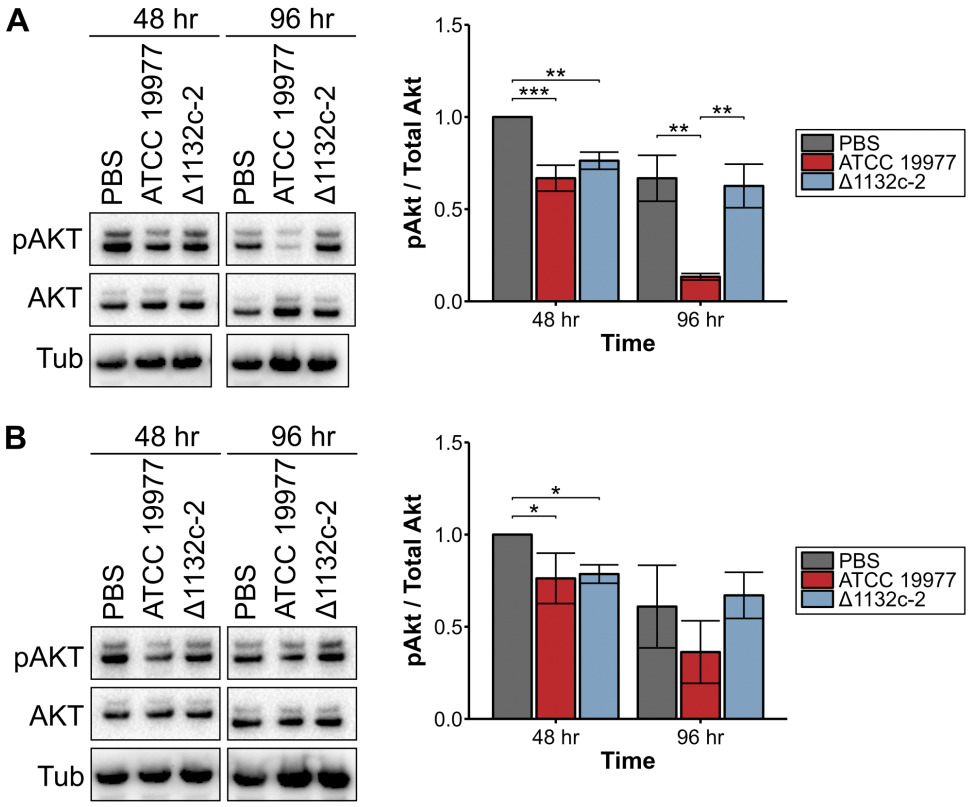


Figure 6.11. Reduction of *D. melanogaster* Akt activity by *M. abscessus* is dependent on asparagine uptake. Systemic levels of Ser505 phosphorylated and total Akt protein of (**A**) w^{1118} and (**B**) $upd2^{\Delta}$ flies at 48 and 96 hours post-infection with *M. abscessus* ATCC 19977 (red) or Δ1132c-2 (blue), measured by Western Blot. Data represents one independent experiment, n = 3 per strain per genotype. Groups were compared with one-way ANOVA with Tukey's test. ∗, P < 0.05; ∗∗, P < 0.01; ∗∗∗, P < 0.001; ∗∗∗∗, P < 0.0001.

6.4 Discussion

MAB_1132c was originally identified from a high-dimensional phenogenomic analysis of *M. abscessus*, with changes in MAB_1132c being associated with differences in clofazimine resistance[581]. The results of this chapter show the importance of MAB_1132c during an *in vivo* infection of *D. melanogaster*, providing insight into how metabolic regulation in *M. abscessus* contributes to its immune evasion strategies by altering host-pathogen interactions. Because of the nature of *M. abscessus* infection, acquisition from environmental sources followed by intra-host adaptation and further transmission via environmental intermediates[153], understanding how the metabolic adaptations of *M. abscessus* result in changes to interactions with host immune systems is essential.

The findings from this chapter confirm the role of MAB_1132c as an asparagine transporter, however similar to *M. tuberculosis* it appears that *M. abscessus* also possesses additional transporters capable of asparagine uptake, albeit not enough to fully compensate for the loss of MAB_1132c in low asparagine conditions. Despite this *in vitro* growth defect, the reduction in asparagine uptake during *in vivo* infection has minimal impact on growth of Δ1132c strains within *D. melanogaster*. This is consistent with previous studies into the role of asparagine transport in *M. tuberculosis* that found the asparagine permease transporter AnsP2 was not required for *in vivo* growth in infected mice lungs and spleens[764]. This is possibly due to the uptake of glutamine, which is considered to act as the predominant nitrogen donor to fuel de novo synthesis of other amino acids[774]. Whilst there was a slight impairment of *in vitro* growth of the Δ1132c strains with glutamine with the sole nitrogen source, this evidently was not sufficient to cause any *in vivo* growth defect.

Beyond the function of MAB_1132c during *M. abscessus* infection, these results shed light on a more general role of asparagine uptake by *M. abscessus* and how this leads to fundamental changes in host-pathogen interactions. Intriguingly, by restricting asparagine in *M. abscessus*, either by mutating MAB_1132c or by using asparagine-limited media, infected *D. melanogaster* were longer lived without significant alteration to *in vivo* bacterial growth. This suggests that while *M. abscessus* is not reliant on prior asparagine uptake for replicative fitness *in vivo*, there is a key changed *M. abscessus* factor which is driving the host survival advantage stemming from differences in the host immune response. I observed these host immune response differences in the reduced transcription of key antimicrobial peptides associated with both the Toll and Imd pathways in *D. melanogaster* when infected with the Δ1132c strains compared with wild-type *M. abscessus*. It is possible that this represents an immune evasion strategy by *M. abscessus*, allowing for increased numbers of bacteria by altering host tolerance to promote survival and further spread of *M. abscessus*. Our results indicate that whatever the change occurring in *M. abscessus* by asparagine availability, the host survival differences

are being driven by Upd cytokine signalling, with possible links to dysregulation of insulin signalling, suggesting that when *M. abscessus* infects with sufficient asparagine levels the cytokine signalling driven by Upd is normally inhibited or ineffectual.

I have been unable to identify what *M. abscessus* factor is being changed by asparagine availability, and how this causes the observed differences in the host response. Triacylglycerol accumulation is not occurring in the Δ1132c strains in rich media, nor in wild-type *M. abscessus* in low-asparagine media, indicating that this is not a general nitrogen limitation phenotype. Nevertheless, the work by Santucci *et al.* on triacylglycerol accumulation during nitrogen limitation is exemplary of how environmental conditions can drive metabolic changes in *M. abscessus* and subsequent differences in infection dynamics[762]. I also confirmed that there is no difference in the morphotype of the Δ1132c strains, which are also known to drive differing host immune responses[122,600]. This suggests that the difference in *M. abscessus* caused by asparagine availability is either in relation to the production of a virulence factor which may normally interact with *D. melanogaster* Upd signalling, or a change in a pathogen-associated molecular pattern altering host recognition of *M. abscessus*. Changes in nitrogen metabolism in other pathogenic mycobacteria have been shown to lead to changes in cell wall structure due to GlnR regulation of the poly-L-glutamine (PLG) layer[775]. This would explain the reduction of antimicrobial peptide transcription in the Δ1132c infected flies despite carrying a similar bacterial load.

The possible role of GlnR in the phenotype of asparagine-limited *M. abscessus* is an interesting question. The *M. abscessus* homologue of global nitrogen regulator GlnR (MAB_0744) has been linked to transcriptional regulation of the other asparagine transporter MAB_2914, as well as nitrite reductase gene MAB_3522c and nitrite extrusion protein MAB_3523c, but not MAB_1132c[662]. Knockout of GlnR results in reduced biofilm formation and increased antibiotic susceptibility, with these phenotypes being rescued upon addition of glutamine or

glutamate[662]. Despite MAB_1132c not being identified in this study, the impact of the other asparagine permease gene on biofilm formation suggests MAB_1132c may also contribute to this phenotype. Bioinformatic analyses could identify whether MAB_1132c contains any putative GlnR binding sites, and biofilm assays and MIC experiments using the Δ1132c, Δ3522c and Δ3523c strains would also inform about the role of these genes individually.

Another outstanding question is how changing the asparagine levels in *M. abscessus* prior to infection may change the *in vivo* competition for asparagine. Limited availability of nutrients creates intense competition between host and pathogen for resources, including amino acids which are highly beneficial to both the host defence and for bacterial virulence. *M. tuberculosis* infections cause consistent metabolic changes in infected hosts, conserved across humans, mice and zebrafish, including a decrease in host asparagine levels during infection[776]. It is unknown if this same asparagine decrease occurs in flies infected with *M. abscessus*, and if so how the asparagine is being utilised.

In summary, this chapter outlines how the metabolic status of *M. abscessus* can influence the host immune response, specifically by altering cytokine signalling and insulin pathways. These findings imply that pathogen nutrient availability can have far-reaching consequences on host defence, providing new avenues for exploring host-pathogen interactions and the manipulation of host immune responses in the treatment of mycobacterial infections. The key outstanding question from this work is what specific *M. abscessus* factor is being altered by asparagine availability and subsequently causing this change in interaction with the host immune systems. I have confirmed that it is not simply a nitrogen limitation or morphotype specific phenotype, and so in-depth transcriptomic or proteomic studies may shed further light on this.

Chapter 7: Discussion

7.1 Summary of work presented

7.1.1 Background and aim of the project

Mycobacterium abscessus is an emerging pathogen with extremely high levels of both intrinsic and acquired resistance, making it extremely challenging to treat. Patients with CF are at greatest risk from *M. abscessus* infection, and as infection rates rise there is the ever-increasing risk of evolution by *M. abscessus* towards becoming a more virulent human pathogen. Very little is understood about the mechanisms of pathogenesis in *M. abscessus* nor about the host immune response to infection. Intensive screening of clinical strains has identified mutations in *M. abscessus* genes that are associated with clinically relevant phenotypes. However, the lack of genetic tools to manipulate the *M. abscessus* genome has severely hampered study into the function of these genes, preventing the development of mutant strains to understand the genetic determinants of pathogenesis and the molecular components involved in interactions with the host.

The aims of this project were twofold. Firstly, I sought to develop an infection model of *M. abscessus* which would allow for both prokaryotic and eukaryotic genetic manipulation in order to probe the host-pathogen interactions at a genetic level. To do this, I used the model organism *Drosophila melanogaster*, allowing me to characterise the consequences of *M. abscessus* infection entirely within the context of an innate immune response. I was then able to combine the wide variety of genetic tools available for use in *D. melanogaster* with a novel CRISPR-Cas9 system for genetic editing of *M. abscessus* to specifically assess the role of targeted *M. abscessus* genes during infection.

The second aim of the project was then to use this system to study the selected *M. abscessus* genes of interest and identify *D. melanogaster* host factors involved in the changes to infection outcomes. I would then combine this with traditional microbiological techniques to

understand the role of these genes in *M. abscessus* biology and consider how differences in the physiological or metabolic status of a pathogen can have far-reaching immune and metabolic consequences during infection of a host.

7.1.2 Key findings

In **Chapter 3**, I characterised the *D. melanogaster* response to *M. abscessus* infection. I found that *M. abscessus* is almost entirely fatal, killing flies in a dose-dependent manner from 4 days post-infection. Using *D. melanogaster* lines with loss-of-function mutations in key components of a variety of innate immune signalling pathways, I found that each pathway individually offers very little protection to the host against *M. abscessus*, despite evidence of activation of both the Toll and Imd pathways from 48 hours post-infection shown by transcriptional levels of AMPs and Bom effectors. These results also showed that there was no benefit of these immune signalling pathways against either of the *M. abscessus* morphotypes, however, it remains unknown whether there is differential detection and subsequent pathway activation based on morphotype in *D. melanogaster*. Experiments manipulating the *D. melanogaster* haemocytes showed that loss of haemocytes also had no effect on survival during *M. abscessus* infection, whereas the presence of haemocytes without phagocytic ability was detrimental and decreased fly survival. These results highlighted key differences in the behaviour of *M. abscessus* compared with *M. marinum*, another mycobacterial pathogen that has been studied in the *D. melanogaster* model.

Chapter 4 focused on the use of a CRISPR-Cas9 two-plasmid system to introduce frameshift mutations within targeted *M. abscessus* genes of interest to create loss-of-function mutant strains. This method makes use of the NHEJ repair system present within mycobacteria. Of the 18 *M. abscessus* genes targeted, selected based on identification from clinical isolates with phenogenomic associations, homology to key *M. tuberculosis* virulence factors, or involvement in a key metabolic pathway, successful frameshift mutations were identified in 11 genes. Screening the mutant strains to identify changes in *D. melanogaster* survival or bacterial load

revealed information about the contribution of each of these genes towards *in vivo* growth and virulence of *M. abscessus*, and how these two characteristics are not always coupled. Particularly interesting findings included the impact on *M. abscessus* virulence caused by loss of the as-yet unidentified WGX-100 protein MAB_1283c, and the observation that whilst nitrite reduction by MAB_3522c is required for *in vivo* growth, nitrite extrusion by MAB_3523c contributes to virulence without an effect on *in vivo* growth. The distinct survival and bacterial load phenotypes also reinforced the usefulness of the *D. melanogaster* model in studying *M. abscessus* host-pathogen interactions.

Following the screen of mutant *M. abscessus* strains produced, I decided to continue studying the role of MAB_0471 and MAB_0472 during infection in **Chapter 5**. As deletion mutations in these genes in clinical isolates were associated with more persistent infections in CF patients, but prolonged survival during *D. melanogaster* infection, I wanted to understand the possible causes underlying this discrepancy. I identified these genes as part of the *tad* operon, not previously described in *M. abscessus*, encoding the flp pilus assembly membrane proteins TadB and TadC, respectively. Due to the role of the Tad/Flp pilus in adhesion and biofilm formation described in other bacterial species, I tested the Δ0471 and Δ0472 strains capacity for biofilm formation. Unexpectedly I found that the mutant *M. abscessus* strains displayed increased surface attachment and decreased intercellular adhesion, resulting in increased pellicle biofilm formation at the air-liquid interface. This phenotype likely underpins the increased persistence of strains with mutations in these genes within CF patients, whereas pellicle biofilm formation is unlikely to occur within *D. melanogaster* haemolymph. *D. melanogaster* survival experiments showed that the increase in survival during infection with the Δ0471 and Δ0472 strains was dependent on Egr signalling and Imd signalling but not Tak1. I tested the hypothesis that the proteins predicted to be secreted by the Tad system, MAB_0474 and MAB_0475 were involved in inhibition of apoptosis, but individual expression of these proteins did not restore the fly survival phenotype or inhibit egr-induced apoptosis.

Finally, in **Chapter 6**, I examined how asparagine acquisition by *M. abscessus* can drive changes in *D. melanogaster* tolerance due to differences in immune signalling and metabolic responses. I selected the Δ1132c strains due to the strong increase in *D. melanogaster* survival that was not coupled with an equivalent change in bacterial load, suggesting a change in bacterial virulence and/or host tolerance. I confirmed that the MAB_1132c gene was functioning as one of multiple non-redundant asparagine transporters in *M. abscessus*, highlighting the importance of asparagine acquisition. Infecting flies with bacteria grown in asparagine-limiting conditions, either by loss of function of MAB_1132c or low-asparagine media, resulted in prolonged survival. As a result of this, bacteria continued to grow to greater levels than those reached under high-asparagine acquisition conditions. This was also accompanied by a reduction in innate immune signalling as measured by AMP transcript levels and was not correlated with changes in morphotype or triacylglycerol accumulation due to general nitrogen limitation. In the case of the Δ1132c strains, the increase in fly survival was shown to be dependent on Upd2 and Upd3 cytokine signalling by *D. melanogaster*.

7.2 *D. melanogaster* as a model for *M. abscessus* infection

A key aspect of the work presented is the usefulness of the *D. melanogaster* model in studying *M. abscessus* infection. *D. melanogaster* has proven to be an excellent model for identifying *M. abscessus* strains with reduced virulence, and subsequently elucidating the host factors responsible for the observed shifts in survival. This has provided new information about clinically relevant host-pathogen interactions of *M. abscessus*. A limitation, however, is the distinctly different host environment. This is exemplified by the results shown in Chapter 5, in which *M. abscessus* strains with deletions in MAB_0471 and MAB_0472 cause more persistent infections in CF patients, but result in increased survival with decreased bacterial loads in *D. melanogaster*. Nevertheless, the *D. melanogaster* model for *M. abscessus* infection offers insight into the cellular interactions with macrophages and the subsequent host immune

and metabolic responses, mirroring deep tissue infection rather than the initial colonisation conditions.

There are currently very few suitable models for studying infections in the context of the CF lung environment, and so combining the findings from the *D. melanogaster* model with other experimental methods such as *in vitro* cell culture, lung-on-a-chip platforms, murine models and bioinformatic analyses from clinical strains can validate the relevance of the host-pathogen interactions identified.

7.2.1 The role of haemocytes

M. abscessus is a facultative intracellular pathogen, which primarily infects haemocytes within the *D. melanogaster* model. Uptake of *M. abscessus* appears to involve the opsonisation factor Tep4[488], and possibly also the phagocytosis receptors NimC1 and Eater. Following phagocytosis, *M. abscessus* is likely capable of replicating intracellularly, in part by inhibiting maturation and acidification of the phagolysosomes in which it is contained[14]. Recent evidence suggests that, like other pathogenic mycobacteria *M. marinum* or *M. tuberculosis*, *M. abscessus* may be capable of phagosome escape and spread into adjacent cells[313]. It is likely that containment within the intracellular phagolysosome vesicle offers a form of protection to *M. abscessus*, preventing detection of the bacteria by *D. melanogaster* PRRs. This would explain the relatively low and slow transcriptional activation of AMPs in response to *M. abscessus* compared to infection with other bacterial pathogens. Following phagosomal growth, *M. abscessus* can cause phagosomal rupture, escaping into the cytosol resulting in increased immune responses and apoptotic cell death, promoting spread to nearby host cells[14].

Based on my results and the findings from other published literature, I have developed a simple model outlining the possible role of haemocytes during *M. abscessus* infection of *D. melanogaster*. Removal of haemocytes by expression of pro-apoptotic genes shows mixed

results on the outcome of *M. abscessus* infection. My findings, by expressing reaper under the control of the haemolectin driver, showed no difference in survival suggesting the presence of haemocytes was neither detrimental nor beneficial to the host during infection. Work by Touré *et al.* found that expression of Debcl under the croquemort driver decreased fly survival and increased bacterial load indicating that, at least during the early phase of infection, phagocytic haemocytes are protective for the host[118]. However, expression of Debcl using either the Hemese driver or ance driver, both highly expressed in a subpopulation of haemocytes, resulted in long-lived flies[118].

Using *D. melanogaster* lines to prevent phagocytosis of *M. abscessus*, but retain the haemocytes along with their signalling capabilities, clearly shows the protective role phagocytic uptake has for the host. Preventing phagocytosis either with *NimC1*^{1}*;eater*^{1} double mutant flies or depletion of phagocytic haemocytes by clodronate results in decreased survival upon infection with *M. abscessus*[118]. Taken together, these data suggest that phagocytic uptake of *M. abscessus* is beneficial to the host, however, the presence of haemocytes in the absence of phagocytosis can be detrimental. This is possibly due to the amount of controlled apoptotic destruction of infected haemocytes that occurs when *M. abscessus* is phagocytosed versus necrotic cell death and other inflammatory damage when *M. abscessus* remains extracellular, which is potentially exaggerated by haemocytes. However, even controlled destruction of infected cells by apoptosis cannot protect *D. melanogaster* from succumbing to *M. abscessus* infection. Inhibition of apoptosis by expression of caspase inhibitor baculovirus protein p35 increases fly survival, but *M. abscessus* is capable of surviving lysis of host cells[118] and uses its release into the haemolymph as an opportunity to spread to further host cells. As with *M. marinum* infection, the inflammatory damage and loss of haemocytes by either apoptosis or necrosis likely contributes to the death of infected flies[470].

7.2.2 *M. abscessus* interactions with *D. melanogaster* differ from those with *M. marinum*

Throughout the results presented in this project, and results from other experiments, many hypotheses about the behaviour of *M. abscessus* were based on information known about *M. marinum* infection of *D. melanogaster*. Whilst some aspects of *M. abscessus* and *M. marinum* infection are consistent, such as a progressive reduction in Akt activity over the course of the infection, many key differences have also been identified. This is perhaps not surprising, *M. abscessus* is a RGM known for causing pulmonary infection of CF patients whereas *M. marinum* is a SGM that very rarely causes pulmonary infection; there are clearly important differences in the environmental location, metabolism and infective behaviour between these species. A comparison between *M. abscessus* and *M. marinum* infection of *D. melanogaster* is shown in Table 7.1.

Table 7.1. Comparison of *M. abscessus* and *M. marinum* infection of *D. melanogaster*.

***D. melanogaster* line**	***M. abscessus***	***M. marinum***
egr^{3}	No survival change (this study)	Increased survival[452]
SC35^{KG}	No survival change (unpublished data, Dionne Lab)	Increased survival (unpublished data, Dionne Lab)
Δ*Tep4*	Increased survival, decreased bacterial load[488]	No survival change[488]
Upd3$^{\Delta}$	No survival change (this study)	Increased survival, decreased bacterial load[470]
w^{1118}	Reduction in pAkt (this study)	Reduction in pAkt[494]
w^{1118}	Mild induction of Toll and Imd genes late during infection (this study)	Mild induction of Toll and Imd genes late during infection[494]
w^{1118}	No change in upd3, Atg2, or other Stat92E target transcription (this study)	Increase in upd3 transcription, increase in Stat92E activity, decrease in Atg2 expression[470]

Given the lack of information about the possible function of *M. abscessus* genes and their roles during infection, the comparatively highly studied and well-characterised *M. tuberculosis*

represents a starting point for identifying the possible function of homologous genes. Also, researchers studying mycobacterial pathophysiology in the context of *M. tuberculosis* infection are increasingly turning to *M. abscessus*. The reasons for this are understandable, *M. abscessus* is a biosafety level 2 organism that requires less stringent laboratory conditions and is considerably faster to grow than *M. tuberculosis*. However, as highlighted by the differences between *M. abscessus* and *M. marinum* infection of *D. melanogaster*, these are fundamentally different pathogens. *M. abscessus* has evolved from the earliest branching lineage of *Mycobacteria* and remains an opportunistic environmental pathogen as opposed to an obligate human pathogen. As such, and as shown from the results of *M. abscessus* mutant strains, the function and role of many *M. abscessus* genes is not entirely comparable to their *M. tuberculosis* homologues. *M. abscessus* has fundamentally different metabolic requirements for its lifestyle compared to *M. tuberculosis*, and this is likely reflected in the host-pathogen interactions and immune consequences during infection. Therefore, any insight into the pathophysiology of *M. abscessus* cannot be assumed to be the same in *M. tuberculosis*, and vice versa.

7.3 Insights into *M. abscessus* pathogenesis

7.3.1 Pathogenic evolution of *M. abscessus*

Biofilm formation is a key step in the initial colonisation of a host by many bacteria, including *M. abscessus*, and especially within the CF lung. *M. abscessus* aggregated into biofilms can tolerate higher antibiotic concentrations leading to treatment failure and the establishment of persistent infections, with bacteria from the biofilm seeding deeper tissue infections. The identification of the *tad* locus within *M. abscessus* and the distinct phenotypes of the Δ0471 and Δ0472 strains in terms of biofilm formation and *D. melanogaster* infection suggests a possible role of this gene locus in the pathogenic evolution of *M. abscessus*. Given the increased pellicle biofilm formation by the Δ0471 and Δ0472 strains *in vitro*, it is possible that this is the cause of the more persistent infections observed in CF patients infected with strains with

deletion mutations in MAB_0471. This would also explain why deletion mutations in MAB_0471 arose in the ancestor of DCC2[581], contributing to the increased fitness and transmission of this DCC[153].

Based on the results in Chapter 5, it appears that the potentially increased capacity to form biofilm and colonise the host environment has a trade-off at the level of interaction with macrophages which occurs during deep tissue infection. The Δ0471 and Δ0472 strains are more susceptible to the activity of TNFα, which may currently restrict the virulence of DCC2. Whilst this is consistent with previous analyses suggesting that the pathogenic evolution of *M. abscessus* is restricted by the competing requirement to maintain transmission fitness[153], it does raise concerns about the potential for within-host adaptation leading to greater virulence. An alternative mechanism may be that the rapid formation of biofilm by DCC2 strains during initial colonisation, whilst itself disadvantaged in terms of establishing deeper tissue infections due to the interaction with macrophages, may offer a safe haven for other *M. abscessus* strains to enter the lung.

7.3.2 Impact of microbial metabolic status on host-pathogen interactions

The results from Chapters 4 and 6 emphasise how changes in microbial metabolism can cause changes in infection outcomes, both in relation to and decoupled from *in vivo* growth, the latter highlighting how the balance of microbial virulence and host tolerance can be shifted. It is being increasingly recognised that the composition of culture medium and laboratory culture conditions impact bacterial phenotypes and experimental outcomes, as has been shown in *M. abscessus* in relation to amino acid uptake or synthesis[662]. It is therefore essential to not only understand the metabolic pathways utilised for intracellular survival during infection of a host cell, but how the metabolic status of the bacterium prior to infection can prime or enhance certain features to promote infectivity and virulence.

Different amino acids clearly play important and specific roles in the behaviour of *M. abscessus*.

This is seen in the results of Chapter 6 showing that asparagine limitation decreases virulence independent of general nitrogen limitation and triacylglycerol accumulation, and reduced growth rate and altered biofilm phenotypes seen in Δ*glnR M. abscessus* strains are specifically linked to glutamine and glutamate, not simply from the lack of a nitrogen source[662]. Whether the changes in the *D. melanogaster* immune response during infection with asparagine-limited *M. abscessus* is due to a change in the production of a specific protein such as a virulence factor, or as a result of changed physical properties due to a global change in nitrogen regulation is unknown. Understanding the bacterial metabolic changes that are occurring to cause the observed host effects is an important factor, and will contribute to knowing whether such changes impact *M. abscessus* transmission or infectivity within patients.

7.4 Conclusions, future questions, and outlook

In this project, I used the *D. melanogaster* model to study the host-pathogen interactions occurring during infection with *M. abscessus* to better understand how this pathogen evades, subverts and survives the innate immune response to establish infections. By using a CRISPR-Cas9 technique I was able to efficiently generate gene knockout *M. abscessus* mutant strains, leading to a better understanding of the role of eleven different genes during infection. This led to the identification of the *M. abscessus tad* locus and showed the importance of TNFα signalling against strains with mutations in these genes, and how asparagine availability prior to infection can lead to essential changes in the metabolic status of the bacteria leading to changes in the host immune response and infection outcome. These results reinforce the usefulness of the *D. melanogaster* model to combine genetic manipulation of both the host and the pathogen to probe interactions at a molecular level. It is also important to consider how the plasticity of environmental pathogens such as *M. abscessus* can produce subtle phenotypic changes that result in profound differences in host responses, highlighting how standard laboratory conditions are not representative of real-world infection conditions.

There are many questions that remain outstanding, including:

1. What is the role and impact of host cell death during *M. abscessus* infection?
    (a) Does intracellular *M. abscessus* secrete virulence factors to inhibit apoptosis?
    (b) Does extracellular *M. abscessus* induce necrotic cell death?
2. What is the role of the *tad* locus in *M. abscessus* infection?
    (a) Does it secrete apoptosis inhibitors? If so, what host factor do they target?
    (b) Do the *tad* locus mutant strains show impaired attachment to host cells?
3. What change is triggered by asparagine limitation that decreases *M. abscessus* virulence?
    (a) Is it the loss of a virulence factor that interferes with JAK/STAT signalling?
    (b) Are asparagine-limited strains simply more susceptible to host JAK/STAT activity?
    (c) Is there a change in biofilm-producing capacity in asparagine-limited strains?

These questions can, in part, be addressed using the genetic tractability of the *D. melanogaster* model combined with the CRISPR-Cas9 approach to produce gene knockout *M. abscessus* strains. Additional experiments to identify the widespread changes occurring in the knockout mutant strains and in infected *D. melanogaster*, such as RNAseq and metabolomics, will shed further light on the specific host-pathogen interactions at play.

References

[1] David E. Griffith, Timothy Aksamit, Barbara A. Brown-Elliott, Antonino Catanzaro, Charles Daley, Fred Gordin, Steven M. Holland, Robert Horsburgh, Gwen Huitt, Michael F. Iademarco, Michael Iseman, Kenneth Olivier, Stephen Ruoss, C. Fordham Von Reyn, Richard J. Wallace, and Kevin Winthrop. An official ATS/IDSA statement: Diagnosis, treatment, and prevention of nontuberculous mycobacterial diseases, 2 2007.

[2] R. Andres Floto, Kenneth N. Olivier, Lisa Saiman, Charles L. Daley, Jean Louis Herrmann, Jerry A. Nick, Peadar G. Noone, Diana Bilton, Paul Corris, Ronald L. Gibson, Sarah E. Hempstead, Karsten Koetz, Kathryn A. Sabadosa, Isabelle Sermet-Gaudelus, Alan R. Smyth, Jakko van Ingen, Richard J. Wallace, Kevin L. Winthrop, Bruce C. Marshall, and Charles S. Haworth. US Cystic Fibrosis Foundation and European Cystic Fibrosis Society consensus recommendations for the management of non-tuberculous mycobacteria in individuals with cystic fibrosis. *Thorax*, 71 Suppl 1(Suppl 1):i1–i22, 1 2016.

[3] Charles S Haworth, John Banks, Toby Capstick, Andrew J Fisher, Thomas Gorsuch, Ian F Laurenson, Andrew Leitch, Michael R Loebinger, Heather J Milburn, Mark Nightingale, Peter Ormerod, Delane Shingadia, David Smith, Nuala Whitehead, Robert Wilson, and R Andres Floto. British Thoracic Society guidelines for the management of non-tuberculous mycobacterial pulmonary disease (NTM-PD). *Thorax*, 72(Suppl 2):ii1–ii64, 11 2017.

[4] E. H. Runyon. Typical Mycobacteria: Their classification. *The American review of respiratory disease*, 91:288–289, 1965.

[5] Stacey L. Martiniano, Jerry A. Nick, and Charles L. Daley. Nontuberculous Mycobacterial Infections in Cystic Fibrosis. *Thoracic surgery clinics*, 29(1):95–108, 2 2019.

[6] Christopher J. Richards and Kenneth N. Olivier. Nontuberculous Mycobacteria in Cystic Fibrosis. *Seminars in Respiratory and Critical Care Medicine*, 40(6):737–750, 2019.

[7] Rachid Nessar, Emmanuelle Cambau, Jean Marc Reyrat, Alan Murray, and Brigitte Gicquel. Mycobacterium abscessus: A new antibiotic nightmare. *Journal of Antimicrobial Chemotherapy*, 67(4):810–818, 4 2012.

[8] In Kwon Park and Kenneth N. Olivier. Nontuberculous mycobacteria in cystic fibrosis and non-cystic fibrosis bronchiectasis. *Seminars in respiratory and critical care medicine*, 36 (2):217–224, 4 2015.

[9] Byung Woo Jhun, Seong Mi Moon, Kyeongman Jeon, O. Jung Kwon, Heejin Yoo, Keumhee C. Carriere, Hee Jae Huh, Nam Yong Lee, Sung Jae Shin, Charles L. Daley, and Won Jung Koh. Prognostic factors associated with long-term mortality in 1445 patients with nontuberculous mycobacterial pulmonary disease: a 15-year follow-up study. *The European respiratory journal*, 55(1), 1 2020.

[10] Charles L. Daley, Jonathan M. Iaccarino, Christoph Lange, Emmanuelle Cambau, Richard J. Wallace, Claire Andrejak, Erik C. Böttger, Jan Brozek, David E. Griffith, Lorenzo Guglielmetti, Gwen A. Huitt, Shandra L. Knight, Philip Leitman, Theodore K. Marras, Kenneth N. Olivier, Miguel Santin, Jason E. Stout, Enrico Tortoli, Jakko Van Ingen, Dirk Wagner, and Kevin L. Winthrop. Treatment of nontuberculous mycobacterial pulmonary disease: An official ATS/ERS/ESCMID/IDSA clinical practice guideline. *European Respiratory Journal*, 56(1), 7 2020.

[11] Charles R. Esther, Denise A. Esserman, Peter Gilligan, Alan Kerr, and Peadar G. Noone. Chronic Mycobacterium abscessus infection and lung function decline in cystic fibrosis. *Journal of Cystic Fibrosis*, 9(2):117–123, 3 2010.

[12] Tavs Qvist, David Taylor-Robinson, Elisabeth Waldmann, Hanne Vebert Olesen, Christine Rønne Hansen, Inger Hee Mathiesen, Niels Høiby, Terese L. Katzenstein, Rosalind L. Smyth, Peter J. Diggle, and Tania Pressler. Comparing the harmful effects of nontuberculous mycobacteria and Gram negative bacteria on lung function in patients with cystic fibrosis. *Journal of cystic fibrosis : official journal of the European Cystic Fibrosis Society*, 15(3):380–385, 5 2016.

[13] Ema Kavaliunaite, Kathryn A. Harris, Paul Aurora, Garth Dixon, Delane Shingadia, Nagarajan Muthialu, and Helen Spencer. Outcome according to subspecies following lung transplantation in cystic fibrosis pediatric patients infected with Mycobacterium abscessus. *Transplant Infectious Disease*, 22(3), 6 2020.

[14] Matt D. Johansen, Jean Louis Herrmann, and Laurent Kremer. Non-tuberculous mycobacteria and the rise of Mycobacterium abscessus, 7 2020.

[15] Christian Hoffmann, Andrew Leis, Michael Niederweis, Jürgen M. Plitzko, and Harald Engelhardt. Disclosure of the mycobacterial outer membrane: cryo-electron tomography and vitreous sections reveal the lipid bilayer structure. *Proceedings of the National Academy of Sciences of the United States of America*, 105(10):3963–3967, 3 2008.

[16] Benoît Zuber, Mohamed Chami, Christine Houssin, Jacques Dubochet, Gareth Griffiths, and Mamadou Daffé. Direct Visualization of the Outer Membrane of Mycobacteria and Corynebacteria in Their Native State. *Journal of Bacteriology*, 190(16):5672, 8 2008.

[17] Antony T. Vincent, Sammy Nyongesa, Isabelle Morneau, Michael B. Reed, Elitza I. Tocheva, and Frederic J. Veyrier. The mycobacterial cell envelope: A relict from the past or the result of recent evolution?, 10 2018.

[18] Charles L. Dulberger, Eric J. Rubin, and Cara C. Boutte. The mycobacterial cell envelope — a moving target. *Nature Reviews Microbiology 2019 18:1*, 18(1):47–59, 11 2019.

[19] L. M. Fu and C. S. Fu-Liu. Is Mycobacterium tuberculosis a closer relative to Gram-positive or Gram-negative bacterial pathogens? *Tuberculosis*, 82(2-3):85–90, 2002.

[20] Megan H. Touchette and Jessica C. Seeliger. Transport of outer membrane lipids in mycobacteria. *Biochimica et biophysica acta. Molecular and cell biology of lipids*, 1862 (11):1340–1354, 11 2017.

[21] P. Chen, R. E. Ruiz, Q. Li, R. F. Silver, and W. R. Bishai. Construction and characterization of a Mycobacterium tuberculosis mutant lacking the alternate sigma factor gene, sigF. *Infection and immunity*, 68(10):5575–5580, 2000.

[22] Pascal Ludwiczak, Martine Gilleron, Yann Bordat, Carlos Martin, Brigitte Gicquel, and Germain Puzo. Mycobacterium tuberculosis phoP mutant: lipoarabinomannan molecular structure. *Microbiology (Reading, England)*, 148(Pt 10):3029–3037, 2002.

[23] Gerard A. Cangelosi, Julie S. Do, Robert Freeman, John G. Bennett, Makeda Semret, and Marcel A. Behr. The two-component regulatory system mtrAB is required for morphotypic multidrug resistance in Mycobacterium avium. *Antimicrobial agents and chemotherapy*, 50(2):461–468, 2 2006.

[24] Roberta Provvedi, Dana Kocíncová, Valentina Donà, Daniel Euphrasie, Mamadou Daffé, Gilles Etienne, Riccardo Manganelli, and Jean Marc Reyrat. SigF controls carotenoid pigment production and affects transformation efficiency and hydrogen peroxide sensitivity in Mycobacterium smegmatis. *Journal of bacteriology*, 190(23):7859–7863, 12 2008.

[25] Robert B. Abramovitch, Kyle H. Rohde, Fong Fu Hsu, and David G. Russell. aprABC: a Mycobacterium tuberculosis complex-specific locus that modulates pH-driven adaptation to the macrophage phagosome. *Molecular microbiology*, 80(3):678–694, 5 2011.

[26] Sladjana Prisic and Robert N. Husson. Mycobacterium tuberculosis Serine/Threonine Protein Kinases . *Microbiology Spectrum*, 2(5), 9 2014.

[27] Joseph O. Falkinham. Mycobacterial aerosols and respiratory disease. *Emerging infectious diseases*, 9(7):763–767, 7 2003.

[28] S. Prinzis, B. Rivoire, and P. J. Brennan. Search for the molecular basis of morphological variation in Mycobacterium avium. *Infection and immunity*, 62(5):1946–1951, 1994.

[29] J. T. Belisle and P. J. Brennan. Chemical basis of rough and smooth variation in mycobacteria. *Journal of bacteriology*, 171(6):3465–3470, 1989.

[30] Gemma Agustí, Oihane Astola, Elisabeth Rodríguez-Güell, Esther Julián, and Marina Luquin. Surface spreading motility shown by a group of phylogenetically related, rapidly growing pigmented mycobacteria suggests that motility is a common property of mycobacterial species but is restricted to smooth colonies. *Journal of bacteriology*, 190 (20):6894–6902, 10 2008.

[31] Annick Ortalo-Magné, Anne Lemassu, Marie-Antoinette Lané Elle, Fabienne Bardou, Gaby Silve, Pierre Gounon, Gilles Marchal, and Mamadou Daffé. Identification of the Surface-Exposed Lipids on the Cell Envelopes of Mycobacterium tuberculosis and Other Mycobacterial Species. *JOURNAL OF BACTERIOLOGY*, 178(2):456–461, 1996.

[32] Susan T. Howard, Elizabeth Rhoades, Judith Recht, Xiuhua Pang, Anny Alsup, Roberto Kolter, C. Rick Lyons, and Thomas F. Byrd. Spontaneous reversion of Mycobacterium abscessus from a smooth to a rough morphotype is associated with reduced expression of glycopeptidolipid and reacquisition of an invasive phenotype. *Microbiology*, 152(6): 1581–1590, 6 2006.

[33] Anne Laure Roux, Albertus Viljoen, Aïcha Bah, Roxane Simeone, Audrey Bernut, Laura Laencina, Therese Deramaudt, Martin Rottman, Jean Louis Gaillard, Laleh Majlessi, Roland Brosch, Fabienne Girard-Misguich, Isabelle Vergne, Chantal de Chastellier, Laurent Kremer, and Jean Louis Herrmann. The distinct fate of smooth and rough Mycobacterium abscessus variants inside macrophages. *Open Biology*, 6(11), 2016.

[34] E. Catherinot, J. Clarissou, G. Etienne, F. Ripoll, J. F. Emile, M. Daffé, C. Perronne, C. Soudais, J. L. Gaillard, and M. Rottman. Hypervirulence of a rough variant of the Mycobacterium abscessus type strain. *Infection and Immunity*, 75(2):1055–1058, 2007.

[35] Emilie Catherinot, Anne Laure Roux, Edouard Macheras, Dominique Hubert, Moussa Matmar, Luc Dannhoffer, Thierry Chinet, Philippe Morand, Claire Poyart, Beate Heym, Martin Rottman, Jean Louis Gaillard, and Jean Louis Herrmann. Acute respiratory failure involving an R variant of mycobacterium abscessus. *Journal of Clinical Microbiology*, 47 (1):271–274, 2009.

[36] Robert Lee Hunter, Nandagopal Venkataprasad, and Margaret R. Olsen. The role of trehalose dimycolate (cord factor) on morphology of virulent M. tuberculosis in vitro. *Tuberculosis (Edinburgh, Scotland)*, 86(5):349–356, 9 2006.

[37] Augusto Cesar Hunt-Serracin, Brian J. Parks, Joseph Boll, and Cara C. Boutte. Mycobacterium abscessus Cells Have Altered Antibiotic Tolerance and Surface Glycolipids in Artificial Cystic Fibrosis Sputum Medium. *Antimicrobial agents and chemotherapy*, 63 (7), 2019.

[38] Gilles Etienne, Christelle Villeneuve, Helen Billman-Jacobe, Catherine Astarie-Dequeker, Marie Ange Dupont, and Mamadous Daffé. The impact of the absence of glycopeptidolipids on the ultrastructure, cell surface and cell wall properties, and phagocytosis of Mycobacterium smegmatis. *Microbiology (Reading, England)*, 148(Pt 10):3089–3100, 2002.

[39] Wassim Daher, Louis David Leclercq, Albertus Viljoen, Jona Karam, Yves F. Dufrêne, Yann Guérardel, and Laurent Kremer. O-Methylation of the Glycopeptidolipid Acyl Chain Defines Surface Hydrophobicity of Mycobacterium abscessus and Macrophage Invasion. *ACS infectious diseases*, 6(10):2756–2770, 10 2020.

[40] Albertus Viljoen, Felipe Viela, Laurent Kremer, and Yves F. Dufrêne. Fast chemical force microscopy demonstrates that glycopeptidolipids define nanodomains of varying hydrophobicity on mycobacteria. *Nanoscale horizons*, 5(6):944–953, 6 2020.

[41] Kaj M. Kreutzfeldt, Paul R. McAdam, Pauline Claxton, Anne Holmes, A. Louise Seagar, Ian F. Laurenson, and J. Ross Fitzgerald. Molecular Longitudinal Tracking of Mycobacterium abscessus spp. during Chronic Infection of the Human Lung. *PLoS ONE*, 8(5):e63237, 5 2013.

[42] In Kwon Park, Amy P. Hsu, Hervé Tettelin, Shamira J. Shallom, Steven K. Drake, Li Ding, Un In Wu, Nick Adamo, D. Rebecca Prevots, Kenneth N. Olivier, Steven M. Holland, Elizabeth P. Sampaio, and Adrian M. Zelazny. Clonal Diversification and Changes in Lipid Traits and Colony Morphology in Mycobacterium abscessus Clinical Isolates. *Journal of Clinical Microbiology*, 53(11):3438, 11 2015.

[43] Wassim Daher, Louis David Leclercq, Matt D. Johansen, Claire Hamela, Jona Karam, Xavier Trivelli, Jérôme Nigou, Yann Guérardel, and Laurent Kremer. Glycopeptidolipid glycosylation controls surface properties and pathogenicity in Mycobacterium abscessus. *Cell chemical biology*, 29(5):910–924, 5 2022.

[44] Alexandre Pawlik, Guillaume Garnier, Mickael Orgeur, Pin Tong, Amanda Lohan, Fabien Le Chevalier, Guillaume Sapriel, Anne Laure Roux, Kevin Conlon, Nadine Honoré, Marie Agnès Dillies, Laurence Ma, Christiane Bouchier, Jean Yves Coppée, Jean Louis Gaillard, Stephen V. Gordon, Brendan Loftus, Roland Brosch, and Jean Louis Herrmann. Identification and characterization of the genetic changes responsible for the characteristic smooth-to-rough morphotype alterations of clinically persistent Mycobacterium abscessus. *Molecular Microbiology*, 90(3):612–629, 11 2013.

[45] Byoung Jun Kim, Bo Ram Kim, So Young Lee, Yoon Hoh Kook, and Bum Joon Kim. Rough colony morphology of Mycobacterium massiliense Type II genotype is due to the deletion of glycopeptidolipid locus within its genome. *BMC genomics*, 14(1), 12 2013.

[46] Rachid Nessar, Jean Marc Reyrat, Lisa B. Davidson, and Thomas F. Byrd. Deletion of the mmpL4b gene in the Mycobacterium abscessus glycopeptidolipid biosynthetic pathway

results in loss of surface colonization capability, but enhanced ability to replicate in human macrophages and stimulate their innate immune response. *Microbiology*, 157(4): 1187–1195, 4 2011.

[47] Audrey Bernut, Albertus Viljoen, Christian Dupont, Guillaume Sapriel, Mickaël Blaise, Christiane Bouchier, Roland Brosch, Chantal de Chastellier, Jean Louis Herrmann, and Laurent Kremer. Insights into the smooth-to-rough transitioning in Mycobacterium bolletii unravels a functional Tyr residue conserved in all mycobacterial MmpL family members. *Molecular Microbiology*, 99(5):866–883, 3 2016.

[48] Morgane Illouz, Louis David Leclercq, Clara Dessenne, Graham Hatfull, Wassim Daher, Laurent Kremer, and Yann Guérardel. Multiple Mycobacterium abscessus O-acetyltransferases influence glycopeptidolipid structure and colony morphotype. *The Journal of biological chemistry*, 299(8), 8 2023.

[49] Sheng Hui Tsai, Gwan Han Shen, Chao Hsiung Lin, Jiue Ru Liau, Hsin Chih Lai, and Shiau Ting Hu. Mab_3168c, a Putative Acetyltransferase, Enhances Adherence, Intracellular Survival and Antimicrobial Resistance of Mycobacterium abscessus. *PLoS ONE*, 8(6), 6 2013.

[50] Elizabeth R. Rhoades, Angela S. Archambault, Rebecca Greendyke, Fong-Fu Hsu, Cassandra Streeter, and Thomas F. Byrd. Mycobacterium abscessus Glycopeptidolipids Mask Underlying Cell Wall Phosphatidyl- myo -Inositol Mannosides Blocking Induction of Human Macrophage TNF-α by Preventing Interaction with TLR2. *The Journal of Immunology*, 183(3):1997–2007, 8 2009.

[51] Nishant Nandanwar, Joy E. Gibson, and Michael N. Neely. Growth medium and nitric oxide alter Mycobacterium abscessus morphotype and virulence. *Microbiological research*, 253, 12 2021.

[52] Sheng Hui Tsai, Hsin Chih Lai, and Shiau Ting Hu. Subinhibitory doses of aminoglycoside antibiotics induce changes in the phenotype of Mycobacterium abscessus. *Antimicrobial Agents and Chemotherapy*, 59(10):6161–6169, 10 2015.

[53] Kelley Hurst-Hess, Paulami Rudra, and Pallavi Ghosh. Mycobacterium abscessus WhiB7 regulates a species-specific repertoire of genes to confer extreme antibiotic resistance. *Antimicrobial Agents and Chemotherapy*, 61(11), 11 2017.

[54] Heui Dong Park, Kristi M. Guinn, Maria I. Harrell, Reiling Liao, Martin I. Voskuil, Martin Tompa, Gary K. Schoolnik, and David R. Sherman. Rv3133c/dosR is a transcription factor that mediates the hypoxic response of Mycobacterium tuberculosis. *Molecular microbiology*, 48(3):833, 5 2003.

[55] Rachel L. Leistikow, Russell A. Morton, Iona L. Bartek, Isaac Frimpong, Karleen Wagner, and Martin I. Voskuil. The Mycobacterium tuberculosis DosR Regulon Assists in Metabolic Homeostasis and Enables Rapid Recovery from Nonrespiring Dormancy. *Journal of Bacteriology*, 192(6):1662, 3 2010.

[56] Breven S. Simcox, Brooke R. Tomlinson, Lindsey N. Shaw, and Kyle H. Rohde. Mycobacterium abscessus DosRS two-component system controls a species-specific regulon required for adaptation to hypoxia. *Frontiers in cellular and infection microbiology*, 13, 2023.

[57] Ting Yu Liu, Sheng Hui Tsai, Jenn Wei Chen, Yu Ching Wang, Shiau Ting Hu, and Yih Yuan Chen. Mab_3083c Is a Homologue of RNase J and Plays a Role in Colony Morphotype,

Aggregation, and Sliding Motility of Mycobacterium abscessus. *Microorganisms*, 9(4), 2021.

[58] Renuka Kapoor and Jagjit S. Yadav. Expanding the mycobacterial diversity of metalworking fluids (MWFs): evidence showing MWF colonization by Mycobacterium abscessus. *FEMS microbiology ecology*, 79(2):392–399, 2 2012.

[59] Rebecca Greendyke and Thomas F. Byrd. Differential antibiotic susceptibility of Mycobacterium abscessus variants in biofilms and macrophages compared to that of planktonic bacteria. *Antimicrobial Agents and Chemotherapy*, 52(6):2019–2026, 6 2008.

[60] Dana Kocíncová, Nathalie Winter, Daniel Euphrasie, Mamadou Daffé, Jean Marc Reyrat, and Gilles Etienne. The cell surface-exposed glycopeptidolipids confer a selective advantage to the smooth variants of Mycobacterium smegmatis in vitro. *FEMS microbiology letters*, 290(1):39–44, 1 2009.

[61] Marion Lagune, Cecile Petit, Flor Vásquez Sotomayor, Matt D. Johansen, Kathrine S.H. Beckham, Christina Ritter, Fabienne Girard-Misguich, Matthias Wilmanns, Laurent Kremer, Florian P. Maurer, and Jean Louis Herrmann. Conserved and specialized functions of Type VII secretion systems in non-tuberculous mycobacteria. *Microbiology (Reading, England)*, 167(7), 2021.

[62] Angel Rivera-Calzada, Nikolaos Famelis, Oscar Llorca, and Sebastian Geibel. Type VII secretion systems: structure, functions and transport models. *Nature reviews. Microbiology*, 19(9):567–584, 9 2021.

[63] Fabienne Ripoll, Sophie Pasek, Chantal Schenowitz, Carole Dossat, Valérie Barbe, Martin Rottman, Edouard Macheras, Beate Heym, Jean Louis Hermann, Mamadou Daffé, Roland Brosch, Jean Loup Risler, and Jean Louis Gaillard. Non mycobacterial virulence genes in the genome of the emerging pathogen Mycobacterium abscessus. *PLoS ONE*, 4(6), 6 2009.

[64] M. Sloan Siegrist, Meera Unnikrishnan, Matthew J. McConnell, Mark Borowsky, Tan Yun Cheng, Noman Siddiqi, Sarah M. Fortune, D. Branch Moody, and Eric J. Rubin. Mycobacterial Esx-3 is required for mycobactin-mediated iron acquisition. *Proceedings of the National Academy of Sciences of the United States of America*, 106(44):18792–18797, 11 2009.

[65] Jo Ann M. Tufariello, Jessica R. Chapman, Christopher A. Kerantzas, Ka Wing Wong, Catherine Vilchèze, Christopher M. Jones, Laura E. Cole, Emir Tinaztepe, Victor Thompson, David Fenyö, Michael Niederweis, Beatrix Ueberheide, Jennifer A. Philips, and William R. Jacobs. Separable roles for Mycobacterium tuberculosis ESX-3 effectors in iron acquisition and virulence. *Proceedings of the National Academy of Sciences of the United States of America*, 113(3):E348–E357, 1 2016.

[66] Emilie Dumas, Eva Christina Boritsch, Mathias Vandenbogaert, Ricardo C.Rodríguez De La Vega, Jean Michel Thiberge, Valerie Caro, Jean Louis Gaillard, Beate Heym, Fabienne Girard-Misguich, Roland Brosch, and Guillaume Sapriel. Mycobacterial pan-genome analysis suggests important role of plasmids in the radiation of type VII secretion systems. *Genome Biology and Evolution*, 8(2):387–402, 2 2016.

[67] Mae Newton-Foot, Robin Mark Warren, Samantha Leigh Sampson, Paul David Van Helden, and Nicolaas Claudius Gey Van Pittius. The plasmid-mediated evolution of the mycobacterial ESX (Type VII) secretion systems. *BMC evolutionary biology*, 16(1), 3 2016.

[68] Laura Laencina, Violaine Dubois, Vincent Le Moigne, Albertus Viljoen, Laleh Majlessi, Justin Pritchard, Audrey Bernut, Laura Piel, Anne Laure Roux, Jean Louis Gaillard, Bérengère Lombard, Damarys Loew, Eric J. Rubin, Roland Brosch, Laurent Kremer, Jean Louis Herrmann, and Fabienne Girard-Misguich. Identification of genes required for Mycobacterium abscessus growth in vivo with a prominent role of the ESX-4 locus. *Proceedings of the National Academy of Sciences of the United States of America*, 115(5): E1002–E1011, 1 2018.

[69] Marion Lagune, Vincent Le Moigne, Matt D. Johansen, Flor Vásquez Sotomayor, Wassim Daher, Cécile Petit, Gina Cosentino, Laura Paulowski, Thomas Gutsmann, Matthias Wilmanns, Florian P. Maurer, Jean Louis Herrmann, Fabienne Girard-Misguich, and Laurent Kremer. The ESX-4 substrates, EsxU and EsxT, modulate Mycobacterium abscessus fitness. *PLoS Pathogens*, 18(8), 8 2022.

[70] Fabienne Girard-Misguich, Laura Laencina, Violaine Dubois, Vincent Le Moigne, Laurent Kremer, Laleh Maljessi, Roland Brosch, and Jean Louis Herrmann. [The most ancestral mycobacterial ESX-4 secretion system is essential for intracellular growth of Mycobacterium abscessus within environmental and human phagocytes]. *Medecine sciences : M/S*, 34(10):795–797, 10 2018.

[71] Julia Lienard, Esther Nobs, Victoria Lovins, Elin Movert, Christine Valfridsson, and Fredric Carlsson. The Mycobacterium marinum ESX-1 system mediates phagosomal permeabilization and type I interferon production via separable mechanisms. *Proceedings of the National Academy of Sciences of the United States of America*, 117(2):1160–1166, 1 2020.

[72] Alka Mehra, Aleena Zahra, Victor Thompson, Natalie Sirisaengtaksin, Ashley Wells, Maura Porto, Stefan Köster, Kristen Penberthy, Yoshihisha Kubota, Amelie Dricot, Daniel Rogan, Marc Vidal, David E. Hill, Andrew J. Bean, and Jennifer A. Philips. Mycobacterium tuberculosis type VII secreted effector EsxH targets host ESCRT to impair trafficking. *PLoS pathogens*, 9(10), 10 2013.

[73] Ekansh Mittal, Michael L. Skowyra, Grace Uwase, Emir Tinaztepe, Alka Mehra, Stefan Köster, Phyllis I. Hanson, and Jennifer A. Philips. Mycobacterium tuberculosis Type VII Secretion System Effectors Differentially Impact the ESCRT Endomembrane Damage Response. *mBio*, 9(6), 11 2018.

[74] Yi Sak Kim, Chul Su Yang, Loi T. Nguyen, Jin Kyung Kim, Hyo Sun Jin, Jin ho Choe, Soo Yeon Kim, Hye Mi Lee, Mingyu Jung, Jin Man Kim, Myung Hee Kim, Eun Kyeong Jo, and Ji Chan Jang. Mycobacterium abscessus ESX-3 plays an important role in host inflammatory and pathological responses during infection. *Microbes and Infection*, 19(1): 5–17, 1 2017.

[75] Louis S. Ates, Roy Ummels, Susanna Commandeur, Robert van der Weerd, Marion Sparrius, Eveline Weerdenburg, Marina Alber, Rainer Kalscheuer, Sander R. Piersma, Abdallah M. Abdallah, Moataz Abd El Ghany, Alyaa M. Abdel-Haleem, Arnab Pain, Connie R. Jiménez, Wilbert Bitter, and Edith N.G. Houben. Essential Role of the ESX-5 Secretion System in Outer Membrane Permeability of Pathogenic Mycobacteria. *PLoS Genetics*, 11(5):1005190, 5 2015.

[76] Li Yin Lai, Tzu Lung Lin, Yi Yin Chen, Pei Fang Hsieh, and Jin Town Wang. Role of the Mycobacterium marinum ESX-1 secretion system in sliding motility and biofilm formation. *Frontiers in Microbiology*, 9(MAY):1160, 5 2018.

[77] Yutika Nath, Suvendra Kumar Ray, and Alak Kumar Buragohain. Essential role of the ESX-3 associated eccD3 locus in maintaining the cell wall integrity of Mycobacterium smegmatis. *International journal of medical microbiology : IJMM*, 308(7):784–795, 10 2018.

[78] Shweta Parmar and Elitza I. Tocheva. The cell envelope of Mycobacterium abscessus and its role in pathogenesis. *PLOS Pathogens*, 19(5), 5 2023.

[79] Robert Koch. The Etiology of Tuberculosis. *Reviews of Infection Diseases*, 4(6), 1982.

[80] E. Löwenstein. Vorlesungen über Bakteriologie, Immunität, spezifische Diagnostik und Therapie der Tuberkulose. *Fischer*, 1920.

[81] Albert Calmette. L'infection bacillaire et la tuberculose chez l'homme et chez les animaux: processus d'infection et de défense, étude biologique et expérimentale. *Masson et Cie*, 1922.

[82] Anil K. Ojha, Anthony D. Baughn, Dhinakaran Sambandan, Tsungda Hsu, Xavier Trivelli, Yann Guerardel, Anuradha Alahari, Laurent Kremer, William R. Jacobs, and Graham F. Hatfull. Growth of Mycobacterium tuberculosis biofilms containing free mycolic acids and harbouring drug-tolerant bacteria. *Molecular Microbiology*, 69(1):164, 7 2008.

[83] René J. Dubos and Bernard D. Davis. Factors affecting the growth of tubercle bacilli in liquid media. *The Journal of Experimental Medicine*, 83(5):409, 4 1946.

[84] Cynthia Pierce, Rene J. Dubos, and Gardner Middlebrook. Infection of mice with tubercle bacilli grown in tween-albumin liquid medium. *Proceedings of the Society for Experimental Biology and Medicine. Society for Experimental Biology and Medicine (New York, N.Y.)*, 64(2):173–174, 1947.

[85] R. J. Dubos and G. Middlebrook. The effect of wetting agents on the growth of tubercle bacilli. *The Journal of experimental medicine*, 88(1):81–88, 1948.

[86] H. BLOCH and H. NOLL. Studies on the virulence of tubercle bacilli; variations in virulence effected by tween 80 and thiosemicarbazone. *The Journal of experimental medicine*, 97 (1):1–16, 1 1953.

[87] Rebecca M Van Boxtel, Randall S Lambrecht, Michael T Collins, and isoniazid E R Squibb. Effects of Colonial Morphology and Tween 80 on Antimicrobial Susceptibility of Mycobacterium paratuberculosis. Technical Report 12, 1990.

[88] Jacobs P. Richards and Anil K. Ojha. Mycobacterial Biofilms. *Microbiology Spectrum*, 2 (5), 9 2014.

[89] Luanne Hall-Stoodley and Hilary Lappin-Scott. Biofilm formation by the rapidly growing mycobacterial species Mycobacterium fortuitum. *FEMS microbiology letters*, 168(1): 77–84, 11 1998.

[90] R. Schulze-Röbbecke, B. Janning, and R. Fischeder. Occurrence of mycobacteria in biofilm samples. *Tubercle and lung disease : the official journal of the International Union against Tuberculosis and Lung Disease*, 73(3):141–144, 1992.

[91] Joseph O. Falkinham, Cheryl D. Norton, and Mark W. Lechevallier. Factors Influencing Numbers of Mycobacterium avium, Mycobacterium intracellulare, and Other Mycobacteria in Drinking Water Distribution Systems. *Applied and Environmental Microbiology*, 67(3): 1225–1231, 3 2001.

[92] Leah M Feazel, Laura K Baumgartner, Kristen L Peterson, Daniel N Frank, J Kirk Harris, and Norman R Pace. Opportunistic pathogens enriched in showerhead biofilms. Technical report, 2009.

[93] M. Dailloux, M. Albert, C. Laurain, S. Andolfatto, A. Lozniewski, P. Hartemann, and L. Mathieu. Mycobacterium xenopi and drinking water biofilms. *Applied and environmental microbiology*, 69(11):6946–6948, 11 2003.

[94] Roland Schulze-Robbecke and Katrin Buchholtz. Heat Susceptibility of Aquatic Mycobacteria. Technical Report 6, 1992.

[95] Mario J.M. Vaerewijck, Geert Huys, Juan Carlos Palomino, Jean Swings, and Françoise Portaels. Mycobacteria in drinking water distribution systems: Ecology and significance for human health, 11 2005.

[96] Keesha A. Steed and Joseph O. Falkinham. Effect of growth in biofilms on chlorine susceptibility of Mycobacterium avium and Mycobacterium intracellulare. *Applied and environmental microbiology*, 72(6):4007–4011, 6 2006.

[97] Alfred H. Stammers and Jeffrey B. Riley. The Heater Cooler as a Source of Infection from Nontuberculous Mycobacteria. *The Journal of Extra-corporeal Technology*, 48(2):55, 2016.

[98] Jasjit Singh, Kathleen O'Donnell, Delma J. Nieves, Felice C. Adler-Shohet, Antonio C. Arrieta, Negar Ashouri, Gurpreet Ahuja, Michele Cheung, W. Nathan Holmes, Kevin Huoh, Lisa Tran, M. Tuan Tran, Nguyen Pham, and Matthew Zahn. Invasive Mycobacterium abscessus Outbreak at a Pediatric Dental Clinic. *Open Forum Infectious Diseases*, 8(6), 6 2021.

[99] J. Recht and R. Kolter. Glycopeptidolipid Acetylation Affects Sliding Motility and Biofilm Formation in Mycobacterium smegmatis. *Journal of Bacteriology*, 183(19):5718, 2001.

[100] Anil Ojha, Mridula Anand, Apoorva Bhatt, Laurent Kremer, William R. Jacobs, and Graham F. Hatfull. GroEL1: A dedicated chaperone involved in mycolic acid biosynthesis during biofilm formation in mycobacteria. *Cell*, 123(5):861–873, 12 2005.

[101] Anil Ojha and Graham F. Hatfull. The role of iron in Mycobacterium smegmatis biofilm formation: the exochelin siderophore is essential in limiting iron conditions for biofilm formation but not for planktonic growth. *Molecular Microbiology*, 66(2):468, 10 2007.

[102] Dhinakaran Sambandan, Dee N. Dao, Brian C. Weinrick, Catherine Vilchèze, Sudagar S. Gurcha, Anil Ojha, Laurent Kremer, Gurdyal S. Besra, Graham F. Hatfull, and William R. Jacobs. Keto-Mycolic Acid-Dependent Pellicle Formation Confers Tolerance to Drug-Sensitive Mycobacterium tuberculosis. *mBio*, 4(3), 2013.

[103] Jennifer M. Pang, Emilie Layre, Lindsay Sweet, Ashley Sherrid, D. Branch Moody, Anil Ojha, and David R. Sherman. The Polyketide Pks1 Contributes to Biofilm Formation in Mycobacterium tuberculosis. *Journal of Bacteriology*, 194(3):715, 2 2012.

[104] Jacob P. Richards, Wenlong Cai, Nicholas A. Zill, Wenjun Zhang, and Anil K. Ojha. Adaptation of Mycobacterium tuberculosis to Biofilm Growth Is Genetically Linked to Drug Tolerance. *Antimicrobial Agents and Chemotherapy*, 63(11), 2019.

[105] Takahiro Totani, Yukiko Nishiuchi, Yoshitaka Tateishi, Yutaka Yoshida, Hiromi Kitanaka, Mamiko Niki, Yukihiro Kaneko, and Sohkichi Matsumoto. Effects of nutritional and ambient

oxygen condition on biofilm formation in Mycobacterium avium subsp. Hominissuis via altered glycolipid expression. *Scientific Reports*, 7, 2 2017.

[106] Margaret M. Williams, Mitchell A. Yakrus, Matthew J. Arduino, Robert C. Cooksey, Christina B. Crane, Shailen N. Banerjee, Elizabeth D. Hilborn, and Rodney M. Donlan. Structural Analysis of Biofilm Formation by Rapidly and Slowly Growing Nontuberculous Mycobacteria. *Applied and Environmental Microbiology*, 75(7):2091, 4 2009.

[107] Tavs Qvist, Steffen Eickhardt, Kasper N. Kragh, Claus B. Andersen, Martin Iversen, Niels Høiby, and Thomas Bjarnsholt. Chronic pulmonary disease with Mycobacterium abscessus complex is a biofilm infection, 12 2015.

[108] Erin S. Gloag, Daniel J. Wozniak, Paul Stoodley, and Luanne Hall-Stoodley. Mycobacterium abscessus biofilms have viscoelastic properties which may contribute to their recalcitrance in chronic pulmonary infections. *Scientific Reports*, 11(1):5020, 12 2021.

[109] Gillian Clary, Smitha J. Sasindran, Nathan Nesbitt, Laurel Mason, Sara Cole, Abul Azad, Karen McCoy, Larry S. Schlesinger, and Luanne Hall-Stoodley. Mycobacterium abscessus smooth and rough morphotypes form antimicrobial-tolerant biofilm phenotypes but are killed by acetic acid. *Antimicrobial Agents and Chemotherapy*, 62(3), 3 2018.

[110] Anja Dokic, Eliza Peterson, Mario L. Arrieta-Ortiz, Min Pan, Alessandro Di Maio, Nitin Baliga, and Apoorva Bhatt. Mycobacterium abscessus biofilms produce an extracellular matrix and have a distinct mycolic acid profile. *The Cell Surface*, 7:100051, 12 2021.

[111] Moirangthem Veigyabati Devi and Anil Kumar Singh. Delineation of transcriptional regulators involve in biofilm formation cycle of Mycobacterium abscessus. *Gene*, 882, 10 2023.

[112] William H Depas, Megan Bergkessel, and Dianne K Newman. Aggregation of Nontuberculous Mycobacteria Is Regulated by Carbon-Nitrogen Balance. Technical report, 2019.

[113] Juan M. Belardinelli, Wei Li, Charlotte Avanzi, Shiva K. Angala, Elena Lian, Crystal J. Wiersma, Zuzana Palčeková, Kevin H. Martin, Bhanupriya Angala, Vinicius C.N. de Moura, Callan Kerns, Victoria Jones, Mercedes Gonzalez-Juarrero, Rebecca M. Davidson, Jerry A. Nick, Bradley R. Borlee, and Mary Jackson. Unique Features of Mycobacterium abscessus Biofilms Formed in Synthetic Cystic Fibrosis Medium. *Frontiers in microbiology*, 12, 10 2021.

[114] Bailey F. Keefe and Luiz E. Bermudez. Environment in the lung of cystic fibrosis patients stimulates the expression of biofilm phenotype in Mycobacterium abscessus. *Journal of medical microbiology*, 71(1), 2022.

[115] Anne Laure Roux, Aurélie Ray, Alexandre Pawlik, Halima Medjahed, Gilles Etienne, Martin Rottman, Emilie Catherinot, Jean Yves Coppée, Karima Chaoui, Bernard Monsarrat, Antoine Toubert, Mamadou Daffé, Germain Puzo, Jean Louis Gaillard, Roland Brosch, Nicolas Dulphy, Jérôme Nigou, and Jean Louis Herrmann. Overexpression of proinflammatory TLR-2-signalling lipoproteins in hypervirulent mycobacterial variants. *Cellular Microbiology*, 13(5):692–704, 2011.

[116] Lisa B. Davidson, Rachid Nessar, Prakasha Kempaiah, Douglas J. Perkins, and Thomas F. Byrd. Mycobacterium abscessus glycopeptidolipid prevents respiratory epithelial TLR2 signaling as measured by HβD2 gene expression and IL-8 release. *PLoS ONE*, 6(12), 12 2011.

[117] Bodil Jönsson, Malin Ridell, and Agnes E. Wold. Phagocytosis and cytokine response to rough and smooth colony variants of Mycobacterium abscessus by human peripheral blood mononuclear cells. *APMIS*, 121(1):45–55, 1 2013.

[118] Hamadoun Touré, Lee Ann Galindo, Marion Lagune, Simon Glatigny, Robert M. Waterhouse, Isabelle Guénal, Jean Louis Herrmann, Fabienne Girard-Misguich, and Sébastien Szuplewski. Mycobacterium abscessus resists the innate cellular response by surviving cell lysis of infected phagocytes. *PLOS Pathogens*, 19(3), 3 2023.

[119] Violaine Dubois, Albertus Viljoen, Laura Laencina, Vincent Le Moigne, Audrey Bernut, Faustine Dubar, Mickaël Blaise, Jean Louis Gaillard, Yann Guérardel, Laurent Kremer, Jean Louis Herrmann, and Fabienne Girard-Misguich. MmpL8MAB controls Mycobacterium abscessus virulence and production of a previously unknown glycolipid family. *Proceedings of the National Academy of Sciences of the United States of America*, 115(43):E10147–E10156, 10 2018.

[120] Jake Whang, Yong Woo Back, Kang In Lee, Nagatoshi Fujiwara, Seungwha Paik, Chul Hee Choi, Jeong Kyu Park, and Hwa Jung Kim. Mycobacterium abscessus glycopeptidolipids inhibit macrophage apoptosis and bacterial spreading by targeting mitochondrial cyclophilin D. *Cell death & disease*, 8(8):e3012, 8 2017.

[121] Cecilia Brambilla, Marta Llorens-Fons, Esther Julián, Estela Noguera-Ortega, Cristina Tomàs-Martínez, Miriam Pérez-Trujillo, Thomas F. Byrd, Fernando Alcaide, and Marina Luquin. Mycobacteria Clumping Increase Their Capacity to Damage Macrophages. *Frontiers in microbiology*, 7(OCT), 10 2016.

[122] Audrey Bernut, Jean-Louis Herrmann, Karima Kissa, Jean-François Dubremetz, Jean-Louis Gaillard, Georges Lutfalla, and Laurent Kremer. Mycobacterium abscessus cording prevents phagocytosis and promotes abscess formation. *Proceedings of the National Academy of Sciences*, 111(10):E943–E952, 3 2014.

[123] Iman Halloum, Séverine Carrère-Kremer, Mickael Blaise, Albertus Viljoen, Audrey Bernut, Vincent Le Moigne, Catherine Vilchèze, Yann Guérardel, Georges Lutfalla, Jean Louis Herrmann, William R. Jacobs, and Laurent Kremer. Deletion of a dehydratase important for intracellular growth and cording renders rough Mycobacterium abscessus avirulent. *Proceedings of the National Academy of Sciences of the United States of America*, 113 (29):E4228–E4237, 7 2016.

[124] Marta Llorens-Fons, Míriam Pérez-Trujillo, Esther Julián, Cecilia Brambilla, Fernando Alcaide, Thomas F. Byrd, and Marina Luquin. Trehalose polyphleates, external cell wall lipids in Mycobacterium abscessus, are associated with the formation of clumps with cording morphology, which have been associated with virulence. *Frontiers in Microbiology*, 8(JUL), 7 2017.

[125] Volker Brinkmann, Ulrike Reichard, Christian Goosmann, Beatrix Fauler, Yvonne Uhlemann, David S. Weiss, Yvette Weinrauch, and Arturo Zychlinsky. Neutrophil extracellular traps kill bacteria. *Science (New York, N.Y.)*, 303(5663):1532–1535, 3 2004.

[126] Kenneth C. Malcolm, Silvia M. Caceres, Kerstin Pohl, Katie R. Poch, Audrey Bernut, Laurent Kremer, Donna L. Bratton, Jean Louis Herrmann, and Jerry A. Nick. Neutrophil killing of Mycobacterium abscessus by intra- and extracellular mechanisms. *PLoS ONE*, 13(4), 4 2018.

[127] Thomas F Byrd and C Rick Lyons. Preliminary Characterization of a Mycobacterium abscessus Mutant in Human and Murine Models of Infection. Technical Report 9, 1999.

[128] Jong Seok Kim, Min Jung Kang, Woo Sik Kim, Seung Jung Han, Hong Min Kim, Ho Won Kim, Kee Woong Kwon, So Jeong Kim, Seung Bin Cha, Seok Yong Eum, Won Jung Koh, Sang Nae Cho, Jong Hwan Park, and Sung Jae Shin. Essential engagement of toll-like receptor 2 in initiation of early protective Th1 response against rough variants of Mycobacterium abscessus. *Infection and Immunity*, 83(4):1556–1567, 2015.

[129] Tae Sung Kim, Yi Sak Kim, Heekyung Yoo, Young Kil Park, and Eun Kyeong Jo. Mycobacterium massiliense induces inflammatory responses in macrophages through toll-like receptor 2 and c-Jun N-terminal Kinase. *Journal of Clinical Immunology*, 34(2): 212–223, 2 2014.

[130] Anna Aulicino, Adam M. Dinan, Aleksandra A. Miranda-CasoLuengo, John A. Browne, Kévin Rue-Albrecht, David E. MacHugh, and Brendan J. Loftus. High-throughput transcriptomics reveals common and strain-specific responses of human macrophages to infection with Mycobacterium abscessus Smooth and Rough variants. *BMC Genomics*, 16(1), 12 2015.

[131] Hans D. Brightbill, Daniel H. Libraty, Stephan R. Krutzik, Ruey Bing Yang, John T. Belisle, Joshua R. Bleharski, Michael Maitland, Michael V. Norgard, Scott E. Plevy, Stephen T. Smale, Patrick J. Brennan, Barry R. Bloom, Paul J. Godowski, and Robert L. Modlin. Host defense mechanisms triggered by microbial lipoproteins through toll-like receptors. *Science (New York, N.Y.)*, 285(5428):732–736, 7 1999.

[132] Mi Sun Jin and Jie Oh Lee. Structures of the toll-like receptor family and its ligand complexes. *Immunity*, 29(2):182–191, 8 2008.

[133] Iain C. Sutcliffe and Dean J. Harrington. Lipoproteins of Mycobacterium tuberculosis: an abundant and functionally diverse class of cell envelope components. *FEMS Microbiology Reviews*, 28(5):645–659, 11 2004.

[134] Renan Marrichi Mauch, Peter Østrup Jensen, Tavs Qvist, Mette Kolpen, Claus Moser, Tacjana Pressler, Marcos Tadeu Nolasco da Silva, Niels Høiby, Daniel Faurholt-Jepsen, Marco Gelpi, Neval Ete Wareham, and Terese Katzenstein. Adaptive Immune Response to Mycobacterium abscessus Complex (MABSC) in Cystic Fibrosis and the Implications of Cross-Reactivity. *Frontiers in Cellular and Infection Microbiology*, 12, 4 2022.

[135] Penelope K. Ellis, Willam J. Martin, and Peter J. Dodd. CD4 count and tuberculosis risk in HIV-positive adults not on ART: A systematic review and meta-analysis. *PeerJ*, 2017(12), 2017.

[136] Jeana Benwill, Michael Babineaux, and Juan C. Sarria. Pulmonary Mycobacterium abscessus in an AIDS patient. *The American journal of the medical sciences*, 339(5): 495–496, 5 2010.

[137] Sarah K. Browne, Peter D. Burbelo, Ploenchan Chetchotisakd, Yupin Suputtamongkol, Sasisopin Kiertiburanakul, Pamela A. Shaw, Jennifer L. Kirk, Kamonwan Jutivorakool, Rifat Zaman, Li Ding, Amy P. Hsu, Smita Y. Patel, Kenneth N. Olivier, Viraphong Lulitanond, Piroon Mootsikapun, Siriluck Anunnatsiri, Nasikarn Angkasekwinai, Boonmee Sathapatayavongs, Po-Ren Hsueh, Chi-Chang Shieh, Margaret R. Brown, Wanna Thongnoppakhun, Reginald Claypool, Elizabeth P. Sampaio, Charin Thepthai, Duangdao Waywa, Camilla Dacombe, Yona Reizes, Adrian M. Zelazny, Paul Saleeb, Lindsey B. Rosen, Allen Mo, Michael Iadarola, and Steven M. Holland. Adult-onset immunodeficiency in Thailand and Taiwan. *The New England journal of medicine*, 367(8):725–734, 8 2012.

[138] Tavs Qvist, Tania Pressler, David Taylor-Robinson, Terese L. Katzenstein, and Niels Høiby. Serodiagnosis of Mycobacterium abscessus complex infection in cystic fibrosis. *The European respiratory journal*, 46(3):707–716, 9 2015.

[139] Chi Eun Oh, Edgar Ortiz-Brizuela, Mayara L. Bastos, and Dick Menzies. Comparing the Diagnostic Performance of QuantiFERON-TB Gold Plus to Other Tests of Latent Tuberculosis Infection: A Systematic Review and Meta-analysis. *Clinical Infectious Diseases: An Official Publication of the Infectious Diseases Society of America*, 73(5): e1116, 9 2021.

[140] Getahun Abate, Fahreta Hamzabegovic, Christopher S. Eickhoff, and Daniel F. Hoft. BCG vaccination induces M. Avium and M. Abscessus cross-protective immunity. *Frontiers in Immunology*, 10(FEB), 2019.

[141] Talita B. Aiello, Carlos E. Levy, Tânia R. Zaccariotto, Ilma A. Paschoal, Mônica C. Pereira, Marcos T.Nolasco da Silva, José D. Ribeiro, Antônio F. Ribeiro, Adyléia A.D.C. Toro, and Renan M. Mauch. Prevalence and clinical outcomes of nontuberculous mycobacteria in a Brazilian cystic fibrosis reference center. *Pathogens and disease*, 76(5), 7 2018.

[142] Karsten Hjelt, Niels Højlyng, Peter Howitz, Niels Illum, Erik Munk, Niels H. Valerius, Kurt Fursted, Karen N. Hansen, Ivar Heltberg, and Christian Koch. The role of Mycobacteria Other Than Tuberculosis (MOTT) in patients with cystic fibrosis. *Scandinavian journal of infectious diseases*, 26(5):569–576, 1994.

[143] Hazel M. Dockrell and Steven G. Smith. What Have We Learnt about BCG Vaccination in the Last 20 Years? *Frontiers in Immunology*, 8(SEP):1134, 9 2017.

[144] Sarah Prentice, Beatrice Nassanga, Emily L. Webb, Florence Akello, Fred Kiwudhu, Hellen Akurut, Alison M. Elliott, Rob J.W. Arts, Mihai G. Netea, Hazel M. Dockrell, Stephen Cose, Emily Webb, Alison Elliott, Irene Nabaweesi, Christopher Zziwa, Milly Namutebi, Benigna Namarra, Esther Nakazibwe, Susan Amongi, Grace Kamukama, Susan Iwala, Caroline Ninsiima, Josephine Tumusiime, Fred Kiwanuka, Saadn Nsubuga, Justin Akello, Sebastian Owilla, Jonathan Levin, Stephen Nash, Prossy Kabuubi Nakawungu, Elson Abayo, Grace Nabakooza, Zephyrian Kaushaaga, and Miriam Akello. BCG-induced non-specific effects on heterologous infectious disease in Ugandan neonates: an investigator-blind randomised controlled trial. *The Lancet. Infectious Diseases*, 21(7):993, 7 2021.

[145] Takehiko Kobayashi, Kazunari Tsuyuguchi, Shiomi Yoshida, Yu Kurahara, Shojiro Minomo, Yoshikazu Inoue, and Katsuhiro Suzuki. Serum immunoglobulin a antibodies to glycopeptidolipid core antigen for Mycobacteroides abscessus complex lung disease. *International Journal of Mycobacteriology*, 9(1):76–82, 1 2020.

[146] Radhey S. Gupta, Brian Lo, and Jeen Son. Phylogenomics and comparative genomic studies robustly support division of the genus Mycobacterium into an emended genus Mycobacterium and four novel genera. *Frontiers in Microbiology*, 9(FEB), 2 2018.

[147] Nathan L. Bachmann, Rauf Salamzade, Abigail L. Manson, Richard Whittington, Vitali Sintchenko, Ashlee M. Earl, and Ben J. Marais. Key Transitions in the Evolution of Rapid and Slow Growing Mycobacteria Identified by Comparative Genomics. *Frontiers in Microbiology*, 10:495775, 1 2020.

[148] Yansheng Zhang, Mitchell A. Yakrus, Edward A. Graviss, Natalie Williams-Bouyer, Christine Turenne, Amin Kabani, and Richard J. Wallace. Pulsed-field gel electrophoresis

study of Mycobacterium abscessus isolates previously affected by DNA degradation. *Journal of Clinical Microbiology*, 42(12):5582–5587, 12 2004.

[149] Silvia E. Smith, Patrice Showers-Corneli, Caitlin N. Dardenne, Henry H. Harpending, Darren P. Martin, and Robert G. Beiko. Comparative Genomic and Phylogenetic Approaches to Characterize the Role of Genetic Recombination in Mycobacterial Evolution. *PLoS ONE*, 7(11), 11 2012.

[150] Veronica Marcos, Zhe Zhou-Suckow, Ali Önder Yildirim, Alexander Bohla, Andreas Hector, Ljubomir Vitkov, Wolf Dietrich Krautgartner, Walter Stoiber, Matthias Griese, Oliver Eickelberg, Marcus A. Mall, and Dominik Hartl. Free DNA in cystic fibrosis airway fluids correlates with airflow obstruction. *Mediators of Inflammation*, 2015, 2015.

[151] Gee W. Lau, Daniel J. Hassett, Huimin Ran, and Fansheng Kong. The role of pyocyanin in Pseudomonas aeruginosa infection. *Trends in molecular medicine*, 10(12):599–606, 12 2004.

[152] Jean Claude Bakala N'Goma, Vincent Le Moigne, Nathalie Soismier, Laura Laencina, Fabien Le Chevalier, Anne Laure Roux, Isabelle Poncin, Carole Serveau-Avesque, Martin Rottman, Jean Louis Gaillard, Gilles Etienne, Roland Brosch, Jean Louis Herrmann, Stéphane Canaan, and Fabienne Girard-Misguich. Mycobacterium abscessus phospholipase C expression is induced during coculture within amoebae and enhances M. abscessus virulence in mice. *Infection and Immunity*, 83(2):780–791, 2015.

[153] Josephine M. Bryant, Karen P. Brown, Sophie Burbaud, Isobel Everall, Juan M. Belardinelli, Daniela Rodriguez-Rincon, Dorothy M. Grogono, Chelsea M. Peterson, Deepshikha Verma, Ieuan E. Evans, Christopher Ruis, Aaron Weimann, Divya Arora, Sony Malhotra, Bridget Bannerman, Charlotte Passemar, Kerra Templeton, Gordon MacGregor, Kasim Jiwa, Andrew J. Fisher, Tom L. Blundell, Diane J. Ordway, Mary Jackson, Julian Parkhill, and R. Andres Floto. Stepwise pathogenic evolution of Mycobacterium abscessus. *Science*, 372(6541), 4 2021.

[154] Linda M. Parsons, Craig S. Jankowski, and Keith M. Derbyshire. Conjugal transfer of chromosomal DNA in Mycobacterium smegmatis. *Molecular microbiology*, 28(3):571–582, 1998.

[155] Jan Madacki, Mickael Orgeur, Guillem Mas Fiol, Wafa Frigui, Laurence Ma, and Roland Brosch. ESX-1-Independent Horizontal Gene Transfer by Mycobacterium tuberculosis Complex Strains. *mBio*, 12(3), 2021.

[156] Todd A. Gray, Janet A. Krywy, Jessica Harold, Michael J. Palumbo, and Keith M. Derbyshire. Distributive Conjugal Transfer in Mycobacteria Generates Progeny with Meiotic-Like Genome-Wide Mosaicism, Allowing Mapping of a Mating Identity Locus. *PLoS Biology*, 11(7), 7 2013.

[157] Guillaume Sapriel, Julie Konjek, Mickael Orgeur, Laurent Bouri, Lise Frézal, Anne Laure Roux, Emilie Dumas, Roland Brosch, Christiane Bouchier, Sylvain Brisse, Mathias Vandenbogaert, Jean Michel Thiberge, Valérie Caro, Yun Fong Ngeow, Joon Liang Tan, Jean Louis Herrmann, Jean Louis Gaillard, Beate Heym, and Thierry Wirth. Genome-wide mosaicism within Mycobacterium abscessus: Evolutionary and epidemiological implications. *BMC Genomics*, 17(1), 2 2016.

[158] Jessica L. Flint, Joseph C. Kowalski, Pavan K. Karnati, and Keith M. Derbyshire. The RD1 virulence locus of Mycobacterium tuberculosis regulates DNA transfer in Mycobacterium

smegmatis. *Proceedings of the National Academy of Sciences of the United States of America*, 101(34):12598, 8 2004.

[159] Kiet T. Nguyen, Kristina Piastro, and Keith M. Derbyshire. LpqM, a Mycobacterial Lipoprotein-Metalloproteinase, Is Required for Conjugal DNA Transfer in Mycobacterium smegmatis. *Journal of Bacteriology*, 191(8):2721, 4 2009.

[160] Abbie Coros, Brian Callahan, Eric Battaglioli, and Keith M. Derbyshire. The specialized secretory apparatus ESX-1 is essential for DNA transfer in Mycobacterium smegmatis. *Molecular Microbiology*, 69(4):794–808, 8 2008.

[161] Kiet T. Nguyen, Kristina Piastro, Todd A. Gray, and Keith M. Derbyshire. Mycobacterial biofilms facilitate horizontal DNA transfer between strains of Mycobacterium smegmatis. *Journal of Bacteriology*, 192(19):5134–5142, 10 2010.

[162] Todd A. Gray, Ryan R. Clark, Nathalie Boucher, Pascal Lapierre, Carol Smith, and Keith M. Derbyshire. Intercellular communication and conjugation are mediated by ESX secretion systems in mycobacteria. *Science (New York, N.Y.)*, 354(6310):347, 10 2016.

[163] Josephine M. Bryant, Dorothy M. Grogono, Daniela Rodriguez-Rincon, Isobel Everall, Karen P. Brown, Pablo Moreno, Deepshikha Verma, Emily Hill, Judith Drijkoningen, Peter Gilligan, Charles R. Esther, Peadar G. Noone, Olivia Giddings, Scott C. Bell, Rachel Thomson, Claire E. Wainwright, Chris Coulter, Sushil Pandey, Michelle E. Wood, Rebecca E. Stockwell, Kay A. Ramsay, Laura J. Sherrard, Timothy J. Kidd, Nassib Jabbour, Graham R. Johnson, Luke D. Knibbs, Lidia Morawska, Peter D. Sly, Andrew Jones, Diana Bilton, Ian Laurenson, Michael Ruddy, Stephen Bourke, Ian C.J.W. Bowler, Stephen J. Chapman, Andrew Clayton, Mairi Cullen, Owen Dempsey, Miles Denton, Maya Desai, Richard J. Drew, Frank Edenborough, Jason Evans, Jonathan Folb, Thomas Daniels, Helen Humphrey, Barbara Isalska, Søren Jensen-Fangel, Bodil Jönsson, Andrew M. Jones, Terese L. Katzenstein, Troels Lillebaek, Gordon MacGregor, Sarah Mayell, Michael Millar, Deborah Modha, Edward F. Nash, Christopher O'Brien, Deirdre O'Brien, Chandra Ohri, Caroline S. Pao, Daniel Peckham, Felicity Perrin, Audrey Perry, Tania Pressler, Laura Prtak, Tavs Qvist, Ali Robb, Helen Rodgers, Kirsten Schaffer, Nadia Shafi, Jakko Van Ingen, Martin Walshaw, Danie Watson, Noreen West, Joanna Whitehouse, Charles S. Haworth, Simon R. Harris, Diane Ordway, Julian Parkhill, and R. Andres Floto. Emergence and spread of a humantransmissible multidrug-resistant nontuberculous mycobacterium. *Science*, 354(6313):751–757, 11 2016.

[164] Pamela B. Davis. Cystic fibrosis since 1938. *American journal of respiratory and critical care medicine*, 173(5):475–482, 3 2006.

[165] J. A. Dodge, P. A. Lewis, M. Stanton, and J. Wilsher. Cystic fibrosis mortality and survival in the UK: 1947-2003. *The European respiratory journal*, 29(3):522–526, 3 2007.

[166] Christopher Ruis, Josephine M. Bryant, Scott C. Bell, Rachel Thomson, Rebecca M. Davidson, Nabeeh A. Hasan, Jakko van Ingen, Michael Strong, R. Andres Floto, and Julian Parkhill. Dissemination of Mycobacterium abscessus via global transmission networks. *Nature Microbiology*, 6(10):1279, 10 2021.

[167] Nakwon Kwak, Margareth Pretti Dalcolmo, Charles L. Daley, Geoffrey Eather, Regina Gayoso, Naoki Hasegawa, Byung Woo Jhun, Won Jung Koh, Ho Namkoong, Jimyung Park, Rachel Thomson, Jakko Van Ingen, Sanne M.H. Zweijpfenning, and Jae Joon Yim. Mycobacterium abscessus pulmonary disease: individual patient data meta-analysis. *The European respiratory journal*, 54(1), 2019.

[168] Morris Moore, Pn D And, and John B Frerichs. An unusual acid-fast infection of the knee with subcutaneous, abscess-like lesions of the gluteal region. Report of a case with a study of the organism, Mycobacterium abscessus, n. sp. Technical report, 1953.

[169] Barbara A. Brown-Elliott and Richard J. Wallace. Clinical and taxonomic status of pathogenic nonpigmented or late-pigmenting rapidly growing mycobacteria, 10 2002.

[170] J. L. Stanford, S. R. Pattyn, F. Portaels, and W. J. Gunthorpe. Studies on Mycobacterium chelonei. *Journal of medical microbiology*, 5(2):177–182, 5 1972.

[171] S. Kusunoki and T. Ezaki. Proposal of Mycobacterium peregrinum sp. nov., nom. rev., and elevation of Mycobacterium chelonae subsp. abscessus (Kubica et al.) to species status: Mycobacterium abscessus comb. nov. *International Journal of Systematic Bacteriology*, 42(2):240–245, 4 1992.

[172] Edouard Macheras, Anne Laure Roux, Fabienne Ripoll, Valérie Sivadon-Tardy, Cristina Gutierrez, Jean Louis Gaillard, and Beate Heym. Inaccuracy of Single-Target Sequencing for Discriminating Species of the Mycobacterium abscessus Group. *Journal of Clinical Microbiology*, 47(8):2596–2600, 2009.

[173] Sylvia Cardoso Leao, Enrico Tortoli, Jean Paul Euzé, and Maria Jesus Garcia. Proposal that Mycobacterium massiliense and Mycobacterium bolletii be united and reclassified as Mycobacterium abscessus subsp. bolletii comb. nov., designation of Mycobacterium abscessus subsp. abscessus subsp. nov. and emended description of Mycobacterium abscessus. *International Journal of Systematic and Evolutionary Microbiology*, 61(9): 2311–2313, 9 2011.

[174] Yong Joon Cho, Hana Yi, Jongsik Chun, Sang Nae Cho, Charles L. Daley, Won Jung Koh, and Sung Jae Shin. The Genome Sequence of 'Mycobacterium massiliense' Strain CIP 108297 Suggests the Independent Taxonomic Status of the Mycobacterium abscessus Complex at the Subspecies Level. *PLOS ONE*, 8(11):e81560, 11 2013.

[175] Edouard Macheras, Julie Konjek, Anne Laure Roux, Jean Michel Thiberge, Sylvaine Bastian, Sylvia Cardoso Leão, Moises Palaci, Valérie Sivadon-Tardy, Cristina Gutierrez, Elvira Richter, Sabine Rüsch-Gerdes, Gaby E. Pfyffer, Thomas Bodmer, Vincent Jarlier, Emmanuelle Cambau, Sylvain Brisse, Valérie Caro, Nalin Rastogi, Jean Louis Gaillard, and Beate Heym. Multilocus sequence typing scheme for the Mycobacterium abscessus complex. *Research in Microbiology*, 165(2):82–90, 2 2014.

[176] Mohamed Sassi and Michel Drancourt. Genome analysis reveals three genomospecies in Mycobacterium abscessus. Technical report, 2014.

[177] Joon Liang Tan, Yun Fong Ngeow, and Siew Woh Choo. Support from phylogenomic networks and subspecies signatures for separation of Mycobacterium massiliense from Mycobacterium bolletii. *Journal of Clinical Microbiology*, 53(9):3042–3046, 9 2015.

[178] Enrico Tortoli, Thomas A. Kohl, Barbara A. Brown-Elliott, Alberto Trovato, Sylvia Cardoso Leão, Maria Jesus Garcia, Sruthi Vasireddy, Christine Y. Turenne, David E. Griffith, Julie V. Philley, Rossella Baldan, Silvia Campana, Lisa Cariani, Carla Colombo, Giovanni Taccetti, Antonio Teri, Stefan Niemann, Richard J. Wallace, and Daniela M. Cirillo. Emended description of mycobacterium abscessus mycobacterium abscessus subsp. Abscessus and mycobacterium abscessus subsp. bolletii and designation of mycobacterium abscessus subsp. massiliense comb. nov. *International Journal of Systematic and Evolutionary Microbiology*, 66(11):4471–4479, 11 2016.

[179] Jeana L. Benwill and Richard J. Wallace. Mycobacterium abscessus: Challenges in diagnosis and treatment, 2014.

[180] Virginie Rollet-Cohen, Anne Laure Roux, Muriel Le Bourgeois, Guillaume Sapriel, Manele El Bahri, Jean Philippe Jais, B. Heym, F. Mougari, Laurent Raskine, Nicolas Véziris, Jean Louis Gaillard, and Isabelle Sermet-Gaudelus. Mycobacterium bolletii Lung Disease in Cystic Fibrosis. *Chest*, 156(2):247–254, 8 2019.

[181] Alina Minias, Lidia Żukowska, Jakub Lach, Tomasz Jagielski, Dominik Strapagiel, Su Young Kim, Won Jung Koh, Heather Adam, Ruth Bittner, Sara Truden, Manca Žolnir-Dovč, and Jarosław Dziadek. Subspecies-specific sequence detection for differentiation of Mycobacterium abscessus complex. *Scientific Reports 2020 10:1*, 10 (1):1–9, 10 2020.

[182] Hee Youn Kim, Byoung Jun Kim, Yoonwon Kook, Yeo Jun Yun, Jeong Hwan Shin, Bum Joon Kim, and Yoon Hoh Kook. Mycobacterium massiliense is differentiated from Mycobacterium abscessus and Mycobacterium bolletii by erythromycin ribosome methyltransferase gene (erm) and clarithromycin susceptibility patterns. *Microbiology and immunology*, 54(6):347–353, 6 2010.

[183] Toshiyuki Harada, Yasushi Akiyama, Atsuyuki Kurashima, Hideaki Nagai, Kazunari Tsuyuguchi, Takashi Fujii, Syuichi Yano, Eriko Shigeto, Toshihiko Kuraoka, Akira Kajiki, Yoshihiro Kobashi, Fumio Kokubu, Atsuo Sato, Shiomi Yoshida, Tomotada Iwamoto, and Hajime Saito. Clinical and microbiological differences between Mycobacterium abscessus and Mycobacterium massiliense lung diseases. *Journal of clinical microbiology*, 50(11): 3556–3561, 11 2012.

[184] Won Jung Koh, Kyeongman Jeon, Nam Yong Lee, Bum Joon Kim, Yoon Hoh Kook, Seung Heon Lee, Young Kil Park, Chang Ki Kim, Sung Jae Shin, Gwen A. Huitt, Charles L. Daley, and O. Jung Kwon. Clinical significance of differentiation of Mycobacterium massiliense from Mycobacterium abscessus. *American Journal of Respiratory and Critical Care Medicine*, 183(3):405–410, 2 2011.

[185] Enrico Tortoli, Barbara A. Brown-Elliott, James D. Chalmers, Daniela M. Cirillo, Charles L. Daley, Stefan Emler, R. Andres Floto, Maria J. Garcia, Wouter Hoefsloot, Won Jung Koh, Christoph Lange, Michael Loebinger, Florian P. Maurer, Kozo Morimoto, Stefan Niemann, Elvira Richter, Christine Y. Turenne, Ravikiran Vasireddy, Sruthi Vasireddy, Dirk Wagner, Richard J. Wallace, Nancy Wengenack, and Jakko Van Ingen. Same meat, different gravy: ignore the new names of mycobacteria. *European Respiratory Journal*, 54(1), 7 2019.

[186] Conor J. Meehan, Roman A. Barco, Yong Hwee E. Loh, Sari Cogneau, and Leen Rigouts. Reconstituting the genus mycobacterium. *International Journal of Systematic and Evolutionary Microbiology*, 71(9):004922, 9 2021.

[187] Meng Rui Lee, Wang Huei Sheng, Chien Ching Hung, Chong Jen Yu, Li Na Lee, and Po Ren Hsueh. Mycobacterium abscessus complex infections in humans. *Emerging Infectious Diseases*, 21(9):1638–1646, 9 2015.

[188] R. W. Wilson, V. A. Steingrube, E. C. Böttger, B. Springer, B. A. Brown-Elliott, V. Vincent, Jr Jost, Y. Zhang, M. J. Garcia, S. H. Chiu, G. O. Onyi, H. Rossmoore, D. R. Nash, and Jr Wallace. Mycobacterium immunogenum sp. nov., a novel species related to Mycobacterium abscessus and associated with clinical disease, pseudo-outbreaks and contaminated metalworking fluids: an international cooperative study on mycobacterial

taxonomy. *International journal of systematic and evolutionary microbiology*, 51(Pt 5): 1751–1764, 2001.

[189] J. O. Falkinham. Surrounded by mycobacteria: Nontuberculous mycobacteria in the human environment, 8 2009.

[190] Jennifer R. Honda, Nabeeh A. Hasan, Rebecca M. Davidson, Myra D. Williams, L. Elaine Epperson, Paul R. Reynolds, Terry Smith, Elena Iakhiaeva, Matthew J. Bankowski, Richard J. Wallace, Edward D. Chan, Joseph O. Falkinham, and Michael Strong. Environmental Nontuberculous Mycobacteria in the Hawaiian Islands. *PLoS Neglected Tropical Diseases*, 10(10), 10 2016.

[191] Matthew J. Gebert, Manuel Delgado-Baquerizo, Angela M. Oliverio, Tara M. Webster, Lauren M. Nichols, Jennifer R. Honda, Edward D. Chan, Jennifer Adjemian, Robert R. Dunn, and Noah Fierer. Ecological analyses of mycobacteria in showerhead biofilms and their relevance to human health. *mBio*, 9(5):1–15, 2018.

[192] Richard A. Kirschner, Bruce C. Parker, and Joseph O. Falkinham. Humic and fulvic acids stimulate the growth of Mycobacterium avium. *FEMS microbiology ecology*, 30(4): 327–332, 1 1999.

[193] Robert H Taylor, Joseph O Falkinham Iii, Cheryl D Norton, and Mark W Lechevallier. Chlorine, Chloramine, Chlorine Dioxide, and Ozone Susceptibility of Mycobacterium avium. Technical Report 4, 2000.

[194] Vincent Jarlier and Hiroshi Nikaido. Mycobacterial cell wall: structure and role in natural resistance to antibiotics. *FEMS microbiology letters*, 123(1-2):11–18, 10 1994.

[195] S. N. Mullis and J. O. Falkinham. Adherence and biofilm formation of Mycobacterium avium, Mycobacterium intracellulare and Mycobacterium abscessus to household plumbing materials. *Journal of Applied Microbiology*, 115(3):908–914, 9 2013.

[196] Mary Ann De Groote, Norman R. Pace, Kayte Fulton, and Joseph O. Falkinham. Relationships between Mycobacterium isolates from patients with pulmonary mycobacterial infection and potting soils. *Applied and Environmental Microbiology*, 72(12):7602–7606, 12 2006.

[197] Joseph O. Falkinham, Michael D. Iseman, Petra de Haas, and Dick van Soolingen. Mycobacterium avium in a shower linked to pulmonary disease. *Journal of Water and Health*, 6(2):209–213, 6 2008.

[198] Rachel Thomson, Carla Tolson, Robyn Carter, Chris Coulter, Flavia Huygens, and Megan Hargreaves. Isolation of nontuberculous mycobacteria (NTM) from household water and shower aerosols in patients with pulmonary disease caused by NTM. *Journal of Clinical Microbiology*, 51(9):3006–3011, 9 2013.

[199] Joseph O. Falkinham. Nontuberculous mycobacteria from household plumbing of patients with nontuberculous mycobacteria disease. *Emerging Infectious Diseases*, 17 (3):419–424, 3 2011.

[200] Patrick J. Brennan and Hiroshi Nikaido. The envelope of mycobacteria. *Annual review of biochemistry*, 64:29–63, 1995.

[201] Maura J. Donohue, Jatin H. Mistry, Joyce M. Donohue, Katharine Oconnell, Dawn King, Jules Byran, Terry Covert, and Stacy Pfaller. Increased frequency of nontuberculous

mycobacteria detection at potable water taps within the United States. *Environmental Science and Technology*, 49(10):6127–6133, 5 2015.

[202] Corinne Le Dantec, Jean Pierre Duguet, Antoine Montiel, Nadine Dumoutier, Sylvie Dubrou, and Véronique Vincent. Chlorine disinfection of atypical mycobacteria isolated from a water distribution system. *Applied and Environmental Microbiology*, 68(3): 1025–1032, 2002.

[203] M. Pryor, S. Springthorpe, S. Riffard, T. Brooks, Y. Huo, G. Davis, and S. A. Sattar. Investigation of opportunistic pathogens in municipal drinking water under different supply and treatment regimes. *Water Science and Technology*, 50(1):83–90, 7 2004.

[204] Jaana Kusnetsov, Eila Torvinen, Outi Perola, Tapio Nousiainen, and Marja-Leena Katila. Colonization of hospital water systems by legionellae, mycobacteria and other heterotrophic bacteria potentially hazardous to risk group patients. *APMIS*, 111:546–56, 2003.

[205] Terry C Covert, Mark R Rodgers, Antolin L Reyes, and Gerard N Stelma. Occurrence of Nontuberculous Mycobacteria in Environmental Samples. Technical Report 6, 1999.

[206] M. B. Kaelin, S. P. Kuster, B. Hasse, B. Schulthess, F. Imkamp, M. Halbe, P. Sander, H. Sax, and P. W. Schreiber. Diversity of non-tuberculous mycobacteria in heater-cooler devices: results from prospective surveillance. *Journal of Hospital Infection*, 105(3):480–485, 7 2020.

[207] Gail Bolan, Arthur L Reingold, Loretta A Carson, Vella A Silcox, Charles L Woodley, Peggy S Hayes, Allen W Hightower, Louise McFarland, Joseph W Brown III, Norman J Petersen, Martin S Favero, Robert C Good, and Claire V Broome. Infections with Mycobacterium chelonei in Patients Receiving Dialysis and Using Processed Hemodialyzers. Technical report, 1985.

[208] Jennifer R. Honda, Ravleen Virdi, and Edward D. Chan. Global environmental nontuberculous mycobacteria and their contemporaneous man-made and natural niches, 8 2018.

[209] J. van Ingen, M. J. Boeree, P. N.R. Dekhuijzen, and D. van Soolingen. Environmental sources of rapid growing nontuberculous mycobacteria causing disease in humans. *Clinical Microbiology and Infection*, 15(10):888–893, 10 2009.

[210] Joseph O. Falkinham. Environmental sources of nontuberculous mycobacteria, 3 2015.

[211] F. C. Bange, B. A. Brown, C. Smaczny, Jr Wallace, and E. C. Böttger. Lack of transmission of mycobacterium abscessus among patients with cystic fibrosis attending a single clinic. *Clinical infectious diseases : an official publication of the Infectious Diseases Society of America*, 32(11):1648–1650, 6 2001.

[212] Kenneth N. Olivier, David J. Weber, Richard J. Wallace, Ali R. Faiz, Ji Hyun Lee, Yansheng Zhang, Barbara A. Brown-Elliot, Allison Handler, Rebecca W. Wilson, Michael S. Schechter, Lloyd J. Edwards, Subha Chakraborti, and Michael R. Knowles. Nontuberculous mycobacteria. I: multicenter prevalence study in cystic fibrosis. *American journal of respiratory and critical care medicine*, 167(6):828–834, 3 2003.

[213] Bodil E. Jönsson, Marita Gilljam, Anders Lindblad, Malin Ridell, Agnes E. Wold, and Christina Welinder-Qlsson. Molecular epidemiology of Mycobacterium abscessus, with focus on cystic fibrosis. *Journal of Clinical Microbiology*, 45(5):1497–1504, 5 2007.

[214] Moira L. Aitken, Ajit Limaye, Paul Pottinger, Estella Whimbey, Christopher H. Goss, Mark R. Tonelli, Gerard A. Cangelosi, M. Ashworth Dirac, Kenneth N. Olivier, Barbara A. Brown-Elliott, Steven McNulty, and Richard J. Wallace. Respiratory outbreak of Mycobacterium abscessus subspecies massiliense in a lung transplant and cystic fibrosis center. *American journal of respiratory and critical care medicine*, 185(2):231–232, 1 2012.

[215] Wei Chang Huang, Chien Shun Chiou, Jiann Hwa Chen, and Gwan Han Shen. Molecular epidemiology of Mycobacterium abscessus infections in a subtropical chronic ventilatory setting. *Journal of Medical Microbiology*, 59(10):1203–1211, 10 2010.

[216] Kathryn A. Harris, Dervla T.D. Kenna, Cornelis Blauwendraat, John C. Hartley, Jane F. Turton, Paul Aurora, and Garth L.J. Dixon. Molecular fingerprinting of Mycobacterium abscessus strains in a cohort of pediatric cystic fibrosis patients. *Journal of Clinical Microbiology*, 50(5):1758–1761, 5 2012.

[217] Josephine M. Bryant, Dorothy M. Grogono, Daniel Greaves, Juliet Foweraker, Iain Roddick, Thomas Inns, Mark Reacher, Charles S. Haworth, Martin D. Curran, Simon R. Harris, Sharon J. Peacock, Julian Parkhill, and R. Andres Floto. Whole-genome sequencing to identify transmission of Mycobacterium abscessus between patients with cystic fibrosis: A retrospective cohort study. *The Lancet*, 381(9877):1551–1560, 2013.

[218] Kathryn A. Harris and Dervla T.D. Kenna. Mycobacterium abscessus infection in cystic fibrosis: Molecular typing and clinical outcomes, 10 2014.

[219] Yansheng Zhang, Malini Rajagopalan, Barbara A Brown, † And, and Richard J Wallace. Randomly Amplified Polymorphic DNA PCR for Comparison of Mycobacterium abscessus Strains from Nosocomial Outbreaks. Technical Report 12, 1997.

[220] Kenneth C. Malcolm, Silvia M. Caceres, Jennifer R. Honda, Rebecca M. Davidson, L. Elaine Epperson, Michael Strong, Edward D. Chan, and Jerry A. Nick. Mycobacterium abscessus displays fitness for fomite transmission. *Applied and Environmental Microbiology*, 83(19), 10 2017.

[221] S. L. Wendt, K. L. George, B. C. Parker, H. Gruft, and J. O. Falkinham IIIrd. Epidemiology of infection by nontuberculous Mycobacteria. III. Isolation of potentially pathogenic mycobacteria from aerosols. *The American review of respiratory disease*, 122(2):259–263, 1980.

[222] Rebecca M. Davidson, Jeanne B. Benoit, Sara M. Kammlade, Nabeeh A. Hasan, L. Elaine Epperson, Terry Smith, Sruthi Vasireddy, Barbara A. Brown-Elliott, Jerry A. Nick, Kenneth N. Olivier, Adrian M. Zelazny, Charles L. Daley, Michael Strong, and Richard J. Wallace. Genomic characterization of sporadic isolates of the dominant clone of Mycobacterium abscessus subspecies massiliense. *Scientific Reports*, 11(1):15336, 12 2021.

[223] Izzy Everall, Christiane Lourenço Nogueira, Josephine M. Bryant, Leonor Sánchez-Busó, Erica Chimara, Rafael da Silva Duarte, Jesus Pais Ramos, Karla Valéria Batista Lima, Maria Luíza Lopes, Moises Palaci, Andre Kipnis, Fernanda Monego, R. Andres Floto, Julian Parkhill, Sylvia Cardoso Leão, and Simon R. Harris. Genomic epidemiology of a national outbreak of post-surgical Mycobacterium abscessus wound infections in Brazil. *Microbial genomics*, 3(5):e000111, 5 2017.

[224] Hervé Tettelin, Rebecca M. Davidson, Sonia Agrawal, Moira L. Aitken, Shamira Shallom, Nabeeh A. Hasan, Michael Strong, Vinicius Calado Nogueira de Moura, Mary Ann

De Groote, Rafael S. Duarte, Erin Hine, Sushma Parankush, Qi Su, Sean C. Daugherty, Claire M. Fraser, Barbara A. Brown-Elliott, Richard J. Wallace, Steven M. Holland, Elizabeth P. Sampaio, Kenneth N. Olivier, Mary Jackson, and Adrian M. Zelazny. High-level relatedness among Mycobacterium abscessus subsp. massiliense strains from widely separated outbreaks. *Emerging Infectious Diseases*, 20(3):364–371, 3 2014.

[225] Aristine Cheng, Hsin-Yun Sun, Yi-Tzu Tsai, Po-Liang Lu, Susan Shin-Jung Lee, Yi-Tzu Lee, Yung-Chih Wang, Po-Yu Liu, Jung-Yien Chien, Po-Ren Hsueh, Shu-Yuan Chang, Un-In Wu, Wang-Huei Sheng, Yee-Chun Chen, and Shan-Chwen Chang. Longitudinal non-cystic fibrosis trends of pulmonary Mycobacterium abscessus disease from 2010 to 2017: spread of the “globally successful clone” in Asia. *ERJ Open Research*, 7(1): 00191–2020, 1 2021.

[226] Jennifer Adjemian, Kenneth N. Olivier, Amy E. Seitz, Steven M. Holland, and D. Rebecca Prevots. Prevalence of nontuberculous mycobacterial lung disease in U.S. medicare beneficiaries. *American Journal of Respiratory and Critical Care Medicine*, 185(8): 881–886, 4 2012.

[227] Meng Rui Lee, Li Ta Keng, Chin Chung Shu, Shih Wei Lee, Chih Hsin Lee, Jann Yuan Wang, Li Na Lee, Chong Jen Yu, and Pan Chyr Yang. Risk factors for Mycobacterium chelonae-abscessus pulmonary disease persistence and deterioration, 2 2012.

[228] Ronan M. Doyle, Marc Rubio, Garth Dixon, John Hartley, Nigel Klein, Pere Coll, and Kathryn A. Harris. Cross-transmission is not the source of new mycobacterium abscessus infections in a multicenter cohort of cystic fibrosis patients. *Clinical Infectious Diseases*, 70(9):1855–1864, 5 2020.

[229] Sanne M.H. Zweijpfenning, Jakko Van Ingen, and Wouter Hoefsloot. Geographic Distribution of Nontuberculous Mycobacteria Isolated from Clinical Specimens: A Systematic Review. *Seminars in respiratory and critical care medicine*, 39(3):336–342, 2018.

[230] Jennifer Adjemian, Kenneth N. Olivier, Amy E. Seitz, Joseph O. Falkinham, Steven M. Holland, and D. Rebecca Prevots. Spatial clusters of nontuberculous mycobacterial lung disease in the United States. *American journal of respiratory and critical care medicine*, 186(6):553–558, 9 2012.

[231] Julia E. Marshall, Rachel A. Mercaldo, Ettie M. Lipner, and D. Rebecca Prevots. Incidence of nontuberculous mycobacteria infections among persons with cystic fibrosis in the United States (2010–2019). *BMC Infectious Diseases*, 23(1):1–5, 12 2023.

[232] Wouter Hoefsloot, Jakko Van Ingen, Claire Andrejak, Kristian Ängeby, Rosine Bauriaud, Pascale Bemer, Natalie Beylis, Martin J. Boeree, Juana Cacho, Violet Chihota, Erica Chimara, Gavin Churchyard, Raquel Cias, Rosa Daza, Charles L. Daley, P. N.Richard Dekhuijzen, Diego Domingo, Francis Drobniewski, Jaime Esteban, Maryse Fauville-Dufaux, Dorte Bek Folkvardsen, Noel Gibbons, Enrique Gómez-Mampaso, Rosa Gonzalez, Harald Hoffmann, Po Ren Hsueh, Alexander Indra, Tomasz Jagielski, Frances Jamieson, Mateja Jankovic, Eefje Jong, Joseph Keane, Wo Jung Koh, Berit Lange, Sylvia Leao, Rita Macedo, Turid Mannsåker, Theodore K. Marras, Jeannette Maugein, Heather J. Milburn, Tamas Mlinkó, Nora Morcillo, Kozo Morimoto, Dimitrios Papaventsis, Elia Palenque, Mar Paez-Peña, Claudio Piersimoni, Monika Polanová, Nalin Rastogi, Elvira Richter, Maria Jesus Ruiz-Serrano, Anabela Silva, M. Pedro Da Silva, Hulya Simsek, Dick Van Soolingen, Nora Szabó, Rachel Thomson, Teresa Tórtola Fernandez, Enrico Tortoli, Sarah E. Totten, Greg Tyrrell, Tuula Vasankari, Miguel Villar, Renata Walkiewicz,

Kevin L. Winthrop, and Dirk Wagner. The geographic diversity of nontuberculous mycobacteria isolated from pulmonary samples: an NTM-NET collaborative study. *The European respiratory journal*, 42(6):1604–1613, 12 2013.

[233] Prabha Desikan, Karuna Tiwari, Nikita Panwalkar, Saima Khaliq, Manju Chourey, Reeta Varathe, Shaina Beg Mirza, Arun Sharma, Sridhar Anand, and Manoj Pandey. Public health relevance of non-tuberculous mycobacteria among AFB positive sputa. *Germs*, 7 (1):10–18, 3 2017.

[234] Chih Cheng Lai, Che Kim Tan, Chien Hong Chou, Hsiao Leng Hsu, Chun Hsing Liao, Yu Tsung Huang, Pan Chyr Yang, Kwen Tay Luh, and Po Ren Hsueh. Increasing incidence of nontuberculous mycobacteria, Taiwan, 2000-2008. *Emerging infectious diseases*, 16(2): 294–296, 2 2010.

[235] Hung Ling Huang, Meng Hsuan Cheng, Po Liang Lu, Chin Chung Shu, Jann Yuan Wang, Jann Tay Wang, Inn Wen Chong, and Li Na Lee. Epidemiology and Predictors of NTM Pulmonary Infection in Taiwan - a Retrospective, Five-Year Multicenter Study. *Scientific reports*, 7(1), 12 2017.

[236] Ngula Monde, Musso Munyeme, Adrian Muwonge, John Bwalya Muma, and Sydney Malama. Characterization of non-tuberculous mycobacterium from humans and water in an Agropastoral area in Zambia. *BMC infectious diseases*, 18(1), 1 2018.

[237] Rachel Thomson, Ellen Donnan, and Anastasios Konstantinos. Notification of Nontuberculous Mycobacteria: An Australian Perspective. *Annals of the American Thoracic Society*, 14(3):318–323, 3 2017.

[238] Mamoudou Maiga, Sophia Siddiqui, Souleymane Diallo, Bassirou Diarra, Brehima Traoré, Yvonne R. Shea, Adrian M. Zelazny, Bindongo P.P. Dembele, Drissa Goita, Hamadoun Kassambara, Abdulrahman S. Hammond, Michael A. Polis, and Anatole Tounkara. Failure to recognize nontuberculous mycobacteria leads to misdiagnosis of chronic pulmonary tuberculosis. *PloS one*, 7(5), 5 2012.

[239] Abdolrazagh Hashemi Shahraki, Parvin Heidarieh, Saeed Zaker Bostanabad, Azar Dokht Khosravi, Mohammad Hashemzadeh, Solmaz Khandan, Maryam Biranvand, Dean E. Schraufnagel, and Mehdi Mirsaeidi. “Multidrug-resistant tuberculosis” may be nontuberculous mycobacteria. *European journal of internal medicine*, 26(4):279, 5 2015.

[240] D. Rebecca Prevots and Theodore K. Marras. Epidemiology of human pulmonary infection with nontuberculous mycobacteria a review, 3 2015.

[241] Kevin L. Winthrop, Eric Chang, Shellie Yamashita, Michael F. Iademarco, and Philip A. LoBue. Nontuberculous mycobacteria infections and anti-tumor necrosis factor-α therapy. *Emerging Infectious Diseases*, 15(10):1556–1561, 10 2009.

[242] D. Rebecca Prevots, Pamela A. Shaw, Daniel Strickland, Lisa A. Jackson, Marsha A. Raebel, Mary Ann Blosky, Ruben Montes De Oca, Yvonne R. Shea, Amy E. Seitz, Steven M. Holland, and Kenneth N. Olivier. Nontuberculous mycobacterial lung disease prevalence at four integrated health care delivery systems. *American Journal of Respiratory and Critical Care Medicine*, 182(7):970–976, 10 2010.

[243] S. K. Brode, C. L. Daley, and T. K. Marras. The epidemiologic relationship between tuberculosis and nontuberculous mycobacterial disease: A systematic review, 11 2014.

[244] Maura J. Donohue and Larry Wymer. Increasing prevalence rate of nontuberculous mycobacteria infections in five states, 2008-2013. *Annals of the American Thoracic Society*, 13(12):2143–2150, 12 2016.

[245] Hyewon Lee, Woojae Myung, Won Jung Koh, Seong Mi Moon, and Byung Woo Jhun. Epidemiology of nontuberculous mycobacterial infection, South Korea, 2007-2016. *Emerging Infectious Diseases*, 25(3):569–572, 3 2019.

[246] Seon Cheol Park, Min Jin Kang, Chang Hoon Han, Sun Min Lee, Cheong Ju Kim, Jung Mo Lee, and Young Ae Kang. Prevalence, incidence, and mortality of nontuberculous mycobacterial infection in Korea: A nationwide population-based study. *BMC Pulmonary Medicine*, 19(1), 8 2019.

[247] Kamran Khan, Jun Wang, and Theodore K. Marras. Nontuberculous mycobacterial sensitization in the United States: National trends over three decades. *American Journal of Respiratory and Critical Care Medicine*, 176(3):306–313, 1 2007.

[248] Santiago Moreno, Rosa Blázquez, Abel Novoa, Isabel Carpena, Ana Menasalvas, Cristóbal Ramírez, and Carmen Guerrero. The effect of BCG vaccination on tuberculin reactivity and the booster effect among hospital employees. *Archives of internal medicine*, 161(14):1760–1765, 2001.

[249] Petra Zimmermann, Adam Finn, and Nigel Curtis. Does BCG vaccination protect against nontuberculous mycobacterial infection? A systematic review and meta-analysis, 7 2018.

[250] Emilie Catherinot, Anne Laure Roux, Marie Anne Vibet, Gil Bellis, Sophie Ravilly, Lydie Lemonnier, Evelyne Le Roux, Claire Bernède-Bauduin, Muriel Le Bourgeois, Jean Louis Herrmann, Didier Guillemot, and Jean Louis Gaillard. Mycobacterium avium and Mycobacterium abscessus complex target distinct cystic fibrosis patient subpopulations. *Journal of cystic fibrosis : official journal of the European Cystic Fibrosis Society*, 12(1): 74–80, 1 2013.

[251] M. Wickremasinghe, L. J. Ozerovitch, G. Davies, T. Wodehouse, M. V. Chadwick, S. Abdallah, P. Shah, and R. Wilson. Non-tuberculous mycobacteria in patients with bronchiectasis. *Thorax*, 60(12):1045–1051, 12 2005.

[252] C. T. Huang, Y. J. Tsai, H. D. Wu, J. Y. Wang, C. J. Yu, L. N. Lee, and P. C. Yang. Impact of non-tuberculous mycobacteria on pulmonary function decline in chronic obstructive pulmonary disease. *The international journal of tuberculosis and lung disease : the official journal of the International Union against Tuberculosis and Lung Disease*, 16(4):539–545, 4 2012.

[253] Jacinta Bustamante, Stéphanie Boisson-Dupuis, Laurent Abel, and Jean Laurent Casanova. Mendelian susceptibility to mycobacterial disease: Genetic, immunological, and clinical features of inborn errors of IFN-γ immunity. *Seminars in Immunology*, 26(6): 454–470, 12 2014.

[254] Abderrahmane Errami, Jamila El Baghdadi, Fatima Ailal, Ibtihal Benhsaien, Kaoutar Ouazahrou, Laurent Abel, Jean Laurent Casanova, Stephanie Boisson-Dupuis, Jacinta Bustamante, and Ahmed Aziz Bousfiha. Mendelian susceptibility to mycobacterial disease: an overview. *Egyptian Journal of Medical Human Genetics 2023 24:1*, 24(1):1–12, 1 2023.

[255] Areej H. Mufti, Baldwin W. Toye, Robert R.J. Mckendry, and Jonathan B. Angel. Mycobacterium abscessus infection after use of tumor necrosis factor α inhibitor therapy:

Case report and review of infectious complications associated with tumor necrosis factor α inhibitor use. *Diagnostic Microbiology and Infectious Disease*, 53(3):233–238, 2005.

[256] Cystic Fibrosis Trust. UK Cystic Fibrosis Registry 2022 Annual Data Report. 2023.

[257] Rose C. Lopeman, James Harrison, Maya Desai, and Jonathan A.G. Cox. Mycobacterium abscessus: Environmental bacterium turned clinical nightmare. *Microorganisms*, 7(3), 3 2019.

[258] Aaron I. Gardner, Elliot McClenaghan, Gemma Saint, Paul S. McNamara, Malcolm Brodlie, and Matthew F. Thomas. Epidemiology of nontuberculous mycobacteria infection in children and young people with cystic fibrosis: Analysis of UK cystic fibrosis registry. *Clinical Infectious Diseases*, 68(5):731–737, 2 2019.

[259] Cecilie Ravnholt, Mette Kolpen, Marianne Skov, Claus Moser, Terese L. Katzenstein, Tania Pressler, Niels Høiby, and Tavs Qvist. The importance of early diagnosis of Mycobacterium abscessus complex in patients with cystic fibrosis. *APMIS*, 126(12):885–891, 12 2018.

[260] H. F. Schiff, S. Jones, A. Achaiah, A. Pereira, G. Stait, and B. Green. Clinical relevance of non-tuberculous mycobacteria isolated from respiratory specimens: seven year experience in a UK hospital. *Scientific Reports*, 9(1), 12 2019.

[261] Gabriel Thabut, Jason D. Christie, Hervé Mal, Michel Fournier, Olivier Brugière, Guy Leseche, Yves Castier, and Dimitris Rizopoulos. Survival benefit of lung transplant for cystic fibrosis since lung allocation score implementation. *American Journal of Respiratory and Critical Care Medicine*, 187(12):1335–1340, 6 2013.

[262] Jason D. Christie, Leah B. Edwards, Anna Y. Kucheryavaya, Christian Benden, Fabienne Dobbels, Richard Kirk, Axel O. Rahmel, Josef Stehlik, and Marshall I. Hertz. The Registry of the International Society for Heart and Lung Transplantation: Twenty-eighth Adult Lung and Heart-Lung Transplant Report—2011. *The Journal of Heart and Lung Transplantation*, 30(10):1104–1122, 10 2011.

[263] M. N. Samano, P. M. Pêgo-Fernandes, A. K. Fonseca Ribeiro, K. Turaça, L. G. Abdalla, L. M. Fernandes, A. T. Correia, and F. B. Jatene. Lung Transplantation in Patients With Cystic Fibrosis. *Transplantation Proceedings*, 45(3):1137–1141, 4 2013.

[264] Marita Gilljam, Henrik Scherstén, Martin Silverborn, Bodil Jönsson, and Annika Ericsson Hollsing. Lung transplantation in patients with cystic fibrosis and Mycobacterium abscessus infection. *Journal of cystic fibrosis : official journal of the European Cystic Fibrosis Society*, 9(4):272–276, 7 2010.

[265] Leonard J. Lobo, Lydia C. Chang, Charles R. Esther, Peter H. Gilligan, Zeynep Tulu, and Peadar G. Noone. Lung transplant outcomes in cystic fibrosis patients with pre-operative Mycobacterium abscessus respiratory infections. *Clinical Transplantation*, 27(4):523–529, 7 2013.

[266] Rebekah M. Dedrick, Carlos A. Guerrero-Bustamante, Rebecca A. Garlena, Daniel A. Russell, Katrina Ford, Kathryn Harris, Kimberly C. Gilmour, James Soothill, Deborah Jacobs-Sera, Robert T. Schooley, Graham F. Hatfull, and Helen Spencer. Engineered bacteriophages for treatment of a patient with a disseminated drug-resistant Mycobacterium abscessus. *Nature Medicine*, 25(5):730–733, 5 2019.

[267] Jerry A. Nick, Rebekah M. Dedrick, Alice L. Gray, Eszter K. Vladar, Bailey E. Smith, Krista G. Freeman, Kenneth C. Malcolm, L. Elaine Epperson, Nabeeh A. Hasan,

Jo Hendrix, Kimberly Callahan, Kendra Walton, Brian Vestal, Emily Wheeler, Noel M. Rysavy, Katie Poch, Silvia Caceres, Valerie K. Lovell, Katherine B. Hisert, Vinicius Calado de Moura, Delphi Chatterjee, Prithwiraj De, Natalia Weakly, Stacey L. Martiniano, David A. Lynch, Charles L. Daley, Michael Strong, Fan Jia, Graham F. Hatfull, and Rebecca M. Davidson. Case Study: Host and Pathogen Response to Bacteriophage Engineered Against Mycobacterium abscessus Lung Infection. *Cell*, 185(11):1860, 5 2022.

[268] Satish Chandrashekaran, Patricio Escalante, and Cassie C. Kennedy. Mycobacterium abscessus disease in lung transplant recipients: Diagnosis and management. *Journal of Clinical Tuberculosis and Other Mycobacterial Diseases*, 9:10, 12 2017.

[269] Clemence Martin, Camille Legeai, Lucile Regard, Christelle Cantrelle, Richard Dorent, Nicolas Carlier, François Kerbaul, and Pierre Regis Burgel. Major Decrease in Lung Transplantation for Patients with Cystic Fibrosis in France. *American Journal of Respiratory and Critical Care Medicine*, 205(5):585–587, 3 2022.

[270] Yuansu Jiang, Xia Lei, and Weiping Lu. Outbreak of Cosmetology-Acquired Mycobacterium abscessus Skin Infection. *JAMA Dermatology*, 159(7):780–781, 7 2023.

[271] Alison J. Beech, Sharon E. Weinberg, Alice E. Mortimer, Fiona Lynch, James Bedford, and Giorgio Calisti. Mycobacterium abscessus skin and soft tissue infection following autologous fat grafting in Kurdistan treated with an antibiotic combination including Imipenem-Relebactam and Rifabutin. *Journal of clinical tuberculosis and other mycobacterial diseases*, 32, 8 2023.

[272] X. Garcia-Navarro, M. A. Barnadas, J. Dalmau, P. Coll, M. Gurguí, and A. Alomar. Mycobacterium abscessus infection secondary to mesotherapy, 9 2008.

[273] Antònia Galmés-Truyols, Jaume Giménez-Duran, Catalina Bosch-Isabel, Antonio Nicolau-Riutort, Joana Vanrell-Berga, Margarita Portell-Arbona, Bartolomé Seguí-Prat, Mercedes Gumá-Torá, Isabel Martí-Alomar, María Ángeles Rojo-Arias, and Mikel Ruiz-Veramendi. An outbreak of cutaneous infection due to Mycobacterium abscessus associated to mesotherapy. *Enfermedades infecciosas y microbiologia clinica*, 29(7): 510–514, 8 2011.

[274] Rou yu Fang and Qiu ning Sun. Mycobacterium abscessus infections following injection of botulinum toxin. *Journal of Cosmetic Dermatology*, 19(4):817–819, 4 2020.

[275] Congying Li, Chen Shen, and Wei Zhang. Infectious Granuloma With Mycobacterium abscessus After Facial Injection of Botulinum Toxin: A Case Report. *The Journal of craniofacial surgery*, 10 2023.

[276] Hwa Jung Ryu, Woo Joo Kim, Chil Hwan Oh, and Hae J. Song. Iatrogenic Mycobacterium abscessus infection associated with acupuncture: clinical manifestations and its treatment. *International journal of dermatology*, 44(10):846–850, 10 2005.

[277] Patrick Tang, Scott Walsh, Christian Murray, Cecilia Alterman, Monali Varia, George Broukhanski, Pamela Chedore, Joel DeKoven, Dalal Assaad, Wayne L. Gold, Danny Ghazarian, Michael Finkelstein, Marjolyn Pritchard, Barbara Yaffe, Frances Jamieson, Bonnie Henry, and Elizabeth Phillips. Outbreak of acupuncture-associated cutaneous Mycobacterium abscessus infections. *Journal of cutaneous medicine and surgery*, 10(4): 166–169, 7 2006.

[278] Chadi Bechara, Edouard MacHeras, Beate Heym, Adele Pages, and Nicole Auffret. Mycobacterium abscessus skin infection after tattooing: first case report and review of the literature. *Dermatology (Basel, Switzerland)*, 221(1):1–4, 8 2010.

[279] Pétra Pereira de Sousa, Rossilene Conceição da Silva Cruz, Antonio Pedro Mendes Schettini, and Danielle Cristine Westphal. Mycobacterium abscessus skin infection after tattooing - Case report. *Anais Brasileiros de Dermatologia*, 90(5):741–743, 2015.

[280] Kazue Nakanaga, Yoshihiko Hoshino, Yuko Era, Kentaro Matsumoto, Yuji Kanazawa, Atsuko Tomita, Masanari Furuta, Motohisa Washizu, Masahiko Makino, and Norihisa Ishii. Multiple cases of cutaneous Mycobacterium massiliense infection in a ”hot spa” in Japan. *Journal of clinical microbiology*, 49(2):613–617, 2 2011.

[281] Miguel Costa-Silva, Artur César, Nuno Preto Gomes, and Filomena Azevedo. Mycobacterium abscessus infection in a SPA worker. *Acta Dermatovenerologica Alpina, Pannonica et Adriatica*, 27(3):159–160, 2018.

[282] Jiwon Lyu, Bum Joon Kim, Byeong Joon Kim, Jin Woo Song, Chang Min Choi, Yeon Mok Oh, Sang Do Lee, Woo Sung Kim, Dong Soon Kim, and Tae Sun Shim. A shorter treatment duration may be sufficient for patients with Mycobacterium massiliense lung disease than with Mycobacterium abscessus lung disease. *Respiratory Medicine*, 108(11):1706–1712, 11 2014.

[283] Anne Laure Roux, Emilie Catherinot, Nathalie Soismier, Beate Heym, Gil Bellis, Lydie Lemonnier, Raphaël Chiron, Brigitte Fauroux, Muriel Le Bourgeois, Anne Munck, Isabelle Pin, Isabelle Sermet, Cristina Gutierrez, Nicolas Véziris, Vincent Jarlier, Emmanuelle Cambau, Jean Louis Herrmann, Didier Guillemot, and Jean Louis Gaillard. Comparing Mycobacterium massiliense and Mycobacterium abscessus lung infections in cystic fibrosis patients. *Journal of Cystic Fibrosis*, 14(1):63–69, 1 2015.

[284] Jimyung Park, Jaeyoung Cho, Chang Hoon Lee, Sung Koo Han, and Jae Joon Yim. Progression and Treatment Outcomes of Lung Disease Caused by Mycobacterium abscessus and Mycobacterium massiliense. *Clinical Infectious Diseases*, 64(3):301–308, 2 2017.

[285] David E. Griffith and Charles L. Daley. Treatment of Mycobacterium abscessus Pulmonary Disease. *Chest*, 161(1):64–75, 1 2022.

[286] Saima Aslam, Elizabeth Lampley, Darcy Wooten, Maile Karris, Constance Benson, Steffanie Strathdee, and Robert T. Schooley. Lessons Learned From the First 10 Consecutive Cases of Intravenous Bacteriophage Therapy to Treat Multidrug-Resistant Bacterial Infections at a Single Center in the United States. *Open Forum Infectious Diseases*, 7(9), 9 2020.

[287] Joaquim Trias and Roland Benz. Permeability of the cell wall of Mycobacterium smegmatis. *Molecular microbiology*, 14(2):283–290, 1994.

[288] V. Jarlier and H. Nikaido. Permeability barrier to hydrophilic solutes in Mycobacterium chelonei. *Journal of bacteriology*, 172(3):1418–1423, 1990.

[289] Matthias Richard, Ana Victoria Gutiérrez, Albertus Viljoen, Daniela Rodriguez-Rincon, Françoise Roquet-Baneres, Mickael Blaise, Isobel Everall, Julian Parkhill, R. Andres Floto, and Laurent Kremer. Mutations in the MAB_2299c TetR regulator confer cross-resistance to Clofazimine and Bedaquiline in Mycobacterium abscessus. *Antimicrobial Agents and Chemotherapy*, 63(1), 1 2019.

[290] Ana Victoria Gutiérrez, Matthias Richard, Françoise Roquet-Banères, Albertus Viljoen, and Laurent Kremer. The TetR Family Transcription Factor MAB_2299c Regulates the Expression of Two Distinct MmpS-MmpL Efflux Pumps Involved in Cross-Resistance to Clofazimine and Bedaquiline in Mycobacterium abscessus. Technical report, 2019.

[291] Anna Rominski, Anna Roditscheff, Petra Selchow, Erik C. Böttger, and Peter Sander. Intrinsic rifamycin resistance of Mycobacterium abscessus is mediated by ADP-ribosyltransferase MAB_0591. *The Journal of antimicrobial chemotherapy*, 72(2): 376–384, 2 2017.

[292] Saiko Obata, Zofia Zwolska, Emiko Toyota, Koichiro Kudo, Akio Nakamura, Tetsuo Sawai, Tadatoshi Kuratsuji, and Teruo Kirikae. Association of rpoB mutations with rifampicin resistance in Mycobacterium avium. *International journal of antimicrobial agents*, 27(1): 32–39, 1 2006.

[293] Daria Soroka, Vincent Dubée, Olivia Soulier-Escrihuela, Guillaume Cuinet, Jean Emmanuel Hugonnet, Laurent Gutmann, Jean Luc Mainardi, and Michel Arthur. Characterization of broad-spectrum Mycobacterium abscessus class A β-lactamase. *The Journal of antimicrobial chemotherapy*, 69(3):691–696, 3 2014.

[294] Vincent Dubée, Audrey Bernut, Mélanie Cortes, Tiffany Lesne, Delphine Dorchene, Anne Laure Lefebvre, Jean Emmanuel Hugonnet, Laurent Gutmann, Jean Luc Mainardi, Jean Louis Herrmann, Jean Louis Gaillard, Laurent Kremer, and Michel Arthur. β-Lactamase inhibition by avibactam in Mycobacterium abscessus. *The Journal of antimicrobial chemotherapy*, 70(4):1051–1058, 9 2015.

[295] Anne Laure Lefebvre, Vincent Le Moigne, Audrey Bernut, Carole Veckerlé, Fabrice Compain, Jean Louis Herrmann, Laurent Kremer, Michel Arthur, and Jean Luc Mainardi. Inhibition of the β-Lactamase BlaMab by Avibactam Improves the In Vitro and In Vivo Efficacy of Imipenem against Mycobacterium abscessus. *Antimicrobial agents and chemotherapy*, 61(4), 4 2017.

[296] Anna Rominski, Petra Selchow, Katja Becker, Juliane K. Brülle, Michael Dal Molin, and Peter Sander. Elucidation of Mycobacterium abscessus aminoglycoside and capreomycin resistance by targeted deletion of three putative resistance genes. *The Journal of antimicrobial chemotherapy*, 72(8):2191–2200, 8 2017.

[297] Michael Dal Molin, Myriam Gut, Anna Rominski, Klara Haldimann, Katja Becker, and Peter Sander. Molecular Mechanisms of Intrinsic Streptomycin Resistance in Mycobacterium abscessus. *Antimicrobial agents and chemotherapy*, 62(1), 1 2017.

[298] Violaine Dubois, Alexandre Pawlik, Anouchka Bories, Vincent Le Moigne, Odile Sismeiro, Rachel Legendre, Hugo Varet, María del Pilar Rodríguez-Ordóñez, Jean-Louis Gaillard, Jean-Yves Coppée, Roland Brosch, Jean-Louis Herrmann, and Fabienne Girard-Misguich. Mycobacterium abscessus virulence traits unraveled by transcriptomic profiling in amoeba and macrophages. *PLoS Pathogens*, 15(11):e1008069, 11 2019.

[299] Kien Lam Ung, Husam M.A.B. Alsarraf, Vincent Olieric, Laurent Kremer, and Mickaël Blaise. Crystal structure of the aminoglycosides N-acetyltransferase Eis2 from Mycobacterium abscessus. *The FEBS journal*, 286(21):4342–4355, 11 2019.

[300] Aron Gagliardi, Petra Selchow, Sakshi Luthra, Daniel Schäfle, Bettina Schulthess, and Peter Sander. KatG as counterselection marker for nontuberculous mycobacteria. *Antimicrobial Agents and Chemotherapy*, 64(5), 5 2020.

[301] Kevin A. Nash, A. Barbara Brown-Elliott, and Richard J. Wallace. A Novel gene, erm(41), confers inducible macrolide resistance to clinical isolates of mycobacterium abscessus but is absent from mycobacterium chelonae. *Antimicrobial Agents and Chemotherapy*, 53(4): 1367–1376, 4 2009.

[302] Matthias Richard, Ana Victoria Gutiérrez, and Laurent Kremer. Dissecting erm(41)-Mediated Macrolide-Inducible Resistance in Mycobacterium abscessus. *Antimicrobial Agents and Chemotherapy*, 64(2), 1 2020.

[303] Santiago Ramón-García, Carol Ng, Pernille R. Jensen, Manisha Dosanjh, Jan Burian, Rowan P. Morris, Marc Folcher, Lindsay D. Eltis, Stephan Grzesiek, Liem Nguyen, and Charles J. Thompson. WhiB7, an Fe-S-dependent Transcription Factor That Activates Species-specific Repertoires of Drug Resistance Determinants in Actinobacteria. *The Journal of Biological Chemistry*, 288(48):34514, 11 2013.

[304] Mark Pryjma, Ján Burian, Kevin Kuchinski, and Charles J. Thompson. Antagonism between front-line antibiotics clarithromycin and amikacin in the treatment of Mycobacterium abscessus infections is mediated by the whiB7 gene. *Antimicrobial Agents and Chemotherapy*, 61(11), 11 2017.

[305] Hien Fuh Ng and Yun Fong Ngeow. Genetic Determinants of Tigecycline Resistance in Mycobacteroides abscessus. *Antibiotics (Basel, Switzerland)*, 11(5), 5 2022.

[306] Dinah Binte Aziz, Mei Lin Go, and Thomas Dick. Rifabutin Suppresses Inducible Clarithromycin Resistance in Mycobacterium abscessus by Blocking Induction of whiB7 and erm41. *Antibiotics*, 9(2), 2 2020.

[307] Therdsak Prammananan, Peter Sander, Barbara A. Brown, Klaus Frischkorn, Grace O. Onyi, Yansheng Zhang, Erik C. Böttger, and Richard J. Wallace. A single 16S ribosomal RNA substitution is responsible for resistance to amikacin and other 2-deoxystreptamine aminoglycosides in Mycobacterium abscessus and Mycobacterium chelonae. *The Journal of infectious diseases*, 177(6):1573–1581, 1998.

[308] Sylvaine Bastian, Nicolas Veziris, Anne Laure Roux, Florence Brossier, Jean Louis Gaillard, Vincent Jarlier, and Emmanuelle Cambau. Assessment of clarithromycin susceptibility in strains belonging to the Mycobacterium abscessus group by erm(41) and rrl sequencing. *Antimicrobial Agents and Chemotherapy*, 55(2):775–781, 2 2011.

[309] Florian P. Maurer, Vera Rüegger, Claudia Ritter, Guido V. Bloemberg, and Erik C. Böttger. Acquisition of clarithromycin resistance mutations in the 23S rRNA gene of Mycobacterium abscessus in the presence of inducible erm(41). *The Journal of antimicrobial chemotherapy*, 67(11):2606–2611, 11 2012.

[310] Richard J. Wallace, Albrecht Meier, Barbara A. Brown, Yansheng Zhang, Peter Sander, Grace O. Onyi, and Erik C. Böttger. Genetic basis for clarithromycin resistance among isolates of Mycobacterium chelonae and Mycobacterium abscessus. *Antimicrobial Agents and Chemotherapy*, 40(7):1676, 1996.

[311] Marc Rubio, Francesca March, Montserrat Garrigó, Carmen Moreno, Montserrat Español, and Pere Coll. Inducible and Acquired Clarithromycin Resistance in the Mycobacterium abscessus Complex. *PLoS ONE*, 10(10), 10 2015.

[312] Susan Realegeno, Ruel Mirasol, Omai B. Garner, and Shangxin Yang. Clinical Whole Genome Sequencing for Clarithromycin and Amikacin Resistance Prediction

and Subspecies Identification of Mycobacterium abscessus. *The Journal of Molecular Diagnostics*, 23(11):1460–1467, 11 2021.

[313] Bo Ram Kim, Byoung Jun Kim, Yoon Hoh Kook, and Bum Joon Kim. Phagosome escape of rough Mycobacterium abscessus strains in murine macrophage via phagosomal rupture can lead to type I interferon production and their cell-to-cell spread. *Frontiers in Immunology*, 10(JAN), 2019.

[314] E. Mendoza-Coronel and M. Castañón-Arreola. Comparative evaluation of in vitro human macrophage models for mycobacterial infection study. *Pathogens and Disease*, 74(6), 8 2016.

[315] J. S. Passmore, P. T. Lukey, and S. R. Ress. The human macrophage cell line U937 as an in vitro model for selective evaluation of mycobacterial antigen-specific cytotoxic T-cell function. *Immunology*, 102(2):146–156, 2001.

[316] Abhilasha Madhvi, Hridesh Mishra, G. R. Leisching, P. Z. Mahlobo, and B. Baker. Comparison of human monocyte derived macrophages and THP1-like macrophages as in vitro models for M. tuberculosis infection. *Comparative Immunology, Microbiology and Infectious Diseases*, 67, 12 2019.

[317] Philemon Ubanako, Ntombikayise Xelwa, and Monde Ntwasa. LPS induces inflammatory chemokines via TLR-4 signalling and enhances the Warburg Effect in THP-1 cells. *PLoS ONE*, 14(9), 9 2019.

[318] Nanthapon Ruangkiattikul, D. Rys, Ketema Abdissa, Manfred Rohde, Torsten Semmler, P. K. Tegtmeyer, Ulrich Kalinke, Carsten Schwarz, Astrid Lewin, and R. Goethe. Type I interferon induced by TLR2-TLR4-MyD88-TRIF-IRF3 controls Mycobacterium abscessus subsp. abscessus persistence in murine macrophages via nitric oxide. *International Journal of Medical Microbiology*, 309(5):307–318, 7 2019.

[319] Seishiro Hirano, Quan Zhou, Akiko Furuyama, and Sanae Kanno. Differential Regulation of IL-1β and IL-6 Release in Murine Macrophages. *Inflammation*, 40(6):1933–1943, 12 2017.

[320] Irène B. Caire-Brändli, Alexia Papadopoulos, Wladimir Malaga, David Marais, Stéphane Canaan, Lutz Thilo, and Chantal De Chastelliera. Reversible Lipid Accumulation and Associated Division Arrest of Mycobacterium avium in Lipoprotein-Induced Foamy Macrophages May Resemble Key Events during Latency and Reactivation of Tuberculosis. *Infection and Immunity*, 82(2):476, 2 2014.

[321] Pierre Santucci, Feriel Bouzid, Nabil Smichi, Isabelle Poncin, Laurent Kremer, Chantal De Chastellier, Michel Drancourt, and Stéphane Canaan. Experimental Models of Foamy Macrophages and Approaches for Dissecting the Mechanisms of Lipid Accumulation and Consumption during Dormancy and Reactivation of Tuberculosis. *Frontiers in Cellular and Infection Microbiology*, 6(OCT):122, 10 2016.

[322] Pascale Peyron, Julien Vaubourgeix, Yannick Poquet, Florence Levillain, Catherine Botanch, Fabienne Bardou, Mamadou Daffé, Jean François Emile, Bruno Marchou, Pere Joan Cardona, Chantal De Chastellier, and Frédéric Altare. Foamy Macrophages from Tuberculous Patients' Granulomas Constitute a Nutrient-Rich Reservoir for M. tuberculosis Persistence. *PLoS Pathogens*, 4(11):1000204, 2008.

[323] Albertus Viljoen, Mickael Blaise, Chantal de Chastellier, and Laurent Kremer. MAB_3551c encodes the primary triacylglycerol synthase involved in lipid accumulation in Mycobacterium abscessus. *Molecular Microbiology*, 102(4):611–627, 11 2016.

[324] Adrian Richter, Tirosh Shapira, and Yossef Av-Gay. THP-1 and Dictyostelium Infection Models for Screening and Characterization of Anti-Mycobacterium abscessus Hit Compounds. *Antimicrobial Agents and Chemotherapy*, 64(1), 2020.

[325] Joas L. da Silva, Jan Nguyen, Kevin P. Fennelly, Adrian M. Zelazny, and Kenneth N. Olivier. Survival of pathogenic Mycobacterium abscessus subsp. massiliense in Acanthamoeba castellanii. *Research in Microbiology*, 169(1):56–60, 1 2018.

[326] Vincent Le Moigne, Claudine Belon, Céline Goulard, Geoffrey Accard, Audrey Bernut, Bruno Pitard, Jean Louis Gaillard, Laurent Kremer, Jean Louis Herrmann, and Anne Béatrice Blanc-Potard. MgtC as a host-induced factor and vaccine candidate against Mycobacterium abscessus infection. *Infection and Immunity*, 84(10):2895–2903, 2016.

[327] Andrés Obregón-Henao, Kimberly A. Arnett, Marcela Henao-Tamayo, Lisa Massoudi, Elizabeth Creissen, Koen Andries, Anne J. Lenaerts, and Diane J. Ordway. Susceptibility of mycobacterium abscessus to antimycobacterial drugs in preclinical models. *Antimicrobial Agents and Chemotherapy*, 59(11):6904–6912, 11 2015.

[328] D. Ordway, M. Henao-Tamayo, E. Smith, C. Shanley, M. Harton, J. Troudt, X. Bai, R. J. Basaraba, I. M. Orme, and E. D. Chan. Animal model of Mycobacterium abscessus lung infection. *Journal of Leukocyte Biology*, 83(6):1502–1511, 3 2008.

[329] Martin Rottman, Emilie Catherinot, Patrick Hochedez, Jean François Emile, Jean Laurent Casanova, Jean Louis Gaillard, and Claire Soudais. Importance of T cells, gamma interferon, and tumor necrosis factor in immune control of the rapid grower Mycobacterium abscessus in C57BL/6 mice. *Infection and Immunity*, 75(12):5898–5907, 12 2007.

[330] Lindsay J. Caverly, Silvia M. Caceres, Cori Fratelli, Carrie Happoldt, Kelley M. Kidwell, Kenneth C. Malcolm, Jerry A. Nick, and David P. Nichols. Mycobacterium abscessus morphotype comparison in a murine model. *PLoS ONE*, 10(2), 2 2015.

[331] Vincent Le Moigne, Clément Raynaud, Flavie Moreau, Christian Dupont, Jérôme Nigou, Olivier Neyrolles, Laurent Kremer, and Jean Louis Herrmann. Efficacy of Bedaquiline, alone or in combination with imipenem, against Mycobacterium abscessus in C3HeB/FeJ mice. *Antimicrobial Agents and Chemotherapy*, 64(6), 6 2020.

[332] Camilla Riva, Enrico Tortoli, Federica Cugnata, Francesca Sanvito, Antonio Esposito, Marco Rossi, Anna Colarieti, Tamara Canu, Cristina Cigana, Alessandra Bragonzi, Nicola Ivan Loré, Paolo Miotto, and Daniela Maria Cirillo. A New Model of Chronic Mycobacterium abscessus Lung Infection in Immunocompetent Mice. *International Journal of Molecular Sciences*, 21(18):1–12, 9 2020.

[333] Audrey Bernut, Mai Nguyen-Chi, Iman Halloum, Jean Louis Herrmann, Georges Lutfalla, and Laurent Kremer. Mycobacterium abscessus-Induced Granuloma Formation Is Strictly Dependent on TNF Signaling and Neutrophil Trafficking. *PLoS Pathogens*, 12(11), 11 2016.

[334] J. Muse Davis, Hilary Clay, Jessica L. Lewis, Nafisa Ghori, Philippe Herbomel, and Lalita Ramakrishnan. Real-time visualization of mycobacterium-macrophage interactions leading to initiation of granuloma formation in zebrafish embryos. *Immunity*, 17(6): 693–702, 12 2002.

[335] M. D. Adams, S. E. Celniker, R. A. Holt, C. A. Evans, J. D. Gocayne, P. G. Amanatides, S. E. Scherer, P. W. Li, R. A. Hoskins, R. F. Galle, R. A. George, S. E. Lewis, S. Richards, M. Ashburner, S. N. Henderson, G. G. Sutton, J. R. Wortman, M. D. Yandell, Q. Zhang, L. X. Chen, R. C. Brandon, Y. H.C. Rogers, R. G. Blazej, M. Champe, B. D. Pfeiffer, K. H. Wan, C. Doyle, E. G. Baxter, G. Helt, C. R. Nelson, G. L. Gabor Miklos, J. F. Abril, A. Agbayani, H. J. An, C. Andrews-Pfannkoch, D. Baldwin, R. M. Ballew, A. Basu, J. Baxendale, L. Bayraktaroglu, E. M. Beasley, K. Y. Beeson, P. V. Benos, B. P. Berman, D. Bhandari, S. Bolshakov, D. Borkova, M. R. Botchan, J. Bouck, P. Brokstein, P. Brottier, K. C. Burtis, D. A. Busam, H. Butler, E. Cadieu, A. Center, I. Chandra, J. Michael Cherry, S. Cawley, C. Dahlke, L. B. Davenport, P. Davies, B. de Pablos, A. Delcher, Z. Deng, A. Deslattes Mays, I. Dew, S. M. Dietz, K. Dodson, L. E. Doup, M. Downes, S. Dugan-Rocha, B. C. Dunkov, P. Dunn, K. J. Durbin, C. C. Evangelista, C. Ferraz, S. Ferriera, W. Fleischmann, C. Fosler, A. E. Gabrielian, N. S. Garg, W. M. Gelbart, K. Glasser, A. Glodek, F. Gong, J. Harley Gorrell, Z. Gu, P. Guan, M. Harris, N. L. Harris, D. Harvey, T. J. Heiman, J. R. Hernandez, J. Houck, D. Hostin, K. A. Houston, T. J. Howland, M. H. Wei, C. Ibegwam, M. Jalali, F. Kalush, G. H. Karpen, Z. Ke, J. A. Kennison, K. A. Ketchum, B. E. Kimmel, C. D. Kodira, C. Kraft, S. Kravitz, D. Kulp, Z. Lai, P. Lasko, Y. Lei, A. A. Levitsky, J. Li, Z. Li, Y. Liang, X. Lin, X. Liu, B. Mattei, T. C. McIntosh, M. P. McLeod, D. McPherson, G. Merkulov, N. V. Milshina, C. Mobarry, J. Morris, A. Moshrefi, S. M. Mount, M. Moy, B. Murphy, L. Murphy, D. M. Muzny, D. L. Nelson, D. R. Nelson, K. A. Nelson, K. Nixon, D. R. Nusskern, J. M. Pacleb, M. Palazzolo, G. S. Pittman, S. Pan, J. Pollard, V. Puri, M. G. Reese, K. Reinert, K. Remington, R. D.C. Saunders, F. Scheeler, H. Shen, B. Christopher Shue, I. Siden-Kiamos, M. Simpson, M. P. Skupski, T. Smith, E. Spier, A. C. Spradling, M. Stapleton, R. Strong, E. Sun, R. Svirskas, C. Tector, R. Turner, E. Venter, A. H. Wang, X. Wang, Z. Y. Wang, D. A. Wassarman, G. M. Weinstock, J. Weissenbach, S. M. Williams, T. Woodage, K. C. Worley, D. Wu, S. Yang, Q. Alison Yao, J. Ye, R. F. Yeh, J. S. Zaveri, M. Zhan, G. Zhang, Q. Zhao, L. Zheng, X. H. Zheng, F. N. Zhong, W. Zhong, X. Zhou, S. Zhu, X. Zhu, H. O. Smith, R. A. Gibbs, E. W. Myers, G. M. Rubin, and J. Craig Venter. The genome sequence of Drosophila melanogaster. *Science (New York, N.Y.)*, 287(5461):2185–2195, 3 2000.

[336] Lawrence T. Reiter, Lorraine Potocki, Sam Chien, Michael Gribskov, and Ethan Bier. A Systematic Analysis of Human Disease-Associated Gene Sequences In Drosophila melanogaster. *Genome Research*, 11(6):1114, 2001.

[337] Sirlei Daffre, Per Kylsten, Christos Samakovlis, and Dan Hultmark. The lysozyme locus in Drosophila melanogaster: an expanded gene family adapted for expression in the digestive tract. *Molecular & general genetics : MGG*, 242(2):152–162, 1 1994.

[338] D. Hultmark. Insect lysozymes. *EXS*, 75:87–102, 1996.

[339] Bruno Lemaitre and Jules Hoffmann. The Host Defense of Drosophila melanogaster. *https://doi.org/10.1146/annurev.immunol.25.022106.141615*, 25:697–743, 3 2007.

[340] Tatsushi Muta and Sadaaki Iwanaga. The role of hemolymph coagulation in innate immunity. *Current opinion in immunology*, 8(1):41–47, 1996.

[341] Kenneth Söderhäll and Lage Cerenius. Role of the prophenoloxidase-activating system in invertebrate immunity. *Current opinion in immunology*, 10(1):23–28, 1998.

[342] U. Theopold, D. Li, M. Fabbri, C. Scherfer, and O. Schmidt. The coagulation of insect hemolymph. *Cellular and molecular life sciences : CMLS*, 59(2):363–372, 2002.

[343] Lage Cerenius and Kenneth Söderhäll. The prophenoloxidase-activating system in invertebrates. *Immunological Reviews*, 198(1):116–126, 4 2004.

[344] Mark Austin Hanson and Bruno Lemaitre. New insights on Drosophila antimicrobial peptide function in host defense and beyond. *Current opinion in immunology*, 62:22–30, 2 2020.

[345] Mark Austin Hanson, Anna Dostálová, Camilla Ceroni, Mickael Poidevin, Shu Kondo, and Bruno Lemaitre. Synergy and remarkable specificity of antimicrobial peptides in vivo using a systematic knockout approach. *eLife*, 8, 2 2019.

[346] Dominique Ferrandon, Jean Luc Imler, Charles Hetru, and Jules A. Hoffmann. The Drosophila systemic immune response: sensing and signalling during bacterial and fungal infections. *Nature reviews. Immunology*, 7(11):862–874, 11 2007.

[347] Estela L. Arrese and Jose L. Soulages. Insect fat body: energy, metabolism, and regulation. *Annual review of entomology*, 55:207–225, 1 2010.

[348] Alexa W. Clemmons, Scott A. Lindsay, and Steven A. Wasserman. An Effector Peptide Family Required for Drosophila Toll-Mediated Immunity. *PLOS Pathogens*, 11 (4):e1004876, 4 2015.

[349] Scott A. Lindsay, Samuel J.H. Lin, and Steven A. Wasserman. Short-Form Bomanins Mediate Humoral Immunity in Drosophila. *Journal of Innate Immunity*, 10(4):306, 9 2018.

[350] Jules A. Hoffmann and Jean Marc Reichhart. Drosophila innate immunity: an evolutionary perspective. *Nature immunology*, 3(2):121–126, 2002.

[351] Phoebe Tzou, Ennio De Gregorio, and Bruno Lemaitre. How Drosophila combats microbial infection: A model to study innate immunity and host-pathogen interactions. *Current Opinion in Microbiology*, 5(1):102–110, 2002.

[352] Bruno Lemaitre, Jean Marc Reichhart, and Jules A. Hoffmann. Drosophila host defense: differential induction of antimicrobial peptide genes after infection by various classes of microorganisms. *Proceedings of the National Academy of Sciences of the United States of America*, 94(26):14614–14619, 12 1997.

[353] Nicolas Buchon, Neal Silverman, and Sara Cherry. Immunity in Drosophila melanogaster-from microbial recognition to whole-organism physiology, 12 2014.

[354] Peter Mellroth, Jenny Karlsson, Janet Håkansson, Niklas Schultz, William E. Goldman, and Håkan Steiner. Ligand-induced dimerization of Drosophila peptidoglycan recognition proteins in vitro. *Proceedings of the National Academy of Sciences of the United States of America*, 102(18):6455, 5 2005.

[355] Filipa Vaz, Ilias Kounatidis, Gonçalo Covas, Richard M. Parton, Maria Harkiolaki, Ilan Davis, Sergio Raposo Filipe, and Petros Ligoxygakis. Accessibility to Peptidoglycan Is Important for the Recognition of Gram-Positive Bacteria in Drosophila. *Cell Reports*, 27 (8):2480, 5 2019.

[356] François Leulier, Claudine Parquet, Sebastien Pili-Floury, Ji Hwan Ryu, Martine Caroff, Won Jae Lee, Dominique Mengin-Lecreulx, and Bruno Lemaitre. The Drosophila immune system detects bacteria through specific peptidoglycan recognition. *Nature immunology*, 4(5):478–484, 5 2003.

[357] Yang Yu, Ji Won Park, Hyun Mi Kwon, Hyun Ok Hwang, In Hwan Jang, Akiko Masuda, Kenji Kurokawa, Hiroshi Nakayama, Won Jae Lee, Naoshi Dohmae, Jinghai Zhang, and

Bok Luel Lee. Diversity of Innate Immune Recognition Mechanism for Bacterial Polymeric meso-Diaminopimelic Acid-type Peptidoglycan in Insects. *The Journal of Biological Chemistry*, 285(43):32937, 10 2010.

[358] Tatiana Michel, Jean Marc Relchhart, Jules A. Hoffmann, and Julien Royet. Drosophila Toll is activated by Gram-positive bacteria through a circulating peptidoglycan recognition protein. *Nature*, 414(6865):756–759, 12 2001.

[359] Vanessa Gobert, Marie Gottar, Alexey A. Matskevich, Sophie Rutschmann, Julien Royet, Marcia Belvin, Jules A. Hoffmann, and Dominique Ferrandon. Dual Activation of the Drosophila Toll Pathway by Two Pattern Recognition Receptors. *Science*, 302(5653): 2126–2130, 12 2003.

[360] Sebastien Pili-Floury, François Leulier, Kuniaki Takahashi, Kaoru Saigo, Emmanuel Samain, Ryu Ueda, and Bruno Lemaitre. In vivo RNA interference analysis reveals an unexpected role for GNBP1 in the defense against Gram-positive bacterial infection in Drosophila adults. *The Journal of biological chemistry*, 279(13):12848–12853, 3 2004.

[361] Marie Gottar, Vanessa Gobert, Alexey A. Matskevich, Jean Marc Reichhart, Chengshu Wang, Tariq M. Butt, Marcia Belvin, Jules A. Hoffmann, and Dominique Ferrandon. Dual Detection of Fungal Infections in Drosophila via Recognition of Glucans and Sensing of Virulence Factors. *Cell*, 127(7):1425–1437, 12 2006.

[362] Lihui Wang, Alexander N.R. Weber, Magda L. Atilano, Sergio R. Filipe, Nicholas J. Gay, and Petros Ligoxygakis. Sensing of Gram-positive bacteria in Drosophila: GNBP1 is needed to process and present peptidoglycan to PGRP-SA. *The EMBO journal*, 25(20): 5005–5014, 10 2006.

[363] Nicolas Buchon, Mickael Poidevin, Hyun Mi Kwon, Auré Lien Guillou, Valentin Sottas, Bok Luel Lee, and Bruno Lemaitrea. A single modular serine protease integrates signals from pattern-recognition receptors upstream of the Drosophila Toll pathway. *Proceedings of the National Academy of Sciences of the United States of America*, 106 (30):12442–12447, 7 2009.

[364] Vincent Bischoff, Cécile Vignal, Ivo G. Boneca, Tatiana Michel, Jules A. Hoffmann, and Julien Royet. Function of the drosophila pattern-recognition receptor PGRP-SD in the detection of Gram-positive bacteria. *Nature immunology*, 5(11):1175–1180, 11 2004.

[365] Philippe Leone, Vincent Bischoff, Christine Kellenberger, Charles Hetru, Julien Royet, and Alain Roussel. Crystal structure of Drosophila PGRP-SD suggests binding to DAP-type but not lysine-type peptidoglycan. *Molecular immunology*, 45(9):2521–2530, 5 2008.

[366] Alexey A. Matskevich, Jessica Quintin, and Dominique Ferrandon. The Drosophila PRR GNBP3 assembles effector complexes involved in antifungal defenses independently of its Toll pathway activation function. *European journal of immunology*, 40(5):1244, 5 2010.

[367] Zakaria Kambris, Sylvain Brun, In Hwan Jang, Hyuck Jin Nam, Yves Romeo, Kuniaki Takahashi, Won Jae Lee, Ryu Ueda, and Bruno Lemaitre. Drosophila Immunity: A Large-Scale In Vivo RNAi Screen Identifies Five Serine Proteases Required for Toll Activation. *Current Biology*, 16(8):808–813, 4 2006.

[368] Jan Paul Dudzic, Mark Austin Hanson, Igor Iatsenko, Shu Kondo, and Bruno Lemaitre. More Than Black or White: Melanization and Toll Share Regulatory Serine Proteases in Drosophila. *Cell Reports*, 27(4):1050–1061, 4 2019.

[369] Laure El Chamy, Vincent Leclerc, Isabelle Caldelari, and Jean Marc Reichhart. Danger signal and PAMP sensing define binary signaling pathways upstream of Toll. *Nature immunology*, 9(10):1165, 2008.

[370] Najwa Issa, Nina Guillaumot, Emilie Lauret, Nicolas Matt, Christine Schaeffer-Reiss, Alain Van Dorsselaer, Jean Marc Reichhart, and Florian Veillard. The Circulating Protease Persephone Is an Immune Sensor for Microbial Proteolytic Activities Upstream of the Drosophila Toll Pathway. *Molecular Cell*, 69(4):539, 2 2018.

[371] In Hwan Jang, Naoyuki Chosa, Sung Hee Kim, Hyuck Jin Nam, Bruno Lemaitre, Masanori Ochiai, Zakaria Kambris, Sylvain Brun, Carl Hashimoto, Masaaki Ashida, Paul T. Brey, and Won Jae Lee. A Spätzle-processing enzyme required for toll signaling activation in Drosophila innate immunity. *Developmental cell*, 10(1):45–55, 1 2006.

[372] Alexander N.R. Weber, Servane Tauszig-Delamasure, Jules A. Hoffmann, Eric Lelièvre, Hugues Gascan, Keith P. Ray, Mary A. Morse, Jean Luc Imler, and Nicholas J. Gay. Binding of the Drosophila cytokine Spätzle to Toll is direct and establishes signaling. *Nature Immunology 2003 4:8*, 4(8):794–800, 7 2003.

[373] Monique Gangloff, Ayaluru Murali, Jin Xiong, Christopher J. Arnot, Alexander N. Weber, Alan M. Sandercock, Carol V. Robinson, Robert Sarisky, Andreas Holzenburg, Cheng Kao, and Nicholas J. Gay. Structural Insight into the Mechanism of Activation of the Toll Receptor by the Dimeric Ligand Spätzle. *Journal of Biological Chemistry*, 283(21):14629–14635, 5 2008.

[374] Tiffany Horng and Ruslan Medzhitov. Drosophila MyD88 is an adapter in the Toll signaling pathway. *Proceedings of the National Academy of Sciences of the United States of America*, 98(22):12654–12658, 10 2001.

[375] Servane Tauszig-Delamasure, Hana Bilak, Maria Capovilla, Jules A. Hoffmann, and Jean Luc Imler. Drosophila MyD88 is required for the response to fungal and Gram-positive bacterial infections. *Nature Immunology*, 3(1):91–97, 12 2001.

[376] Bruno Lemaitre, Emmanuelle Nicolas, Lydia Michaut, Jean Marc Reichhart, and Jules A. Hoffmann. The dorsoventral regulatory gene cassette spatzle/Toll/Cactus controls the potent antifungal response in Drosophila adults. *Cell*, 86(6):973–983, 9 1996.

[377] Par Towb, Rene L. Galindo, and Steven A. Wasserman. Recruitment of Tube and Pelle to signaling sites at the surface of the Drosophila embryo. *Development*, 125(13):2443–2450, 7 1998.

[378] Huaiyu Sun, Benjamin N. Bristow, Guowei Qu, and Steven A. Wasserman. A heterotrimeric death domain complex in Toll signaling. *Proceedings of the National Academy of Sciences of the United States of America*, 99(20):12871–12876, 10 2002.

[379] Martin C. Moncrieffe, J. Günter Grossmann, and Nicholas J. Gay. Assembly of Oligomeric Death Domain Complexes during Toll Receptor Signaling. *Journal of Biological Chemistry*, 283(48):33447–33454, 11 2008.

[380] Jessica Daigneault, Liv Klemetsaune, and Steven A. Wasserman. The IRAK homolog Pelle is the functional counterpart of IκB kinase in the Drosophila Toll pathway. *PloS one*, 8(9), 9 2013.

[381] Y. Tony Ip, Michael Reach, Ylva Engstrom, Latha Kadalayil, Haini Cai, Sergio González-Crespo, Kazuaki Tatei, and Michael Levine. Dif, a dorsal-related gene that mediates an immune response in Drosophila. *Cell*, 75(4):753–763, 11 1993.

[382] Pascal Manfruelli, Jean Marc Reichhart, Ruth Steward, Jules A. Hoffmann, and Bruno Lemaitre. A mosaic analysis in Drosophila fat body cells of the control of antimicrobial peptide genes by the Rel proteins Dorsal and DIF. *The EMBO journal*, 18(12):3380–3391, 6 1999.

[383] Olivier Binggeli, Claudine Neyen, Mickael Poidevin, and Bruno Lemaitre. Prophenoloxidase Activation Is Required for Survival to Microbial Infections in Drosophila. *PLOS Pathogens*, 10(5):e1004067, 2014.

[384] Jan P. Dudzic, Shu Kondo, Ryu Ueda, Casey M. Bergman, and Bruno Lemaitre. Drosophila innate immunity: regional and functional specialization of prophenoloxidases. *BMC Biology*, 13(1), 10 2015.

[385] Viktor Honti, Gábor Csordás, Éva Kurucz, Róbert Márkus, and István Andó. The cell-mediated immunity of Drosophila melanogaster: Hemocyte lineages, immune compartments, microanatomy and regulation. *Developmental & Comparative Immunology*, 42(1):47–56, 1 2014.

[386] Won Park Ji, Byung Rok Je, Shunfu Piao, Seiichi Inamura, Yukari Fujimoto, Koichi Fukase, Shoichi Kusumoto, Kenneth Söderhäll, Nam Chul Ha, and Bok Luel Lee. A synthetic peptidoglycan fragment as a competitive inhibitor of the melanization cascade. *The Journal of biological chemistry*, 281(12):7747–7755, 3 2006.

[387] Jennifer Volz, Hans Michael Müller, Agnieszka Zdanowicz, Fotis C. Kafatos, and Mike A. Osta. A genetic module regulates the melanization response of Anopheles to Plasmodium. *Cellular microbiology*, 8(9):1392–1405, 9 2006.

[388] Hongnan Kan, Chan Hee Kim, Hyun Mi Kwon, Ji Won Park, Kyung Baeg Roh, Hanna Lee, Bum Joon Park, Rong Zhang, Jinghai Zhang, Kenneth Söderhäll, Nam Chul Ha, and Bok Luel Lee. Molecular control of phenoloxidase-induced melanin synthesis in an insect. *The Journal of biological chemistry*, 283(37):25316–25323, 9 2008.

[389] Petros Ligoxygakis, Nadège Pelte, Chuanyi Ji, Vincent Leclerc, Bernard Duvic, Marcia Belvin, Haobo Jiang, Jules A. Hoffmann, and Jean Marc Reichhart. A serpin mutant links Toll activation to melanization in the host defence of Drosophila. *The EMBO Journal*, 21 (23):6330, 12 2002.

[390] Casimiro Castillejo-López and Udo Häcker. The serine protease Sp7 is expressed in blood cells and regulates the melanization reaction in Drosophila. *Biochemical and Biophysical Research Communications*, 338(2):1075–1082, 12 2005.

[391] Huaping Tang, Zakaria Kambris, Bruno Lemaitre, and Carl Hashimoto. Two proteases defining a melanization cascade in the immune system of Drosophila. *The Journal of biological chemistry*, 281(38):28097–28104, 9 2006.

[392] Hyuck Jin Nam, In Hwan Jang, Hyejin You, Kyung Ah Lee, and Won Jae Lee. Genetic evidence of a redox-dependent systemic wound response via Hayan protease-phenoloxidase system in Drosophila. *The EMBO journal*, 31(5):1253–1265, 3 2012.

[393] Thomas Werner, Karin Borge-Renberg, Peter Mellroth, Håkan Steiner, and Dan Hultmark. Functional diversity of the Drosophila PGRP-LC gene cluster in the response to lipopolysaccharide and peptidoglycan. *Journal of Biological Chemistry*, 278(29): 26319–26322, 7 2003.

[394] Takashi Kaneko, William E. Goldman, Peter Mellroth, Håkan Steiner, Koichi Fukase, Shoichi Kusumoto, William Harley, Alvin Fox, Douglas Golenbock, and Neal Silverman. Monomeric and polymeric gram-negative peptidoglycan but not purified LPS stimulate the Drosophila IMD pathway. *Immunity*, 20(5):637–649, 5 2004.

[395] Carolyn R. Stenbak, Ji-Hwan Ryu, François Leulier, Sebastien Pili-Floury, Claudine Parquet, Mireille Hervé, Catherine Chaput, Ivo G. Boneca, Won-Jae Lee, Bruno Lemaitre, and Dominique Mengin-Lecreulx. Peptidoglycan molecular requirements allowing detection by the Drosophila immune deficiency pathway. *Journal of immunology (Baltimore, Md. : 1950)*, 173(12):7339–7348, 12 2004.

[396] François Leulier, Antony Rodriguez, Ranjiv S. Khush, John M. Abrams, and Bruno Lemaitre. The Drosophila caspase Dredd is required to resist Gram-negative bacterial infection. *EMBO Reports*, 1(4):353, 10 2000.

[397] Marie Gottar, Vanessa Gobert, Tatiana Michel, Marcla Belvin, Geoffrey Duyk, Jules A. Hoffmann, Dominique Ferrandon, and Jullen Royet. The Drosophila immune response against Gram-negative bacteria is mediated by a peptidoglycan recognition protein. *Nature*, 416(6881):640–644, 4 2002.

[398] Kwang Min Choe, Thomas Werner, Svenja Stöven, Dan Hultmark, and Kathryn V. Anderson. Requirement for a peptidoglycan recognition protein (PGRP) in Relish activation and antibacterial immune responses in Drosophila. *Science (New York, N.Y.)*, 296(5566): 359–362, 4 2002.

[399] Aya Takehana, Tomonori Katsuyama, Tamaki Yano, Yoshiteru Oshima, Haruhiko Takada, Toshiro Aigaki, and Shoichiro Kurata. Overexpression of a pattern-recognition receptor, peptidoglycan-recognition protein-LE, activates imd/relish-mediated antibacterial defense and the prophenoloxidase cascade in Drosophila larvae. *Proceedings of the National Academy of Sciences of the United States of America*, 99(21):13705, 10 2002.

[400] Aya Takehana, Tamaki Yano, Shizuka Mita, Atsushi Kotani, Yoshiteru Oshima, and Shoichiro Kurata. Peptidoglycan recognition protein (PGRP)-LE and PGRP-LC act synergistically in Drosophila immunity. *The EMBO Journal*, 23(23):4690, 11 2004.

[401] Kwang Min Choe, Hyangkyu Lee, and Kathryn V. Anderson. Drosophila peptidoglycan recognition protein LC (PGRP-LC) acts as a signal-transducing innate immune receptor. *Proceedings of the National Academy of Sciences of the United States of America*, 102 (4):1122–1126, 1 2005.

[402] Takashi Kaneko, Tamaki Yano, Kamna Aggarwal, Jae Hong Lim, Kazunori Ueda, Yoshiteru Oshima, Camilla Peach, Deniz Erturk-Hasdemir, William E. Goldman, Byung Ha Oh, Shoichiro Kurata, and Neal Silverman. PGRP-LC and PGRP-LE have essential yet distinct functions in the drosophila immune response to monomeric DAP-type peptidoglycan. *Nature immunology*, 7(7):715–723, 7 2006.

[403] Marina Martin, Aoi Hiroyasu, R. Marena Guzman, Steven A. Roberts, and Alan G. Goodman. Analysis of Drosophila STING Reveals an Evolutionarily Conserved Antimicrobial Function. *Cell reports*, 23(12):3537, 6 2018.

[404] François Leulier, Sheila Vidal, Kaoru Saigo, Ryu Ueda, and Bruno Lemaitre. Inducible expression of double-stranded RNA reveals a role for dFADD in the regulation of the antibacterial response in Drosophila adults. *Current Biology*, 12(12):996–1000, 6 2002.

[405] Silvia Naitza, Carine Rossé, Christine Kappler, Philippe Georgel, Marcia Belvin, David Gubb, Jacques Camonis, Jules A. Hoffmann, and Jean Marc Reichhart. The Drosophila Immune Defense against Gram-Negative Infection Requires the Death Protein dFADD. *Immunity*, 17(5):575–581, 11 2002.

[406] Shimin Hu and Xiaolu Yang. dFADD, a novel death domain-containing adapter protein for the Drosophila caspase DREDD. *The Journal of biological chemistry*, 275(40): 30761–30764, 10 2000.

[407] Svenja Stöven, Istvan Ando, Latha Kadalayil, Ylva Engström, and Dan Hultmark. Activation of the Drosophila NF-κB factor Relish by rapid endoproteolytic cleavage. *EMBO Reports*, 1(4):347, 10 2000.

[408] Svenja Stöven, Neal Silverman, Anna Junell, Marika Hedengren-Olcott, Deniz Erturk, Ylva Engström, Tom Maniatis, and Dan Hultmark. Caspase-mediated processing of the drosophila NF-κB factor relish. *Proceedings of the National Academy of Sciences of the United States of America*, 100(10):5991–5996, 5 2003.

[409] Sheila Vidai, Ranjiv S. Khush, François Leulier, Phoebe Tzou, Makoto Nakamura, and Bruno Lemaitre. Mutations in the Drosophila dTAK1 gene reveal a conserved function for MAPKKKs in the control of rel/NF-κB-dependent innate immune responses. *Genes & Development*, 15(15):1900, 8 2001.

[410] Neal Silverman, Rui Zhou, Rachel L. Erlich, Mike Hunter, Erik Bernstein, David Schneider, and Tom Maniatis. Immune activation of NF-kappaB and JNK requires Drosophila TAK1. *The Journal of biological chemistry*, 278(49):48928–48934, 2003.

[411] Anni Kleino, Susanna Valanne, Johanna Ulvila, Jenni Kallio, Henna Myllymäki, Heidi Enwald, Svenja Stöven, Mickael Poidevin, Ryu Ueda, Dan Hultmark, Bruno Lemaitre, and Mika Rämet. Inhibitor of apoptosis 2 and TAK1-binding protein are components of the Drosophila Imd pathway. *The EMBO Journal*, 24(19):3423, 10 2005.

[412] Viola Gesellchen, David Kuttenkeuler, Michael Steckel, Nadège Pelte, and Michael Boutros. An RNA interference screen identifies Inhibitor of Apoptosis Protein 2 as a regulator of innate immune signalling in Drosophila. *EMBO Reports*, 6(10):979, 10 2005.

[413] Nicholas Paquette, Meike Broemer, Kamna Aggarwal, Li Chen, Marie Husson, Deniz Ertürk-Hasdemir, Jean Marc Reichhart, Pascal Meier, and Neal Silverman. Caspase-mediated cleavage, IAP binding, and ubiquitination: linking three mechanisms crucial for Drosophila NF-kappaB signaling. *Molecular cell*, 37(2):172–182, 1 2010.

[414] Chen Wang, Li Deng, Mei Hong, Giridhar R. Akkaraju, Jun Ichiro Inoue, and Zhijian J. Chen. TAK1 is a ubiquitin-dependent kinase of MKK and IKK. *Nature 2001 412:6844*, 412 (6844):346–351, 7 2001.

[415] Sophie Rutschmann, Alain C. Jung, Rui Zhou, Neal Silverman, Jules A. Hoffmann, and Dominique Ferrandon. Role of Drosophila IKKγ in a Toll-independent antibacterial immune response. *Nature Immunology 2000 1:4*, 1(4):342–347, 2000.

[416] Neal Silverman, Rui Zhou, Svenja Stöven, Niranjan Pandey, Dan Hultmark, and Tom Maniatis. A Drosophila IκB kinase complex required for Relish cleavage and antibacterial immunity. *Genes & Development*, 14(19):2461, 10 2000.

[417] Yiran Lu, Louisa P. Wu, and Kathryn V. Anderson. The antibacterial arm of the Drosophila innate immune response requires an IκB kinase. *Genes & Development*, 15(1):104, 1 2001.

[418] Tatsushi Igaki, Hiroshi Kanda, Yuki Yamamoto-Goto, Hirotaka Kanuka, Erina Kuranaga, Toshiro Aigaki, and Masayuki Miura. Eiger, a TNF superfamily ligand that triggers the Drosophila JNK pathway. *The EMBO Journal*, 21(12):3009, 6 2002.

[419] Eduardo Moreno, Minhong Yan, and Konrad Basler. Evolution of TNF signaling mechanisms: JNK-dependent apoptosis triggered by Eiger, the Drosophila homolog of the TNF superfamily. *Current biology : CB*, 12(14):1263–1268, 7 2002.

[420] Saila Kauppila, Walid S.A. Maaty, Po Chen, Raghuvir S. Tomar, Michael T. Eby, Joe Chapo, Sukit Chew, Nisha Rathore, Sunny Zachariah, Suwan K. Sinha, John M. Abrams, and Preet M. Chaudhary. Eiger and its receptor, Wengen, comprise a TNF-like system in Drosophila. *Oncogene 2003 22:31*, 22(31):4860–4867, 7 2003.

[421] Neha Agrawal, Renald Delanoue, Alessandra Mauri, Davide Basco, Matthieu Pasco, Bernard Thorens, and Pierre Léopold. The Drosophila TNF Eiger Is an Adipokine that Acts on Insulin-Producing Cells to Mediate Nutrient Response. *Cell Metabolism*, 23(4): 675–684, 4 2016.

[422] Hiroshi Kanda, Tatsushi Igaki, Hirotaka Kanuka, Takeshi Yagi, and Masayuki Miura. Wengen, a member of the Drosophila tumor necrosis factor receptor superfamily, is required for eiger signaling. *Journal of Biological Chemistry*, 277(32):28372–28375, 8 2002.

[423] Ditte S. Andersen, Julien Colombani, Valentina Palmerini, Krittalak Chakrabandhu, Emilie Boone, Michael Röthlisberger, Janine Toggweiler, Konrad Basler, Marina Mapelli, Anne Odile Hueber, and Pierre Léopold. The Drosophila TNF receptor Grindelwald couples loss of cell polarity and neoplastic growth. *Nature*, 522(7557):482–486, 6 2015.

[424] Valentina Palmerini, Silvia Monzani, Quentin Laurichesse, Rihab Loudhaief, Sara Mari, Valentina Cecatiello, Vincent Olieric, Sebastiano Pasqualato, Julien Colombani, Ditte S. Andersen, and Marina Mapelli. Drosophila TNFRs Grindelwald and Wengen bind Eiger with different affinities and promote distinct cellular functions. *Nature Communications*, 12 (1), 12 2021.

[425] Guang-Ho Cha, Kyoung Sang Cho, Jun Hee Lee, Myungjin Kim, Euysoo Kim, Jeehye Park, Sung Bae Lee, and Jongkyeong Chung. Discrete Functions of TRAF1 and TRAF2 in Drosophila melanogaster Mediated by c-Jun N-Terminal Kinase and NF-κB-Dependent Signaling Pathways. *Molecular and Cellular Biology*, 23(22):7982, 11 2003.

[426] Peter Geuking, Rajesh Narasimamurthy, and Konrad Basler. A Genetic Screen Targeting the Tumor Necrosis Factor/Eiger Signaling Pathway: Identification of Drosophila TAB2 as a Functionally Conserved Component. *Genetics*, 171(4):1683, 12 2005.

[427] Lei Xue, Tatsushi Igaki, Erina Kuranaga, Hiroshi Kanda, Masayuki Miura, and Tian Xu. Tumor Suppressor CYLD Regulates JNK-Induced Cell Death in Drosophila. *Developmental Cell*, 13(3):446–454, 9 2007.

[428] Peter Geuking, Rajesh Narasimamurthy, Bruno Lemaitre, Konrad Basler, and François Leulier. A Non-Redundant Role for Drosophila Mkk4 and Hemipterous/Mkk7 in TAK1-Mediated Activation of JNK. *PLoS ONE*, 4(11), 11 2009.

[429] Juan R. Riesgo-Escovar, Mario Jenni, Andreas Fritz, and Ernst Hafen. The Drosophila Jun-N-terminal kinase is required for cell morphogenesis but not for DJun-dependent cell fate specification in the eye. *Genes & development*, 10(21):2759–2768, 1996.

[430] Hayla K. Sluss, Zhiqiang Han, Tamera Barrett, Roger J. Davis, and Y. Tony Ip. A JNK signal transduction pathway that mediates morphogenesis and an immune response in Drosophila. *Genes & development*, 10(21):2745–2758, 1996.

[431] Julia Zeitlinger, Lutz Kockel, Fiorenzo A. Peverali, David B. Jackson, Marek Mlodzik, and Dirk Bohmann. Defective dorsal closure and loss of epidermal decapentaplegic expression in Drosophila fos mutants. *The EMBO journal*, 16(24):7393–7401, 12 1997.

[432] Enrique Martín-Blanco, Alexandra Gampel, Jenny Ring, Kanwar Virdee, Nikolai Kirov, Aviva M. Tolkovsky, and Alfonso Martinez-Arias. puckered encodes a phosphatase that mediates a feedback loop regulating JNK activity during dorsal closure in Drosophila. *Genes & development*, 12(4):557–670, 2 1998.

[433] Meng C. Wang, Dirk Bohmann, and Heinrich Jasper. JNK extends life span and limits growth by antagonizing cellular and organism-wide responses to insulin signaling. *Cell*, 121(1):115–125, 4 2005.

[434] Ghada Tafesh-Edwards and Ioannis Eleftherianos. JNK signaling in Drosophila immunity and homeostasis. *Immunology Letters*, 226:7–11, 10 2020.

[435] Pascal Meier, John Silke, Sally J. Leevers, and Gerard I. Evan. The Drosophila caspase DRONC is regulated by DIAP1. *The EMBO Journal*, 19(4):598, 2 2000.

[436] Zhiwei Song, Kimberly McCall, and Hermann Steller. DCP-1, a Drosophila Cell Death Protease Essential for Development. *Science*, 275(5299):536–540, 1 1997.

[437] Andrew G. Fraser and Gerard I. Evan. Identification of a Drosophila melanogaster ICE/CED-3-related protease, drICE. *The EMBO journal*, 16(10):2805–2813, 5 1997.

[438] Andrew G. Fraser, Nicola J. McCarthy, and Gerard I. Evan. drICE is an essential caspase required for apoptotic activity in Drosophila cells. *The EMBO Journal*, 16(20):6192–6199, 10 1997.

[439] Jin Mo Park, Helen Brady, Maria Grazia Ruocco, Huaiyu Sun, Dee Ann Williams, Susan J. Lee, Tomohisa Kato, Normand Richards, Kyle Chan, Frank Mercurio, Michael Karin, and Steven A. Wasserman. Targeting of TAK1 by the NF-κB protein Relish regulates the JNK-mediated immune response in Drosophila. *Genes & Development*, 18(5):584, 3 2004.

[440] Xianjue Ma, Jiuhong Huang, Lixia Yang, Yang Yang, Wenzhe Li, and Lei Xue. NOPO modulates Egr-induced JNK-independent cell death in Drosophila. *Cell Research*, 22(2): 425, 2 2012.

[441] Xianjue Ma, Lixia Yang, Yang Yang, Maoquan Li, Wenzhe Li, and Lei Xue. dUev1a modulates TNF-JNK mediated tumor progression and cell death in Drosophila. *Developmental Biology*, 380(2):211–221, 8 2013.

[442] X. Ma, W. Li, H. Yu, Y. Yang, M. Li, L. Xue, and T. Xu. Bendless modulates JNK-mediated cell death and migration in Drosophila. *Cell Death & Differentiation 2014 21:3*, 21(3): 407–415, 10 2013.

[443] Hiroshi Kanda, Tatsushi Igaki, Hideyuki Okano, and Masayuki Miura. Conserved metabolic energy production pathways govern Eiger/TNF-induced nonapoptotic cell death. *Proceedings of the National Academy of Sciences of the United States of America*, 108 (47):18977–18982, 11 2011.

[444] Mingli Li, Shiyao Sun, Jessica Priest, Xiaolin Bi, and Yun Fan. Characterization of TNF-induced cell death in Drosophila reveals caspase- and JNK-dependent necrosis and its role in tumor suppression. *Cell Death & Disease*, 10(8), 8 2019.

[445] Rihab Loudhaief, Rouba Jneid, Christian Fokdal Christensen, Duncan J. Mackay, Ditte S. Andersen, and Julien Colombani. The Drosophila tumor necrosis factor receptor,Wengen, couples energy expenditure with gut immunity. *Science Advances*, 9(23), 6 2023.

[446] Baohe Shen, H. Liu, Edward Y. Skolnik, and James L. Manley. Physical and functional interactions between Drosophila TRAF2 and Pelle kinase contribute to Dorsal activation. *Proceedings of the National Academy of Sciences of the United States of America*, 98(15): 8596–8601, 7 2001.

[447] Gökhan S. Hotamisligil, Pascal Peraldi, Adriane Budavari, Ramsey Ellis, Morris F. White, and Bruce M. Spiegelman. IRS-1-mediated inhibition of insulin receptor tyrosine kinase activity in TNF-alpha- and obesity-induced insulin resistance. *Science (New York, N.Y.)*, 271(5249):665–668, 2 1996.

[448] K. Teoman Uysal, Sarah M. Wiesbrock, Michael W. Marino, and Gökhan S. Hotamisligil. Protection from obesity-induced insulin resistance in mice lacking TNF-alpha function. *Nature*, 389(6651):610–614, 1997.

[449] Jim Hirosumi, Gürol Tuncman, Lufen Chang, Cem Z. Görgün, K. Teoman Uysal, Kazuhisa Maeda, Michael Karin, and Gökhan S. Hotamisligil. A central role for JNK in obesity and insulin resistance. *Nature*, 420(6913):333–336, 11 2002.

[450] Hong Ruan and Harvey F. Lodish. Insulin resistance in adipose tissue: Direct and indirect effects of tumor necrosis factor-α. *Cytokine and Growth Factor Reviews*, 14(5):447–455, 2003.

[451] Kyung Ah Lee, Kyu Chan Cho, Boram Kim, In Hwan Jang, Kibum Nam, Young Eun Kwon, Myungjin Kim, Do Young Hyeon, Daehee Hwang, Jae Hong Seol, and Won Jae Lee. Inflammation-Modulated Metabolic Reprogramming Is Required for DUOX-Dependent Gut Immunity in Drosophila. *Cell Host & Microbe*, 23(3):338–352, 3 2018.

[452] David S. Schneider, Janelle S. Ayres, Stephanie M. Brandt, Alexandre Costa, Marc S. Dionne, Michael D. Gordon, Eric M. Mabery, Madeleine G. Moule, Linh N. Pham, and Mimi M. Shirasu-Hiza. Drosophila eiger Mutants Are Sensitive to Extracellular Pathogens. *PLoS Pathogens*, 3(3), 3 2007.

[453] Reginaldo G. Bastos, Zachary P. Howard, Aoi Hiroyasu, and Alan G. Goodman. Host and Bacterial Factors Control Susceptibility of Drosophila melanogaster to Coxiella burnetii Infection. *Infection and Immunity*, 85(7), 7 2017.

[454] Eric M. Mabery and David S. Schneider. The Drosophila TNF Ortholog Eiger Is Required in the Fat Body for a Robust Immune Response. *Journal of Innate Immunity*, 2(4):371, 6 2010.

[455] Albana Kodra, Claire de la Cova, Abigail R. Gerhold, and Laura A. Johnston. Widely Used Mutants of eiger, Encoding the Drosophila Tumor Necrosis Factor, Carry Additional Mutations in the NimrodC1 Phagocytosis Receptor. *G3: Genes|Genomes|Genetics*, 10 (12):4707, 12 2020.

[456] Douglas A. Harrison, Patricia E. McCoon, Richard Binari, Michael Gilman, and Norbert Perrimon. Drosophila unpaired encodes a secreted protein that activates the JAK signaling pathway. *Genes & development*, 12(20):3252–3263, 10 1998.

[457] Hervé Agaisse, Ulla Maja Petersen, Michael Boutros, Bernard Mathey-Prevot, and Norbert Perrimon. Signaling role of hemocytes in Drosophila JAK/STAT-dependent response to septic injury. *Developmental Cell*, 5(3):441–450, 9 2003.

[458] M. Melissa Gilbert, Brian K. Weaver, J. Peter Gergen, and Nancy C. Reich. A novel functional activator of the Drosophila JAK/STAT pathway, unpaired2, is revealed by an in vivo reporter of pathway activation. *Mechanisms of development*, 122(7-8):939–948, 7 2005.

[459] James Castelli Gair Hombría, Stephen Brown, Sabine Häder, and Martin P. Zeidler. Characterisation of Upd2, a Drosophila JAK/STAT pathway ligand. *Developmental biology*, 288(2):420–433, 12 2005.

[460] Victoria M. Wright, Katja L. Vogt, Elizabeth Smythe, and Martin P. Zeidler. Differential activities of the Drosophila JAK/STAT pathway ligands Upd, Upd2 and Upd3. *Cellular signalling*, 23(5):920–927, 5 2011.

[461] Stephen Brown, Nan Hu, and James Castelli Gair Hombría. Identification of the first invertebrate interleukin JAK/STAT receptor, the Drosophila gene domeless. *Current biology : CB*, 11(21):1700–1705, 10 2001.

[462] Hua Wei Chen, Xiu Chen, Su Wan Oh, Maria J. Marinissen, J. Silvio Gutkind, and Steven X. Hou. mom identifies a receptor for the Drosophila JAK/STAT signal transduction pathway and encodes a protein distantly related to the mammalian cytokine receptor family. *Genes & development*, 16(3):388–398, 2 2002.

[463] Xianyu Steven Hou, Michael B. Melnick, and Norbert Perrimon. Marelle acts downstream of the Drosophila HOP/JAK kinase and encodes a protein similar to the mammalian STATs. *Cell*, 84(3):411–419, 2 1996.

[464] Riqiang Yan, Stephen Small, Claude Desplan, Charles R. Dearolf, and James E. Darnell. Identification of a Stat gene that functions in Drosophila development. *Cell*, 84(3):421–430, 2 1996.

[465] Hiu Kiu and Sandra E. Nicholson. Biology and significance of the JAK/STAT signalling pathways. *Growth factors (Chur, Switzerland)*, 30(2):88–106, 4 2012.

[466] H. Myllymäki and M. Rämet. JAK/STAT Pathway in Drosophila Immunity. *Scandinavian Journal of Immunology*, 79(6):377–385, 6 2014.

[467] Bernard A. Callus and Bernard Mathey-Prevot. SOCS36E, a novel Drosophila SOCS protein, suppresses JAK/STAT and EGF-R signalling in the imaginal wing disc. *Oncogene*, 21(31):4812–4821, 2002.

[468] Peter Karsten, Sabine Häder, and Martin P. Zeidler. Cloning and expression of Drosophila SOCS36E and its potential regulation by the JAK/STAT pathway. *Mechanisms of Development*, 117(1-2):343–346, 9 2002.

[469] Marie Lagueux, Emmanuel Perrodou, Elena A. Levashina, Maria Capovilla, and Jules A. Hoffmann. Constitutive expression of a complement-like protein in Toll and JAK gain-of-function mutants of Drosophila. *Proceedings of the National Academy of Sciences of the United States of America*, 97(21):11427, 10 2000.

[470] Claire B. Peán, Mark Schiebler, Sharon W.S. Tan, Jessica A. Sharrock, Katrin Kierdorf, Karen P. Brown, M. Charlotte Maserumule, Shinelle Menezes, Martina Pilátová, Kévin Bronda, Pierre Guermonprez, Brian M. Stramer, R. Andres Floto, and Marc S. Dionne. Regulation of phagocyte triglyceride by a STAT-ATG2 pathway controls mycobacterial infection. *Nature Communications*, 8, 3 2017.

[471] Akhila Rajan and Norbert Perrimon. The Drosophila cytokine Unpaired 2 regulates physiological homeostasis by remotely controlling Insulin secretion. *Cell*, 151(1):123, 9 2012.

[472] Fernanda Lourido, Daniela Quenti, Daniela Salgado-Canales, and Nicolás Tobar. Domeless receptor loss in fat body tissue reverts insulin resistance induced by a high-sugar diet in Drosophila melanogaster. *Scientific Reports*, 11(1):3263, 12 2021.

[473] René Lanot, Daniel Zachary, François Holder, and Marie Meister. Postembryonic hematopoiesis in Drosophila. *Developmental biology*, 230(2):243–257, 2 2001.

[474] Cory J. Evans, Volker Hartenstein, and Utpal Banerjee. Thicker than blood: conserved mechanisms in Drosophila and vertebrate hematopoiesis. *Developmental cell*, 5(5): 673–690, 11 2003.

[475] Michael J. Williams. Drosophila hemopoiesis and cellular immunity. *Journal of immunology (Baltimore, Md. : 1950)*, 178(8):4711–4716, 4 2007.

[476] Bernard Charroux and Julien Royet. Elimination of plasmatocytes by targeted apoptosis reveals their role in multiple aspects of the Drosophila immune response. *Proceedings of the National Academy of Sciences of the United States of America*, 106(24):9797–9802, 6 2009.

[477] Utpal Banerjee, Juliet R. Girard, Lauren M. Goins, and Carrie M. Spratford. Drosophila as a Genetic Model for Hematopoiesis. *Genetics*, 211(2):367–417, 2 2019.

[478] Róbert Márkus, Barbara Laurinyecz, Éva Kurucz, Viktor Honti, Izabella Bajusz, Botond Sipos, Kálmán Somogyi, Jesper Kronhamn, Dan Hultmark, and István Andó. Sessile hemocytes as a hematopoietic compartment in Drosophila melanogaster. *Proceedings of the National Academy of Sciences of the United States of America*, 106(12):4805, 3 2009.

[479] Kalpana Makhijani, Brandy Alexander, Tsubasa Tanaka, Eric Rulifson, and Katja Brückner. The peripheral nervous system supports blood cell homing and survival in the Drosophila larva. *Development*, 138(24):5379–5391, 12 2011.

[480] Katrina S. Gold and Katja Brückner. Drosophila as a model for the two myeloid blood cell systems in vertebrates. *Experimental hematology*, 42(8):717–727, 2014.

[481] Katrina S. Gold and Katja Brückner. Macrophages and cellular immunity in Drosophila melanogaster. *Seminars in immunology*, 27(6):357, 12 2015.

[482] Seung Hye Jung, Cory J. Evans, Christine Uemura, and Utpal Banerjee. The Drosophila lymph gland as a developmental model of hematopoiesis. *Development (Cambridge, England)*, 132(11):2521–2533, 6 2005.

[483] Manon Letourneau, Francois Lapraz, Anurag Sharma, Nathalie Vanzo, Lucas Waltzer, and Michèle Crozatier. Drosophila hematopoiesis under normal conditions and in response to immune stress. *FEBS letters*, 590(22):4034–4051, 11 2016.

[484] Pablo Sanchez Bosch, Kalpana Makhijani, Leire Herboso, Katrina S. Gold, Rowan Baginsky, Katie J. Woodcock, Brandy Alexander, Katelyn Kukar, Sean Corcoran, Thea Jacobs, Debra Ouyang, Corinna Wong, Elodie J.V. Ramond, Christa Rhiner, Eduardo Moreno, Bruno Lemaitre, Frederic Geissmann, and Katja Brückner. Adult Drosophila lack hematopoiesis, but rely on a blood cell reservoir at the respiratory epithelia to relay infection signals to surrounding tissues. *Developmental cell*, 51(6):787, 12 2019.

[485] Monicia Elrod-Erickson, Smita Mishra, and David Schneider. Interactions between the cellular and humoral immune responses in Drosophila. *Current Biology*, 10(13):781–784, 6 2000.

[486] Éva Kurucz, B. Váczi, R. Márkus, Barbara Laurinyecz, P. Vilmos, J. Zsámboki, Kinga Csorba, Elisabeth Gateff, D. Hultmark, and I. Andó. Definition of Drosophila hemocyte subsets by cell-type specific antigens. *Acta biologica Hungarica*, 58 Suppl(SUPPL. 1): 95–111, 11 2007.

[487] C. Melcarne, B. Lemaitre, and E. Kurant. Phagocytosis in Drosophila: From molecules and cellular machinery to physiology. *Insect Biochemistry and Molecular Biology*, 109:1–12, 6 2019.

[488] Hamadoun Touré, Nicolas Durand, Isabelle Guénal, Jean-Louis Herrmann, Fabienne Girard-Misguich, and Sébastien Szuplewski. Mycobacterium abscessus Opsonization Allows an Escape from the Defensin Bactericidal Action in Drosophila. *Microbiology Spectrum*, 11(4), 8 2023.

[489] Yumi Hashimoto, Yukichika Tabuchi, Kenji Sakurai, Mayumi Kutsuna, Kenji Kurokawa, Takeshi Awasaki, Kazuhisa Sekimizu, Yoshinobu Nakanishi, and Akiko Shiratsuchi. Identification of Lipoteichoic Acid as a Ligand for Draper in the Phagocytosis of Staphylococcus aureus by Drosophila Hemocytes. *The Journal of Immunology*, 183(11): 7451–7460, 12 2009.

[490] Lynda M. Stuart, Jiusheng Deng, Jessica M. Silver, Kazue Takahashi, Anita A. Tseng, Elizabeth J. Hennessy, R. Alan B. Ezekowitz, and Kathryn J. Moore. Response to Staphylococcus aureus requires CD36-mediated phagocytosis triggered by the COOH-terminal cytoplasmic domain. *Journal of Cell Biology*, 170(3):477–485, 8 2005.

[491] Nirmalya Chatterjee and Norbert Perrimon. What fuels the fly: Energy metabolism in Drosophila and its application to the study of obesity and diabetes. *Science Advances*, 7(24):4336–4345, 6 2021.

[492] Charles Géminard, Eric J. Rulifson, and Pierre Léopold. Remote Control of Insulin Secretion by Fat Cells in Drosophila. *Cell Metabolism*, 10(3):199–207, 9 2009.

[493] Edward Owusu-Ansah and Norbert Perrimon. Modeling metabolic homeostasis and nutrient sensing in Drosophila: implications for aging and metabolic diseases. *Disease Models & Mechanisms*, 7(3):343, 2014.

[494] Marc S. Dionne, Linh N. Pham, Mimi Shirasu-Hiza, and David S. Schneider. Akt and foxo Dysregulation Contribute to Infection-Induced Wasting in Drosophila. *Current Biology*, 16 (20):1977–1985, 10 2006.

[495] Charles Géminard, Nathalie Arquier, Sophie Layalle, Marc Bourouis, Maija Slaidina, Renald Delanoue, Marianne Bjordal, Mickael Ohanna, May Ma, Julien Colombani, and Pierre Léopold. Control of Metabolism and Growth Through Insulin-Like Peptides in Drosophila. *Diabetes*, 55(Supplement_2):S5–S8, 12 2006.

[496] Aurelio A. Teleman. Molecular mechanisms of metabolic regulation by insulin in Drosophila. *The Biochemical journal*, 425(1):13–26, 1 2009.

[497] Eric J. Rulifson, Seung K. Kim, and Roel Nusse. Ablation of insulin-producing neurons in flies: growth and diabetic phenotypes. *Science (New York, N.Y.)*, 296(5570):1118–1120, 5 2002.

[498] Tomoatsu Ikeya, Milos Galic, Priyanka Belawat, Knud Nairz, and Ernst Hafen. Nutrient-dependent expression of insulin-like peptides from neuroendocrine cells in the CNS contributes to growth regulation in Drosophila. *Current biology : CB*, 12(15): 1293–1300, 8 2002.

[499] Susan J. Broughton, Matthew D.W. Piper, Tomoatsu Ikeya, Timothy M. Bass, Jake Jacobson, Yasmine Driege, Pedro Martinez, Ernst Hafen, Dominic J. Withers, Sally J. Leevers, and Linda Partridge. Longer lifespan, altered metabolism, and stress resistance in Drosophila from ablation of cells making insulin-like ligands. *Proceedings of the National Academy of Sciences of the United States of America*, 102(8):3105–3110, 2 2005.

[500] Rafael Fernandez, Diane Tabarini, Natalia Azpiazu, Manfred Frasch, and Joseph Schlessinger. The Drosophila insulin receptor homolog: a gene essential for embryonic development encodes two receptor isoforms with different signaling potential. *The EMBO journal*, 14(14):3373–3384, 1995.

[501] Ruth Böhni, Juan Riesgo-Escovar, Sean Oldham, Walter Brogiolo, Hugo Stocker, Bernard F. Andruss, Kathy Beckingham, and Ernst Hafen. Autonomous control of cell and organ size by CHICO, a Drosophila homolog of vertebrate IRS1-4. *Cell*, 97(7):865–875, 6 1999.

[502] Christine C. Milburn, Maria Deak, Sharon M. Kelly, Nick C. Price, Dario R. Alessi, and Daan M.F. Van Aalten. Binding of phosphatidylinositol 3,4,5-trisphosphate to the pleckstrin homology domain of protein kinase B induces a conformational change. *The Biochemical journal*, 375(Pt 3):531–538, 11 2003.

[503] Dario R. Alessi, Stephen R. James, C. Peter Downes, Andrew B. Holmes, Piers R.J. Gaffney, Colin B. Reese, and Philip Cohen. Characterization of a 3-phosphoinositide-dependent protein kinase which phosphorylates and activates protein kinase Balpha. *Current biology : CB*, 7(4):261–269, 1997.

[504] Dos D. Sarbassov, David A. Guertin, Siraj M. Ali, and David M. Sabatini. Phosphorylation and regulation of Akt/PKB by the rictor-mTOR complex. *Science (New York, N.Y.)*, 307 (5712):1098–1101, 2 2005.

[505] Ville Hietakangas and Stephen M. Cohen. Re-evaluating AKT regulation: role of TOR complex 2 in tissue growth. *Genes & Development*, 21(6):632, 3 2007.

[506] Lars P. Van Der Heide, Marco F.M. Hoekman, and Marten P. Smidt. The ins and outs of FoxO shuttling: mechanisms of FoxO translocation and transcriptional regulation. *Biochemical Journal*, 380(Pt 2):297, 6 2004.

[507] Boris Gershman, Oscar Puig, Lilian Hang, Robert M. Peitzsch, Marc Tatar, and Robert S. Garofalo. High-resolution dynamics of the transcriptional response to nutrition in Drosophila: a key role for dFOXO. *Physiological genomics*, 29(1):24–34, 3 2007.

[508] Aurelio A. Teleman, Ville Hietakangas, Aram C. Sayadian, and Stephen M. Cohen. Nutritional control of protein biosynthetic capacity by insulin via Myc in Drosophila. *Cell metabolism*, 7(1):21–32, 1 2008.

[509] Brendan D. Manning and Alex Toker. AKT/PKB Signaling: Navigating the Network. *Cell*, 169(3):381, 4 2017.

[510] Robert A. Saxton and David M. Sabatini. mTOR Signaling in Growth, Metabolism, and Disease. *Cell*, 168(6):960, 3 2017.

[511] Sara Cherry. Genomic RNAi screening in Drosophila S2 cells: what have we learned about host-pathogen interactions?, 6 2008.

[512] Jennifer A. Philips, Eric J. Rubin, and Norbert Perrimon. Drosophila RNAi screen reveals CD36 family member required for mycobacterial infection. *Science (New York, N.Y.)*, 309 (5738):1251–1253, 8 2005.

[513] Jennifer A. Philips, Maura C. Porto, Hui Wang, Eric J. Rubin, and Norbert Perrimon. ESCRT factors restrict mycobacterial growth. *Proceedings of the National Academy of Sciences of the United States of America*, 105(8):3070–3075, 2 2008.

[514] Eleanor K.P. Marshall and Marc S. Dionne. Drosophila versus Mycobacteria: A model for mycobacterial host–pathogen interactions. *Molecular Microbiology*, 117(3):600–609, 3 2022.

[515] Ingrid Chou Koo, Yamini M. Ohol, Ping Wu, J. Hiroshi Morisaki, Jeffery S. Cox, and Eric J. Brown. Role for lysosomal enzyme β-hexosaminidase in the control of mycobacteria infection. *Proceedings of the National Academy of Sciences of the United States of America*, 105(2):710, 1 2008.

[516] Marc S. Dionne, Nafisa Ghori, and David S. Schneider. Drosophila melanogaster is a genetically tractable model host for Mycobacterium marinum. *Infection and Immunity*, 71 (6):3540–3550, 6 2003.

[517] Chun Taek Oh, Cheol Moon, Myeong Seon Jeong, Seung Hae Kwon, and Jichan Jang. Drosophila melanogaster model for Mycobacterium abscessus infection. *Microbes and Infection*, 15(12):788–795, 11 2013.

[518] Rebecca L. Belmonte, Mary Kate Corbally, David F. Duneau, and Jennifer C. Regan. Sexual Dimorphisms in Innate Immunity and Responses to Infection in Drosophila melanogaster. *Frontiers in immunology*, 10, 1 2020.

[519] Crystal M. Vincent and Marc S. Dionne. Disparate regulation of IMD signaling drives sex differences in infection pathology in Drosophila melanogaster. *Proceedings of the National Academy of Sciences of the United States of America*, 118(32), 8 2021.

[520] Marie Lavollay, Martine Fourgeaud, Jean Louis Herrmann, Lionel Dubost, Arul Marie, Laurent Gutmann, Michel Arthur, and Jean Luc Mainardi. The peptidoglycan of

Mycobacterium abscessus is predominantly cross-linked by L,D-transpeptidases. *Journal of Bacteriology*, 193(3):778–782, 2011.

[521] Elizabeth Story-Roller, Emily C. Maggioncalda, Keira A. Cohen, and Gyanu Lamichhane. Mycobacterium abscessus and β-lactams: Emerging insights and potential opportunities, 9 2018.

[522] Takahiro Tanji, Xiaodi Hu, Alexander N. R. Weber, and Y. Tony Ip. Toll and IMD pathways synergistically activate an innate immune response in Drosophila melanogaster. *Molecular and cellular biology*, 27(12):4578–4588, 6 2007.

[523] Kaman Chan, Timothy Knaak, Laura Satkamp, Olivier Humbert, Stanley Falkow, and Lalita Ramakrishnan. Complex pattern of Mycobacterium marinum gene expression during long-term granulomatous infection. *Proceedings of the National Academy of Sciences of the United States of America*, 99(6):3920–3925, 3 2002.

[524] Shintaro Okada and John S. O'Brien. Tay-Sachs disease: generalized absence of a beta-D-N-acetylhexosaminidase component. *Science (New York, N.Y.)*, 165(3894): 698–700, 1969.

[525] B. Spyropoulos. Tay-Sachs carriers and tuberculosis resistance. *Nature*, 331(6158):666, 1988.

[526] K. Utsumi, A. Tsuji, R. Kase, A. Tanaka, T. Tanaka, E. Uyama, T. Ozawa, H. Sakuraba, Y. Komaba, M. Kawabe, Y. Iino, and Y. Katayama. Western blotting analysis of the beta-hexosaminidase alpha- and beta-subunits in cultured fibroblasts from cases of various forms of GM2 gangliosidosis. *Acta neurologica Scandinavica*, 105(6):427–430, 2002.

[527] Evgueni A. Sevrioukov, Nabil Moghrabi, Mary Kuhn, and Helmut Krämer. A mutation in dVps28 reveals a link between a subunit of the endosomal sorting complex required for transport-I complex and the actin cytoskeleton in Drosophila. *Molecular biology of the cell*, 16(5):2301–2312, 5 2005.

[528] Ana T. López-Jiménez, Elena Cardenal-Muñoz, Florence Leuba, Lilli Gerstenmaier, Caroline Barisch, Monica Hagedorn, Jason S. King, and Thierry Soldati. The ESCRT and autophagy machineries cooperate to repair ESX-1-dependent damage at the Mycobacterium-containing vacuole but have opposite impact on containing the infection. *PLoS pathogens*, 14(12), 12 2018.

[529] Cynthia Portal-Celhay, JoAnn M. Tufariello, Smita Srivastava, Aleena Zahra, Thais Klevorn, Patricia S. Grace, Alka Mehra, Heidi S. Park, Joel D. Ernst, William R. Jacobs, Jr, and Jennifer A. Philips. Mycobacterium tuberculosis EsxH inhibits ESCRT-dependent CD4+ T-cell activation. *Nature microbiology*, 2:16232, 12 2016.

[530] Jacqueline M. Kimmey, Jeremy P. Huynh, Leslie A. Weiss, Sunmin Park, Amal Kambal, Jayanta Debnath, Herbert W. Virgin, and Christina L. Stallings. Unique role for ATG5 in neutrophil-mediated immunopathology during M. tuberculosis infection. *Nature*, 528 (7583):565–569, 12 2015.

[531] Alessandra Romagnoli, Marilena P. Etna, Elena Giacomini, Manuela Pardini, Maria Elena Remoli, Marco Corazzari, Laura Falasca, Delia Goletti, Valérie Gafa, Roxane Simeone, Giovanni Delogu, Mauro Piacentini, Roland Brosch, Gian Maria Fimia, and Eliana M. Coccia. ESX-1 dependent impairment of autophagic flux by Mycobacterium tuberculosis in human dendritic cells. *Autophagy*, 8(9):1357–1370, 2012.

[532] Ryan C. Scott, Oren Schuldiner, and Thomas P. Neufeld. Role and regulation of starvation-induced autophagy in the Drosophila fat body. *Developmental cell*, 7(2): 167–178, 8 2004.

[533] Fergal O'Farrell, Shenqiu Wang, Nadja Katheder, Tor Erik Rusten, and Christos Samakovlis. Two-tiered control of epithelial growth and autophagy by the insulin receptor and the ret-like receptor, stitcher. *PLoS biology*, 11(7), 7 2013.

[534] G. Juhász, L. G. Puskás, O. Komonyi, B. Érdi, P. Maróy, T. P. Neufeld, and M. Sass. Gene Expression Profiling Identifies FKBP39 as an Inhibitor of Autophagy in Larval Drosophila Fat Body. *Cell death and differentiation*, 14(6):1181, 6 2007.

[535] Fabio Demontis and Norbert Perrimon. FOXO/4E-BP signaling in Drosophila muscles regulates organism-wide proteostasis during aging. *Cell*, 143(5):813–825, 11 2010.

[536] Shintaro Maeda, Chinatsu Otomo, and Takanori Otomo. The autophagic membrane tether ATG2A transfers lipids between membranes. *eLife*, 8, 7 2019.

[537] Hajnalka Laczkó-Dobos, Asha Kiran Maddali, András Jipa, Arindam Bhattacharjee, Attila Gergely Végh, and Gábor Juhász. Lipid profiles of autophagic structures isolated from wild type and Atg2 mutant Drosophila. *Biochimica et biophysica acta. Molecular and cell biology of lipids*, 1866(3):158868, 3 2021.

[538] Paulina Fernandez-Soto, Alexander J.E. Bruce, Alistair J. Fielding, Jennifer S. Cavet, and Lydia Tabernero. Mechanism of catalysis and inhibition of Mycobacterium tuberculosis SapM, implications for the development of novel antivirulence drugs. *Scientific Reports 2019 9:1*, 9(1):1–14, 7 2019.

[539] Isabelle Vergne, Jennifer Chua, and Vojo Deretic. Tuberculosis toxin blocking phagosome maturation inhibits a novel Ca2+/calmodulin-PI3K hVPS34 cascade. *The Journal of experimental medicine*, 198(4):653–659, 8 2003.

[540] Isabelle Vergne and Vojo Deretic. The role of PI3P phosphatases in the regulation of autophagy. *FEBS letters*, 584(7):1313–1318, 4 2010.

[541] Jwa Jin Kim, Hye Mi Lee, Dong Min Shin, Wonho Kim, Jae Min Yuk, Hyo Sun Jin, Sang Hee Lee, Guang Ho Cha, Jin Man Kim, Zee Won Lee, Sung Jae Shin, Heekyung Yoo, Young Kil Park, Jin Bong Park, Jongkyeong Chung, Tamotsu Yoshimori, and Eun Kyeong Jo. Host cell autophagy activated by antibiotics is required for their effective antimycobacterial drug action. *Cell Host and Microbe*, 11(5):457–468, 5 2012.

[542] Tae Sung Kim, Yern Hyerk Shin, Hye Mi Lee, Jin Kyung Kim, Jin Ho Choe, Ji Chan Jang, Soohyun Um, Hyo Sun Jin, Masaaki Komatsu, Guang Ho Cha, Han Jung Chae, Dong Chan Oh, and Eun Kyeong Jo. Ohmyungsamycins promote antimicrobial responses through autophagy activation via AMP-Activated protein kinase pathway. *Scientific Reports*, 7(1), 12 2017.

[543] Gábor Juhász, Balázs Érdi, Miklós Sass, and Thomas P. Neufeld. Atg7-dependent autophagy promotes neuronal health, stress tolerance, and longevity but is dispensable for metamorphosis in Drosophila. *Genes & development*, 21(23):3061–3066, 12 2007.

[544] Péter Nagy, Krisztina Hegedus, Karolina Pircs, Ágnes Varga, and Gábor Juhász. Different effects of Atg2 and Atg18 mutations on Atg8a and Atg9 trafficking during starvation in Drosophila. *FEBS letters*, 588(3):408–413, 1 2014.

[545] Stefan Köster, Sandeep Upadhyay, Pallavi Chandra, Kadamba Papavinasasundaram, Guozhe Yang, Amir Hassan, Steven J. Grigsby, Ekansh Mittal, Heidi S. Park, Victoria Jones, Fong Fu Hsu, Mary Jackson, Christopher M. Sassetti, and Jennifer A. Philips. Mycobacterium tuberculosis is protected from NADPH oxidase and LC3-associated phagocytosis by the LCP protein CpsA. *Proceedings of the National Academy of Sciences of the United States of America*, 114(41):E8711–E8720, 10 2017.

[546] Denise A. Rozwarski, Gregory A. Grant, Derek H.R. Barton, William R. Jacobs, and James C. Sacchettini. Modification of the NADH of the isoniazid target (InhA) from Mycobacterium tuberculosis. *Science (New York, N.Y.)*, 279(5347):98–102, 1 1998.

[547] Annabel Guichard, Shauna M. McGillivray, Beatriz Cruz-Moreno, Nina M. Van Sorge, Victor Nizet, and Ethan Bier. Anthrax toxins cooperatively inhibit endocytic recycling by the Rab11/Sec15 exocyst. *Nature*, 467(7317):854–858, 10 2010.

[548] David L. Erickson, J. Louise Lines, Everett C. Pesci, Vittorio Venturi, and Douglas G. Storey. Pseudomonas aeruginosa relA contributes to virulence in Drosophila melanogaster. *Infection and immunity*, 72(10):5638–5645, 10 2004.

[549] Kate E. Broderick, Adriano Chan, Maheswari Balasubramanian, Jake Feala, Sharon L. Reed, Markandeswar Panda, Vijay S. Sharma, Renate B. Pilz, Timothy D. Bigby, and Gerry R. Boss. Cyanide produced by human isolates of Pseudomonas aeruginosa contributes to lethality in Drosophila melanogaster. *The Journal of infectious diseases*, 197(3):457–464, 2 2008.

[550] Siriwan Boonma, Adisak Romsang, Jintana Duang-Nkern, Sopapan Atichartpongkul, Wachareeporn Trinachartvanit, Paiboon Vattanaviboon, and Skorn Mongkolsuk. The FinR-regulated essential gene fprA, encoding ferredoxin NADP+ reductase: Roles in superoxide-mediated stress protection and virulence of Pseudomonas aeruginosa. *PloS one*, 12(2), 2 2017.

[551] Magda L. Atilano, James Yates, Marcus Glittenberg, Sergio R. Filipe, and Petros Ligoxygakis. Wall teichoic acids of Staphylococcus aureus limit recognition by the drosophila peptidoglycan recognition protein-SA to promote pathogenicity. *PLoS pathogens*, 7(12), 12 2011.

[552] Dingding An, Yiorgos Apidianakis, Ana Laura Boechat, Regina L. Baldini, Boyan C. Goumnerov, and Laurence G. Rahme. The pathogenic properties of a novel and conserved gene product, KerV, in proteobacteria. *PloS one*, 4(9), 9 2009.

[553] Janelle S. Ayres and David S. Schneider. Two ways to survive an infection: what resistance and tolerance can teach us about treatments for infectious diseases. *Nature reviews. Immunology*, 8(11):889, 11 2008.

[554] Arturo Casadevall and Liise anne Pirofski. Host□Pathogen Interactions: The Attributes of Virulence. *The Journal of Infectious Diseases*, 184(3):337–344, 8 2001.

[555] Aditya Kumar Sharma, Neha Dhasmana, Neha Dubey, Nishant Kumar, Aakriti Gangwal, Meetu Gupta, and Yogendra Singh. Bacterial Virulence Factors: Secreted for Survival. *Indian Journal of Microbiology*, 57(1):1, 3 2017.

[556] Uday Tak, Jiri Vlach, Acely Garza-Garcia, Doreen William, Olga Danilchanka, Luiz Pedro Sório de Carvalho, Jamil S. Saad, and Michael Niederweis. The tuberculosis necrotizing toxin is an NAD+ and NADP+ glycohydrolase with distinct enzymatic properties. *The Journal of Biological Chemistry*, 294(9):3024, 3 2019.

[557] Bavesh D. Kana and Valerie Mizrahi. Molecular genetics of Mycobacterium tuberculosis in relation to the discovery of novel drugs and vaccines. *Tuberculosis*, 84(1-2):63–75, 1 2004.

[558] Krishnamoorthy Gopinath, Digby F. Warner, and Valerie Mizrahi. Targeted gene knockout and essentiality testing by homologous recombination. *Methods in molecular biology (Clifton, N.J.)*, 1285:131–149, 2015.

[559] Fabian M. Arnold, Michael Hohl, Sille Remm, Hendrik Koliwer-Brandl, Sophia Adenau, Sasitorn Chusri, Peter Sander, Hubert Hilbi, and Markus A. Seeger. A uniform cloning platform for mycobacterial genetics and protein production. *Scientific Reports 2018 8:1*, 8 (1):1–16, 6 2018.

[560] D. K. Armianinova, D. S. Karpov, M. S. Kotliarova, and A. V. Goncharenko. Genetic Engineering in Mycobacteria. *Molecular Biology*, 56(6):830–841, 12 2022.

[561] Eira Choudhary, Preeti Thakur, Madhu Pareek, and Nisheeth Agarwal. Gene silencing by CRISPR interference in mycobacteria. *Nature Communications*, 6, 2 2015.

[562] Eira Choudhary, Ajitesh Lunge, and Nisheeth Agarwal. Strategies of genome editing in mycobacteria: Achievements and challenges, 5 2016.

[563] T. Parish and N. G. Stoker. Use of a flexible cassette method to generate a double unmarked Mycobacterium tuberculosis tlyA plcABC mutant by gene replacement. *Microbiology (Reading, England)*, 146 (Pt 8)(8):1969–1975, 2000.

[564] Nyaradzai Mitchell Chimukuche and Monique J. Williams. Genetic Manipulation of Non-tuberculosis Mycobacteria. *Frontiers in Microbiology*, 12:633510, 2 2021.

[565] Vladimir Pelicic, Jean Marc Reyrat, and Brigitte Gicquel. Expression of the Bacillus subtilis sacB gene confers sucrose sensitivity on mycobacteria. *Journal of Bacteriology*, 178(4): 1197, 1996.

[566] Vladimir Pelicic, Jean Marc Reyrat, and Brigitte Gicquel. Generation of unmarked directed mutations in mycobacteria, using sucrose counter-selectable suicide vectors. *Molecular microbiology*, 20(5):919–925, 1996.

[567] Vladimir Pelicic, Mary Jackson, Jean Marc Reyrat, William R. Jacobs, Brigitte Gicquel, and Christophe Guilhot. Efficient allelic exchange and transposon mutagenesis in Mycobacterium tuberculosis. *Proceedings of the National Academy of Sciences of the United States of America*, 94(20):10955, 9 1997.

[568] Joachim Stephan, Volker Stemmer, and Michael Niederweis. Consecutive gene deletions in Mycobacterium smegmatis using the yeast FLP recombinase. *Gene*, 343(1):181–190, 12 2004.

[569] Ganjam V. Kalpana, Barry R. Bloom, and William R. Jacobs. Insertional mutagenesis and illegitimate recombination in mycobacteria. *Proceedings of the National Academy of Sciences*, 88(12):5433–5437, 6 1991.

[570] A. Aldovini, R. N. Husson, and R. A. Young. The uraA locus and homologous recombination in Mycobacterium bovis BCG. *Journal of Bacteriology*, 175(22):7282–7289, 1993.

[571] Taek Park Kun, John L. Dahl, John P. Bannantine, Raúl G. Barletta, Jongsam Ahn, Andrew J. Allen, Mary Jo Hamilton, and William C. Davis. Demonstration of allelic

exchange in the slow-growing bacterium Mycobacterium avium subsp. paratuberculosis, and generation of mutants with deletions at the pknG, relA, and lsr2 loci. *Applied and environmental microbiology*, 74(6):1687–1695, 3 2008.

[572] Stan J.J. Brouns, Matthijs M. Jore, Magnus Lundgren, Edze R. Westra, Rik J.H. Slijkhuis, Ambrosius P.L. Snijders, Mark J. Dickman, Kira S. Makarova, Eugene V. Koonin, and John Van Der Oost. Small CRISPR RNAs guide antiviral defense in prokaryotes. *Science*, 321 (5891):960–964, 8 2008.

[573] F. J.M. Mojica, C. Díez-Villaseñor, J. García-Martínez, and C. Almendros. Short motif sequences determine the targets of the prokaryotic CRISPR defence system. *Microbiology*, 155(3):733–740, 3 2009.

[574] Matthew H. Larson, Luke A. Gilbert, Xiaowo Wang, Wendell A. Lim, Jonathan S. Weissman, and Lei S. Qi. CRISPR interference (CRISPRi) for sequence-specific control of gene expression. *Nature protocols*, 8(11):2180–2196, 2013.

[575] Jeremy M. Rock, Forrest F. Hopkins, Alejandro Chavez, Marieme Diallo, Michael R. Chase, Elias R. Gerrick, Justin R. Pritchard, George M. Church, Eric J. Rubin, Christopher M. Sassetti, Dirk Schnappinger, and Sarah M. Fortune. Programmable transcriptional repression in mycobacteria using an orthogonal CRISPR interference platform. *Nature Microbiology*, 2, 2 2017.

[576] Bingbing Sun, Junjie Yang, Sheng Yang, Richard D. Ye, Daijie Chen, and Yu Jiang. A CRISPR-Cpf1-Assisted Non-Homologous End Joining Genome Editing System of Mycobacterium smegmatis. *Biotechnology Journal*, 13(9), 9 2018.

[577] Nicolas C. Stephanou, Feng Gao, Paola Bongiorno, Sabine Ehrt, Dirk Schnappinger, Stewart Shuman, and Michael S. Glickman. Mycobacterial Nonhomologous End Joining Mediates Mutagenic Repair of Chromosomal Double-Strand DNA Breaks. *Journal of Bacteriology*, 189(14):5237, 7 2007.

[578] Amandeep Singh. Guardians of the mycobacterial genome: A review on DNA repair systems in Mycobacterium tuberculosis. *Microbiology (United Kingdom)*, 163(12): 1740–1758, 12 2017.

[579] Mei Yi Yan, Si Shang Li, Xin Yuan Ding, Xiao Peng Guo, Qi Jin, and Yi Cheng Sun. A CRISPR-Assisted Nonhomologous End-Joining Strategy for Efficient Genome Editing in Mycobacterium tuberculosis. *mBio*, 11(1), 1 2020.

[580] Aniek S. Meijers, Ran Troost, Roy Ummels, Janneke Maaskant, Alexander Speer, Sergey Nejentsev, Wilbert Bitter, and Coenraad P. Kuijl. Efficient genome editing in pathogenic mycobacteria using Streptococcus thermophilus CRISPR1-Cas9. *Tuberculosis (Edinburgh, Scotland)*, 124:101983, 9 2020.

[581] Lucas Boeck, Sophie Burbaud, Marcin Skwark, Will H. Pearson, Jasper Sangen, Andreas W. Wuest, Eleanor K.P. Marshall, Aaron Weimann, Isobel Everall, Josephine M. Bryant, Sony Malhotra, Bridget P. Bannerman, Katrin Kierdorf, Tom L. Blundell, Marc S. Dionne, Julian Parkhill, and R. Andres Floto. Mycobacterium abscessus pathogenesis identified by phenogenomic analyses. *Nature Microbiology*, 7(9):1431, 9 2022.

[582] Danny E. Miller, Kevin R. Cook, and R. Scott Hawley. The joy of balancers. *PLoS Genetics*, 15(11), 2019.

[583] Sergey A. Sinenko and Bernard Mathey-Prevot. Increased expression of Drosophila tetraspanin, Tsp68C, suppresses the abnormal proliferation of ytr-deficient and Ras/Raf-activated hemocytes. *Oncogene*, 23(56):9120–9128, 12 2004.

[584] A. H. Brand and N. Perrimon. Targeted gene expression as a means of altering cell fates and generating dominant phenotypes. *Development (Cambridge, England)*, 118(2): 401–415, 1993.

[585] Chun Taek Oh, Cheol Moon, Ok Kyu Park, Seung Hae Kwon, and Jichan Jang. Novel drug combination for Mycobacterium abscessus disease therapy identified in a Drosophila infection model. *Journal of Antimicrobial Chemotherapy*, 69(6):1599–1607, 6 2014.

[586] Abigail M. McGuire, Brian Weiner, Sang T. Park, Ilan Wapinski, Sahadevan Raman, Gregory Dolganov, Matthew Peterson, Robert Riley, Jeremy Zucker, Thomas Abeel, Jared White, Peter Sisk, Christian Stolte, Mike Koehrsen, Robert T. Yamamoto, Milena Iacobelli-Martinez, Matthew J. Kidd, Andreia M. Maer, Gary K. Schoolnik, Aviv Regev, and James Galagan. Comparative analysis of mycobacterium and related actinomycetes yields insight into the evolution of mycobacterium tuberculosis pathogenesis. *BMC Genomics*, 13(1), 3 2012.

[587] J. F. Petit, A. Adam, J. Wietzerbin-Falszpan, E. Lederer, and J. M. Ghuysen. Chemical structure of the cell wall of Mycobacterium smegmatis. I. Isolation and partial characterization of the peptidoglycan. *Biochemical and biophysical research communications*, 35(4):478–485, 5 1969.

[588] J. Wietzerbin-Falszpan, B. C. Das, I. Azuma, A. Adam, J. F. Petit, and E. Lederer. Isolation and mass spectrometric identification of the peptide subunits of mycobacterial cell walls. *Biochemical and biophysical research communications*, 40(1):57–63, 7 1970.

[589] Sergio R. Filipe, Alexander Tomasz, and Petros Ligoxygakis. Requirements of peptidoglycan structure that allow detection by the Drosophila Toll pathway. *EMBO Reports*, 6(4):327, 4 2005.

[590] Sophie Rutschmann, Alain C. Jung, Charles Hetru, Jean Marc Reichhart, Jules A. Hoffmann, and Dominique Ferrandon. The Rel Protein DIF Mediates the Antifungal but Not the Antibacterial Host Defense in Drosophila. *Immunity*, 12(5):569–580, 5 2000.

[591] Mark Austin Hanson, Lianne B. Cohen, Alice Marra, Igor Iatsenko, Steven A. Wasserman, and Bruno Lemaitre. The Drosophila Baramicin polypeptide gene protects against fungal infection. *PLOS Pathogens*, 17(8):e1009846, 8 2021.

[592] Yosuke Seto and Koichiro Tamura. Extensive Differences in Antifungal Immune Response in Two Drosophila Species Revealed by Comparative Transcriptome Analysis. *International Journal of Genomics*, 2013:15, 2013.

[593] Brian P. Lazzaro and Madeline R R. Galac. Disease Pathology: Wasting Energy Fighting Infection, 11 2006.

[594] François Leulier, Nouara Lhocine, Bruno Lemaitre, and Pascal Meier. The Drosophila Inhibitor of Apoptosis Protein DIAP2 Functions in Innate Immunity and Is Essential To Resist Gram-Negative Bacterial Infection. *Molecular and Cellular Biology*, 26(21): 7821–7831, 11 2006.

[595] Dani Osman, Nicolas Buchon, Sveta Chakrabarti, Yu Ting Huang, Wan Chi Su, Mickaël Poidevin, Yu Chen Tsai, and Bruno Lemaitre. Autocrine and paracrine unpaired signaling

regulate intestinal stem cell maintenance and division. *Journal of Cell Science*, 125(24): 5944–5949, 12 2012.

[596] Claudia Melcarne, Elodie Ramond, Jan Dudzic, Andrew J. Bretscher, Éva Kurucz, István Andó, and Bruno Lemaitre. Two Nimrod receptors, NimC1 and Eater, synergistically contribute to bacterial phagocytosis in Drosophila melanogaster. *The FEBS Journal*, 286 (14):2670–2691, 7 2019.

[597] Crystal M. Vincent, Carolina J. Simoes da Silva, Ashima Wadhawan, and Marc S. Dionne. Origins of Metabolic Pathology in Francisella-Infected Drosophila. *Frontiers in Immunology*, 11:514637, 7 2020.

[598] Lianne B. Cohen, Scott A. Lindsay, Yangyang Xu, Samuel J.H. Lin, and Steven A. Wasserman. The Daisho Peptides Mediate Drosophila Defense Against a Subset of Filamentous Fungi. *Frontiers in Immunology*, 11:506003, 1 2020.

[599] Jyothsna Ramesh Kumar, Jessica P. Smith, Hyeogsun Kwon, and Ryan C. Smith. Use of Clodronate Liposomes to Deplete Phagocytic Immune Cells in Drosophila melanogaster and Aedes aegypti. *Frontiers in Cell and Developmental Biology*, 9, 2 2021.

[600] Julia Y. Kam, Elinor Hortle, Elizabeth Krogman, Sherridan E. Warner, Kathryn Wright, Kaiming Luo, Tina Cheng, Pradeep Manuneedhi Cholan, Kazu Kikuchi, James A. Triccas, Warwick J. Britton, Matt D. Johansen, Laurent Kremer, and Stefan H. Oehlers. Rough and smooth variants of Mycobacterium abscessus are differentially controlled by host immunity during chronic infection of adult zebrafish. *Nature Communications 2022 13:1*, 13(1):1–11, 2 2022.

[601] Otmane Lamrabet and Michel Drancourt. Genetic engineering of Mycobacterium tuberculosis: A review. *Tuberculosis*, 92(5):365–376, 9 2012.

[602] Katlyn Borgers, Kristof Vandewalle, Nele Festjens, and Nico Callewaert. A guide to Mycobacterium mutagenesis. *The FEBS Journal*, 286(19):3757–3774, 10 2019.

[603] Stoyan Bardarov, Jordan Kriakov, Christian Carriere, Shengwei Yu, Carlos Vaamonde, Ruth A. Mcadam, Barry R. Bloom, Graham F. Hatfull, and William R. Jacobs. Conditionally replicating mycobacteriophages: A system for transposon delivery to Mycobacterium tuberculosis. *Proceedings of the National Academy of Sciences of the United States of America*, 94(20):10961, 9 1997.

[604] Halima Medjahed and Jean Marc Reyrat. Construction of mycobacterium abscessus defined glycopeptidolipid mutants: Comparison of genetic tools. *Applied and Environmental Microbiology*, 75(5):1331–1338, 2009.

[605] Mélanie Cortes, Anil Kumar Singh, Jean Marc Reyrat, Jean Louis Gaillard, Xavier Nassif, and Jean Louis Herrmann. Conditional gene expression in mycobacterium abscessus. *PLoS ONE*, 6(12), 12 2011.

[606] Albertus Viljoen, Ana Victoria Gutiérrez, Christian Dupont, Eric Ghigo, and Laurent Kremer. A simple and rapid gene disruption strategy in Mycobacterium abscessus: On the design and application of glycopeptidolipid mutants. *Frontiers in Cellular and Infection Microbiology*, 8(MAR), 3 2018.

[607] Natalia Kurepina, Liang Chen, Kaelea Composto, Dalin Rifat, Eric L. Nuermberger, and Barry N. Kreiswirth. CRISPR Inhibition of Essential Peptidoglycan Biosynthesis Genes in

Mycobacterium abscessus and Its Impact on β-Lactam Susceptibility. *Antimicrobial agents and chemotherapy*, 66(4), 4 2022.

[608] Dalin Rifat, Liang Chen, Barry N. Kreiswirth, and Eric L. Nuermberger. Genome-wide essentiality analysis of mycobacterium abscessus by saturated transposon mutagenesis and deep sequencing. *mBio*, 12(3), 6 2021.

[609] F. Bigi, A. Alito, J. C. Fisanotti, M. I. Romano, and A. Cataldi. Characterization of a novel Mycobacterium bovis secreted antigen containing PGLTS repeats. *Infection and Immunity*, 63(7):2581, 1995.

[610] François Xavier Berthet, Micheline Lagranderie, Pierre Gounon, Christine Laurent-Winter, Danielle Ensergueix, Pierre Chavarot, Françoise Thouron, Eddie Maranghi, Vladimir Pelicic, Denis Portnoï, Gilles Marchal, and Brigitte Gicquel. Attenuation of virulence by disruption of the Mycobacterium tuberculosis erp gene. *Science*, 282(5389):759–762, 10 1998.

[611] L. de Mendonça-Lima, M. Picardeau, C. Raynaud, J. Rauzier, Y. O. Goguet de la Salmonière, L. Barker, F. Bigi, A. Cataldi, B. Gicquel, and J. M. Reyrat. Erp, an extracellular protein family specific to mycobacteria. *Microbiology*, 147(8):2315–2320, 8 2001.

[612] Leila de Mendonça-Lima, Yann Bordat, Elisabeth Pivert, Chiara Recchi, Olivier Neyrolles, Aboubakar Maitournam, Brigitte Gicquel, and Jean Marc Reyrat. The allele encoding the mycobacterial Erp protein affects lung disease in mice. *Cellular Microbiology*, 5(1):65–73, 1 2003.

[613] Dana Kocíncová, Berit Sondén, Leila De Mendonça-Lima, Brigitte Gicquel, and Jean Marc Reyrat. The Erp protein is anchored at the surface by a carboxy-terminal hydrophobic domain and is important for cell-wall structure in Mycobacterium smegmatis. *FEMS Microbiology Letters*, 231(2):191–196, 2 2004.

[614] Christine L. Cosma, Kathryn Klein, Rosa Kim, Dana Beery, and Lalita Ramakrishnan. Mycobacterium marinum Erp Is a Virulence Determinant Required for Cell Wall Integrity and Intracellular Survival. *Infection and Immunity*, 74(6):3125, 6 2006.

[615] Dana Kocíncová, Berit Sondén, Yann Bordat, Elisabeth Pivert, Leila De Mendonça-Lima, Brigitte Gicquel, and Jean Marc Reyrat. The Hydrophobic Domain of the Mycobacterial Erp Protein Is Not Essential for the Virulence of Mycobacterium tuberculosis. *Infection and Immunity*, 72(4):2379, 4 2004.

[616] F. Bigi, A. Gioffré, L. Klepp, M. P. Santangelo, C. A. Velicovsky, G. H. Giambartolomei, C. A. Fossati, M. I. Romano, T. Mendum, J. J. McFadden, and A. Cataldi. Mutation in the P36 gene of Mycobacterium bovis provokes attenuation of the bacillus in a mouse model. *Tuberculosis*, 85(4):221–226, 7 2005.

[617] Sergio Arruda, Gloria Bomfim, Ronald Knights, Tellervo Huima-Byron, and Lee W. Riley. Cloning of an M. tuberculosis DNA fragment associated with entry and survival inside cells. *Science*, 261(5127):1454–1457, 1993.

[618] Bruno Flesselles, Naveen N. Anand, Jack Remani, Sheena M. Loosmore, and Michel H. Klein. Disruption of the mycobacterial cell entry gene of Mycobacterium bovis BCG results in a mutant that exhibits a reduced invasiveness for epithelial cells. *FEMS Microbiology Letters*, 177(2):237–242, 8 1999.

[619] Nobuyuki Shimono, Lisa Morici, Nicola Casali, Sally Cantrell, Ben Sidders, Sabine Ehrt, and Lee W. Riley. Hypervirulent mutant of Mycobacterium tuberculosis resulting from disruption of the mce1 operon. *Proceedings of the National Academy of Sciences of the United States of America*, 100(26):15918–15923, 12 2003.

[620] Andrea Gioffré, Eduardo Infante, Diana Aguilar, María De La Paz Santangelo, Laura Klepp, Ariel Amadio, Virginia Meikle, Ignacio Etchechoury, María Isabel Romano, Angel Cataldi, Rogelio Pando Hernández, and Fabiana Bigi. Mutation in mce operons attenuates Mycobacterium tuberculosis virulence. *Microbes and Infection*, 7(3):325–334, 3 2005.

[621] Jun Ishikawa, Atsushi Yamashita, Yuzuru Mikami, Yasutaka Hoshino, Haruyo Kurita, Kunimoto Hotta, Tadayoshi Shiba, and Masahira Hattori. The complete genomic sequence of Nocardia farcinica IFM 10152. Technical report, 2004.

[622] Ryan H. Senaratne, Ben Sidders, Patricia Sequeira, Grainne Saunders, Kathleen Dunphy, Olivera Marjanovic, J. Rachel Reader, Patricia Lima, Stephen Chan, Sharon Kendall, Johnjoe McFadden, and Lee W. Riley. Mycobacterium tuberculosis strains disrupted in mce3 and mce4 operons are attenuated in mice. *Journal of medical microbiology*, 57(Pt 2):164–170, 2 2008.

[623] Amit K. Pandey and Christopher M. Sassetti. Mycobacterial persistence requires the utilization of host cholesterol. *Proceedings of the National Academy of Sciences of the United States of America*, 105(11):4376, 3 2008.

[624] Nicola Casali and Lee W. Riley. A phylogenomic analysis of the Actinomycetales mce operons. *BMC Genomics*, 8(1):1–23, 2 2007.

[625] Ashwani Kumar, Amita Chandolia, Uma Chaudhry, Vani Brahmachari, and Mridula Bose. Comparison of mammalian cell entry operons of mycobacteria: in silico analysis and expression profiling. *FEMS immunology and medical microbiology*, 43(2):185–195, 2 2005.

[626] Laura I. Klepp, Julia Sabio y Garcia, and FabianaBigi. Mycobacterial MCE proteins as transporters that control lipid homeostasis of the cell wall. *Tuberculosis*, 132:102162, 1 2022.

[627] William W. Mohn, Robert Van Der Geize, Gordon R. Stewart, Sachi Okamoto, Jie Liu, Lubbert Dijkhuizen, and Lindsay D. Eltis. The actinobacterial mce4 locus encodes a steroid transporter. *The Journal of biological chemistry*, 283(51):35368–35374, 12 2008.

[628] Laura I. Klepp, Marina A. Forrellad, Ana V. Osella, Federico C. Blanco, Emma J. Stella, María Verónica Bianco, María de la Paz Santangelo, Cristopher Sassetti, Mary Jackson, Angel A. Cataldi, Fabiana Bigi, and Héctor R. Morbidoni. Impact of the deletion of the six mce operons in Mycobacterium smegmatis. *Microbes and infection*, 14(7-8):590–599, 7 2012.

[629] Evgeniya V. Nazarova, Christine R. Montague, Thuy La, Kaley M. Wilburn, Neelima Sukumar, Wonsik Lee, Shannon Caldwell, David G. Russell, and Brian C. VanderVen. Rv3723/LucA coordinates fatty acid and cholesterol uptake in Mycobacterium tuberculosis. *eLife*, 6, 6 2017.

[630] Laura Rank, Laura E. Herring, and Miriam Braunstein. Evidence for the mycobacterial mce4 transporter being a multiprotein complex. *Journal of Bacteriology*, 203(10), 5 2021.

[631] Jieru Wang, Xiaojie Zhu, Yongchong Peng, Tingting Zhu, Han Liu, Yifan Zhu, Xuekai Xiong, Xi Chen, Changmin Hu, Huanchun Chen, Yingyu Chen, and Aizhen Guo. Mycobacterium tuberculosis YrbE3A Promotes Host Innate Immune Response by Targeting NF-κB/JNK Signaling. *Microorganisms*, 8(4):584, 4 2020.

[632] Yushu Chen, Yuchun Wang, and Shu-Sin Chng. A conserved membrane protein negatively regulates Mce1 complexes in mycobacteria. *Nature Communications 2023 14:1*, 14(1): 1–11, 9 2023.

[633] Philip S. Renshaw, Parthena Panagiotidou, Adam Whelan, Stephen V. Gordon, R. Glyn Hewinson, Richard A. Williamson, and Mark D. Carr. Conclusive evidence that the major T-cell antigens of the Mycobacterium tuberculosis complex ESAT-6 and CFP-10 form a tight, 1:1 complex and characterization of the structural properties of ESAT-6, CFP-10, and the ESAT-6*CFP-10 complex. Implications for pathogenesis and virulence. *The Journal of biological chemistry*, 277(24):21598–21603, 6 2002.

[634] Christian Poulsen, Santosh Panjikar, Simon J. Holton, Matthias Wilmanns, and Young Hwa Song. WXG100 Protein Superfamily Consists of Three Subfamilies and Exhibits an α-Helical C-Terminal Conserved Residue Pattern. *PLOS ONE*, 9(2):e89313, 2 2014.

[635] N. C. Gey Van Pittius, J. Gamieldien, W. Hide, G. D. Brown, R. J. Siezen, and A. D. Beyers. The ESAT-6 gene cluster of Mycobacterium tuberculosis and other high G+C Gram-positive bacteria. *Genome biology*, 2(10), 2001.

[636] Mark J. Pallen. The ESAT-6/WXG100 superfamily - And a new Gram-positive secretion system? *Trends in Microbiology*, 10(5):209–212, 5 2002.

[637] Monica L. Burts, Wade A. Williams, Kristin DeBord, and Dominique M. Missiakas. EsxA and EsxB are secreted by an ESAT-6-like system that is required for the pathogenesis of Staphylococcus aureus infections. *Proceedings of the National Academy of Sciences of the United States of America*, 102(4):1169–1174, 1 2005.

[638] Oren S. Rosenberg, Dustin Dovala, Xueming Li, Lynn Connolly, Anastasia Bendebury, Janet Finer-Moore, James Holton, Yifan Cheng, Robert M. Stroud, and Jeffery S. Cox. Substrates Control Multimerization and Activation of the Multi-Domain ATPase Motor of Type VII Secretion. *Cell*, 161(3):501–512, 4 2015.

[639] Maria H. Daleke, Roy Ummels, Punto Bawono, Jaap Heringa, Christina M.J.E. Vandenbroucke-Grauls, Joen Luirink, and Wilbert Bitter. General secretion signal for the mycobacterial type VII secretion pathway. *Proceedings of the National Academy of Sciences of the United States of America*, 109(28):11342–11347, 7 2012.

[640] Benjamin Gold, G. Marcela Rodriguez, Salvatore A.E. Marras, Mickey Pentecost, and Issar Smith. The Mycobacterium tuberculosis IdeR is a dual functional regulator that controls transcription of genes involved in iron acquisition, iron storage and survival in macrophages. *Molecular microbiology*, 42(3):851–865, 2001.

[641] Dirk Schnappinger, Sabine Ehrt, Martin I. Voskuil, Yang Liu, Joseph A. Mangan, Irene M. Monahan, Gregory Dolganov, Brad Efron, Philip D. Butcher, Carl Nathan, and Gary K. Schoolnik. Transcriptional Adaptation of Mycobacterium tuberculosis within Macrophages: Insights into the Phagosomal Environment. *The Journal of Experimental Medicine*, 198(5): 693, 9 2003.

[642] Juliano Timm, Frank A. Post, Linda Gail Bekker, Gabriele B. Walther, Helen C. Wainwright, Riccardo Manganelli, Wai Tsing Chan, Liana Tsenova, Benjamin Gold, Issar Smith,

Gilla Kaplan, and John D. McKinney. Differential expression of iron-, carbon-, and oxygen-responsive mycobacterial genes in the lungs of chronically infected mice and tuberculosis patients. *Proceedings of the National Academy of Sciences of the United States of America*, 100(24):14321, 11 2003.

[643] G. A. Snow and A. J. White. Chemical and biological properties of mycobactins isolated from various mycobacteria. *Biochemical Journal*, 115(5):1031, 1969.

[644] Jovana Gobin, Christopher H. Moore, Joseph R. Reeve, Diane K. Wong, Bradford W. Gibson, and Marcus A. Horwitz. Iron acquisition by Mycobacterium tuberculosis: isolation and characterization of a family of iron-binding exochelins. *Proceedings of the National Academy of Sciences of the United States of America*, 92(11):5189, 5 1995.

[645] Glennon V. Bythrow, Manal F. Farhat, Keith Levendosky, Poornima Mohandas, Gabrielle A. Germain, Barney Yoo, and Luis E.N. Quadri. Mycobacterium abscessus Mutants with a Compromised Functional Link between the Type VII ESX-3 System and an Iron Uptake Mechanism Reliant on an Unusual Mycobactin Siderophore. *Pathogens*, 11(9), 9 2022.

[646] G. Marcela Rodriguez and Issar Smith. Identification of an ABC Transporter Required for Iron Acquisition and Virulence in Mycobacterium tuberculosis. *Journal of Bacteriology*, 188 (2):424, 1 2006.

[647] Fabian M. Arnold, Miriam S. Weber, Imre Gonda, Marc J. Gallenito, Sophia Adenau, Pascal Egloff, Iwan Zimmermann, Cedric A.J. Hutter, Lea M. Hürlimann, Eike E. Peters, Jörn Piel, Gabriele Meloni, Ohad Medalia, and Markus A. Seeger. The ABC exporter IrtAB imports and reduces mycobacterial siderophores. *Nature*, 580(7803):413–417, 4 2020.

[648] Michelle B. Ryndak, Shuishu Wang, Issar Smith, and G. Marcela Rodriguez. The Mycobacterium tuberculosis High-Affinity Iron Importer, IrtA, Contains an FAD-Binding Domain. *Journal of Bacteriology*, 192(3):861, 2 2010.

[649] Aisha Farhana, Sandeep Kumar, Shailendra S. Rathore, Prahlad C. Ghosh, Nasreen Z. Ehtesham, Anil K. Tyagi, and Seyed E. Hasnain. Mechanistic Insights into a Novel Exporter-Importer System of Mycobacterium tuberculosis Unravel Its Role in Trafficking of Iron. *PLoS ONE*, 3(5), 5 2008.

[650] Juan M Belardinelli, Divya Arora, Charlotte Avanzi, William H Wheat, Josephine M Bryant, John S Spencer, Tom L Blundell, Julian Parkhill, R Andres Floto, and Mary Jackson. Clinically relevant mutations in the PhoR sensor kinase of host-adapted Mycobacterium abscessus isolates impact response to acidic pH and virulence. *Microbiology spectrum*, page e0158823, 10 2023.

[651] Sujatha M. Santhanagopalan and G. Marcela Rodriguez. Examining the role of Rv2895c (viuB) in iron acquisition in Mycobacterium tuberculosis. *Tuberculosis (Edinburgh, Scotland)*, 92(1):60, 1 2012.

[652] Lawrence G. Wayne and L. G. Hayes. Nitrate reduction as a marker for hypoxic shiftdown of Mycobacterium tuberculosis. *Tubercle and Lung Disease*, 79(2):127–132, 1 1998.

[653] Rajoana Rojony, Lia Danelishvili, Anaamika Campeau, Jacob M. Wozniak, David J. Gonzalez, and Luiz E. Bermudez. Exposure of mycobacterium abscessus to environmental stress and clinically used antibiotics reveals common proteome response among pathogenic mycobacteria. *Microorganisms*, 8(5), 5 2020.

[654] Sven Malm, Yvonne Tiffert, Julia Micklinghoff, Sonja Schultze, Insa Joost, Isabel Weber, Sarah Horst, Birgit Ackermann, Mascha Schmidt, Wolfgang Wohlleben, Stefan Ehlers, Robert Geffers, Jens Reuther, and Franz Christoph Bange. The roles of the nitrate reductase NarGHJI, the nitrite reductase NirBD and the response regulator GlnR in nitrate assimilation of Mycobacterium tuberculosis. *Microbiology*, 155(4):1332–1339, 4 2009.

[655] Shamim Akhtar, Arshad Khan, Charles D. Sohaskey, Chinnaswamy Jagannath, and Dhiman Sarkar. Nitrite reductase NirBD is induced and plays an important role during in vitro dormancy of Mycobacterium tuberculosis. *Journal of Bacteriology*, 195(20): 4592–4599, 2013.

[656] Mai Ping Tan, Patricia Sequeira, Wen Wei Lin, Wai Yee Phong, Penelope Cliff, Seow Hwee Ng, Boon Heng Lee, Luis Camacho, Dirk Schnappinger, Sabine Ehrt, Thomas Dick, Kevin Pethe, and Sylvie Alonso. Nitrate Respiration Protects Hypoxic Mycobacterium tuberculosis Against Acid- and Reactive Nitrogen Species Stresses. *PLoS ONE*, 5(10): 13356, 2010.

[657] Shubhada R. Hegde. Computational Identification of the Proteins Associated With Quorum Sensing and Biofilm Formation in Mycobacterium tuberculosis. *Frontiers in Microbiology*, 10:479640, 1 2020.

[658] S. T. Cole, R. Brosch, J. Parkhill, T. Garnier, C. Churcher, D. Harris, S. V. Gordon, K. Eiglmeier, S. Gas, C. E. Barry, F. Tekaia, K. Badcock, D. Basham, D. Brown, T. Chillingworth, R. Connor, R. Davies, K. Devlin, T. Feltwell, S. Gentles, N. Hamlin, S. Holroyd, T. Hornsby, K. Jagels, A. Krogh, J. McLean, S. Moule, L. Murphy, K. Oliver, J. Osborne, M. A. Quail, M. A. Rajandream, J. Rogers, S. Rutter, K. Seeger, J. Skelton, R. Squares, S. Squares, J. E. Sulston, K. Taylor, S. Whitehead, and B. G. Barrell. Deciphering the biology of Mycobacterium tuberculosis from the complete genome sequence. *Nature*, 393(6685):537–544, 6 1998.

[659] Amy Cunningham-Bussel, Tuo Zhang, and Carl F. Nathan. Nitrite produced by Mycobacterium tuberculosis in human macrophages in physiologic oxygen impacts bacterial ATP consumption and gene expression. *Proceedings of the National Academy of Sciences of the United States of America*, 110(45), 11 2013.

[660] Kerstin J. Williams, Victoria A. Jenkins, Geraint R. Barton, William A. Bryant, Nitya Krishnan, and Brian D. Robertson. Deciphering the metabolic response of Mycobacterium tuberculosis to nitrogen stress. *Molecular Microbiology*, 97(6):1142–1157, 9 2015.

[661] Victoria A. Jenkins, Geraint R. Barton, Brian D. Robertson, and Kerstin J. Williams. Genome wide analysis of the complete GlnR nitrogen-response regulon in Mycobacterium smegmatis. *BMC Genomics*, 14(1):301, 5 2013.

[662] Junsheng Fan, Yaping Jia, Siyuan He, Zhili Tan, Anqi Li, Juan Li, Zhemin Zhang, Bing Li, and Haiqing Chu. GlnR Activated Transcription of Nitrogen Metabolic Pathway Genes Facilitates Biofilm Formation by Mycobacterium abscessus. *International Journal of Antimicrobial Agents*, 63(1):107025, 1 2024.

[663] Robert Van Der Geize, Katherine Yam, Thomas Heuser, Maarten H Wilbrink, Hirofumi Hara, Matthew C Anderton, Edith Sim, Lubbert Dijkhuizen, Julian E Davies, William W Mohn, and Lindsay D Eltis. A gene cluster encoding cholesterol catabolism in a soil actinomycete provides insight into Mycobacterium tuberculosis survival in macrophages. Technical report, 2007.

[664] Katherine C. Yam, Igor D'Angelo, Rainer Kalscheuer, Haizhong Zhu, Jian Xin Wang, Victor Snieckus, Lan H. Ly, Paul J. Converse, William R. Jacobs, Natalie Strynadka, and Lindsay D. Eltis. Studies of a Ring-Cleaving Dioxygenase Illuminate the Role of Cholesterol Metabolism in the Pathogenesis of Mycobacterium tuberculosis. *PLoS Pathogens*, 5(3): 1000344, 3 2009.

[665] Jennifer C. Chang, Maurine D. Miner, Amit K. Pandey, Wendy P. Gill, Nada S. Harik, Christopher M. Sassetti, and David R. Sherman. igr Genes and Mycobacterium tuberculosis Cholesterol Metabolism. *Journal of Bacteriology*, 191(16):5232, 8 2009.

[666] Yanmin Hu, Robert Van Der Geize, Gurdyal S. Besra, Sudagar S. Gurcha, Alexander Liu, Manfred Rohde, Mahavir Singh, and Anthony Coates. 3-Ketosteroid 9alpha-hydroxylase is an essential factor in the pathogenesis of Mycobacterium tuberculosis. *Molecular microbiology*, 75(1):107–121, 1 2010.

[667] Jennifer E. Griffin, Amit K. Pandey, Sarah A. Gilmore, Valerie Mizrahi, John D. McKinney, Carolyn R. Bertozzi, and Christopher M. Sassetti. Cholesterol catabolism by Mycobacterium tuberculosis requires transcriptional and metabolic adaptations. *Chemistry & biology*, 19(2):218, 2 2012.

[668] Wonsik Lee, Brian C. VanderVen, Ruth J. Fahey, and David G. Russell. Intracellular Mycobacterium tuberculosis Exploits Host-derived Fatty Acids to Limit Metabolic Stress. *The Journal of Biological Chemistry*, 288(10):6788, 3 2013.

[669] Jennifer E. Griffin, Jeffrey D. Gawronski, Michael A. DeJesus, Thomas R. Ioerger, Brian J. Akerley, and Christopher M. Sassetti. High-Resolution Phenotypic Profiling Defines Genes Essential for Mycobacterial Growth and Cholesterol Catabolism. *PLoS Pathogens*, 7(9): 1002251, 9 2011.

[670] Kaley M. Wilburn, Rachael A. Fieweger, and Brian C. VanderVen. Cholesterol and fatty acids grease the wheels of Mycobacterium tuberculosis pathogenesis. *Pathogens and Disease*, 76(2):21, 3 2018.

[671] Rochelle van Wyk, Mari van Wyk, Samson Sitheni Mashele, David R. Nelson, and Khajamohiddin Syed. Comprehensive Comparative Analysis of Cholesterol Catabolic Genes/Proteins in Mycobacterial Species. *International Journal of Molecular Sciences*, 20(5), 3 2019.

[672] Israël Casabon, Kendra Swain, Adam M. Crowe, Lindsay D. Eltis, and William W. Mohn. Actinobacterial acyl coenzyme A synthetases involved in steroid side-chain catabolism. *Journal of bacteriology*, 196(3):579–587, 2 2014.

[673] Natalia Wrońska, Anna Brzostek, Rafał Szewczyk, Adrian Soboń, Jarosław Dziadek, and Katarzyna Lisowska. The Role of fadD19 and echA19 in Sterol Side Chain Degradation by Mycobacterium smegmatis. *Molecules*, 21(5), 5 2016.

[674] Xinxin Yang, Natasha M. Nesbitt, Eugenie Dubnau, Issar Smith, and Nicole S. Sampson. Cholesterol Metabolism Increases the Metabolic Pool of Propionate in M. tuberculosis. *Biochemistry*, 48(18):3819, 5 2009.

[675] Suzanne T. Thomas, Brian C. VanderVen, David R. Sherman, David G. Russell, and Nicole S. Sampson. Pathway Profiling in Mycobacterium tuberculosis: ELUCIDATION OF CHOLESTEROL-DERIVED CATABOLITE AND ENZYMES THAT CATALYZE ITS METABOLISM*. *The Journal of Biological Chemistry*, 286(51):43668, 12 2011.

[676] Ernesto J. Muñoz-Elías, Anna M. Upton, Joseph Cherian, and John D. McKinney. Role of the methylcitrate cycle in Mycobacterium tuberculosis metabolism, intracellular growth, and virulence. *Molecular Microbiology*, 60(5):1109–1122, 6 2006.

[677] Anna M. Upton and John D. McKinney. Role of the methylcitrate cycle in propionate metabolism and detoxification in Mycobacterium smegmatis. *Microbiology (Reading, England)*, 153(Pt 12):3973–3982, 12 2007.

[678] Suzana Savvi, Digby F. Warner, Bavesh D. Kana, John D. McKinney, Valerie Mizrahi, and Stephanie S. Dawes. Functional Characterization of a Vitamin B12-Dependent Methylmalonyl Pathway in Mycobacterium tuberculosis: Implications for Propionate Metabolism during Growth on Fatty Acids. *Journal of Bacteriology*, 190(11):3886, 6 2008.

[679] Hyungjin Eoh and Kyu Y. Rhee. Methylcitrate cycle defines the bactericidal essentiality of isocitrate lyase for survival of mycobacterium tuberculosis on fatty acids. *Proceedings of the National Academy of Sciences of the United States of America*, 111(13):4976–4981, 4 2014.

[680] Ty A. Gould, Helmus Van De Langemheen, Ernesto J. Muñoz-Elías, John D. McKinney, and James C. Sacchettini. Dual role of isocitrate lyase 1 in the glyoxylate and methylcitrate cycles in Mycobacterium tuberculosis. *Molecular Microbiology*, 61(4):940–947, 8 2006.

[681] John D Mckinney, Kerstin Ho, È Ner Zu Bentrup[23], Ernesto J Mun Ä Oz-Elõ Âas, Andras Miczak[23], Bing Chen, Wai-Tsing Chan, Dana Swenson[23], James C Sacchettinik, William R Jacobs, and David G Russell[23]. Persistence of Mycobacterium tuberculosis in macrophages and mice requires the glyoxylate shunt enzyme isocitrate lyase. Technical report, 2000.

[682] D. L. Rainwater and P. E. Kolattukudy. Isolation and Characterization of Acyl Coenzyme A Carboxylases from Mycobacterium tuberculosis and Mycobacterium bovis, Which Produce Multiple Methyl-Branched Mycocerosic Acids. *Journal of Bacteriology*, 151(2):905, 1982.

[683] Madhulika Jain, Christopher J. Petzold, Michael W. Schelle, Michael D. Leavell, Joseph D. Mougous, Carolyn R. Bertozzi, Julie A. Leary, and Jeffery S. Cox. Lipidomics reveals control of Mycobacterium tuberculosis virulence lipids via metabolic coupling. *Proceedings of the National Academy of Sciences of the United States of America*, 104(12):5133, 3 2007.

[684] Jeffery S. Cox, Bing Chess, Michael McNeil, and William R. Jacobs. Complex lipid determines tissue-specific replication of Mycobacterium tuberculosis in mice. *Nature*, 402 (6757):79–83, 11 1999.

[685] Rachel E. Geisel, Kaori Sakamoto, David G. Russell, and Elizabeth R. Rhoades. In Vivo Activity of Released Cell Wall Lipids of Mycobacterium bovis Bacillus Calmette-Guérin Is Due Principally to Trehalose Mycolates. *The Journal of Immunology*, 174(8):5007–5015, 4 2005.

[686] Mi Jeong Kim, Helen C. Wainwright, Michael Locketz, Linda Gail Bekker, Gabriele B. Walther, Corneli Dittrich, Annalie Visser, Wei Wang, Fong Fu Hsu, Ursula Wiehart, Liana Tsenova, Gilla Kaplan, and David G. Russell. Caseation of human tuberculosis granulomas correlates with elevated host lipid metabolism. *EMBO Molecular Medicine*, 2(7):258, 7 2010.

[687] Jaiyanth Daniel, Hédia Maamar, Chirajyoti Deb, Tatiana D. Sirakova, and Pappachan E. Kolattukudy. Mycobacterium tuberculosis Uses Host Triacylglycerol to Accumulate Lipid

Droplets and Acquires a Dormancy-Like Phenotype in Lipid-Loaded Macrophages. *PLoS Pathogens*, 7(6), 6 2011.

[688] Cody R. Ruhl, Breanna L. Pasko, Haaris S. Khan, Lexy M. Kindt, Chelsea E. Stamm, Luis H. Franco, Connie C. Hsia, Min Zhou, Colton R. Davis, Tian Qin, Laurent Gautron, Michael D. Burton, Galo L. Mejia, Dhananjay K. Naik, Gregory Dussor, Theodore J. Price, and Michael U. Shiloh. Mycobacterium tuberculosis Sulfolipid-1 Activates Nociceptive Neurons and Induces Cough. *Cell*, 181(2):293–305, 4 2020.

[689] Alisha M. Block, Sarah B. Namugenyi, Nagendra P. Palani, Alyssa M. Brokaw, Leanne Zhang, Kenneth B. Beckman, and Anna D. Tischler. Mycobacterium tuberculosis Requires the Outer Membrane Lipid Phthiocerol Dimycocerosate for Starvation-Induced Antibiotic Tolerance. *mSystems*, 8(1), 2 2023.

[690] Alessandro Michelucci, Thekla Cordes, Jenny Ghelfi, Arnaud Pailot, Norbert Reiling, Oliver Goldmann, Tina Binz, André Wegner, Aravind Tallam, Antonio Rausell, Manuel Buttini, Carole L. Linster, Eva Medina, Rudi Balling, and Karsten Hiller. Immune-responsive gene 1 protein links metabolism to immunity by catalyzing itaconic acid production. *Proceedings of the National Academy of Sciences of the United States of America*, 110(19):7820–7825, 5 2013.

[691] R. B. Clayton. The utilization of sterols by insects. *Journal of Lipid Research*, 5(1):3–19, 1 1964.

[692] Zhonghua Liu and Xun Huang. Lipid metabolism in Drosophila: development and disease. *Acta Biochimica et Biophysica Sinica*, 45(1):44–50, 1 2013.

[693] Sonali Srivastava, Sarika Chaudhary, Lipi Thukral, Ce Shi, Rinkoo D. Gupta, Radhika Gupta, K. Priyadarshan, Archana Vats, Asfarul S. Haque, Rajan Sankaranarayanan, Vivek T. Natarajan, Rakesh Sharma, Courtney C. Aldrich, and Rajesh S. Gokhale. Unsaturated Lipid Assimilation by Mycobacteria Requires Auxiliary cis-trans Enoyl CoA Isomerase. *Chemistry & Biology*, 22(12):1577–1587, 12 2015.

[694] Ida Rosenkrands, Claus Aagaard, Karin Weldingh, Inger Brock, Morten H. Dziegiel, Mahavir Singh, Søren Hoff, Pernille Ravn, and Peter Andersen. Identification of Rv0222 from RD4 as a novel serodiagnostic target for tuberculosis. *Tuberculosis*, 88(4):335–343, 7 2008.

[695] Ningning Ren, Jingfang JinLi, Yingyu Chen, Xia Zhou, Jieru Wang, Pan Ge, Farhan Anwar Khan, Li Zhang, Changmin Hu, Ian D. Robertson, Huanchun Chen, and Aizhen Guo. Identification of new diagnostic biomarkers for Mycobacterium tuberculosis and the potential application in the serodiagnosis of human tuberculosis. *Microbial biotechnology*, 11(5):893–904, 9 2018.

[696] Lin Wang, Juehui Wu, Jun Li, Hua Yang, Tianqi Tang, Haijiao Liang, Mianyong Zuo, Jie Wang, Haipeng Liu, Feng Liu, Jianxia Chen, Zhonghua Liu, Yang Wang, Cheng Peng, Xiangyang Wu, Ruijuan Zheng, Xiaochen Huang, Yajun Ran, Zihe Rao, and Baoxue Ge. Host-mediated ubiquitination of a mycobacterial protein suppresses immunity. *Nature*, 577 (7792):682–688, 1 2020.

[697] Tina Truong and Bennett H. Penn. An M. tuberculosis Metabolic Enzyme Moonlights as an Anti-Inflammatory Effector Protein. *Cell Host & Microbe*, 27(3):310–312, 3 2020.

[698] Michal Bar-Oz, Michal Meir, and Daniel Barkan. Virulence-Associated Secretion in Mycobacterium abscessus. *Frontiers in Immunology*, 13:938895, 7 2022.

[699] Kenan C. Murphy, Samantha J. Nelson, Subhalaxmi Nambi, Kadamba Papavinasasundaram, Christina E. Baer, and Christopher M. Sassetti. Orbit: A new paradigm for genetic engineering of mycobacterial chromosomes. *mBio*, 9(6):1–20, 2018.

[700] G. Marcela Rodriguez, Martin I. Voskuil, Benjamin Gold, Gary K. Schoolnik, and Issar Smith. ideR, an Essential Gene in Mycobacterium tuberculosis: Role of IdeR in Iron-Dependent Gene Expression, Iron Metabolism, and Oxidative Stress Response. *Infection and Immunity*, 70(7):3371, 2002.

[701] Ernesto J. Muñoz-Elías and John D. McKinney. Mycobacterium tuberculosis isocitrate lyases 1 and 2 are jointly required for in vivo growth and virulence. *Nature Medicine*, 11 (6):638–644, 6 2005.

[702] Ruchi Pandey and G. Marcela Rodriguez. IdeR is required for iron homeostasis and virulence in Mycobacterium tuberculosis. *Molecular Microbiology*, 91(1):98–109, 1 2014.

[703] Marina A. Forrellad, Cristina L. Vázquez, Federico C. Blanco, Laura I. Klepp, Elizabeth A. García, Rosana V. Rocha, Villafañe Luciana, María M. Bigi, Maximiliano G. Gutierrez, and Fabiana Bigi. Rv2617c and P36 are virulence factors of pathogenic mycobacteria involved in resistance to oxidative stress. *Virulence*, 10(1):1026, 1 2019.

[704] Arsheed Ahmad Ganaie, Garima Trivedi, Amanpreet Kaur, Sidharth Shankar Jha, Shashi Anand, Vibhuti Rana, Amit Singh, Shekhar Kumar, and Charu Sharma. Interaction of Erp Protein of Mycobacterium tuberculosis with Rv2212 Enhances Intracellular Survival of Mycobacterium smegmatis. *Journal of Bacteriology*, 198(20):2841, 10 2016.

[705] P. Vineel Reddy, Rupangi Verma Puri, Priyanka Chauhan, Ritika Kar, Akshay Rohilla, Aparna Khera, and Anil K. Tyagi. Disruption of Mycobactin Biosynthesis Leads to Attenuation of Mycobacterium tuberculosis for Growth and Virulence. *The Journal of Infectious Diseases*, 208(8):1255–1265, 10 2013.

[706] Brian C. VanderVen, Ruth J. Fahey, Wonsik Lee, Yancheng Liu, Robert B. Abramovitch, Christine Memmott, Adam M. Crowe, Lindsay D. Eltis, Emanuele Perola, David D. Deininger, Tiansheng Wang, Christopher P. Locher, and David G. Russell. Novel Inhibitors of Cholesterol Degradation in Mycobacterium tuberculosis Reveal How the Bacterium's Metabolism Is Constrained by the Intracellular Environment. *PLoS Pathogens*, 11(2), 2015.

[707] Kaley M. Wilburn, Christine R. Montague, Bo Qin, Ashley K. Woods, Melissa S. Love, Case W. McNamara, Peter G. Schultz, Teresa L. Southard, Lu Huang, H. Michael Petrassi, and Brian C. VanderVen. Pharmacological and genetic activation of cAMP synthesis disrupts cholesterol utilization in Mycobacterium tuberculosis. *PLOS Pathogens*, 18(2): e1009862, 2 2022.

[708] Monique E. Theriault, Davide Pisu, Kaley M. Wilburn, Gabrielle Lê-Bury, Case W. MacNamara, H. Michael Petrassi, Melissa Love, Jeremy M. Rock, Brian C. VanderVen, and David G. Russell. Iron limitation in M. tuberculosis has broad impact on central carbon metabolism. *Communications Biology*, 5(1), 12 2022.

[709] Lisa Craig, Michael E. Pique, and John A. Tainer. Type IV pilus structure and bacterial pathogenicity. *Nature Reviews Microbiology 2004 2:5*, 2(5):363–378, 5 2004.

[710] Mladen Tomich, Paul J. Planet, and David H. Figurski. The tad locus: postcards from the widespread colonization island. *Nature Reviews Microbiology 2007 5:5*, 5(5):363–375, 5 2007.

[711] Scott C Kachlany, Paul J Planet, Mrinal K Bhattacharjee, Evyenia Kollia, Rob Desalle, Daniel H Fine, and David H Figurski. Nonspecific Adherence by Actinobacillus actinomycetemcomitans Requires Genes Widespread in Bacteria and Archaea. Technical Report 21, 2000.

[712] Scott C. Kachlany, Paul J. Planet, Rob DeSalle, Daniel H. Fine, David H. Figurski, and Jeffrey B. Kaplan. flp-1, the first representative of a new pilin gene subfamily, is required for non-specific adherence of Actinobacillus actinomycetemcomitans. *Molecular microbiology*, 40(3):542–554, 2001.

[713] Helen C. Schreiner, Kathy Sinatra, Jeffrey B. Kaplan, David Furgang, Scott C. Kachlany, Paul J. Planet, Brenda A. Perez, David H. Figurski, and Daniel H. Fine. Tight-adherence genes of Actinobacillus actinomycetemcomitans are required for virulence in a rat model. *Proceedings of the National Academy of Sciences of the United States of America*, 100 (12):7295, 6 2003.

[714] Lia Danelishvili, Yoshitaka Yamazaki, Jeannie Selker, and Luiz E. Bermudez. Secreted Mycobacterium tuberculosis Rv3654c and Rv3655c Proteins Participate in the Suppression of Macrophage Apoptosis. *PLoS ONE*, 5(5), 2010.

[715] Katherine M. Mann, Aaron C. Pride, Kelly Flentie, Jacqueline M. Kimmey, Leslie A. Weiss, and Christina L. Stallings. Analysis of the contribution of MTP and the predicted Flp pilus genes to Mycobacterium tuberculosis pathogenesis. *Microbiology*, 162(10):1784, 10 2016.

[716] Scott C. Kachlany, Paul J. Planet, Rob DeSalle, Daniel H. Fine, and David H. Figurski. Genes for tight adherence of Actinobacillus actinomycetemcomitans: from plaque to plague to pond scum. *Trends in microbiology*, 9(9):429–437, 9 2001.

[717] Matteo Tassinari, Marta Rudzite, Alain Filloux, and Harry H. Low. Assembly mechanism of a Tad secretion system secretin-pilotin complex. *Nature Communications 2023 14:1*, 14 (1):1–13, 9 2023.

[718] Mladen Tomich, Daniel H. Fine, and David H. Figurski. The TadV protein of Actinobacillus actinomycetemcomitans is a novel aspartic acid prepilin peptidase required for maturation of the Flp1 pilin and TadE and TadF pseudopilins. *Journal of bacteriology*, 188(19): 6899–6914, 10 2006.

[719] Mikkel Klausen, Arne Heydorn, Paula Ragas, Lotte Lambertsen, Anders Aaes-Jørgensen, Søren Molin, and Tim Tolker-Nielsen. Biofilm formation by Pseudomonas aeruginosa wild type, flagella and type IV pili mutants. *Molecular Microbiology*, 48(6):1511–1524, 6 2003.

[720] Sophie De Bentzmann, Marianne Aurouze, Geneviève Ball, and Alain Filloux. FppA, a Novel Pseudomonas aeruginosa Prepilin Peptidase Involved in Assembly of Type IVb Pili. *Journal of Bacteriology*, 188(13):4851, 7 2006.

[721] Kyosuke Yamamoto, Hiroyuki Arai, Masaharu Ishii, and Yasuo Igarashi. Involvement of Flagella-Driven Motility and Pili in Pseudomonas aeruginosa Colonization at the Air-Liquid Interface. *Microbes and Environments*, 27(3):320, 2012.

[722] Nam Vo, Benjamin S. Sidner, Yafan Yu, and Kurt H. Piepenbrink. Type IV Pilus-Mediated Inhibition of Acinetobacter baumannii Biofilm Formation by Phenothiazine Compounds. *Microbiology spectrum*, 11(4), 8 2023.

[723] Christopher J. Alteri, Nora Rios-Sarabia, Miguel A. De la Cruz, Jorge A. González-y Merchand, Jorge Soria-Bustos, Carmen Maldonado-Bernal, María L. Cedillo, Jorge A.

Yáñez-Santos, Ygnacio Martínez-Laguna, Javier Torres, Richard L. Friedman, Jorge A. Girón, and Miguel A. Ares. The Flp type IV pilus operon of Mycobacterium tuberculosis is expressed upon interaction with macrophages and alveolar epithelial cells. *Frontiers in Cellular and Infection Microbiology*, 12:916247, 9 2022.

[724] Dario R. Alessi, Mirjana Andjelkovic, Barry Caudwell, Peter Cron, Nick Morrice, Philip Cohen, and Brian A. Hemmings. Mechanism of activation of protein kinase B by insulin and IGF-1. *The EMBO Journal*, 15(23):6541, 12 1996.

[725] Michael P. Scheid, Paola A. Marignani, and James R. Woodgett. Multiple phosphoinositide 3-kinase-dependent steps in activation of protein kinase B. *Molecular and cellular biology*, 22(17):6247–6260, 9 2002.

[726] S. J. Snipas, M. Drag, H. R. Stennicke, and G. S. Salvesen. Activation mechanism and substrate specificity of the Drosophila initiator caspase DRONC. *Cell Death & Differentiation 2008 15:5*, 15(5):938–945, 2 2008.

[727] Chan Hee Kim, Donggi Paik, Florentina Rus, and Neal Silverman. The Caspase-8 Homolog Dredd Cleaves Imd and Relish but Is Not Inhibited by p35. *The Journal of Biological Chemistry*, 289(29):20092, 7 2014.

[728] Rui Zhou, Neal Silverman, Mei Hong, Dorothy S. Liao, Yvonne Chung, Zhijian J. Chen, and Tom Maniatis. The role of ubiquitination in Drosophila innate immunity. *Journal of Biological Chemistry*, 280(40):34048–34055, 10 2005.

[729] Silvia Guntermann and Edan Foley. The protein Dredd is an essential component of the c-Jun N-terminal kinase pathway in the Drosophila immune response. *Journal of Biological Chemistry*, 286(35):30284–30294, 9 2011.

[730] Po Chen, Antony Rodriguez, Robert Erskine, Tien Thach, and John M. Abrams. Dredd,a Novel Effector of the Apoptosis ActivatorsReaper, Grim,andHidinDrosophila. *Developmental Biology*, 201(2):202–216, 9 1998.

[731] Inma González and Ana Busturia. High levels of dRYBP induce apoptosis in Drosophila imaginal cells through the activation of reaper and the requirement of trithorax, dredd and dFADD. *Cell Research 2009 19:6*, 19(6):747–757, 3 2009.

[732] Christopher J. Alteri, Juan Xicohténcatl-Cortes, Sonja Hess, Guillermo Caballero-Olin, Jorge A. Girón, and Richard L. Friedman. Mycobacterium tuberculosis produces pili during human infection. *Proceedings of the National Academy of Sciences of the United States of America*, 104(12):5145, 3 2007.

[733] Albertus Viljoen, Yves F. Dufrêne, and Jérôme Nigou. Mycobacterial Adhesion: From Hydrophobic to Receptor-Ligand Interactions. *Microorganisms*, 10(2), 2 2022.

[734] Cynthia B. Whitchurch, Tim Tolker-Nielsen, Paula C. Ragas, and John S. Mattick. Extracellular DNA required for bacterial biofilm formation. *Science (New York, N.Y.)*, 295 (5559):1487, 2 2002.

[735] Marie Allesen-Holm, Kim Bundvig Barken, Liang Yang, Mikkel Klausen, Jeremy S. Webb, Staffan Kjelleberg, Søren Molin, Michael Givskov, and Tim Tolker-Nielsen. A characterization of DNA release in Pseudomonas aeruginosa cultures and biofilms. *Molecular microbiology*, 59(4):1114–1128, 2 2006.

[736] Erin S. Gloag, Lynne Turnbull, Alan Huang, Pascal Vallotton, Huabin Wang, Laura M. Nolan, Lisa Mililli, Cameron Hunt, Jing Lu, Sarah R. Osvath, Leigh G. Monahan, Rosalia

Cavaliere, Ian G. Charles, Matt P. Wand, Michelle L. Gee, Ranganathan Prabhakar, and Cynthia B. Whitchurch. Self-organization of bacterial biofilms is facilitated by extracellular DNA. *Proceedings of the National Academy of Sciences of the United States of America*, 110(28):11541–11546, 7 2013.

[737] Davide Campoccia, Lucio Montanaro, and Carla Renata Arciola. Extracellular DNA (eDNA). A Major Ubiquitous Element of the Bacterial Biofilm Architecture. *International Journal of Molecular Sciences 2021, Vol. 22, Page 9100*, 22(16):9100, 8 2021.

[738] L. W. Matthews, S. Spector, J. Lemm, and J. L. Potter. Studies on pulmonary secretions. I. The overall chemical composition of pulmonary secretions from patients with cystic fibrosis, bronchiectasis, and laryngectomy. *The American review of respiratory disease*, 88:199–204, 8 1963.

[739] Eric A. Jones, Glen McGillivary, and Lauren O. Bakaletz. Extracellular DNA within a nontypeable Haemophilus influenzae-induced biofilm binds human beta defensin-3 and reduces its antimicrobial activity. *Journal of innate immunity*, 5(1):24–38, 1 2013.

[740] Giovanna Batoni, Giuseppantonio Maisetta, and Semih Esin. Antimicrobial peptides and their interaction with biofilms of medically relevant bacteria. *Biochimica et biophysica acta*, 1858(5):1044–1060, 5 2016.

[741] Reuben Ramphal, Michel Lhermitte, M. Filliat, and Philippe Roussel. The binding of anti-pseudomonal antibiotics to macromolecules from cystic fibrosis sputum. *Journal of Antimicrobial Chemotherapy*, 22(4):483–490, 10 1988.

[742] Heidi Mulcahy, Laetitia Charron-Mazenod, and Shawn Lewenza. Extracellular DNA Chelates Cations and Induces Antibiotic Resistance in Pseudomonas aeruginosa Biofilms. *PLoS Pathogens*, 4(11):1000213, 11 2008.

[743] Wen Chi Chiang, Martin Nilsson, Peter Østrup Jensen, Niels Høiby, Thomas E. Nielsen, Michael Givskov, and Tim Tolker-Nielsen. Extracellular DNA shields against aminoglycosides in Pseudomonas aeruginosa biofilms. *Antimicrobial Agents and Chemotherapy*, 57(5):2352–2361, 5 2013.

[744] Natalya Doroshenko, Boo Shan Tseng, Robert P. Howlin, Jill Deacon, Julian A. Wharton, Philipp J. Thurner, Brendan F. Gilmore, Matthew R. Parsek, and Paul Stoodley. Extracellular DNA impedes the transport of vancomycin in Staphylococcus epidermidis biofilms preexposed to subinhibitory concentrations of vancomycin. *Antimicrobial agents and chemotherapy*, 58(12):7273–7282, 12 2014.

[745] Mike Wilton, Laetitia Charron-Mazenod, Richard Moore, and Shawn Lewenza. Extracellular DNA Acidifies Biofilms and Induces Aminoglycoside Resistance in Pseudomonas aeruginosa. *Antimicrobial agents and chemotherapy*, 60(1):544–553, 1 2015.

[746] Søren Molin and Tim Tolker-Nielsen. Gene transfer occurs with enhanced efficiency in biofilms and induces enhanced stabilisation of the biofilm structure. *Current Opinion in Biotechnology*, 14(3):255–261, 6 2003.

[747] Jeremy S. Webb, Lyndal S. Thompson, Sally James, Tim Charlton, Tim Tolker-Nielsen, Birgit Koch, Michael Givskov, and Staffan Kjelleberg. Cell Death in Pseudomonas aeruginosa Biofilm Development. *Journal of Bacteriology*, 185(15):4585, 8 2003.

[748] Lynne Turnbull, Masanori Toyofuku, Amelia L. Hynen, Masaharu Kurosawa, Gabriella Pessi, Nicola K. Petty, Sarah R. Osvath, Gerardo Cárcamo-Oyarce, Erin S. Gloag, Raz Shimoni, Ulrich Omasits, Satoshi Ito, Xinhui Yap, Leigh G. Monahan, Rosalia Cavaliere, Christian H. Ahrens, Ian G. Charles, Nobuhiko Nomura, Leo Eberl, and Cynthia B. Whitchurch. Explosive cell lysis as a mechanism for the biogenesis of bacterial membrane vesicles and biofilms. *Nature Communications*, 7, 4 2016.

[749] Alejandra L. Ibáñez de Aldecoa, Olga Zafra, and José E. González-Pastor. Mechanisms and Regulation of Extracellular DNA Release and Its Biological Roles in Microbial Communities. *Frontiers in microbiology*, 8(JUL), 7 2017.

[750] Ali Tahrioui, Rachel Duchesne, Emeline Bouffartigues, Sophie Rodrigues, Olivier Maillot, Damien Tortuel, Julie Hardouin, Laure Taupin, Marie Christine Groleau, Alain Dufour, Eric Déziel, Gerald Brenner-Weiss, Marc Feuilloley, Nicole Orange, Olivier Lesouhaitier, Pierre Cornelis, and Sylvie Chevalier. Extracellular DNA release, quorum sensing, and PrrF1/F2 small RNAs are key players in Pseudomonas aeruginosa tobramycin-enhanced biofilm formation. *NPJ Biofilms and Microbiomes*, 5(1), 12 2019.

[751] Paul J. Planet, Scott C. Kachlany, Rob DeSalle, and David H. Figurski. Phylogeny of genes for secretion NTPases: identification of the widespread tadA subfamily and development of a diagnostic key for gene classification. *Proceedings of the National Academy of Sciences of the United States of America*, 98(5):2503–2508, 2 2001.

[752] P. J. Christie, J. E. Ward, M. P. Gordon, and E. W. Nester. A gene required for transfer of T-DNA to plants encodes an ATPase with autophosphorylating activity. *Proceedings of the National Academy of Sciences of the United States of America*, 86(24):9677–9681, 1989.

[753] Leslie A. Ronish, Ben Sidner, Yafan Yu, and Kurt H. Piepenbrink. Recognition of extracellular DNA by type IV pili promotes biofilm formation by Clostridioides difficile. *Journal of Biological Chemistry*, 298(10):102449, 10 2022.

[754] Christophe S. Bernard, Christophe Bordi, Elise Termine, Alain Filloux, and Sophie De Bentzmann. Organization and PprB-Dependent Control of the Pseudomonas aeruginosa tad Locus, Involved in Flp Pilus Biology. *Journal of Bacteriology*, 191(6):1961, 3 2009.

[755] Poushali Chakraborty, Sapna Bajeli, Deepak Kaushal, Bishan Dass Radotra, and Ashwani Kumar. Biofilm formation in the lung contributes to virulence and drug tolerance of Mycobacterium tuberculosis. *Nature Communications*, 12(1), 12 2021.

[756] Juan M. Zapata, Shu Ichi Matsuzawa, Adam Godzik, Eugen Leo, Steven A. Wasserman, and John C. Reed. The Drosophila tumor necrosis factor receptor-associated factor-1 (DTRAF1) interacts with Pelle and regulates NFkappaB activity. *The Journal of biological chemistry*, 275(16):12102–12107, 4 2000.

[757] Natalia Kozlova, José Braga, Josefin Lundgren, José Rino, Patrick Young, Maria Carmo-Fonseca, and Neus Visa. Studies on the role of NonA in mRNA biogenesis. *Experimental Cell Research*, 312(13):2619–2630, 8 2006.

[758] Sabine Ehrt, Dirk Schnappinger, and Kyu Y. Rhee. Metabolic principles of persistence and pathogenicity in Mycobacterium tuberculosis, 8 2018.

[759] Juanmei He, Xiaoman Kang, Jiacheng Wu, Zhihui Shao, Zhenhua Zhang, Yuqian Wu, Hua Yuan, Guoping Zhao, and Jin Wang. Transcriptional Self-Regulation of the Master

Nitrogen Regulator GlnR in Mycobacteria. *Journal of bacteriology*, 205(4):e0047922, 4 2023.

[760] Mehak Zahoor Khan, Ashima Bhaskar, Sandeep Upadhyay, Pooja Kumari, Raju S. Rajmani, Preeti Jain, Amit Singh, Dhiraj Kumar, Neel Sarovar Bhavesh, and Vinay Kumar Nandicoori. Protein kinase G confers survival advantage to Mycobacterium tuberculosis during latency-like conditions. *The Journal of Biological Chemistry*, 292(39):16093, 9 2017.

[761] Yong Yang, Jacob P. Richards, Jennifer Gundrum, and Anil K. Ojha. GlnR Activation Induces Peroxide Resistance in Mycobacterial Biofilms. *Frontiers in microbiology*, 9(JUL), 7 2018.

[762] Pierre Santucci, Matt D. Johansen, Vanessa Point, Isabelle Poncin, Albertus Viljoen, Jean François Cavalier, Laurent Kremer, and Stéphane Canaan. Nitrogen deprivation induces triacylglycerol accumulation, drug tolerance and hypervirulence in mycobacteria. *Scientific Reports*, 9(1), 12 2019.

[763] Alexandre Gouzy, Gérald Larrouy-Maumus, Ting Di Wu, Antonio Peixoto, Florence Levillain, Geanncarlo Lugo-Villarino, Jean Luc Gerquin-Kern, Luiz Pedro Sório De Carvalho, Yannick Poquet, and Olivier Neyrolles. Mycobacterium tuberculosis nitrogen assimilation and host colonization require aspartate. *Nature Chemical Biology*, 9(11): 674–676, 2013.

[764] Alexandre Gouzy, Gérald Larrouy-Maumus, Daria Bottai, Florence Levillain, Alexia Dumas, Joshua B. Wallach, Irène Caire-Brandli, Chantal de Chastellier, Ting Di Wu, Renaud Poincloux, Roland Brosch, Jean Luc Guerquin-Kern, Dirk Schnappinger, Luiz Pedro Sório de Carvalho, Yannick Poquet, and Olivier Neyrolles. Mycobacterium tuberculosis Exploits Asparagine to Assimilate Nitrogen and Resist Acid Stress during Infection. *PLoS Pathogens*, 10(2), 2014.

[765] P. O. Oluboyo and R. T. Erasmus. The significance of glucose intolerance in pulmonary tuberculosis. *Tubercle*, 71(2):135–138, 1990.

[766] Soren Kaeseler Andersen, Jakob Gjedsted, Christian Christiansen, and Else Tønnesen. The roles of insulin and hyperglycemia in sepsis pathogenesis. *Journal of leukocyte biology*, 75(3):413–421, 3 2004.

[767] David M. Higgins, Joaquin Sanchez-Campillo, Adrian G. Rosas-Taraco, Jonathan R. Higgins, Eric J. Lee, Ian M. Orme, and Mercedes Gonzalez-Juarrero. Relative levels of M-CSF and GM-CSF influence the specific generation of macrophage populations during infection with Mycobacterium tuberculosis. *Journal of immunology (Baltimore, Md. : 1950)*, 180(7):4892–4900, 4 2008.

[768] David G. Russell, Pere Joan Cardona, Mi Jeong Kim, Sophie Allain, and Frédéric Altare. Foamy macrophages and the progression of the human tuberculosis granuloma. *Nature immunology*, 10(9):943–948, 2009.

[769] Julius Brandenburg, Sebastian Marwitz, Simone C. Tazoll, Franziska Waldow, Barbara Kalsdorf, Tim Vierbuchen, Thomas Scholzen, Annette Gross, Svenja Goldenbaum, Alexandra Hölscher, Martina Hein, Lara Linnemann, Maja Reimann, Andreas Kispert, Michael Leitges, Jan Rupp, Christoph Lange, Stefan Niemann, Jochen Behrends, Torsten Goldmann, Holger Heine, Ulrich E. Schaible, Christoph Hölscher, Dominik Schwudke, and Norbert Reiling. WNT6/ACC2-induced storage of triacylglycerols in macrophages is exploited by Mycobacterium tuberculosis. *The Journal of clinical investigation*, 131(16), 8 2021.

[770] Helmy Rachman, Michael Strong, Timo Ulrichs, Leander Grode, Johannes Schuchhardt, Hans Mollenkopf, George A. Kosmiadi, David Eisenberg, and Stefan H.E. Kaufmann. Unique Transcriptome Signature of Mycobacterium tuberculosis in Pulmonary Tuberculosis. *Infection and Immunity*, 74(2):1233, 2 2006.

[771] Eduardo A. Troian, Heather M. Maldonado, Unnati Chauhan, Valdir C. Barth, and Nancy A. Woychik. Mycobacterium abscessus VapC5 toxin potentiates evasion of antibiotic killing by ribosome overproduction and activation of multiple resistance pathways. *Nature Communications 2023 14:1*, 14(1):1–15, 6 2023.

[772] Katrin Kierdorf, Fabian Hersperger, Jessica Sharrock, Crystal M. Vincent, Pinar Ustaoglu, Jiawen Dou, Attila Gyoergy, Olaf Groß, Daria E. Siekhaus, and Marc S. Dionne. Muscle function and homeostasis require cytokine inhibition of AKT activity in Drosophila. *eLife*, 9, 1 2020.

[773] Deniz Ertekin, Leonie Kirszenblat, Richard Faville, and Bruno Van Swinderen. Down-regulation of a cytokine secreted from peripheral fat bodies improves visual attention while reducing sleep in Drosophila. *PLoS biology*, 18(8), 8 2020.

[774] Khushboo Borah, Martin Beyß, Axel Theorell, Huihai Wu, Piyali Basu, Tom A. Mendum, Katharina Nöh, Dany J.V. Beste, and Johnjoe McFadden. Intracellular Mycobacterium tuberculosis Exploits Multiple Host Nitrogen Sources during Growth in Human Macrophages. *Cell Reports*, 29(11):3580–3591, 12 2019.

[775] Deeksha Tripathi, Harish Chandra, and Rakesh Bhatnagar. Poly-L-glutamate/glutamine synthesis in the cell wall of Mycobacterium bovis is regulated in response to nitrogen availability. *BMC microbiology*, 13(1), 2013.

[776] Yi Ding, Robert Jan Raterink, Rubén Marín-Juez, Wouter J. Veneman, Koen Egbers, Susan van den Eeden, Mariëlle C. Haks, Simone A. Joosten, Tom H.M. Ottenhoff, Amy C. Harms, A. Alia, Thomas Hankemeier, and Herman P. Spaink. Tuberculosis causes highly conserved metabolic changes in human patients, mycobacteria-infected mice and zebrafish larvae. *Scientific reports*, 10(1), 12 2020.

[777] Vivek Sharma, Sujata Sharma, Kerstin Hoener Zu Bentrup, John D. McKinney, David G. Russell, William R. Jacobs, and James C. Sacchettini. Structure of isocitrate lyase, a persistence factor of Mycobacterium tuberculosis. *Nature Structural Biology 2000 7:8*, 7 (8):663–668, 8 2000.

Appendix

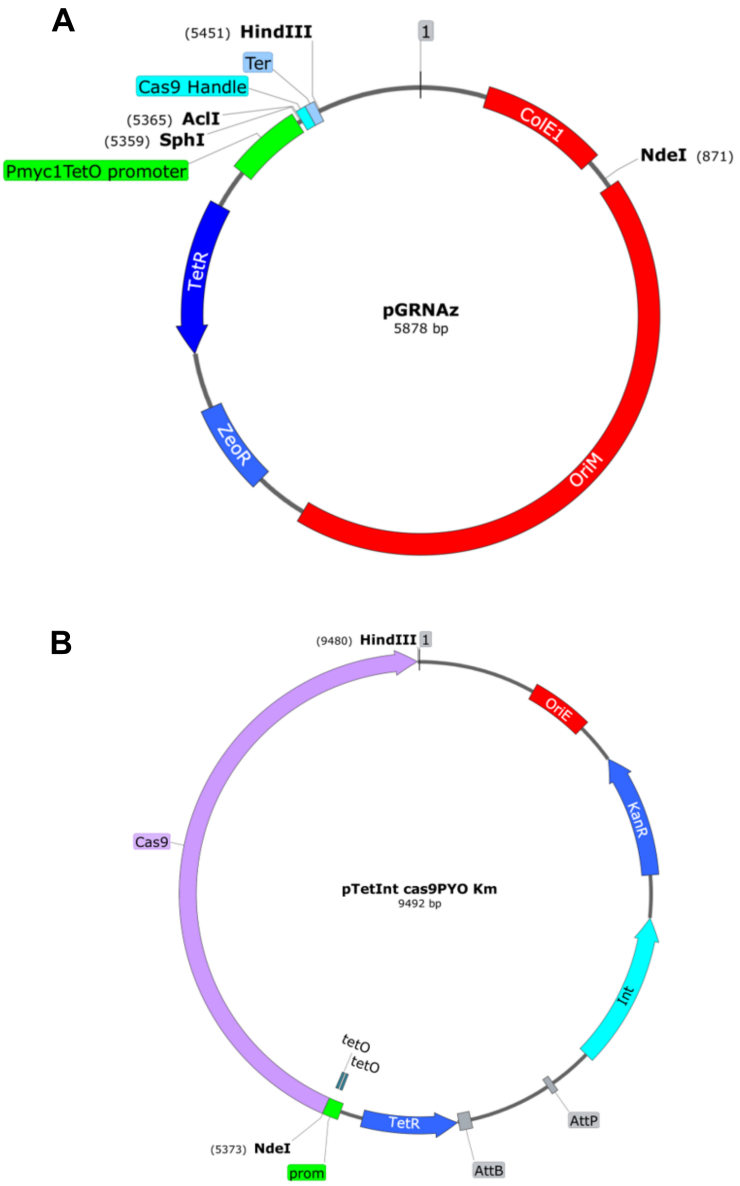


Figure S2.1. Plasmids used to produce *M. abscessus* knockout mutants using CRISPR-Cas9. (**A**) pGRNAz plasmid containing zeocin resistance gene. Guide RNA sequences were inserted between SphI and AclI restriction sites, upstream of the Cas9 handle and terminator sequence. Expression is under the control of tetracycline. (**B**) pTetInt-*cas9*PYO containing kanamycin resistance gene and Cas9, also under transcriptional control of tetracycline. Produced with SnapGene.

ATGGACAAGAAGTACAGCATCGGCCTGGACATCGGCACCAACAGCGTGGGCTGGGCG
GTCATCACGGACGAGTACAAGGTCCCCTCCAAGAAGTTCAAGGTCCTGGGCAACACCG
ACCGGCACAGCATCAAGAAGAACCTGATCGGCGCCCTGCTGTTCGACTCCGGCGAGA
CCGCCGAGGCGACGCGCCTGAAGCGGACCGCGCGGCGCCGATACACGCGGCGCAAG
AACCGCATCTGCTACCTCCAGGAAATCTTCTCGAACGAGATGGCCAAGGTGGACGACA
GCTTCTTCCACCGGCTGGAGGAGTCCTTCCTGGTGGAGGAGGACAAGAAGCACGAGC
GCCACCCGATCTTCGGCAACATCGTGGACGAGGTGGCCTACCACGAGAAGTACCCCA
CGATCTACCACCTGCGCAAGAAGCTGGTGGACAGCACCGACAAGGCGGACCTGCGGC
TGATCTACCTGGCCCTGGCGCACATGATCAAGTTCCGCGGCCACTTCCTGATCGAGGG
CGACCTGAACCCGGACAACTCGGACGTGGACAAGCTGTTCATCCAGCTGGTGCAGACC
TACAACCAGCTGTTCGAGGAGAACCCCATCAACGCCTCCGGCGTGGACGCCAAGGCG
ATCCTGTCGGCGCGCCTGTCCAAGTCGCGGCGCCTGGAGAACCTGATCGCCCAGCTG
CCGGGCGAGAAGAAGAACGGCCTGTTCGGCAACCTGATCGCGCTGAGCCTGGGCCTG
ACGCCCAACTTCAAGTCCAACTTCGACCTGGCCGAGGACGCGAAGCTCCAGCTGTCGA
AGGACACCTACGACGACGACCTGGACAACCTGCTGGCCCAGATCGGCGACCAGTACG
CGGACCTGTTCCTGGCCGCCAAGAACCTGAGCGACGCCATCCTGCTGTCCGACATCCT
GCGGGTCAACACCGAGATCACGAAGGCCCCGCTGAGCGCGTCCATGATCAAGCGGTA
CGACGAGCACCACCAGGACCTGACCCTGCTGAAGGCGCTGGTGCGCCAGCAGCTGCC
CGAGAAGTACAAGGAAATCTTCTTCGACCAGTCGAAGAACGGCTACGCCGGCTACATC
GACGGCGGCGCGAGCCAGGAGGAGTTCTACAAGTTCATCAAGCCGATCCTGGAGAAG
ATGGACGGCACGGAGGAGCTGCTGGTCAAGCTGAACCGCGAGGACCTGCTGCGCAAG
CAGCGGACCTTCGACAACGGCTCGATCCCGCACCAGATCCACCTGGGCGAGCTGCAC
GCCATCCTGCGGCGCCAGGAGGACTTCTACCCCTTCCTGAAGGACAACCGCGAGAAG
ATCGAGAAGATCCTGACGTTCCGCATCCCGTACTACGTCGGCCCGCTGGCCCGCGGC
AACTCGCGCTTCGCGTGGATGACCCGGAAGAGCGAGGAGACCATCACGCCGTGGAAC
TTCGAGGAGGTCGTGGACAAGGGCGCCTCGGCGCAGAGCTTCATCGAGCGCATGACC
AACTTCGACAAGAACCTGCCGAACGAGAAGGTCCTGCCCAAGCACAGCCTGCTGTACG
AGTACTTCACCGTGTACAACGAGCTGACGAAGGTCAAGTACGTGACCGAGGGTATGCG
CAAGCCGGCCTTCCTGTCGGGCGAGCAGAAGAAGGCGATCGTGGACCTGCTGTTCAA
GACCAACCGCAAGGTCACGGTGAAGCAGCTGAAGGAGGACTACTTCAAGAAGATCGAG
TGTTTCGACTCGGTCGAGATCAGCGGCGTGGAGGACCGCTTCAACGCCAGCCTGGGC
ACCTACCACGACCTGCTGAAGATCATCAAGGACAAGGACTTCCTGGACAACGAGGAGA
ACGAGGACATCCTGGAGGACATCGTCCTGACCCTGACGCTGTTCGAGGACCGCGAGA
TGATCGAGGAGCGGCTGAAGACGTACGCCCACCTGTTCGACGACAAGGTGATGAAGC
AGCTGAAGCGGCGCCGATACACCGGCTGGGGCCGCCTGTCGCGGAAGCTGATCAACG
GCATCCGGGACAAGCAGTCCGGCAAGACCATCCTGGACTTCCTGAAGTCGGACGGCTT

Figure S2.2. Sequence of *S. pyogenes cas9* enzyme expressed by plasmid pTetInt-*cas9*PYO.

CGCGAACCGCAACTTCATGCAGCTGATCCACGACGACAGCCTGACCTTCAAGGAGGAC
ATCCAGAAGGCCCAAGTGAGCGGCCAGGGCGACTCCCTGCACGAGCACATCGCCAAC
CTGGCGGGCTCGCCGGCGATCAAGAAGGGCATCCTCCAGACCGTCAAGGTCGTGGAC
GAGCTGGTCAAGGTGATGGGCCGCCACAAGCCCGAGAACATCGTGATCGAGATGGCC
CGGGAGAACCAGACCACGCAGAAGGGCCAGAAGAACAGCCGCGAGCGGATGAAGCG
CATCGAGGAGGGCATCAAGGAGCTGGGCTCCCAGATCCTGAAGGAGCACCCGGTCGA
GAACACCCAGCTCCAGAACGAGAAGCTGTACCTGTACTACCTCCAGAACGGCCGCGAC
ATGTACGTGGACCAGGAGCTGGACATCAACCGGCTGAGCGACTACGACGTGGACCAC
ATCGTGCCGCAGTCGTTCCTGAAGGACGACAGCATCGACAACAAGGTCCTGACCCGCT
CGGACAAGAACCGGGGCAAGTCGGACAACGTGCCCAGCGAGGAGGTCGTGAAGAAGA
TGAAGAACTACTGGCGCCAGCTGCTGAACGCCAAGCTGATCACGCAGCGCAAGTTCGA
CAACCTGACCAAGGCCGAGCGGGGCGGCCTGAGCGAGCTGGACAAGGCGGGCTTCA
TCAAGCGCCAGCTGGTCGAGACCCGGCAGATCACGAAGCACGTGGCGCAGATCCTGG
ACTCGCGGATGAACACGAAGTACGACGAGAACGACAAGCTGATCCGCGAGGTCAAGG
TGATCACCCTGAAGTCCAAGCTGGTCTCGGACTTCCGCAAGGACTTCCAGTTCTACAAG
GTCCGGGAGATCAACAACTACCACCACGCCCACGACGCGTACCTGAACGCCGTCGTG
GGCACCGCGCTGATCAAGAAGTACCCGAAGCTGGAGTCGGAGTTCGTCTACGGCGAC
TACAAGGTCTACGACGTGCGCAAGATGATCGCCAAGTCCGAGCAGGAGATCGGCAAG
GCCACCGCGAAGTACTTCTTCTACTCGAACATCATGAACTTCTTCAAGACCGAGATCAC
GCTGGCCAACGGCGAGATCCGCAAGCGCCCGCTGATCGAGACCAACGGCGAGACGG
GCGAGATCGTCTGGGACAAGGGCCGCGACTTCGCGACCGTCCGGAAGGTGCTGTCGA
TGCCGCAGGTCAACATCGTGAAGAAGACCGAGGTGCAGACGGGCGGCTTCTCCAAGG
AGTCGATCCTGCCCAAGCGCAACTCGGACAAGCTGATCGCCCGGAAGAAGGACTGGG
ACCCGAAGAAGTACGGCGGCTTCGACTCCCCCACCGTCGCCTACTCGGTGCTGGTCG
TGGCGAAGGTCGAGAAGGGCAAGTCCAAGAAGCTGAAGTCGGTGAAGGAGCTGCTGG
GCATCACCATCATGGAGCGCTCGTCGTTCGAGAAGAACCCGATCGACTTCCTGGAGGC
GAAGGGCTACAAGGAGGTCAAGAAGGACCTGATCATCAAGCTGCCCAAGTACTCCCTG
TTCGAGCTGGAGAACGGCCGCAAGCGGATGCTGGCCTCGGCGGGCGAGCTGCAAAAG
GGCAACGAGCTGGCCCTGCCGAGCAAGTACGTCAACTTCCTGTACCTGGCGTCGCACT
ACGAGAAGCTGAAGGGCAGCCCCGAGGACAACGAGCAGAAGCAGCTGTTCGTGGAGC
AGCACAAGCACTACCTGGACGAGATCATCGAGCAGATCAGCGAGTTCTCCAAGCGCGT
CATCCTGGCCGACGCGAACCTGGACAAGGTGCTGAGCGCCTACAACAAGCACCGCGA
CAAGCCGATCCGGGAGCAGGCGGAGAACATCATCCACCTGTTCACCCTGACGAACCTG
GGTGCCCCGGCCGCCTTCAAGTACTTCGACACCACGATCGACCGCAAGCGGTACACCT
CGACGAAGGAGGTGCTGGACGCGACCCTGATCCACCAGTCCATCACGGGCCTGTACG
AGACGCGGATCGACCTGAGCCAGCTGGGCGGCGACTAA

Figure S2.2. Sequence of *S. pyogenes cas9* enzyme expressed by plasmid pTetInt-*cas9*PYO continued.

```
# Paste in gene of interest sequence 5' - 3'
sequence = list("")
print("Sequence length:", (len(sequence)))
print("Primers identified:")

# Set minimum and maximum length of primers and desired GC content
x = 19
while x <= 21:
    def sliding_window_analysis(sequence, function, window_size=x, step_size=1):
        for start in range(0, len(sequence), step_size):
            end = start + window_size
            if end > len(sequence):
                break
            yield start, end, function(sequence[start:end])

    def gc_content(sequence):
        gc_count = sequence.count("G") + sequence.count("C")
        return gc_count

    for start, end, gc in sliding_window_analysis(sequence, gc_content):
        if gc == (30 - x) and (sequence[end - 2] == "C" or sequence[end - 2] == "G")
        and (sequence[end - 1] == "C" or sequence[end - 1] == "G"):
            print(*sequence[start:end])
            print("Start:", start, "End:", end,"Length:", len(sequence[start:end]),
            "GC Count:", gc)
        else:
            pass
    x = x + 1
```

Figure S2.3. Python script for design of PCR primers to amplify *M. abscessus* target genes. The script is designed to search the inputted nucleotide sequence to identify primer sequences between 19 and 21 nucleotides long and calculate the GC content, producing a list of possible primer target sequences.

Table S2.1. R studio packages.

Package	Function
bdsmatrix	Matrices used by coxme
broom	Summarises statistical information in tibbles
cowplot	Themes and functions to align plots into complex compound figures (alternative to patchwork)
coxme	Fit Cox proportional hazards models containing both fixed and random effects
dplyr	For working with data frame like objects
emmeans	Obtain estimated marginal means for linear, generalized linear, and mixed models
FSA	Functions for data import, manipulation, statistical analysis, and result visualization
ggfortify	Plotting tools for statistics used in survival analysis
gggenes	Extension of ggplot2 for producing gene arrow maps
ggplot2	For producing graphics
ggprism	Aesthetic functions for plots
ggpubr	For customising ggplot2 graphics
ggsignif	To show statistical comparisons between groups on ggplots
ggtext	ggplot2 extension for formatting of plot labels
gridExtra	Functions to work with grid graphics and tables
lubridate	Functions to work with date-times and time-spans
magrittr	Forward pipe operator
pacman	Wrap library and package related functions
ranger	To analyse data from genome-wide association studies
readxl	To import excel data files
reshape	Reshape and aggregate data
rio	Data import and export
rstatix	For performing basic statistical tests
patchwork	Build a compound figure containing multiple plots (alternative to cowplot)
scales	Map data to aesthetics for data visualisation
simplevis	Wrapper function for visualisation
stringr	For text wrapping and formatting

Package	Function
survival	Contains the core survival analysis routines
survminer	Contains the function ’ggsurvplot()’ for drawing survival curves
tidyverse	Collection of packages for data manipulation and visualisation

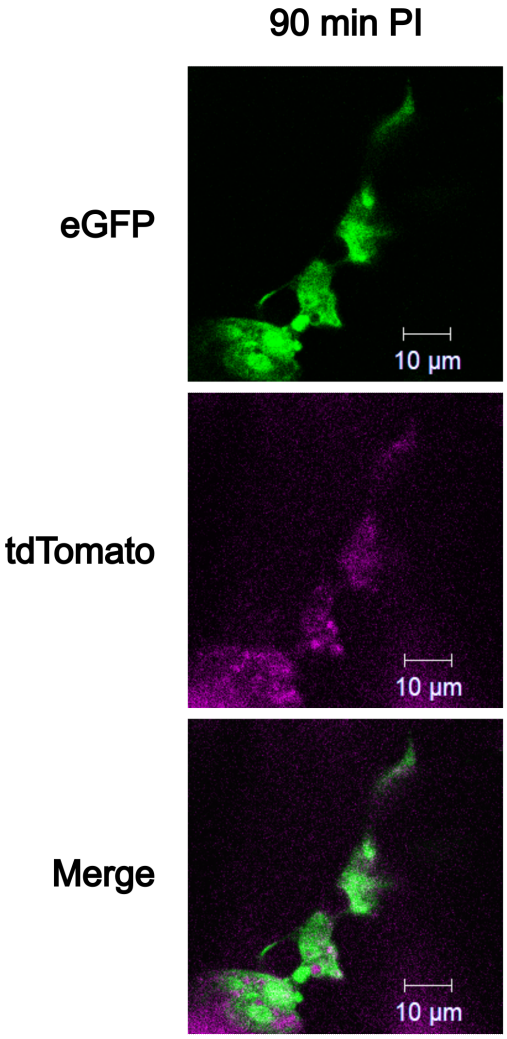


Figure S3.1. Confocal images of *D. melanogaster* haemocytes infected with *M. abscessus*. Confocal images taken of live *D. melanogaster* with *in vivo M. abscessus* tdTomato Smooth infection. Flies with haemocytes expressing eGFP (Hml$^{\Delta}$-Gal4, UAS-2x-eGFP) were injected with *M. abscessus* tdTomato Rough (magenta) and imaged 90 minutes post infection. Scale bar represents 10 μm.

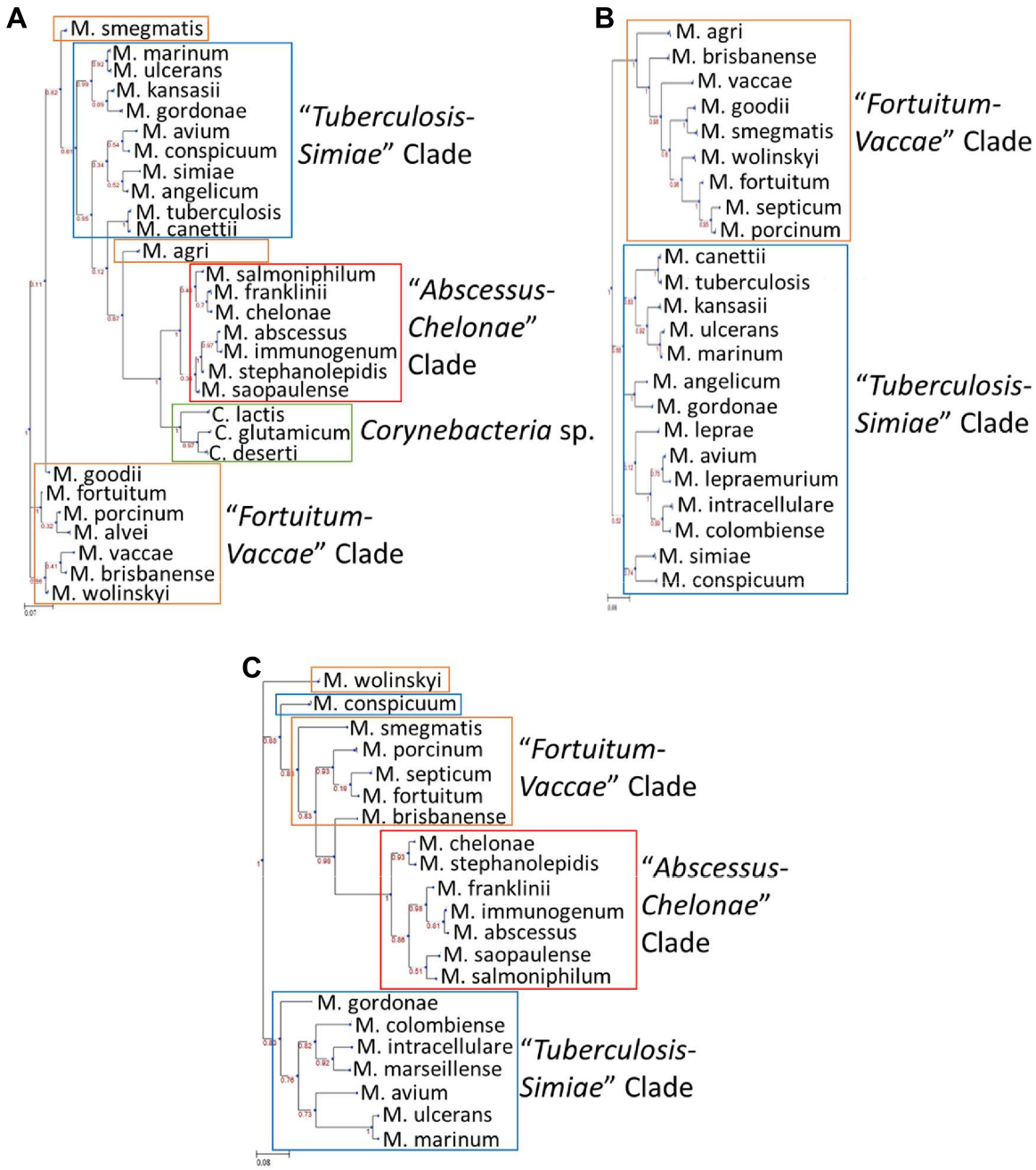


Figure S4.1. Isocitrate lyase enzymes in *Mycobacteria*. (**A**) Phylogenetic analysis of isocitrate lyase 1 (ICL1) in *Mycobacteria*. Produced using homologues of *M. abscessus* isocitrate lyase MAB_4095c. Most *Mycobacteria* have ICL1 enzymes closely related to those in other bacterial species, seen by the similarity to the *Corynebacteria* sp. ICL1, with the exception of *M. leprae*. (**B**) Phylogenetic analysis of mycobacterial isocitrate lyase 2 (ICL2, also known as AceA), which is more similar to plant and fungal isocitrate lyase enzymes. This enzyme is completely absent from the "*Abscessus-Chelonae*" clade. Produced using homologues of *M. tuberculosis* Erdman ICL2. (**C**) Phylogenetic analysis of methylisocitrate lyase (MCL) in *Mycobacteria*. Produced using homologues of *M. abscessus* methylisocitrate lyase MAB_4618. Several species including *M. tuberculosis*, *M. leprae*, and *M. kansasii* are lacking MCL. Produced with TREND.

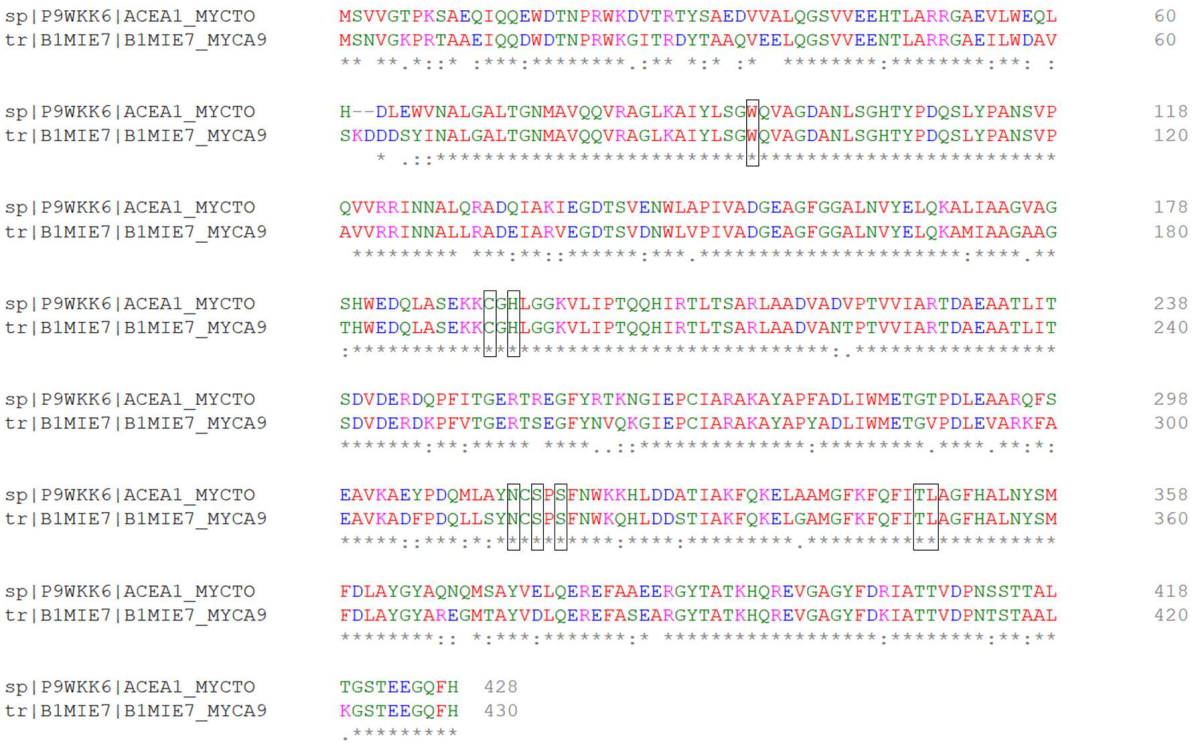


Figure S4.2. Multiple sequence alignment of isocitrate lyase 1 in *M. abscessus* and *M. tuberculosis*. Multiple sequence alignment of *M. tuberculosis* ICL1 (MYCTO) and *M. abscessus* isocitrate lyase MAB_4095c (MYCA9). Black boxes indicate active site residues of *M. tuberculosis*[777]. Produced with Clustal Omega.

Table S6.1. Statistically significant comparisons for Figure 6.7.

Gene	Time	Comparison	P-value
Drs	6 hr	UI vs PBS	0.5 (∗)
Drs	6 hr	UI vs ATCC19977	0.1 (∗∗)
Drs	6 hr	UI vs Δ1132c-1	0.31 (∗)
Drs	6 hr	UI vs Δ1132c-2	0.5 (∗)
Drs	6 hr	UI vs Δ1132c-3	0.017 (∗∗)
Drs	48 hr	UI vs ATCC19977	0.00021 (∗∗∗∗)
Drs	48 hr	PBS vs ATCC19977	0.013 (∗∗∗)
Drs	48 hr	ATCC19977 vs Δ1132c-1	0.017 (∗∗)
Drs	48 hr	ATCC19977 vs Δ1132c-2	0.000044 (∗∗∗∗)
Drs	48 hr	ATCC19977 vs Δ1132c-3	0.021 (∗∗)
Drs	80 hr	UI vs ATCC19977	0.000011 (∗∗∗∗)
Drs	80 hr	UI vs Δ1132c-1	0.0015 (∗∗∗)
Drs	80 hr	UI vs Δ1132c-2	0.1 (∗∗)
Drs	80 hr	UI vs Δ1132c-3	0.0098 (∗∗∗)
Drs	80 hr	PBS vs ATCC19977	0.000011 (∗∗∗∗)
Drs	80 hr	PBS vs Δ1132c-1	0.0015 (∗∗∗)
Drs	80 hr	PBS vs Δ1132c-2	0.083 (∗∗)
Drs	80 hr	PBS vs Δ1132c-3	0.027 (∗∗)
Drs	80 hr	ATCC19977 vs Δ1132c-1	0.035 (∗∗)
Drs	80 hr	ATCC19977 vs Δ1132c-2	0.0015 (∗∗∗)
Drs	80 hr	ATCC19977 vs Δ1132c-3	0.003 (∗∗∗)
Mtk	6 hr	UI vs PBS	0.000078 (∗∗∗∗)
Mtk	6 hr	UI vs ATCC19977	0.000078 (∗∗∗∗)
Mtk	6 hr	UI vs Δ1132c-1	0.000022 (∗∗∗∗)
Mtk	6 hr	UI vs Δ1132c-2	0.000022 (∗∗∗∗)
Mtk	6 hr	UI vs Δ1132c-3	0.000011 (∗∗∗∗)
Mtk	48 hr	UI vs ATCC19977	0.000011 (∗∗∗∗)
Mtk	48 hr	UI vs Δ1132c-1	0.021 (∗∗)
Mtk	48 hr	UI vs Δ1132c-2	0.12 (∗∗)
Mtk	48 hr	UI vs Δ1132c-3	0.0041 (∗∗∗)
Mtk	48 hr	PBS vs ATCC19977	0.044 (∗∗)

Gene	Time	Comparison	P-value
Mtk	48 hr	ATCC19977 vs Δ1132c-1	0.0011 (∗∗∗∗)
Mtk	48 hr	ATCC19977 vs Δ1132c-2	0.003 (∗∗∗)
Mtk	48 hr	ATCC19977 vs Δ1132c-3	0.027 (∗∗)
Mtk	80 hr	UI vs ATCC19977	0.000011 (∗∗∗∗)
Mtk	80 hr	UI vs Δ1132c-1	0.0011 (∗∗∗∗)
Mtk	80 hr	UI vs Δ1132c-2	0.0022 (∗∗∗)
Mtk	80 hr	UI vs Δ1132c-3	0.013 (∗∗∗)
Mtk	80 hr	PBS vs ATCC19977	0.000011 (∗∗∗∗)
Mtk	80 hr	PBS vs Δ1132c-1	0.00033 (∗∗∗∗)
Mtk	80 hr	PBS vs Δ1132c-2	0.0011 (∗∗∗∗)
Mtk	80 hr	PBS vs Δ1132c-3	0.0056 (∗∗∗)
Mtk	80 hr	ATCC19977 vs Δ1132c-2	0.000078 (∗∗∗∗)
Mtk	80 hr	ATCC19977 vs Δ1132c-3	0.00021 (∗∗∗∗)
IM1	6 hr	UI vs PBS	0.31 (∗)
IM1	6 hr	UI vs ATCC19977	0.0056 (∗∗∗)
IM1	6 hr	UI vs Δ1132c-1	0.055 (∗∗)
IM1	6 hr	UI vs Δ1132c-2	0.044 (∗∗)
IM1	6 hr	UI vs Δ1132c-3	0.00013 (∗∗∗∗)
IM1	48 hr	UI vs ATCC19977	0.000011 (∗∗∗∗)
IM1	48 hr	UI vs Δ1132c-1	0.26 (∗)
IM1	48 hr	UI vs Δ1132c-3	0.013 (∗∗∗)
IM1	48 hr	PBS vs ATCC19977	0.000011 (∗∗∗∗)
IM1	48 hr	PBS vs Δ1132c-1	0.5 (∗)
IM1	48 hr	PBS vs Δ1132c-3	0.044 (∗∗)
IM1	48 hr	ATCC19977 vs Δ1132c-1	0.0011 (∗∗∗∗)
IM1	48 hr	ATCC19977 vs Δ1132c-2	0.003 (∗∗∗)
IM1	48 hr	ATCC19977 vs Δ1132c-3	0.00021 (∗∗∗∗)
IM1	80 hr	UI vs ATCC19977	0.000011 (∗∗∗∗)
IM1	80 hr	UI vs Δ1132c-1	0.000044 (∗∗∗∗)
IM1	80 hr	UI vs Δ1132c-2	0.013 (∗∗∗)
IM1	80 hr	UI vs Δ1132c-3	0.003 (∗∗∗)
IM1	80 hr	PBS vs ATCC19977	0.000011 (∗∗∗∗)

Gene	Time	Comparison	P-value
IM1	80 hr	PBS vs Δ1132c-1	0.000011 (∗∗∗∗)
IM1	80 hr	PBS vs Δ1132c-2	0.017 (∗∗)
IM1	80 hr	PBS vs Δ1132c-3	0.0041 (∗∗∗)
IM1	80 hr	ATCC19977 vs Δ1132c-2	0.0015 (∗∗∗)
IM1	80 hr	ATCC19977 vs Δ1132c-3	0.021 (∗∗)
IM2	6 hr	UI vs PBS	0.5 (∗)
IM2	6 hr	UI vs ATCC19977	0.00021 (∗∗∗∗)
IM2	6 hr	UI vs Δ1132c-1	0.013 (∗∗∗)
IM2	6 hr	UI vs Δ1132c-2	0.017 (∗∗)
IM2	6 hr	UI vs Δ1132c-3	0.0022 (∗∗∗)
IM2	6 hr	PBS vs ATCC19977	0.26 (∗)
IM2	48 hr	UI vs ATCC19977	0.000011 (∗∗∗∗)
IM2	48 hr	UI vs Δ1132c-1	0.22 (∗)
IM2	48 hr	UI vs Δ1132c-2	0.43 (∗)
IM2	48 hr	UI vs Δ1132c-3	0.035 (∗∗)
IM2	48 hr	PBS vs ATCC19977	0.000011 (∗∗∗∗)
IM2	48 hr	PBS vs Δ1132c-3	0.055 (∗∗)
IM2	48 hr	ATCC19977 vs Δ1132c-1	0.0005 (∗∗∗∗)
IM2	48 hr	ATCC19977 vs Δ1132c-2	0.00074 (∗∗∗∗)
IM2	48 hr	ATCC19977 vs Δ1132c-3	0.0022 (∗∗∗)
IM2	80 hr	UI vs ATCC19977	0.000011 (∗∗∗∗)
IM2	80 hr	UI vs Δ1132c-1	0.000011 (∗∗∗∗)
IM2	80 hr	UI vs Δ1132c-2	0.017 (∗∗)
IM2	80 hr	UI vs Δ1132c-3	0.021 (∗∗)
IM2	80 hr	PBS vs ATCC19977	0.000011 (∗∗∗∗)
IM2	80 hr	PBS vs Δ1132c-1	0.000011 (∗∗∗∗)
IM2	80 hr	PBS vs Δ1132c-2	0.027 (∗∗)
IM2	80 hr	PBS vs Δ1132c-3	0.068 (∗∗)
IM2	80 hr	ATCC19977 vs Δ1132c-2	0.0022 (∗∗∗)
IM2	80 hr	ATCC19977 vs Δ1132c-3	0.22 (∗)
IM4	6 hr	UI vs ATCC19977	0.044 (∗∗)
IM4	6 hr	UI vs Δ1132c-2	0.26 (∗)

Gene	Time	Comparison	P-value
IM4	6 hr	UI vs Δ1132c-3	0.1 (∗∗)
IM4	48 hr	UI vs ATCC19977	0.000044 (∗∗∗∗)
IM4	48 hr	UI vs Δ1132c-3	0.027 (∗∗)
IM4	48 hr	PBS vs ATCC19977	0.0011 (∗∗∗∗)
IM4	48 hr	PBS vs Δ1132c-3	0.58 (∗)
IM4	48 hr	ATCC19977 vs Δ1132c-1	0.013 (∗∗∗)
IM4	48 hr	ATCC19977 vs Δ1132c-2	0.021 (∗∗)
IM4	48 hr	ATCC19977 vs Δ1132c-3	0.013 (∗∗∗)
IM4	80 hr	UI vs ATCC19977	0.000044 (∗∗∗∗)
IM4	80 hr	UI vs Δ1132c-1	0.003 (∗∗∗)
IM4	80 hr	UI vs Δ1132c-2	0.12 (∗∗)
IM4	80 hr	UI vs Δ1132c-3	0.15 (∗)
IM4	80 hr	PBS vs ATCC19977	0.000022 (∗∗∗∗)
IM4	80 hr	PBS vs Δ1132c-1	0.00074 (∗∗∗∗)
IM4	80 hr	PBS vs Δ1132c-2	0.15 (∗)
IM4	80 hr	PBS vs Δ1132c-3	0.18 (∗)
IM4	80 hr	ATCC19977 vs Δ1132c-1	0.26 (∗)
IM4	80 hr	ATCC19977 vs Δ1132c-2	0.0041 (∗∗∗)
IM4	80 hr	ATCC19977 vs Δ1132c-3	0.068 (∗∗)
IM10	6 hr	UI vs ATCC19977	0.0015 (∗∗∗)
IM10	6 hr	UI vs Δ1132c-1	0.18 (∗)
IM10	6 hr	UI vs Δ1132c-2	0.055 (∗∗)
IM10	6 hr	UI vs Δ1132c-3	0.0015 (∗∗∗)
IM10	6 hr	ATCC19977 vs Δ1132c-1	0.67 (∗)
IM10	48 hr	UI vs ATCC19977	0.00033 (∗∗∗∗)
IM10	48 hr	UI vs Δ1132c-3	0.1 (∗∗)
IM10	48 hr	PBS vs ATCC19977	0.00074 (∗∗∗∗)
IM10	48 hr	PBS vs Δ1132c-3	0.18 (∗)
IM10	48 hr	ATCC19977 vs Δ1132c-1	0.0098 (∗∗∗)
IM10	48 hr	ATCC19977 vs Δ1132c-2	0.0074 (∗∗∗)
IM10	48 hr	ATCC19977 vs Δ1132c-3	0.027 (∗∗)
IM10	80 hr	UI vs ATCC19977	0.000011 (∗∗∗∗)

Gene	Time	Comparison	P-value
IM10	80 hr	UI vs Δ1132c-1	0.000022 (∗∗∗∗)
IM10	80 hr	UI vs Δ1132c-2	0.0056 (∗∗∗)
IM10	80 hr	UI vs Δ1132c-3	0.0041 (∗∗∗)
IM10	80 hr	PBS vs ATCC19977	0.000011 (∗∗∗∗)
IM10	80 hr	PBS vs Δ1132c-1	0.000011 (∗∗∗∗)
IM10	80 hr	PBS vs Δ1132c-2	0.0074 (∗∗∗)
IM10	80 hr	PBS vs Δ1132c-3	0.0015 (∗∗∗)
IM10	80 hr	ATCC19977 vs Δ1132c-1	0.18 (∗)
IM10	80 hr	ATCC19977 vs Δ1132c-2	0.15 (∗)
IM10	80 hr	ATCC19977 vs Δ1132c-3	0.027 (∗∗)

Table S6.2. Statistically significant comparisons for Figure 6.8.

Gene	Time	Comparison	P-value
AttA	6 hr	UI vs PBS	0.00013 (∗∗∗∗)
AttA	6 hr	UI vs ATCC19977	0.000022 (∗∗∗∗)
AttA	6 hr	UI vs Δ1132c-1	0.000078 (∗∗∗∗)
AttA	6 hr	UI vs Δ1132c-2	0.000011 (∗∗∗∗)
AttA	6 hr	UI vs Δ1132c-3	0.000011 (∗∗∗∗)
AttA	48 hr	UI vs ATCC19977	0.000011 (∗∗∗∗)
AttA	48 hr	UI vs Δ1132c-1	0.027 (∗∗)
AttA	48 hr	UI vs Δ1132c-2	0.31 (∗)
AttA	48 hr	UI vs Δ1132c-3	0.0022 (∗∗∗)
AttA	48 hr	PBS vs ATCC19977	0.0022 (∗∗∗)
AttA	48 hr	PBS vs Δ1132c-3	0.36 (∗)
AttA	48 hr	ATCC19977 vs Δ1132c-1	0.000011 (∗∗∗∗)
AttA	48 hr	ATCC19977 vs Δ1132c-2	0.003 (∗∗∗)
AttA	48 hr	ATCC19977 vs Δ1132c-3	0.044 (∗∗)
AttA	80 hr	UI vs ATCC19977	0.000011 (∗∗∗∗)
AttA	80 hr	UI vs Δ1132c-1	0.00074 (∗∗∗∗)
AttA	80 hr	UI vs Δ1132c-2	0.013 (∗∗∗)
AttA	80 hr	UI vs Δ1132c-3	0.0015 (∗∗∗)
AttA	80 hr	PBS vs ATCC19977	0.000011 (∗∗∗∗)
AttA	80 hr	PBS vs Δ1132c-1	0.0005 (∗∗∗∗)
AttA	80 hr	PBS vs Δ1132c-2	0.021 (∗∗)
AttA	80 hr	PBS vs Δ1132c-3	0.0022 (∗∗∗)
AttA	80 hr	ATCC19977 vs Δ1132c-1	0.000078 (∗∗∗∗)
AttA	80 hr	ATCC19977 vs Δ1132c-2	0.000078 (∗∗∗∗)
AttA	80 hr	ATCC19977 vs Δ1132c-3	0.00074 (∗∗∗∗)
Dipt	6 hr	UI vs PBS	0.000044 (∗∗∗∗)
Dipt	6 hr	UI vs ATCC19977	0.000044 (∗∗∗∗)
Dipt	6 hr	UI vs Δ1132c-1	0.00013 (∗∗∗∗)
Dipt	6 hr	UI vs Δ1132c-2	0.000011 (∗∗∗∗)
Dipt	6 hr	UI vs Δ1132c-3	0.000011 (∗∗∗∗)
Dipt	6 hr	Δ1132c-1 vs Δ1132c-3	0.58 (∗)

Gene	Time	Comparison	P-value
Dipt	48 hr	UI vs ATCC19977	0.0011 (∗∗∗∗)
Dipt	48 hr	UI vs Δ1132c-3	0.36 (∗)
Dipt	48 hr	PBS vs ATCC19977	0.36 (∗)
Dipt	48 hr	ATCC19977 vs Δ1132c-1	0.0098 (∗∗∗)
Dipt	48 hr	ATCC19977 vs Δ1132c-2	0.021 (∗∗)
Dipt	80 hr	UI vs ATCC19977	0.000011 (∗∗∗∗)
Dipt	80 hr	UI vs Δ1132c-1	0.5 (∗)
Dipt	80 hr	UI vs Δ1132c-2	0.1 (∗∗)
Dipt	80 hr	UI vs Δ1132c-3	0.055 (∗∗)
Dipt	80 hr	PBS vs ATCC19977	0.000011 (∗∗∗∗)
Dipt	80 hr	PBS vs Δ1132c-1	0.58 (∗)
Dipt	80 hr	PBS vs Δ1132c-2	0.22 (∗)
Dipt	80 hr	PBS vs Δ1132c-3	0.12 (∗∗)
Dipt	80 hr	ATCC19977 vs Δ1132c-1	0.0011 (∗∗∗∗)
Dipt	80 hr	ATCC19977 vs Δ1132c-2	0.0056 (∗∗∗)
Dipt	80 hr	ATCC19977 vs Δ1132c-3	0.027 (∗∗)
Dro	6 hr	UI vs PBS	0.00013 (∗∗∗∗)
Dro	6 hr	UI vs ATCC19977	0.00013 (∗∗∗∗)
Dro	6 hr	UI vs Δ1132c-1	0.00033 (∗∗∗∗)
Dro	6 hr	UI vs Δ1132c-2	0.00033 (∗∗∗∗)
Dro	6 hr	UI vs Δ1132c-3	0.00013 (∗∗∗∗)
Dro	48 hr	UI vs PBS	0.18 (∗)
Dro	48 hr	UI vs ATCC19977	0.000022 (∗∗∗∗)
Dro	48 hr	UI vs Δ1132c-1	0.0098 (∗∗∗)
Dro	48 hr	UI vs Δ1132c-2	0.021 (∗∗)
Dro	48 hr	UI vs Δ1132c-3	0.00074 (∗∗∗∗)
Dro	48 hr	PBS vs ATCC19977	0.67 (∗)
Dro	48 hr	ATCC19977 vs Δ1132c-1	0.027 (∗∗)
Dro	48 hr	ATCC19977 vs Δ1132c-2	0.0022 (∗∗∗)
Dro	48 hr	ATCC19977 vs Δ1132c-3	0.58 (∗)
Dro	80 hr	UI vs ATCC19977	0.000011 (∗∗∗∗)
Dro	80 hr	UI vs Δ1132c-1	0.0022 (∗∗∗)

Gene	Time	Comparison	P-value
Dro	80 hr	UI vs Δ1132c-2	0.0098 (∗∗∗)
Dro	80 hr	UI vs Δ1132c-3	0.0074 (∗∗∗)
Dro	80 hr	PBS vs ATCC19977	0.000011 (∗∗∗∗)
Dro	80 hr	PBS vs Δ1132c-1	0.0056 (∗∗∗)
Dro	80 hr	PBS vs Δ1132c-2	0.035 (∗∗)
Dro	80 hr	PBS vs Δ1132c-3	0.013 (∗∗∗)
Dro	80 hr	ATCC19977 vs Δ1132c-1	0.15 (∗)
Dro	80 hr	ATCC19977 vs Δ1132c-2	0.000011 (∗∗∗∗)
Dro	80 hr	ATCC19977 vs Δ1132c-3	0.000022 (∗∗∗∗)
CecA1	6 hr	UI vs ATCC19977	0.055 (∗∗)
CecA1	6 hr	UI vs Δ1132c-2	0.0022 (∗∗∗)
CecA1	6 hr	UI vs Δ1132c-3	0.027 (∗∗)
CecA1	48 hr	UI vs ATCC19977	0.5 (∗)
CecA1	48 hr	UI vs Δ1132c-3	0.43 (∗)
CecA1	48 hr	PBS vs Δ1132c-3	0.22 (∗)
CecA1	48 hr	ATCC19977 vs Δ1132c-2	0.1 (∗∗)
CecA1	48 hr	ATCC19977 vs Δ1132c-3	0.013 (∗∗∗)
CecA1	48 hr	Δ1132c-1 vs Δ1132c-2	0.67 (∗)
CecA1	48 hr	Δ1132c-1 vs Δ1132c-3	0.055 (∗∗)
CecA1	80 hr	UI vs ATCC19977	0.0015 (∗∗∗)
CecA1	80 hr	PBS vs ATCC19977	0.0015 (∗∗∗)
CecA1	80 hr	ATCC19977 vs Δ1132c-1	0.0098 (∗∗∗)
CecA1	80 hr	ATCC19977 vs Δ1132c-2	0.027 (∗∗)
CecA1	80 hr	ATCC19977 vs Δ1132c-3	0.1 (∗∗)
Def	80 hr	ATCC19977 vs Δ1132c-2	0.035 (∗∗)

Table S6.3. Statistically significant comparisons for Figure 6.9.

Gene	Time	Comparison	P-value
Upd2	6 hr	UI vs Δ1132c-3	0.068 (∗∗)
Upd2	6 hr	PBS vs Δ1132c-3	0.1 (∗∗)
Upd2	6 hr	ATCC19977 vs Δ1132c-3	0.055 (∗∗)
Upd2	6 hr	Δ1132c-1 vs Δ1132c-3	0.5 (∗)
Upd2	6 hr	Δ1132c-2 vs Δ1132c-3	0.31 (∗)
Upd2	48 hr	UI vs ATCC19977	0.055 (∗∗)
Upd2	48 hr	PBS vs ATCC19977	0.055 (∗∗)
Upd2	48 hr	ATCC19977 vs Δ1132c-2	0.67 (∗)
Upd2	48 hr	ATCC19977 vs Δ1132c-3	0.26 (∗)
Upd2	80 hr	PBS vs ATCC19977	0.26 (∗)
Upd2	80 hr	ATCC19977 vs Δ1132c-2	0.18 (∗)
Upd2	80 hr	Δ1132c-1 vs Δ1132c-2	0.58 (∗)
Upd2	80 hr	Δ1132c-2 vs Δ1132c-3	0.26 (∗)
Upd3	6 hr	UI vs Δ1132c-3	0.31 (∗)
Upd3	6 hr	ATCC19977 vs Δ1132c-3	0.26 (∗)
Upd3	6 hr	Δ1132c-2 vs Δ1132c-3	0.67 (∗)
Upd3	48 hr	ATCC19977 vs Δ1132c-2	0.055 (∗∗)
Upd3	48 hr	ATCC19977 vs Δ1132c-3	0.017 (∗∗)
Upd3	80 hr	PBS vs ATCC19977	0.58 (∗)
Upd3	80 hr	PBS vs Δ1132c-1	0.5 (∗)
Upd3	80 hr	PBS vs Δ1132c-3	0.22 (∗)
Upd3	80 hr	ATCC19977 vs Δ1132c-2	0.58 (∗)
Upd3	80 hr	Δ1132c-2 vs Δ1132c-3	0.58 (∗)
Socs36E	6 hr	UI vs Δ1132c-1	0.58 (∗)
Socs36E	6 hr	PBS vs Δ1132c-2	0.18 (∗)
Socs36E	6 hr	Δ1132c-1 vs Δ1132c-2	0.068 (∗∗)
Socs36E	6 hr	Δ1132c-2 vs Δ1132c-3	0.044 (∗∗)
Socs36E	80 hr	UI vs ATCC19977	0.31 (∗)
Socs36E	80 hr	PBS vs ATCC19977	0.43 (∗)
Stat92E	48 hr	UI vs ATCC19977	0.083 (∗∗)
Stat92E	48 hr	UI vs Δ1132c-1	0.044 (∗∗)

Gene	Time	Comparison	P-value
Stat92E	48 hr	UI vs Δ1132c-2	0.055 (∗∗)
Stat92E	48 hr	UI vs Δ1132c-3	0.044 (∗∗)
Atg2	6 hr	UI vs Δ1132c-1	0.43 (∗)
Atg2	6 hr	UI vs Δ1132c-2	0.12 (∗∗)
Atg2	6 hr	UI vs Δ1132c-3	0.58 (∗)
Atg2	6 hr	PBS vs Δ1132c-2	0.18 (∗)
Atg2	6 hr	ATCC19977 vs Δ1132c-2	0.18 (∗)
Atg2	6 hr	ATCC19977 vs Δ1132c-3	0.31 (∗)
Atg2	48 hr	UI vs Δ1132c-2	0.5 (∗)
Atg2	48 hr	UI vs Δ1132c-3	0.068 (∗∗)
Atg2	80 hr	UI vs Δ1132c-1	0.31 (∗)
TotA	6 hr	UI vs Δ1132c-2	0.0015 (∗∗∗)
TotA	6 hr	PBS vs Δ1132c-2	0.044 (∗∗)
TotA	6 hr	ATCC19977 vs Δ1132c-2	0.15 (∗)
TotA	6 hr	Δ1132c-1 vs Δ1132c-2	0.31 (∗)
TotA	48 hr	PBS vs Δ1132c-2	0.43 (∗)
TotA	48 hr	PBS vs Δ1132c-3	0.43 (∗)
TotA	80 hr	UI vs PBS	0.083 (∗∗)
TotA	80 hr	UI vs ATCC19977	0.0098 (∗∗∗)
TotA	80 hr	UI vs Δ1132c-2	0.5 (∗)
TotA	80 hr	PBS vs ATCC19977	0.000011 (∗∗∗∗)
TotA	80 hr	PBS vs Δ1132c-2	0.000044 (∗∗∗∗)
TotA	80 hr	PBS vs Δ1132c-3	0.0005 (∗∗∗∗)
TotA	80 hr	ATCC19977 vs Δ1132c-1	0.0041 (∗∗∗)
TotA	80 hr	ATCC19977 vs Δ1132c-2	0.43 (∗)
TotA	80 hr	ATCC19977 vs Δ1132c-3	0.36 (∗)
TotA	80 hr	Δ1132c-1 vs Δ1132c-2	0.22 (∗)
TotA	80 hr	Δ1132c-1 vs Δ1132c-3	0.67 (∗)
egr-RA	6 hr	UI vs ATCC19977	0.26 (∗)
egr-RA	6 hr	UI vs Δ1132c-2	0.068 (∗∗)
egr-RA	6 hr	UI vs Δ1132c-3	0.31 (∗)
egr-RA	6 hr	PBS vs Δ1132c-2	0.5 (∗)

Gene	Time	Comparison	P-value
egr-RA	48 hr	UI vs Δ1132c-2	0.43 (∗)
egr-RA	48 hr	PBS vs Δ1132c-2	0.22 (∗)
egr-RA	48 hr	PBS vs Δ1132c-3	0.083 (∗∗)
egr-RA	48 hr	ATCC19977 vs Δ1132c-2	0.5 (∗)
egr-RA	48 hr	ATCC19977 vs Δ1132c-3	0.58 (∗)
egr-RA	48 hr	Δ1132c-1 vs Δ1132c-2	0.58 (∗)
egr-RA	80 hr	UI vs Δ1132c-2	0.5 (∗)
egr-RA	80 hr	PBS vs Δ1132c-2	0.12 (∗∗)
egr-RA	80 hr	Δ1132c-2 vs Δ1132c-3	0.43 (∗)
Tace	6 hr	ATCC19977 vs Δ1132c-1	0.58 (∗)
Tace	6 hr	ATCC19977 vs Δ1132c-2	0.035 (∗∗)
Tace	6 hr	Δ1132c-2 vs Δ1132c-3	0.36 (∗)
Tace	48 hr	ATCC19977 vs Δ1132c-1	0.58 (∗)
Tace	48 hr	ATCC19977 vs Δ1132c-2	0.67 (∗)
Tace	80 hr	UI vs Δ1132c-2	0.26 (∗)
Tace	80 hr	UI vs Δ1132c-3	0.26 (∗)
Tace	80 hr	PBS vs Δ1132c-2	0.055 (∗∗)
Tace	80 hr	PBS vs Δ1132c-3	0.083 (∗∗)
Tace	80 hr	ATCC19977 vs Δ1132c-2	0.26 (∗)
Tace	80 hr	ATCC19977 vs Δ1132c-3	0.58 (∗)
Tace	80 hr	Δ1132c-1 vs Δ1132c-2	0.31 (∗)